A biomechanical study of lateral ankle sprain

David Christopher Rochelle

Submitted in accordance with the requirements for the degree of Doctor of Philosophy

The University of Leeds

Institute of Medical and Biological Engineering

School of Mechanical Engineering

October 2020

The candidate confirms that the work submitted is their own, except where work which has formed part of jointly authored publications has been included. The contribution of the candidate and the other authors to this work has been explicitly indicated below. The candidate confirms that appropriate credit has been given within the thesis where reference has been made to the work of others.

The work within the section titled 'Characterisation of the Lateral Collateral Ligament Complex at Realistic Sprain-inducing Strain Rates' within Chapter 3 is based on work from jointly authored publications, shown in Appendix H – Author's Journal Article. The contents of the following publication contributed to the entire chapter (Rochelle, D.C., Herbert, A., Ktistakis, I., Redmond, A.C., Chapman, G.J. and Brockett, C.L. 2020. Mechanical characterisation of the lateral collateral ligament complex of the ankle at realistic sprain-like strain rates. Journal of the Mechanical Behavior of Biomedical Materials. 102, p.103473).

Acknowledgements

As with many before me, the road to completing my PhD was not without an obstacle or two (or twenty) along the way. But on the bright side, at least the current global pandemic did not interfere with the practical elements of my project. The journey to completion was made through persistence, hard work and a bit of luck but was only possible due to the support from those around me to whom I will be forever grateful.

Firstly, I must thank all of my many supervisors Claire, Tony, Tony and Graham for their continued guidance and motivation to pursue through the challenges, I seriously would not have completed my project without their dedication. I am also thankful for the contributions of Robin, John and Derrick, my industrial sponsors from Xiros, for their product insight, active involvement and additional resources provided.

To the human tissue donors and their families, who were progressively minded and selfless in their actions to willingly aid the advancement of engineering and scientific research, I am ever so grateful for your sacrifice.

There are many others who contributed to my personal development and the progression of the project who I sincerely thank. Both Ioannis and Ippokratis provided surgical training and performed surgical procedures for my project without whom a large extent of the human tissue testing would not have been possible. Also contributing to my ability to perform human tissue research from a university perspective were Nagitha, Dan and Stacy, thank you guys.

Phil the lab manager and the amazing technicians (Irvin, Keith, Sam, Jane, Dec, Lee, Camille and Rhys) all moved mountains (or at least a 12 ft drop-rig) when called upon, even in the 11th hour. Their hard work ensured the testing performed in this project was possible. After a long laboratory session and breaking/bending another part of my sprain simulator, yet again, they were always there to offer a smile or sometimes a sweet which really did pick me up, I cannot thank you guys enough for your support. Crucially important to performing motion capture were Qualisys AB, particularly Ian and Daniel, who were incredibly generous and flexible throughout the project offering an exemplary level of service.

Then there are the most important people in my life, my family, close friends and Ultimate Frisbee teammates. Whilst they mostly didn't know much beyond the fact I work with dead feet their ability to release the stresses of a PhD were second to none, exactly what I needed from them. I apologise for my moaning and the accidental exposures to images of partly dissected feet, I promise it won't happen again.

I owe my sanity to everyone involved in the making of The American Office which provided necessary interruption to thesis writing. Finally, to everyone who continuously asked over the last four years "have you finished you PhD yet?" you didn't help, but at least next time you ask I can thankfully now say "yes I have".

Abstract

Lateral ankle sprain is amongst the most common musculoskeletal injuries posing a significant economic and resource burden on healthcare systems. The high prevalence of chronic residual symptoms following ankle sprain can severely impact patient quality of life and contribute to the development of post-traumatic osteoarthritis.

The research presented hereinafter aimed to advance the development of synthetic interventions for ankle sprain by mechanically characterising the lateral ankle ligaments, analysing changes in joint stability following simulated sprain and evaluating the effectiveness of synthetic interventions to restore joint stability.

Strain rate was identified to significantly influence the failure load of ligaments demonstrating the importance of mechanically characterising ligaments at appropriate rates of loading. Characterising the lateral ankle ligaments determined that the ultimate failure load and stiffness of the lateral ankle ligaments do not differ systematically, however a tendency toward greater strength in people with a higher body mass index was identified.

A sectioning study of the lateral ankle ligaments analysed joint stability changes using anterior drawer and talar tilt tests determining lateral ankle stability to decrease with increasing damage. When repaired successfully synthetic intervention was able to adequately restore joint stability however catastrophic failure of suture tape fixation was frequent, particularly during inversion motion.

Suture anchor fixation of synthetic interventions was mechanically characterised in both porcine bone and a Sawbone model. Sawbone, used routinely for manufacturer testing, was determined to be an inadequate model of human bone. Loads achieved by the suture anchor fixation for the InternalBrace (Arthrex Inc, Naples, FL, USA) were below that of native lateral ankle ligaments but could be doubled by a simple adaptation proposed to prevent suture tape slippage.

This thesis advances the development of suture tapes and their fixation for the treatment of lateral ankle sprain however further research is required to seek benefit in their use.

Contents

List of Figures

List of Tables

Abbreviations

AIM	Automatic identification of markers
AiTFL	Anteroinferior tibiofibular ligament
AOFAS	American Orthopaedic Foot and Ankle Society
ATFL	Anterior talofibular ligament
BLB	Bone-ligament-bone
BMI	Body mass index
BW	Body weight
CAI	Chronic ankle instability
CFL	Calcaneofibular ligament
CI	Confidence interval
CT	Computed tomography
DOF	Degrees of freedom
FAAM	Foot and Ankle Ability Measure
FAOS	Visual analogue scale
GAGs	Glycosaminoglycans
iMBE	Institute of Medical and Biological Engineering
LAS	Lateral ankle sprain
LCL	Lateral collateral ligament
MRI	Magnetic resonance imaging
NHS	National Health Service
PBS	Phosphate buffered saline
PEG	Polyethylene glycol
PiTFL	Posteroinferior tibiofibular ligament
PLLA	Polylactic acid
PMMA	Polymethyl methacrylate
PRICE	Protection, rest, ice, compression and elevation
PTFL	Posterior talofibular ligament
PTOA	Post-traumatic osteoarthritis
QTM	Qualisys Track Manager
ROM	Range of motion
SPEG	Mixture of sodium chloride and polyethylene glycol

UHMWPE	Ultra-high molecular weight polyethylene
VAS	Visual Analog Scale

Chapter 1 – Literature Review

1.1 Epidemiology of Sprain

Lateral ankle sprain (LAS) is one of the most common musculoskeletal injuries accounting for three to five percent of all Accident and Emergency visits in the UK, equating to around 300,000 reported injuries per year (Bridgman, 2003; Cooke, 2003). These figures are however thought to be underestimates with the incidence rate of ankle sprains being 5.5 times higher than reported to healthcare professionals (Kemler et al., 2015). Often ankle sprains go unreported as they are considered benign injuries that do not require professional treatment, evidenced by 44 % of individuals returning to sport within 24 hours of injury (Roos et al., 2017). Approximately 14 % of sprains are considered severe ankle sprains which require further assessment and treatment (Bridgman, 2003). Ankle sprain treatment costs, on average, approximately €360 in the Netherlands (Verhagen et al., 2005) therefore, assuming the same cost in the UK, the total annual cost of ankle sprains is estimated to be £98M.

A previous ankle sprain is however one of the most common predispositions to a LAS (12 % to 47 %), hence the repetitive nature of sprains (Herzog et al., 2019). A prior sprain is believed to increase re-injury risk by 21% (Pefanis et al., 2009). Up to 70 % of individuals who suffer a LAS may develop residual physical disability such as chronic ankle instability (CAI) (Gribble et al., 2016a). Functional ankle instability has been attributed as a risk factor for post-traumatic ankle osteoarthritis (PTOA) (Golditz et al., 2014). Early development of PTOA could be detrimental to the young individuals prone to ankle sprain and therefore present an even larger economic burden (Hirose et al., 2004; Valderrabano et al., 2006; Bitton, 2009; Croy et al., 2012).

There is therefore an argument for early surgical intervention following LAS, once conservative treatment options have been exhausted, to better prevent the development of PTOA and the previously stated incurring economic costs. Research into the cause, prevention and treatment of LAS can assist in alleviating the long-term health and economic implications of LAS.

1.2 Anatomical Planes

The foot and ankle work harmoniously to provide considerable and complex motion at their many joints. The ankle joint complex is capable of multiaxial motion in all three anatomical planes of motion: the sagittal, frontal (coronal) and transverse planes, shown in Figure 1.

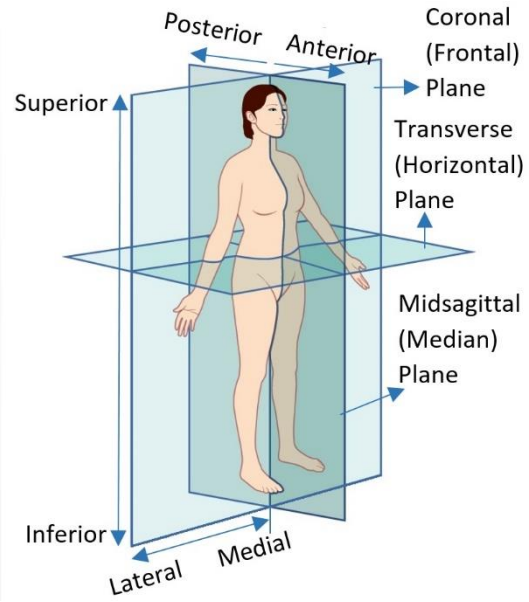

Figure 1. Anatomical planes of the body. Adapted from: (Connexions, 2013).

1.3 Ankle Complex Anatomy

The ankle complex is a multifaceted joint consisting of three joints. The talocrural (tibiotalar or "true ankle") joint and subtalar (talocalcaneal) joint are responsible for the majority of joint articulation for the ankle complex, shown in Figure 2. The distal tibiofibular syndesmosis (distal tibiofibular or inferior tibiofibular) joint, is the third joint of the ankle complex. The tibiofibular syndesmosis is not a synovial articulating joint but does allow accessory gliding which is crucial to the normal mechanics of the ankle (Hertel, 2002). The ankle complex has three major components of stability which are the congruity of the articulating surfaces when loaded, ligamentous restraints, and musculotendinous units (Hertel, 2002).

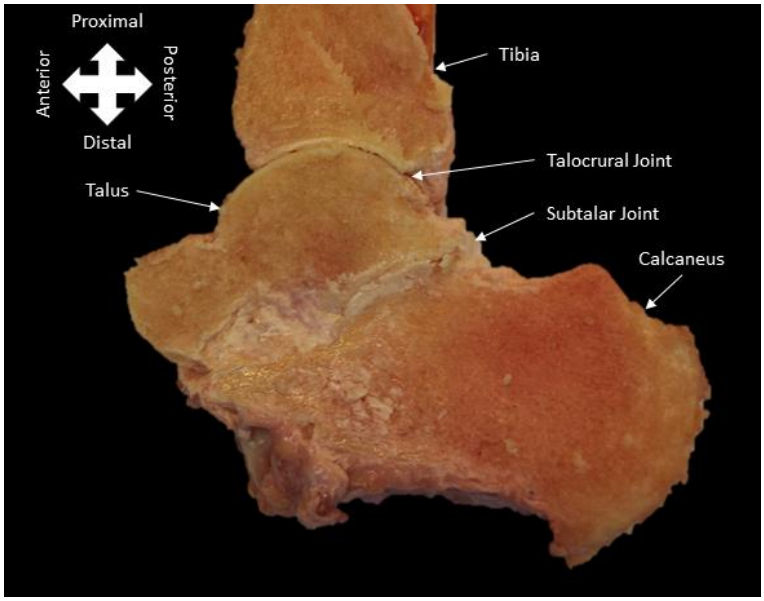

Figure 2. Medial view of a right foot where a midsagittal cut has been made through the ankle complex.

Reported in this review is the typical anatomy of the ankle however anatomical variations are frequent within the ankle and hindfoot (Aparisi Gómez et al., 2019). The anatomy varies in terms of size, orientation or even presence of structures including additional sesamoid bones, accessory ossicles, bipartitions, coalitions and accessory muscles (Aparisi Gómez et al., 2019). Anatomical variations are typically a by-product of a developmental abnormality that constitute an incidental radiographic finding (Sarrafian, 2011).

1.3.1 Talocrural Joint

The talocrural joint is formed by the articulation of the dome of the talus, medial malleolus, tibial plafond and lateral malleolus (Hertel, 2002). The joint forms a bracket-shape, known as a mortise, which can mostly be considered as a hinge joint allowing dorsi-/plantar flexion, yet a degree of motion occurs in all three anatomical planes, shown in Figure 3 (Hertel, 2002). The joint is most stable when in dorsiflexion due to the talus being on average 4.2 mm wider anteriorly (Sarrafian, 1993).

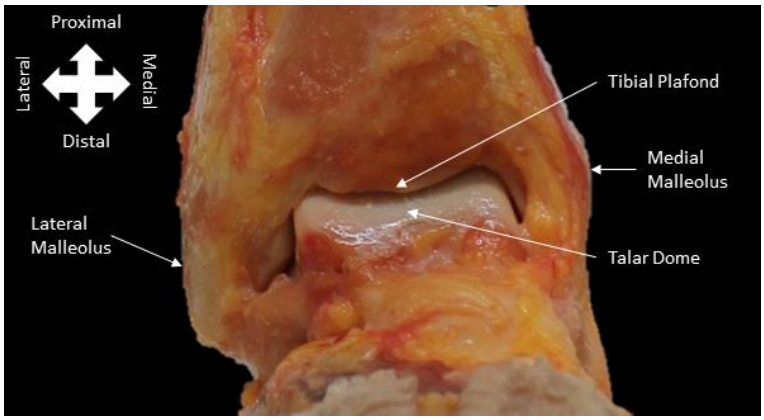

Figure 3. Anterior view of the talocrural joint.

When the ankle complex is fully loaded in a neutral or dorsiflexed position the congruity of articular surfaces provides 100 % of translational and 60 % of rotational stability (Watanabe et al., 2012). The static stabilisation provided by the ligaments is however crucial (Hertel, 2002) if the ankle is unloaded or in a plantar flexed position. When the ankle is unloaded the lateral ligaments contribute 70 to 80 % of anterior stability and the medial ligaments contribute 50 to 80 % of posterior stability (Watanabe et al., 2012). The medial and lateral ligaments together account for 50 to 80 % of rotational stability (Watanabe et al., 2012). The talocrural joint is statically stabilised by the joint capsule, the anterior talofibular ligament (ATFL), posterior talofibular ligament (PTFL), calcaneofibular ligament (CFL) and deltoid ligament (Hertel, 2002). The ATFL, PTFL and CFL stabilise the lateral side whereas the deltoid ligament stabilises the medial side. The tibiofibular syndesmosis ligaments also play a crucial role in the stabilisation of the lateral side of the talocrural joint by maintaining the distal joint between the tibia and fibula (Brockett and Chapman, 2016).

1.3.2 Subtalar Joint

Articulations between the talus and the calcaneus form the subtalar joint, shown in Figure 2 (Hertel, 2002). The three articulating facets of the inferior aspect of the talus are concave and the superior aspects of the calcaneus are concentrically convex allowing inversion and eversion (Brockett and Chapman, 2016). The subtalar joint consists of an intricate structure, having two separate joint cavities and allows for the motions of pronation and supination (Hertel, 2002). The posterior subtalar joint is formed between the inferior posterior facet of the talus and the superior posterior facet of the calcaneus (Rockar, 1995). Whereas the anterior subtalar joint is formed by the articulations between the anterior-superior facets of the talus (talar head) and the sustentaculum tali of the calcaneus (Hertel, 2002). Static stabilisation of the subtalar joint provided by ligamentous tissue is vast and provides a great contribution however it is not fully understood.

1.3.3 Ligaments

1.3.3.1 Lateral Collateral Ligament Complex

The lateral collateral ligament (LCL) complex consists of the ATFL, CFL and PTFL, shown in Figure 4. Ligaments in their own right the ATFL, CFL and PTFL can be considered as a complex due to their interconnecting fibres and proximity of insertion point to the fibula (Khawaji and Soames, 2015; Golanó et al., 2016; Matsui et al., 2017; Edama et al., 2018; Kakegawa et al., 2019; Dalmau-Pastor et al., 2020; Vega et al., 2020). Connecting fibres have been identified between the ATFL and PTFL, ATFL and CFL, and CFL and PTFL, shown in Figure 5 (Taser et al., 2006; Dalmau-Pastor et al., 2020).

The ATFL presents as an intra-capsular single, double or triple band fibre bundle at a frequency of 23 to 62 %, 36 to 70 % and 3 to 21 %, respectively (Milner and Soames, 1997; Khawaji and Soames, 2015; Matsui et al., 2017; Edama et al., 2018; Kakegawa et al., 2019). Irrespective of the number of fibre bundles, the overall width of the ATFL does not vary greatly (Milner and Soames, 1997). The ATFL is quadrilateral in shape and approximately 11 to 25 mm long, 5 to 11 mm wide and 2 mm thick (Taser et al., 2006; Snedeker et al., 2012; Matsui et al., 2017). The fibular origin of the ATFL is at the inferior aspect of the anterior border of the distal fibula laterally to the articular cartilage of the fibula (Matsui et al., 2017). The ATFL runs anteromedially and inserts on the body of the talus immediately anterior to the lateral articular surface, shown in Figure 4 (Harper, 1991; Sarrafian, 1993; Golanó et al., 2016). The ATFL forms a mean angle of 25 degrees (range 5 degrees to 45 degrees) with the transverse plane and 47 degrees (range 45 degrees to 56 degrees) with the sagittal plane (Taser et al., 2006).

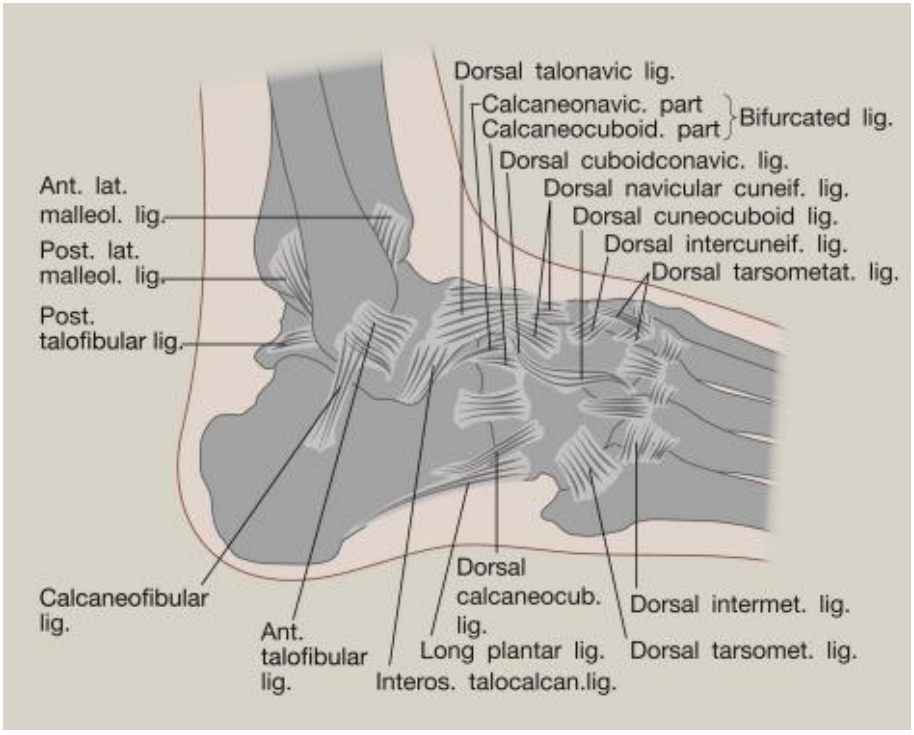

Figure 4. An illustration of the lateral ankle ligaments. Here the anterior talofibular ligament, abbreviated to ATFL throughout, is labelled (Ant. Talofibular lig.). The calcaneofibular ligament, abbreviated to CFL throughout, is labelled (Calcaneofibular lig.). The posterior talofibular ligament, abbreviated to PTFL throughout, is labelled (Post. talofibular lig.). The anteroinferior tibiofibular ligament, abbreviated to AiFTL throughout, is labelled (Ant. lat. malleol. lig.). The posteroinferior tibiofibular ligament, abbreviated to PiTFL throughout, is labelled (Post. lat. malleol. lig.). Source: (Gray and Lewis, 2000).

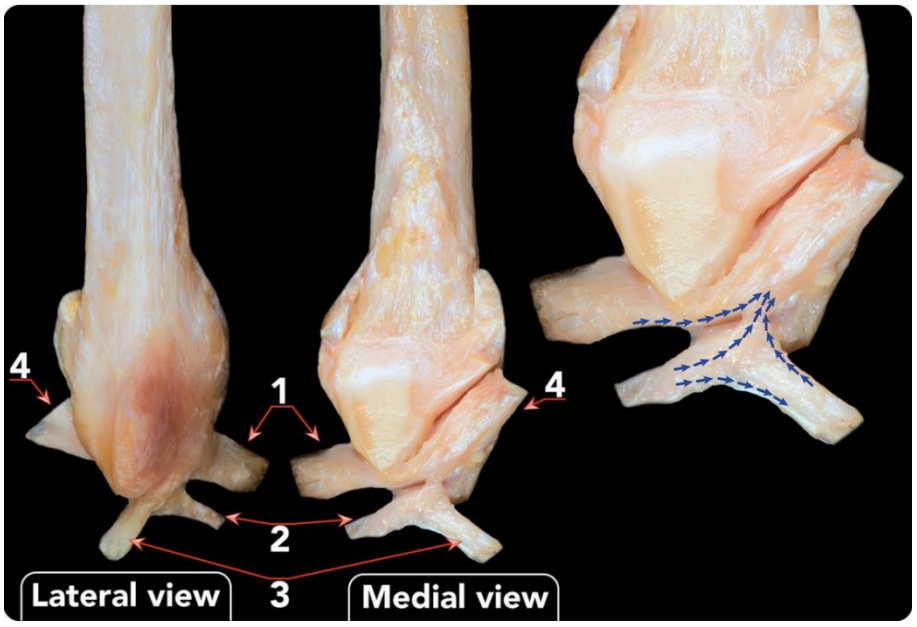

Figure 5. Lateral and medial view of the fibular malleolus showing connecting fibres between the superior (1) and inferior (2) bands of the ATFL, CFL (3) and PTFL (4). Blue arrows = the direction of interconnecting ligament fibres. Source: (Dalmau-Pastor et al., 2020).

The CFL, an extra-capsular ligament, can either have a cord-like structure with a consistent diameter or a flat fanning out structure getting wider towards calcaneal insertion (Matsui et

al., 2017; Kakegawa et al., 2019). Frequency of the various morphologies is argued in the literature with a meta-analysis by Matsui et al. 2017 reporting 66 % and 34 % occurrence of the cord-like and fanned out morphology, respectively (Matsui et al., 2017). In contrast studies performed by anatomists detailed the opposite findings with 67 % of ligaments being flat and 33 % cylindrical (Golanó et al., 2016; Kakegawa et al., 2019). Cross-sectional dimensions of the CFL do not vary greatly between flat and cylindrical cross-section morphologies. The width and diameter measurements quoted in the literature are 5 to 8 mm for both morphologies (Golanó et al., 2016; Matsui et al., 2017). Length measurements of the CFL are quoted from 15 to 35 mm in the meta-analysis by Matsui et al. 2017 with Golano et al. 2016 quoting 20 mm as the average length of the CFL (Golanó et al., 2016; Matsui et al., 2017). Fibular origin of the CFL is at the anterior border of the distal lateral malleolus and calcaneal insertion is at a small tubercle distal and posterior to the subtalar joint line, shown in Figure 4 (Snedeker et al., 2012). The CFL forms a mean angle of 40 degrees (range 30 degrees to 58 degrees) with the transverse plane and 51 degrees (range 32 degrees to 60 degrees) with the sagittal plane (Taser et al., 2006).

Fibular origin points of the ATFL and CFL have been identified to be independent, with connective tissue and fat separating the two ligaments (Kakegawa et al., 2019). In contrast, computed tomography (CT) analysis determined the ATFL and CFL to have a mutual point of origin on the fibula (Neuschwander et al., 2013). The ability to distinguish small thin layers of connective tissue and fat amongst other soft tissues is extremely challenging via dissection and using 3-dimensional CT. Whilst the findings regarding the origin of the ligaments are still unclear, the ligaments are definitely interconnected, shown by the blue arrows in Figure 5. The angle formed between the ATFL and CFL is approximately 105 degrees and between 90 to 100 degrees in the sagittal and frontal planes, respectively (Snedeker et al., 2012).

The PTFL originates on the posteromedial side of lateral malleolus and travels medially and close to horizontally to insert on the posterior side of the talus, shown in Figure 4 (Sarrafian, 2011; Golanó et al., 2016). The PTFL is trapezoidal in shape with a broad and multifascicular insertion points on the posterior surface of the talus, lateral talar process or os trigonum. The os trigonum is a small round, oval or triangular accessory bone present posterior to the talus in up to 25 % of individuals (Mellado et al., 2003; Sarrafian, 2011; Golanó et al., 2016; Aparisi Gómez et al., 2019). Length, width and thickness values of the PTFL are 15.3 ± 0.9 to 23.0 ± 7.0 mm, 5.5 ± 2.5 to 13.0 ± 3.1 mm and 2.3 ± 0.6 mm, respectively (Attarian et al., 1985; Milner and Soames, 1998; Butler and Walsh, 2004). Literature studying the PTFL is scarce in comparison to the ATFL and CFL which are damaged more often (Van Den Bekerom et al., 2008).

1.3.3.2 Medial Collateral Ligament Complex

The deltoid ligament is divided into deep and superficial layers which are anatomically separated (Tochigi et al., 2005; Hintermann et al., 2006; Snedeker et al., 2012). The superficial

layer consists of the tibiospring, tibionavicular, superficial posterior tibiotalar and tibiocalcaneal ligaments (Snedeker et al., 2012). The broad, fan shaped, and continuous structure of the deltoid ligament makes it difficult to differentiate between the superficial ligaments (Snedeker et al., 2012). All ligaments in the superficial layer of the deltoid ligament originate from the tibia, shown in Figure 6. The tibionavicular inserts onto the navicular bone blending its fibres with the tibiospring ligament which extends to the calcaneonavicular (spring) ligament (Mengiardi et al., 2005; Mengiardi et al., 2007; Sarrafian, 2011; Golanó et al., 2016). The tibiocalcaneal ligament runs vertically and inferiorly inserting onto the sustentaculum tali, a tubercle on the medial side of the calcaneus, shown in Figure 6 (Mengiardi et al., 2005; Mengiardi et al., 2007; Sarrafian, 2011; Golanó et al., 2016). The deep layer of the deltoid ligament consists of the deep anterior tibiotalar and deep posterior tibiotalar ligaments (Snedeker et al., 2012). The deep anterior tibiotalar ligament originates from the anterior aspect of the medial malleolus attaching to the medial aspect of talus and the deep posterior tibiotalar ligament originates from the distal tip of the medial malleolus immediately medial to the articulation surface and extends posterolaterally to its insertion point on the medial tubercle of the talus (Sarrafian, 2011; Snedeker et al., 2012).

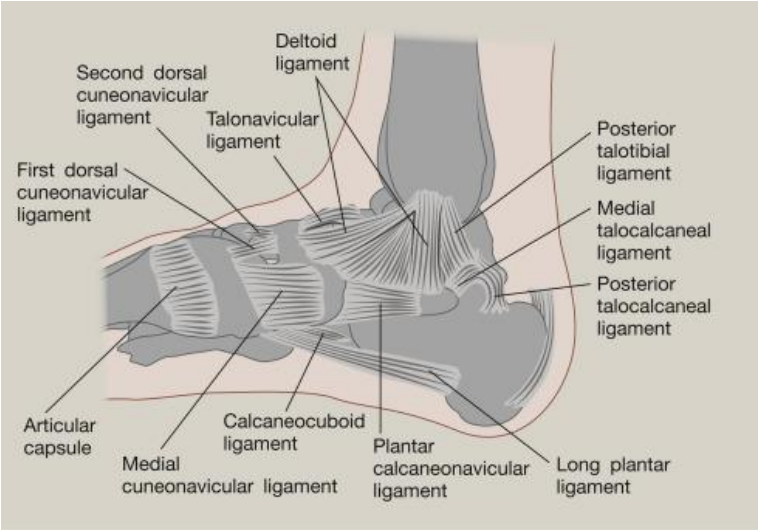

Figure 6. An illustration of the medial ankle ligaments of the ankle complex. The deltoid ligament and the posterior tibiotalar ligament labelled (Posterior talotibial ligament) are shown. Source: (Gray and Lewis, 2000).

The posterior intermalleolar ligament is another less-researched ligament in the literature. Originating at the fibula between the PTFL and transverse ligament the multifascicular ligament extends horizontally inserting medially on the posterior border of the tibia, the medial malleolus and the posterior of the talus (Golanó et al., 2016). The presence of the ligament is quoted from 19 % to 100 % however the size of the ligaments and proximity to the posterior joint capsule pose difficulties for assessment during dissection (Golanó et al., 2016).

1.3.3.3 Distal Tibiofibular Syndesmosis

The distal tibiofibular syndesmosis is formed between the tibia and fibula at the distal end. Minimal motion occurs between the tibia and fibular at the distal tibiofibular syndesmosis satisfying the definition of a syndesmosis, which is an immovable joint where bones are joined by connective tissue. The tibiofibular syndesmosis consists of the anteroinferior tibiofibular ligament (AiTFL), the posteroinferior tibiofibular ligament (PiTFL), the transverse ligament and the interosseous tibiofibular ligament (Golanó et al., 2016). Additional support to the tibiofibular syndesmosis is provided by the inferior segment of the interosseous membrane (Golanó et al., 2016). The tibial origin of the AiTFL is at the anterior tubercle of the tibia around 5 mm above the articular surface, shown in Figure 4 (Van Den Bekerom and Raven, 2007). The ligament runs distally and laterally to its fibular insertion on the anterior margin immediately lateral to the articulation surface (Golanó et al., 2016). When taking a frontal view of the foot, the angle created between the AiTFL and the tibial plafond is between 30 to 50 degrees and an angle of 65 degrees posteriorly with the sagittal plane (Ebraheim et al., 2006). Three slightly converging collagen fibre bands in the lateroinferior direction, separated by fatty tissue, form the AiTFL (Ebraheim et al., 2006; Hermans et al., 2010). The length of the fibres increases distally through the width of the AiTFL from 6 to 9 mm for the proximal band to 17 to 21 mm for the distal band (Hermans et al., 2010). The overall width and thickness dimensions of the AiTFL are 14.4 to 16.9 mm and 1.8 to 4.0 mm, respectively (Hermans et al., 2010).

Both a deep and superficial component of the PiTFL exist, where the deep component is sometimes referred to as the transverse ligament and the PiTFL usually describes the superficial component. The fibular origin of the superficial band is at the posterior edge of the lateral malleolus, shown in Figure 4 (Golanó et al., 2016). The fibres of the ligaments extend proximally and medially to the tibial insertion at the posterior tibial tubercle (Golanó et al., 2016). As the ligament extends from the fibula to the tibia the width of the PiTFL increases considerably giving the ligament a triangular shape. The average fibre length increases from 9.7 mm for the proximal fibres to 21.8 mm for the distal fibres (Hermans et al., 2010). The PiTFL forms an angle between 20 and 40 degrees with the transverse plane and 60 to 85 degrees with the sagittal plane (Hermans et al., 2010). The transverse ligament originates on the medial side of the fibula proximal to the malleolar fossa and inserts at the posterior edge of the tibia immediately posterior to the articular surface (Golanó et al., 2016). Tibial origin of the transverse ligament is at the dorso-distal rim of the tibia and the ligament extends horizontally to the fibular insertion at the malleolar fossa. The fibres of the deep component of the PiTFL are longer than the superficial varying from 22 to 43 mm in length with some distal fibres potentially extending as far as the medial malleolus (Ebraheim et al., 2006; Golanó et al., 2016).

The interosseous membrane connects the tibia and fibula along their entire length from the lateral side of the tibia to the medial side of the fibula. The interosseous tibiofibular ligament is a distal continuation of the interosseous membrane however the ligament is a dense mass of

short fibres (Golanó et al., 2016). The importance of the contribution to stability of the tibiofibular syndesmosis made by the interosseous tibiofibular ligament is disputed however some believe it plays an important role (Hoefnagels et al., 2007). Similarly to the AiTFL and PiTFL the length of the fibres increases distally from 6.6 ± 1.3 mm to 10.4 ± 3.1 mm (Hermans et al., 2010). The average thickness of the interosseous tibiofibular ligament is 4.7 ± 1.1 mm and the width is 21.2 ± 1.7 mm and 17.7 ± 1.0 mm at the fibular and tibial attachment points, respectively (Hermans et al., 2010).

1.3.3.4 Subtalar stability

The subtalar ligaments can be categorised into three groups: deep ligaments, peripheral ligaments and retinacula (Viladot et al., 1984; Harper, 1991). The cervical and interosseous ligaments are deep ligaments which separate the anterior and posterior joint capsules, shown in Figure 7. The ligaments form a barrier by crossing obliquely, similarly to cruciate ligaments of the knee, to stabilise the subtalar joint (Viladot et al., 1984). The interosseous ligament originates on the calcaneus and runs superiorly and medially to insertion point on the talar neck (Viladot et al., 1984). The peripheral ligaments of the subtalar joint include the CFL, lateral talocalcaneal ligament and the fibulotalocalcaneal ligament. The lateral talocalcaneal ligament is present in approximately 52 % of the population (Kakegawa et al., 2019). Of those occurrences, 61 % act as a reinforcement connecting the inferior aspect of the ATFL and the anterior aspect of the CFL (Kakegawa et al., 2019). The remaining were found to run in parallel with the CFL slightly anterior between the talus and calcaneus (Kakegawa et al., 2019). The lateral talocalcaneal ligament is smaller and weaker than the CFL but still contributes to the resistance of excessive supination of the subtalar joint (Viladot et al., 1984; Stephens and Sammarco, 1992; Burks and Morgan, 1994).

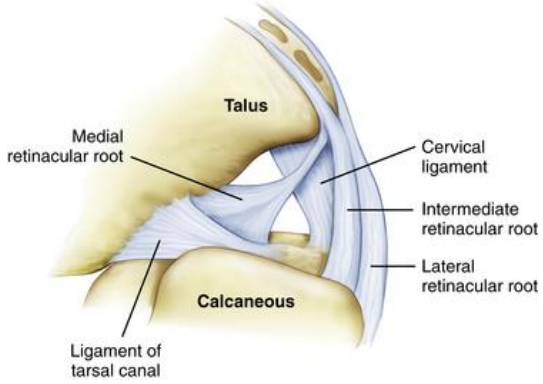

Figure 7. The deep lateral ankle ligaments of the subtalar joint. Source: (Frey, 2015).

The inferior extensor retinaculum attaches to the lateral talus and calcaneus and is formed by the lateral, intermediate and medial fibre bands, shown in Figure 8 (Snedeker et al., 2012). The inferior extensor retinaculum retains the extensor digitorum longus, extensor digitorium brevis and peroneus tertius tendons. The lateral root in conjunction with the CFL provide the ligamentous support to the subtalar joint (Snedeker et al., 2012).

1.3.4 Muscles and Tendons

Movement of the foot and ankle is controlled by muscles which originate in the leg and insert within the foot. The majority of motion is generated by twelve muscles which can be compartmentalised into the anterior, lateral, posterior and deep posterior compartments, shown in Figure 8 (Brockett and Chapman, 2016). The anterior compartment includes four muscles: the tibialis anterior, extensor digitorium longus, extensor hallicus longus and the peroneus tertius (Brockett and Chapman, 2016). The tibialis and extensor hallicus longus generate dorsiflexion and inversion, the peroneus tertius generate dorsiflexion and eversion, and the extensor digitorium longus generates only dorsiflexion of the ankle complex (Zwipp and Randt, 1994). The lateral compartment consists of two muscles the peroneus longus and peroneus brevis, which generate plantar flexion and eversion of the ankle complex (Zwipp and Randt, 1994). The posterior compartment includes three muscles: the gastrocnemius, soleus and plantaris, which assist plantar flexion of the ankle complex (Zwipp and Randt, 1994). The deep posterior compartment also includes three muscles: the tibialis posterior, flexor digitorium longus and flexor hallicus longus, which generate plantar flexion and inversion (Zwipp and Randt, 1994).

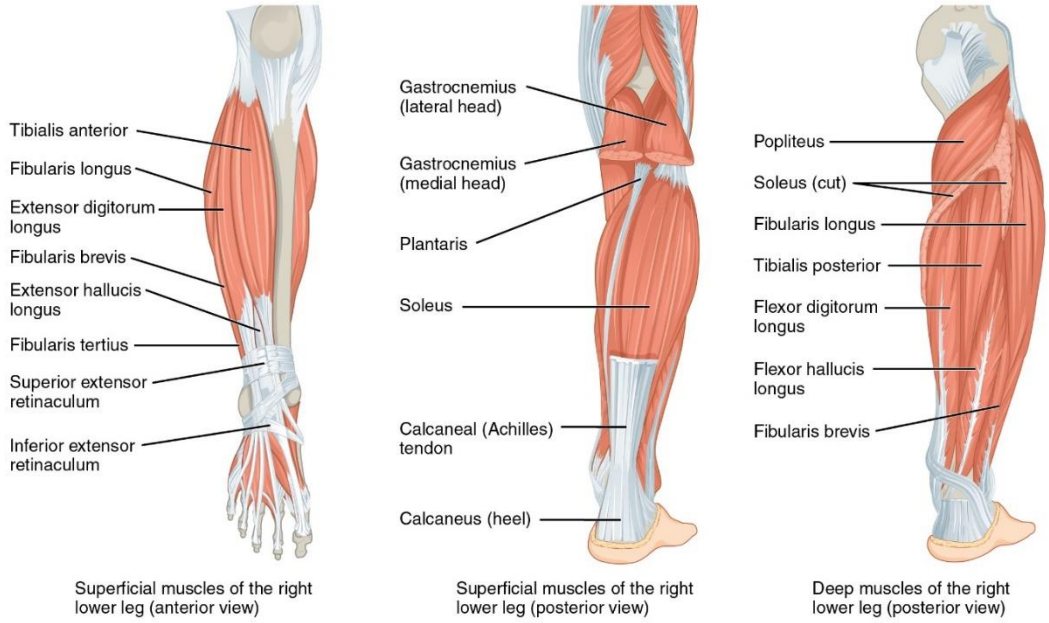

Figure 8. Muscles of the lower leg. Source: (https://opentextbc.ca/anatomyandphysiology/wp-content/uploads/sites/142/2016/03/1123_Muscles_of_the_Leg_that_Move_the_Foot_and_Toes.jpg. Accessed: 27/09/2020).

Musculotendinous units generate a stiffness when they contract, which aids in the dynamic stabilisation of the joints (Hertel, 2002). Integral to the dynamic stabilisation of the lateral side of the ankle and protection against LAS are the peroneus longus, peroneus brevis and the muscles of the anterior compartment of the lower leg (Hertel, 2002). The peroneal longus and brevis muscles can control supination whereas those of the anterior compartment of the lower leg can reduce the rate of plantar flexion (Sinkjaer et al., 1988; Ashton-Miller et al., 2013).

1.4 Biomechanics of the Ankle

Motion at the ankle complex is guided by the joint surface and ligamentous structures; and motion is induced by the forces and moments of the extrinsic muscles as well as external forces. The ankle joint complex can rotate in all three planes of motion allowing dorsi-/plantar flexion, inversion/eversion and internal/external rotation in the sagittal, frontal and transverse planes, respectively, shown in Figure 9 (Brockett and Chapman, 2016). A combination of plantar flexion, inversion and internal rotation is termed supination and causes the sole of the foot to face medially (Donatelli, 1985). Whereas a combination of dorsiflexion, eversion and external rotation, called pronation, causes the sole of the foot to face laterally (Donatelli, 1985).

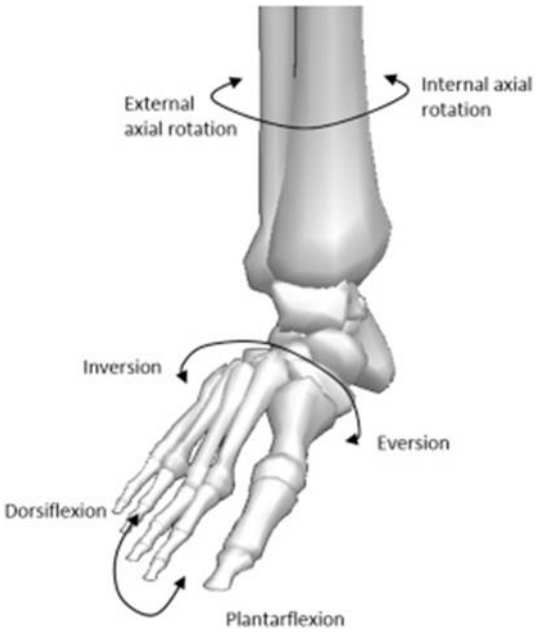

Figure 9. The relative motions of the ankle joint complex. Adapted from: Visual 3D (C-Motion, Rockville, Maryland). Source: (Brockett and Chapman, 2016).

1.4.1 Range of Motion

Total range of motion (ROM) of the ankle complex in the sagittal plane is between 65 to 75 degrees, comprised of 10 to 20 degrees dorsiflexion through to 40 to 55 degrees plantar flexion (Stauffer et al., 1977; Grimston et al., 1993). Overall ROM of the ankle complex in the frontal plane is approximately 35 degrees, moving from 20 to 23 degrees inversion through to 10 to 12 degrees eversion (Stauffer et al., 1977; Root et al., 1977). The ROM of the ankle complex required for daily activities is however much lower with the maximum ROM in the sagittal plane associated with walking being 30 degrees, stair ascent 37 degrees and stair descent 56 degrees (Nordin and Frankel, 2012).

Dorsi-/plantar flexion is the predominant motion occurring at the talocrural joint and inversion/eversion at the subtalar joint. Tuijthof et al. (2009) reported that 63 degrees of dorsi-/plantar flexion occurs at the talocrural joint and 4 degrees at the subtalar joint (Tuijthof et al.,

2009). Understanding of the contributions to inversion/eversion have historically been more contentious. The current belief is that inversion/eversion motion occurs at both the talocrural and subtalar joints. Lundgren et al. (2008) document joint rotations during the stance phase of walking measured in vivo. Joint rotations were found to be on average 15.3 ± 2.0 degrees, 8.1 ± 3.8 degrees and 7.8 ± 2.7 degrees at the talocrural joint and 6.8 ± 1.4 degrees, 9.8 ± 1.8 degrees and 7.5 ± 2.0 degrees at the subtalar joint in the sagittal, frontal and transverse anatomical planes, respectively (Lundgren et al., 2008).

1.4.2 Axis of Rotation

The axis of rotation for the joints of the ankle complex is a historical topic of disagreement. The axis of rotation was originally believed to alter during flexion due to the talus having two different arcs and radii, the shape of the talar trochlea and the action of soft tissues (Barnett and Napier, 1952). During dorsiflexion the axis of rotation had a distal inclination in the lateral direction and through plantar flexion a distal inclination in the medial direction (Barnett and Napier, 1952). Contrary to this it was later believed that a fixed hinge was a more appropriate description of the rotational axis, generating pronation and supination (Isman and Inman, 1969). Further study suggests that the hinge definition is an oversimplification and multiaxial motion occurs in the ankle complex (Lundberg et al., 1989; Leardini et al., 2014). The theory of multiaxial motion is based on internal rotation and external rotation occurring during dorsiflexion and plantar flexion, respectively (Leardini et al., 2014). The literature on the axis of rotation of the ankle complex is conflicting and further research into the topic could provide further insight. The most recent evidence suggests that the instantaneous centre of rotation theory is most likely to be correct and explains somewhat the difficulty faced when interpreting ankle biomechanics.

1.4.3 Forces in the Ankle Joint

The forces acting on the ankle joint complex vary depending on the activity being performed. Ground reaction forces acting on the ankle joint have been estimated to be approximately five times body weight (BW) and 13 times BW during the stance phase of normal walking and running, respectively (Burdett, 1982). Musculoskeletal models however have been found to overestimate joint reaction forces when compared to those measured in vivo using instrumented prostheses (Fregly et al., 2012).

The load applied to the ankle joint complex is distributed across the talocrural joint and fibula, which carry 83 % and 17 % of the load respectively (Calhoun et al., 1994). However these values can vary, with the fibula transmitting more load during dorsiflexion (Brockett and Chapman, 2016). The increase in load transmission during dorsiflexion is proposed to be due to the talus being wider anteriorly increasing the contact area and joint stability. Between 77 % and 90 % of the load transmitted by the talocrural joint is applied to the talar dome with the remaining load carried by the medial and lateral surfaces (Michael et al., 2008). The

distribution of load is determined by ligamentous forces and positional effects (Brockett and Chapman, 2016). During eversion the lateral facet experiences the highest load whereas the medial facet carries more load during inversion (Brockett and Chapman, 2016).

The talus does not have any muscular attachment and is therefore only constrained by ligament and contact forces (Leardini et al., 2014). Although the talus is highly constrained by the geometry of the ankle, there is potential that ligamentous damage induced during an ankle sprain could alter the load distribution on the talus. A redistribution of load could increase the mean contact pressure of the ankle which has been linked to the causation of PTOA in the ankle (Buckwalter et al., 2013).

Although the loads applied to the ankle are relatively high compared to other joints of the lower limb, the ankle has a high level of congruency. Therefore, the large contact area (11 to 13 cm^2) has been suggested produce stresses lower than those in the knee or hip (Nordin and Frankel, 2012). Contact area is greatest during stance phase of gait, with smaller contact areas at both toe-off and heel strike (de Asla et al., 2006).

1.5 Structure of Ligaments

Ligaments are primarily composed of collagen, glycoproteins, protein polysaccharides, elastin, glycolipids, water and cells (mostly fibroblast cells) (Hawkins, 2002). The proportional composition of ligaments is shown in Figure 10. Ligament extracellular matrix is composed of 55 % to 70 % water, whereby a substantial proportion is associated with the proteoglycans in the extracellular matrix (Nordin and Frankel, 2012). The dry weight of ligaments consists of 60 % to 85 % collagen, the majority being type I collagen (Hawkins, 2002).

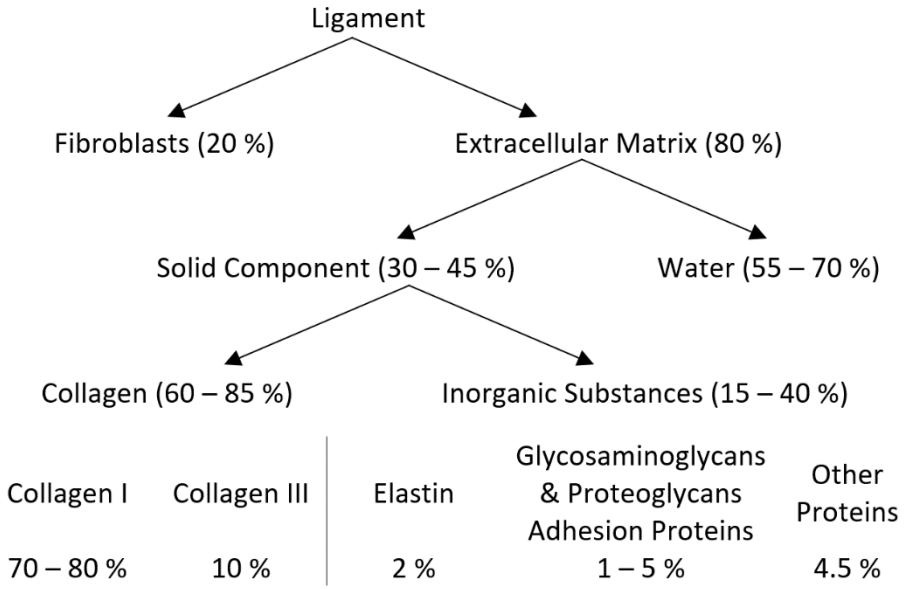

Figure 10. Proportional composition of ligaments. Percentage composition values source: (Kjær, 2004; Nordin and Frankel, 2012; Marieswaran et al., 2018).

Ligament microstructure is hierarchical, collagen molecules group together in a nearly parallel orientation to form progressively larger fibrils. Fibrils form fibres which have a crimped pattern

and group to form fascicles which then form the entire ligament, shown in Figure 11. Surrounding ligaments is an epiligamentous region which acts to provide protection to the collagen fibres and ligamentous neurovascular bundles, supply nutrients to the ligament through its vascular network, and allow for the sliding of the ligament against adjacent tissues (Chowdhury et al., 1991). To enable the sliding over adjacent tissues the epiligament has a multidirectional collagen fibre orientation, allowing pressure and tension to be resisted in a multitude of directions (Chowdhury et al., 1991).

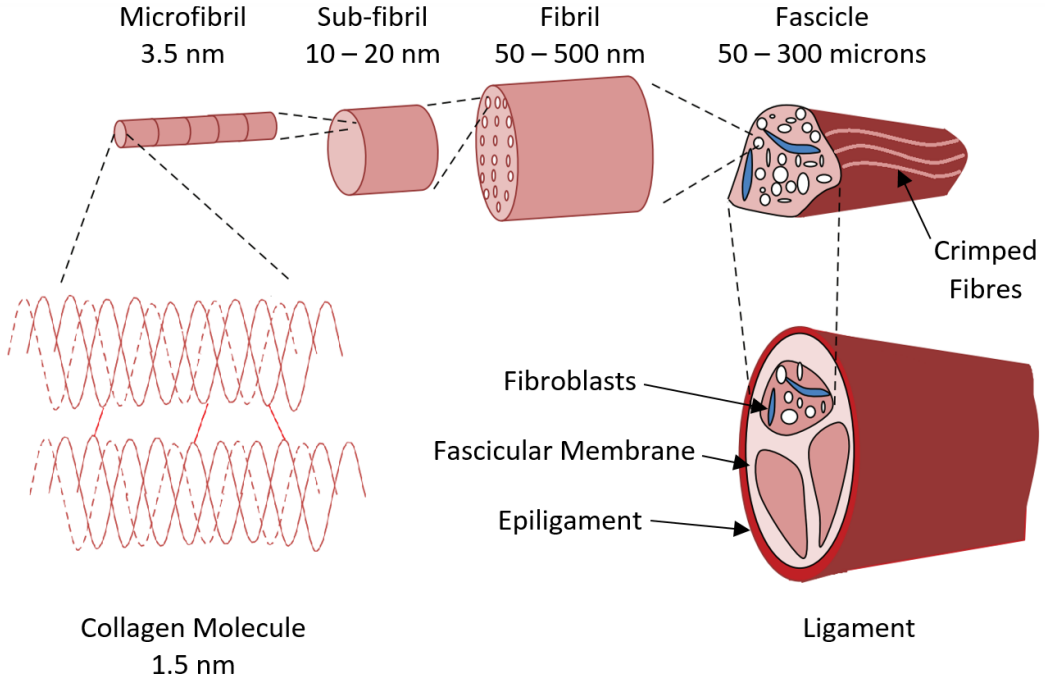

Figure 11. The organisational structure of a ligament. Adapted from (Marieswaran et al., 2018), original source (Kastelic et al., 1978).

Collagen molecules are cross-linked at the fibril level providing strength to ligaments (Nordin and Frankel, 2012). Collagen molecules are theorised to cross-link in a head-to-tail manner, however a more complex inter-fibrillar cross-linking may also exist (Nordin and Frankel, 2012). The internal crimping pattern of fibres decreases from the centre to periphery of the epiligament (Rein et al., 2015). The crimp pattern occurs every 67 nm and 45 µm in collagen fibrils and fascicles, respectively (Kastelic et al., 1978). Crimping of ligaments play a crucial biomechanical role and acts to prevent injury. During increased loading ligaments will uncrimp, thereby affording elongation of the ligament to prevent damage (Rein et al., 2015). Fibroblasts are functionally responsive to the local loading environment and when required to do so can produce the structural constituents of the extracellular matrix (Zitnay and Weiss, 2018). This phenomena is responsible for the mechano-responsive nature of ligaments (Birch et al., 2013).

Ligaments can attach to bones directly or indirectly. Direct insertion of ligaments to bone involves the transition of the ligament to fibrocartilage, mineralised fibrocartilage and finally bone (Marieswaran et al., 2018). Whereas for indirect insertion of ligaments the superficial fibres are connected to periosteum and the deep fibres to bone (Woo et al., 1987).

1.5.1 Lateral Collateral Ligament Complex

There is a scant amount of literature on the structure and composition of the LCL complex. Histological analysis determined that there are three different morphological compositions of ankle ligaments; densely packed parallel, mixed tight and loose parallel, and densely packed interlaced ligaments (Rein et al., 2015). The ATFL, CFL and PTFL are all composed of densely packed parallel collagen bundles, providing high tensile force resistance (Kumai et al., 2002; Rein et al., 2015). No significant difference in the structure of the ATFL, CFL and PTFL has been reported (Rein et al., 2015).

Kumani (2002) reported that the ATFL is composed of types I, III and VI collagens, dermatan and keratin sulphate (Kumai et al., 2002). Type II collagen is absent from most of the ligament except the entheses and sesamoid fibrocartilage (Kumai et al., 2002). Sesamoid fibrocartilage of the ATFL is found where the ligament wraps around the talus. The sesamoid fibrocartilage contributes to protecting the talar insertion from avulsion, along with a greater bone density than at the fibular origin (Kumai et al., 2002).

1.6 Function of Ligaments

Ligaments have three main functions: 1) to act as mechanical passive stabilisers of joints, 2) to have a viscoelastic response to aid in the preservation of joint homeostasis, 3) to have sensory function where ligaments are capable of monitoring and supplying afferent kinaesthetic and proprioceptive information (Rein et al., 2015). Mechano-receptors within ligaments and joint capsules react to changes in joint angle, joint velocity, mechanical distortion and intra-articular pressure providing proprioceptive information to influence the muscular joint stability (Macefield, 2005; Solomonow, 2006; Rein et al., 2015).

1.6.1 Lateral Collateral Ligament Complex

The primary function of the ligaments at the ankle complex is to provide stability to the joint through resisting excessive motion. The role each ligament plays in the stabilisation of the joint has been evaluated by a small number of studies to determine how individual ligaments contribute to the stability of the ankle complex. A cadaveric study using radiographic image analysis found the ATFL and anterior aspect of the CFL to restrict plantar flexion, demonstrated by ligament fibres being straight (taut) in Figure 12 (Stagni et al., 2004). Similarly the posterior aspect of the CFL and PTFL were found to restrict dorsiflexion, shown in Figure 12 (Stagni et al., 2004).

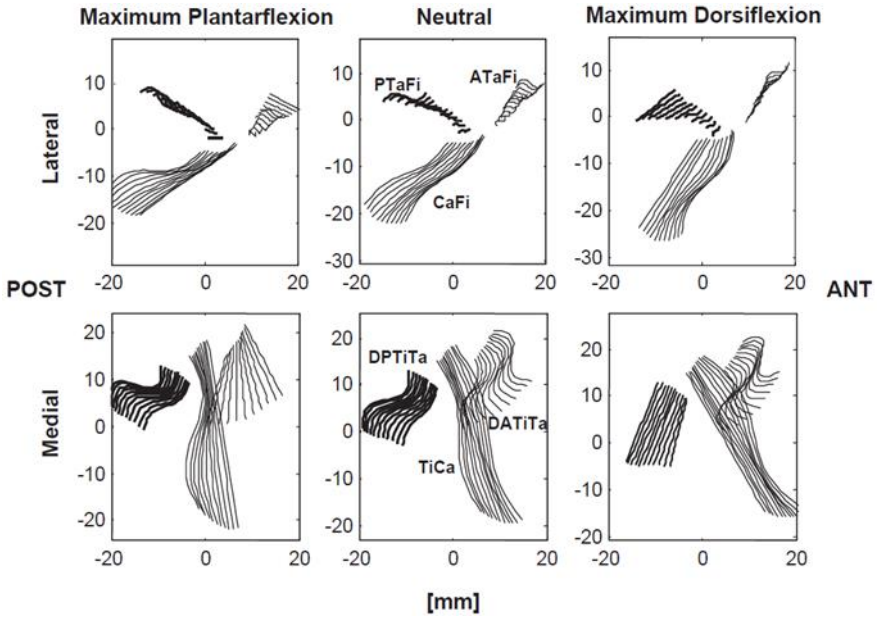

Figure 12. Illustrative representation of ligament fibre recruitment for the calcaneofibular (CaFi), anterior talofibular (ATaFi) and posterior talofibular (PTaFi) of the LCL complex as well as the, tibiocalcaneal (TiCa), deep anterior (DATiTa) and deep posterior (DPTiTa) tibiotalar ligaments of the medial collateral ligament complex. Each ligament is shown in the sagittal plane with 11 modelled fibres which are only represented as straight lines when their maximum length is achieved. Source: (Stagni et al., 2004).

1.6.1.1 Anterior Talofibular Ligament

Length changes of the LCL complex have been determined for healthy individuals using a combined dual-orthogonal fluoroscopic and magnetic resonance imaging (MRI) technique (de Asla et al., 2009). In maximum dorsiflexion, neutral and maximum plantar flexion positions of the ankle the ATFL is 13.9 ± 2.9 mm, 16.3 ± 3.0 mm and 20.8 ± 2.7 mm long, respectively (de Asla et al., 2009). Additionally, from maximal pronation to maximal supination the ATFL extends significantly from 14.8 ± 2.5 mm to 17.4 ± 3.0 mm (de Asla et al., 2009).

Strain in the LCL complex of cadaveric ankle ligaments has been measured using a mercury-filled strain gauge in 10 degree intervals from 20 degrees dorsiflexion through to 30 degrees plantar flexion (Colville et al., 1990). Additional inversion, eversion, internal and external rotation forces were also applied (Colville et al., 1990). Strain in the ATFL generally increased progressively as the ankle moved from 20 degrees dorsiflexion to 30 degrees plantar flexion, additional internal rotation and inversion motion increased the strain recorded (Broström, 1964; Renstrom et al., 1988; Colville et al., 1990; Kannus and Renström, 1991; Kakwani and Siddique, 2014) , shown in Figure 13. The highest ligament forces in the ATFL were observed in plantar flexion and supination (Bahr et al., 1998; Ozeki et al., 2006). The length, strain and force data all indicate that the ATFL acts to restrict plantar flexion, inversion and internal rotation.

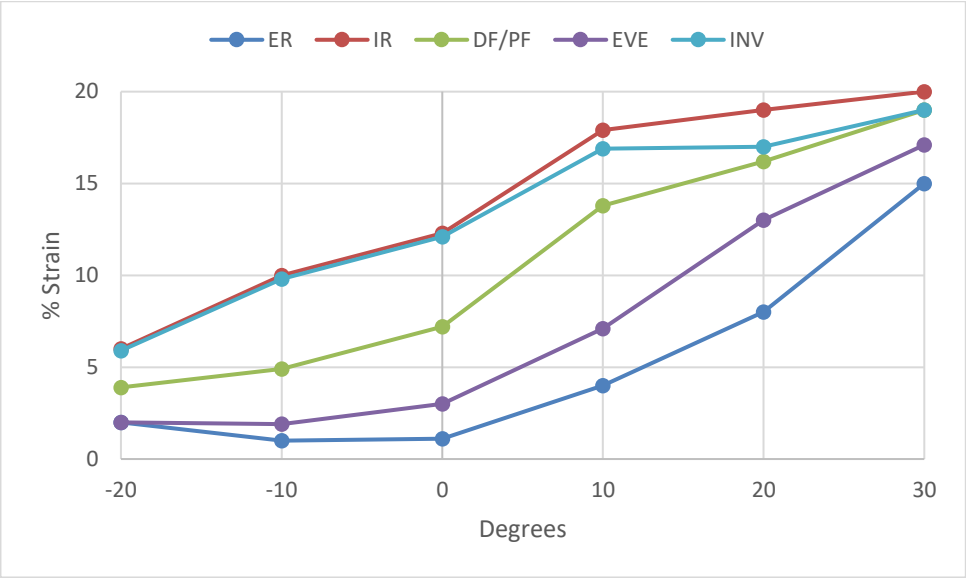

Figure 13. Strain measurements for the ATFL through dorsi-/plantar flexion in 10 degree increments from 20 degrees dorsiflexion (negative values) to 30 degrees plantar flexion (positive values). Results are also shown when 3 Nm moments are applied for external rotation (ER), internal rotation (IR), dorsi-/plantar flexion (DF/PF), eversion (EVE) and inversion (INV). Adapted from: (Colville et al., 1990).

1.6.1.2 Calcaneofibular Ligament

The CFL and ATFL have been described as synergistic as when one is relaxed the other is strained during dorsi-/plantar flexion motion (Renstrom et al., 1988; Colville et al., 1990; Cawley and France, 1991). Length measurements of the CFL in maximum dorsiflexion, neutral and maximal plantar flexion positions are 29.9 ± 3.0 mm, 28.0 ± 2.9 mm and 26.6 ± 2.2 mm (de Asla et al., 2009). Furthermore, the CFL shortens from 31.0 ± 3.8 mm at maximal pronation to 26.9 ± 3.6 mm at maximal supination (de Asla et al., 2009). Strain measurements of the CFL progressively decrease as the ankle moves from 20 degrees dorsiflexion to approximately 10 degrees plantar flexion before increasing slightly up to 30 degrees plantar flexion, shown in Figure 14 (Colville et al., 1990). Only additional inversion increased the strain within the CFL over the whole ROM compared to dorsi-/plantar flexion motion alone, shown in Figure 14 (Colville et al., 1990). Ligament force studies determined the highest CFL force to be in supination during dorsiflexion (Bahr et al., 1998) or pronation during plantar flexion (Ozeki et al., 2006).

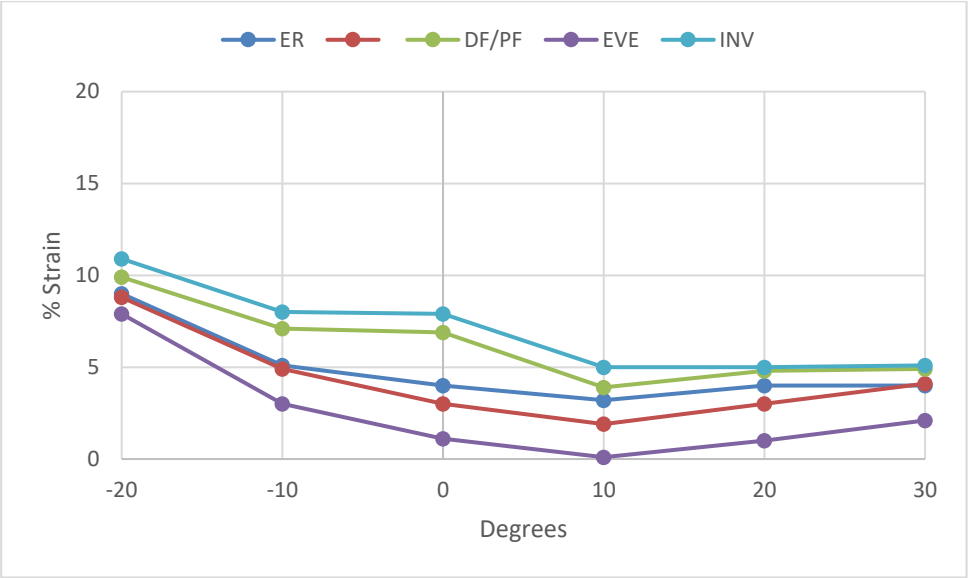

Figure 14. Strain measurements for the CFL through dorsi-/plantar flexion in 10 degree increments from 20 degrees dorsiflexion (negative values) to 30 degrees plantar flexion (positive values). Results are also shown when 3 Nm moments are applied for external rotation (ER), internal rotation (IR), dorsi-/plantar flexion (DF/PF), eversion (EVE) and inversion (INV). Adapted from: (Colville et al., 1990).

Unlike the anterior and posterior ligaments, the CFL rotates isometrically with the tibiocalcaneal ligament of the medial collateral ligament complex about their origins and insertions (Leardini et al., 2014). It has therefore been suggested that the CFL acts primarily as a guide for the axis of subtalar motion (King, 1984; Colville et al., 1990). However, as the ATFL is commonly the first injured ligament in a LAS the CFL may become the subsequent primary restraint to talar inversion (Colville et al., 1990). The CFL stabilises the subtalar joint by resisting excessive inversion and internal rotation and is most taut when dorsiflexed as it reaches a vertical position (Stormont et al., 1985; Kjorsgaard-Andersen et al., 1987; Stephens and Sammarco, 1992; Hølmer et al., 1994; Cass and Settles, 1994; Hollis et al., 1995).

1.6.1.3 Posterior Talofibular Ligament

As the ankle moves from the neutral position into dorsiflexion or plantar flexion the strain within the PTFL generally increases, being most taut in dorsiflexion, shown in Figure 15 (Colville et al., 1990). Uniquely, in comparison to the ATFL and CFL, the strain accumulated by the PTFL is greatest during dorsi-/plantar flexion alone, without additional inversion/eversion or internal/external rotation, shown in Figure 15 (Colville et al., 1990). The PTFL resists both inversion and internal rotation of the loaded talocrural joint but is deemed an insignificant structure in inversion-internal rotation ankle injuries (Grond, 1973). Force within the PTFL is greatest when in dorsiflexion (Ozeki et al., 2006).

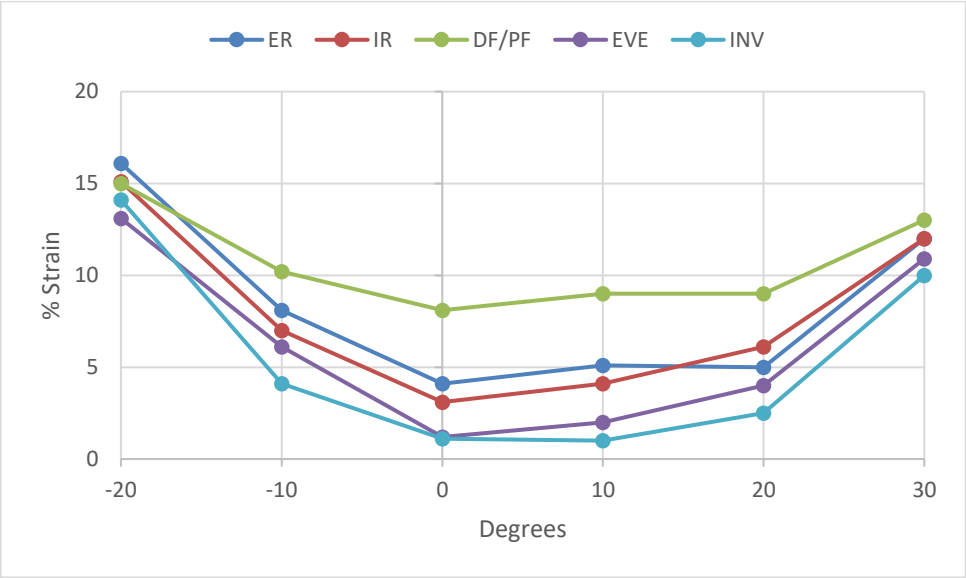

Figure 15. Strain measurements for the PTFL through dorsi-/plantar flexion in 10 degree increments from 20 degrees dorsiflexion (negative values) to 30 degrees plantar flexion (positive values). Results are also shown when 3 Nm moments are applied for external rotation (ER), internal rotation (IR), dorsi-/plantar flexion (DF/PF), eversion (EVE) and inversion (INV). Adapted from: (Colville et al., 1990).

1.7 Mechanical Characteristics of Ligaments

Ligaments exhibit a nonlinear viscoelastic time dependent response to tensile loading, starting with an initial toe region followed by a progressively stiffer loading region, shown in Figure 16 (Funk et al., 2000; Hawkins, 2002; Nordin and Frankel, 2012; Zitnay and Weiss, 2018).

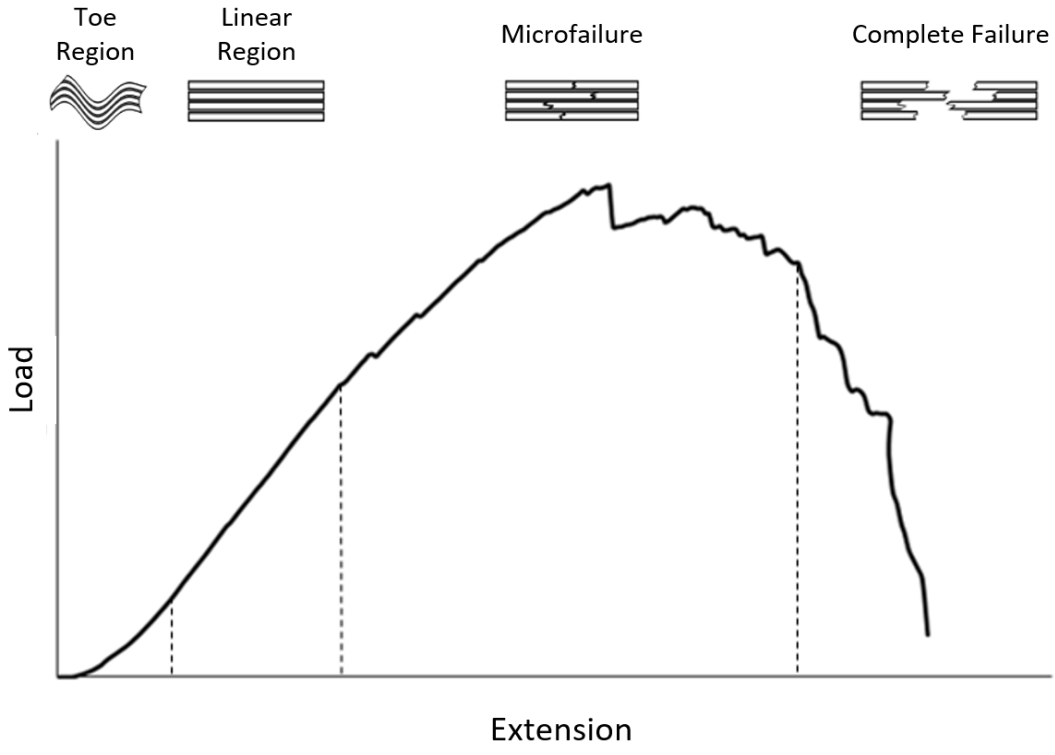

Figure 16. Load-extension profile of ligament separated (dashed lines) into the toe, linear, microfailure and complete failure regions.

The initial nonlinear elastic toe region is attributed to the straightening of the crimped collagen fibres under relatively low load (Abrahams, 1967). Following the straightening of fibres they begin to elongate, producing an almost linear response, until plastic deformation starts to occur at the microscopic level and the profile starts to plateau, shown in Figure 16 (Hawkins, 2002). The fibrous nature of ligaments allows for the independent failure of ligament fibres without complete catastrophic failure of the ligament. The independent failure of fibres is responsible for the characteristic peaks and troughs displayed in the microfailure region of the load-extension curve of ligaments. Complete catastrophic failure of the ligament follows through either intraligamentous failure or bone avulsion. Intraligamentous failure describes the mid-substance rupture of a ligament and is caused by the accumulation of microfailures. Intraligamentous failure is fibrous with a frayed appearance at the site of rupture. Avulsion failures are defined as failure at the insertion of the ligament to bone. Avulsion failures include the separation of the ligament from the bone surface, the separation of the ligament and cartilage from the bone surface, or as a small bone fracture at the insertion of a ligament.

Load-extension results may be used to represent the structural properties of ligaments. Meaning they are dependent on the length and cross-sectional area of the specimen tested. In the case of ligaments, structural properties describe the properties of the entire bone-ligament-bone (BLB) construct, providing load, extension and stiffness results for the construct. Alternatively material properties can be considered, such as stress-strain values, which account for anatomical geometrical variance between specimens. Therefore material properties describe the stress or strain levels achieved by the material(s) that form a construct irrespective of the size of the construct. The stress-strain curve for ligaments contains the same regions (toe, linear, microfailure and complete failure) as the load-extension curve however the shape of the profile is different. Both structural and material properties have their own merits and determining which is most appropriate is dependent on whether you wish to find the properties of the entire construct of the materials that form it.

1.7.1 Viscoelastic Behaviour of Ligaments

Ligaments display stress relaxation, creep, hysteresis and strain rate sensitivity characteristics (Hawkins, 2002). Stress relaxation describes a decreasing load over time when a ligament is held at a constant extension length, shown in Figure 17A. Creep is defined by an increasing deformation of the ligament over time whilst a constant load is being applied, shown in Figure 17B. Whilst ligaments will deform when a load is applied they are able to return to their original geometry once relaxed providing the load was not in excess of the yield load (the load where the linear region ends and microfailure begins).

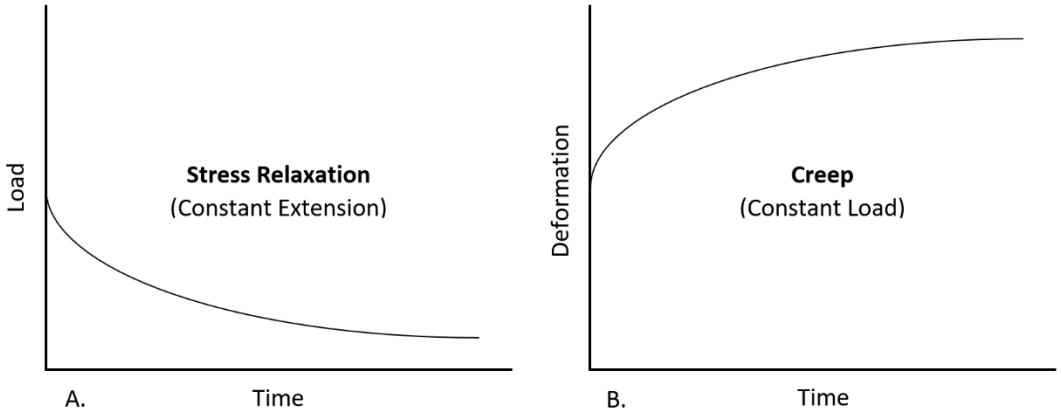

Figure 17. Hypothetical graphs demonstrating stress relaxation (A) and creep (B) characteristics of ligaments.

Hysteresis is a phenomenon which occurs when the fluid component of the ligament is redistributed to reduce the stress carried by the solid component of the ligament, shown in Figure 18. The ligament stores some of the energy spent during elongation causing the relaxation curve to follow a lower energy profile, shown in Figure 18 (Nordin and Frankel, 2012). The area between the elongation curve and relaxation curve represents the energy stored by the ligament. The viscoelastic qualities (stress relaxation, creep and hysteresis) are useful qualities for ligaments as they afford the adaptive nature of ligaments.

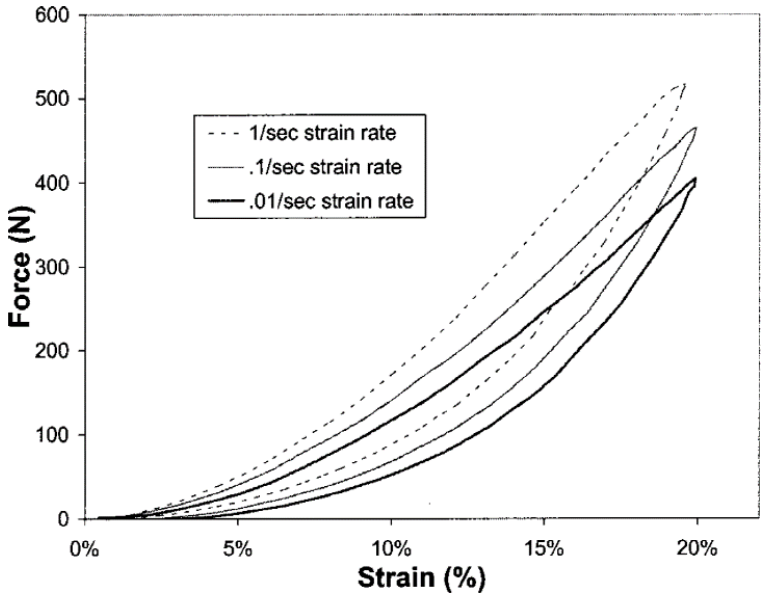

Figure 18. Hysteresis loops for AiTFL. Source: (Funk et al., 2000).

An increased rate of loading results in an increased stiffness, load and energy absorbed with respect to the elongation experienced by the ligament, shown in Figure 19 (Attarian et al., 1985). Strain rate also influences the failure mode of ligaments with a positive correlation identified between strain rate and the frequency of mid-substance failures compared to avulsions (Crowninshield and Pope, 1976). This could be due to the strain rate dependency of the viscoelastic properties of ligaments (Funk et al., 2000). At very fast strain rates (> 100 $\%.s^{-1}$) there is not adequate time for appreciable ligament relaxation (Funk et al., 2000). Whereas at

very slow strain rates (< 0.01 %.s^{-1}) the ligament is essentially fully relaxed throughout testing (Funk et al., 2000). Additionally, the greater strain rate sensitivity of bone than ligaments has been reported to reduce the frequency of avulsion failures at higher strain rates (Hawkins, 2002).

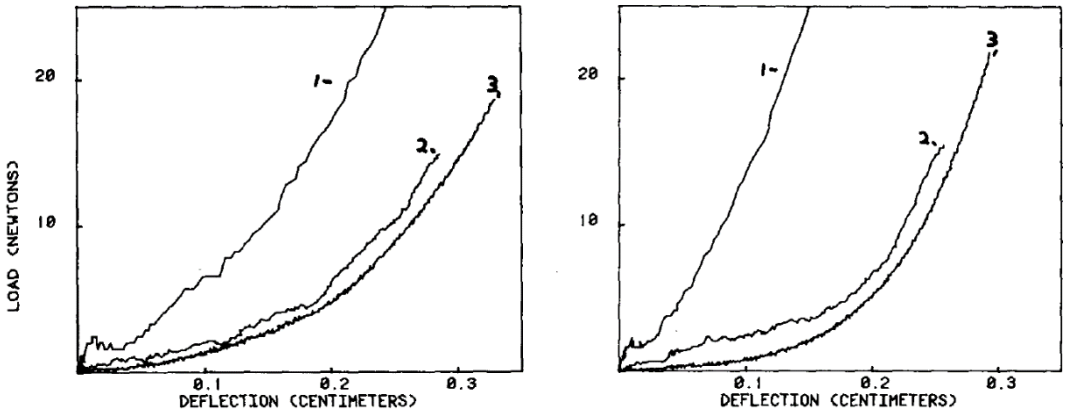

Figure 19. Load-deflection curves of the ATFL (left) and CFL (right) demonstrating the nonlinearity and strain rate dependence. Deflection rates are 1 = 1000 mm.s^{-1}, 2 = 50 mm.s^{-1} and 3 = 0.1 mm.s^{-1} (Attarian et al., 1985).

1.7.2 Animal Models

Ankle osteoarthritis research has been performed on many species of animals over the years including: horse, pig, dog, sheep, rat and mouse, shown in Figure 20 (Delco et al., 2017). Alternatively a goat model has been developed for osteochondral defect of the talus (van Bergen et al., 2013). Although these species have some resemblance of a human ankle, all of the species are quadrupeds and not bipeds like humans. Quadrupeds have a very different gait to biped species with varying biomechanics, loading and anatomy of the ankle. Other biped species such as ostrich and kangaroo have been investigated in ankle locomotion studies however there is very little published with these species (Smith et al., 2006; Snelling et al., 2017).

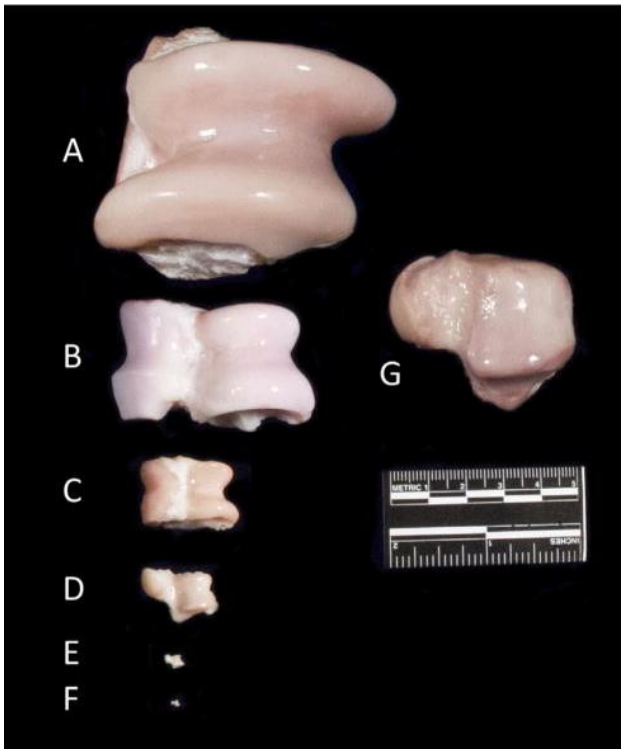

Figure 20. The tali from species commonly used as ankle models for comparison of size. A) Horse, B) pig, C) sheep, D) dog, E) rat, F) mouse and G) human. Source: (Delco et al., 2017).

The use of mice in research on ankle ligaments has come to the fore recently, particularly with respect to ankle sprain modelling (Hubbard-Turner et al., 2013; Wikstrom et al., 2015; Chang et al., 2016; Wikstrom et al., 2018). However, when considering xenograft materials for ligament replacement procedures, porcine tissue is predominantly used due to ease of supply and appropriate dimensions (Herbert et al., 2015). Of the animal models previously used, the porcine ankle is closest in size to that of the human, shown in Figure 20.

1.7.3 Experimental Conditions

1.7.3.1 Strain Rate

Whether the mechanical properties of ligamentous tissue are influenced by strain rate is debated in the literature. There are those that believe an increased strain rate causes an increase in ultimate failure load/stress and linear stiffness/modulus (Noyes et al., 1974; Neumann et al., 1994; Yamamoto et al., 1999; Bonner et al., 2015; Karunaratne et al., 2018). In contrast, there are some that propose ligaments are generally insensitive to strain rate (Woo et al., 1981; Blevins et al., 1994; Pioletti et al., 1999; Funk et al., 2000). The potential factors that could explain this discrepancy are multifactorial and vast, factors such as age, species, hydration level and ligament tested; in addition to whether material or structural properties were analysed, testing was to failure or non-destructive and the strain rates employed. The results of studies investigating the effect of strain rate are summarised in Table 1.

Table 1. Previously published results on the effect of strain rate on mechanical properties of ligamentous structures of the knee, unless otherwise stated, tested to failure. *statistically significant difference (p < .05), **statistically significant difference (p < .01), * statistically significant difference (p < .005) & †data is an estimation from graphical data calculated using WebPlot Digitizer.**

First Author, Year	Species, Structure	Sample Size	Strain Rate (%.s^{-1})	Stiffness (N.mm^{-1})	Ultimate Failure Load (N)	Elastic Modulus (MPa)	Ultimate Failure Stress (MPa)
(Blevins et al., 1994)	Human, Patellar Tendon	40	10	603 ± 182	1693 ± 567	302 ± 83	35.9 ± 10.9
			100	519 ± 156	1790 ± 601	310 ± 95	37.1 ± 11.8
(Bonner et al., 2015)	Pig, Lateral Collateral Ligament	7	1	-	-	288** ± 83.9	39.9** ± 11.0
		7	10	-	-	364 ± 86.6	56.5 ± 8.2
		7	94	-	-	656** ± 82.4	72.8** ± 11.1
		7	1006	-	-	763 ± 141.3	75.9 ± 9.6
		12	12990	-	-	906 ± 195.2	77.4 ± 15.4
(Neumann et al., 1994)	Human, Anterior Longitudinal Ligament (Spine)	54	0.1 (mm.s^{-1})	81.7 ± 37.2	742 ± 384	-	-
			1 – 4 (mm.s^{-1})	85.2* ± 32.6	843* ± 356	-	-
			170 – 230 (mm.s^{-1})	200* ± 99.6	1261* ± 369	-	-
(Noyes et al., 1974)	Monkey, Anterior Cruciate Ligament	34	0.662	156.5 ± 30.9	805.1*** ± 175.5	-	-
			66.2	151.4 ± 30.5	997.3*** ± 164.8	-	-

First Author, Year	Species, Structure	Sample Size	Strain Rate (%.s^{-1})	Stiffness (N.mm^{-1})	Ultimate Failure Load (N)	Elastic Modulus (MPa)	Ultimate Failure Stress (MPa)
(Yamamoto et al., 1999)	Rabbit, Patellar Tendon	6	0.01			183 ± 26	14.0* ± 1.3
			0.1			218*† ± 30	16.6*† ± 2.2
			1			248* ± 13	19.1 ± 2.8

Scrutinising the literature further does not yield an obvious explanation for the disagreement in findings. The two studies most similar in design, yet contradictory in result, are those of Blevins et al. (1994) and Yamamoto et al. (1999), where both analysed the material properties of patellar tendon samples tested to failure (Blevins et al., 1994; Yamamoto et al., 1999). The main differences in design were that Blevins et al. (1994) analysed patellar tendons from humans whereas Yamamoto et al. (1999) analysed patellar tendons from rabbits (Blevins et al., 1994; Yamamoto et al., 1999). All studies within Table 1 show a positive correlation between strain rate and ultimate failure stress as well as elastic modulus. With the exception of Blevins et al. (1994), all studies show a positive correlation between strain rate and ultimate tensile load and all except Noyes et al. (1974) found a positive correlation between strain rate and stiffness.

Unfortunately, the findings of Yamamoto et al. (1999) are not fully documented and their results for 0.1 %.s^{-1} strain rate are not reported textually. The results for 0.1 %.s^{-1} have been estimated in Table 1 using an online digitiser (WebPlot Digitizer) (Rohatgi, n.d.). The estimations were validated using the ultimate failure stress and elastic modulus results for 0.01 %.s^{-1} (183 ± 27 MPa and 14.0 ± 1.2 MPa, respectively) and 1 %.s^{-1} (248 ± 12 MPa and 19.0 ± 2.7 MPa, respectively) which agree well with the published results. The elastic modulus results at 0.1 %.s^{-1} were found to be significantly lower than at 1 %.s^{-1} and the failure stress results at 0.1 %.s^{-1} were reported as significantly higher than at 0.01 %.s^{-1} (Yamamoto et al., 1999). This discrepancy in the literature requires further investigation.

1.7.3.2 Tissue Hydration

The state of tissue hydration affects the mechanical properties of ligamentous and tendinous tissues due to the role of water content under an applied tensile load. The fluid component of the extracellular matrix, which accounts for 65 - 75 % wet weight of the extracellular matrix, is redistributed throughout the tissue upon an applied load (Rumian et al., 2007). Water is a

further influence on the mechanical properties of ligamentous tissue due to the interaction with GAGs. GAGs are predominantly important to compressive mechanical properties however they also have a role in tensile mechanical properties where they span the interfibrillar space (Franchi et al., 2010). It is therefore important in mechanical characterisation studies to attempt to replicate the natural hydration level of the tissue being characterised. There have been various hydration mediums and methods of hydration proposed for natural tissue testing. The current protocols within the Institute of Medical and Biological Engineering (iMBE) at the University of Leeds propose using phosphate buffered saline (PBS) as the medium and either continuously spraying the sample, wrapping the sample in PBS soaked gauze, or testing the sample within a PBS bath. There is no evidence, to the author's knowledge, for any difference between the two methods on the mechanical properties of ligamentous tissues.

1.7.4 Mechanical Properties of the Lateral Collateral Ligament Complex

The limited amount of comparable published data on material and structural properties for the LCL complex is shown in Table 2. The ATFL, the most frequently injured ankle ligament, has the lowest ultimate failure load of the ligaments of the LCL complex (Attarian et al., 1985; Siegler et al., 1988). Mean values for ultimate failure load of the ATFL range in the literature from 138.9 ± 23.5 to 297.1 ± 80.3 N (Attarian et al., 1985; Funk et al., 2000). Such broad ranging results emphasise the difficulty faced when comparing results between studies within the literature, particularly where different strain rates are employed. Large inter-subject variation also exists within studies however, with a relatively large study (n = 36) characterising the ATFL to failure, reporting a mean ultimate failure load of 206 N ranging from 58 N to 556 N (St Pierre et al., 1983).

The studies of Attarian et al. (1985) and Siegler et al. (1988), are the main focus of this review as they compare the tensile mechanical properties of the ATFL, CFL and PTFL when ligaments were aligned with the axis of loading. There were however differences between the two studies in terms of the testing protocol followed. Attarian et al. (1985) performed preconditioning "at 20 Hz for 10 s at physiological deflections (20 to 30 % maximum strain)", followed by "several load-deflection tests at a constant velocity, varying from 0.01 to 10 cm/s" prior to a test to failure at strain rates shown in Table 2 (Attarian et al., 1985). Siegler et al. (1988) performed 15 preconditioning cycles followed by several loading-unloading cycles where the maximum tensile force increased by 44.5 N per cycle until failure (Siegler et al., 1988).

Table 2. The material and structural properties of the LCL complex reported in literature. For avulsion failures the location of avulsion is denoted. (T) = Talus, (F) = Fibula and (C) = Calcaneus. Attarian et al. (1985) quote mean ± standard error of the mean whereas Siegler et al. (1988) quote mean ± standard deviation.

		ATFL		CFL		PTFL	
		Attarian et al., 1985	Siegler et al., 1988	Attarian et al., 1985	Siegler et al., 1988	Attarian et al., 1985	Siegler et al., 1988
Sample size		12	20	16	20	4	20
Mean age (years)		57.9	67.8 ± 15.2	57.9	67.8 ± 15.2	57.9	67.8 ± 15.2
Length (mm)		10.5 ± 0.1	17.8 ± 0.3	17.5 ± 0.1	27.7 ± 0.3	15.3 ± 0.1	21.2 ± 0.4
Strain rate used ($mm.s^{-1}$)		1010	3.2	1060	3.2	820	3.2
Ultimate failure load (N)		139 ± 24	231 ± 129	346 ± 55	307 ± 142	261 ± 32	418 ± 191
Ultimate elongation (mm)		5.1 ± 0.5	2.5 ± 0.8	6.3 ± 0.5	3.7 ± 0.7	13.1 ± 1.6	3.5 ± 0.9
Stiffness ($N.mm^{-1}$)		40.0 ± 8.5	-	70.5 ± 6.9	-	39.8 ± 13.8	-
Ultimate tensile strength (MPa)		-	24.2 ± 16.9	-	46.2 ± 36.6	-	26.0 ± 24.8
Strain to failure		0.53 ± 0.06	0.15 ± 0.06	0.38 ± 0.03	0.13 ± 0.03	1.00 ± 0.15	0.17 ± 0.05
Elastic modulus (MPa)		-	256 ± 181	-	512 ± 334	-	217 ± 170
Yield stress (MPa)		-	22.6 ± 16.6	-	43.6 ± 35.9	-	25.0 ± 24.0
Yield strain		-	0.14 ± 0.07	-	0.13 ± 0.02	-	0.16 ± 0.04
Failure Mode	**Mid-substance**	67 %	42 %	50 %	30 %	100 %	30 %
	Avulsion	33 % (T)	58 %	25 % (C) 25 % (F)	70 %	0 %	70 %

The CFL and PTFL are both reported as having the highest ultimate failure load of the LCLs, with the majority favouring the CFL (Attarian et al., 1985; Siegler et al., 1988; Funk et al., 2000). When normalised by the cross-sectional area of the ligaments the CFL is considerably stronger than the ATFL and PTFL, which have similar ultimate tensile strengths (46 ± 36, 24 ±

17 and 26 ± 25, respectively) (Siegler et al., 1988). The strain rate effect on failure load previously described for ligamentous tissue is not witnessed for the ATFL and PTFL when comparing the two studies, shown in Table 2. Testing protocol differences could however explain the higher failure load when characterised at a lower strain rate. By performing a loading-unloading tensile test at a relatively low strain rate (3.2 $mm.s^{-1}$) sufficient time is given for the viscoelastic properties of the ligament to be enabled (Siegler et al., 1988). Furthermore, when ligaments were characterised to a pre-failure extension limit of 3 mm at varying strain rates (0.15 $mm.s^{-1}$, 15 $mm.s^{-1}$ and 1000 $mm.s^{-1}$) an increased strain rate was demonstrated to increase the load achieved by both the ATFL and CFL (Attarian et al., 1985). The load approximately doubled for both the ATFL and CFL when tested at 1000 $mm.s^{-1}$ compared to 15 $mm.s^{-1}$ (equivalent to 9524 $\%.s^{1-}$ and 143 $\%.s^{-1}$, respectively) (Attarian et al., 1985). These results clarify the importance of selecting an appropriate strain rate for the conditions to be modelled by a mechanical characterisation study.

The ATFL has the lowest ultimate elongation of the LCLs however when normalised by ligament length the CFL has the lowest strain to failure (Attarian et al., 1985; Siegler et al., 1988). The ultimate elongation is however likely of more value in the context of LAS at the ultimate elongation of the ligaments can be related to displacements achieved during sprain motion to determine the likelihood of ligament rupture. The stiffness of the ATFL is around 40 $N.mm^{-1}$, similar to the PTFL but much less than the CFL (40 $N.mm^{-1}$ and 71 $N.mm^{-1}$, respectively) (Attarian et al., 1985). The results for the elastic modulus follow a similar trend to the stiffness results, being highest for the CFL, attributed to the high density and axial fibre orientation of its collagenous fibres (Siegler et al., 1988).

The failure mode of the ATFL is documented as either mid-substance failure or talar avulsion with frequencies varying dependent on the strain rate (Attarian et al., 1985; Siegler et al., 1988). The failure mode results for the LCL complex agree with those previously documented within this review for general ligamentous tissue, that avulsions are more prevalent when characterised at lower strain rates. The CFL was reported to avulse between 50 to 70 % of the time with the location of avulsion equally split between the calcaneal and fibular insertions (Attarian et al., 1985; Siegler et al., 1988). Avulsion of the PTFL varies between 0 to 70 % of failures with remaining failures being mid-substance (Attarian et al., 1985; Siegler et al., 1988). Unfortunately, Siegler et al. (1988) did not report the location of PTFL avulsions.

1.8 Lateral Ankle Sprain

1.8.1 Ligament Failure Mechanisms

Ligament failure can occur due to excessive loading (contact injury), load being applied at an excessive rate (sudden inversion walking in high heels), or a combination of excessive loads applied at excessive rates (sudden inversion during cutting motion). Ligament injuries, or

sprains, are clinically categorised into three grades by their severity, shown in Figure 21 (Magee, 2008). Grade I (mild) sprain represents small microfailure without macroscopic alterations to the ligament or instability to the joint. Grade II (moderate) sprains present as a partial ligament rupture with some joint instability. Grade III (severe) sprain represents a complete rupture of a ligament resulting in total instability of the joint.

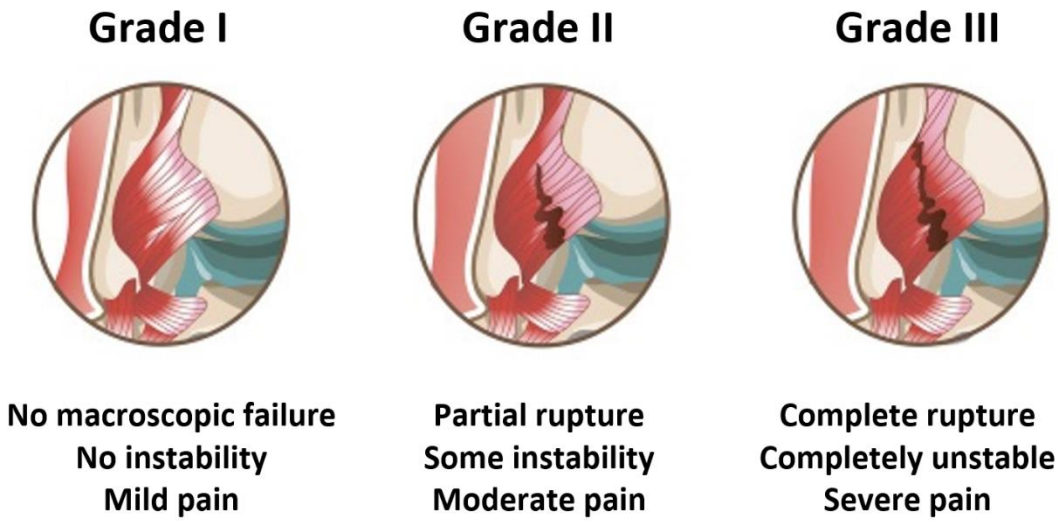

Figure 21. Grades of ankle sprain. Adapted From: (https://www.betterbraces.com/media/wysiwyg/degrees-of-ankle-sprains-rs.jpg. Accessed: 27/09/2020).

The ATFL is the most frequently injured ligament in the LCL complex followed by the CFL and subsequently the PTFL (Kumai et al., 2002). Injury to the PTFL is rare and typically occurs in severe LASs in conjunction with bone fracture or dislocation (Safran et al., 1999). Rotational instability increases after the rupture of the ATFL due to the amount of internal rotation of the rearfoot increasing dramatically and the remaining ligaments are subjected to further stresses (Kjærsgaard-Andersen et al., 1988). The rupture of the ATFL induces a strain increase in the CFL and the subsequent rupture of the CFL increases the strain within the cervical ligament (Martin et al., 1998). Isolated injury of the CFL has also been presented in a small number of cases (Rigby et al., 2015).

1.8.2 Biomechanics of Lateral Ankle Sprain

As previously described, strain increases in the ATFL due to plantar flexion, inversion and internal rotation motion (Colville et al., 1990). Therefore excessive degrees of such rotations will induce ATFL sprain. The same is true for the CFL in inversion and dorsiflexion and the PTFL in dorsiflexion (Colville et al., 1990). Lateral ankle sprain has also been associated with excessive supination of the rearfoot about an externally rotated shank soon after heel strike during gait or landing a jump (Bahr and Bahr, 2014); excessive plantar flexion at initial contact with the ground (Wright et al., 2000; Gehring et al., 2013; Bahr and Bahr, 2014) and a lateral centre of pressure at initial contact (Willems et al., 2005). There is therefore likely not only one motion responsible for instigating LASs.

Lateral ankle sprain events have been captured within biomechanics laboratories and at filmed sports events, affording the kinematic analysis of LAS shown in Table 3 (Fong et al., 2009b; Mok et al., 2011; Kristianslund et al., 2011; Gehring et al., 2013; Terada and Gribble, 2015; Panagiotakis et al., 2017).

Table 3. The kinematic data published within literature relating to LAS captured using marker-based motion analysis (MB) and marker-based image-matching motion analysis (IM). Bolded results are estimations produced through the digitisation of graphical data using WebPlot Digitizer software (https://apps.automeris.io/wpd/. Accessed: 27/09/2020). Max = maximum, PF = plantar flexion, DF = dorsiflexion, INV = inversion, EVE = eversion, IR = internal rotation, ER = external rotation, deg = degrees and s = seconds.

Author, year	**Fong et al., 2009b**	**Kristianslund et al., 2011**	**Mok et al., 2011**	**Mok et al., 2011**	**Gehring et al., 2013**	**Terada et al., 2015**	**Panagiotakis et al., 2017**			
Motion	Cut	Cut	High jump	Contact injury hockey	Cut	Stop-jump	Contact injury basketball			
Injury	Mild ATFL sprain	LAS	LAS	LAS	Mild LAS	Mild LAS	LAS			
Method	MB	MB	IM	IM	MB	MB	IM			
Max PF (deg)	1	**19**	**52**	**14**	50	**47**	3	27	12	54
Max PF/DF velocity ($deg.s^{-1}$)	370	**353**	-	-	1240	**270**	-	-	-	-
Max INV (deg)	48	**33**	142	78	45	**13**	93	77	96	107
Max INV/EVE velocity ($deg.s^{-1}$)	632	559	1752	1397	1290	**96**	-	-	-	-
Max IR (deg)	10	**56**	**51**	**45**	24	-	3	38	28	47
Max IR/ER velocity ($deg.s^{-1}$)	271	**690**	-	-	580	-	-	-	-	-

The variation in kinematic data for the generation of LAS between studies is considerable due to the vastly different motions possible to induce LAS injury. The data suggests that neither

plantar flexion, inversion nor internal rotation independently are essential motions required for LAS, yet all three can be influential. Excessive inversion was the primary motion quoted within the majority of these studies, particularly those where a contact injury had occurred due to another players foot landing on the affected ankle (Mok et al., 2011; Panagiotakis et al., 2017). Other studies found plantar flexion to be the predominant motion (Gehring et al., 2013; Terada and Gribble, 2015) and one study reported internal rotation to be responsible for LAS (Kristianslund et al., 2011). The largest rotation within each study is associated with the highest rotational velocity, highlighting the influence of rotational velocity on sprain events.

Only the study by Fong et al. (2009b) details which ligaments were damaged due to sprain. A mild ATFL sprain was reported during a sharp left turn performed at maximum running speed. Increased inversion and internal rotation occurred at foot strike during the injury trial compared to previous non-injury trials (15 degrees vs 9 degrees and 21 degrees vs 14 degrees, respectively) (Fong et al., 2009b). The ankle complex then progressed to achieve 18 degrees of dorsiflexion, 48 degrees of inversion and 10 degrees of internal rotation 0.2 s later, shown in Figure 22 (Fong et al., 2009b).

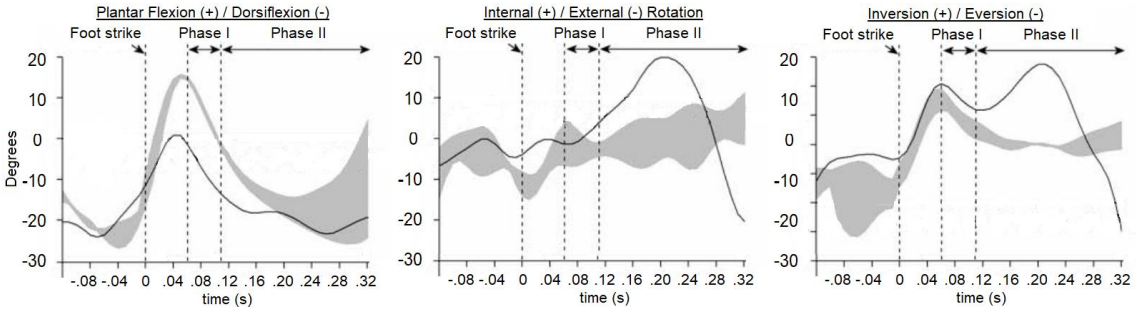

Figure 22. Kinematic data of the ankle complex when performing a sharp left turn cutting pattern. The mean and standard deviation of the normal trials (grey band) and the injury trial (black line) are shown. Phase I = pre-injury phase and phase II = injury phase. Figure adapted from (Fong et al., 2009b).

In a similar study by Kristianslund et al. (2011) a substantial and rapid increase in both inversion and internal rotation angles and moments occurred during the sprain event, shown in Figure 23. At initial contact, the ankle complex inverted 16 degrees, 6 degrees and 5 degrees and internally rotated 8 degrees, 4 degrees and -1 degrees in the sprain and two preceding non-injury trials, respectively (Kristianslund et al., 2011). A 2 cm lateral shift in the centre of pressure was observed in the first 50 ms of the contact phase which extended during the stance phase to 8.4 cm in the injury trial compared to 3.3 cm and 3.0 cm in the two non-injury trials (Kristianslund et al., 2011). The variation in kinematics and kinetics between the injury and non-injury trials signifies the causation of the LAS as being a lateral shift in centre of pressure, increased inversion and increased internal rotation, shown in Figure 23.

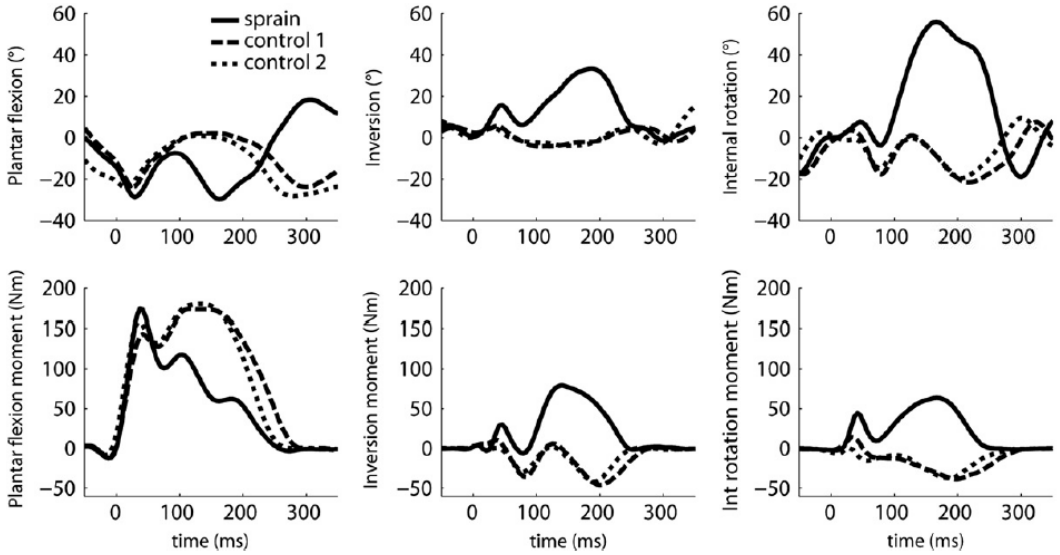

Figure 23. Kinematic and kinetic data for sprain trial and two preceding non-injury trials when performing a cut movement. Source: (Kristianslund et al., 2011).

Another study analysing LAS during a cutting movement reported considerably high velocities for plantar flexion (1240 degrees.s^{-1}), in addition to inversion (1290 degrees.s^{-1}) and internal rotation (580 degrees), shown in Figure 24 (Gehring et al., 2013). Explosive activation of the tibialis anterior muscle and the peroneus longus muscle occurred 40 to 45 ms after contact with the ground during the injury trial, prior to that of the two preceding non-injury trials (62 ms and 74 ms) (Gehring et al., 2013). The role that the tibialis anterior muscle plays is speculated by Gehring et al. (2013) to be either counteracting plantar flexion or contributing to additional inversion and internal rotation (Lee and Piazza, 2008; McCullough et al., 2011).

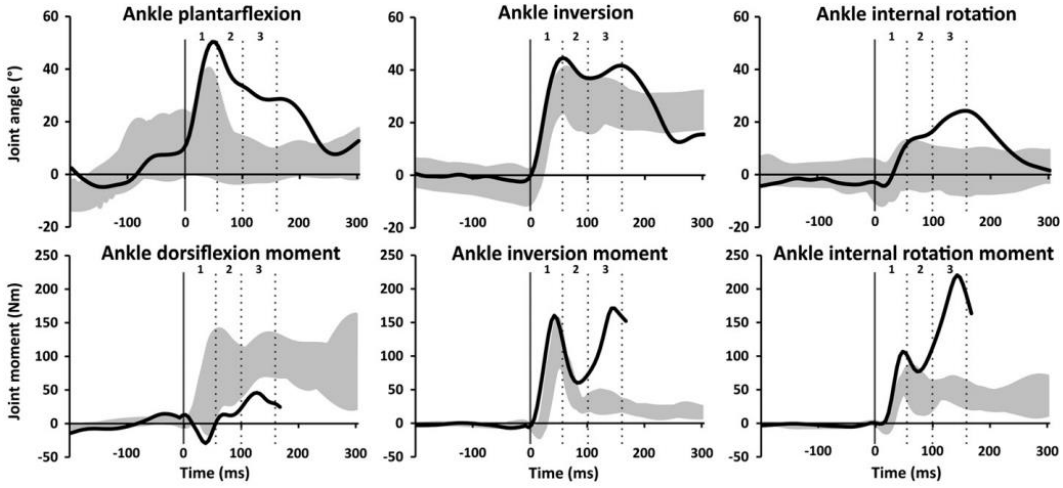

Figure 24. Ankle kinematics and kinetics for a LAS injury trial (black line) and of 16 control trials (grey band represents the range). Source: (Gehring et al., 2013).

A common characteristics of the trials resulting in LAS within the three cutting movement studies is a simultaneous second peak in inversion ROM and a peak in internal rotation ROM. Where reported, the inversion and internal rotation moments peaked a similar time point to the peak in ROM. There is no definitive value of inversion angle or velocity required to sprain

the ligaments of the ankle however it is known that as inversion velocities increase so does the severity of ankle injury (Lynch et al., 1996).

An alternative method affording the analysis of a greater number of video captured ankle sprain injuries is a model-based image-matching motion analysis method (Krosshaug and Bahr, 2005). This method involved placing a skeletal model onto a subject recorded from at least two different angles whilst ankle sprain occurred to analyse the kinematics. Contact injury sprains such as those reported by Mok et al. (2011) and Panagiotakis et al. (2017) can be analysed using such a method, which otherwise could not be analysed. The accuracy of such a method is however less than traditional optical motion capture analysis, shown in Figure 25. Results from studies using the marker-based image-matching technique should therefore be interpreted with caution and only used as estimates for ankle sprain ROM. However, the technique offers great opportunity to expand the understanding of ankle sprain biomechanics which still requires a large amount of basic understanding.

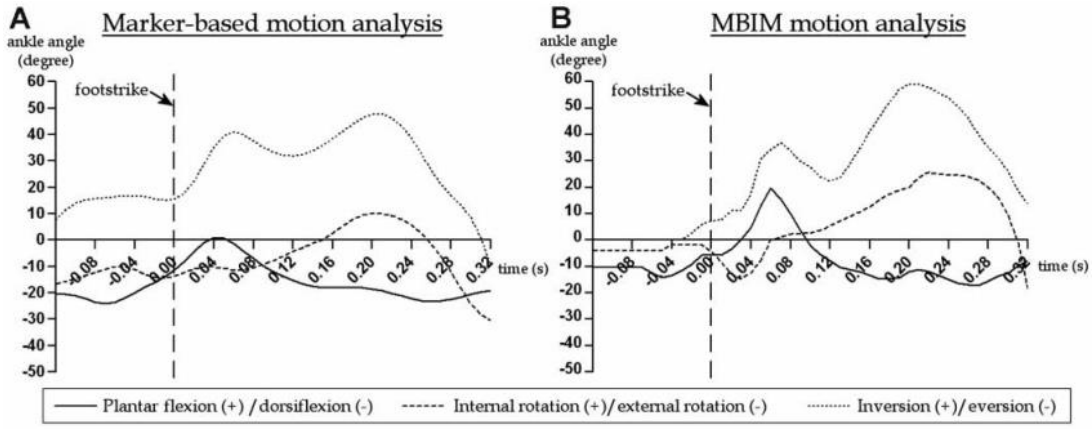

Figure 25. A comparison of traditional marker-based motion capture analysis (A) and marker-based image-matching motion analysis (B) techniques within the ankle joint. Source: (Fong et al., 2009b).

1.8.3 Simulation of Lateral Ankle Sprain

Given the rarity of accidental ankle sprains within biomechanics laboratories, researchers have attempted to replicate ankle sprain in cadaver tissue. Such devices offer an opportunity to investigate LAS biomechanics under controlled conditions and at a greater intensity. To the author's knowledge a device capable of simulating LAS in cadaver tissue with realistic kinematic profiles does not exist. Furthermore, the author is only aware of one passive device capable of inducing damage to the lateral ankle ligaments (Konradsen and Voigt, 2002). The device was able to induce ATFL and CFL rupture in specimens fixed at 20 degrees tibial inclination, 30 degrees plantar flexion, 30 degrees inversion and 10 degrees internal rotation (Konradsen and Voigt, 2002). The rate of loading used in the study and the failure loads are unfortunately not included within the research article.

Several dynamic robotic gait simulators exist for the biomechanical analysis of cadaver ankles (Sharkey and Hamel, 1998; Hurschler et al., 2003; Nester et al., 2007; Aubin et al., 2008; Lee

and Davis, 2009; Peeters et al., 2013; Baxter et al., 2016). Muscle actuators allow for the muscular response and active dynamic stability of muscles to be incorporated into testing. The advancement in gait simulation of the ankle has progressed well over the past 20 years however the devices investigate biomechanics of standard gait cycles opposed to traumatic events. Simulation of sprain requires considerably higher loads to be applied at much greater rates of loading than employed in these studies.

The biomechanics of LAS have been investigated in living patients using devices which replicate sprain motion to a pre-injury degree of ROM (≤ 35 degrees inversion) (Nawoczenski et al., 1985; Johnson and Johnson, 1993; Ha et al., 2015). Sprain inducing biomechanical studies cannot be performed on patients due to the obvious ethical implications of causing harm to patients. The ethics surrounding exposing patients to pre-injury ROMs are questionable yet many studies exist where this has occurred (Ha et al., 2015). Devices such as tilting platforms (Sheth et al., 1997; Chan et al., 2008; Mitchell et al., 2008; Fong et al., 2009a; Alfuth et al., 2014; Jain et al., 2014; Bhaskaran et al., 2015; Agres et al., 2019) and fulcrum soles (Knight and Weimar, 2012) have previously been used as shown in Figure 26 and Figure 27, respectively.

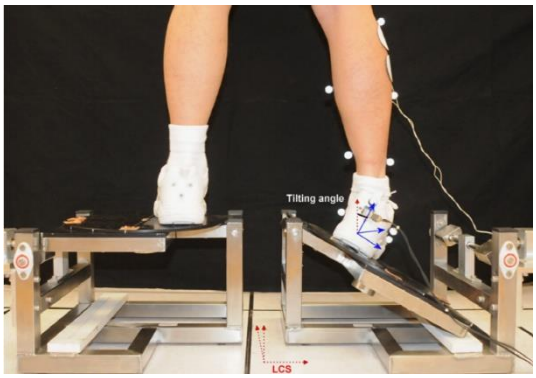

Figure 26. A tilting platform device used to analyse LAS motion. Source: (Fong et al., 2012).

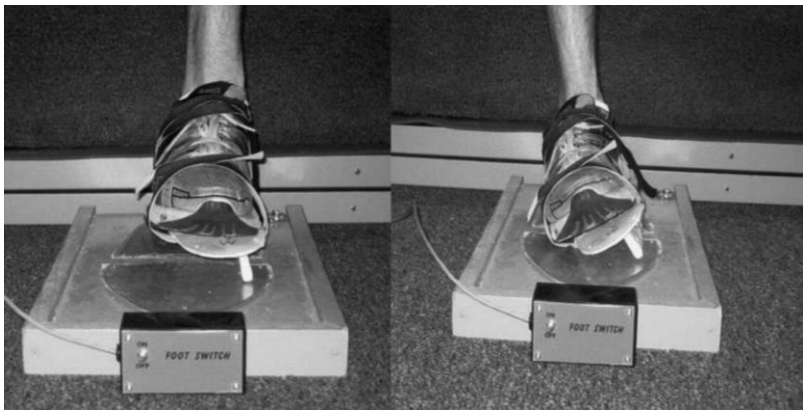

Figure 27. A fulcrum sole device used to analyse LAS motion. Source: (Knight and Weimar, 2012).

The findings of such studies have numerous limitations when attempting to simulate ankle sprain. Most significant is that the participants are in bipedal stance with their body weight unevenly distributed onto the supporting limb, opposite to the reality of sprain events (Jain et

al., 2014). Furthermore, participants have reacted to the sudden inversion quicker than biologically possible for a neuromuscular response suggesting a potential anticipatory response to other stimuli (Jain et al., 2014). Anticipatory responses have been reported to alter the kinetic response in sprain analysis (Simpson et al., 2019). The kinematic and kinetic responses of participants performing a sprain simulation tasks could therefore differ quite considerably to those of actual sprain events.

1.8.4 Sprain Diagnosis

Sprain diagnosis can be performed using clinical outcomes, clinical tests and imaging techniques. Outcome scores capture the impact of an injury or the effectiveness of a treatment. The most common functional outcome measures for LAS are the American Orthopaedic Foot and Ankle Society (AOFAS) Ankle-Hindfoot Scale, Karlsson score, Foot and Ankle Outcome Score (FAOS) and Foot and Ankle Ability Measure (FAAM) (Spennacchio et al., 2020). To assess pain the Visual Analog Scale (VAS) is typically used (Spennacchio et al., 2020). Since the studies of this project will be using cadaveric tissue the opportunity to perform such analysis is not feasible.

Clinical tests can be performed by a trained clinician to subjectively test the extent of physical injury. An anterior drawer and talar tilt test are the most commonly used clinical tests for ankle sprain (Song et al., 2019). Anterior translation and talar tilt tests allow a clinician to manually assess the stability of the ankle in a qualitative manner. There is evidence however, to suggest that an anterolateral drawer test is superior to the anterior drawer test when analysing lateral ankle stability (Phisitkul et al., 2009; Miller et al., 2016). Devices have been developed which quantify the stability of the ankle joint by determining the ROM achieved under a certain load in anterior displacement and inversion rotation (Kovaleski et al., 1999; Kerkhoffs et al., 2005; El. Daou et al., 2018). This objective style of analysis would be possible with cadaveric tissue and would allow for the quantification of joint stability, these devices are discussed in more detail in the relevant section of Chapter 5.

Medical imaging can also assess the extent of physical injury but more objectively than clinical tests. Techniques such as CT, MRI arthrography, ultrasound and radiography have all been used to assess ankle sprain previously (Tanaka and Mason, 2011; Tourné and Mabit, 2017). Ultrasound is the most favourable imaging technique for ligaments due to its improved ability to capture soft tissues compared to other techniques. Quantitative imaging methods, stress radiography and stress ultrasonography, have both been used to analyse ankle stability quantitatively. This method of analysis should be explored for the studies to be performed in this project due to the nonintrusive nature of imaging.

1.9 Ankle Ligament Repair

1.9.1 Natural Healing Process

The biological healing potential of damaged ligaments is extremely poor, this is attributed to the lack of vascularisation of the tissue (Moshiri and Oryan, 2012). Often, the healing response of tendons and ligaments are reported together due to their similar physiology and ultrastructure (Tozer and Duprez, 2005). The ligamentous region has three overlapping healing stages which are inflammation, fibroplasia and remodelling, shown in Figure 28 (Moshiri and Oryan, 2013). The remodelling stage can be subdivided into early and late remodelling, shown in Figure 28 (Hope and Saxby, 2007; Moshiri and Oryan, 2013).

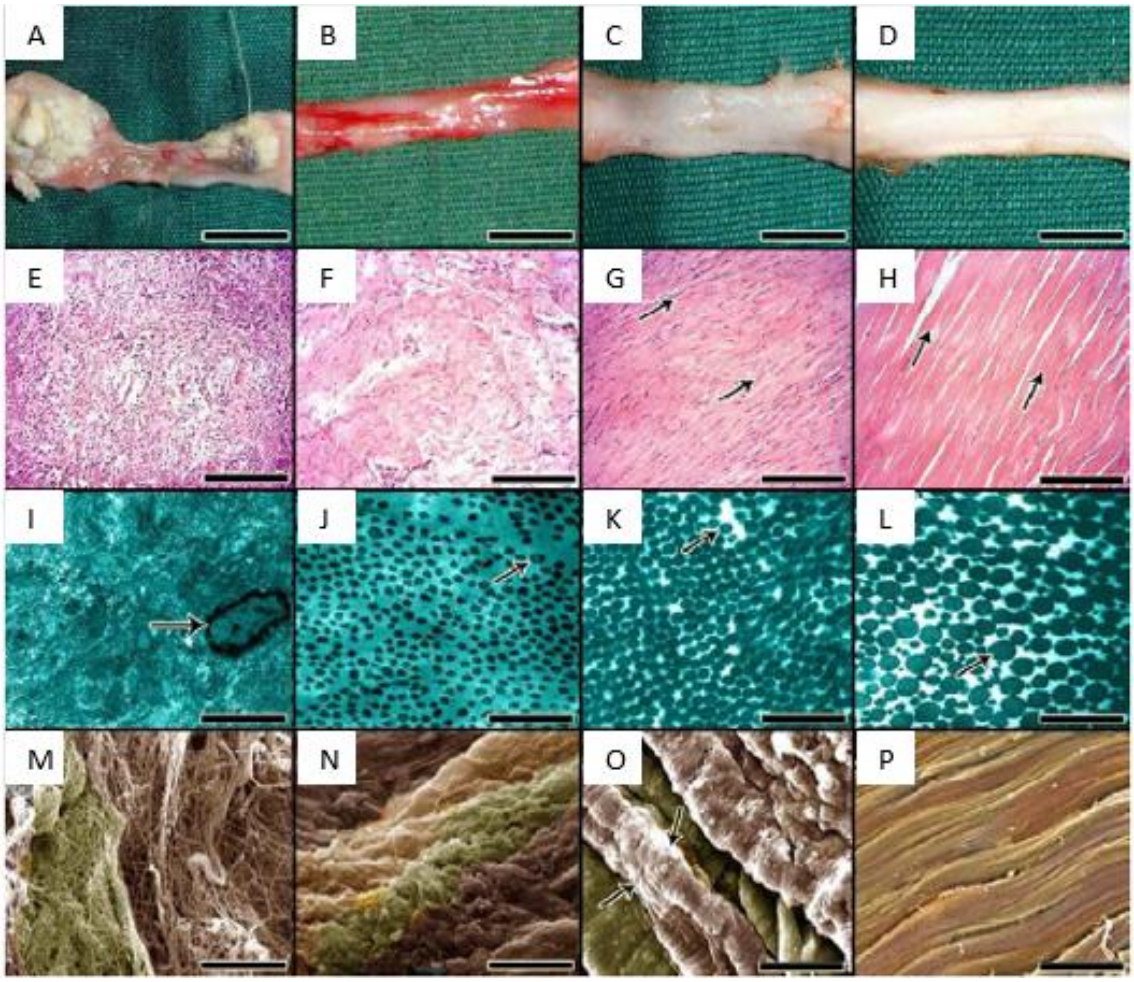

Figure 28. Inflammation (first column), fibroplasia (second column), early remodelling (third column) and late remodelling (fourth column) under gross morphology (first row), light microscope (second row), transmission electron microscope (third row) and scanning electron microscope (fourth row). "Scale bar: A to D: 1 cm, E to H: 50 µm, I to L: 900 nm, M to P: 2 µm." Source: (Moshiri and Oryan, 2013).

The inflammatory stage is initiated at the point of ligament rupture. Platelets aggregate at the rupture site of the ligament, causing a blood clot, and the release of chemoattractant is activated (Yang et al., 2013). The blood clot acts as a scaffold creating a platform enabling cell migration, attachment, proliferation and other pathophysiological duties (Moshiri and Oryan,

2012). Platelets release growth factors and pro inflammatory mediators while injured cells release pro inflammatory cytokines which regulate the migration and activation of inflammatory cells (Moshiri and Oryan, 2013). Necrotic cells are phagocytosed by inflammatory cells which migrate from the surrounding tissues (Yang et al., 2013).

The proliferation stage or fibroplasia follows, approximately two days after injury (Voleti et al., 2012). Fibroblasts, responsible for the synthesis of the extracellular matrix, start to be recruited to the injury site and proliferate (Garner et al., 1989; James et al., 2008; Yang et al., 2013). Concurrently, neutrophil levels drop while growth factors continue to be released by macrophages, mediating cell recruitment and activity (Voleti et al., 2012). A collagenous matrix forms and the presence of collagen type III fibrils (arrow, Figure 28J) as well as the concentrations of water and glycosaminoglycans (GAGs) are starting to be elevated (Juneja et al., 2013). Figure 28N shows that collagen fibrils have been formed but they are not yet fibres as shown in Figure 28O.

The final stage, remodelling, succeeds one to two months after injury involving the alignment of collagen and fibroblasts in the direction of stress (Yang et al., 2013). During early remodelling collagen fibres are formed increasing the density of collagen fibres, shown in Figure 28K, and are arranged uni-directionally, shown by the arrows in Figure 28G. In late remodelling, the collagen fibre bundles are present and are highly aligned, shown in Figure 28L and Figure 28H, respectively. Gradually, over a period of years, the healing tissue forms a fibrovascular scar, which possesses inferior mechanical and biochemical properties compared to the previously uninjured tissue (Yang et al., 2013).

During the remodelling stage the ligament could be at increased risk of recurrent sprain due to the inferior mechanical properties of the ligamentous tissue. Why some people have recurrent sprain and others do not is unclear.

1.9.2 Conservative Treatment

Mild and moderate LAS can, at least initially, be treated conservatively. Conservative treatment will initially involve protect, rest, ice, compression and elevation (PRICE) methods in order to alleviate pain and reduce the inflammatory response. The use of non-steroidal anti-inflammatory drugs, such as Ibuprofen, is commonly recommended to reduce inflammation. Inflammation is however the first necessary step of the natural healing process and its suppression could delay ligament recovery (Stovitz and Johnson, 2003). Therefore current National Health Service (NHS) guidance suggests that non-steroidal anti-inflammatory drugs should be commenced after 48 hours from the point of injury as to not inhibit platelet action during the inflammatory response to injury and thus slowing the healing process (https://www.nhs.uk/conditions/sprains-and-strains/. Accessed: 27/09/20). If the severity of pain allows, the joint should remain mobilised through the unloaded rotation of the ankle through the ROM in dorsi-/plantar flexion, inversion/eversion and internal/external rotation.

After 48 hours physiotherapy can be started, guided by pain, to restore full ROM, strength and proprioception. Physiotherapy should be light initially and build over the following weeks. Most patients can return to more intense exercise such as running from eight weeks after a mild to moderate sprain. Techniques such as kinesiotaping, non-elastic taping and prophylactic bracing are often used to protect the ankle upon return to sport.

1.9.3 Surgical Treatment

Once conservative methods have been exhausted over a period of at least three months, and anterior drawer or talar tilt test results are positive or CAI is confirmed by stress radiography or MRI, surgical treatment should be considered (Song et al., 2019). A minimum of six months of conservative treatment has also been recommended prior to considering surgical treatment as the duration between injury and surgery does not affect surgical outcomes (Hassan et al., 2018; Song et al., 2019). Over 80 repair procedures for the surgical treatment of ankle instability have been described (Tourné and Mabit, 2017). Selection of the most appropriate method is dependent on the quality of the ligament remnant (Yasui et al., 2018). The procedures can be categorised as either anatomic repairs, anatomic reconstructions or as non-anatomic reconstructions (Tourné and Mabit, 2017). Anatomic stabilisation techniques restore stability to the ankle whilst maintaining the original anatomy of the ligaments whereas non-anatomic do not maintain original anatomy. Most often open procedures are performed however arthroscopic techniques are gaining popularity as evidence of their success builds.

1.9.3.1 Anatomic Repair

Broström originally proposed a method of imbrication of the ligament to the bone, defined by overlapping a layer of tissue to surgically close a wound, reconstructing the natural anatomy, shown in Figure 29A. Karlsson et al. (1989) suggested shortening and reinserting the lateral ligaments of the ankle, which often elongate during failure, into the fibular malleolus (Karlsson et al., 1989). Reinforced anatomic stabilisation procedures exist using the extensor retinaculum, periosteum and synthetic reinforcements.

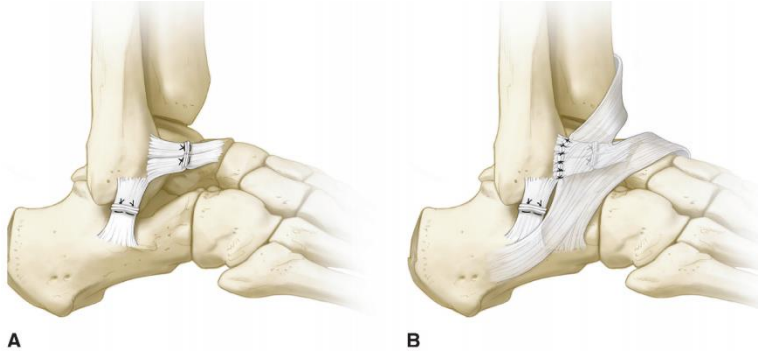

Figure 29. Illustrations of the traditional Broström (A) and modified Broström-Gould techniques (B). Source: (Yasui et al., 2018).

Since the advent of the Broström procedure it has been modified many times. Gould et al. (1980) contributed the addition of overlapping the extensor retinaculum as reinforcement and fixing it transosseously to the anterior aspect of the fibular malleolus, shown in Figure 29B (Gould et al., 1980). Biomechanical analysis of the Broström and the Gould modified Broström procedures found both methods to reduce inversion and translation at all ankle positions compared to untreated sectioned ankles when analysed using the anterior drawer and talar tilt tests (Behrens et al., 2013). However, no significant biomechanical difference or difference in mechanical stability between either surgical method and the intact ankle was found (Behrens et al., 2013). Arthroscopic techniques have also been developed for this procedure (Guillo et al., 2013).

Synthetic materials were originally proposed as prosthetics to replace the damaged ligaments, however due to many complications such procedures have been abandoned for ankle ligament replacement. For example, devices developed by the industrial sponsors of the project include a synthetic suture tape (Jones et al., 2007) and the Leeds-Keio artificial ligament (Xiros Ltd, Leeds, UK) (Usami et al., 2000). Synthetic materials are however currently being used as an attachment or reinforcement for traditional Broström procedures, shown in Figure 30. The suture anchor technique can be used where the ligament does not tear mid-substance or close to the enthesis of the ligament, shown in Figure 30A. Both a single and double anchor technique exist for suture anchor repair. Often when performing an augmented procedure it is done so with the modified Broström-Gould technique utilising the extensor retinaculum for additional support. Arthrex are the leading brand in the field and their InternalBrace™ (Arthrex Inc, Naples, Florida) is currently the only device used to augment a modified Broström-Gould repair procedure (Viens et al., 2014; Coetzee et al., 2019).

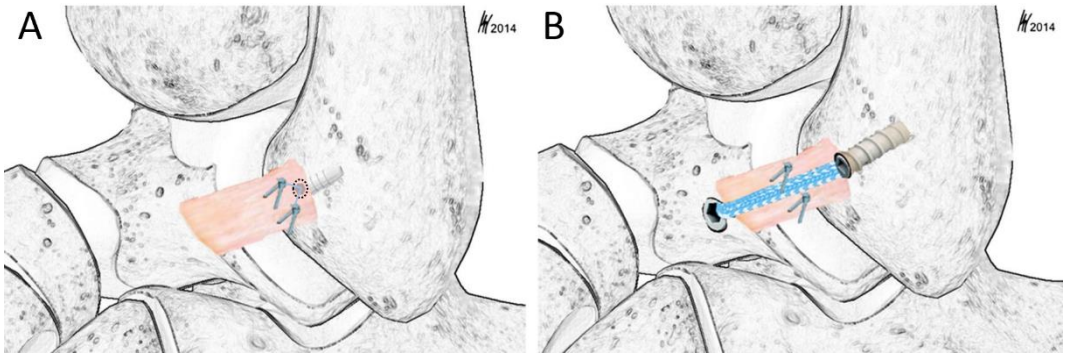

Figure 30. Illustrations of a suture anchor repair (A) and augmented Broström repair with InternalBrace (B). Adapted from (Schuh et al., 2016).

An anatomic approach is the recommended procedure over non-anatomic as it has been shown to be more stable and has success rates between 87 % to 95 % (Gould et al., 1980; Ahlgren and Larsson, 1989; Tanaka and Mason, 2011; Schepers et al., 2011; Kakwani and Siddique, 2014). The modified Broström technique is considered as the gold standard against which new techniques are often compared.

1.9.3.2 Anatomic Reconstruction

Reconstruction techniques are used where the remnants of ligament following damage are insufficient for a repair procedure. A variety of tendons have been used including the plantaris, Achilles, peroneus tertius and peroneus brevis tendons, shown in Figure 31 (Tourné and Mabit, 2017). The location and orientation of the tendons should closely reproduce those of the ligaments being reconstructed, shown in Figure 31.

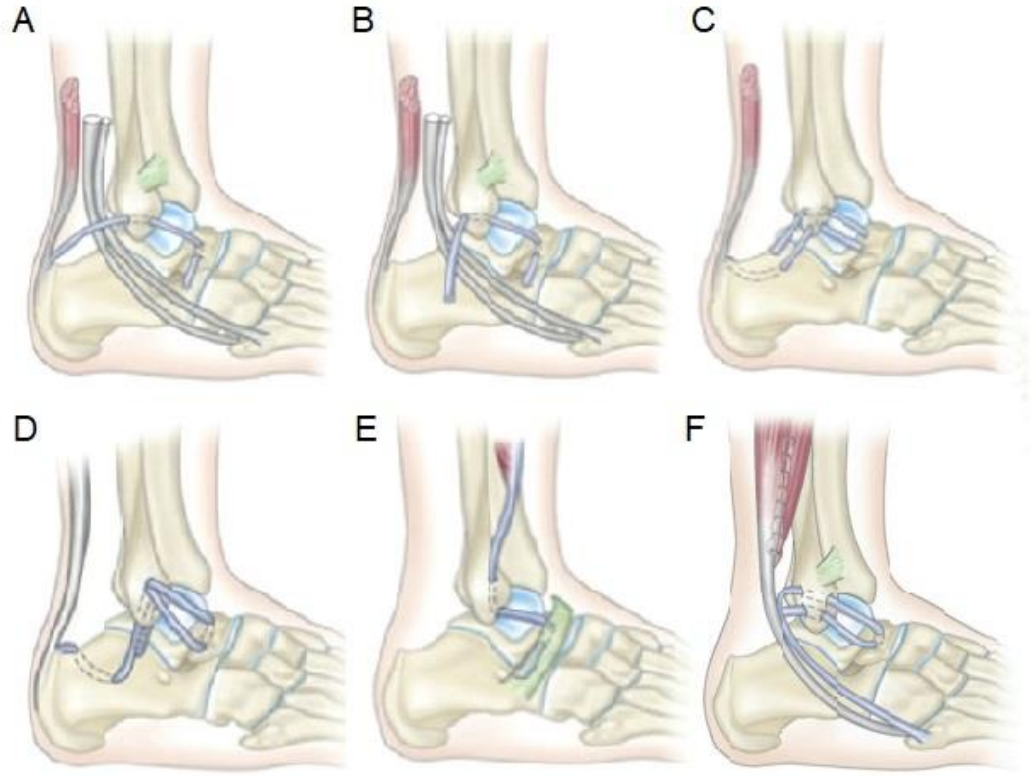

Figure 31. Illustrations of anatomic reconstruction procedures. A) Storen procedure using Achilles (ATFL only) (Storen, 1959)**, B) Storen procedure using Achilles (ATFL and CFL)** (Storen, 1959)**, C) Niethard procedure using plantaris, D) Anderson procedure using plantaris (Anderson, 1985), E) Mabit procedure using peroneus tertius and F) Watson-Jones procedure using peroneus brevis (Watson-Jones, 1940). Adapted from: (Tourné and Mabit, 2015).**

1.9.3.3 Non-anatomic Reconstruction

The peroneus brevis tendon is used in non-anatomic reconstruction also and several techniques have been described. The two frequently utilised non-anatomic procedures are the Evans and the Chrisman-Snook procedures (Tanaka and Mason, 2011). Although anatomic approaches are preferred, non-anatomic approaches are used when the anatomic approach fails or tissue damage is too severe for anatomic procedures to be performed (Schepers et al., 2011).

The Evans approach is a Hemi-Castaing approach where half of the peroneus brevis tendon is harvested and threaded anteroposteriorly through a tunnel drilled through the lateral malleolus and sutured to the remaining intact half of the tendon, shown in Figure 32A (Evans,

1953). Similarly, the Chrisman-Snook technique weaves half of the peroneus brevis tendon through a drilled tunnel in the lateral malleolus anteroposteriorly and then through a tunnel drilled through the lateral side of the calcaneus before being sutured back together (Chrisman and Snook, 1969).

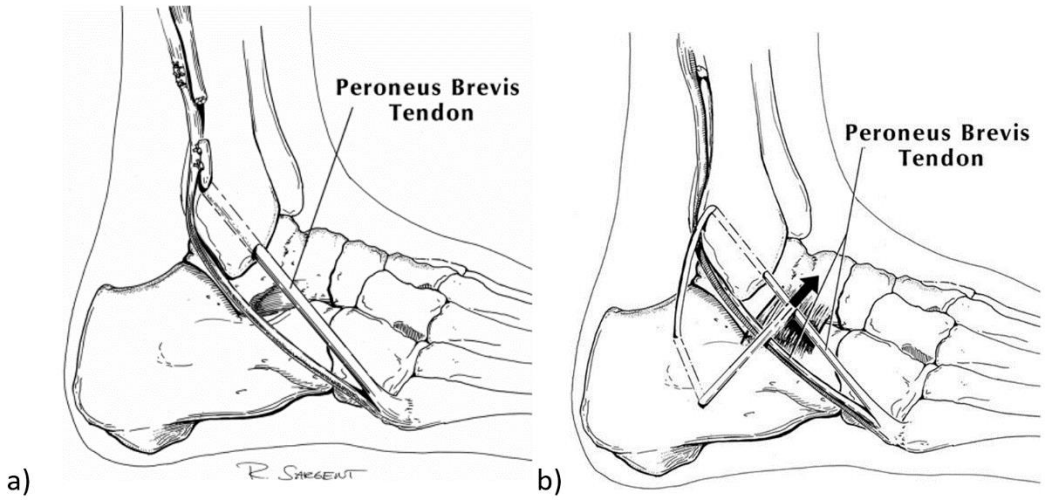

Figure 32. Illustrations of the non-anatomic approaches a) Evans and b) Chrisman-Snook. Source: (Baumhauer and O'Brien, 2002).

1.9.3.4 Outcomes for Surgical Treatment

Clinicians most commonly use the AOFAS Ankle-Hindfoot Scale and Karlsson score to assess functional outcomes (Vuurberg et al., 2018b; Song et al., 2019). The AOFAS Ankle-Hindfoot Scale combines patient perception and physician assessment for pain, function and alignment of the ankle (Kitaoka et al., 1994). The Karlsson score analyses patient outcomes by pain, swelling, instability, stiffness, stair climbing, running, work activities and requirement of additional support (Karlsson and Peterson, 1991). Also frequently reported are the FAOS and the patient-reported FAAM and VAS. The FAOS rates the patient outcomes on symptoms, stiffness, pain, function during activities of daily living, function during sporting activities and quality of life (Roos et al., 2001). The FAAM assesses a patient's ability to perform activities of daily living and sporting participation (Carcia et al., 2008).

1.9.3.4.1 Open Versus Arthroscopic

No statistical significance exists between the outcomes of open and arthroscopic anatomic repair procedures however the complication rate of arthroscopic procedures is much higher (8 % vs 15 %, respectively) (Guelfi et al., 2018; Brown et al., 2018; Song and Hua, 2019). Single-stage arthroscopy however has a much lower complication rate (11 %) than double-stage arthroscopy (47 %) (Araoye et al., 2017).

1.9.3.4.2 Anatomic Versus Non-anatomic

Anatomic repair and reconstruction produce better functional outcomes than non-anatomical reconstruction, with anatomical repair slightly better than reconstruction (Noailles et al., 2018; Vuurberg et al., 2018b). Anatomic repair is also associated with reduced secondary osteoarthritis and nerve damage compared to non-anatomic repair (Noailles et al., 2018; Cao et al., 2018).

1.9.3.5 Outcomes of Anatomic Repair

The outcomes of anatomic repair techniques are rated as very good or excellent by 86 to 100 % of patients having received the treatment, shown in Table 4. The traditional Broström anatomic repair procedure is slightly less favourable than the modified Brostöm-Gould procedure which has become the gold standard for ankle ligament surgical treatment.

Outcome measure scores for suture anchor repair are similar to the modified Broström-Gould procedure but with a lower percentage of good or excellent ratings, shown in Table 4 (Cho et al., 2013). The percentage of patients suffering from residual instability is however lower for suture anchor repair technique compared to the modified Broström-Gould procedure. Single-anchor and double-anchor attachment of a suture repair show similar clinical and functional outcomes with double anchor repair benefitting from improved talar tilt, Karlsson score and sporting participation (Cho et al., 2013; Li et al., 2020).

Evidence for the suture tape augmentation procedure is also comparable to that of the Broström-Gould procedure. Follow-up periods for the two synthetic approaches are considerably shorter than the traditional Broström and modified Broström procedures. Whilst this does not make them inferior techniques the results should be interpreted cautiously.

Table 4. The range of outcomes reported in the literature for different surgical treatments. AOFAS = American Orthopaedic Foot and Ankle Society Ankle-Hindfoot Scale, FAOS = Foot and Ankle Outcome Score, FAAM = Foot and Ankle Ability Measure, RI = residual instability and OA = osteoarthritis. Sources: [1] = (Bell et al., 2006), [2] = (Maffulli et al., 2013), [3] = (Nery et al., 2011), [4] = (Tourné et al., 2012), [5] = (Russo et al., 2016), [6] = (Cho et al., 2013), [7] = (Cottom and Rigby, 2013), [8] = (Ulku et al., 2020), [9] = (Cho et al., 2015), [10] = (Yoo and Yang, 2016), [11] = (Cho et al., 2017), [12] = (Coetzee et al., 2018), [13] = (Cho et al., 2019), [14] = (Xu et al., 2019).

Procedure	Source	Follow-up (years)	AOFAS/ Karlsson score	Good or excellent rating (%)	FAOS/ FAAM score	RI (%)	OA (%)
Anatomic repair							
Broström	[1-2]	9 - 26	89 - 90	86 - 91	92	9 - 16	4 - 11
Repair & reinforcement							
Broström-Gould	[3-5]	10 - 15	90 - 99/ 95	93 - 100	-	5 - 9	0 - 3
Suture anchor repair	[6-8]	1 - 3	95/ 90 - 94	88 - 92	92/ 90	3	-
Suture tape augmentation	[9-14]	0.5 - 2	94 - 98	91	91 - 93/ 89 - 93	0 - 7	-

1.9.3.5.1 Risk Factors

On average 8 % of surgical treatments for lateral ankle injury fail with a complication rate of 17.6 % (Araoye et al., 2017). The systemic condition of generalised ligament laxity can cause a significant four- to six-fold increase in the failure rate of the modified Broström-Gould procedure (Park et al., 2016; Xu and Lee, 2016). The outcome measures AOFAS Ankle-Hindfoot Scale, Karlsson score, talar tilt and anterior talar translation are all significantly worse for patients with generalised ligament laxity (Xu and Lee, 2016). Generalised ligament laxity as well as tibiofibular syndesmosis widening, osteochondral lesion of the talus, high pre-operative talar tilt angle (>15 degrees) and high anterior talar translation (>10 mm) are all associated with clinical failure (Park et al., 2016).

1.9.3.6 Postoperative Management

Partial weight bearing with a brace can be initiated two days after surgery providing benefits over the traditional immobilisation approach (Song et al., 2019). Should immobilisation be required to treat pain or oedema it should not surpass 10 days and be followed by functional support for four to six weeks (Vuurberg et al., 2018a). An effective rehabilitation programme should be followed as in conservative treatment for LAS utilising manual mobilisation and exercise therapy (Vuurberg et al., 2018a).

1.9.3.7 Pre-clinical Evaluation of Synthetic Interventions

To the author's knowledge, no literature exists within peer-reviewed journals reporting the mechanical properties of synthetic interventions and their attachments which are currently being used to augment modified Broström procedures. Industrial manufacturers have however performed their own pre-clinical testing of their devices, with some publishing white papers. In a study investigating implantation methods, the InternalBrace suture tape (Arthrex Inc, Naples, FL, USA) achieved a maximum failure load of 352.31 ± 57.61 N, shown in Appendix Arthrex White Paper 2. A subsequent study performed by Arthrex following the manufacturer's currently recommended implantation technique found the ultimate failure load of the InternalBrace to be 249 ± 47 N, shown in Appendix Arthrex White Paper 3. Both studies were performed using human cadaveric samples with relatively small sample sizes of six and five, respectively. Mechanical characterisation was performed through a linear extension load to failure test at a rate of 20 mm/min.

The Infinity-Lock tube tape (Xiros Ltd, Leeds, UK), developed by the industrial sponsors of this project, has been mechanically characterised during pre-clinical testing but the research has not been published. Their mechanical characterisation studies have been performed mainly on the synthetic tape alone with fewer studies looking at fixation into a Sawbone model similar to that used by Arthrex, shown in Appendix Arthrex White Paper 1. No testing of the product has previously been performed in human tissue.

1.10 Summary

The ankle joint complex is comprised of the talocrural, subtalar and tibiofibular syndesmosis joints which work harmoniously to perform complex multiaxial motion. The conformity of the bones, ligamentous structures and muscles are the major stabilising factors of the ankle. The ATFL restricts plantar flexion, inversion and internal rotation, the CFL restricts dorsiflexion and inversion and the PTFL restricts dorsi-/plantar flexion. Excessive degrees of such motions instigate damage to the respective ligaments. The biomechanics of LAS are not fully understood and are likely multifactorial and highly variable, dependent on the action being performed. Further clarity is required on the biomechanics of LAS including ROM, rotational velocities and moment forces. A device capable of replicating LAS effectively would add great value to the field, however such a device does not exist to the knowledge of the author.

Patients suffering LAS can develop chronic lateral ankle instability. Chronic ankle instability has been attributed to be the leading cause of PTOA. Conservative treatment should be the first treatment option for a LAS however after at least three months of effective functional rehabilitation and the persistent presence of instability, surgical approaches can be considered. The modified Broström procedure, a reinforced anatomical repair, is the gold standard for surgical treatment of lateral ligament injuries. Recently an augmented version of the procedure using a synthetic suture tape has been proposed with surgical outcomes similar

to that of the gold standard procedure. Such an outcome would however be expected as the addition of a suture tape is the only technical variant between the two procedures. Further investigation into the mechanical contribution of the suture tape to joint stability is required.

To effectively assess the mechanical contributions of the suture tapes to the stability of the lateral ankle the mechanical characteristics of the natural tissue must first be understood. The mechanical characteristics of ankle ligaments are scantily reported and have not been performed at realistic strain rates associated with ankle sprain. Further research is required to determine the mechanical characteristics of the LCL complex ligaments and this review identified gaps in the knowledge base that will be met by fulfilling the following aims and objectives.

1.11 Research Aims

The aims of this research project are centred around the progression in understanding of the severe LAS of the human ankle. This project aims to develop appropriate testing protocols in terms of dissection, storage and mechanical characterisation of the individual lateral ankle ligaments for human cadaveric samples. This project also aims to simulate severe LAS in cadaveric samples to analyse the change in joint stability post-sprain before evaluating the effectiveness of synthetic interventions to restore lateral ankle joint stability. Finally, this project aims to identify an appropriate fixation technique for the Infinity-Lock suture tape (Xiros Ltd, Leeds, UK), mechanically characterise the fixation and compare it to the most popular synthetic ligament used in lateral ankle ligament repair, the InternalBrace suture tape (Arthrex Inc, Naples, FL, USA).

1.12 Research Objectives

- To perform a mechanical investigation into the effects of experimental conditions (strain rate, tissue hydration and temperature) and storage conditions (number of freeze-thaw cycles, freezing pre-/post-dissection and freeze duration) on the ultimate failure stress/load and elastic modulus/stiffness of porcine patellar tendon. – Chapter 2.
- To develop a dissection protocol for the biomechanical characterisation of individual lateral ankle ligament BLB complexes from the same human cadaveric specimen. – Chapter 3.
- To determine the ultimate failure load, stiffness and failure mode of individual lateral ankle ligament BLB complexes from the same human cadaveric specimen at strain rates representative of LAS. – Chapter 3.
- To design and manufacture a device capable of replicating the motions associated with LAS using human cadaveric specimens to investigate the biomechanics of LAS. – Chapter 4.
- To investigate the change in anterior translation and inversion rotation of the ankle joint complex following sequential sectioning of the ATFL and CFL to

characterise the alterations to lateral ankle joint stability following severe LAS. – Chapter 5.

- To evaluate the contributions of the Infinity-Lock suture tape (Xiros Ltd, Leeds, UK) and InternalBrace suture tape (Arthrex Inc, Naples, FL, USA) to the restoration of natural lateral ankle joint stability (anterior translation and inversion rotation displacements) in an augmented modified Broström repair of a severe LAS. – Chapter 5.
- To explore the most appropriate tunnel preparatory method for the implantation of the Infinity-Lock suture tape (Xiros Ltd, Leeds, UK) when implanted into natural bone using SwiveLock suture anchors (Arthrex Inc, Naples, FL, USA). – Chapter 5.
- To investigate the ultimate failure load, stiffness and failure mode of the Infinity-Lock suture tape (Xiros Ltd, Leeds, UK) and InternalBrace suture tape (Arthrex Inc, Naples, FL, USA) when implanted following manufacturer guidelines into porcine fibula and a Sawbone model. – Chapter 5.

Chapter 2 – The Effect of Storage and Experimental Conditions on Material and Structural Properties of Porcine Patellar Tendon

2.1 Introduction

The mechanical properties analysed in this study include both material and structural properties. Structural properties are defined as the properties associated to load-extension results describing the characteristics of the entire structure and are dependent on the dimensions and components of the structure. Material properties are defined as the properties associated to stress-strain results describing the characteristics of the material(s) which form the structure and are independent of the dimensions of the structure.

The aim of this study was to identify the effect of experimental conditions (strain rate, tissue hydration and temperature) and storage conditions (number of freeze-thaw cycles, freezing pre-/post-dissection and freeze duration) on the ultimate failure stress/load and elastic modulus/stiffness of porcine patellar tendon. A secondary motivation of this study was to validate the methods for future mechanical characterisation research on human cadaver ankle tissue.

2.2 Study Rationale

The human ankle ligament characterisation study, performed after this preliminary study, planned to use frozen cadaveric specimens imported from the United States of America. The post-mortem processing cycle of the US-derived donor specimens to be used in the study was uncertain, however a likely lifecycle of the specimens is shown in Figure 33. It was anticipated to likely include cycles of freeze and thaw, the impact of which on the material and structural properties of the tissue warranted further investigation. The human specimens arrive as intact whole specimens dissected from the donor inferior to the knee joint. The duration for which the specimens would be frozen was dependent on the time between death and being shipped, but also on the success of the preliminary study. The effects of strain rate and tissue hydration on material properties have previously been explored however there is some contradiction in the results. The literature surrounding the topics investigated is summarised below.

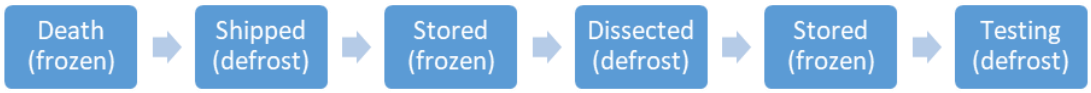

Figure 33. The likely lifecycle of donor specimens from point of death though to testing.

2.2.1 Storage Conditions

The number of freeze-thaw cycles do not significantly affect the mechanical properties of ligamentous tissue when compared to fresh unfrozen samples (Huang et al., 2011; Jung et al., 2011; Suto et al., 2012). Research conducted on rat patellar tendon and bone identified that

up to five freeze-thaw cycles have been shown to have no significant effect on the ultimate failure stress (46.1 ± 17.9 MPa), Young's modulus (211.4 ± 108.3 MPa) and strain at failure (23.8 ± 4.9 %) when compared to fresh samples (42.6 ± 16.3 MPa, 206.8 ± 99.2 MPa and 22.0 ± 4.8 %, respectively) (Suto et al., 2012). Similar findings were reported when human patellar tendon was characterised after one, four and eight freeze-thaw cycles, however the results were not compared to a fresh control group (Jung et al., 2011). Contrary, when human flexor digitorium superficialis tendon was characterised fresh and after one, two, three, five and ten freeze-thaw cycles a significant difference in mechanical properties was identified for more than five freeze-thaw cycles compared to fresh specimens (Huang et al., 2011). The contradictory findings determined it necessary to investigate the effect of freeze-thaw specifically in relation to the post-mortem processing cycle likely observed for the human donor tissue in subsequent study. Unknown, to the author's knowledge, is the effect of the tissue being frozen pre-dissection compared to post-dissection or the duration of the freezing period on the mechanical properties of ligamentous tissue.

2.2.2 Porcine Patellar Tendon

It was deemed unnecessary and wasteful to use human tissue for the method development stage of the larger research project. Suitable animal models were therefore identified and explored for the preliminary study, described in Animal Models within Chapter 1. For the reasons described within the Animal Models section of the literature review, as well as the existing expertise within iMBE working with porcine tissue and an established gripping technique for the patellar tendon, the porcine patellar tendon was selected as the specimen for the preliminary study. Unlike most tendons which attach the belly of a given muscle directly to a respective bone at the muscle attachment site, the patellar tendon originates at the patellar apex and inserts at the tibial tuberosity, shown in Figure 34. The patellar tendon is therefore often referred to as a ligament as it spans between two bones. The patellar tendon is called a tendon however because the patella is a sesamoid bone. Meaning the patella is independent from the femur and formed between the patellar tendon and quadriceps tendon, which are collectively responsible for the connectivity of the quadriceps muscle to the tibia.

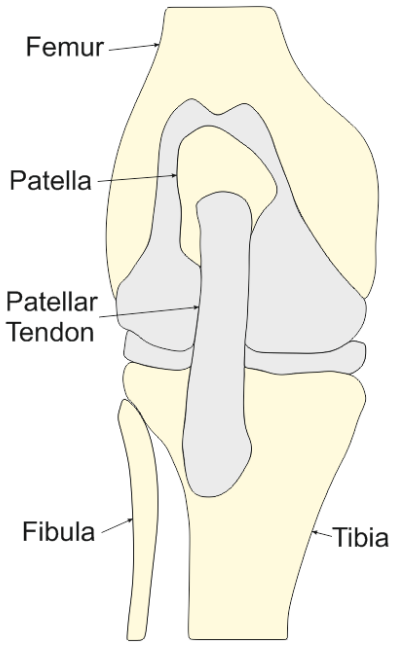

Figure 34. Illustration of the porcine knee joint including patellar tendon.

The classification of the patellar tendon as a tendon was of little importance to this study as the main testing requirement was a bone-tendon/ligament-bone construct. The structural properties of the patellar tendon are superior to the ligaments of the LCL complex with a mean failure load of 1790 N (Blevins et al., 1994). Ligaments and tendons have similar structure and the structure of the patellar tendon is more akin to a ligament than tendon (Nordin and Frankel, 2012). Thinning of the patellar tendon could achieve similar dimensions to the ankle ligaments, resulting in closer structural property results. Methods established and outcomes of the preliminary study should therefore be applicable to testing of the ankle ligaments.

2.3 Method

2.3.1 Study Design

Twenty-seven porcine right hind legs from six-month old pigs, sourced from John Penny & Sons (Leeds, UK), were used in this study. Ethical approval was not required for the testing as all porcine legs were sourced from the food chain. Each of the 27 specimens were randomly divided into nine independent test groups with a sample size n = 3.

The independent test groups were arranged to form five different testing condition subsets. The subsets identify the effect of strain rate, testing environment, number of freeze-thaw cycles, freeze duration and freezing condition on the material and structural properties of the porcine patellar tendon, shown in Table 5.

Table 5. The testing conditions investigated in this study are shown including the different test groups within a testing condition and their respective variables. PBS = phosphate buffered saline. †'Standard condition' independent test group.

Testing Condition	Test Group Name	Variable
Strain Rate	**25 % Strain**	25 %.s^{-1} strain rate
	100 % Strain†	100 %.s^{-1} strain rate
Testing Environment	**PBS Sprayed†**	Tested exposed to air after hydration with PBS spray
	Water Bath	Tested submerged in PBS bath at 37 °C
Number of Freeze-thaw Cycles	**Fresh**	Not frozen
	2 Cycles	Frozen and thawed 2x
	3 Cycles†	Frozen and thawed 3x
	4 Cycles	Frozen and thawed 4x
Freeze Duration	**Fresh**	Not frozen
	117 days†	Frozen for a total of 117 days
	151 days	Frozen for a total of 151 days
Freezing Condition	**Dissected†**	Frozen and thawed 3x after dissection
	1 in-situ	Frozen and thawed 1x intact and 2x after dissection
	2 in-situ	Frozen and thawed 2x intact and 1x after dissection

A ‘standard condition’ test group was established which was used for comparison within each of the testing condition subsets. The standard condition was tested exposed to air after hydration with PBS (Oxoid Ltd, Basingstoke, UK) spray at a strain rate of 100%.s^{-1} after three cycles of freeze-thaw as a dissected BLB constructs over a duration of 117 days. The ‘Fresh’ independent test group was used within the number of freeze-thaw cycles and freeze duration testing condition subsets. The ‘standard condition’ independent test group was named differently for ease of comparison within testing condition subsets, highlighted in Table 5.

2.3.2 Sample Preparation

Porcine right hind legs arrived from the abattoir as intact whole limbs, shown in Figure 35. The specimens requiring an intact in-situ freeze-thaw cycle, where the whole leg was frozen, were placed directly into a -20 °C freezer for 24 hours for the appropriate amount of cycles. These specimens were subsequently defrosted on a dissection table at 21 °C for 48 hours prior to subsequent freeze-thaw cycles and dissection. The weight of the pig was provided by the abattoir and recorded for reference.

Figure 35. Lateral view of an intact porcine leg as delivered into the laboratory from the abattoir.

To prepare the BLB specimen a cut was first made through the skin along the lateral side of the leg from the superior border of the leg distally to approximately 50 mm inferior to the knee joint. The cut through the skin was then continued transversely to the medial side of the leg before continuing superiorly on the medial side to the superior border of the leg. The skin within the cut section was then removed from the leg, exposing the patellar tendon. The glassy white appearance of the patellar tendon and the surrounding fat pad allowed for easy identification. The patella and anterior aspect of the tibial tuberosity were located through palpation of the knee joint. Once all aspects of the patellar tendon BLB construct were located the patella was dissected away from the quadriceps muscle. The patellar tendon was then removed from the fat pad by dissecting along the edges of the patellar tendon parallel with the orientation of the ligament fibres, shown in Figure 36A.

The patella was separated from the quadriceps muscle and the anterior and posterior cruciate ligaments, lateral and medial collateral ligaments, and the meniscus of the knee were severed with a scalpel at their insertion to the tibia. This separated the tibia from the femur as shown in Figure 36B. The soft tissue surrounding the tibia and fibula was removed down to approximately 50 mm inferior to the knee joint. The superior tibiofibular syndesmosis joint was divided with a scalpel and a transverse cut was made through the fibula and tibia 50 mm inferior to the knee using an oscillating bone saw. The shaft of the tibia was gripped within a vice and a transverse cut was made directly above the insertion point of the patellar tendon to the tibia. The transverse cut was made with an oscillating bone saw anteroposteriorly, to avoid damaging the patellar tendon. The anterior aspect of the tibial tuberosity was cut from the tibia with a frontal cut approximately 3 mm posterior to the growth plate present in the tibia, producing a suitable BLB sample, shown in Figure 36C.

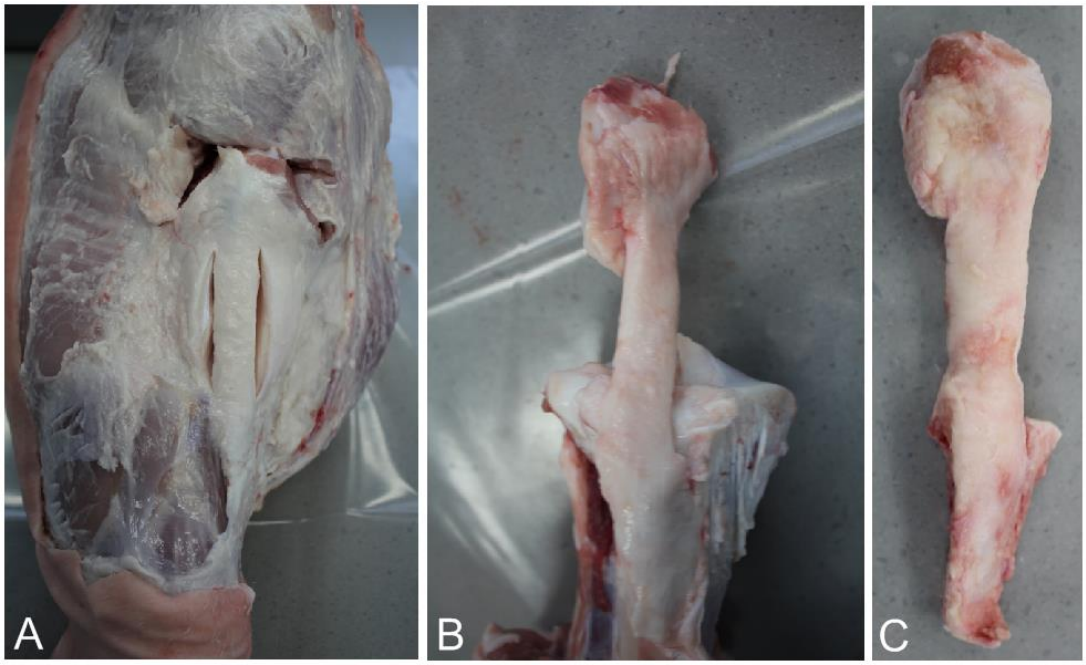

Figure 36. Dissection protocol followed to remove the patellar tendon from a porcine knee joint. A) Removal of skin and isolation of patellar tendon, B) patellar tendon and tibia separated from the femur and C) a BLB patellar tendon sample.

At this stage specimens which were required to be frozen as dissected BLB specimens were wrapped in PBS soaked gauze, sealed within a polythene bag and stored in a -20 °C freezer for the appropriate number of cycles. The specimens were thawed within the sealed polythene bag for three hours at 21 °C prior to subsequent freeze-thaw cycles or testing.

To prepare the sample for testing, fatty tissue surrounding the ligament and bone was removed and the ligament was thinned to create a cross-sectional area of approximately 13 mm^2, matching that of the ATFL (Siegler et al., 1988). To calculate the cross-sectional area of the specimens their cross-section was assumed to be a rectangle. This assumption was made because, when thinned, the highly fibrous tissue can be removed in uniform straight lines producing a cross-section similar to a rectangle, shown in Figure 37.

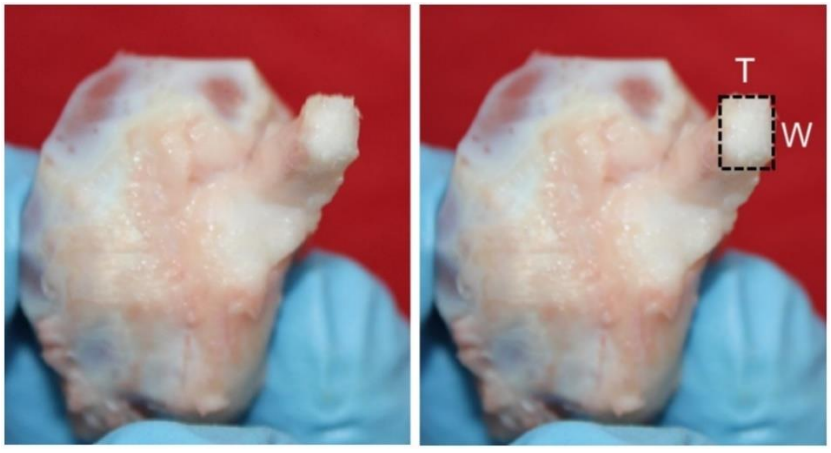

Figure 37. Inferior view of a BLB porcine patellar tendon specimen thinned to approximately 13 mm^2 and severed with a scalpel to show the rectangular cross-section. T = tendon thickness and W = tendon width.

In order to produce the correct cross-sectional area first the thickness was measured, using a Vernier calliper (accurate to 0.02 mm), and the desired cross-sectional area was divided by the thickness of the ligament as this varied between specimens. The resulting width was then set on the Vernier calliper and positioned over the central region of the ligament. A scalpel was then used to dissect along the length of the patellar tendon. The ligament width was then measured to determine the final cross-sectional area. Remaining non-ligamentous soft tissue was removed from the BLB specimens producing a specimen similar to that shown in Figure 38.

Figure 38. Bone-ligament-bone porcine patellar tendon specimen thinned to approximately 13 mm^2.

The soft tissue and articular cartilage from the bony attachments was removed to afford sufficient interaction with Polymethyl methacrylate (PMMA) bone cement. Two small 20 x 4 mm screws were inserted into each of the bony attachments, perpendicular to the orientation of ligament fibres, to further augment the bone prior to cementing. The ligament was wrapped in PBS soaked gauze to protect and hydrate it during the exothermic reaction of the cement setting, shown in Figure 39.

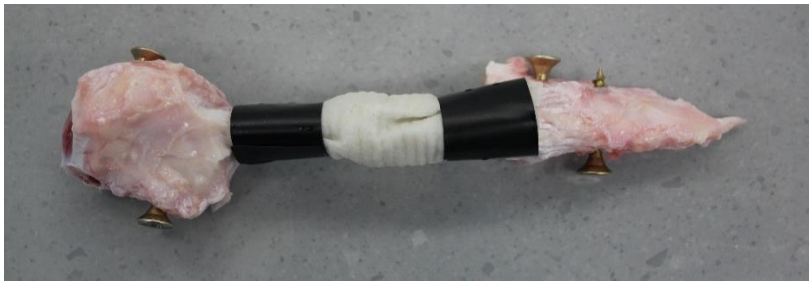

Figure 39. Bone-ligament-bone porcine patellar tendon specimen prepared for bone cementing.

A standard PMMA mixture (WHW Plastics, Hull, UK) with a ratio of two parts powder to one part solvent was used to cement the specimens into potting devices previously developed within iMBE, following a previously established methodology (Herbert et al., 2016). The bony extremity was secured within the potting devices using four bolts, one on each side of the potting device, and the end-caps were attached. The PMMA mixture was poured into a pot containing one bony attachment, with the ligament and other bony attachment suspended

above using a clamp stand, and left to set for 25 minutes. This process was repeated for the other bony attachment resulting in a fully cemented specimen, shown in Figure 41.

2.3.3 Testing Protocol

An Instron ElectroPuls E10000 (Instron, Buckinghamshire, UK) was used in this study, shown in Figure 40. The ElectroPuls E1000 is a linear-torsion all-electric dynamic test instrument with a dynamic linear load capacity of ±10 kN and a dynamic torque capacity of ±100 Nm. The stroke length of the ElectroPuls E10000 is 60 mm and linear displacement can occur at a rate of 1 $m.s^{-1}$. Upon exchange of the load cells, the ElectroPuls E10000 was calibrated following the iMBE standard operating procedure. Calibration was performed using the Calibration wizard, an electronic auto-calibration system built into the device's software, prior to the attachment of any other fixtures. The auto-calibration was performed for both linear and torsional load and involved a three stages process including a course balance, span and fine balance. The calibration data was saved and stored for future reference.

Figure 40. Instron ElectroPuls E10000 electromechanical testing device (Instron, Buckinghamshire, UK).

The cemented patellar tendon was fixed into the potting devices using four bolts into the sides of the pot and an end cap. The individual pots were affixed to the Instron ElectroPuls E10000 using an M8 threaded bar attached to a floating joint, shown in Figure 41. The floating joints allowed five degrees of motion in any direction and an unlimited degree of rotation at each end of the specimen. The floating joints were used to minimise any alignment errors when potting, ensuring load was transmitted equally through the specimen similarly to previously published literature (Siegler et al., 1988).

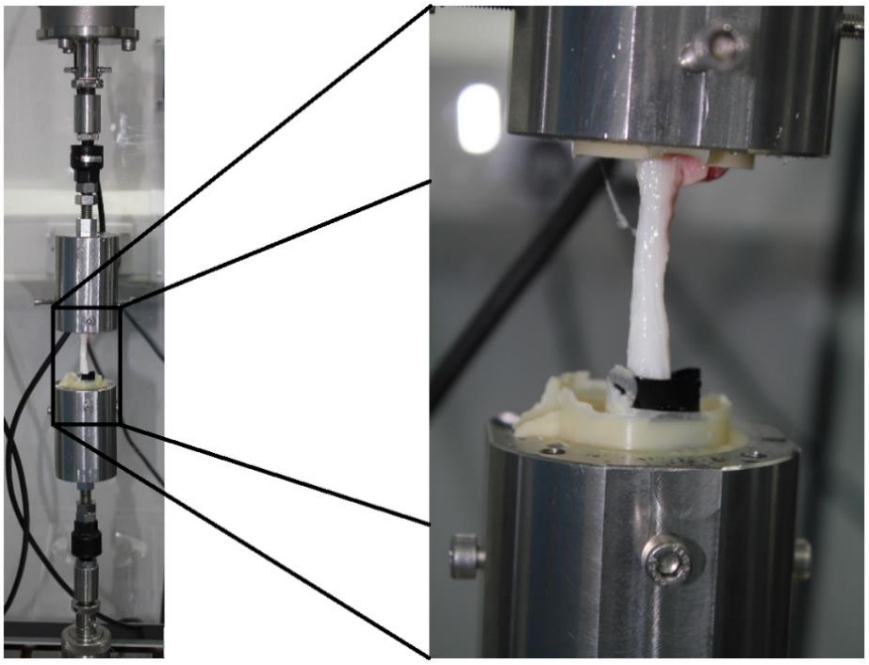

Figure 41. Porcine patellar tendon cemented into potting devices and attached to an Instron ElectroPuls E10000 mechanical testing device (Instron, Buckinghamshire, UK) with floating joints.

Throughout the preparation stages prior to testing, specimens were sprayed with PBS to keep the tissue hydrated. For PBS bath trials specimens were submerged in a PBS filled temperature-controlled water bath at 37 ± 0.5 °C. The temperature was measured and regulated using a custom-built Instron temperature controller pumping unit throughout the setup and testing (Instron, Buckinghamshire, UK). The unit connected to the water bath with flexible polymer tubing and the temperature was measured using a thermocouple placed within the water bath.

The mechanical characterisation was performed through a standard tensile test performed in load control using an Instron ElectroPuls E10000, shown in Figure 40 (Instron, Buckinghamshire, UK). A 10 kN load cell was used, with a 0.5 % accuracy down to 1 % of full scale, as the maximum failure load of human patellar tendon is quoted in literature to be around 3 kN (Herbert et al., 2016). Prior to testing each specimen the ElectroPuls E10000 was tuned to the specific specimen to be tested. This process optimised the performance and control of the testing system for the specific specimen being tested. Tuning of the testing system was performed by applying a load of 20 N to the specimen and measuring the linear stiffness of the testing setup. A pre-load of approximately 10 N was applied to the specimens to ensure they were taut prior to testing and the digital extension was zeroed.

Preconditioning was completed to ensure specimens were in an appropriate physiological state of readiness prior to failure testing and fluid redistribution had occurred within the specimens (Quinn and Winkelstein, 2011). Fifteen cycles of preconditioning with a sinusoidal waveform application, ranging between 0 – 3 mm of digital extension, were performed at a rate of 0.5 $mm.s^{-1}$. The displacement of 3 mm was chosen for preconditioning as it was

approximately equal to 5 % strain for the patellar tendon. Five percent strain represents a value determined to safely load the specimen without damage whilst being greater than the transition point from the toe-region to the linear region of loading (2 % strain) (Johnson et al., 1994).

The specimens were then ramp loaded to failure at either 100 $\%.s^{-1}$ or 25 $\%.s^{-1}$ depending on the strain rate appropriate for the independent group. A strain rate of 100 $\%.s^{-1}$ was selected for injury as it has previously been suggested to be the injury strain rate of the anterior cruciate ligament and medial collateral ligament of the knee (Blevins et al., 1994). A strain rate of 100 $\%.s^{-1}$ was appropriate for ankle ligament characterisation also as detailed in Chapter 3 Testing Protocol. A strain rate of 25 $\%.s^{-1}$ was chosen as it is within the range of 7-28 % proposed to be representative of normal walking (Blevins et al., 1994).

2.3.4 Data Analysis

The mode of failure was determined via physical and visual examination of the specimens. Any specimens where the patellar tendon had torn away from bone, torn cartilage away from bone or torn a small fragment of bone away from bone were categorised as an avulsion. Any intra-ligamentous failures were defined as mid-substance failures. After the experimental testing, post-processing was completed to calculate the ultimate failure load/stress and ultimate failure extension/strain of each patellar tendon from each specimen. A custom MATLAB bi-linear fitting tool was used to calculate toe-region elastic stiffness/modulus (K_0/E_0), linear elastic stiffness/modulus (K_1/E_1), load/stress value of the transition point between toe-region and linear region ($\sigma_{structural}/\sigma_{material}$), extension/strain value of the transition point ($\varepsilon_{structural}/\varepsilon_{material}$) and the goodness of fit value for the model (R^2), defined in Table 6 (Herbert et al., 2016).

Table 6. Definitions of the terms used for the custom MATLAB bi-linear fitting tool.

Term	Symbol	Definition
Toe-region elastic stiffness/modulus	K_0/E_0	The stiffness/modulus of the non-linear toe-region of the load-extension/stress-strain curve.
Linear elastic stiffness/modulus	K_1/E_1	The stiffness/modulus of the linear region of the load-extension/stress-strain curve.
Load/stress value of the transition point	$\sigma_{structural}/\sigma_{material}$	The load/stress value of the transition point between toe-region and linear region.
Extension/strain value of the transition point	$\varepsilon_{structural}/\varepsilon_{material}$	The extension/strain value of the transition point between toe-region and linear region.
Goodness of fit value	R^2	How well the model fits to the data.

First the interval of data to be fitted was selected by highlighting the start of the toe-region and end of the linear region. The MATLAB bi-linear fitting tool then calculated the slope of the toe and linear regions and identified the transition point between the two regions, finally the load/stress and extension/strain values of the transition point were calculated. The results were generated and a graph was produced as shown in Figure 42. The model also reported the goodness of fit for each test.

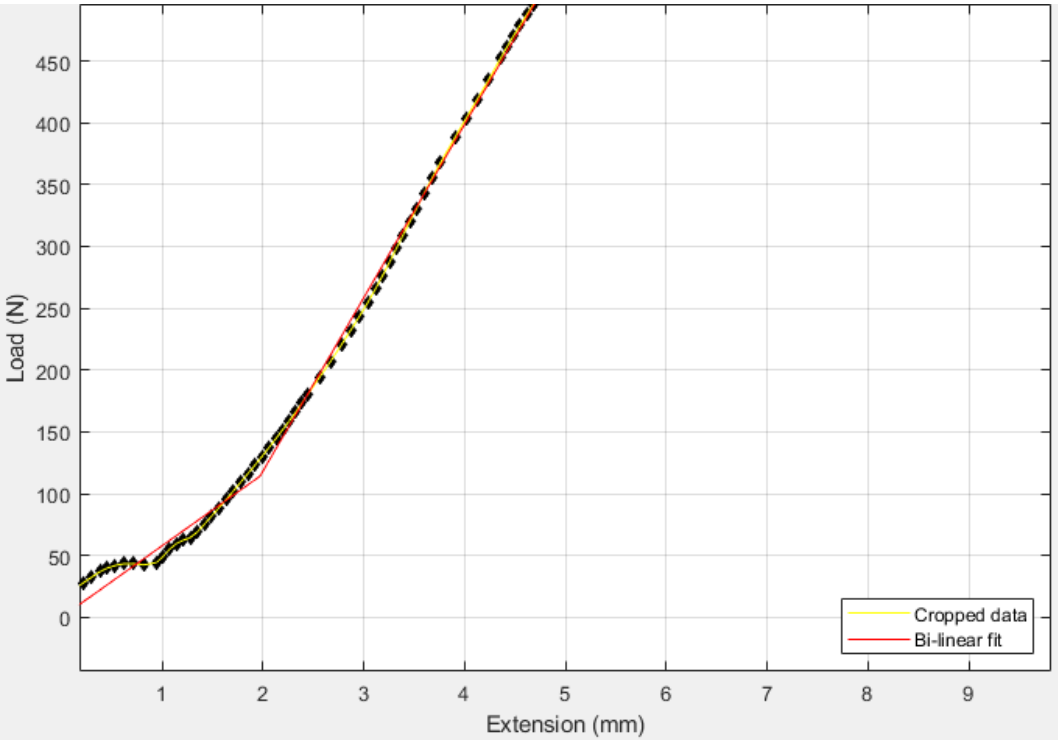

Figure 42. The output of the custom bi-linear fitting tool given the mechanical data input. The two gradients of the red line show the toe and linear regions and the point at which the slope gradient changes is the transition point.

Mean values and 95 % confidence intervals (CI) for the ligament ultimate failure load/stress, ultimate extension/strain, bi-linear elastic stiffness/modulus and transition point between the toe and linear regions were calculated for each of the independent test groups. For each experimental condition subset statistical analysis was performed between the relevant independent test groups, as in Table 5. The statistical analysis performed was a one-way ANOVA followed by a Tukey test where there were more than two independent groups within an experimental condition subset.

2.4 Results

The average cross-sectional area and ligament length measured for samples and recorded average weight of the pigs are reported for each independent test group in Table 7.

Table 7. The average (and range) of cross-sectional area (CSA) and length of the thinned porcine patellar tendon samples as well as the average (and range) weight of the pigs used within each independent test group. †'Standard group' also called 100 % strain, PBS Sprayed, 117 days and dissected.

Test Group Name	Average CSA (mm^2)	Average Length (mm)	Average Weight (kg)
Fresh	13.06 (12.04 – 14.81)	58.55 (56.20 – 59.80)	84.8 (82.6 – 88.9)
2 Cycles	13.66 (13.02 – 14.28)	61.53 (59.06 – 65.48)	84.4 (82.7 – 86.3)
3 Cycles†	12.69 (11.54 – 13.68)	59.30 (58.80 – 59.80)	84.0 (82.5 – 85.2)
4 Cycles	13.37 (12.59 – 13.84)	59.45 (53.62 – 64.72)	76.5 (74.1 – 80.7)
25 % Strain	13.45 (12.93 – 14.42)	58.84 (56.88 – 60.80)	77.5 (74.8 – 79.4)
1 in-situ	12.86 (11.75 – 13.89)	58.73 (55.74 – 60.84)	69.0 (66.1 – 74.4)
2 in-situ	12.51 (11.33 – 13.56)	59.82 (59.52 – 60.32)	75.3 (73.9 – 76.9)
Water Bath	12.55 (11.21 – 13.54)	58.24 (53.16 – 61.38)	84.2 (78.3 – 90.3)
151 days	12.11 (11.20 – 13.42)	54.53 (53.66 – 56.26)	75.7 (70.0 – 83.6)

The structural and material properties of porcine patellar tendon tested to investigate the effects of different experimental, environmental and storage conditions are detailed below. The results are split into the experimental condition subsets as described in Table 5 for ease of comparison.

2.4.1 Strain Rate

The structural and material properties of porcine patellar tendon tested at strain rates of 25 $\%.s^{-1}$ and 100 $\%.s^{-1}$ are displayed in Table 8. The load-displacement and stress-strain curves are shown in Figure 43 and Figure 44, respectively.

Table 8. The mean value ± 95 % CI for the structural and material properties of porcine patellar tendon tested at strain rates of 25 %.s^{-1} and 100 %.s^{-1}. K_0/E_0 = toe-region elastic stiffness/modulus, K_1/E_1 = linear region elastic stiffness/modulus, $\varepsilon_{structural}/\varepsilon_{material}$ = extension/strain coordinate of transition point, $\sigma_{structural}/\sigma_{material}$ = load/stress coordinate of transition point, R^2 = mean value for the goodness of fit for the K_0/E_0 and K_1/E_1 calculations. *Significant results (P < 0.05). †'Standard group'.

Test Group	Ultimate Failure Load (N)	Ultimate Extension (mm)	K_0 (N.mm^{-1})	K_1 (N.mm^{-1})	$\varepsilon_{structural}$ (mm)	$\sigma_{structural}$ (N)	R^2
25 % Strain	902.6 ± 525.1	10.4 ± 1.1	36.2 ± 32.5	123.0 ± 61.9	1.3* ± 0.5	43.9 ± 28.9	0.996
100 % Strain†	1270.7 ± 367.0	10.9 ± 4.9	43.3 ± 30.1	140.1 ± 58.9	1.6* ± 0.1	69.5 ± 42.9	0.997
Test Group	**Ultimate Failure Stress (Mpa)**	**Ultimate Strain**	**E_0 (MPa)**	**E_1 (MPa)**	**$\varepsilon_{material}$**	**$\sigma_{material}$ (MPa)**	**R^2**
25 % Strain	66.7* ± 30.3	0.177 ± 0.005	158.9 ± 146.1	534.8 ± 246.9	0.021 ± 0.008	3.3* ± 2.4	0.996
100 % Strain†	100.0* ± 9.3	0.184 ± 0.081	206.5 ± 76.2	712.1 ± 153.5	0.029 ± 0.013	5.9* ± 0.9	0.997

The mean ultimate failure load increased by 40.8 % from 25 %.s^{-1} to 100 %.s^{-1} but the difference was not significant (p = 0.731). The ultimate failure stress was significantly higher when tested at a higher strain rate of 100 %.s^{-1} (100.0 ± 9.3) compared to 25 %.s^{-1} (66.7 ± 30.3) (p = 0.011). An increased strain rate, from 25 %.s^{-1} to 100 %.s^{-1}, also exhibited a non-significant 33 % increase in linear elastic modulus (p = 0.059). No significant difference in the stiffness of the porcine patellar tendon was found when tested at 25 %.s^{-1} and 100 %.s^{-1}. The stress and extension values for the transition point from the toe-region to the linear region were significantly higher at a strain rate of 100 %.s^{-1} (5.9 ± 0.9 MPa and 1.6 ± 0.1 mm) than at 25 %.s^{-1} (3.3 ± 2.4 MPa and 1.3 ± 0.5 mm) (p = 0.012; p = 0.030, respectively). No significant differences were found for ultimate strain or ultimate extension when tested at the two strain rates.

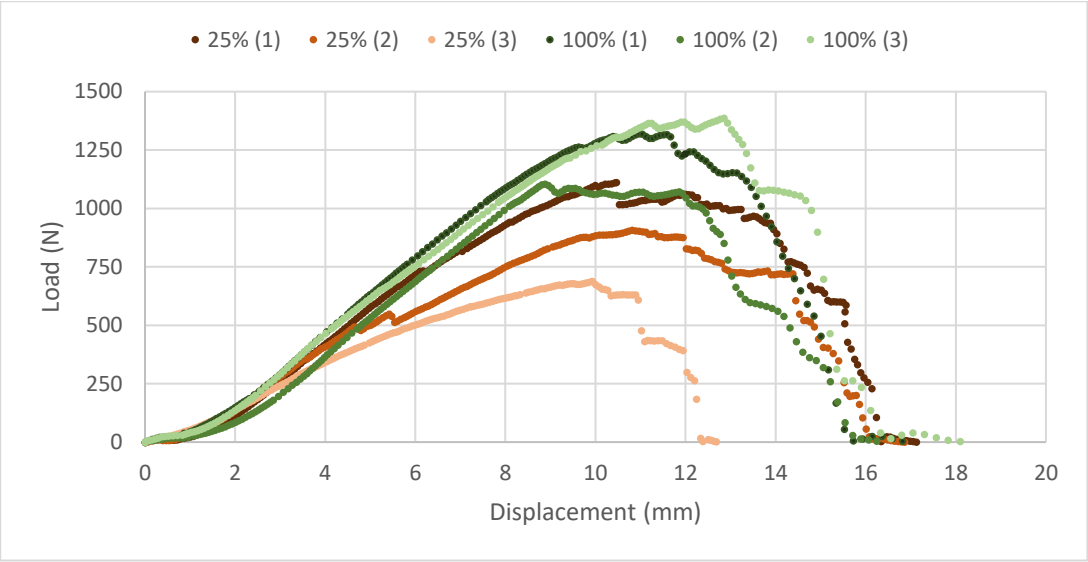

Figure 43. The load-displacement curves for each of the three porcine patellar tendons, as indicated within the brackets, characterised at strain rate of 25 %.s^{-1} and 100 %.s^{-1}.

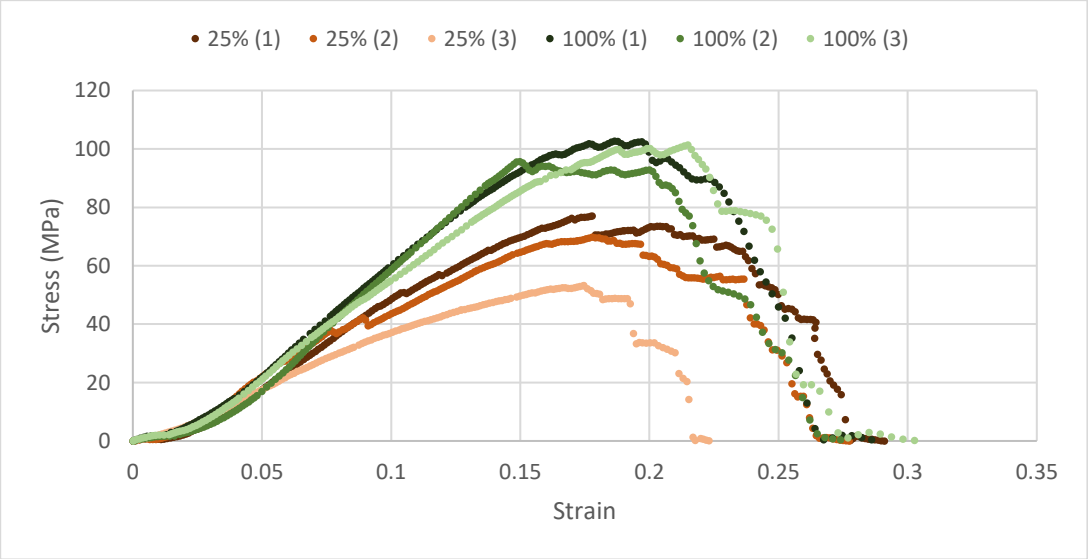

Figure 44. The stress-strain curves for each of the three porcine patellar tendons, as indicated within the brackets, characterised at strain rate of 25 %.s^{-1} and 100 %.s^{-1}.

2.4.2 Testing Environment

The structural and material properties of porcine patellar tendon tested under different environmental conditions are given in Table 9.

Table 9. The mean value ± 95 % CI for the structural and material properties of porcine patellar tendon tested when sprayed with PBS and submerged in PBS. K_0/E_0 = toe-region elastic stiffness/modulus, K_1/E_1 = linear region elastic stiffness/modulus, $\varepsilon_{structural}/\varepsilon_{material}$ = extension/strain coordinate of transition point, $\sigma_{structural}/\sigma_{material}$ = load/stress coordinate of transition point, R^2 = mean value for the goodness of fit for the K_0/E_0 and K_1/E_1 calculations. *Significant results (P < 0.05). †'Standard group'.

Test Group	Ultimate Failure Load (N)	Ultimate Extension (mm)	K_0 ($N.mm^{-1}$)	K_1 ($N.mm^{-1}$)	$\varepsilon_{structural}$ (mm)	$\sigma_{structural}$ (N)	R^2
PBS Sprayed†	1270.7 ± 367.0	10.9 ± 4.9	43.3 ± 30.1	140.1 ± 58.9	1.6 ± 0.1	69.5 ± 42.9	0.997
PBS Bath	1066.0 ± 422.8	11.5 ± 7.5	57.7 ± 12.8	141.7 ± 24.9	1.7 ± 0.7	98.5 ± 30.1	0.9987
Test Group	**Ultimate Failure Stress (Mpa)**	**Ultimate Strain**	**E_0 (MPa)**	**E_1 (MPa)**	**$\varepsilon_{material}$**	**$\sigma_{material}$ (MPa)**	**R^2**
PBS Sprayed†	100.0 ± 9.3	0.184 ± 0.081	206.5 ± 76.2	712.1 ± 153.5	0.029 ± 0.013	5.9* ± 0.9	0.997
PBS Bath	85.9 ± 46.5	0.198 ± 0.121	269.9 ± 85.9	670.5 ± 185.3	0.030 ± 0.009	8.0* ± 1.1	0.999

No significant difference was found for any of the structural properties between samples sprayed with PBS and tested at 21 °C compared to samples tested in a temperature controlled PBS bath at 37 °C. The stress value of the transition point was significantly higher for samples tested in a PBS bath compared to those sprayed with PBS ($p = 0.003$). No other significant differences were found for the material properties of samples sprayed with PBS compared to being tested in a PBS bath.

2.4.3 Storage Conditions

2.4.3.1 Number of Freeze-thaw Cycles

The structural and material properties of the specimens tested after zero, two, three and four freeze-thaw cycles are shown in Table 10. The load-displacement and stress-strain curves are shown in Figure 45 and Figure 46, respectively.

Table 10. The mean value ± 95 % CI for the structural and material properties of porcine patellar tendon tested after zero, two, three and four freeze-thaw cycles. K_0/E_0 = toe-region elastic stiffness/modulus, K_1/E_1 = linear region elastic stiffness/modulus, $\varepsilon_{structural}/\varepsilon_{material}$ = extension/strain coordinate of transition point, $\sigma_{structural}/\sigma_{material}$ = load/stress coordinate of transition point, R^2 = mean value for the goodness of fit for the K_0/E_0 and K_1/E_1 calculations. *Significant results (P < 0.05). †'Standard group'.

Test Group	Ultimate Failure Load (N)	Ultimate Extension (mm)	K_0 ($N.mm^{-1}$)	K_1 ($N.mm^{-1}$)	$\varepsilon_{structural}$ (mm)	$\sigma_{structural}$ (N)	R^2
Fresh	997.3 ± 357.7	10.4 ± 7.3	39.3 ± 8.3	131.4 ± 33.0	2.1 ± 1.2	82.8 ± 34.6	0.998
2 Cycles	1031.6 ± 230.2	11.2 ± 2.0	72.3* ± 21.4	132.2 ± 38.1	1.6 ± 0.9	111.3* ± 31.5	0.999
3 Cycles†	1270.7 ± 367.0	10.9 ± 4.9	43.3 ± 30.1	140.1 ± 58.9	1.6 ± 0.1	69.5* ± 42.9	0.997
4 Cycles	1089.3 ± 204.1	9.0 ± 0.6	48.7 ± 15.4	145.2 ± 7.6	1.8 ± 1.3	85.4 ± 38.3	0.998

Test Group	Ultimate Failure Stress (Mpa)	Ultimate Strain	E_0 (MPa)	E_1 (MPa)	$\varepsilon_{material}$	$\sigma_{material}$ (MPa)	R^2
Fresh	76.6 ± 28.0	0.178 ± 0.135	177.2 ± 45.1	594.2 ± 300.3	0.036 ± 0.015	6.4 ± 3.5	0.998
2 Cycles	75.4 ± 9.1	0.182 ± 0.018	326.3* ± 54.3	599.7 ± 71.1	0.026 ± 0.015	8.4 ± 3.6	0.999
3 Cycles†	100.0* ± 9.3	0.184 ± 0.081	206.5 ± 76.2	712.1 ± 153.5	0.029 ± 0.013	5.9 ± 0.9	0.997
4 Cycles	81.4 ± 5.7	0.152 ± 0.045	225.3 ± 131.5	669.3 ± 248.4	0.032 ± 0.026	6.8 ± 1.5	0.998

The ultimate failure stress results were significantly different between the test groups for number of freeze thaw cycles (p = 0.005). Post-hoc analysis identified that the ultimate failure stress results of the samples tested after three freeze-thaw cycles (100.0 ± 9.3 MPa), was significantly higher than those not frozen (76.6 ± 28.0 MPa), frozen twice (75.4 ± 9.1 MPa) and frozen four times (81.4 ± 5.7 MPa) (p = 0.008; p = 0.006; p = 0.029, respectively). The ultimate failure stress of the fresh samples and samples frozen twice and four times did not differ significantly. The stiffness and elastic modulus values for the toe-region differed significantly

between groups (p = 0.005 and p = 0.003, respectively). Post-hoc analysis revealed that the stiffness result for samples frozen twice (72.3 ± 21.4 $N.mm^{-1}$) was significantly higher than those tested fresh (39.9 ± 7.3 $N.mm^{-1}$), frozen three times (43.3 ± 30.1 $N.mm^{-1}$) and frozen four times (48.7 ± 15.4 $N.mm^{-1}$) (p = 0.005, p = 0.011 and p = 0.032, respectively). The same pattern was found for elastic modulus of the toe-region too, shown in Table 8 (p = 0.003, p = 0.010 and p = 0.026, respectively). The transition point of the toe-region to the linear region had a significantly higher load value for two cycles of freeze-thaw (111.3 ± 31.5 N) than three cycles (69.5 ± 42.9 N) (p = 0.037). No significant differences were found for ultimate failure load, ultimate extension, linear stiffness, ultimate strain or linear elastic modulus for the number of freeze thaw cycles.

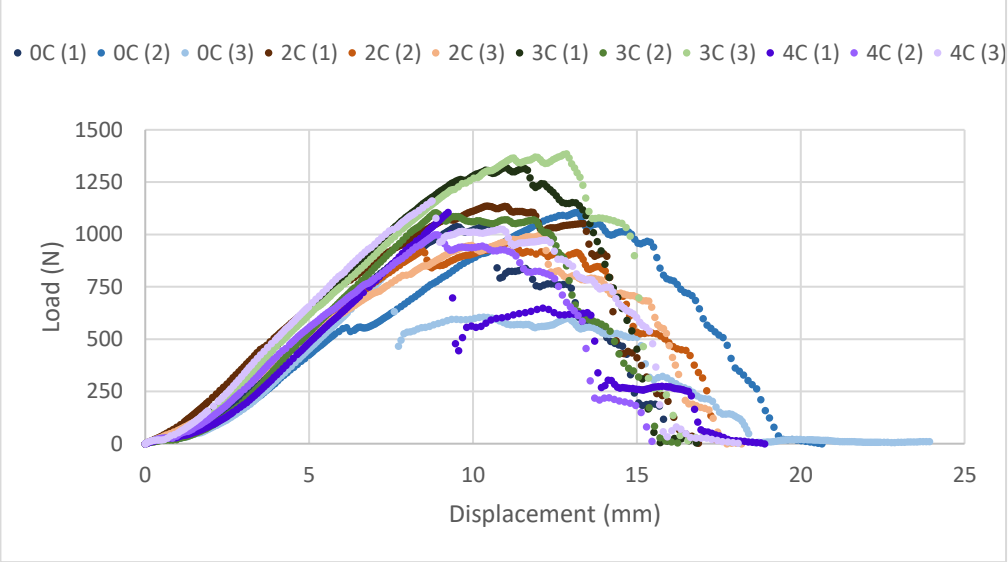

Figure 45. The load-displacement curves for each of the three porcine patellar tendons, as indicated within the brackets, characterised fresh (0C), after two (2C), three (3C) and four (4C) cycles of freeze-thaw.

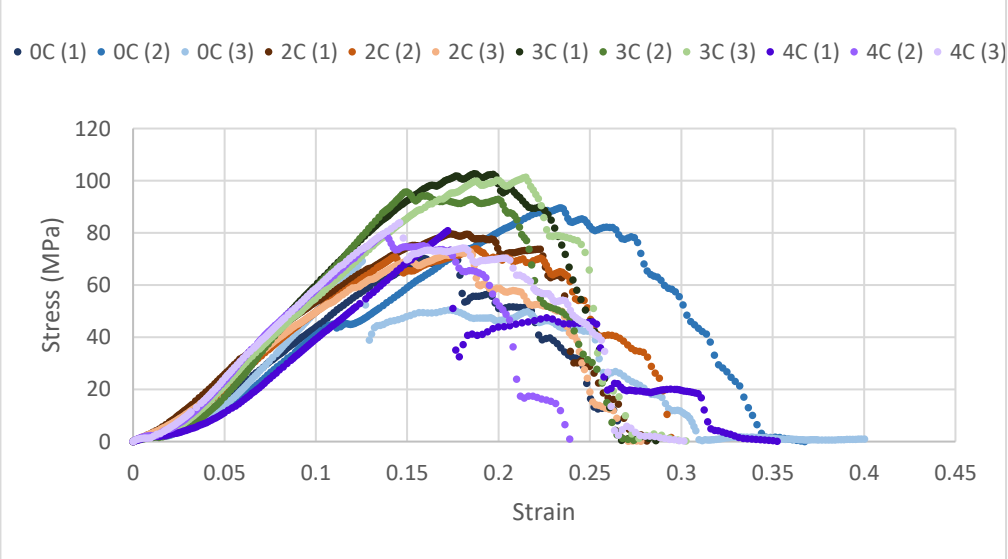

Figure 46. The stress-strain curves for each of the three porcine patellar tendons, as indicated within the brackets, characterised fresh (0C), after two (2C), three (3C) and four (4C) cycles of freeze-thaw.

2.4.3.2 Freezing Duration

The structural and material properties of the specimens tested after zero, 117 and 151 days frozen are shown in Table 11.

Table 11. The mean value ± 95 % CI for the structural and material properties of porcine patellar tendon tested after zero, 117 and 151 days frozen. K_0/E_0 = toe-region elastic stiffness/modulus, K_1/E_1 = linear region elastic stiffness/modulus, $\varepsilon_{structural}/\varepsilon_{material}$ = extension/strain coordinate of transition point, $\sigma_{structural}/\sigma_{material}$ = load/stress coordinate of transition point, R^2 = mean value for the goodness of fit for the K_0/E_0 and K_1/E_1 calculations. *Significant results (P < 0.05). †'Standard group'.

Test Group	Ultimate Failure Load (N)	Ultimate Extension (mm)	K_0 ($N.mm^{-1}$)	K_1 ($N.mm^{-1}$)	$\varepsilon_{structural}$ (mm)	$\sigma_{structural}$ (N)	R^2
Fresh	997.3 ± 357.7	10.4 ± 7.3	39.3 ± 8.3	131.4 ± 33.0	2.1 ± 1.2	82.8 ± 34.6	0.998
117 days†	1270.7 ± 367.0	10.9 ± 4.9	43.3 ± 30.1	140.1 ± 58.9	1.6 ± 0.1	69.5 ± 42.9	0.997
151 days	1140.1 ± 189.8	10.4 ± 3.2	62.1 ± 28.3	177.5 ± 163.4	1.9 ± 0.5	123.4* ± 12.3	0.999
Test Group	**Ultimate Failure Stress (Mpa)**	**Ultimate Strain**	**E_0 (MPa)**	**E_1 (MPa)**	**$\varepsilon_{material}$**	**$\sigma_{material}$ (MPa)**	**R^2**
Fresh	76.6 ± 28.0	0.178 ± 0.135	177.2* ± 45.1	594.2 ± 300.3	0.036 ± 0.015	6.4 ± 3.5	0.998
117 days†	100.0 ± 9.3	0.184 ± 0.081	206.5 ± 76.2	712.1 ± 153.5	0.029 ± 0.013	5.9 ± 0.9	0.997
151 days	94.9 ± 30.6	0.190 ± 0.069	277.1* ± 101.0	637.2 ± 157.5	0.037 ± 0.020	10.0* ± 1.84	0.998

No significant differences were found in any of the structural or material failure properties for samples frozen for zero, 117 or 151 days. A significant difference was identified for the modulus of the toe-region between groups (p = 0.02), shown in Table 11. Post-hoc analysis confirmed that the modulus of the toe-region for samples frozen for 151 days (277.1 ± 101.0 MPa) was significantly higher than fresh samples (177.2 ± 45.1 MPa) (p = 0.018). A significant difference was also observed for the transition point load value between groups (p = 0.006). Post-hoc testing indicated that the transition point load value for samples frozen for 151 days (123.4 ± 12.3 N) was significantly higher than those frozen for 117 days (69.5 ± 42.9 N) and

those tested fresh (82.8 ± 34.6 N) (p = 0.006; p = 0.021, respectively). A similar main effect was found for the stress value (p = 0.004) with post-hoc results between samples frozen for 151 days (10.0 ± 1.84 MPa) being significantly higher than those frozen for 117 days (5.9 ± 0.9 MPa) or tested fresh (6.4 ± 3.5 MPa) (p = 0.005; p = 0.009, respectively).

2.4.3.3 Freezing Condition

The structural and material properties of porcine patellar tendon specimens tested after being frozen in different states of dissection are shown in Figure 47 and Figure 48, respectively as well as collectively in Table 12.

Table 12. The mean value ± 95 % CI for the structural and material properties of porcine patellar tendon tested after three cycles of freeze-thaw. Frozen as either fully dissected (3 cycles), once as a whole leg and twice dissected (1 in-situ) or twice as a whole leg and once dissected (2 in-situ). K_0/E_0 = toe-region elastic stiffness/modulus, K_1/E_1 = linear region elastic stiffness/modulus, $\varepsilon_{structural}/\varepsilon_{material}$ = extension/strain coordinate of transition point, $\sigma_{structural}/\sigma_{material}$ = load/stress coordinate of transition point, R^2 = mean value for the goodness of fit for the K_0/E_0 and K_1/E_1 calculations. *Significant results (P < 0.05). †'Standard group'.

Test Group	Ultimate Failure Load (N)	Ultimate Extension (mm)	K_0 ($N.mm^{-1}$)	K_1 ($N.mm^{-1}$)	$\varepsilon_{structural}$ (mm)	$\sigma_{structural}$ (N)	R^2
3 Cycles†	1270.7 ± 367.0	10.9 ± 4.9	43.3 ± 30.1	140.1 ± 58.9	1.6 ± 0.1	69.5 ± 42.9	0.997
1 in-situ	1219.8 ± 277.6	12.3 ± 1.3	42.6 ± 3.4	149.6 ± 20.4	1.8 ± 0.2	76.2 ± 9.0	0.997
2 in-situ	939.3 ± 389.0	9.3 ± 1.6	43.4 ± 15.6	134.2 ± 50.5	1.8 ± 0.5	78.5 ± 9.7	0.998
Test Group	**Ultimate Failure Stress (Mpa)**	**Ultimate Strain**	**E_0 (MPa)**	**E_1 (MPa)**	**$\varepsilon_{material}$**	**$\sigma_{material}$ (MPa)**	**R^2**
3 Cycles†	100.0 ± 9.3	0.184 ± 0.081	206.5 ± 76.2	712.1 ± 153.5	0.029 ± 0.013	5.9 ± 0.9	0.997
1 in-situ	94.8 ± 4.1	0.210 ± 0.047	195.7 ± 56.0	690.5 ± 240.7	0.031 ± 0.008	5.8 ± 1.3	0.997
2 in-situ (8)	74.8* ± 18.8	0.155 ± 0.028	205.0 ± 86.3	615.2 ± 142.2	0.030 ± 0.007	6.0 ± 1.5	0.997

Specimens were either frozen intact once and dissected twice (1 in-situ), intact twice and dissected once (2 in-situ) or dissected for all three freeze-thaw cycles (3 Cycles). No significant differences were found for any of the structural properties or any of the material properties

other than ultimate failure stress. A significant difference was found between groups for the ultimate failure stress (p = 0.002), shown in Table 12. The ultimate failure stress of samples frozen twice in-situ followed by once post-dissection was significantly lower (74.8 ± 18.8 MPa) than those which were frozen three times post-dissection (100.0 ± 9.3 MPa) and those frozen once in-situ followed by twice post-dissection (94.8 ± 4.1 MPa) (p = 0.002; p = 0.006, respectively).

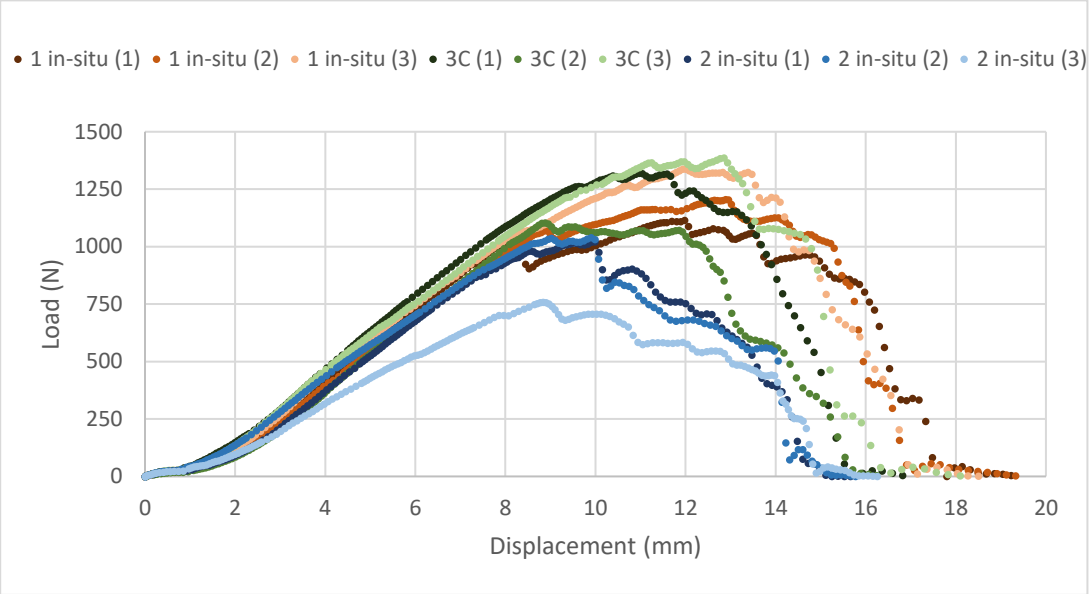

Figure 47. The load-displacement curves for each of the three porcine patellar tendons, as indicated within the brackets, characterised after three freeze-thaw cycles dissected (3C), once intact and twice dissected (1 in-situ) and twice intact and once dissected (2 in-situ).

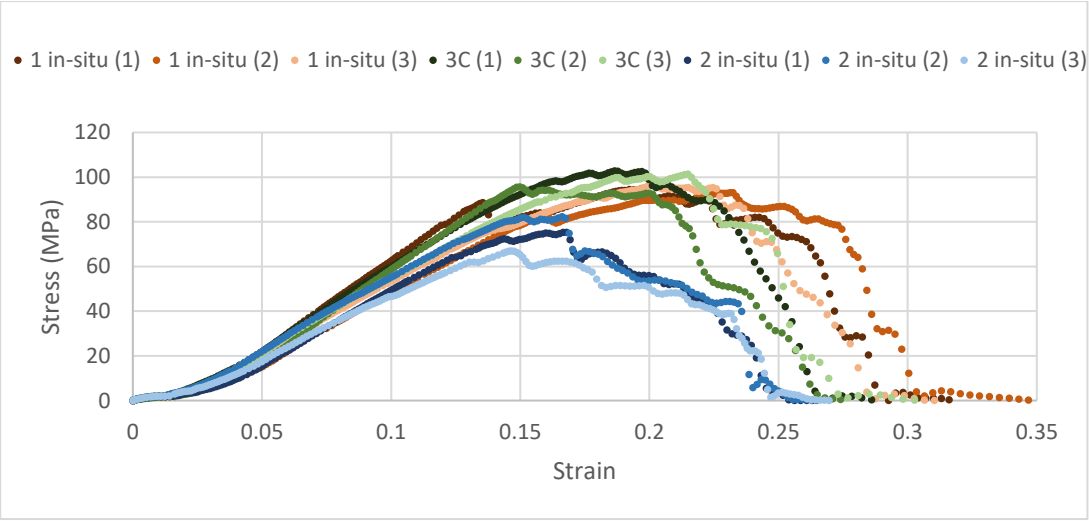

Figure 48. The stress-strain curves for each of the three porcine patellar tendons, as indicated within the brackets, characterised after three freeze-thaw cycles dissected (3C), once intact and twice dissected (1 in-situ) and twice intact and once dissected (2 in-situ).

2.4.4 Failure Mode

The failure mode and observed frequency is recorded in Table 13. Two types of failure were observed, either a mid-substance failure or an avulsion of the patella which occurred in 51.8 %

and 48.2 % of specimens across all trials, respectively. Mid-substance failure of the porcine patellar tendon was very fibrous (Figure 49A) and avulsions included the tearing away of ligament, cartilage or bone from the bone surface at the attachment point of the ligament (Figure 49B). Fibres fail independently of one another, which is why the load/extension graphs have many peaks and troughs in the plastic deformation region of the graph, as shown in Figure 47.

Table 13. The frequency of avulsion and mid-substance failures for each independent group. †'Standard group'.

Observed failure	Fresh	2 Cycles	3 Cycles†	4 Cycles	25 % Strain	1 in-situ	2 in-situ	Water Bath	151 days	Total
Mid-substance	1	3	3	0	1	1	2	1	2	**14 (51.8 %)**
Avulsion (Patella)	2	0	0	3	2	2	1	2	1	**13 (48.2 %)**

Figure 49. A) An example of a mid-substance failure for porcine patellar tendon. B) An example of an avulsion for porcine patellar tendon where a small bone fragment (1) has avulsed from the patella (2).

2.5 Discussion

This study explored the effects of strain rate, environmental conditions and storage conditions on both the structural and material properties of immature porcine patellar tendon. None of the failure structural properties investigated, the ultimate failure load, ultimate extension and stiffness, were significantly affected by any of the experimental or storage conditions evaluated in this study. The high prevalence of avulsions highlights the relevance of structural properties when characterising ligamentous structures to failure. The characterisation results of the porcine patellar tendon will inform future mechanical characterisation studies on the effects of such conditions, including the study described in Chapter 3. The results are discussed further within their respective subsections.

2.5.1 Strain Rate

The observed increase in ultimate failure load/stress and linear stiffness/modulus with an increased strain rate from 25 $\%.s^{-1}$ to 100 $\%.s^{-1}$ supports previously published literature, shown in Table 1 (Noyes et al., 1974; Neumann et al., 1994; Bonner et al., 2015; Karunaratne et al., 2018). A statistically significant difference was only identified for the ultimate failure stress within this study amongst all failure properties. Whilst the increase in ultimate failure load and elastic modulus were not statistically significant a trend was observed. A larger sample size could alter the result which is currently influenced by the small sample size and large variability.

The decrease in load and extension values of the transition point between the toe-region and linear region of the load-extension curve, reported in Table 8, support a previous hypothesis that strain rate-effects are present in the toe-region (Pioletti et al., 1999). These findings were also reported in a recent study characterising porcine super flexor tendon (Edwards et al., 2019). This phenomenon is likely due to the greater redistribution of water content possible within the structure of the ligament at the lower strain rates. Thus, a greater load is required to achieve the same extension value due to the increased role of water and GAGs at the lower strain rate.

Importantly for future work, significant differences have been identified in this study between lower strain rates associated with walking and higher strain rates associated with sprain. In order to effectively characterise and understand the mechanical behaviour of ligaments during sprain events they must be tested at realistic sprain inducing strain rates.

2.5.2 Testing Environment

The lack of a significant difference in the characterisation results, between samples sprayed with PBS prior to testing and samples tested within a water bath, suggests that either method is appropriate for the mechanical characterisation of ligamentous tissue. Spraying samples with PBS however reduces PBS requirements and necessitates less time to set-up and is

therefore favourable. It is worth noting that this characterisation study took less than ten minutes from the final application of PBS, after fixing the specimen into the mechanical testing device, to the completion of the test. This result may therefore not be true for longer mechanical characterisation tests which are at an increased risk of dehydration.

The limited exposure to PBS is also beneficial as there is some evidence that the use of PBS at high concentrations or for prolonged periods of time is not appropriate for the characterisation of tendinous tissue (Screen et al., 2005; Screen et al., 2006; Han et al., 2012; Edwards et al., 2019). These studies found large exposures to PBS to confound the outcome and interpretation of investigations into mechanical properties (Screen et al., 2005; Screen et al., 2006; Han et al., 2012). When soaked in PBS the water content of tendinous tissue increases, causing significant swelling of fibrils and the inter-fibrillar matrix and a significant reduction in sliding between adjacent fibres (Screen et al., 2005; Screen et al., 2006). This causes failure to be initiated between fibrils and sub-fibrils, leading to a reduction in ultimate tensile load and elastic modulus (Screen et al., 2006). Solutes within the PBS can also diffuse into the tissue, interacting with its structure, and altering the mechanics (Hannafin and Arnoczky, 1994; Safa et al., 2017).

A study reported subsequent to the present one found other hydration mediums such as polyethylene glycol (PEG) and a mixture of sodium chloride (NaCl) and PEG (SPEG) to be more appropriate buffer solutions for long-term testing (Safa et al., 2017). Both PEG and SPEG sufficiently hydrate tendinous tissue without solute diffusion to produce consistent characterisation results (Safa et al., 2017). An increased solute concentration was correlated to a decreased apparent water content (Safa et al., 2017). The duration of the hydration soak was however eight hours in the previous study compared to 30 minutes in this study. The effects reported by Safa et al. (2017) are likely magnified by the considerable length of time for the medium soak.

2.5.3 Storage Conditions

2.5.3.1 Number of Freeze-thaw Cycles

Samples frozen for three cycles compared to fresh samples, two cycles and four cycles of freeze-thaw demonstrated a significantly higher ultimate failure stress (100.0 ± 9.3 MPa; 76.6 ± 28.0 MPa; 75.4 ± 9.1 MPa; 81.4 ± 5.7 MPa, respectively) ($p = 0.008$; $p = 0.006$; $p = 0.029$, respectively). No significant difference was found between the two cycle and four cycle groups indicating that the significance found for three cycles is not due to the number of freeze-thaw cycles but some other artefact or the small sample size. This lack of a discernible pattern and the fact that the specimens which were tested fresh do not significantly differ from the samples frozen twice or four times ($p = 0.984$; $p = 0.787$, respectively), suggests that the number of freeze-thaw cycles has no effect on the mechanical properties of porcine patellar tendon. This hypothesis would agree with previously published research of the effect of the

number of freeze-thaw cycles (Huang et al., 2011; Jung et al., 2011; Suto et al., 2012; Arnout et al., 2013; Quirk et al., 2018).

2.5.3.2 Freeze Duration

Freezing BLB porcine patellar tendon samples for up to five months had no significant effect on the structural or material properties when compared to fresh samples. No previous literature existed, to the author's knowledge, on the effect of freeze-duration on the mechanical properties of ligamentous tissue. This is likely due to the majority of studies characterising the tissue they receive promptly after the death of the donor. With the frequent use of tissue stored in tissue banks, more research is required on this topic to investigate the effects of freeze duration.

A previous study analysed the effect of freeze duration on the compressive structural and material properties of porcine trabecular bone (Lee and Jasiuk, 2014). The study found both one and five years of freezing to lower the Young's modulus compared to fresh samples by approximately 39 % and 42 %, respectively (Lee and Jasiuk, 2014). The ultimate compressive strength was also significantly reduced by around 28 % after five years of freezing compared to fresh samples (Lee and Jasiuk, 2014). The reduction in ultimate compressive strength after one year was approximately 11 % lower when compared to fresh samples although this difference did not reach statistical significance (Lee and Jasiuk, 2014). This could be important to the results for failure mode of ligamentous structures as avulsion is more likely to be present in those with inferior bone quality.

A study subsequent to the one detailed in this chapter identified that freezing rat Achilles tendon for nine months significantly reduced the tear resistance of the tendon when compared to fresh samples (74.3 ± 18.4 N and 125.4 ± 16.4 N, respectively) (Quirk et al., 2018). The findings of neither study are contradictory to the results reported in this chapter as the longest freezing period was five months in this study. The results of these papers would however be of great importance and possible concern when using tissue sourced from tissue banks. The tissue used in future studies is expected to be frozen for durations considerably closer to the present study than for five years. This finding should however be a concern of tissue banks who should potentially look to limit the duration tissue samples are frozen for.

2.5.3.3 Freeze Condition

The ultimate failure stress for specimens frozen in-situ twice (74.8 ± 18.8 MPa) was significantly lower than once in-situ (94.8 ± 4.1 MPa) and three cycles dissected (100.0 ± 9.3 MPa) ($p = 0.006$; $p = 0.002$, respectively). Each additional freeze in-situ appears to have lowered the mean failure load/stress of porcine patellar tendon samples. The cause of a reduction in failure stress due to freeze cycles as an intact limb are unclear. One potential hypothesis is that the dimensions of the sample change due to increased swelling of the ligament during the intact freeze-thaw cycles reducing the material properties of the sample.

An alternative hypothesis could be that during freezing the formation of ice crystals under natural joint tension has caused damage to the patellar tendon. The duration of the freezing period was much shorter for two cycles in-situ (46 days) compared to three cycles post-dissection and one cycle in-situ (117 days and 116 days, respectively). If previously published literature is applicable to porcine patellar tendon then an extended duration should reduce the strength properties of the ligament.

When comparing the ultimate failure stress results for two in-situ freeze-thaw cycles to fresh samples, not originally included in this subset, no significantly difference was observed ($p = 0.988$). This finding suggests that freezing intact specimens does not affect the failure mechanical properties. Other than the condition in which the samples were frozen, the other most noticeable variable capable of providing an explanation was the duration of the freeze period. The samples frozen in-situ twice were however frozen for a shorter length of time than the other frozen samples in this subset. This contradicts the proposed effect of longer freezing durations which potentially cause a reduction in mechanical properties (Quirk et al., 2018). The small sample size of three cannot provide conclusive evidence and a larger, more appropriately powered study, with structural analysis would provide further insight for this particular investigation.

2.5.4 Failure Mode

Avulsions accounted for 48.2 % of all observed failures, a typical result for BLB construct material characterisation. Avulsion failure was more prevalent at the slower strain rate of 25 $\%.s^{-1}$ (2/3) compared to the higher strain rate of 100 $\%.s^{-1}$ (0/3). These findings support previously published literature by Noyes et al. (1974) who reported 46.3 % of all failures to be avulsions and identified an increased prevalence of avulsions at lower strain rates (Noyes et al., 1974). The authors found avulsions to occur in 30 % of samples at a higher strain rate (66.2 $\%.s^{-1}$) compared to 67 % at a slower strain rate (0.662 $\%.s^{-1}$) (Noyes et al., 1974). Whereas in a study by Blevins et al. (1994) avulsions occurred in 32 % of patellar tendon samples taken from human donors and strain rate was determined to have no effect of the failure mode when tested at 10 $\%.s^{-1}$ and 100 $\%.s^{-1}$ (Blevins et al., 1994). The general consensus in the literature is that strain rate does influence the failure mode of BLB constructs (Noyes et al., 1974; Crowninshield and Pope, 1976; Hawkins, 2002). The large sample size (n = 81) of the Blevins et al. (1994) study does however raise questions. In particular what is the definition of avulsion, a term which differs in meaning between papers? Blevins et al. (1994) distinguishes between mid-substance, insertion failures and bony avulsions and details the location of insertion and avulsion failures. Many others however simply define the failure mechanism of ligaments as either mid-substance or avulsion. Whilst the classification of purely mid-substance and bone avulsion failures are clear, the location of failures at insertions could be included in either the mid-substance or avulsion categories depending on the examiners definition and judgement. A

consensus should be sought for an appropriate classification of failure modes of ligaments to improve current understand and afford better comparison between studies.

In the current study the avulsions were found to occur on the patellar side only and were small in nature, as shown in Figure 49B. The samples had however been thinned along their entire length which could likely influence the failure mode. Often sprained ligaments are depicted as a snapped ligament with a clean break, whereas this study found mid-substance failure to be fibrous, and even after complete rupture the ligament was still loosely attached. The fibrous failure of ligaments is not well visualised within literature and therefore is often misunderstood in the clinical environment. An understanding of the failure mode of ligaments is fundamental for clinicians wishing to treat and surgically repair damaged ligaments. The type of failure has implications on the surgical approach selected to repair the ligaments of the ankle. Ankle ligaments are routinely repaired surgically by attaching the two ruptured elements of the ligament, in a procedure called the modified Broström procedure, however this technique is not possible where failure occurs at the insertion of the ligament.

The large prevalence of avulsions highlights the potential irrelevance of failure material properties in this study due to the results not being solely representative of patellar tendon. The material properties were calculated only considering the intra-ligamentous cross-sectional area of the patellar tendon. The material properties do not consider the geometries of the bone or, perhaps more importantly, of the insertion point of the ligament onto the bone. Structural properties however, are unaffected by avulsions as the bone attachment and ligament combine to form a BLB construct which structural properties aim to describe mechanically. Structural properties are therefore more clinically relevant for future ankle characterisation as the concern is the risk of an ankle sprain, whereby avulsion can be present.

2.5.5 Limitations of the study

A noteworthy point for all results from this study, but particularly for the evaluation of failure mode, is that the specimens were not in their natural geometry and were intentionally thinned to match the dimensions of the ATFL. The results should therefore not be interpreted as results representative of natural porcine patellar tendon. The failure mode results did however generally agree with published literature, therefore the effect of thinning the samples does not appear to have influenced the failure mode results. Bearing in mind the importance of these results attempting to mimic those of human ankle ligaments, an argument could be made that immature porcine patellar tendon is not representative of mature human ankle ligaments. Whilst this may be true to some extent, the purpose of this study was primarily to identify the effects of testing and storage conditions on the mechanical properties of ligamentous tissue rather than define values for specific ligaments.

In terms of study design, many measures were taken to ensure that the testing groups addressed the aims of this study and identified the effects of various test parameters. One

factor which was difficult to control due to the size of the study and the number of variable factors was the freezing duration of samples. The variation is greater than desired, however it should not be detrimental to the study as the freezing duration results suggest that up to five months of freezing do not have a significant effect on mechanical properties. It could also be argued that the water bath trials assess not only tissue hydration, but also temperature effects. This was not due to a lack of foresight but instead a case of purposeful improved efficiency. Had a significant difference been identified then the exact reasons could have been explored in further testing.

2.6 Conclusion

The mechanical properties of BLB constructs which have been freeze-thawed up to four times over a period of up to 5 months, are comparable to fresh samples. Testing ligaments exposed to air during short standard tensile testing after being rehydrated with PBS is suitable for the characterisation of ligaments. Structural properties in particular, should be examined in studies using BLB testing where avulsions are present and sprain characterisation studies should be performed at representative strain rates. A concern from this chapter for the planned future work is the use of samples from tissue banks where samples are frozen for longer durations and the impact this may have on mechanical properties. The lack of significant effects determined in this study for various storage conditions and testing environments enable future human tissue testing to be performed with confidence. Taking the practicality of laboratory practice and time efficiency into consideration, optimum test conditions for subsequent human tissue testing were developed. The optimum testing conditions include testing ligaments exposed to air after consistent hydration with PBS solution at appropriate strain rates using tissues that have been freeze-thawed as BLB constructs up to four times for a period of up to five months.

Chapter 3 – Mechanical Characterisation of Lateral Ankle Ligaments

3.1 Introduction

Having identified suitable storage and mechanical testing protocols for BLB constructs an efficient dissection protocol and effective gripping technique were required specifically for the characterisation of lateral ankle ligaments. This chapter has two parts, firstly the LCL complex is mechanically characterised at strain rates representative of LAS. A novel dissection protocol and gripping technique are described for the LCL complex alongside the mechanical characterisation results. Secondly, characterisation of the distal tibiofibular syndesmosis is explored and the determination of an appropriate gripping technique is investigated.

3.2 Characterisation of the Lateral Collateral Ligament Complex at Realistic Sprain-inducing Strain Rates

3.2.1 Introduction

Some studies exist which report the mechanical properties of the lateral ankle ligaments (St Pierre et al., 1983; Attarian et al., 1985; Siegler et al., 1988; Funk et al., 2000; Beumer et al., 2003; Butler and Walsh, 2004; Viens et al., 2014). The methodology of each study varies including the ligaments tested, as well as the material testing device, gripping technique and strain rate used. The general set-up tests BLB specimens using a mechanical testing device. None of these studies determine the failure mechanical properties for the intact LCL complex (ATFL, CFL and PTFL), or the AiTFL and the PiTFL from the same donor foot. The absence of literature detailing such information is likely due to the difficulty faced isolating and gripping ankle ligaments, as previously reported (Siegler et al., 1988; Funk et al., 2000). A lack of published work on this topic has hindered the understanding of the mechanical requirements of repair techniques for ankle sprain and the failure mechanisms of natural ligaments during ankle sprain.

The detailed anatomy of the lateral ankle ligaments is provided in Chapter 1 Ankle Complex Anatomy. Of importance to this chapter are the location of fibular insertions as well as the orientation and geometry of the ligaments, shown in Figure 50A and Figure 50B.

This study aimed to improve understanding of the ultimate failure load, stiffness and failure modes of the human LCL complex characterised individually at strain rates representative of LAS.

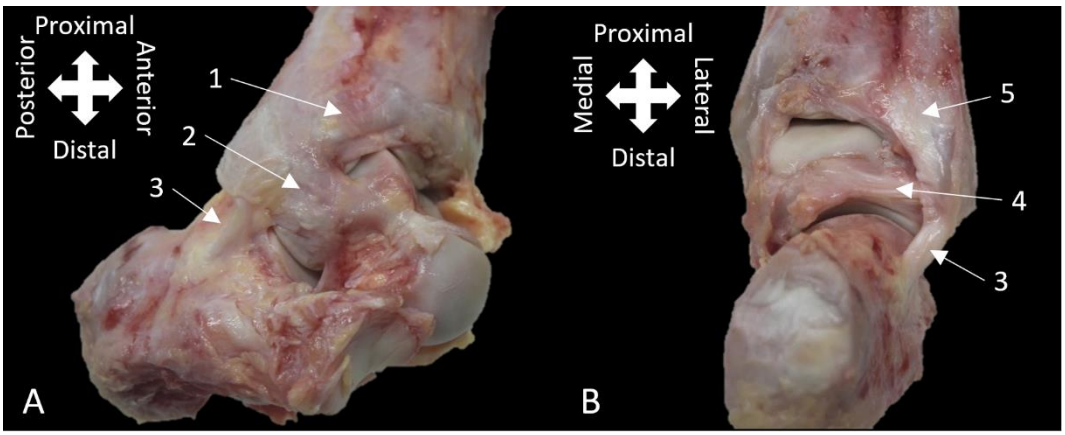

Figure 50. A) Anterolateral view and B) posterolateral view of a dissected human ankle showing the lateral ankle ligaments. Ligaments shown are the AiTFL (1), anterior talofibular ligament (2), calcaneofibular ligament (3), posterior talofibular ligament (4) and PiTFL (5).

3.2.2 Materials and Methods

3.2.2.1 Specimens

Ethical approval for this study was granted by the University of Leeds Research Ethics Committee (MEEC 15-020). Eight fresh frozen human cadaver feet, sourced from MedCure (USA), were used in the study. Exclusion criteria for the cadaver tissue included a reported prior lower limb trauma or surgery, or a history of diabetes. Two samples were excluded from the study, one due to a fibular fracture and another because of the presence of an os trigonum accessory bone, both identified during initial dissection. The mean ± 95 % CI donor age was 56.2 ± 12.2 years, body mass index (BMI) was 22.3 ± 2.9 $kg.m^{-2}$ and there were three males and three females. A summary of donor information is shown in Table 14.

Table 14. Tissue donor demographic details. The mean and 95 % CI is given for age, weight and BMI. (M – male, F – female, A.A – African American, C – Caucasian, R – right & L – left).

Sample	Age (years)	Sex	Race	Weight (kg)	BMI ($kg.m^{-2}$)	L/R Foot
1	72	M	A.A	71	22.4	R
2	60	F	C	53	18.9	L
3	49	F	C	49	20.9	R
4	61	M	C	66	21.4	R
5	38	M	C	85	27.0	L
6	57	F	C	61	23.2	R
Mean	56.2	-	-	64.1	22.3	-
± CI	± 12.2			± 13.8	± 2.9	

3.2.2.2 Sample Preparation

Following shipping from the United States of America the intact frozen specimens were stored in a -80 °C freezer, compliant with the Human Tissue Act, until they were tested. Specimens were thawed for 48 hours at 4 °C in a refrigerator prior to dissection. After at least 24 hours of thawing, each foot was scanned, at a resolution of 82 µm, using a SCANCO Medical xtreme CT scanner (SCANCO Medical, Brüttisellen, Switzerland). Each scan lasted approximately 90 minutes and was performed to ensure no major undiagnosed damage was present as well as for computational modelling purposes for other projects.

The LCL complex was dissected intact from each foot, whilst preserving the syndesmosis joint for potential future study, following a novel dissection protocol, shown in Figure 51 and Figure 52. The proximity of fibular insertions provided particular difficulty for the dissection protocol as they limited the amount of bone stock available for each of the ligaments. Initially, all ligaments were intended to be isolated as individual BLB constructs for mechanical characterisation. The interconnecting fibres of the ATFL, CFL and PTFL prevented the LCL complex from being isolated for testing (Dalmau-Pastor et al., 2020). Furthermore, particular consideration was given to the fibular insertions of the AiTFL and ATFL as well as the PiTFL and PTFL which are also in close proximity. Due to these factors it was determined that the LCL complex would not be able to be split separately into its constituent structures for testing.

Pre-planning of the dissection protocol was performed with an aim to preserve as much bone stock as possible for each of the BLB constructs. The initial soft tissue dissection to expose the ligaments and bony constructs of the ankle was performed by a foot and ankle specialist consultant orthopaedic surgeon. Firstly, all fascia and soft tissue was dissected from the calcaneocuboid talonavicular joint posteriorly and then proximally to the transverse cut through the tibia and fibula. Next, the forefoot was removed by transecting along the talonavicular calcaneocuboid joint.

From this point onwards the dissection was performed by the author. Using an oscillating bone saw, a sagittal cut was made through the entirety of the calcaneus and talus and approximately 50 mm into the tibia, as shown in Figure 51B. The cut was made approximately one third of the distance between the medial and lateral malleoli on the medial side of the ankle to preserve bone on the lateral side for the tibial, talar and calcaneal insertions. The lateral ankle complex was then removed by a transverse cut through the fibula, separating the LCL complex from the distal tibiofibular syndesmosis, as shown in Figure 51C. The cut was performed between the fibular insertions of the ATFL and AiTFL and the PTFL and PiTFL. The delicate cut was performed ensuring the fibular insertions of the four aforementioned ligaments were not disrupted.

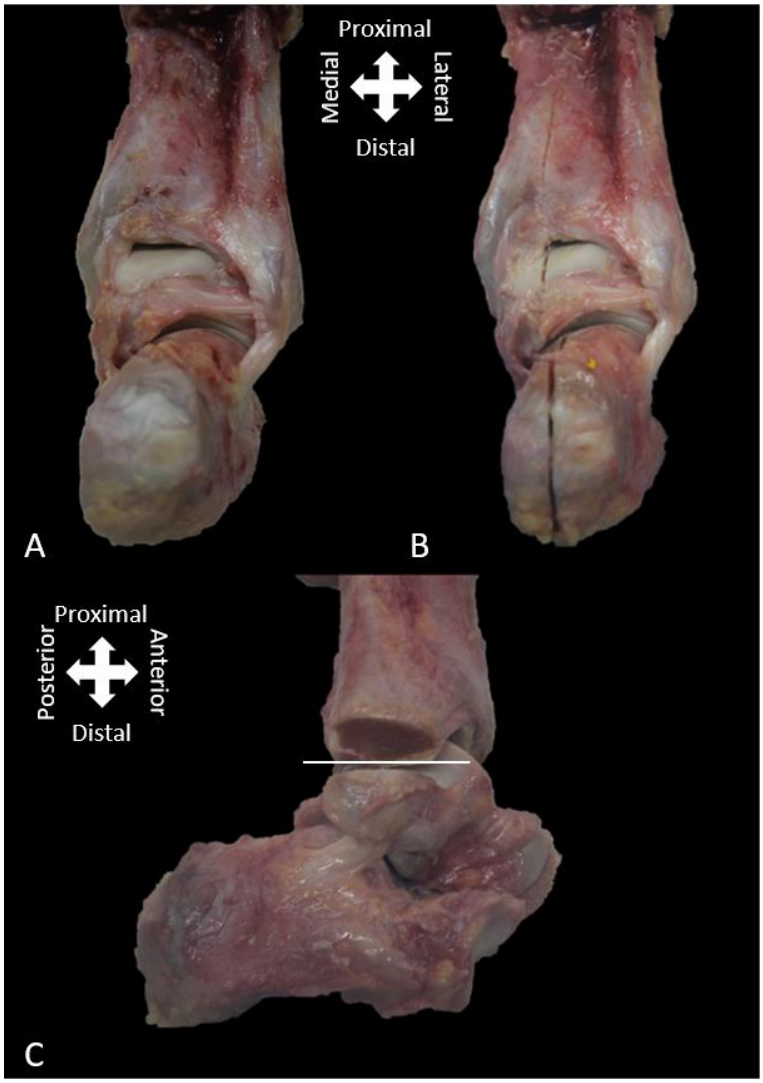

Figure 51. The dissection protocol employed to remove the LCL complex from the ankle complex. A) Posterior view of the intact ankle complex. B) Posterior view of the sagittal cut through the tibia separating the medial and lateral aspects of the rearfoot. C) Lateral view of the transverse cut (white line) made through the fibula to separate the LCL complex and distal tibiofibular syndesmosis.

To further prepare the LCL complex the talus was split in half with a frontal cut creating independent talar insertions for ATFL and PTFL, shown in Figure 52. The calcaneus was then reduced in size and shaped to fit within the gripping fixture. Two parallel frontal cuts, either side of the calcaneal insertion, parallel with the fibres of the CFL were performed. Finally, two transverse cuts, one distal and one proximal to the calcaneal insertion of the CFL were performed. The proximal transverse cut was performed using a small handheld hacksaw for increased precision and was made from directly proximal to the calcaneal insertion in a lateral to medial direction. The final construct for testing was produced, as shown in Figure 52.

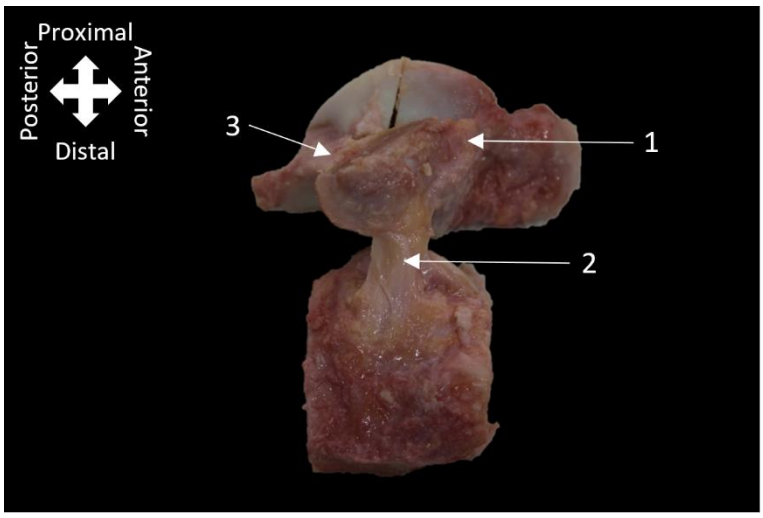

Figure 52. The LCL complex fully dissected prior to testing. The frontal cut into talus has been performed, creating separate bone pieces for the ATFL and PTFL, and the calcaneus has been shaped to fit within the bespoke testing grip. The ATFL (1), CFL (2) and PTFL (3) are shown.

Following this technique, independent BLB samples for the AiTFL and PiTFL could be produced for potential future study. First, a transverse cut through the fibula and tibia was made 50 mm proximal to the tibial plafond as deep as the initial sagittal cut through the tibia, separating the distal tibiofibular syndesmosis from the shank of the leg, shown in Figure 53A. A final frontal cut was made centrally through the fibula and tibia to isolate the AiTFL and PiTFL, shown in Figure 53B.

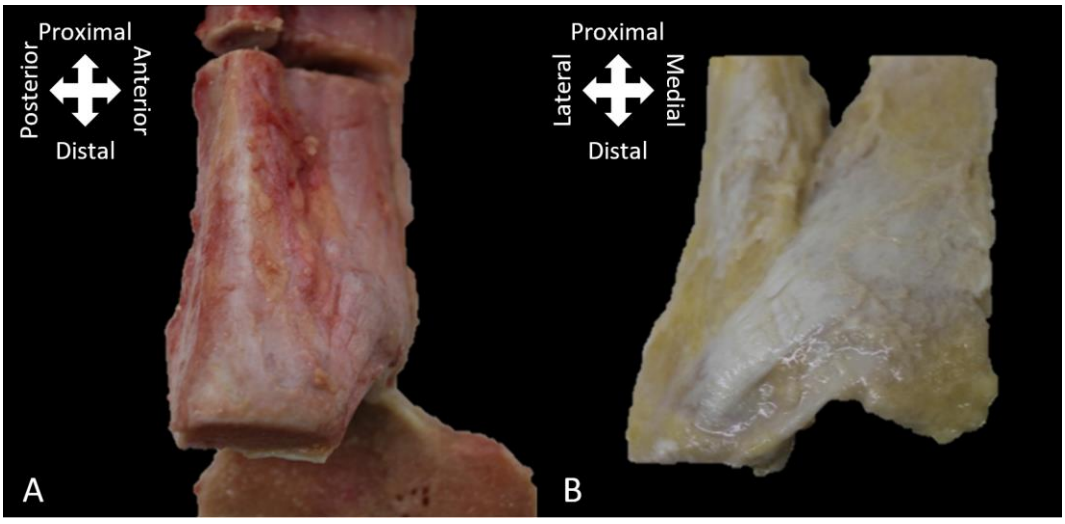

Figure 53. A) Lateral view of the distal tibiofibular syndesmosis dissected from the tibia. B) Anterior view of an isolated AiTFL BLB construct.

Post-dissection ligament lengths were measured using Vernier callipers with the ligaments orientated in line with their collagen fibres and the slack in the ligament was removed by hand. The ligaments were measured once, from the centre of the origin to the centre of the insertion. This measurement technique, was determined to be comparable to laser micrometre systems for similar tissues and is therefore considered acceptable (Woo et al.,

1990). The tissue hydration level of the ankle complex was maintained by wrapping the complex in PBS (Oxoid Ltd, Basingstoke, UK) soaked paper towel (Herbert et al., 2016).

3.2.2.3 Testing Protocol

Each ligament of the LCL complex was tested individually whilst the complex was kept intact. Tissue rehydration was performed to ensure the viscoelastic nature of ligaments could act efficiently during the testing. Immediately before the characterisation of the CFL, the complex was submerged in PBS for 30 minutes. The complex was then submerged for 15 minutes prior to testing the ATFL and a further 15 minutes prior to testing the PTFL due to the short length of time taken for each test.

A bespoke gripping technique was required due to the LCL complex being characterised as an intact complex, rather than as individual BLB constructs. The novel fixation device developed, shown in Figure 54, was a small cubic pot with a removable front cover. Engineering drawings of the design are provided in Appendix A – Lateral Collateral Ligament Complex Pot.

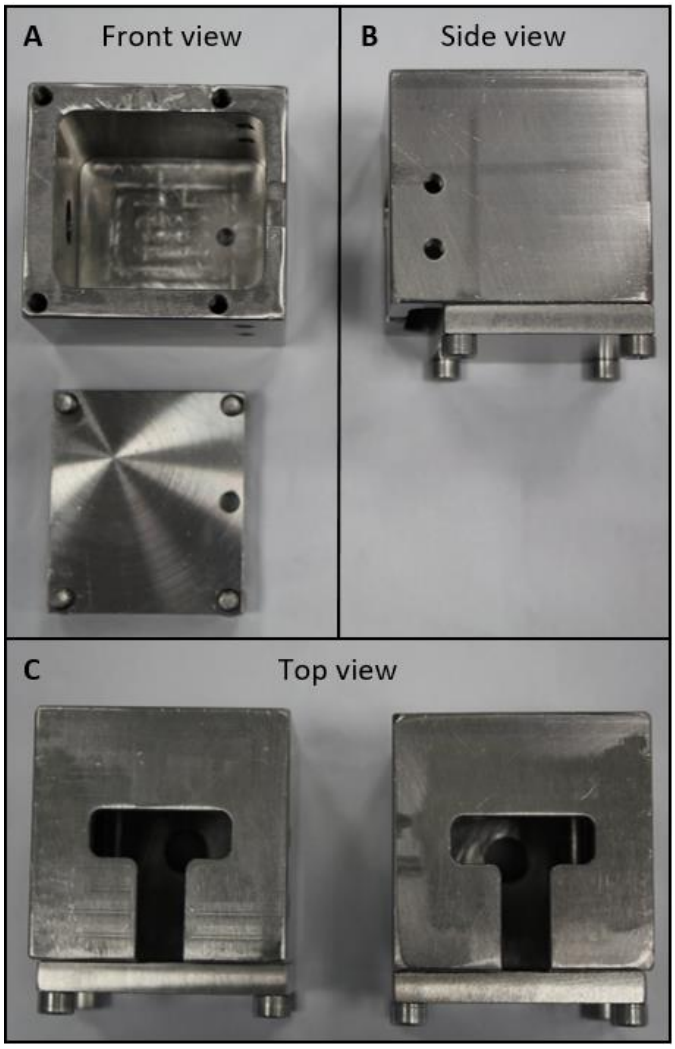

Figure 54. The bespoke fixation device manufactured for the testing of the LCL complex. A) shows the front view of the pot with front cover detached. B) shows a side view of the assembled pot. C) shows the top view of the pot when arranged for testing the T-shaped slots are on opposing faces.

The bone attachments of the ligaments were fixed within the gripping fixture using six gripping bolts for each bone attachment ensuring collagen fibre alignment, as shown in Figure 55. The locating bolts had tapered tips which were partially imbedded into the bone to provide secure fixation. Two locating bolts were inserted from the lateral and medial sides with an additional bolt through the anterior and posterior faces of the fixation device. The cubic pot was designed with a T-shaped slot in the bottom face, between the two pots, to allow the ligament to slide into the pots easily, shown in Figure 54.

The ligaments were too short for the other bone attachments to be located outside of the testing device whilst the first and second ligaments were tested. Therefore, the CFL was characterised first, then the ATFL followed by the PTFL. During testing of the CFL both talar insertions of the ATFL and PTFL were in the same pot as the fibula bone attachment with the calcaneal bone attachment in the other pot to characterise the CFL, shown in Figure 55. The congruency of the talar insertions of the ATFL and PTFL to the fibula also aided in the positioning and fixation of the fibular insertion of the CFL.

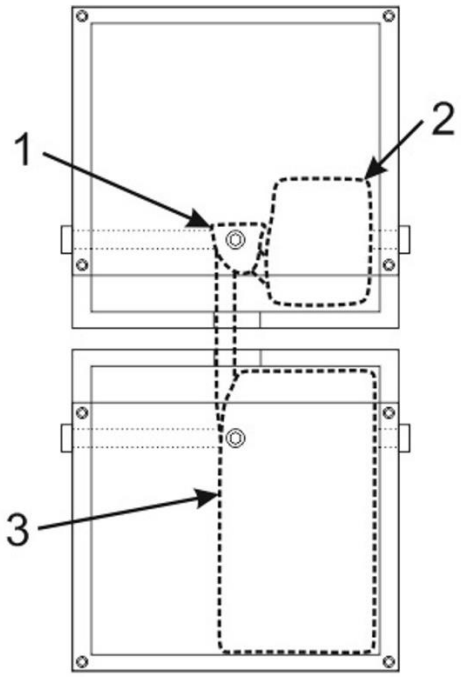

Figure 55. The LCL complex fixed into the bespoke LCL fixation device prior to characterisation of the CFL. The ATFL and PTFL, and their bony attachments from the fibula (1) to the talus (2) are within the top pot and the calcaneus (3) is within the bottom pot.

The mechanical characterisation was performed using an Instron ElectroPuls E10000, with a 1 kN load cell (Instron, Buckinghamshire, UK). A 1 kN load cell was selected as the failure loads previously reported in the literature were considerably lower than 1 kN (Attarian et al., 1985; Siegler et al., 1988). A floating joint was used to attach the top grip to the Instron to correct for any unintended malalignment within the setup.

Preconditioning was completed to ensure specimens were in an appropriate physiological state of readiness and fluid redistribution had occurred within the specimens prior to failure

testing (Quinn and Winkelstein, 2011). Fifteen cycles of preconditioning following a sinusoidal waveform, ranging between 2 N and a load value corresponding to 3.5 % strain, were performed at a frequency of 0.83 Hz. The 3.5 % strain value represents the minimum amount of strain accumulated by any of the LCLs during one step of a normal walking cycle (10 degrees dorsiflexion through to 20 degrees plantar flexion) (Colville et al., 1990). A strain of 3.5 % is also considerably lower than the 20 % strain value quoted as the maximum value for safe physiological loading for ligaments of the LCL complex (Attarian et al., 1985). The preconditioning load values representing 3.5 % strain were determined in a preliminary test of each ligament tested under strain control at a rate of 10 %.s^{-1}. The frequency of 0.83 Hz is equivalent to the rate of normal walking (approximately one full gait cycle per second).

Following preconditioning, the specimens were then ramp loaded to failure at a strain rate of 100 %.s^{-1}. A strain rate of 100 %.s^{-1} was selected to be representative of sprain, having previously been suggested to be a suitable injury strain rate for anterior cruciate ligament injury (Blevins et al., 1994). The following equation, incorporating real-world inputs, also suggests that a strain rate of 100 %.s^{-1} is appropriate to replicate lateral ankle ligament sprain.

$$\dot{\varepsilon} = \frac{\Delta L}{Lt}$$

Where $\dot{\varepsilon}$ is the strain rate, ΔL is the change in length of the ATFL from neutral position to maximum plantar flexion (4.5 mm) (de Asla et al., 2009), L is the length of the ATFL in the neutral position (16.3 mm) (de Asla et al., 2009) and t is the time taken for the sprain motion of an ankle (0.3 s) (Fong et al., 2009b).

3.2.2.4 Data Analysis

The mode of failure was determined via physical palpation and visual examination of the specimens. Any specimens where the ligament had torn away from bone, torn cartilage away from bone or torn a small fragment of bone away from bone were categorised as an avulsion. Any intra-ligamentous failures were defined as mid-substance failures. After the experimental testing, post-processing was completed to calculate the ultimate failure load and stiffness of each ligament from each donor. The linear stiffness value (k1) was calculated using a custom Matlab algorithm (Herbert et al., 2016).

Mean values and 95 % CI for the ligament ultimate failure load, stiffness and length, as well as the donor BMI, weight and age were calculated for the ATFL, CFL and PTFL. A repeated measures ANOVA with a Greenhouse-Geisser correction ($p < 0.01$) was performed to calculate any significant differences in ultimate failure load or stiffness between the ATFL, CFL and PTFL. Analysis of the data stratified by age, weight and BMI was performed to identify any potential correlations with these patient-specific factors and both ultimate failure load and stiffness. Correlations were calculated for the ATFL, CFL and PTFL individually using a two-tailed Pearson correlation test ($p < 0.01$).

3.2.3 Results

The post-dissection ligament lengths used to calculate the ligament specific preconditioning limits are provided in Table 15. The CFL was the longest of the three ligaments forming the LCL complex, with mean ± 95 % CI length of 20.0 ± 1.9 mm. The PTFL and ATFL followed in order but were similar in length with mean lengths of 13.4 ± 3.2 mm and 12.6 ± 0.9 mm, respectively.

Table 15. Ligament lengths (mm) for each individual ligament and the mean ligament length and 95 % CI for ATFL, CFL and PTFL.

Sample	ATFL	CFL	PTFL
1	11.62	17.60	10.50
2	11.76	20.66	14.66
3	12.90	19.24	10.54
4	13.50	23.00	18.34
5	12.08	20.06	14.80
6	13.54	19.66	11.66
Mean ± CI	12.6 ± 0.9	20.0 ± 1.9	13.4 ± 3.2

The mechanical characterisation results for the ATFL, CFL and PTFL are shown in Table 16. The CFL had the highest mean ultimate failure load ± 95 % CI of 367.8 ± 79.8 N followed by the PTFL 351.4 ± 110.8 N, while the ATFL was the weakest 263.6 ± 164.3 N. No significant differences were found for the ultimate failure load (p = 0.24) or stiffness (p = 0.30) between the ATFL, CFL and PTFL.

The ratio of avulsions to mid-substance failures was similar for the ligament types tested, as detailed in Table 16. The ATFL avulsed from the fibula in four of the six tests, the CFL avulsed from the fibula in two of the six tests and the PTFL avulsed from the talus in two of the six tests. No systematic differences in ultimate failure load or stiffness were identified between the different failure modes. When avulsion did occur, the site of avulsion was consistent amongst ligament types, shown in Table 16. Figure 56A and Figure 56B illustrate clear examples of a mid-substance failure and avulsion, respectively.

Table 16. The mean and 95 % CI for the ultimate failure load and stiffness results of the ATFL, CFL and PTFL. As well as the failure mode (A – avulsion and M – mid-substance) and avulsion location.

	ATFL	CFL	PTFL
Ultimate Failure Load Mean ± CI (N)	263.6 ± 164.3	367.8 ± 79.8	351.4 ± 110.8
Stiffness Mean ± CI ($N.mm^{-1}$)	44.7 ± 16.6	45.8 ± 19.0	59.0 ± 10.7
Failure Mode (A/M)	4/2	2/4	2/4
Avulsion Site	Fibula	Fibula	Talus

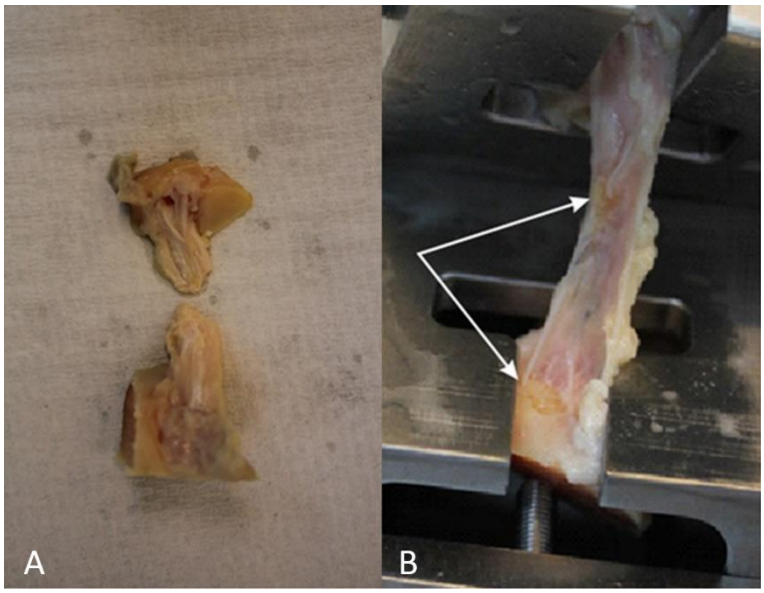

Figure 56. A) A mid-substance failure where intra-ligamentous failure has occurred. B) An avulsion failure where a fragment of bone has also been avulsed from the bone surface (white arrows).

The correlation results for the ultimate failure load and stiffness to the patient-specific factors: BMI, weight and age are presented in Table 17. The ultimate failure load of the CFL was found to have a significant strong positive Pearson correlation with BMI (r = 0.92; p = 0.01). The ultimate failure load of the ATFL and PTFL had non-significant Pearson correlation scores with BMI (r = 0.18; p = 0.73 and r = 0.65; p = 0.16, respectively). No significant relationship was found for either age or weight with relation to both the ultimate failure load and stiffness of

the ATFL, CFL and PTFL. No significant relationship was identified between BMI and stiffness for the ATFL (r = -0.05; p = 0.92), CFL (r = 0.22; p = 0.68) and PTFL (r = -0.01; p = 0.98).

Table 17. The correlation (r-value) and respective significance (p-value) of both ligament ultimate failure load and ligament stiffness against the patient-specific factors (PSF): BMI, weight and age.

Ligament Property		PSF	r-value	p-value
Failure Load	**ATFL**	**BMI**	0.184	0.727
	CFL	**BMI**	0.919*	0.010
	PTFL	**BMI**	0.650	0.162
	ATFL	**Weight**	0.516	0.395
	CFL	**Weight**	0.874	0.023
	PTFL	**Weight**	0.327	0.527
	ATFL	**Age**	0.560	0.248
	CFL	**Age**	-0.273	0.600
	PTFL	**Age**	-0.496	0.317
Stiffness (k1)	**ATFL**	**BMI**	-0.052	0.922
	CFL	**BMI**	0.216	0.681
	PTFL	**BMI**	-0.013	0.981
	ATFL	**Weight**	0.176	0.738
	CFL	**Weight**	0.410	0.419
	PTFL	**Weight**	0.000	0.999
	ATFL	**Age**	0.750	0.086
	CFL	**Age**	-0.397	0.436
	PTFL	**Age**	-0.340	0.510

*indicates result is significant at the 0.01 level (two-tailed).

The ultimate failure load results of the ATFL, CFL and PTFL are plotted against BMI in Figure 57 with the results for all three ligaments of each donor aligned vertically according to the donor's BMI. There is no evidence of a systematic tendency for the ultimate failure load to vary by ligament type either within or between donors.

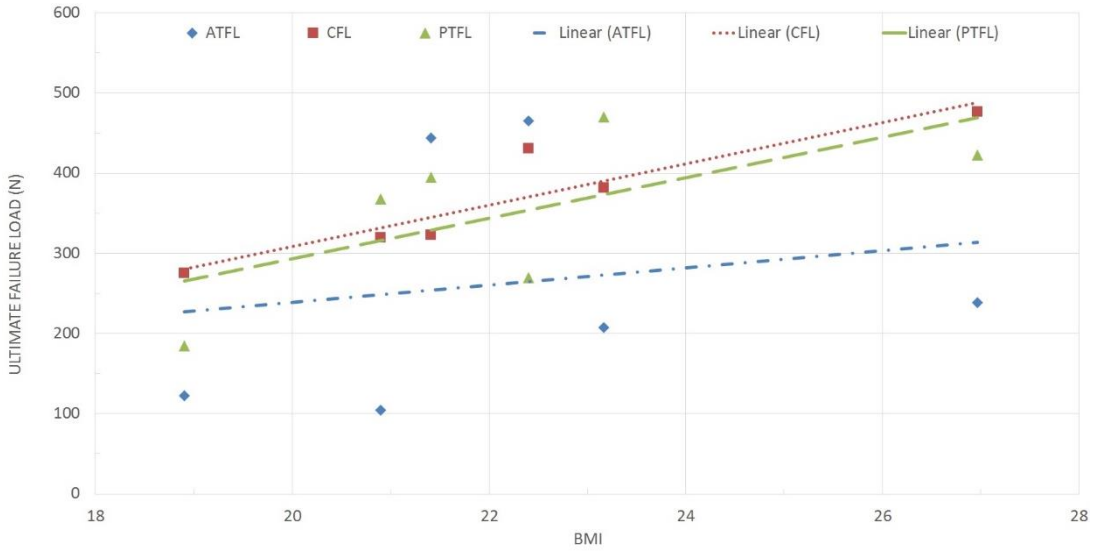

Figure 57. A graphical representation of the relationship between BMI and ultimate failure load. The three ligaments of each donor are vertically aligned according to the BMI of the donor.

3.2.4 Discussion

The aim of this study was to improve understanding of the mechanical properties and failure modes of the LCL complex when strained at a rate representative of LAS. The mechanical characteristics of the entire LCL complex when loaded at a realistic sprain-like strain rate (100 $\%.s^{-1}$) are reported. The mean ultimate failure load results concur with previously published work, that the CFL and PTFL provide similar levels of support under load and that the ATFL is the weakest (Attarian et al., 1985; Siegler et al., 1988). There is however, a large amount variability between specimens, as shown in Figure 57. At the individual donor level there was no clear pattern for which ligament is the strongest or weakest of the LCL complex. This finding can also be shown by the results of St Pierre et al. (1983) for the ATFL, ranging in failure load from 44 N to 556 N, however this was not discussed within the article (St Pierre et al., 1983). Notably, the ATFL, which is widely established as the weakest LCL, was the strongest for two donors in this study, contradicting the general consensus suggested by mean values (Attarian et al., 1985; Siegler et al., 1988). The widely established view that the ATFL is the weakest of the LCLs could therefore be incorrect for some individuals. The cause of this finding is likely multifactorial with possible explanations including unreported prior injuries, BMI and activity level. A much larger sample size and in-depth patient information is required to substantiate any hypothesis.

Stiffness results in this study are similar to those previously reported by Attarian et al. (1985) who strained the LCLs at strain rates considerably higher than 100 $\%.s^{-1}$. This study and the Attarian et al. (1985) paper therefore support the theory that the strain-rate dependency of ligaments can be neglected when tested at strain rates greater than 100 $\%.s^{-1}$ (Funk et al., 2000; Bonner et al., 2015).

Both mid-substance failure and avulsion are abundantly prevalent as failure modes of the LCLs. Categorisation of the failure mode is somewhat subjective due to the fibrous nature of ligamentous failure, the difficulty faced differentiating between failure modes and the lack of a standardised definition of avulsion. The location of ligament avulsion was consistent, at the fibula for the ATFL and CFL and at the talus for the PTFL. Siegler et al. (1988) found the AFTL to avulse 58 % of the time and the CFL and PTFL to avulse in 70 % of tests, with remaining specimen failing mid-substance (Siegler et al., 1988). Attarian et al. (1985) reported eight mid-substance failures and four talar avulsions for the ATFL, eight mid-substance failures, four calcaneal avulsions and four fibula avulsions for the CFL and four mid-substance failures for the PTFL (Attarian et al., 1985). St Pierre et al. (1983) reported 18 talar avulsions, 16 mid-substance failures and two unknown failures for the ATFL (St Pierre et al., 1983).

The location of ATFL avulsion in this study is inconsistent with those previously reported and an explanation as to why is unclear. Possible explanations include the status of the fibula, the orientation of the ligament or the vastly different strain rates. The fibula was intact for testing in the studies by St Pierre et al. (1983) and Attarian et al. (1985) whereas in this study the fibula was split reducing the amount of bone to be gripped. The orientation of the specimen may differ slightly between this study and the two studies highlighted due to the fibula not being intact, although all studies attempted tensile testing with fibre alignment. The orientation of ligaments and alignment of collagen fibres during testing can have a significant effect on the failure properties of ligaments (Von Forell et al., 2014). The similarity in failure load and stiffness results for avulsion and mid-substance failures support previous findings (Noyes et al., 1974).

The prevalence of avulsion and mid-substance failures are however comparable. The high prevalence of avulsions could be due to the significantly higher local strain proximal to the attachment site of ligaments compared to the central region (Stouffer et al., 1985). Alternatively the age of the donors could impact the results as a greater amount of avulsion have been identified in an older population (Noyes and Grood, 1976). The failure mechanism of a ligament is an important consideration prior to a ligament repair being performed as the fixation method may differ depending on whether the ligament needs reattaching to bone or to ligament.

A potentially noteworthy finding was the positive correlation between BMI and ultimate failure load values for the ligaments of the LCL complex, specifically the significant correlation for the CFL. This finding suggests that the CFL of individuals with a higher BMI have a greater load bearing capacity than those with a lower BMI. This is likely due to the adaptive remodelling nature of ligaments as individuals with a greater BMI are likely to apply more stress to the ligament, increasing strength over time (Bonnel et al., 2010). The BMI of an individual could therefore be an important factor when selecting the appropriate material properties of a synthetic intervention, and notably people with a high BMI who are more often candidates for a synthetic ligament replacement (Ajis et al., 2006). Therefore, the load bearing

capacity of the synthetic interventions, and their fixation devices, should at least match the upper boundary of the 95 % CI of ultimate failure load to ensure the synthetic does not subsequently fail. The stiffness of the synthetic material, along with the tension applied upon insertion, is arguably as important. A stiffness that is too high could reduce the joint mobility and too low could affect the stability of the joint. Therefore it could be recommended that the stiffness of the synthetic material is matched to that of the natural tissue results reported here.

The anatomy of ligaments is often depicted incorrectly in illustrations because of stylistic licence. A previously published pictorial essay does however provide detailed images of the ankle ligament anatomy (Golanó et al., 2016). Figure 50 shows the fibular insertions of the ATFL and CFL. These attachments are often illustrated as separate insertion points however, as shown in Figure 50, the two ligaments commonly insert at the same point on the fibula. It is suggested that the inferior aspect of the ATFL and CFL are connected by arciform fibres, thus forming the lateral fibulotalocalcaneal complex (Dalmau-Pastor et al., 2020). This observation was also made when performing the dissections for this study. The results of this study however suggest that the connecting fibres are not of a sufficient strength to cause both the ATFL and CFL to rupture simultaneously. The CFL was tested first in every instance and no macroscopic damage to the ATFL was observed. The mechanical property results of both the ATFL and CFL are also similar to those previously published (Siegler et al., 1988).

The limitations to the study predominantly centre on the use of human cadaveric tissue. The main limitation is the small sample size (n = 6). Research using donor cadaveric tissue should be minimised to only what is essential and performed with maximum efficiency and integrity out of respect for the donors. The characterisation of cadaveric human tissue may not reflect the same response as living tissue. However, ligamentous tissue primarily attributes its strength properties to the collagen fibres which form the majority of ligament structure. The collagen would not be greatly affected by the tissue being alive or dead, providing it remains well hydrated and is stored appropriately to abate tissue degradation. Although the exclusion criteria required donors to have not reported any lower limb trauma, certain that a prior sprain has not occurred at some point during the donor's lifespan cannot be guaranteed. It is estimated that ankle injury rates are approximately five and a half times higher than those registered in emergency departments (Kemler et al., 2015). This could provide some explanation for the inconsistencies in strength between ligament types. Large variations in the results following the mechanical characterisation of ankle ligaments are also reported elsewhere (Siegler et al., 1988).

The use of elderly donor tissue to investigate sprain has previously been suggested to be a limitation of cadaver studies due to deteriorating tissue quality and its impact on mechanical properties (Noyes and Grood, 1976). An effort was therefore made to be provided with the youngest donor specimen's possible (mean 56.2 years). Other previous studies, including ATFL specific literature, have however reported no correlation between mechanical properties and

age (St Pierre et al., 1983; Blevins et al., 1994; Johnson et al., 1994; Flahiff et al., 1995; Couppé et al., 2009). Half of the human tissue specimens used in this study were inherited from a previous researcher who had not used the human tissue. This tissue had been frozen for 23 months prior to its use in the characterisation study which could have significantly reduced the tear resistance of the ligament according to the subsequent findings of another researcher (Quirk et al., 2018). All other human tissue samples had been frozen for no more than four months after their receipt at the university. Among the small sample of n = 3 for longer-term and shorter term freeze, no systematic difference was observed for any of the ligaments of the LCL complex. Finally, the link identified between BMI and ultimate failure load of the CFL and PTFL is based on a narrow range of BMI with only one donor having a BMI outside of the normal range and the trend may not be reflected in a population at the extremities of the BMI scale.

The current findings highlight a range of indicative ultimate failure loading requirements that can further inform the mechanical property specifications for synthetic ankle ligaments. Through improved matching of the mechanical properties, particularly the stiffness, of synthetic ligaments to their natural counterparts joint mobility and stability have the potential to also improve.

3.2.5 Conclusion

Limitations aside, the conditions of this study were carefully defined to reflect those experienced by individuals who would suffer an ankle sprain allowing for the entire LCL complex to be characterised at realistic sprain inducing strain rates. In the current study the ultimate failure load and stiffness of the ATFL, CFL and PTFL did not differ systematically but there was a tendency toward greater strength in people with a higher BMI. The maximum likely exposure loads, the BMI of the patient and the failure mode of the LCLs all appear to be factors to be further considered when selecting the material, repair or reconstruction technique to be used for surgical stabilisation of the sprained ankle.

3.3 Characterisation of the Anterior and Posterior Tibiofibular Ligaments

3.3.1 Introduction

This section describes the various fixation devices explored during this project to characterise the AiTFL and PiTFL of the distal tibiofibular syndesmosis. The differing anatomy of the AiTFL and PiTFL to the ligaments of the LCL complex prevented the technique described in the previous section from being used. Characterisation of the syndesmosis ligaments has previously been performed but not at strain rates representative of ankle sprain. Characterisation of the AiTFL and PiTFL under such conditions can provide insight to the requirements of synthetic interventions, such as those developed by the industrial sponsors of this project, for syndesmosis sprain applications.

A survey of the literature identified previous studies to have characterised the AiTFL and PiTFL (Funk et al., 2000; Beumer et al., 2003; Butler and Walsh, 2004). Butler and Walsh (2004) did not test intact BLB constructs, instead they dissected and tested a 5 mm gauge length of mid-substance (Butler and Walsh, 2004). The study only calculated mechanical properties at strains of 10 % and 30 % opposed to testing to complete failure. Funk et al. (2000) were able to successfully characterise to failure BLB constructs. They were however only successful for one out of six AiTFL samples and zero out of six PiTFL samples, demonstrating the difficulty faced characterising these ligaments (Funk et al., 2000). The article attributed the failed tests to the cutting and drilling of bone attachments leading to failure at the potting.

Beumer et al. (2003) provide the most complete failure characterisation results for the AiTFL and PiTFL (Beumer et al., 2003). Unlike the two studies highlighted above the research focussed on the AiTFL and PiTFL specifically and were able to successfully characterise 10 samples for each ligament. The results of the study are shown in Table 18 and report the AiTFL to fail on average at 499 ± 105 N and the PiTFL at 708 ± 91 N (Beumer et al., 2003). The study also reports the mode of failure as 30 % avulsion and 70 % mid-substance for the AiTFL and 50 % avulsion and 50 % mid-substance for the PiTFL (Beumer et al., 2003). Their method involved splitting the tibia into an anterior and posterior segment using a frontal cut with the fibula remaining intact. Each bone piece was then potted using an epoxy resin which would have covered the fibular insertions of the ATFL, CFL and PTFL. Their method was therefore unfortunately irreproducible for this project as the successful characterisation of the LCL complex would have been compromised. An appropriate gripping technique was therefore required for the testing of the AiTFL and PiTFL after sectioning of the fibula for the LCL complex.

Table 18. The structural properties and failure modes of the anteroinferior tibiofibular and posteroinferior tibiofibular ligaments. Source: (Beumer et al., 2003).

		AiTFL	PiTFL
Sample size		10	10
Mean age (years)		72 ± 8	72 ± 8
Strain rate used ($mm.s^{-1}$)		0.5	0.5
Ultimate load (N)		499 ± 105	708 ± 91
Stiffness ($N.mm^{-1}$)		78 ± 12	101 ± 16
Failure type	**Mid-substance**	70 %	50 %
	Avulsion	30 % (F)	50 % (F)

The aim of this study was to develop an effective gripping technique for the mechanical characterisation of the AiTFL and PiTFL individually at strain rates representative of severe LAS causing complete rupture of the ligament.

3.3.2 Materials and Methods

3.3.2.1 Specimens

Porcine tissue was used for the evaluation of gripping techniques for the AiTFL and PiTFL as the anatomy of porcine distal tibiofibular syndesmosis is similar to that of human tissue, shown in Figure 58. The use of porcine tissue for this exploratory testing prevented wastage of valuable human tissue. Fresh right hind legs of six month old pigs, sourced from John Penny & Sons (Leeds, UK), were used in this study. To prevent wastage of porcine tissue, no specimens were ordered specifically for this testing. Instead, ankles were harvested from porcine specimens ordered for hip projects within iMBE where the ankle is normally disposed of.

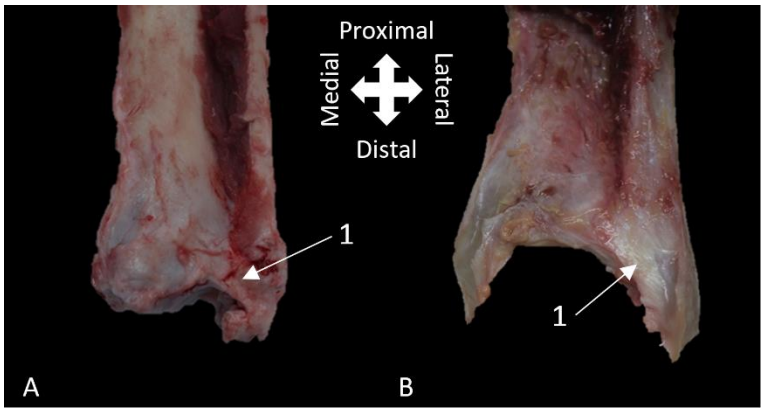

Figure 58. Posterior view of the distal tibiofibular syndesmosis showing the PiTFL (1) in A) porcine and B) human tissue.

3.3.2.2 Sample Preparation

The fresh samples arrived from the abattoir as intact right hind legs and the ankles joint was separated from the remainder of the leg. An incision was made with a scalpel through the skin and musculature, around the circumference of the leg, approximately midway between the knee and ankle joints, shown in Figure 59. An oscillating bone saw was then used to perform a transverse cut through the tibia and fibula at the same point as the incision, shown in Figure 59.

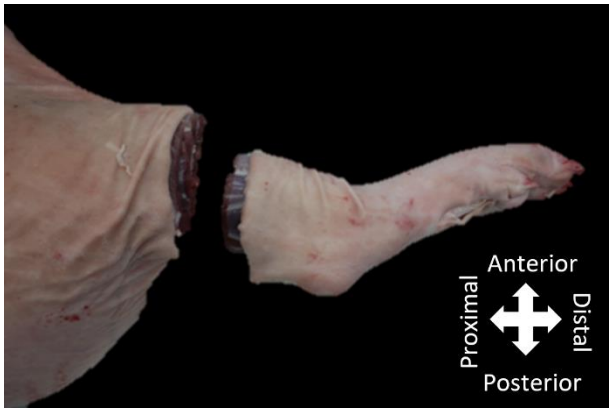

Figure 59. Lateral view of a porcine right hind leg with the ankle joint complex removed approximately midway between the knee and ankle joints.

A second incision was made on the anterior side of the specimen from the most proximal point of the tibia distally to the ankle joint complex. A mediolateral incision was then performed at the most distal point of the second incision and all skin proximal to the third incision was removed. All musculature around the tibia and fibula was removed by severing the Achilles tendon at its calcaneal insertion and the tendons of the tibialis anterior, peroneus tertius, peroneus longus and anterior digital extensor muscles at the point they pass the cruciate ligament, shown in Figure 60. The lateral and medial ligaments of the ankle in addition to the joint capsule were then severed isolating the distal tibiofibular syndesmosis, shown in Figure 58A.

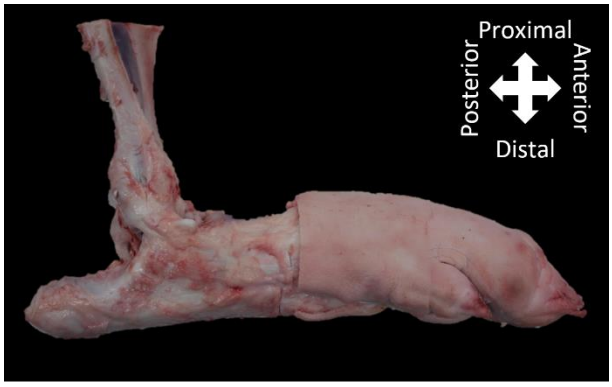

Figure 60. Lateral view of the porcine ankle complex after removal of skin, musculature and associated tendons.

To produce samples replicable of human AiTFL and PiTFL BLB constructs the samples were sectioned further. A midsagittal cut was made through the tibia using an oscillating saw, shown in Figure 61A. A frontal cut followed, made centrally through the fibula and tibia, to isolate the AiTFL and PiTFL, shown in Figure 61B. The distal tip of the fibula was not removed, as with human tissue, as it is much smaller in the immature porcine ankle than in mature human tissue and was deemed unnecessary, shown in Figure 58. Bone-ligament-bone constructs for the AiTFL and PiTFL were produced, shown in Figure 61C and Figure 61D, respectively.

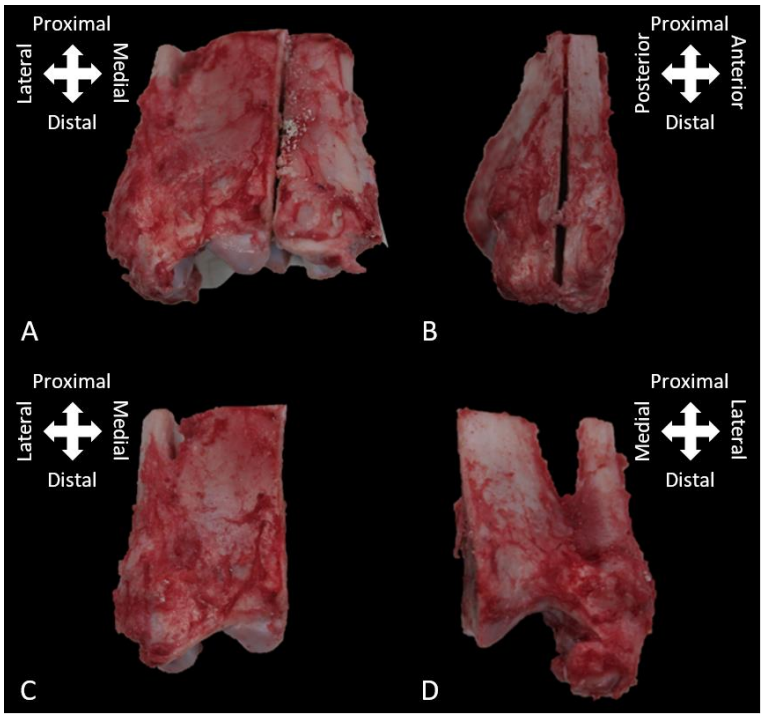

Figure 61. The dissection protocol followed to isolate the AiTFL and PiTFL. A) Anterior view of the midsagittal cut performed through the tibia. B) Lateral view of the frontal cut made through the fibula and tibia. C) Anterior view of an AiTFL sample. D) Posterior view of a PiTFL sample.

3.3.2.3 Testing Protocol

The gripping techniques for the AiTFL and PiTFL were mechanically investigated using an Instron ElectroPuls E10000 equipped with a 5 kN load cell (Instron, Buckinghamshire, UK). The testing protocol was similar to that of the human LCL complex previously described. First, 15 cycles of preconditioning following a sinusoidal waveform, ranging between 2 N and a load value corresponding to 3.5 % strain, were performed at a frequency of 0.83 Hz. The samples were then ramp loaded to failure at a strain rate of 100 %.s^{-1}.

3.3.3 Results and Discussion

Novel custom gripping techniques were developed for the AiTFL and PiTFL of the distal tibiofibular syndesmosis. The lack of tibial and fibular bone available, particularly distally to the fibular insertion for both the AiTFL and PiTFL, is shown in Figure 53. This posed a considerable

challenge in terms of gripping the syndesmosis ligaments sufficiently. Several approaches were made in an attempt to characterise the AiTFL and PiTFL which are described hereinafter.

3.3.3.1 Lateral Collateral Ligament Complex Pot

Initially, an attempt was made to use the same fixation device used for the characterisation of the LCL complex. Due to the shorter ligament length and the lack of a gap between the tibia and fibula at the distal tibiofibular syndesmosis joint, a portion of bone needed to be removed. Using a small handheld hacksaw, a 12 mm wide portion of bone was removed from the medial side of the fibula and tibia perpendicular to the orientation of the collagen fibres of the ligament, shown in Figure 62.

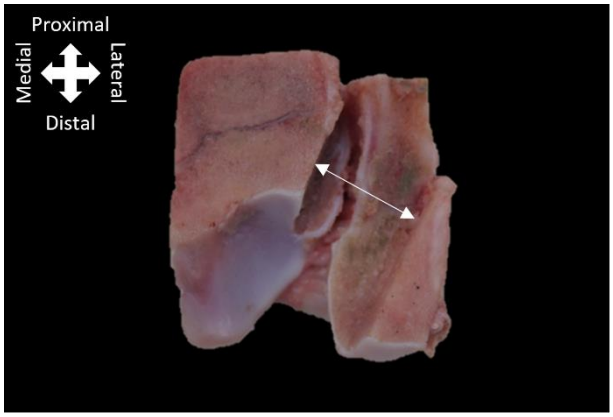

Figure 62. Posterior view of porcine AiTFL sample prepared for testing in the LCL complex testing pot with a 12 mm wide section of bone removed (white arrows).

The width of the bone portion removed was slightly larger than the combined 10 mm thickness of the two walls of the pots. This was purposeful to prevent the pots from touching at the initiation of the test and to afford the balancing of the load cell. The depth of the bone portion was sufficiently deep to allow for the remaining bone and the ligament to slide within the 10 mm gap in the pot, shown in Figure 63. The AiTFL or PiTFL was positioned in the pots and secured with four bolts in each pot, two into each of the lateral and medial sides of the bone piece, shown in Figure 63.

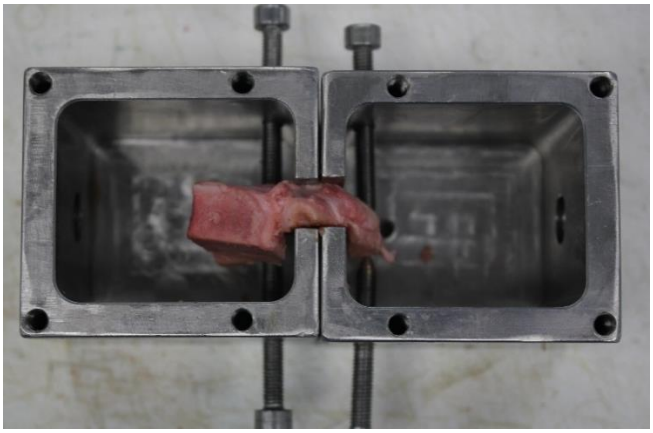

Figure 63. Distal view of a porcine PiTFL sample loaded within the LCL complex pot prior to testing.

Some success occurred with this gripping technique with one AiTFL sample failing through a tibial avulsion, shown in Figure 64A. Other attempts were however unsuccessful with failure often occurring due to fibular bone fracture where the bone interfaced with the pot, shown in Figure 64B. The removal of bone tissue caused a weak point in the fibula where abnormal loading was applied. This type of failure suggested that the locating bolts were ineffective at securing the smaller bone pieces of the AiTFL and PiTFL than those of the LCL complex. Although fibular fracture can occur with distal tibiofibular syndesmosis sprains, this type of failure was determined to be unsuccessful as the fracture was not representative of those associated with natural syndesmosis sprain. Failure loads reached up to 580 N for this gripping technique before failing in a non-representative manner.

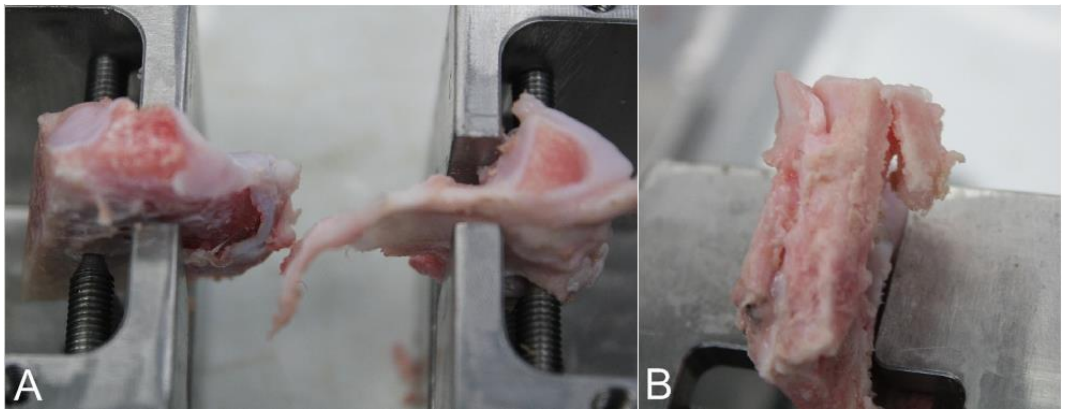

Figure 64. Failed porcine AiTFL specimens that have failed through A) an avulsion and B) a tibial fracture at the interface with the pot.

3.3.3.2 Distal Tibiofibular Syndesmosis Cement Pot

The next approach to characterise the AiTFL and PiTFL involved a fixation device designed specifically for the AiTFL and PiTFL, shown in Figure 65 and – Syndesmosis Pot. This fixation device aimed to capitalise on the larger amount of tibial and fibular bone proximal to the ligaments whilst also ensuring fibre alignment for the ligament during testing.

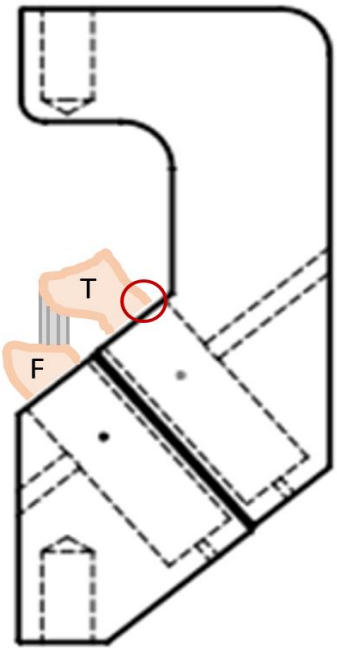

Figure 65. A bespoke fixation device for the testing of the AiTFL and PiTFL. F = Fibula, T = Tibia and the red ring highlights the weak point during testing.

Prior to cementing the proximal bone into small cylindrical cement pots, shown in Figure 66A, the tibial bone insertion of the ligaments needed to be thinned to no more than 10 mm in width and thickness. The bone was secured within the cement pots using one locating bolt into each of the pots from the medial side into the tibia and lateral side into the fibula. The cemented BLB constructs, shown in Figure 66B, could then be inserted into the fixation device and secured by the two bolts through the pots and into the bone cement.

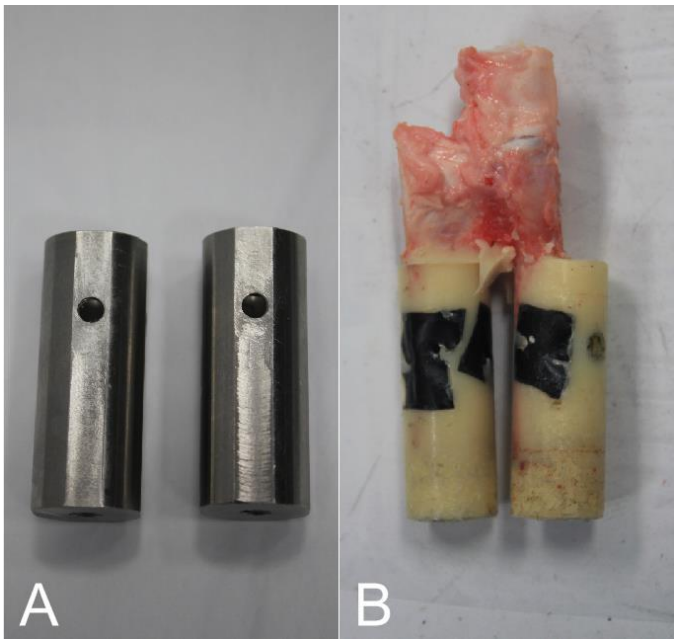

Figure 66. A) Cement pots for the distal tibiofibular cement pot. B) Anterior view of a cemented porcine AiTFL sample prior to loading into the distal tibiofibular syndesmosis pot.

Both porcine AiTFL and PiTFL samples were tested and both ligaments failed through fracture of the fibula at the cement border. Failure occurred at lower loads than the prior gripping

technique at loads of 140 N and 200 N for the AiTFL and PiTFL, respectively. The positioning of the AiTFL and PiTFL was such that the ligament fibres were perfectly aligned with the axis of loading. This however meant that the application of load onto the fibular bone attachment from the top grip was slightly off centre. Subsequently a moment arm force was generated as the two bones were separated. This caused abnormal stresses to occur at the surface of the interface between the fibula and bone cement, shown in Figure 65. The increased flexibility of immature porcine bone aided the generation of a moment arm force and decreased the likelihood of ligament failure. This gripping technology failed to apply load in a manner representative of distal tibiofibular syndesmosis sprain and was therefore determined to be insufficient for AiTFL and PiTFL characterisation.

3.3.3.3 Patellar Tendon Cement Pot

At this point expert external counsel was sought from Dr James Funk, a laboratory and research specialist at the Centre for Applied Biomechanics in Charlottesville, USA. Dr Funk had previously published characterisation results for the AiTFL and PiTFL (Funk et al., 2000). Although their research had low success rates for the characterisation of the AiTFL and PiTFL their research article hinted towards why failures occurred and gave advice for future testing (Funk et al., 2000). This research study epitomises the difficulties faced when characterising the structures of the distal tibiofibular syndesmosis. Dr Funk kindly offered advice and the full methodology implemented during their prior research. Their approach involved cementing the specimens and drilling small holes into the bone to afford improved integration of the potting material within bone.

Further external expert advice was sought from Dr James Rudert from The University of Iowa, USA. Dr Rudert has over 40 years of experience in the mechanical characterisation of musculoskeletal tissues. Dr Rudert was also kind enough to disseminate their wealth of knowledge and described their methods for testing similar musculoskeletal structures. Dr Rudert's suggestion was to screw six to ten very small screws into each bone piece aligned with the orientation of the ligament fibres. The screw heads were then to be cemented using a PMMA cement mixture. It was advised that the PMMA be mixed with a higher fluid content than standard.

Given the similarity of the methods in terms of cementing, and the low success rate of the former method, the method proposed by Dr Rudert was chosen to be pursued. In addition to the previously described dissection protocol a further transverse cut was made no more than 30 mm proximal to the distal tip of the fibula, shown in Figure 67. This produced a smaller bone piece but one which could be cemented into an existing cement pot previously used in the porcine patellar tendon study in Chapter 2. The cementing method was identical to that described in Chapter 2. The cement was however mixed at a 9:5 ratio of solid to fluid components of the PMMA bone cement rather than the 2:1 ratio previously used, following the advice from Dr Rudert.

Figure 67. Porcine AiTFL sample prepared for testing following recommendations by Dr Rudert with three small (20 x 4 mm) screws into each bone piece.

Originally two 25 x 4 mm screws were inserted into each bone piece parallel with the ligament fibre orientation. This method produced the highest failure loads of all methods explored so far for the syndesmosis with the AiTFL failing at 646 N. The failure mode however was still not representable of natural damage as fibula fracture occurred at the interface with the screws into the bone, shown in Figure 68A.

Various combination of smaller (8 x 2 mm) screws were then attempted with up to nine screws into the tibial bone piece and up to eight screws into the fibula bone piece, detailed in Table 19.

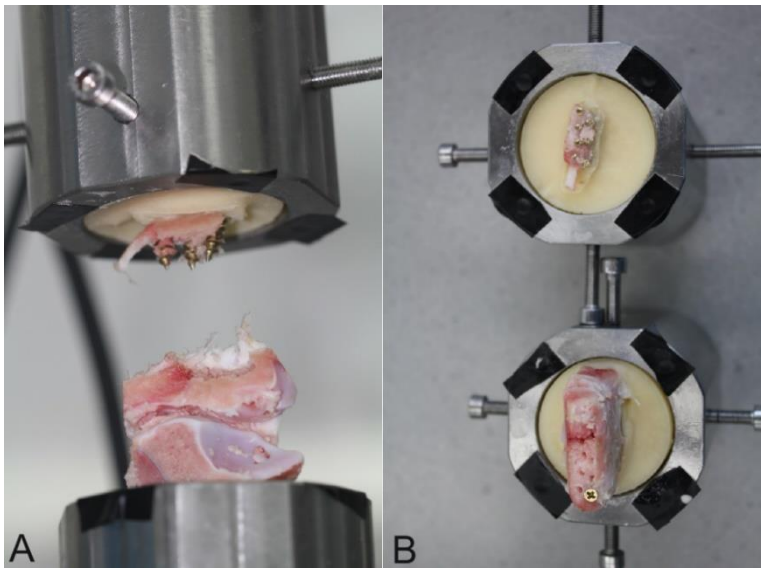

Figure 68. A failed porcine AiTFL specimen prepared with three small (20 x 4 mm) screws into each bone piece (left). A failed porcine AiTFL specimen prepared with eight small (8 x 2 mm) screws into each bone piece (right). Failure has occurred at the bone-screw interface within the fibula for both specimens.

Table 19. Testing iterations, failure load and failure mode for samples tested.

Sample	Ligament	Tibial Screws	Fibular Screws	Failure Load	Failure Mode
1	AiTFL	3x (4 x 25 mm)	3x (4 x 25 mm)	630 N	Fibular fracture at screw interface
	PiTFL	2x (4 x 25 mm)	2x (4 x 25 mm)	284 N	Tibial avulsion
2	AiTFL	2x (4 x 25 mm)	2x (4 x 25 mm)	646 N	Fibular fracture at screw interface
	PiTFL	2x (4 x 25 mm)	2x (4 x 25 mm)	461 N	Tibial fracture
3	AiTFL	6x (2 x 8 mm)	6x (2 x 8 mm)	269 N	Screw pulled out of the fibula or cement
	PiTFL	6x (2 x 8 mm)	6x (2 x 8 mm)	570 N	Screws pulled out of fibula
4	AiTFL	8x (2 x 8 mm)	8x (2 x 8 mm)	781 N	Fibular fracture
	PiTFL	8x (2 x 8 mm)	8x (2 x 8 mm)	739 N	Tibial avulsion
5	AiTFL	8x (2 x 8 mm)	8x (2 x 8 mm)	428 N	Fibular fracture at screw interface
	PiTFL	8x (2 x 8 mm)	8x (2 x 8 mm)	282 N	Tibial fracture at growth plate
6	AiTFL	8x (2 x 8 mm)	8x (2 x 8 mm)	552 N	Tibial fracture at growth plate
	PiTFL	8x (2 x 8 mm)	8x (2 x 8 mm)	507 N	Fibular fracture at screw interface
7	AiTFL	9x (2 x 8 mm)	8x (2 x 8 mm)	645 N	Tibial fracture at screw interface
	PiTFL	9x (2 x 8 mm)	8x (2 x 8 mm)	430 N	Tibial fracture

The highest failure loads occurred when eight 8 x 2 mm screws were inserted into both the fibula and tibia. The maximum load achieved for the AiTFL was 781 N where failure occurred

through a fibular fracture, shown in Figure 68B. Some success was achieved in the characterisation of the PiTFL with a maximum load of 739 N inducing a tibial avulsion.

This method was by far the most promising achieving failure loads close to, and at times exceeding, those of previously published studies on human AiTFLs and PiTFLs (Funk et al., 2000; Beumer et al., 2003). This method was therefore trialled with human AiTFL and PiTFL samples from the same donor. A replica of the pot previously used was required for use with human tissue manufactured from 316 stainless steel, shown in Appendix C – Human Cement Pot. This trial was however made with some reservations as the loads achieved during the porcine testing were somewhat inconsistent, ranging from 270 N to 781 N. The failure mode of specimens tested was also inconsistent with bone fracture occurring at the bone-screw interface in either the fibula or the tibia, shown in Figure 68.

During the human trial of this methodology, failure occurred due to the screws pulling out of the bone at considerably lower loads of 100 N and 97 N for the AiTFL and PiTFL, respectively. Upon visual inspection, the density of the mature human bone appeared to be much lower than that of the immature porcine bone previously trialled, supporting previously published findings (Aerssens et al., 1998; Reinwald and Burr, 2008). The deteriorated trabecular bone quality of the mature human donor tissue determined this method to be insufficient for the characterisation of human AiTFL and PiTFL.

3.3.4 Conclusion

A suitable gripping technique for human AiTFL and PiTFL samples, after the sectioning of the distal tip of the fibula for LCL complex characterisation, is still yet to be determined. The most promising technique of those investigated in this study was the final technique explained. The technique involved the insertion of several small 8 x 2 mm screws into the tibia and fibula parallel with the collagen fibre alignment of the ligaments which were then cemented. This technique produced failure loads up to 781 N in immature porcine tissue exceeding the failure loads of human AiTFL and PiTFL samples reported in the literature. Repeatable characterisation of the intact AiTFL and PiTFL is most likely achievable when testing the AiTFL and PiTFL individually with the cortical shell of the fibula and tibia bones intact. A study using such an approach would benefit from a paired specimen study with contralateral limbs of healthy individuals being used for each ligament to reduce the variability between groups.

Chapter 4 – Development of a Lateral Ankle Sprain Simulation

4.1 Introduction

This chapter describes the design and development of a device capable of simulating LAS in cadaveric tissue. Cadaveric tissue was used in this study given the destructive nature of the testing and the lack of an adequate animal model for ankle complex biomechanics. The use of an artificial model was explored however artificial models were either inadequate or were cost inefficient and untested. Ankle sprain simulation was desired to further investigate the biomechanics of ankle sprain, assess stability changes pre-/post-sprain and to better understand the failure mode of ankle ligaments due to sprain. The novel sprain simulation device was intended to be able to replicate various ankle sprain types including lateral and distal tibiofibular syndesmosis sprain for both left and right feet.

This chapter does not follow the traditional layout of an academic research paper. Rather the topic is introduced and general methods explained prior to a narrative progression of the research performed, results and some discussion within sections 'Sprain Platform Validation' and 'Cadaver Testing', before an overall discussion and final conclusions.

4.1.1 Natural Ankle Sprain Biomechanics

A detailed description of the literature available on the biomechanics of LAS is reported in Chapter 1 Biomechanics of Lateral Ankle Sprain. Two studies captured the biomechanics of LAS during a cutting motion and provided the full ROM values. During a cutting trial where a participant suffered a mild ATFL sprain, the maximum ROM in plantar flexion, inversion and internal rotation was 1 degree, 48 degrees and 10 degrees, respectively (Fong et al., 2009b). Whereas the other study reported a ROM of 50 degrees plantar flexion, 45 degrees inversion and 24 degrees internal rotation to induce a mild LAS injury (Gehring et al., 2013). Even though the two participants were performing similar cutting patterns and the injury diagnosed was similar, if not the same, the biomechanics captured to cause the injury were considerably different. Therefore, potentially suggesting that there may not be specific values for the causation of LAS. More likely there are a multitude of possible combinations of plantar flexion, inversion and internal rotation which can induce LAS. To the knowledge of the author, no studies exist detailing the biomechanics of severe ankle sprain. The minimal and varied data on the biomechanics of natural ankle sprain highlights the significant challenge in the simulation of LAS injury.

4.1.2 Lateral Ankle Sprain Simulation

Experimental simulation provides an alternative approach for the exploration of the biomechanics of LAS. The literature on this subject is described in Chapter 1 Simulation of Lateral Ankle Sprain. Devices which mimic the ROM associated with LAS to a safe non-injury

limits in vivo in live subjects, exist in the form of fulcrum soles and collapsing/tilting platforms (Ha et al., 2015). These devices offer valuable research opportunities into the proprioceptive response and muscle activation in patients during sprain initiation. Although in their current application these devices are limited to safe ROM limits, similar devices could be developed with larger ROM to induce ankle sprain. The potential of these designs for a LAS simulation device is greatest in collapsing platform, shown in Figure 26.

Alternatively, a tilting platform aiming to simulate LAS with cadaveric tissue has previously been developed, shown in Figure 69 (Konradsen and Voigt, 2002). The platform could be pre-set at angles of 0 to 40 degrees for dorsi-/plantar flexion, 0 to 40 degrees inversion/eversion and 0 to 30 degrees internal/external rotation. The platform allowed for the analysis of ligament elongation during the application of a 500 N vertical load using a materials testing device. This approach was deemed unsuitable for this study as the specimens were attached to the platform which was pre-set at the required angles. This prevents the full biomechanics of LAS motion from being investigated. To the author's knowledge, no device exists capable of simulating the biomechanics of LAS through to severe injury of the LCL complex.

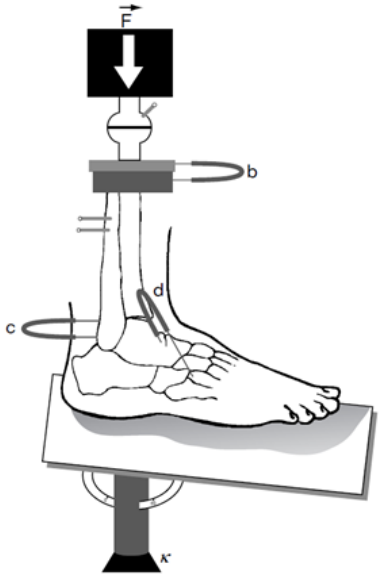

Figure 69. A loading platform designed for the investigation of ankle motions and ligament elongation (Konradsen and Voigt, 2002).

Other devices exist which, although not intended to replicate LAS, do investigate ankle motion through the full ROM. A double-cradle platform, shown in Figure 70, was developed to analyse joint stability (Fujii et al., 2010). The platform is capable of six degrees-of-freedom (DOF) motion affording dorsi-/plantar flexion, inversion/eversion and internal/external rotation as well as anterior-posterior, medial-lateral and proximal-distal translation. The ROM of the platform was not published by the authors however a device similar to this could be produced to be capable of generating the required angles for LAS. Inspiration into device design was also sought from other natural ankle simulations unrelated to sprain briefly discussed in the Simulation of Lateral Ankle Sprain section of Chapter 1.

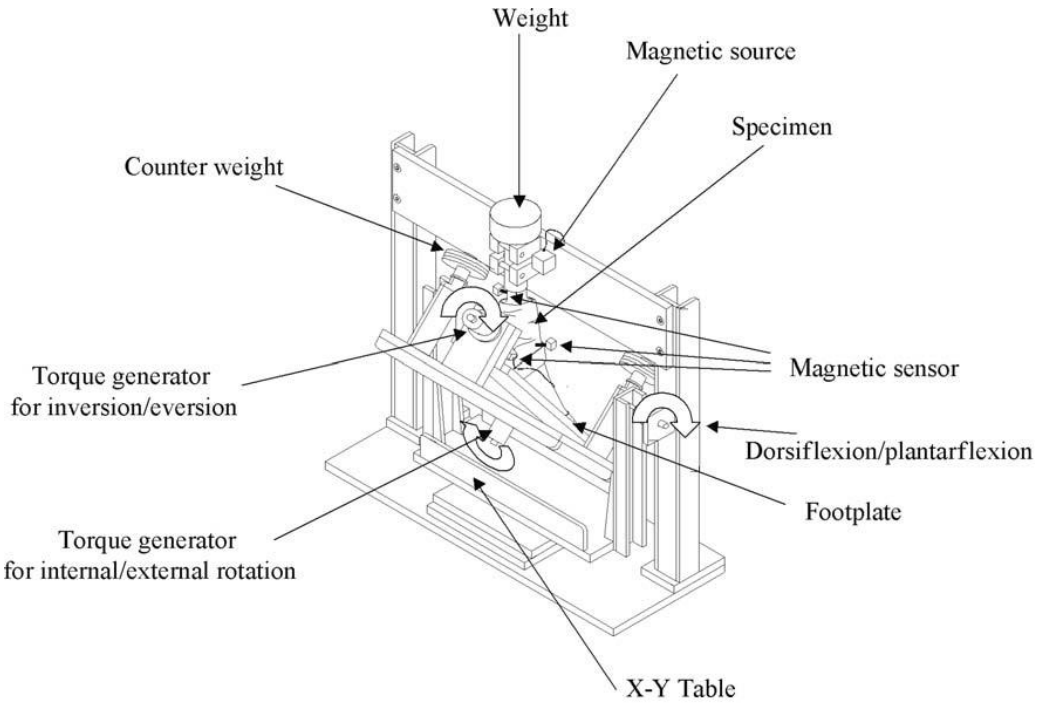

Figure 70. A double-cradle device used for the analysis of joint stability capable of six degrees of freedom motion (Fujii et al., 2010).

The strength of a simulation is defined by its ability to accurately replicate an event. There are many variables to consider for the accurate simulation of LAS to reproduce in vivo conditions. Variables including the ROM, rotational velocity, load and intactness of structures all influence the validity of a simulation of LAS and each have a differing level of significance. The importance of each variable can be argued and is influenced by the aims of the simulation. For this study the most important aspect of a simulation of lateral ankle sprain was the ROM achieved by the ankle joint complex. The previous chapters have emphasised the importance of strain rate for the mechanical performance of the LCL complex and therefore the rotational velocity is also of great importance. Load is an important aspect for the simulation of LAS but is also linked to the ROM as without sufficient load the ankle joint complex will not achieve the desired ROM to induce injury. Of least importance to this study was the intactness of the structures around the ankle joint complex as the focus of this study was on the LCL complex and not the other tissues which may play a role during LAS. This does not however mean that other structures play no role during LAS.

4.1.3 Aim

The aim of this study was to develop a simulation of severe LAS through the design and manufacture a device capable of successfully replicating severe LAS in human cadaveric samples, where a complete rupture of the ATFL and/or CFL occurs.

4.2 Method Development

The extreme novelty of this work, particularly within iMBE at the University of Leeds, meant extensive preparation and development of methods was required for this study. The development of a platform capable of replicating the ROM associated with LAS, a suitable loading device and motion analysis method were all required. These factors and their impacts on one another were simultaneously considered throughout the entire method development procedure.

4.2.1 Device Specification

An ideal device specification was first established, based on the limited published data and protocols associated to the iMBE laboratories.

4.2.1.1 Range of Motion

The literature reporting biomechanics of LAS is highly varied between studies and the severity of injury is vaguely reported, shown in Table 3. It is generally agreed that a combination of plantar flexion, inversion and internal rotation typically occurs during LAS, shown in Figure 71.

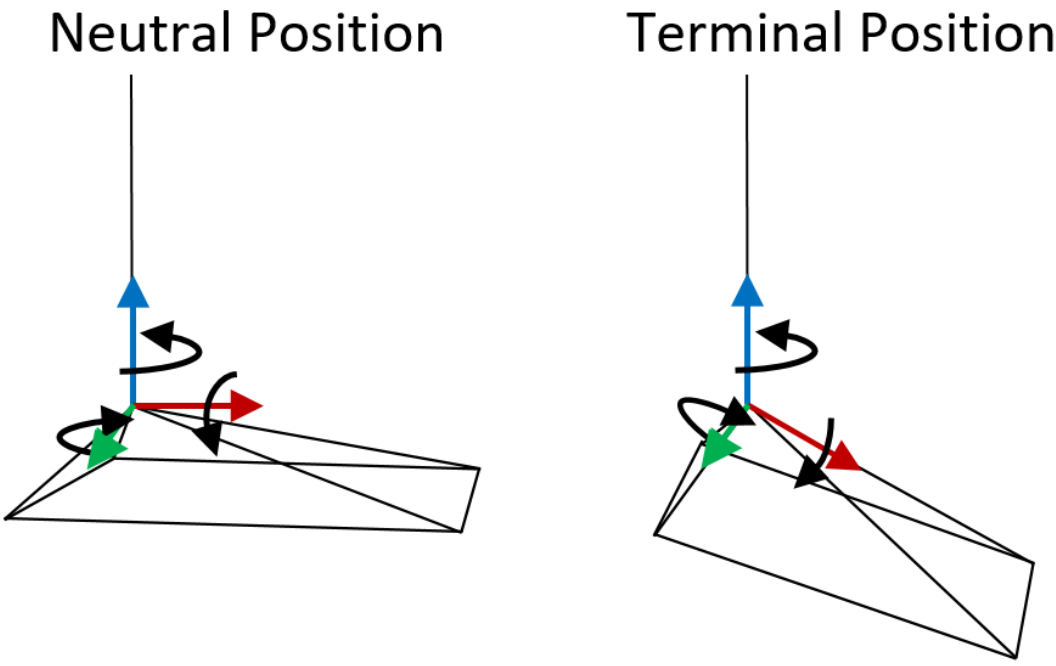

Figure 71. A free body diagram representing the motions associated with LAS. The neutral position is the natural position of the foot relative to the shank of the leg when standing. The terminal position is the position of the foot during a LAS event. The Red arrow = x-axis (anterior/posterior), green arrow = y-axis (medial/lateral) and blue arrow = z-axis (vertical axis).

To the author's knowledge, at the point of developing this specification, no research article reporting the biomechanics of a severe LAS existed. The results of Panagiotakis et al. 2017 had not yet been published and did not come to the author's attention for some time after

publication. The range of values reported for plantar flexion, inversion and internal rotation ROM are shown in Figure 72.

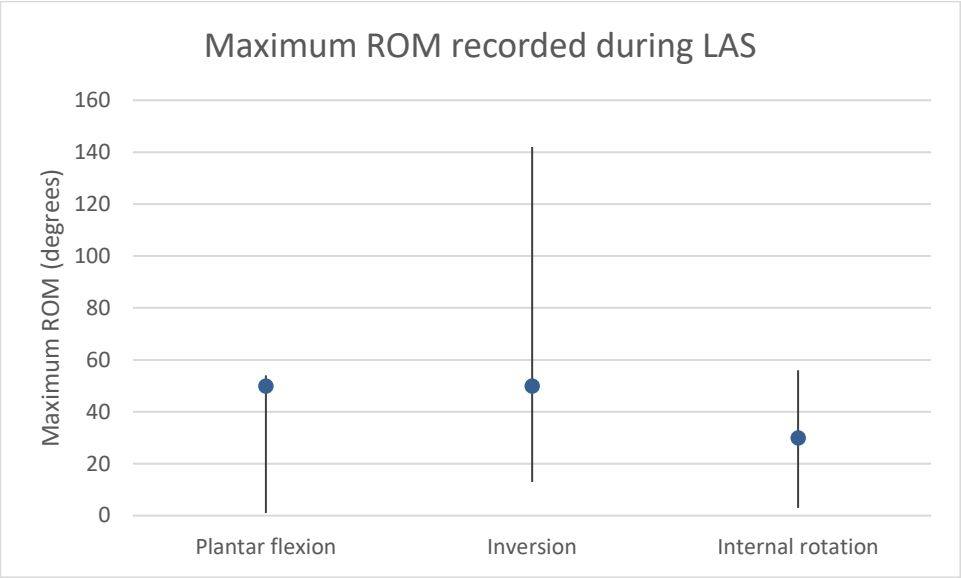

Figure 72. The range in values reported for the maximum ROM achieved during LAS. The blue markers indicate the minimum values chosen for maximum ROM of the simulation device within the device specification.

Those who did specify the severity of injury reported mild LAS injuries, caused by a ROM of up to 50 degrees of plantar flexion, 48 degrees inversion and 24 degrees internal rotation (Fong et al., 2009b; Gehring et al., 2013). It was therefore determined that the ROM achievable by the sprain platform must be at least 50 degrees plantar flexion, 50 degrees inversion and 30 degrees internal rotation, shown in Figure 72. The ROM required must also be able to be performed for both left and right feet specimens.

4.2.1.2 Loading

To the knowledge of the author, the load applied to the ankle complex during LAS is unknown and likely varies considerably given the individual, type of sprain, severity of sprain and the activity being performed during sprain initiation. The load required to initiate LAS in this study was therefore required to be estimated. First, the biomechanics of LAS literature was reviewed, shown in Table 3. The plantar flexion, inversion and internal rotation velocities have been analysed for real-life sprain events and the range in results are summarised in Figure 73.

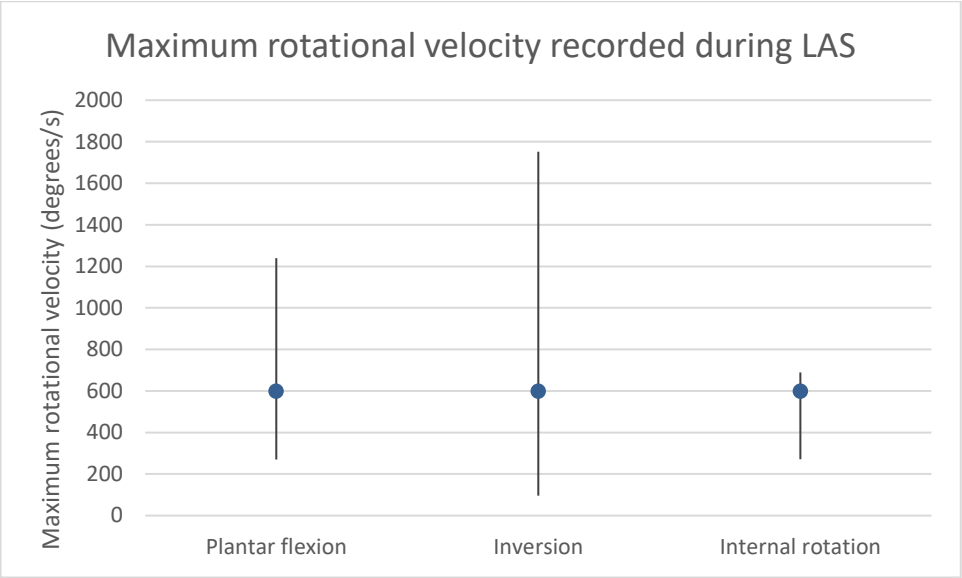

Figure 73. The range in values reported for the maximum rotational velocity achieved during LAS. The blue markers indicate the rotational velocity chosen for all motions performed in this study.

Unfortunately, kinetic data for LAS has not been previously captured, to the author's knowledge. The ground reaction forces of various activities associated to LAS have however been reported. The ground reaction force of walking, jogging, running, landing a jump and cutting range between 1x and 3.5x BW (Rowlands and Stiles, 2012). As a conservative measure, to prevent the wastage of specimens, a load of BW was initially selected for simulation of ankle sprain.

Previous literature, and the results of the two prior studies, indicate the importance of strain rate in the replication of sprain conditions. The rate of loading was therefore considered of particular performance for this study. Ideally, plantar flexion, inversion and internal rotation would each be driven by an independent source affording unique rates of loading for each motion.

4.2.1.3 Motion Capture

In terms of product specification, the main requirement of the motion capture system was a sufficient capture rate to analyse the biomechanics of LAS which occurred at very high rates of rotational velocity. Also required to be considered however was the devices' compatibility with the sprain platform, loading device and human tissue usage as well as the size and portability of the system.

4.2.1.4 Simulation of Sprain Specification

As previously mentioned, the sprain platform, loading device and motion capture system must integrate and be compatible with each other to allow for the full biomechanical analysis of severe LAS motion. The sprain platform must therefore not obstruct the view of the specimen by motion capture cameras and be capable of withstanding the potentially high loads applied

during the testing. Additional considerations were required due to the fact that the specimens were human cadaveric feet. Health and safety protocols within iMBE, to be compliant with the Health and Safety Executive, dictated that the parts contacting human tissue specimens must be disposable or manufactured from a suitable sterilisable material, such as 316 stainless steel. The specifications of the devices used to simulate severe LAS are displayed in Table 20. The success criteria for the simulation of severe LAS would be a complete rupture of the ATFL and/or CFL. Complete rupture could present as an avulsion or mid-substance tear.

Table 20. The overall device specification for the development of a simulation of severe LAS. PF = platar flexion, INV = inversion, IR = internal rotation and deg = degrees.

	Essential	**Desirable**
Range of Motion		
Maximum PF (deg)	50	60
PF velocity (deg.s^{-1})	>370	Up to 1240
Maximum INV (deg)	50	150
INV velocity (deg.s^{-1})	>559	Up to 1752
Maximum IR (deg)	30	60
IR velocity (deg.s^{-1})	>271	Up to 690
Scale of motion limits (deg)	≤5	1
Applicable to left and right footed specimens	✓	
Load		
Load capacity (kg.f)	60	100
Rate of loading	Causes rotational velocity >600 deg.s^{-1}	Causes rotational velocity up to 1752 deg.s^{-1}
Independent loading rates for each motion		✓
Scale of load (kg)	5	0.1
Motion Capture		
Capture rate (Hz)	100	1000
Portable system		✓
Other		
Sterilisable	✓	

4.2.2 Sprain Platform

Given the scarcity of data on the biomechanics of LAS, capable of inducing ligament injury, the development of a sprain platform required an adaptable and agile approach. The design process was initiated with the analysis of previously developed ankle sprain platforms, joint stability and gait motion, described previously in this chapter and in Chapter 1. A collapsing platform or double-cradle design was identified as the most promising concept for a LAS platform. Both approaches had the potential to provide the ROM requirements detailed by the specification and warranted further exploration.

Two potential platform designs were developed whilst on an industrial placement at Instron Ltd (Buckinghamshire, UK). The first design, shown in Figure 74, was a double-cradle fixture driven by hydraulic actuators. This platform could only control motion in the dorsi-/plantar flexion and inversion/eversion directions. The ROM capable in these planes was adaptable in 5 degree increments, using metal pins inserted through the small holes located around the axes of rotation, between ±50 degrees. The platform was intended for use with an ElectroPuls E10000 (Instron, Buckinghamshire, UK) materials testing device which has the capability of applying torsional loads, thus generating the internal/external rotation. Dependent on the placement of the foot and the configuration of the actuators this design could, in theory, drive the foot through the required motions for lateral, medial and syndesmosis sprain of both left and right feet.

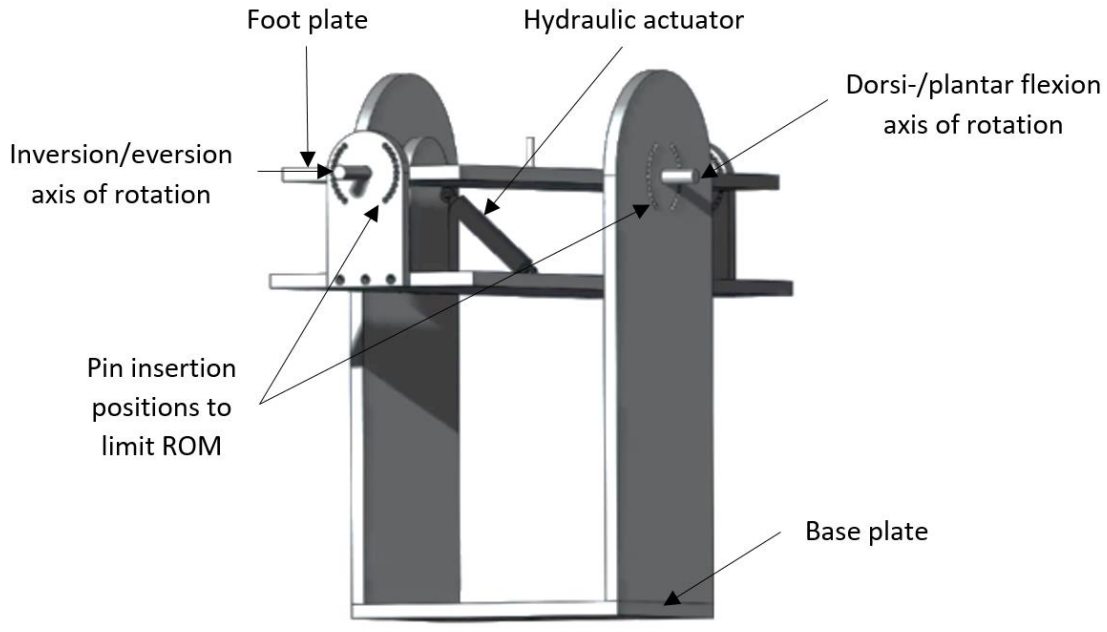

Figure 74. A double-cradle sprain platform concept designed for the simulation of lateral, medial and distal tibiofibular ankle sprain for left and right feet.

The second design, based on the collapsing platform concept, is shown in Figure 75. The design operated as a collapsing platform where the foot plate was supported by solenoids at three corners and a universal joint bracket at the other corner. When triggered, at the point of load

initiation, the solenoids retract allowing the foot plate to fall. During the sprain simulation, only the universal joint supported the foot plate, shown in closer detail in Figure 76. The motion of the foot plate terminated at the point of contact with the hard stop plates below, shown in Figure 75. Similar to the double-cradle design, the collapsing platform could theoretically simulate lateral, medial and distal tibiofibular syndesmosis ankle sprain of both left and right feet.

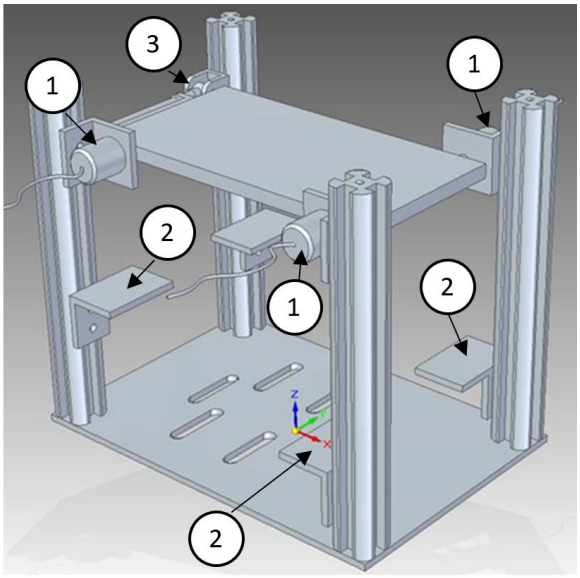

Figure 75. A collapsing platform design for a sprain platform configured for a LAS trial with a right foot. 1 = solenoids, 2 = hard stops, 3 = universal joint, red arrow = x-axis (anterior/ posterior), green arrow = y-axis (medial/lateral) and blue arrow = z-axis (vertical axis).

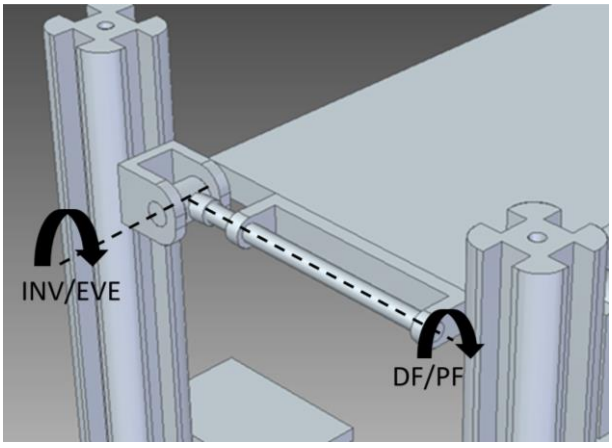

Figure 76. The universal joint designed to attach the foot plate to the fixture and allow motion in both the inversion/eversion (INV/EVE) and dorsi-/plantar flexion (DF/PF) directions.

Unlike the double-cradle design, the universal joint generated internal/external rotation in addition to dorsi-/plantar flexion and inversion/eversion motion. One advantage of this design over the double-cradle design was that the degree of motion could be limited along the full ROM, for dorsi-/plantar flexion and inversion/eversion, rather than in 5 degree increments. This was achieved by altering the position of the hard stops below the footplate which could slide up and down the aluminium extrusion supports and be secured. The degree of

internal/external rotation was a by-product of the amount of dorsi-/plantar flexion and inversion/eversion prescribed and was less controllable. Similar to the previous design the collapsing platform design was developed under the assumption that an Instron ElectroPuls E10000 would be used to apply the load.

Figure 77. The collapsing platform design at the termination point of testing demonstrating the plantar flexion, inversion and internal rotation ROM of the foot plate.

The collapsing platform design was selected as the most favourable design due to the versatility and adaptability of the modular design. The collapsing platform design had many advantages over the double-cradle design, detailed in Table 21. The modularity of the design was particularly important given the unknown ROM required to induce severe LAS and the therefore iterative approach to testing undertook. One limitation to the design was that plantar flexion, inversion and internal rotation would all be driven by the same load source. This therefore determined that the rate of loading, considered to be of particular importance, would have to be compromised for all three ranges of motion. This compromise was considered important though as the ROM achieved by the collapsing platform design was more versatile and replicable of LAS than the double-cradle design and significantly less complex in design. As explained later in the chapter, this compromise became essential due to

the inclusion of internal rotation motion within the platform design as the loading device used was unable to generate internal rotation.

Table 21. The advantages and disadvantages of the collapsing platform compared to the double-cradle design.

Advantages	Disadvantages
• Plantar flexion and inversion ROM can be adapted along the full scale rather than in 5 degree increments • Can generate internal/external rotation motion • Easily modified for left/right feet • Load is applied by an external system opposed to the actuators driving the double-cradle, which may not be able to apply an appropriate load • Modular design to change parts for individual modifications • Less metalwork which could obstruct motion capture analysis.	• Solenoids are an additional complexity which require triggering at the precisely correct moment

The design of the collapsing platform was refined and manufactured within iMBE in accordance with the engineering drawings in Appendix Sprain Platform Assembly v.1. The base plate, foot plate, hard stops and universal joint were manufactured from 316 stainless steel and the frame was constructed using aluminium extrusion. Use of 316 stainless steel was preferable due to the sterilisation and strength capabilities of the material. Aluminium extrusion was selected for the frame to allow for positioning of the other parts, attached to the frame using T-nuts, to be repositioned with ease. The solenoids were replaced with weak sacrificial supports, in the form of wooden golf tees, which gave way under impact, eliminating the complexity of the design. The hard stops, responsible for limiting the motion of the plate were altered from the original design to be cylindrical so that point contact could be initiated with the foot plate, shown in Figure 78. The cylindrical hard stops were reinforced using M5 threaded rod, inserted through the hard stop distal to the attachment to the sprain platform, to the base of the sprain platform. A further M5 threaded rod was used to reinforce the inferior hard stop to the posterior side of the sprain platform. Additional lengths of aluminium extrusion were placed between the vertical extrusion pieces to reinforce the platform, shown in Figure 78. Two further longer lengths of aluminium extrusion were placed on the medial and lateral sides of the platform, positioned in line with the medial and lateral malleoli, shown in

Figure 78. These two pieces of extrusion were to limit the movement of the tibia during testing, restricting all but inferior/superior translation.

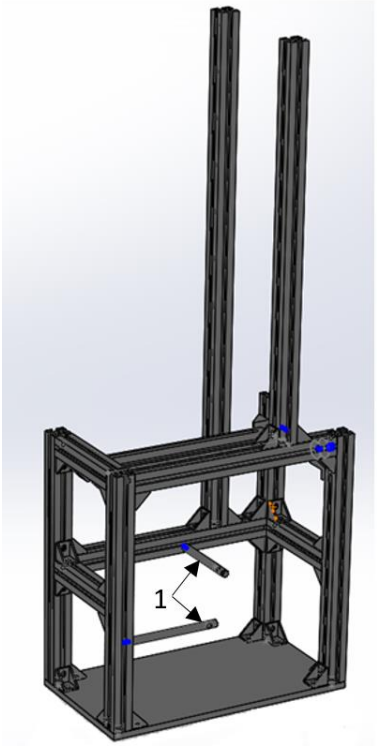

Figure 78. The first version of the sprain platform with the hard stops of the sprain platform configured to generate 40 degrees of inversion and plantar flexion for a right foot. 1 = cylindrical hard stops.

4.2.3 Loading Device

Throughout the design process it was assumed that the sprain platform would be mounted onto an Instron ElectroPuls E10000 (Instron, Buckinghamshire, UK). The ElectroPuls E10000 was proposed due to its ability to apply both axial and torsional controlled loads. The device can apply an axial load up to ±10 kN at a strain rate up to 1 $m.s^{-1}$ over a 60 mm stroke length. It is also capable of applying a rotational torque load up to ±100 Nm over a ±135 degrees ROM. The ElectroPuls E10000 also has the capability to control the loading applied throughout testing, meaning that should an unexpected or abnormal load occur the test can be terminated safely. The ElectroPuls E10000 has the capability to operate in load control (and measure corresponding displacements) or displacement control (and measure corresponding loads). The improved control systems reduce the likelihood of unanticipated damage to the specimens occurring during testing aiding in the prevention of specimen wastage, an important consideration when working with human tissue. The device also has a capture rate of up to 10,000 Hz ensuring as much detail as possible is captured during sprain events. This is of particular importance given the high strain rate and rotational velocity associated with LAS.

Regrettably, however, the ElectroPuls E10000 was determined to be unfeasible for this testing, as it was being used extensively around the proposed time of testing in a collaborative

research project with other university partners. In addition, the position of the ElectroPuls E10000 within the iMBE laboratory restricted the placement of motion capture cameras. The device was positioned in a corner of the laboratory and would need to be moved more centrally in order to position motion capture cameras around the device, shown in Figure 79. Furthermore, the Perspex safety casing of the ElectroPuls E10000 needed to be removed for testing as infrared light emitted from motion capture cameras is not able to pass through Perspex. The combination of these factors and disruption to many laboratory users led to the ElectroPuls E10000 not being used in this study.

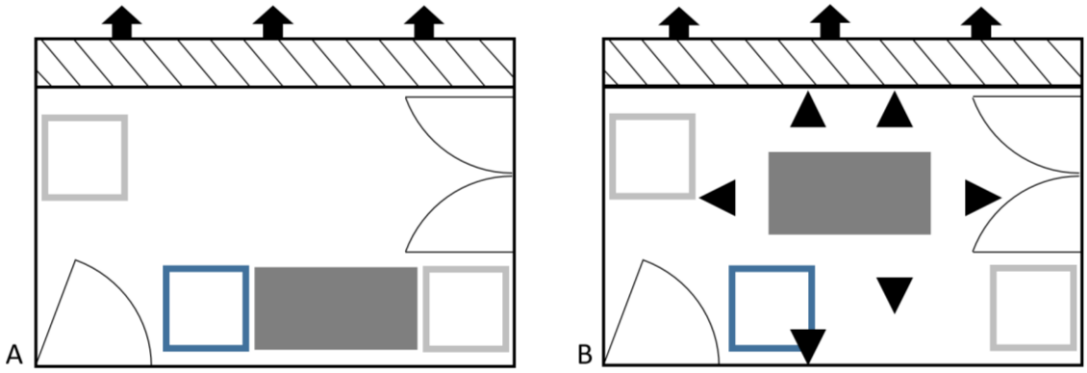

Figure 79 The configuration of the lab A) during normal operation and B) as required for this testing. Single black arc = entrance door, double black arc = fire exit, white square with grey border = refrigerators, grey rectangle = Instron ElectroPuls E10000, white square with blue border = drawer with PC station for Instron ElectroPuls E10000, black triangles = motion capture cameras, black chevron area = other fixed parts and black arrows = the rest of the lab. Not to scale.

As an alternative loading device, a drop-weight test rig was considered, shown in Figure 80. The drop rig is a simple device whereby a mass carrier, loaded between 2.5 kg to 15.5 kg in increments of 1.3 kg, can be suspended at a variable height from 1.0 m to 1.7 m above the ground, shown in Figure 80. The mass carrier is manually released by holding the safety release buttons and pulling the handle supporting the mass carrier out from underneath it. When released the mass carrier slides down the vertical pole to impact with the specimen impactor. The increased portability of the drop rig compared to the Instron ElectroPuls E10000 allowed it to be moved to a quiet area of the laboratory with no footfall required and sufficient space around the device for appropriate placement of the motion capture cameras.

The use of the drop rig did however compromise the loading of the ankle joint complex during the simulation of LAS. The drop rig lacked the ability to control the rate of loading and the load applied independently. The ability of the ElectroPuls E10000 to measure and analyse force and displacement data was also absent from the drop rig.

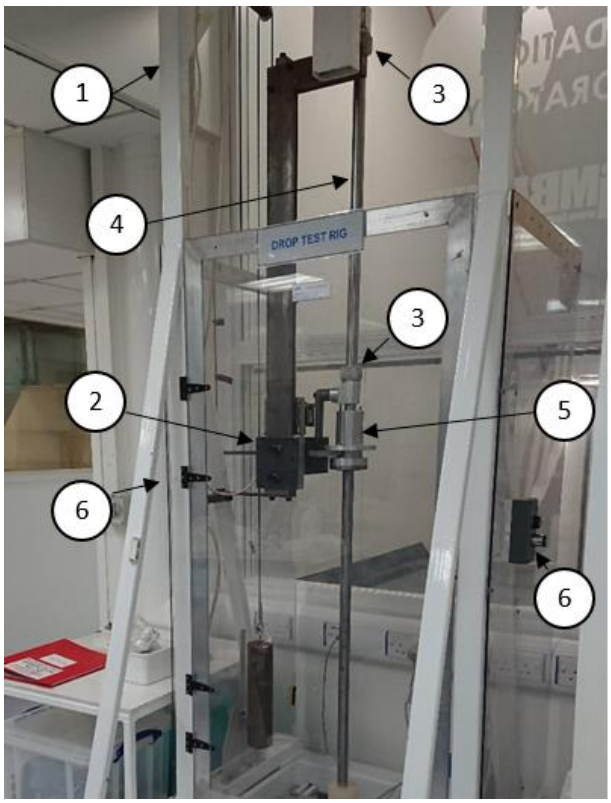

Figure 80. The drop-weight test rig. 1 = main frame, 2 = release mechanism, 3 = clamp, 4 = vertical pole, 5 = mass carrier and 6 = safety release button.

4.2.3.1 Mass-energy Calculations

The design of the collapsing platform, and use of the drop-weight rig, determined that the rotational velocities for plantar flexion, inversion and internal rotation must all be generated by the same falling mass. Based upon the published data, initial testing values for a compromised rotational velocity, plantar flexion angle and inversion angle were selected as 600 degrees per second, 40 degrees and 40 degrees, respectively. The large variability of kinematic data between sprain trials made the selection of appropriate angles very challenging. Only the plantar flexion and inversion angles were selected for the load calculations as the internal rotation angle was a by-product of the two other motions. Inversion angle was given a greater importance in the determination of required values to generate LAS as plantar flexion was not always present, shown in Table 3. In terms of the rotational velocity a value of 600 degrees per second was chosen as it was higher than the values quoted for the majority of sprain scenarios reported in Table 3.

The load capacity of the drop-weight rig (15.5 kg) is considerably lower than the mean BW of the six donor samples expected to be used in the study (60.0 ± 14.4 kg), shown in Table 30. The load capacity of the drop weight rig was restricted by the size of the mass carrier and the release mechanism, shown in Figure 80. The production of slightly wider individual masses was considered, however the mass would have likely been similar as the current masses were lead and new masses would have been steel. The total mass could certainly not be increased sufficiently, matching that of the human donors. This posed an additional limitation to the

simulation of severe LAS causing an unavoidable shift in focus from replicating the rotational velocity of the ankle joint complex, and therefore the strain rate of the lateral ankle ligaments, to matching the energy of sprain. To do so an estimation of the energy experienced during sprain was calculated.

To estimate the energy of sprain the following equations were used:

$$Velocity\ (v) = \frac{\Delta z}{t} \quad (1)$$

$$Kinetic\ Energy\ (KE) = \frac{mv^2}{2} \quad (2)$$

Where Δz = vertical displacement, t = time and m = mass.

Vertical displacement describes the vertical distance the foot plate travels from the neutral position (0 degrees of inversion and plantar flexion) to the simulated sprain position (40 degrees of plantar flexion and inversion). The vertical displacement was 95mm, measured in the laboratory using Vernier callipers, shown in Figure 81.

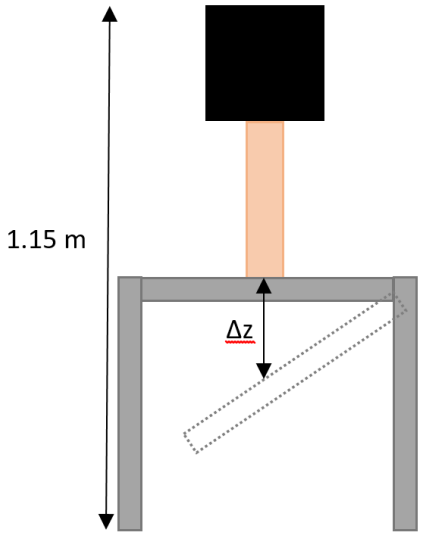

Figure 81. The vertical displacement (Δz) of the footplate from the neutral starting position to the final simulated sprain position. Black square = specimen impactor, beige rectangle = foot, grey rectangles = sprain platform in neutral position and white rectangle with grey dotted border = simulated sprain position of foot plate.

The time taken to rotate 40 degrees at a rotational velocity of 600 degrees per second was calculated by rearranging Equation 1 to solve for time resulting in a time of $0.0\dot{6}$ s. The linear velocity was then calculated by inputting the time ($0.0\dot{6}$ s) and vertical displacement (95 mm) into Equation 1 to give a linear velocity of 1.43 m.s^{-1}. The average mass of donors (59.95 kg) and velocity (1.43 m.s^{-1}) were then input into Equation 2 to calculate an estimation for a sprain inducing energy of 61.3 J.

As previously stated, the maximum mass for the drop test was 15.5 kg and the maximum height the mass could be dropped from was 1.7 m above the ground. The height of the platform, specimen, intramedullary rod and impactor was estimated to total 1.15 m, shown in

Figure 81. The distance between the bottom of the mass carrier and the top of the specimen impactor, the maximum drop height for testing, was therefore 0.55 m.

The mass and height values for the drop test required to produce 61.3 J of energy were calculated using Equation 2 and the following equations:

$$v = v_0 + at \quad (3)$$

$$\Delta z = v_0 t + \frac{1}{2} a t^2 \quad (4)$$

Where v_0 = initial velocity and a = acceleration.

The initial linear velocity was 0 m.s^{-1} for the drop testing, simplifying the equations. Prior to calculating the height from which the maximum mass of 15.5 kg should be dropped from, to create 61.3 J of energy, Equation 2 was rearranged to solve for velocity. Inputting the energy value (61.3 J) and mass value (15.5 kg) resulted in a linear velocity (v) of 2.81 m.s^{-1}. The time taken for the mass to drop, from the initiation of the test until impact with the specimen impactor, was then calculated by rearranging Equation 3 to solve for time and inputting the initial velocity as 0 m.s^{-1}, the linear velocity as 2.81 m.s^{-1} and acceleration as 9.81 m.s^{-2} to give a time of 0.286 s. The time result was input into Equation 4 to give a drop distance required to produce 61.3 J of energy when a 15.5 kg mass is dropped of 0.40 m. The drop-weight loading rig was therefore determined to be capable of applying sufficient energy loads to induce LAS in cadaveric specimens.

4.2.4 Motion Capture

The motions of the ankle complex, talocrural joint and subtalar joint were of importance in this study to analyse the biomechanics of LAS. Both goniometers and optical motion capture analysis exist as techniques to analyse joint motion. Optical motion capture was selected as the most favourable technique for this project due to the 3-dimensional capabilities of the technique. Importantly the motion capture system was able to function at the required capture rate and the existing expertise within the supervisory team was advantageous. Optical motion capture cameras operate using light (usually infrared) to track the motion of reflective markers or LEDs attached to moving objects or bodies.

4.3 Materials and Methods

4.3.1 Samples

Two fresh frozen human cadaveric feet, sourced from MedCure (USA), were used in this study. Ethical approval was granted by the University of Leeds Research Ethics Committee (MEEC 15-020). Exclusion criteria for the tissues included a reported prior lower limb trauma or surgery, or a history of diabetes. The mean donor age was 63 years, BMI was 21.8 kg.m^{-2} and there was one male and one female. A summary of donor information is shown in Table 22.

Table 22. Tissue donor demographic details. (M = male, F = female, R = right & L = left).

Sample	Age (years)	Sex	L/R Foot	Weight (kg)	BMI (kg.m^{-2})
1	68	M	L	97.5	29.1
2	58	F	R	40.8	14.4

4.3.2 Sample Preparation

The feet were stored in a -40 °C freezer, compliant with the Human Tissue Act, until testing. Samples were thawed for 48 hours at 4 °C in a refrigerator prior to dissection. The dissections for this study were performed by the author, who had a large amount of dissection experience and had previously received training from a foot and ankle specialist consultant orthopaedic surgeon during prior ankle dissections. To start the dissection all fascia and soft tissue were dissected posterior to the calcaneocuboid talonavicular joint, except for the fat pad distal to the calcaneus, shown in Figure 82A/B. The skin and fascia were removed around the ankle complex to afford the visualisation of the LCL complex, for visual assessment of damage to the ankle. The removal of skin and fascia around the tibia and fibula was performed as the tissue was providing minimal stabilisation to the ankle joint complex and decreased the difficulty implanting the intramedullary rod. The fat pad was retained to maintain the natural dorsi-/plantar flexion position of the foot.

A 10 mm hole was drilled into the intramedullary cavity of the tibia, perpendicular to the ground, with the foot in the neutral position. Where possible, two 5 mm diameter holes were drilled through the cortex of the tibia into the centre of the cavity. The holes were drilled from the posterior side of the tibia and were vertically spaced 100 mm apart from their centres. The intramedullary rod, shown in Appendix D.3.6 Specimen Impactor Intramedullary Nail, was inserted into the tibial cavity and secured with two M5 bolts through the tibia and intramedullary rod. Where the length of the cavity was insufficient one M5 bolt was used, as shown in Figure 82, which worked as effectively as two bolts in restricting relative motion between the intramedullary rod and the tibia.

An 8 mm medial-lateral hole was drilled through the calcaneus perpendicular to the axis of the intramedullary rod. A metal tube with internal diameter of 5 mm and external diameter of 8 mm was implanted, shown in Figure 82, to aid potential stability analysis. A 1 mm pilot hole was drilled into the fibula, tibia and calcaneus at the positions of the lateral malleolus, medial malleolus and posterior calcaneal static markers, respectively, as shown in Figure 86. A 2 x 8 mm screw was inserted into each pilot hole, flush to the surface of the bone, to provide additional attachment for the static passive markers, shown in Figure 82.

Figure 82. A) medial view and B) posterior view of a dissected sample with the intramedullary rod, calcaneal tube and medial, lateral and posterior static marker screws implanted.

A 2.5 mm hole was then drilled into the calcaneus, talus, fibula and tibia for the implantation of bone pins to anchor the marker triads. The hole into the calcaneus was positioned on the posterolateral side of the proximal surface of the calcaneus, shown in Figure 83. The hole was drilled approximately 45 degrees from the frontal and sagittal planes to prevent the arms of the marker triad from colliding with the tibia or fibula. The hole into the talus was located on the medial side of the articulating surface of the tibiotalar joint on the anterior surface of the talus proximal to the talar head, shown in Figure 83. The hole was drilled at approximately 45 degrees to the vertical axis in the sagittal plane, shown in Figure 83, to avoid collision of the marker triad arms with the tibia or midfoot.

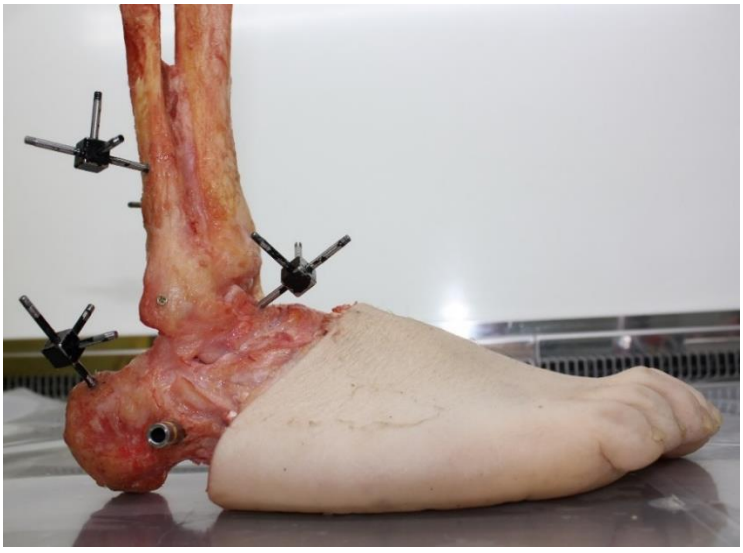

Figure 83. Lateral view of a dissected foot with marker triads implanted.

The holes into the tibia and fibula were drilled approximately 60 mm superior to the medial and lateral malleoli, respectively. The hole into the tibia was drilled perpendicular to the surface of the bone and located posteriorly on the medial side of the tibia, shown in Figure 84. The hole into the fibula was positioned posteriorly on the lateral side of the fibula and drilled perpendicular to the bone surface, shown in Figure 84.

The sample preparation differs between samples one and two at this point in terms of marker triad fixation. For sample one a 6 mm M3 grub screw was screwed into each of the 2.5 mm drilled holes to anchor marker triads. Marker triads could be push-fit into the hexagonal holes of the grub screws. In later trials the grub screws were removed and the marker triads were screwed directly into the bone of the specimen. The latter methodology was performed for the second sample. At this point the samples were fully prepared for testing and were submerged in PBS (Oxoid Ltd, Basingstoke, UK) solution for 30 minutes at room temperature (21 °C), to rehydrate the sample after an extended period exposed to the air.

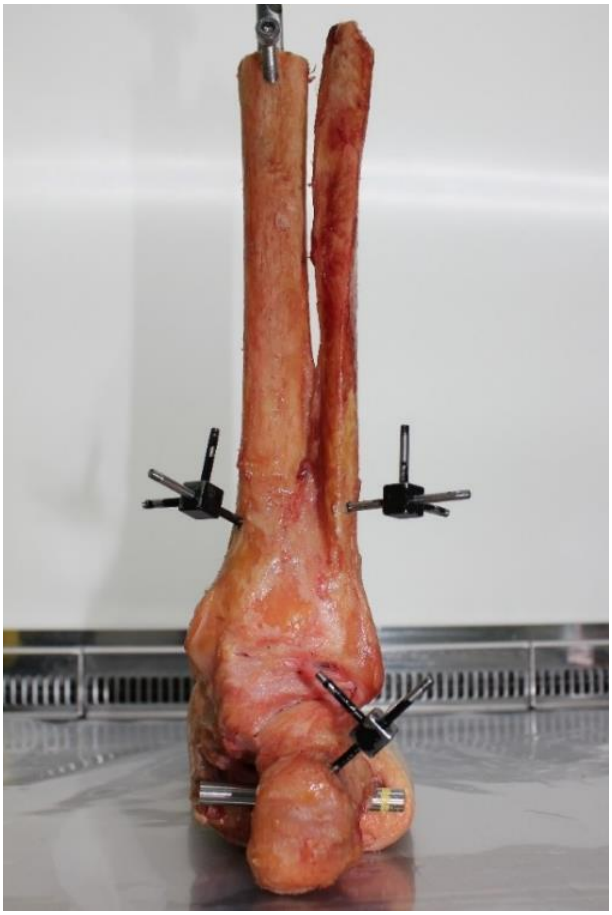

Figure 84. Posterior view of a dissected foot with marker triads implanted.

4.3.3 Foot Model

To allow for biomechanical comparison of ankle joint complex kinematics between specimens the placement of reflective markers must be consistent, achieved by following a model. There are many different foot and ankle multi-segment models that exist, varying in complexity and functionality (Leardini et al., 1999; Carson et al., 2001; Nester et al., 2014; Oosterwaal et al.,

2016). The use of cadaver tissue further affords the implantation of marker triads into the bones of the ankle complex using bone pins. A custom five segment marker model (tibia, fibula, talus, calcaneus and foot) was used in this study, adapted from a previous bone pin study on foot and ankle kinematics, shown in Figure 85 (Lundgren et al., 2008). The previous model was chosen as a guide to build a custom model as the 3-dimensional motion of all bones of the ankle joint complex were able to be tracked from the placement of a single bone pin into each bone.

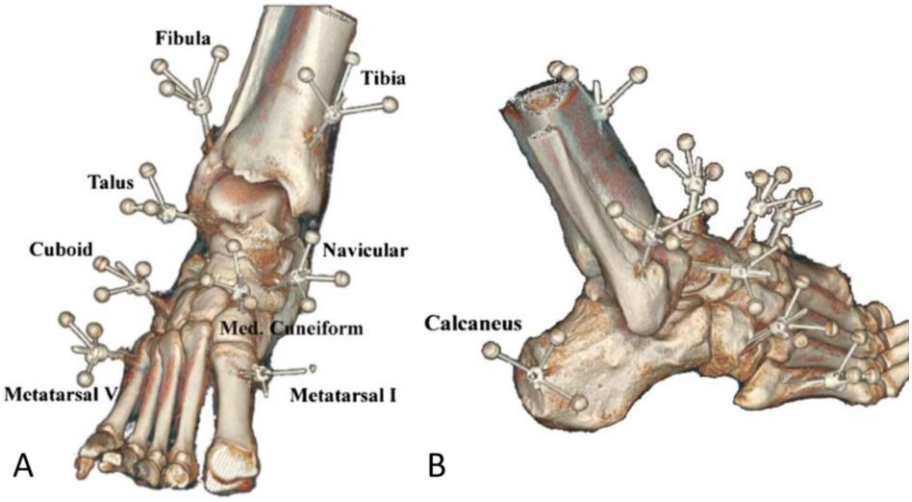

Figure 85. Bone pin and marker placement model previously used for the kinematic analysis of the foot and ankle (Lundgren et al., 2008).

The custom model developed for this study focussed on the talocrural and subtalar joints of the ankle complex, therefore 3-dimensional data for the cuboid, navicular and medial cuneiform was not required. Bone pins with marker triads were inserted into the fibula, tibia, talus and calcaneus, shown in Figure 86. Individual anatomical markers were located on the medial and lateral malleoli, the first, third and fifth metatarsal and the posterior of the calcaneus, in line with the third metatarsal marker, shown in Figure 86. The first, third and fifth metatarsal markers and the posterior calcaneus marker formed a single segment foot model and the medial and lateral malleoli markers determined the centre of rotation for the foot segment. As no past research, to the author's knowledge, has examined the effect of simulated ankle sprain on ankle complex kinematics, a single segment foot model was also used to compare outputs from each bone and the foot plate to ensure that all outputs/kinematics were following similar trends. Individual markers were also placed in the four corners of the foot plate to track the motion of the foot plate as a single segment, shown in Figure 86.

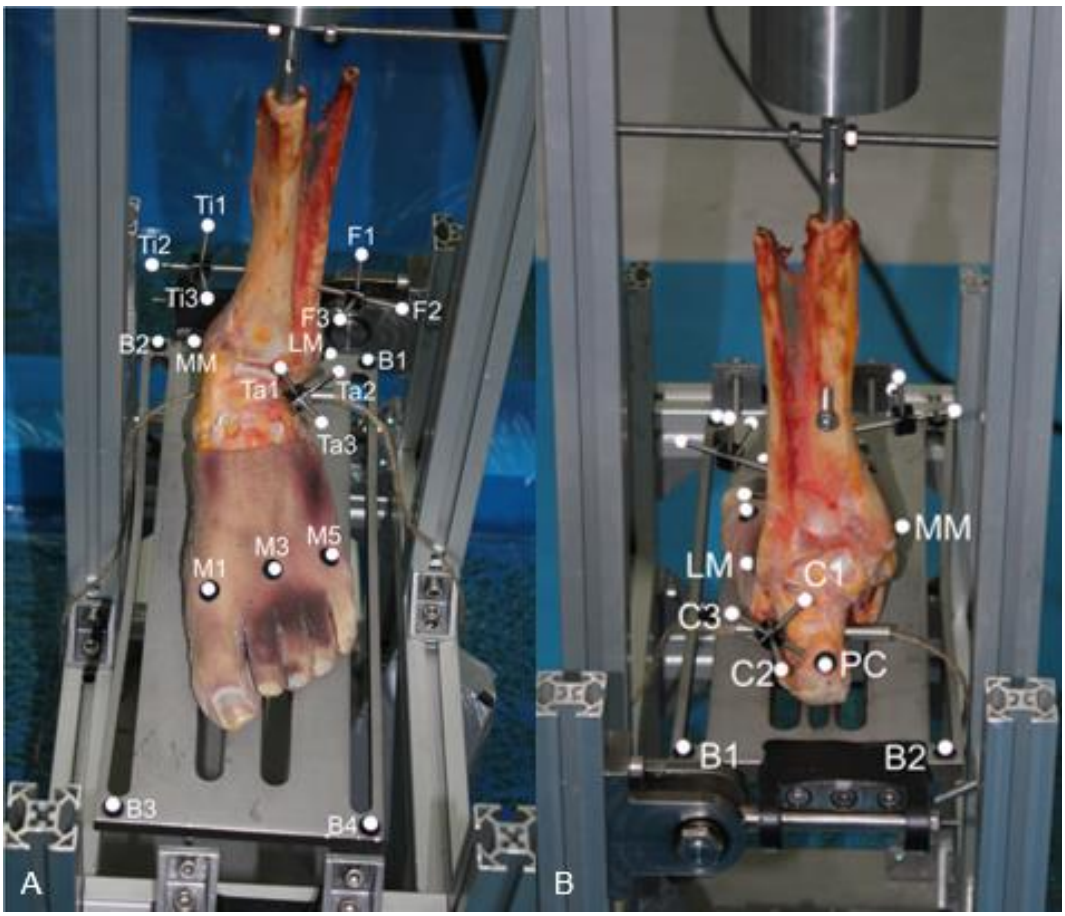

Figure 86. A) Anterior view and B) posterior view of the marker placement of the custom model for this study. B1, B2, B3 and B4 = base marker 1, 2, 3 and 4, M1, M3 and M5 = first, third and fifth metatarsal markers, MM and LM = medial and lateral malleolar markers, PC = posterior calcaneus marker, C1, C2 and C3 = calcaneal markers 1, 2 and 3, Ta1, Ta2 and Ta3 = talar marker 1, 2 and 3, Ti1, Ti2 and Ti3 = tibial markers 1, 2 and 3, F1, F2 and F3 = fibular markers 1, 2 and 3.

4.3.4 Data Collection

Simulated ankle sprain kinematics were captured in this study using a six Miqus M3 camera 3D infrared passive marker motion capture system, integrated with one Miqus video camera (Qualysis AB, Gothenburg, Sweden). The Miqus M3, shown in Figure 87A, acquired data at up to 1000 Hz and to a 0.1 mm accuracy. Whereas the Miqus video camera, shown in Figure 87B, used to potentially identify the time point of ligament rupture operated at 550 Hz.

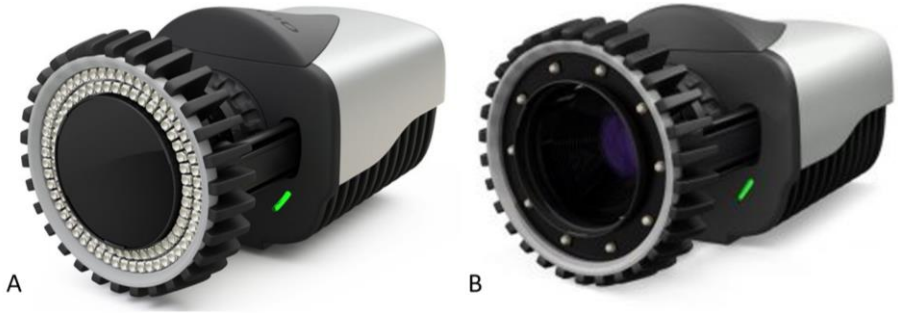

Figure 87. A) Miqus M3 motion capture camera and B) Miqus Video camera.

The motion capture system was set up with the cameras positioned around the collapsing platform for optimal capture dependent on the configuration of the collapsing platform and the type of foot (left/right) being tested, shown in Figure 88. Once positioned the motion capture cameras were individually optimised in terms of focus and exposure and the system was calibrated. The collapsing platform was removed from the capture volume and the calibration L-frame was positioned in the corner where the collapsing platform had been positioned, shown in Figure 88A. The L-frame determines the orientation of the laboratory space and it was therefore important that the placement of the L-frame was consistent between trials. Black electrical tape was placed on the floor of the laboratory to mark the position and orientation of the L-frame.

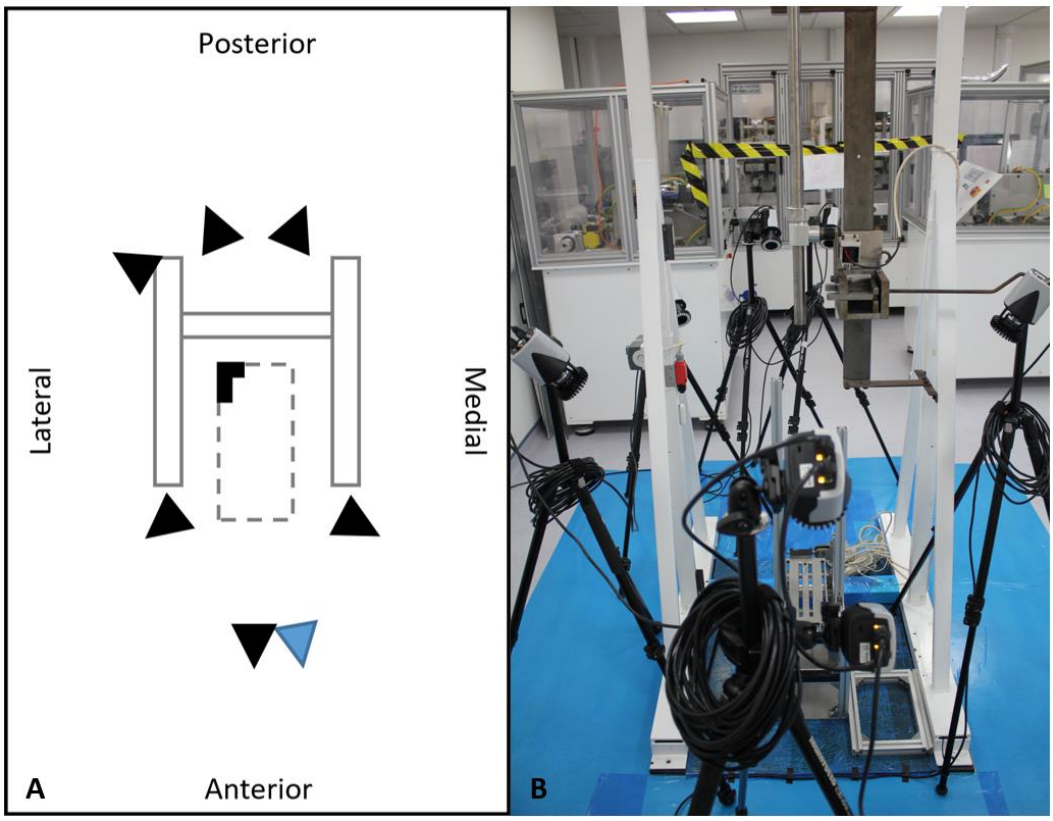

Figure 88. A) Floorplan schematic and B) image of the lab showing the positioning of motion capture cameras for the analysis of a right foot. Also shown is the location of the L-frame during calibration. White rectangle with solid grey border = drop rig frame, white rectangle with dashed grey border = sprain platform, black L = L-frame, black triangle = Qualisys Miqus M3 motion capture camera and blue triangle = Qualisys Miqus video camera. Not to scale.

Calibration was performed, following the standard procedure detailed by Qualisys, using a small carbon fibre calibration kit, shown in Figure 89. The 123.2 mm calibration wand was moved through the entire capture volume for 60 seconds in all directions to cover as much of the capture volume as possible. The system was calibrated before testing each specimen and the calibration data was recorded. On average the standard deviation of the wand length during the calibration was 0.1 mm. Should the calibration require repeating, due to movement of the portable cameras throughout testing, the Qualisys Track Manager (QTM) software (Qualisys AB, Gothenburg, Sweden) provided a prompt and the calibration was repeated. The

calibration volume was checked to ensure that the entire potential volume required for sprain simulation was calibrated, shown in Figure 90

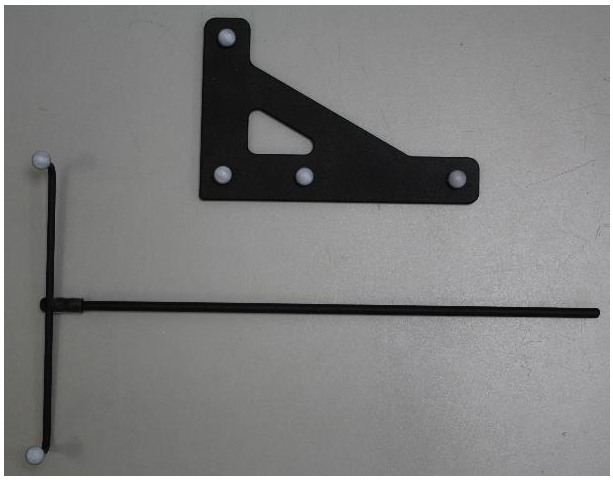

Figure 89. The small carbon fibre calibration kit, comprised of a calibration wand and L-frame, provided by Qualisys.

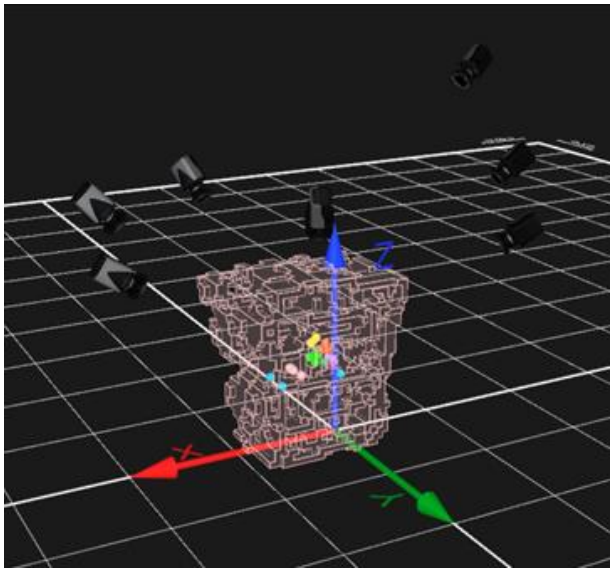

Figure 90. The capture volume for the calibration (pink volume) shown within the virtual laboratory created within QTM. The laboratory origin is at the position of the L-frame during calibration and the axes show the relevant directions.

4.3.4.1 Simulation of Sprain

Following the PBS soak, the skin and bone at the location of the anatomical markers was dried with paper towel to improve the adhesion of the markers to the appropriate anatomical landmarks. Twenty-two super-spherical 6.5 mm diameter reflective markers (Qualisys AB, Gothenburg, Sweden) were then screwed onto the marker triad arms and anatomical marker bases. Individual anatomical markers were then attached to the following anatomical landmarks using double sided adhesive tape; medial and lateral malleoli, the first, third and fifth metatarsal, the posterior of the calcaneus in line with the third metatarsal marker and the four corners of the foot plate, shown in Figure 86.

The collapsing platform was repositioned under the drop rig following the calibration of the motion capture system, ensuring the corner of the platform was aligned with the tape markings on the floor. The foot plate was positioned in zero degrees of dorsi-/plantar flexion and inversion/eversion, measured using a digital angle gauge. The golf tees supporting the foot plate were exchanged for metal bolts to prevent the foot plate from giving way during the preparation stages, shown in Figure 91. The specimen was attached to the sprain platform using a 160 mm long M5 threaded rod inserted through the 5 mm mediolateral hole in the intramedullary rod. A nut was threaded onto each side of the threaded rod to secure the position of the intramedullary rod centrally on the M5 threaded rod and prevent any medial-lateral translation. A T-nut was threaded onto each end of the M5 threaded rod and the T-nuts were slid down the vertical supports to restrict internal/external rotation of the tibia. The specimen impactor, containing a linear bearing, was then screwed onto the intramedullary rod, shown in Figure 91.

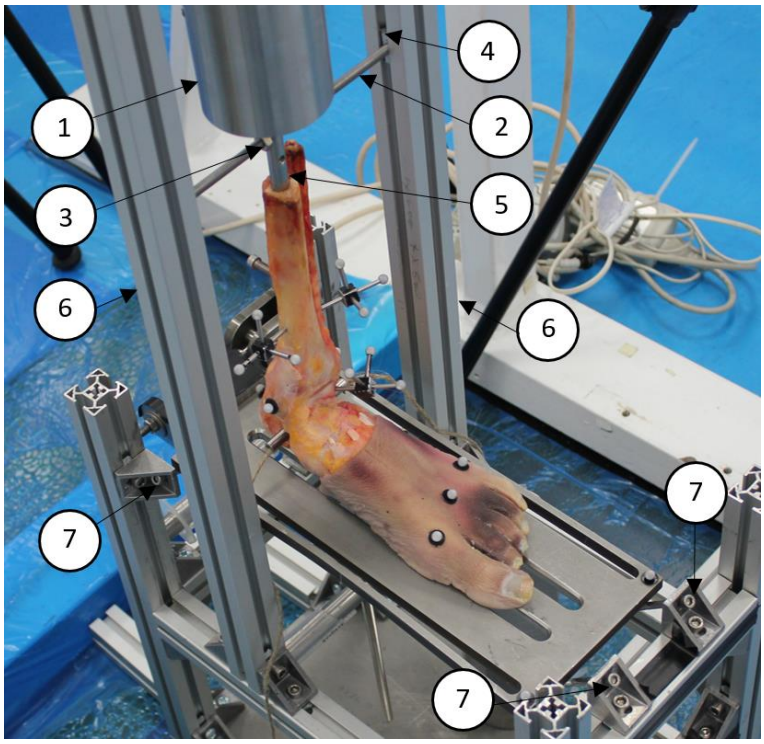

Figure 91. Tibial attachment to the sprain platform and the drop rig. 1 = specimen impactor, 2 = threaded rod, 3 = nut, 4 = T-nut 5 = intramedullary rod, 6 = vertical support and 7 = bolt/golf tee.

The height of the release mechanism was adjusted to the appropriate height by loosening the upper clamp around the vertical pole and releasing the tension bolts attaching the release mechanism to the main frame. The height of the release mechanism was positioned appropriately above the specimen impactor and secured by tightening the tension bolts. The vertical pole was repositioned to allow the mass carrier to be slid onto the pole. Both clamps around the vertical pole were loosened, the pole was raised and the clamps tightened. The mass carrier was loaded with the appropriate mass for the given trial and slid up the vertical

pole and secured in place by the release mechanism. The vertical pole was finally repositioned so that the bottom of the vertical pole was as low as possible.

The metal bolts supporting the foot plate were replaced with wooden golf tees and a static trial of the specimen was taken. Following the first static trial of each specimen an automatic identification of markers (AIM) model was established to quicken the labelling process within QTM, shown in Figure 92. After applying the AIM model to the static trial, a 100 % capture of the markers was ensured for the static trial. When markers were not all visible the marker triads were adjusted and markers were visually inspected for fading/damage, being replaced where necessary. The static trial was then repeated and if markers were still not captured the positioning of the motion capture cameras was adjusted to be optimal for the specimen being tested. The motion capture system was then recalibrated, the sprain platform was repositioned under the drop rig and the static trial was repeated.

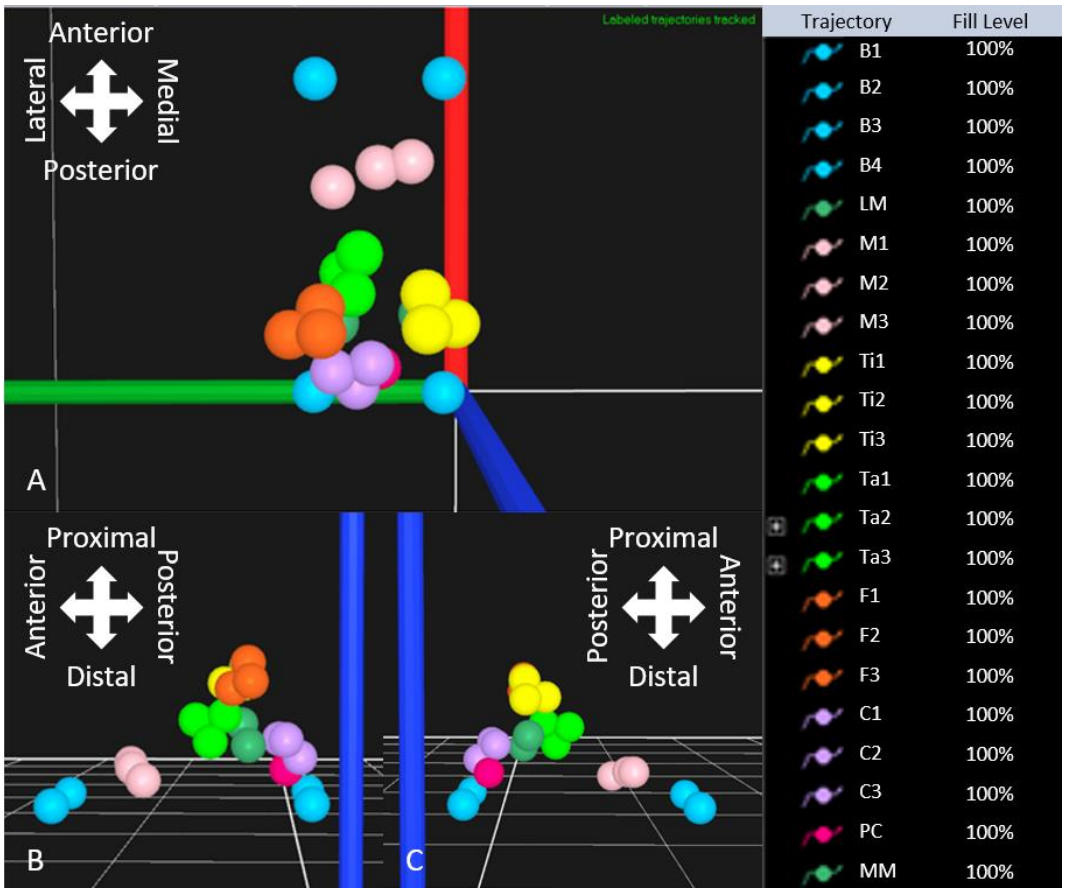

Figure 92. A) Proximal view, B) lateral view and C) medial view of an AIM model produced and applied to a specimen within QTM. B1, B2, B3 and B4 (light blue) = base marker 1, 2, 3 and 4, M1, M3 and M5 (light pink) = first, third and fifth metatarsal markers, MM and LM (forest green) = medial and lateral malleolar markers, PC (bright pink) = posterior calcaneus marker, C1, C2 and C3 (light purple) = calcaneal markers 1, 2 and 3, Ta1, Ta2 and Ta3 (lime green)= talar marker 1, 2 and 3, Ti1, Ti2 and Ti3 (yellow) = tibial markers 1, 2 and 3, F1, F2 and F3 (orange) = fibular markers 1, 2 and 3. Red arrow = x-axis (anterior/posterior), green arrow = y-axis (medial/lateral) and blue arrow = z-axis (vertical axis).

The motion capture system was then initiated to record the dynamic trial of the sprain simulation. Sprain simulation was performed by pressing the safety release buttons and

triggering the release mechanism. The mass carrier fell down the vertical pole, due to gravity, to impact with the specimen impactor below. The dynamic motion capture trial was stopped and the specimen and sprain platform were inspected for damage. The calcaneal bolt, marker triads and intramedullary rod were removed and the specimen returned to the -40 °C freezer.

4.3.5 Data Processing

The motion capture data was captured within the QTM software and the AIM model was applied. The data was exported from QTM as a .c3d file and post-processing of the data was performed within Visual 3D (C-Motion, Maryland, USA). Kinematic data was filtered using a low pass Butterworth filter at 6Hz.

4.3.6 Data Analysis

The markers were grouped to allow for the analysis of the different segments of the foot and ankle as well as the foot plate of the sprain platform, shown in Table 23. When analysing joint motion the convention was established that motion of the distal bone segment was reported in relation to the proximal bone segment. The motion of the talocrural joint segment, for example, was described by the motion of the talus with respect to the tibia.

Table 23. The marker groupings for different segments of the foot and ankle. Wrt = with respect to.

Segment Name	Anatomical Relations	Markers Used
Tibial Triad	3D motion of tibia	Ti1, Ti2 and Ti3
Fibular Triad	3D motion of fibula	F1, F2 and F3
Talar Triad	3D motion of talus	Ta1, Ta2 and Ta3
Calcaneal Triad	3D motion of calcaneus	C1, C2 and C3
Ankle Complex	3D motion of ankle complex	C1, C2 and C3 wrt Ti1, Ti2 and Ti3
Talocrural Joint	3D motion of talocrural joint	Ta1, Ta2 and Ta3 wrt Ti1, Ti2 and Ti3
Subtalar Joint	3D motion of subtalar joint	C1, C2 and C3 wrt Ta1, Ta2 and Ta3
Foot	3D motion of the foot	MM, LM, M1, M5
Foot Plate	3D motion of the foot plate	B1, B2, B3 and B4

A local coordinate system was defined for each of the five foot and ankle segments and the foot plate segment using the markers on the triads and the markers the foot plate, respectively, in combination with some virtual markers. Virtual markers were created from the malleoli markers (defines x-axis, medial/lateral) and the posterior calcaneus and 3rd metatarsal marker (defines y-axis, anterior/posterior) which were projected onto the floor thus the foot,

and all segments, were parallel to the floor. The local coordinate systems for each segment were co-incident with the axes of the global frame when the foot was in the neutral position during the static trial. For the foot plate x-axis (medial/lateral) was determined by base markers two (B2) and three (B3) and the y-axis (anterior/posterior) by base markers two (B2) and one (B1). The z-axis (vertical) was defined to be perpendicular to the x- and y-axes.

Angular motion at the ankle complex, talocrural and subtalar joints was assumed to have six DOF and was formed by the combination of the tibia and calcaneus, tibia and talus, and the talus and calcaneus, respectively, as shown in Table 23. Euler angles were calculated for the ankle complex, talocrural and subtalar joints using the rotation sequence sagittal (x), frontal (y) and transverse (z) plane motion. The data was normalised to be percentage of trial, opposed to simply time, and the peak positive and negative values of plantar flexion, inversion and internal rotation were used to calculate the overall ROM of each segment and intersegment joint during the simulation of sprain.

4.4 Sprain Platform Validation

Validation of the sprain platform was performed prior to use with valuable cadaver specimens to ensure the collapsing platform operated safely and effectively. Two different trials were performed for the validation testing to investigate the foot plate angles achieved, load capacity of the collapsing platform, effectiveness of the weak supports and 3D printed polymer marker triads, shown in Table 24.

Table 24. The testing conditions used for the validation of the sprain platform. Bolded text highlights the unique features of, or changes made between, trials.

	Testing Conditions
Trial 1	• **2.5 kg** dropped from **1 m** equal to **24.5 J** energy • **40 degrees** plantar flexion and **40 degrees** inversion • **Polyurethane block** as specimen • **Wooden golf tees** used as weak supports
Trial 2	• **12.9 kg** dropped from 1 m equal to **126.5 J** energy • 40 degrees plantar flexion and 40 degrees inversion • **Sawbone model foot** as specimen • 3D printed **polymer marker triads**

4.4.1 Trial 1 – Foot Plate Angles and Weak Support

Initial testing investigated the angles achieved by the foot plate and the effectiveness of wooden golf tees as weak supports for the foot plate. The mass carrier (2.5 kg) was dropped

from a height of 1 m (equal to 24.5 J energy). A polyurethane block was used as a replacement for a specimen, secured to the foot plate using two M10 bolts and nuts, shown in Figure 93. Only the static base markers (B1, B2, B3 and B4) were used for the motion capture in this trial to analyse the ROM of the foot plate, expected to achieve 40 degrees of plantar flexion and inversion.

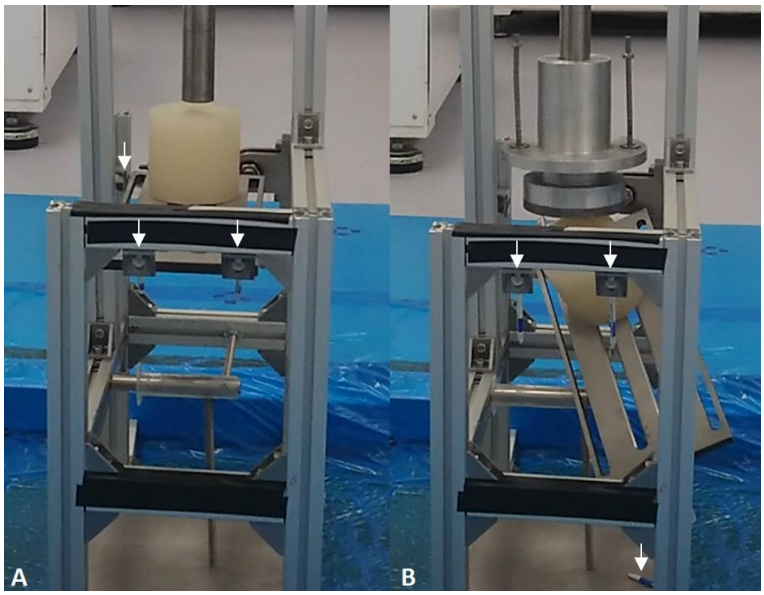

Figure 93. Initial trial testing the weak supports with a polyurethane block at the point of trial initiation (A) and termination (B). The white and blue wooden golf tees (white arrows) supporting the foot plate can be seen intact in (A) and snapped in (B).

4.4.1.1 Outcome

Golf tees successfully gave way under the relatively low load of 24.5 J energy. At the point of terminal impact, the foot plate plantar flexed 38.8 degrees, inverted 33.6 degrees and internally rotated 24.9 degrees. The point of terminal impact was defined as the point where the foot plate made contact with the hard stops at a position closest to the desired degrees of plantar flexion and inversion prior to any evident vibrations of the foot plate. The universal joint arm of the collapsing platform, shown in Appendix D.1.29 Universal Joint Arm 2 v.1, was bent during the drop testing at a relatively low load.

4.4.2 Trial 2 – Marker Placement and Load Capacity

A more substantial universal joint arm was produced, shown in Appendix D.1.30 Universal Joint Arm 2 v.2. An anatomical model foot was used in the second trial to assess the marker placement and to test the 3D printed polymer marker triads, shown in Appendix D.2.1 Marker Triad. The model was prepared for sprain simulation following the protocol previously described for cadaver samples, shown in Figure 94. The model foot was attached to the footplate using a heavy duty cable tie positioned around the metatarsals. The previously estimated maximum drop height of the mass carrier (0.55 m) was conservative. Once set-up with a cadaveric sample a maximum height of 0.85 m was possible which achieved an energy

of 121.6 J when the maximum mass of 15.5 kg was dropped. In this trial an increased mass of 12.9 kg was dropped from a height of 1 m, equal to 126.5 J energy to determine the load capacity of the sprain platform under the maximum possible loading energy for testing.

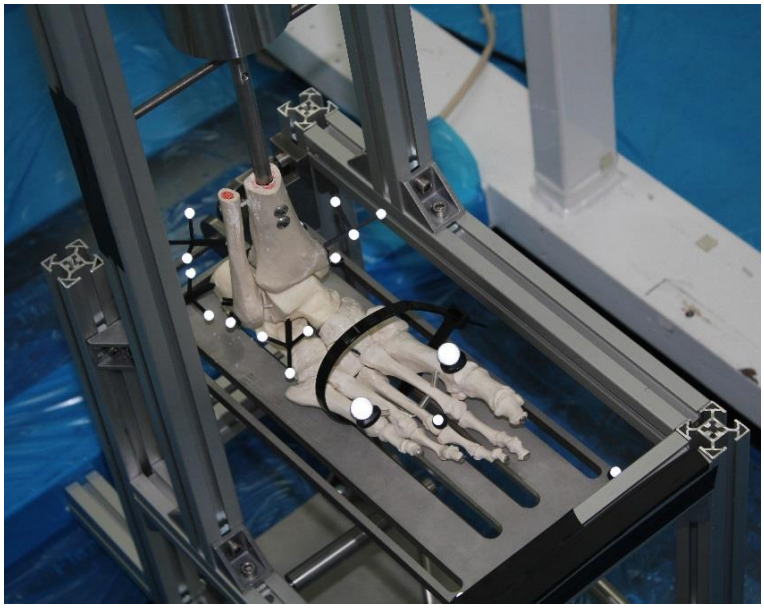

Figure 94. Sawbone model foot mounted to the collapsing platform prior to testing. The model and foot plate markers and triads are attached in the appropriate places.

4.4.2.1 Outcome

The model foot was damaged during testing as the elastic holding the talocrural joint together snapped. The model foot was also deemed to be insufficient for the purpose of this study and therefore its use was discontinued. The lack of an adequate synthetic model determined that cadaver testing was initiated. Damage had also occurred to the universal joint small diameter bracket and medial hard stop as a result of the increased loading. Polymer marker triads were also damaged and although the motion of the model was abnormal their use was discontinued due to the weak and brittle nature of the material.

4.5 Cadaver Testing

Following initial rig validation tests and with the lack of an adequate model for sprain simulation testing, cadaver donor tissue testing was commenced. Trials were performed on different days due to the significant amount of time required to prepare for testing and the replacement/repair of damaged parts between trials, with the exception of trials three and four which were performed within 15 minutes of each other. Where trials were performed on separate days, the 30 minute PBS soak was repeated to rehydrate the sample after an extended period exposed to air without hydration measures being conducted. The use of hydration methods throughout testing was hindered by the reflective markers used for motion capture analysis. The markers were required to remain clean and dry to be captured efficiently

by the infrared cameras. Excess moisture would also cause issues with the adhesion of anatomical markers.

4.5.1 Sample 1

Four trials were performed using sample 1 to investigate fixation of the specimen to the foot plate, anchorage of the marker triads to bone and design iterations to the collapsing platform. Repetitive testing using the same sample was performed until catastrophic damage to the specimens to prevent excessive wastage of human specimens. The testing conditions investigated in the four trials for sample 1 are detailed in Table 25.

Table 25. The testing conditions used for investigation of the simulation of LAS. Bolded text highlights the unique features of, or changes made between, trials.

	Testing Conditions
Trial 1	• **15.5 kg** dropped from **0.4 m** equal to **60.6 J** energy • 40 degrees inversion and 40 degrees plantar flexion • Foot secured to plate with a heavy duty **cable tie** • 316 stainless steel triads - **hex insert** • Universal joint and medial hard stop were **redesigned** • Additional **posterior hard stop**
Trial 2	• 15.5 kg dropped from 0.4 m equal to 60.6 J energy • 40 degrees inversion and 40 degrees plantar flexion • Foot secured to plate with an **M8 bolt into calcaneus** and **two** heavy duty **cable ties** • 316 stainless steel triads - **threaded insert** • Intramedullary rod **realigned**
Trial 3	• 15.5 kg dropped from 0.4 m equal to 60.6 J energy • 40 degrees inversion and 40 degrees plantar flexion • Foot secured to plate with an M8 bolt into calcaneus and two heavy duty cable ties • 316 stainless steel triads - threaded insert **embedded until no relative motion between triad and bone** • Threaded bar **replaced**
Trial 4	• 15.5 kg dropped from **0.8 m** equal to **121.6 J** energy • 40 degrees inversion and 40 degrees plantar flexion • Foot secured to plate with an M8 bolt into calcaneus and two heavy duty cable ties • 316 stainless steel triads - threaded insert embedded until no relative motion between triad and bone

4.5.1.1 Trial 1 – Sprain Platform Version Two, Foot Fixation and Marker Triad Fixation

The medial hard stop and universal joint of the collapsing platform were redesigned and manufactured, shown in Appendix D.1.2 Sprain Platform Assembly v.2. An additional posterior hard stop was also designed and implemented to reinforce the stopping power and reduce the load acting on the universal joint at the attachment point to the sprain platform. Similarly to the other hard stops the posterior hard stop was attached to the sprain platform by screwing it into a T-nut within the aluminium extrusion, additionally a corner bracket was placed under the other end of the hard stop to reinforce it.

Fixation of the specimen to the foot plate was first trialled using a heavy-duty cable tie around the talonavicular calcaneocuboid joint, shown in Figure 95. The marker triads were reproduced from 316 stainless steel with a modular design and a hexagonal insert to the grub screws, shown in Appendix D.2.2 Marker Triad Assembly v.2. The appropriate mass (15.5 kg) and drop height (0.4 m) previously estimated to generate sprain were used in this study, equating to 60.6 J of energy.

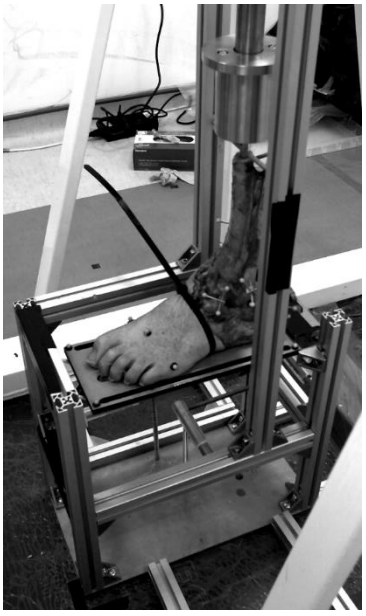

Figure 95. Sample one prepared for testing of the first trial.

4.5.1.1.1 Outcome

The cable tie fixing the specimen to the foot plate snapped upon impact with the hard stops. Marker triads were dislodged from the grub screws during the drop test. No damage to the universal joint occurred at the appropriate loading energy. The full impact may not however have been absorbed by the sprain platform due to the cable tie snapping and the foot sliding. Slippage of the specimen caused abnormal loading to occur within the intramedullary rod bending the intramedullary rod at the insertion to the specimen impactor.

4.5.1.2 Trial 2 – Foot Fixation and Marker Triad Fixation

A second heavy duty cable tie was used to reinforce the attachment of the specimen to the foot plate around the metatarsals, shown in Figure 96. Additionally, the fat pad distal to the calcaneus was removed by scalpel to allow for a 6 mm hole to be drilled into the distal surface of the calcaneus approximately 10 mm medial to the midline of the foot. An M8 bolt was inserted through the medial of the two central slots in the foot plate and into the hole in the calcaneus, shown in Figure 96. Two nuts positioned on the M8 bolt between the foot and the foot plate could be adjusted change the height of the rearfoot to correct for the removed fat pad.

To improve marker triad anchorage the grub screws were removed and the marker triads were inserted directly into the pilot holes. To facilitate this the triad arm with a hexagonal cross-section was replaced with another threaded triad arm, shown in Appendix D.2.3 Marker Triad Assembly v.3. The triads were screwed 3.5 mm into the pilot holes, equal to the threaded length of the triad arm. The damaged intramedullary rod was realigned and the drop test was repeated.

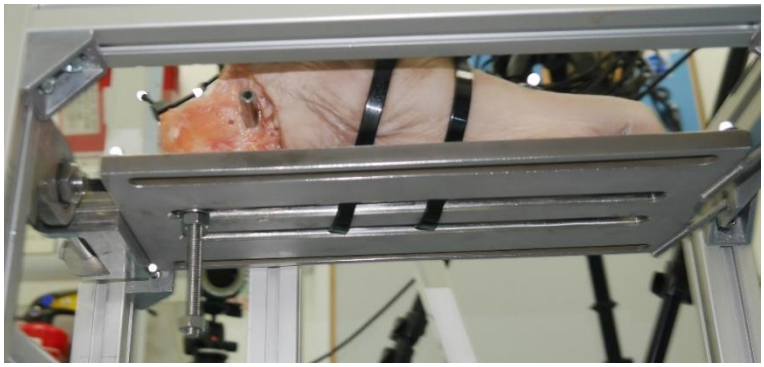

Figure 96. Sample one prepared for the second trial, with a bolt into the calcaneus for addition attachment to the foot plate.

4.5.1.2.1 Outcome

The improved fixation of the specimen to the foot plate proved to be sufficient with no visible slippage of the specimen. The threaded bar through the mediolateral hole in the intramedullary rod, responsible for restricting internal/external rotation of the tibia, was however severely bent. One of the T-nuts within the vertical supports appeared to catch within the aluminium extrusion during testing causing it to be jammed. The load transmitted from the specimen to the foot plate was therefore considerably lower than the anticipated 60.6 J energy. Anchorage of the marker triads was again insufficient with the marker triads into the tibia, fibula and talus falling out.

4.5.1.3 Trial 3 – Marker Triad Fixation

Marker triads were inserted by hand into the bone beyond the thread limit for this trial to improve their integration into the bone. Triads were screwed into bone until resistance was

felt for two full rotations of the marker triad and no relative motion between the triad and the bone occurred upon applied pressure. The threaded rod through the intramedullary rod was replaced and the drop test was repeated.

4.5.1.3.1 Outcome

All markers and triads remained fixed in place, no damage occurred to any parts of the sprain platform and no slippage of the sample occurred. Ligament rupture did not occur and no visible tearing of the ligaments was observed, shown in Figure 97.

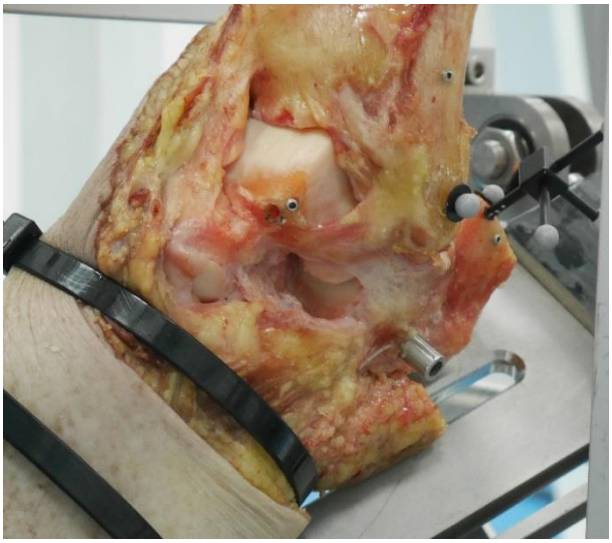

Figure 97. A specimen after drop test and the end point where no noticeable damage to the ligaments had occurred.

The biomechanical data for this sprain simulation trial is tabulated in Table 26 and graphed in Appendix E.1 Sample 1 Trial 3. Analysis of the motion capture data revealed that the foot plate plantar flexed 34.1 degrees, inverted 29.4 degrees and internally rotated 14.7 degrees. These values, below the anticipated ROM for the foot plate, did not cause macroscopic damage to the ligaments.

Table 26. The biomechanical data for the third trial of the first sample during the sprain simulation. Three-dimensional data is reported for each element of the foot, ankle and platform analysed. Min = the minimum value for the respective motion of the element analysed. A negative value represents the opposing motion to the one listed (negative dorsiflexion is positive plantar flexion). Max = the maximum value for the respective motion of the element analysed. ROM = range of motion of the element during the full sprain trial. PF = plantar flexion, INV = inversion and IR = internal rotation. * = data capture was not 100 %.

Element	Motion	Min (Degrees)	Max (Degrees)	ROM (Degrees)
Foot Plate	**PF**	-1.5	34.1	35.6
	INV	-1.5	29.4	30.8
	IR	2.1	14.7	12.6
Foot	**PF**	-0.7	37.3	38.0
	INV	-0.2	29.0	29.1
	IR	-4.6	13.2	17.8
Tibia	**PF**	-8.9	0.6	9.5
	INV	-3.8	2.4	6.2
	IR	-18.4	4.6	23.0
Calcaneus*	**PF**	1.3	50.1	48.8
	INV	-1.0	34.7	35.6
	IR	-10.8	14.0	24.8
Fibula	**PF**	-11.2	3.9	15.2
	INV	-0.6	8.2	8.8
	IR	-21.7	4.9	26.6
Talus*	**PF**	-21.9	18.4	40.3
	INV	-17.0	20.8	37.8
	IR	-17.8	5.5	23.3
Ankle Complex*	**PF**	1.2	57.7	56.5
	INV	-3.0	27.5	30.4
	IR	-11.1	20.1	31.2
Subtalar Joint*	**PF**	-4.5	34.9	39.4
	INV	-18.9	35.9	54.8
	IR	-15.3	12.3	27.7
Talocrural Joint*	**PF**	-20.7	19.9	40.6
	INV	-14.9	19.2	34.0
	IR	-8.9	3.2	12.1

The ankle complex can be split into its independent components of the subtalar and talocrural joints. At the subtalar joint 34.9 degrees of plantar flexion, 35.9 degrees of inversion and 12.3 degrees of internal rotation occurred. At the talocrural joint 19.9 degrees plantar flexion, 19.2 degrees inversion and 8.9 degrees of external rotation occurred. Not all the data was captured during the sprain trial for the subtalar and talocrural joints due to the talus marker triad not being fully tracked for the duration of the trial.

4.5.1.4 Trial 4 – Increased Loading Energy

A decision was made in the laboratory, since the BW load used for energy estimations was conservative, to increase the load applied to the specimen. The increased load experienced by the ligaments was expected to potentially cause damage to the lateral ankle ligaments which had survived loading at the previous lower value. The height from which the 15.5 kg mass was dropped from was increased to 0.8 m, equal to an energy of 121.6 J.

4.5.1.4.1 Outcome

In trial 4, the increased load caused a calcaneal fracture to occur at the insertion point of the M8 bolt into the calcaneus, shown in Figure 98. Subsequent to the calcaneal fracture, the two cable ties around the foot snapped causing the specimen to slip down the platform. The slippage and consequential change in the contact point of loading caused the intramedullary rod to bend near the insertion to the specimen impactor. The abnormal motion of the foot also meant that marker triad arms were bent during the test after collision with the foot plate and sprain platform.

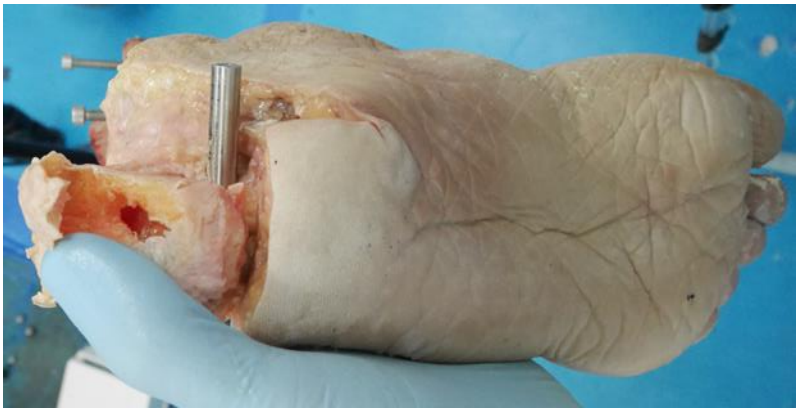

Figure 98. A failed specimen due to calcaneal fracture at the insertion point of an M8 bolt into the bone securing the specimen to the foot plate of the collapsing platform.

4.5.2 Sample 2

Following the catastrophic failure of the first sample, a second sample was assigned for the investigation into the simulation of LAS. Two trials are described in this section however only the second trial was performed with the second sample, the first trial did not use a specimen. The testing conditions of each trial are shown in Table 27.

Table 27. The testing conditions used for investigation of the simulation of LAS. Bolded text highlights the unique features of, or changes made between, trials.

	Testing Conditions
Trial 1	• **No applied force, plate fell under gravity** • **45 degrees inversion and 50 degrees plantar flexion** • **No specimen**
Trial 2	• 15.5 kg dropped from **0.4 m** equal to **60.6 J** energy • **45 degrees** inversion and **50 degrees** plantar flexion • **New hard stop design** • Foot secured to plate with an M8 bolt into calcaneus, **using a calcaneal mount**, and two heavy duty cable ties • 316 stainless steel triads - threaded insert embedded until no relative motion between triad and bone

4.5.2.1 Trial 1 – Increased Range of Motion

Due to an increased impact energy causing a calcaneal fracture in the fourth trial of the first sample increasing the ROM was explored as an alternative approach to cause rupture of the LCLs. The plantar flexion and inversion ROM were increased in an effort to induce LAS. The hard stops of the collapsing platform were repositioned to limit ROM to 50 degrees of plantar flexion and 45 degrees of inversion. No specimen was used, load was not applied to the foot plate and motion capture analysis was not performed in this trial. Golf tees were removed and the foot plate was held in its initial position, the foot plate was then released and allowed to fall under gravity.

4.5.2.1.1 Outcome

The repositioning of the hard stops prevented the plate from being able to travel the intended ROM. Multiple configurations of the medial and inferior hard stops were attempted. The anteromedial corner of the foot plate either collided with the medial hard stop, preventing the appropriate amount of inversion, or the foot plate swung above the medial hard stop, not limiting inversion at all.

4.5.2.2 Trial 2 – New Hard Stop

A new hard stop was manufactured specifically for testing of samples to 50 degrees of plantar flexion and 45 degrees of inversion, shown in Appendix D.1.16 Base Hard Stop. Although this removed somewhat a proportion of the adaptability of the sprain platform, it was deemed a necessary step towards a successful sprain trial. A section of dead rubber was duct taped to the surface of the hard stop to limit the vibrations of the foot plate upon impact with the hard stop, shown in Figure 99.

Figure 99. New hard stop manufactured to limit motion to 45 degrees of inversion and 50 degrees of plantar flexion.

Upon inspection of the sample used for this test it became clear that the previous sample fixation method would not be suitable. The width of the calcaneus was much smaller and did not cover either of the slots in the foot plate. A calcaneal mount was manufactured to attach the calcaneus to the foot plate affording the centralisation of the 6 mm hole drilled into the inferior side of the calcaneus, shown in Appendix D.1.17 Calcaneal Mount. The calcaneal mount was an essential part for smaller samples where a hole could not be drilled 10 mm medially to the midline of the foot. The release height of the mass carrier was returned to 0.4 m, equal to an energy of 60.6 J.

4.5.2.2.1 Outcome

Calcaneal fracture occurred once again followed by the subsequent failure of cable ties and slippage of the specimen. The results for this trial are shown in Table 28 and Appendix E.2 Sample 2 Trial 2. The foot plate plantar flexed 46.7 degrees, inverted 39.7 degrees and internally rotated 19.5 degrees. The foot itself plantar flexed 48.3 degrees, inverted 47.2 degrees and internally rotated 31.4 degrees. These figures are similar to the values the simulation was aiming to replicate. Once again, on visual inspection, the ankle ligaments remained intact.

Table 28. The biomechanical data for the second trial of the second sample during the sprain simulation. Three-dimensional data is reported for each element of the foot, ankle and platform analysed. Min = the minimum value for the respective motion of the element analysed. A negative value represents the opposing motion to the one listed (negative dorsiflexion is positive plantar flexion). Max = the maximum value for the respective motion of the element analysed. ROM = range of motion of the element during the full sprain trial. PF = plantar flexion, INV = inversion and IR = internal rotation. * = data capture was not 100 %.

Element	Motion	Min (Degrees)	Max (Degrees)	ROM (Degrees)
Foot Plate	**PF**	-0.8	46.7	47.5
	INV	0.0	39.7	39.8
	IR	-2.8	19.5	22.3
Foot	**PF**	-0.4	48.3	48.8
	INV	0.0	47.2	47.2
	IR	-7.3	31.4	38.8
Tibia	**PF**	-15.9	1.4	17.2
	INV	-5.1	3.8	8.9
	IR	-14.5	0.8	15.3
Calcaneus	**PF**	-0.0	63.0	63.0
	INV	-3.1	30.6	33.7
	IR	-4.6	15.9	20.5
Fibula	**PF**	-8.4	6.3	14.7
	INV	-6.3	15.5	21.8
	IR	-16.4	20.8	37.1
Talus	**PF**	-10.3	34.0	44.4
	INV	-3.6	54.0	57.6
	IR	-14.2	23.5	37.7
Ankle	**PF**	-0.1	68.6	68.7
Complex	**INV**	-6.9	28.2	35.2
	IR	0.0	22.4	22.4
Subtalar	**PF**	-0.1	42.8	43.0
	INV	-14.9	11.3	26.3
	IR	-50.0	12.8	62.8
Talocrural	**PF**	-5.9	44.8	50.6
	INV	-5.4	50.7	56.1
	IR	-9.1	38.1	47.1

4.6 General Discussion

Although severe sprain was not simulated successfully in this study a sprain platform capable of replicating the ROM associated with lateral, syndesmosis and potentially medial sprain was produced. The sprain platform went through many design iterations throughout this study, capitalising on the adaptable nature afforded by the modularity of the design. The second version of the platform, shown in Appendix D.1.2 Sprain Platform Assembly v.2, is a robust and effective collapsing platform for various general investigations into ankle motion under low loads at angles up to 45 degrees of plantar flexion and inversion. For investigations into ankle motion greater than 45 degrees plantar flexion and inversion a design similar to the third version, shown in Appendix D.1.3 Sprain Platform Assembly v.3, would be required with a hard stop designed for the specific angles to be investigated.

The trial closest to simulating LAS was the third trial of the first sample where no damage occurred to the sprain platform, intramedullary rod, marker triads nor the bones. Ligament rupture was however not initiated during the trial. Analysis of the foot plate ROM determined the foot plate to plantar flex, invert and internally rotate by 34.1 degrees, 29.4 degrees and 14.7 degrees, respectively. These values, below the anticipated ROM for the foot plate, could explain why no macroscopic damage to the ligaments was observed. A possible explanation for the plate not achieving the desired plantar flexion and inversion ROM could be that the natural tissue was providing a greater level of resistance against the natural motion of the plate than expected. Alternatively, the load applied could have been insufficient to drive the ankle complex and attached foot plate through to the desired termination point. There was however no guarantee that rupture of the lateral ankle ligaments would occur even at the expected ROM angles. The unknown nature of the biomechanics of severe LAS at the initiation of this study posed a significant challenge for the effective simulation of LAS. The estimated loads and ROM used in this study were perhaps too conservative to generate ligament rupture, given they were made using data associated to mild LAS.

The ROM of the foot plate dictates the ROM of the foot and the ankle complex, all of which were expected to be equal. Both the foot and ankle complex achieved greater plantar flexion ROM than the foot plate by 3.2 degrees and 23.6 degrees, respectively, in the third trial of the first sample. The considerably higher plantar flexion ROM for the ankle complex was investigated further. Firstly, the tibia was determined to have dorsiflexed 8.9 degrees during this trial, possibly caused by minor anterior slippage of the calcaneus relative to the foot plate. Dorsiflexion of the tibia translates to additional plantar flexion of the ankle complex as it is calculated using the motion of the calcaneal marker triad relative to the tibial marker triad. This 8.9 degrees alone is not sufficient to cause the 23.6 degree increase in plantar flexion between the ankle complex and the foot plate. The calcaneal marker triad plantar flexed 50.1 degrees which is considerably higher than expected given the calcaneus is fixed to the foot plate, which only plantar flexed 34.1 degrees. A small amount of relative ROM between the

calcaneus and the foot plate could have occurred, however the amount would have been minimal and certainly not accountable for the 16.0 degree increase in plantar flexion between the foot plate and calcaneus. Relative motion between the calcaneus and the calcaneal marker triad is therefore likely responsible for this discrepancy due to inadequate fixation of the marker triad into the calcaneus. This theory would also explain why the data tends to a steady-state value after impact with the hard stops of approximately 46.0 degrees, shown in Figure 100.

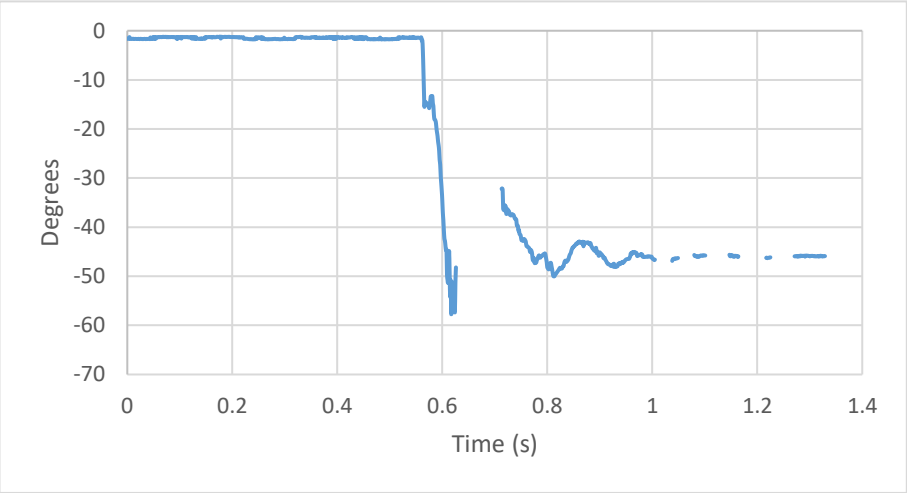

Figure 100. The plantar flexion of the ankle complex during the sprain simulation trial.

A period of missing data occurred for the talus in the third trial of the first sample. It is likely that a marker of the talar triad was not within view of at least two cameras at the points no data was captured due to the foot or framework of the sprain platform obstructing the view. The ability of the motion capture system to capture all data is imperative to the success of this study as all sprain trials, unlike most biomechanics studies, were intended to be single attempt tests to failure.

The increase in load between the third and fourth trial of the first sample, performed as the load estimates were likely lower than required for severe LAS, was considerable. The load was increased to approximately the maximum capacity of the drop weight rig (121.6 J) causing calcaneal fracture. Upon reflection a more measured approach whereby the load was perhaps scaled up using BW would have been more appropriate, given the considerably higher BW of the donor (97.5 kg) compared to the BW used for the estimations (60.0 kg). The maximum load capacity was used however with the aim of determining whether the maximum load was capable of initiating ligament rupture, it was not foreseen that bone fracture would occur prior to ligament rupture. Ligament rupture did not occur in the final trial however this could be expected as the calcaneal fracture would have prevented the full load from being transmitted through the lateral ankle ligaments. Had the fracture not occurred rupture of the ligaments was still not a certainty given the biomechanics of severe LAS are unknown.

The final trial in this study was performed after reducing the load to 60.6 J, where previously no damage occurred to the first sample, yet a calcaneal fracture occurred again. This could possibly highlight the large variability which is associated with natural tissue testing. The two samples were however from considerably different donors with the first sample being from a 97.5 kg donor with a BMI of 29.1 whereas the second sample was from a 40.8 kg donor with a BMI of 14.4 $kg.m^{-2}$. The second sample was also much smaller than the first, therefore the amount of bone between the calcaneal bolt and the cortical shell was reduced. Both the donor BMI and the amount of bone stock could provide an explanation for the difference observed between samples at the lower load of 60.6 J. Alternatively, the outcome could be due to differing mechanics of each trial, shown in Figure 101. In the final trial the calcaneus plantar flexed 63 degrees compared to 50 degrees in the third trial of the first sample. The increased plantar flexion ROM would have caused an increased anterodistal force in the final trial (44.1 J compared to 34.0 J). This load would be absorbed by the calcaneal bone posterior to the M8 bolt. The use of a bolt into the calcaneus was the most effective way to attach the sample to the foot plate while still being able to track the biomechanical data. The abnormal loading through the calcaneus did however result in the failure of the simulation and therefore its effectiveness as a fixation method of the sample to the foot plate is questionable.

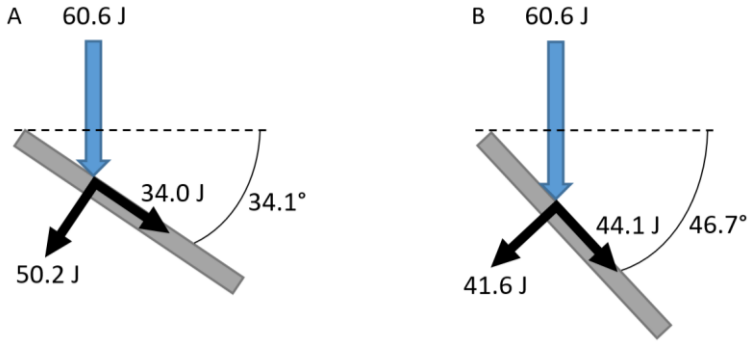

Figure 101. Schematic of the resolved angles for A) the third trial of the first sample and B) the second trial of the second sample. Grey bar = foot plate.

Had LAS been simulated successfully, ligament strain data could have been collected during the simulation of LAS. Such analysis would require further experimental equipment such as buckle transducers previously used for this purpose (Best et al., 2016). Additionally, it would have been beneficial to have imaged the ligaments before and after the simulation of LAS to identify potential microscale damaged to the ligaments or lower grade ligament sprains. Imaging of samples was explored using either MRI or ultrasound. Imaging facilities were however not available during the time of this project due to a shortage of radiographers at the local facility and the author did not possess the required skills to confidently perform the imaging. Analysis of joint stability using drawer tests, typically performed during clinical assessment, was alternatively planned to be performed before and after successful simulation of LAS, detailed in Chapter 5 Stability Assessment.

Insight and lessons learnt from this study can be used to guide future studies into the cadaveric simulation of ankle sprain. A conceptual specification is proposed by the author for those wishing to attempt to replicate LAS in cadaveric tissue in the future based on the experiences of this study, shown in Table 29.

Table 29. A conceptual specification for future simulations of severe LAS. Bold text indicates where the values have changed from the original device specification. PF = platar flexion, INV = inversion, IR = internal rotation and deg = degrees.

	Essential	**Desirable**
Range of Motion		
Maximum PF (deg)	50	60
PF velocity (deg.s^{-1})	>370	Up to 1240
Maximum INV (deg)	**90**	150
INV velocity (deg.s^{-1})	>559	Up to 1752
Maximum IR (deg)	30	60
IR velocity (deg.s^{-1})	>271	Up to 690
Load		
Load capacity (kg.f)	60	160
Rate of loading	Causes rotational velocity >600 deg.s^{-1}	Causes rotational velocity up to 1752 deg.s^{-1}
Independent loading rates for each motion		✓
Scale of load (kg)	5	0.1
Motion Capture		
Capture rate (Hz)	**500**	**≥1000**

The only alterations to the original device specification are an increased degree of inversion motion and a higher capture rate for motion capture. The simulation of sprain configured in this project had the capacity to meet the essential requirements of the conceptual specification. Unfortunately, a lack of resource and time prevented the full exploration into the capacity of the sprain simulation developed in this project. There are however several considerations the author would recommend for future researchers of severe LAS. Firstly, when simulating ankle sprain with cadaver tissue, which is inherently variable, the loading device used should be capable of adapting the load applied based on a feedback loop. The ElectroPuls E10000 and robotic arm devices have previously been used to apply loads to the

ankle joint (Viens et al., 2014; El. Daou et al., 2018). Such devices allow for greater control over the loading capacity and rate of loading applied to individual samples. The loads applied could perhaps be scaled between samples using the foot size of the sample or BMI of the donor, previously determined in this project to affect the strength of the LCL complex.

Secondly, a less severe dissection protocol than that adopted in this study would be beneficial where the desire is to understand the natural response more accurately. As much of the joint capsule, soft tissue and fascia should be retained as possible in such circumstances. This study however sought the contributions of the lateral ankle ligaments only and required the visualisation of the LCL complex, given the lack of an imaging technique to identify ligament rupture. Retaining the joint capsule has the additional benefit of retaining the synovial fluid within the joints for lubrication.

Thirdly, the author believes LAS to be too broad a term. Future researchers would benefit from an increased specificity and should hypothesise which ligaments they aim to severely rupture. Whilst the required biomechanics are currently somewhat unknown, should they become known in the future the researcher should aim to replicate the exact motion first as a proof of concept study.

Fourthly, when performing optical motion capture analysis of cadaver tissue firm implantation of the marker triads is essential to successful capture. This was achieved in this study through the implantation of a rigid bone pin directly into the bone until no relative motion between the bone pin and bone occurred upon applied pressure. Optical motion analysis was effective for the analysis of ankle complex joint motion at the high rates of loading in this study. The use of optimal motion capture for the catastrophic testing performed in this study did however raise some concerns when data was not captured at a 100 % success rate. This could be avoided with the careful and considered placement of motion capture cameras and regular inspection of reflective markers for damage/saturation. The use of the chosen optical motion capture system prevented regular hydration of the sample after placement of the reflective markers. For sprain simulation testing this was not considered an issue as the testing occurred over a short length of time. This factor should however be considered for longer tests performed using optical motion capture.

Finally, medical imaging in the form of ultrasound or MRI should be performed to validate the simulation of sprain and to confirm complete rupture of the ligament. This would also aid in the reduction of soft tissue dissection previously discussed.

4.7 Conclusion

A sprain platform was developed capable of replicating the ROM associated with LAS. The simulation of LAS motion provided insight into the contributions of the talocrural and subtalar joints to the ROM of the ankle during such motions. A reproducible simulation of severe LAS was not achieved and therefore an alternative approach to identify the stability changes due

to severe LAS was explored within the following chapter. Finally, advice to future researchers wishing to simulate ankle sprain with cadaver tissue is described.

Chapter 5 – Joint Stability and Suture Tape Analysis

5.1 Introduction

A study based on surgically sectioning specific ligaments was devised for the stability analysis of the ankle complex following the inconsistent results for the simulation of sprain. A sectioning study allowed individual ligaments to be consistently damaged and their contributions to lateral ankle stability to be evaluated. This chapter has two parts, the first part explores the changes in lateral ankle stability due to the sequential sectioning of the ATFL and CFL. Subsequently, the analysis of synthetic surgical interventions for LAS to restore joint stability are also investigated within this section. The second section characterises the current implantation methods for synthetic surgical interventions for LAS.

5.2 The Effect of Lateral Ankle Sprain on Joint Stability and the Effectiveness of Synthetic Interventions in Restoring Joint Stability

5.2.1 Introduction

The typical ankle sprain injury pathway is believed to be primary injury to the ATFL, followed by damage to the CFL and in extreme circumstances injury to the PTFL (Colville et al., 1990). Ligament sprains are graded as mild, moderate and severe, as described in Chapter 1 Ligament Failure Mechanisms. Grade III ankle sprain describes a complete rupture of a ligament. Ankle sprain can be diagnosed in multiple ways including: clinical examination, the AOFAS Ankle-Hindfoot Scale, Karlsson score, VAS score, talar tilt tests and anterior drawer stress radiographs (Song et al., 2019).

Stress tests are commonly performed by clinicians and physiotherapists to assess the stability of the ankle and to assess whether a sprain has occurred. Commonly anterior drawer and talar tilt tests or an anterolateral drawer test is performed (Song et al., 2019). In an anterior drawer test, the clinician applies an anterior force to the hindfoot with one hand while the other hand restrains the distal tibia. Similarly, a talar tilt test involves restraining the distal tibia with one hand while applying an inversion force with the other. The anterolateral drawer test is similar to the anterior drawer test however the foot is allowed to internally rotate in addition to the anterior force applied to the hindfoot. This prevents potential restriction of anterior displacement due to the medial ligaments of the ankle complex. There is evidence that the anterolateral drawer test is superior to the anterior drawer test when assessing lateral ankle stability (Phisitkul et al., 2009; Miller et al., 2016). Stress radiographs and stress ultrasonography have also both been used to quantitatively assess ankle stability during stress tests. It was determined that for healthy participants, no more than 3 mm of anterior talar translation and no more than 18 degrees of talar tilt should occur under loads of 95 N and 20 Nm, respectively (Seligson et al., 1980). The figure of 3 mm of distal translation has been

longstanding and is often quoted as a threshold for ankle instability when performing a clinical diagnosis.

Alternatively others have developed testing machines to assess the stability of the ankle for both living patients and cadaveric tissue (Kerkhoffs et al., 2005; Kovaleski et al., 2014). These devices are typically used in research settings to quantify joint stability, without the need of imaging equipment, where a consistent and measurable load can be applied. Kovaleski et al. (2014) used an ankle arthrometer, shown in Figure 102A, to analyse anterior and inversion drawer ROM when loads of 125 N and 4 N.m torque were applied, respectively (Kovaleski et al., 2014). Samples were tested intact, after sectioning of the ATFL and after combined sectioning of the ATFL and CFL to investigate stability changes after sequential sectioning of the lateral ankle ligaments (Kovaleski et al., 2014). Kerkhoffs et al. (2005) used a custom device, shown in Figure 102B, to analyse anterior displacement, applying 150 N anterior load through the ankle. In cadaver testing anterior drawer tests were performed on intact, ATFL sectioned, combined ATFL and CFL sectioned and combined ATFL, CFL and PTFL sectioned samples (Kerkhoffs et al., 2005).

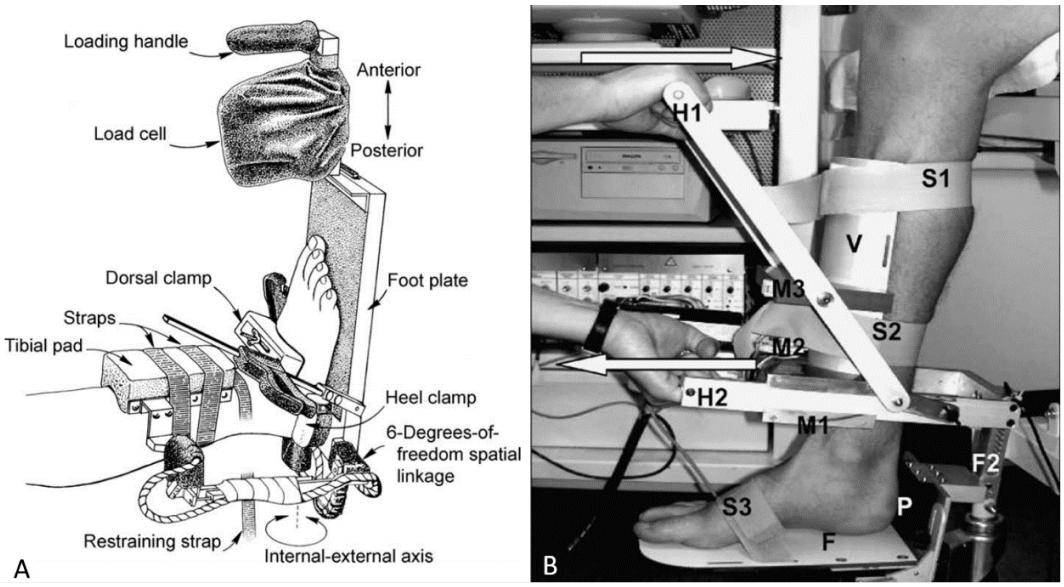

Figure 102. A) An ankle arthrometer developed to assess ankle ROM (Kovaleski et al., 2014). B) A quantitative anterior ankle tester to assess anterior displacement in patients and cadavers (Kerkhoffs et al., 2005).

Following an ankle sprain, should the ankle complex be determined to be unstable, conservative treatment options are first explored, detailed in Chapter 1 Conservative Treatment. Initial treatments focus on reducing inflammation and healing but typically, if after three to six months the ankle complex stability is not restored through conservative treatments or a Grade III severe ankle sprain occurs, surgical treatment can be required (Song et al., 2019). Synthetic interventions gained popularity during the 1980s and 1990s and were explored as replacement ligaments. Long-term follow-up studies of synthetic interventions highlighted poor outcomes and high incidence of complications leading to a rapid decline in

the use of synthetic interventions for ankle ligament repair in the 1990s (Wredmark and Engström, 1993; Miller et al., 2006; Chen et al., 2015; Tourné and Mabit, 2017).

The modified Broström procedure has been considered the gold standard technique for ligament repair for over 50 years (Song et al., 2019). The modified Broström procedure has however been determined to be approximately half the strength of native ATFL (Waldrop et al., 2012; Viens et al., 2014). Patients who have generalised ligament laxity have been shown to have an increased laxity over time after a modified Broström procedure (Xu and Lee, 2016). The repaired ligament stretches under load as the weaker collagen crosslinks do not regenerate and remodel sufficiently to pre-injury levels (Hauser and Dolan, 2011). Synthetic interventions have experienced a recent resurgence, however rather than being a synthetic ligament in their own right they are usually used to augment a natural tissue repair, shown in Figure 103 (Viens et al., 2014; Coetzee et al., 2018). Currently, to the author's knowledge, the InternalBrace (Arthrex Inc, Naples, FL, USA) is the only synthetic intervention routinely used for lateral ankle repair, with a large amount of research-based evidence (Waldrop et al., 2012; Viens et al., 2014; Schuh et al., 2016; Yoo and Yang, 2016; Coetzee et al., 2018; Cho et al., 2019; Boey et al., 2019; Xu et al., 2019). A Broström repair with InternalBrace ligament augmentation (Arthrex Inc, Naples, FL, USA) boasts strengths surpassing that of the native ATFL, earlier mobility during recovery and quicker return to activity (Viens et al., 2014; Coetzee et al., 2018). The InternalBrace prevents over-stretching of the repaired ligament acting as a static brace of the ATFL, shown in Figure 103.

Figure 103. An illustration of a Broström repair augmented with InternalBrace (Arthrex Inc, Naples, FL, USA). Source: (https://www.arthrex.com/foot-ankle/open-brostrom. Accessed: 27/09/2020).

The industrial sponsors of this project (Xiros Ltd, Leeds, UK) have developed their own suture tape, currently used for surgical applications in the shoulder, with the potential to be used for ankle ligament repair. The 3 mm Infinity-Lock tube tape (Xiros Ltd, Leeds, UK) has an open weave structure allowing for cell infiltration within the suture tape, shown in Figure 104. Xiros have characterised the synthetic ligament in-house and analysed suture anchor fixation of the

synthetic within Sawbone models. No testing of the product had however previously been performed in animal or human tissue.

Figure 104. The Infinity-Lock tube tape produced by Xiros. Source: (https://www.neoligaments.com/product/infinity-lock/. Accessed: 27/09/2020)

The first aim of this study was to analyse the change in ankle stability (anterior translation and inversion rotation) after sequential sectioning of the lateral ankle ligaments in human cadaveric samples. The second aim was to evaluate the capability of synthetic interventions to restore ankle joint stability after rupture of the ATFL and CFL.

5.2.2 Materials and Methods

5.2.2.1 Samples

Six fresh frozen human cadaver feet were procured for use in this study from MedCure (USA). Ethical approval was granted by the University of Leeds Research Ethics Committee (MEEC 15-020). Exclusion criteria for the tissues included a reported prior lower limb trauma or surgery, or a history of diabetes. A summary of donor information is shown in Table 30.

Table 30. Tissue donor demographic details. The mean and standard deviation (SD) is given for age, weight and BMI. (M = male, F = female, R = right & L = left).

Sample	Age (years)	Sex	L/R Foot	Weight (kg)	BMI (kg.m^{-2})
1	49	F	L	48.5	20.9
2	38	M	R	85.3	27.0
3	61	M	R	65.8	21.4
4	57	F	L	55.3	19.7
5	33	M	L	50.8	19.2
6	49	F	R	54.0	18.1
Mean ± SD	47.8 ± 10.7	-	-	60.0 ± 13.8	21.1 ± 3.1

5.2.2.2 Sample Preparation

The samples were stored in a -40 °C freezer, compliant with the Human Tissue Act, until they were tested. Samples were thawed for 48 hours at 6 °C in a refrigerator prior to dissection. The sample preparation for this study was identical to the procedure described in Chapter 4 Sample Preparation for the second sample, with the exception of the 6 mm diameter hole drilled into the distal surface of the calcaneus not being performed in this study. Once dissected, the samples were stored in a 6 °C refrigerator overnight and testing commenced the following day. The samples were soaked in PBS (Oxoid Ltd, Basingstoke, UK) for 30 minutes to rehydrate the sample while the motion capture system was calibrated.

5.2.2.3 Motion Capture

5.2.2.3.1 Foot Model

The six segment model (tibia, fibula, talus, calcaneus, foot and foot plate) described in the Foot Model section of Chapter 4 was used to analyse joint kinematics in this study. Twenty-two 6.5 mm passive markers were screwed onto the marker triads and anatomical markers. Marker triads were implanted directly into the bone and anatomical markers affixed using double sided tape, as described for the second sample in the Simulation of Sprain section of Chapter 4.

5.2.2.3.2 Data Collection

A six Miqus M3 camera 3D infrared passive marker motion capture system, intergrated with one Miqus video camera (Qualisys AB, Gothenburg, Sweden), was configured and calibrated as described in Chapter 4 Data Collection. The average standard deviation of the calibration wand length across all trials was 0.08 mm, ranging from 0.064 mm to 0.094 mm.

The specimen was attached to the sprain platform and drop rig following the methods described in the Simulation of Sprain section of Chapter 4. The vertical pole and vertical supports of the sprain platform prevented tibial motion in all directions except inferior and superior translation, shown in Figure 105. Metal bolts replaced golf tees to support the foot plate throughout testing to prevent accidental giving way of the platform.

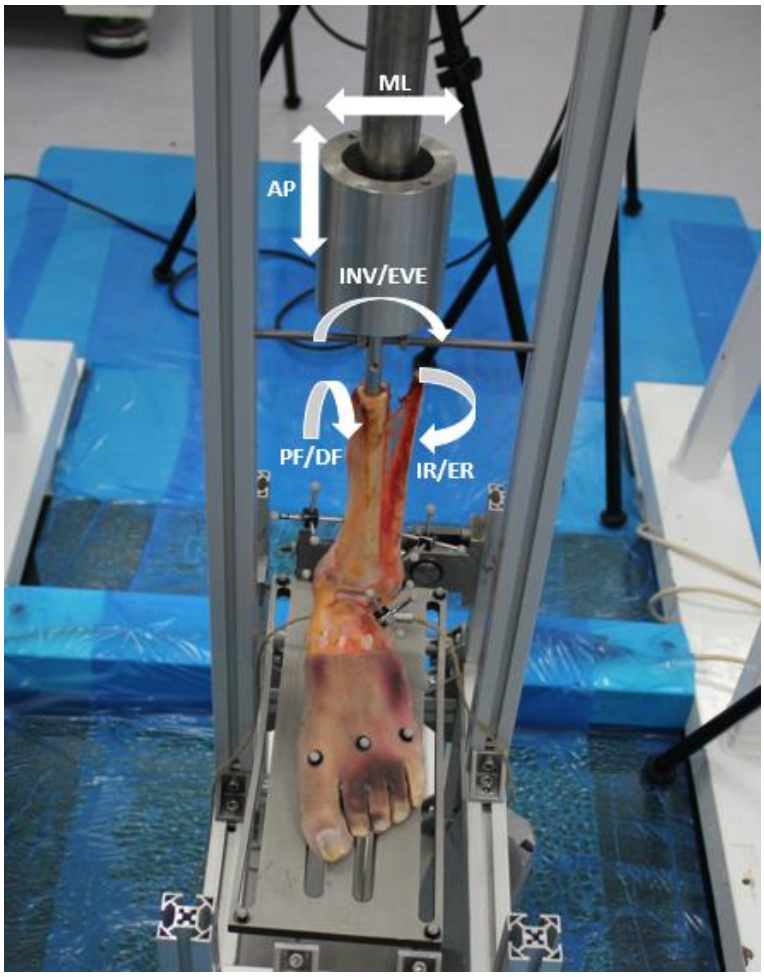

Figure 105. The motions of the tibia restricted by the vertical supports of the sprain platform and the vertical pole of the drop rig. AP = anterior-posterior displacement, ML = medial-lateral displacement, PF/DF = dorsi-/plantar flexion, INV/EVE = inversion/eversion and IR/ER = internal/external rotation.

5.2.2.3.3 Stability Assessment

Stability of the ankle was assessed through four motion drawer stress tests including anterior, posterior, inversion and eversion drawer tests. Once positioned on the sprain platform with all of the markers attached to the sample, the first set of stability analysis tests were performed for the intact specimen, shown in Figure 106.

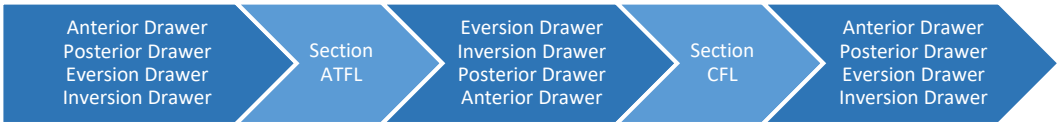

Figure 106. The testing protocol pathway describing the order of stability analyses and ligament sectioning.

A static trial was captured prior to the dynamic trial performed for each drawer test. During the static trial the foot was relaxed in the neutral position (zero degrees on dorsi-/plantar flexion, inversion/eversion and internal/external rotation) and no load was applied to the sample. Each drawer test was performed three times within a dynamic trial to improve the accuracy of the test consistency. At the end of each dynamic trial, the data was briefly analysed to ensure a 100 % capture rate and if data was missing the drawer test was repeated.

A load of 10 kg.f (98.1 N) was applied to the sample using a spring balance for the anterior and posterior drawer tests. The load value was selected based on previously published stability analysis literature (Seligson et al., 1980; Kovaleski et al., 2014). The spring balance was attached to the tube through the calcaneal tube with strong twine, shown in Figure 107. Twine was chosen due to its flexibility, resistance to stretching and cost-efficiency as it was required to be disposed of as clinical waste after contacting human tissue.

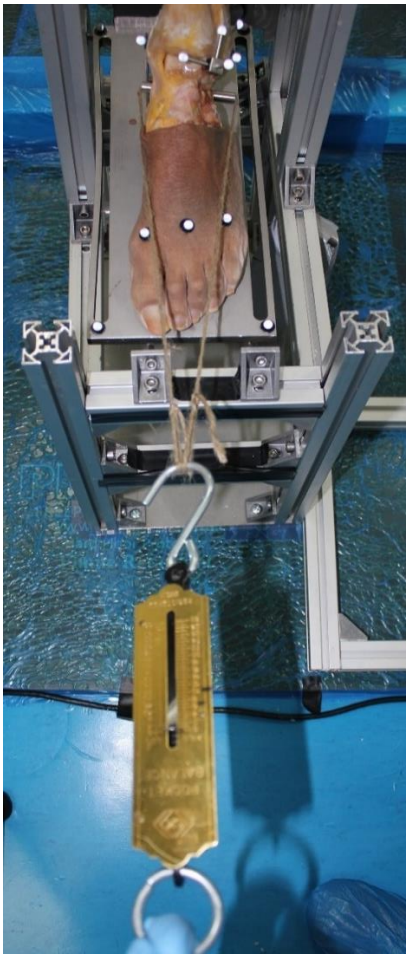

Figure 107. Test setup for an anterior drawer test. A calibrated spring balance is used to apply a load of 10 kg.f to the ankle through the calcaneus.

For the eversion and inversion drawer tests the twine was removed from the calcaneal tube and a custom calcaneal attachment was connected using two 4.9 mm diameter 316 stainless steel pins, shown in Figure 108 and Appendix F – Torque Adapter. A 4 N.m torque load was applied to the specimens using a calibrated dial torque wrench for both the eversion and inversion drawer tests, based on loading values previously used (Kovaleski et al., 2014). During inversion and eversion drawer tests the sample was elevated slightly, by no more than 30 mm, to allow for clearance of the foot, calcaneal tube and calcaneal adapter from the foot plate.

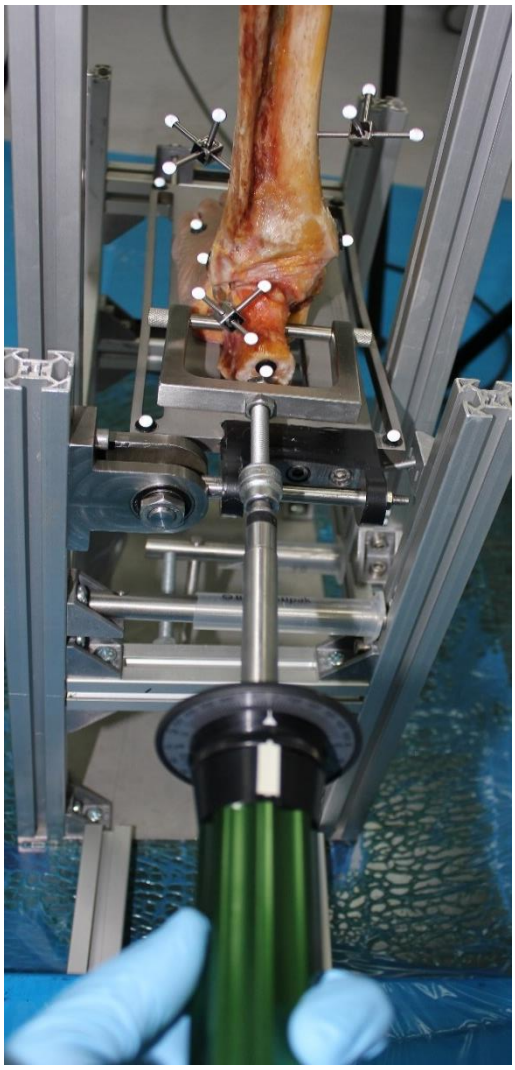

Figure 108. Test setup for an inversion or eversion drawer test. A calibrated dial torque wrench, connected to the calcaneal tube, is used to apply a torque load of 4 N.m to the ankle through the calcaneus.

Following the first set of drawer tests, the ATFL was sectioned with a scalpel. One clean cut was made centrally through the cross-section of the ATFL, shown in Figure 109A. The drawer tests were repeated for the ATFL damage condition. The order of the drawer tests was changed to be eversion drawer, inversion drawer, posterior drawer and anterior drawer (see Figure 106) to improve the efficiency of the testing and reduce the time the sample spent exposed to the dry air. Similarly to the ATFL, the CFL was sectioned with a scalpel, shown in Figure 109B, and the drawer tests were performed a further time in the original order. The

intramedullary rod, marker triads and calcaneal tube were removed and samples were stored in a -20 °C freezer prior to any further testing.

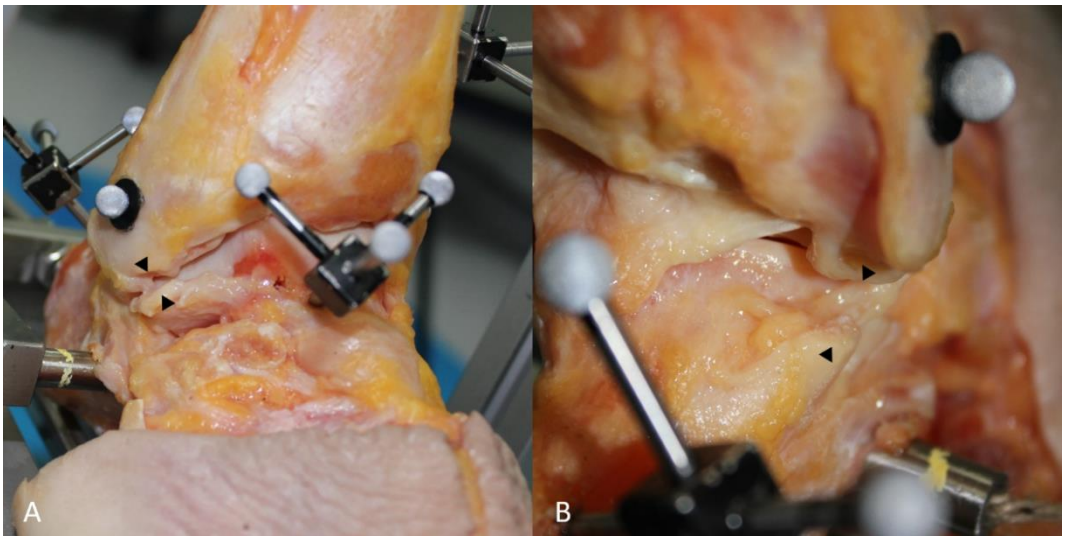

Figure 109. Samples after sectioning of the ATFL (A) and CFL (B). Black arrowheads indicate the where the ligament was sectioned.

5.2.2.3.4 Data Processing

The kinematic data was exported from QTM (Qualisys AB, Gothenburg, Sweden) as a .c3d file and imported into Visual3D (C-Motion, Maryland, USA). Kinematic data was filtered using a low pass Butterworth filter at 6Hz.

5.2.2.4 Suture Tape Repair Surgical Procedure

5.2.2.4.1 Method Development

Repair of the sectioned samples was explored using a synthetic intervention produced by the industrial sponsor of this project. A 3 mm wide synthetic Infinity-Lock suture tape was proposed by the industrial sponsors as an appropriate synthetic intervention for LAS. Although no surgical technique had been determined, fixation of the Infinity-Lock suture tape had been explored by Xiros using a custom SawBone model, previously used by Arthrex Inc, shown in Appendix G.1 Arthrex White Paper 1. The SawBone model was suggested to replicate the densities of human bone with a 40 mm thick lower density (160 $kg.m^{-3}$) region surrounded by two 3 mm thick layers of higher density (320 $kg.m^{-3}$) Sawbone. During their testing, Xiros had successfully implanted the Infinity-Lock suture into the Sawbone model using SwiveLock suture anchors (Arthrex Inc, Naples, FL, USA).

After consultation with the industrial sponsor and a foot and ankle specialist clinical fellow the Broström repair with InternalBrace ligament augmentation procedure was selected as the surgical procedure to be followed. Particularly important to the decision was that the technique was being performed in practice, the surgeon was trained in the technique and the Infinity-Lock suture tape had successfully been implanted into Sawbone using SwiveLock

suture anchors. The suture tape was secured in the talus by a foot and ankle specialist clinical fellow orthopaedic surgeon using a 4.75 x 19.1 mm SwiveLock suture anchor and in the fibula using a 3.5 x 15.8 mm SwiveLock suture anchor.

Upon implantation of the Infinity-Lock suture tape using SwiveLock suture anchors it became evident that the suture anchors were not suitable. Excessive force was required to implant the suture tape into human bone using both the 3.5 x 15.8 mm and 4.75 x 19.1 mm suture anchors. In an attempt to utilise the suture anchors with the Infinity-Lock suture tape the pilot holes were reamed to accommodate the thicker suture tape than the technique was developed for. The suture tapes were then able to be implanted into human bone under excessive force. During implantation the thread of the suture anchor struggled to engage with the bone due to the thickness of the suture tape and/or the widening of the pilot hole, causing the suture anchor to rotate without progressing into the bone at times. This action under high torque loads caused fraying of the suture tape to occur, shown in Figure 110. The strength of the fixation was also low failing under a weak inversion load applied by the surgeon.

Figure 110. A failed ATFL suture tape augmentation using the Infinity-Lock suture tape (Xiros, Ltd, Leeds, UK). Visible fraying of the suture tape is noticeable where the suture tape was originally seated in the fibula.

5.2.2.4.1.1 Outcomes

- The 3 mm Infinity-Lock suture tape (Xiros Ltd, Leeds, UK) could not be implanted into human tissue following the previously described method due to the thickness of the suture tape (Viens et al., 2014).
- Larger pilot holes afforded the implantation of the suture anchors (SwiveLock, Arthrex Inc, Naples, FL, USA) upon excessive force but caused the suture tape to fray, shown in Figure 110. A larger pilot hole and/or the thickness of the suture tape caused the suture anchor to rotate within the pilot hole rather than screw into the bone. Once implanted the fixation failed under a small inversion load applied by the surgeon.

5.2.2.4.2 Main Study

In order to achieve the second aim of the study to evaluate the stability restorative capacity of synthetic interventions for severe LAS a decision was made to use an alternative suture tape (InternalBrace). Although, these findings would not directly benefit the industrial sponsors of this project they could provide argument for the use of synthetic interventions in the ankle. Devices were sourced from a company specialising in the sale of medical devices (eSutures, USA) and from the wastage stock of a local hospital. Some devices were expired products with one suture anchor expiring 17 months before use. All other devices used in this study had expired within 12 months of the study taking place or were still valid.

The synthetic repair procedure was performed by a foot and ankle specialist clinical fellow orthopaedic surgeon on all six samples in this study. The samples were removed from the -20°C freezer and defrosted within a 6 °C fridge for 24 hours. The suture tape augmentation procedure performed was similar to that detailed in previously published literature, with the exception of the soft tissue repair (Viens et al., 2014). The soft tissue repair was omitted to establish the stability contributions of the suture tape alone to the augmentation procedure. The foot was positioned in a neutral position, as previously defined, and secured with a guidewire inserted through the tibia, talus and calcaneus, shown in Figure 111.

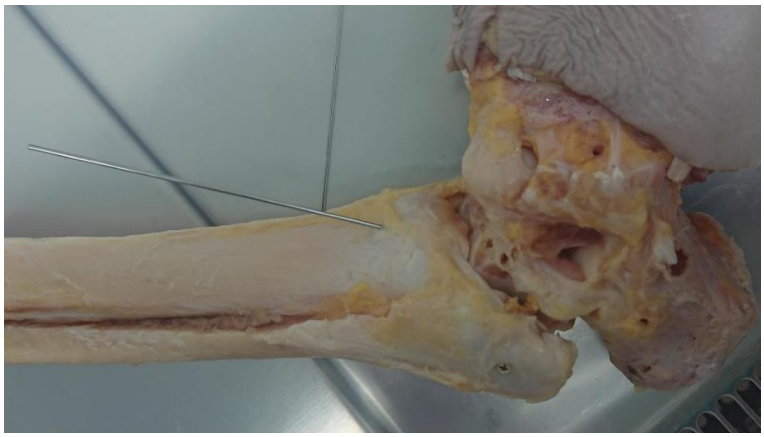

Figure 111. A sample fixed in the neutral position with a guidewire through the tibia, talus and into the calcaneus.

The surgeon does not typically repair the CFL as this is not felt to improve surgical outcomes, however a recent review suggested repair to both the ATFL and CFL should be considered (Song et al., 2019). Opposed to the suggested technique documented on the Arthrex website repair of the ATFL and CFL was performed individually, rather than as a combined augmentation, due to the preference of the surgeon performing the procedure (Arthrex, 2017). The procedures differ with respect to the fibular insertion(s), with the combined approach using one anchor into the fibular for both the ATFL and CFL augmentations and the technique followed in this study having separate fibular anchors for the ATFL and CFL augmentations. It was the opinion of the surgeon that the individual repair allowed for an anatomical repair of both the ATFL and CFL rather than a compromised positioning of the

fibular bone anchor. To the knowledge of the author no literature exists however investigating the strength, stability or biomechanical difference between the procedures.

5.2.2.4.2.1 Anterior Talofibular Ligament Repair

The ATFL was repaired first, a 2.7 mm tunnel was drilled into the talus at the insertion point of the ATFL and a 3.4 mm tunnel at the origin of the ATFL into the fibula. The drilled tunnels were then tapped with a 3.5 mm and 4.75 mm tap (Arthrex Inc, Naples, FL, USA) into the talus and fibula, respectively. A 3.5 x 15.8 mm SwiveLock suture anchor was loaded with a 2 mm wide InternalBrace suture tape. The InternalBrace is a braided ultra-high molecular weight polyethylene (UHMWPE) and polyester suture tape. The anchor was seated into the talus and progressed into the tapped hole until sufficient tension was achieved, signified by an audible squeaking of the suture anchor in the tunnel. The anchor was implanted to be flush with the surface of the bone. A 4.75 x 19.1 mm SwiveLock suture anchor was then loaded with one of the strands of InternalBrace and seated into the tapped hole in the fibula under tension and progressed until flush with the surface of the bone, shown in Figure 112.

5.2.2.4.2.2 Calcaneofibular Ligament Repair

The CFL was then repaired, two 3.4 mm tunnels were drilled into the origin and insertion of the CFL. The holes were then tapped using a 4.75 mm tap. A 4.75 x 19.1 mm SwiveLock suture anchor was loaded with 2 mm wide InternalBrace and seated into the calcaneus tunnel and progressed until tensioned and flush with the bone surface. A second 4.75 mm SwiveLock suture anchor was then loaded onto the InternalBrace, seated into the fibula under appropriate tension and progressed until flush with the bone surface, shown in Figure 112. The excess InternalBrace was removed using a scalpel and the FiberWire within the suture anchors was removed. The length of the sutures was measured using Vernier callipers accurate to 0.02 mm three times for improved accuracy. Following the repair procedure all samples were frozen once again until the final stability analyses could be performed.

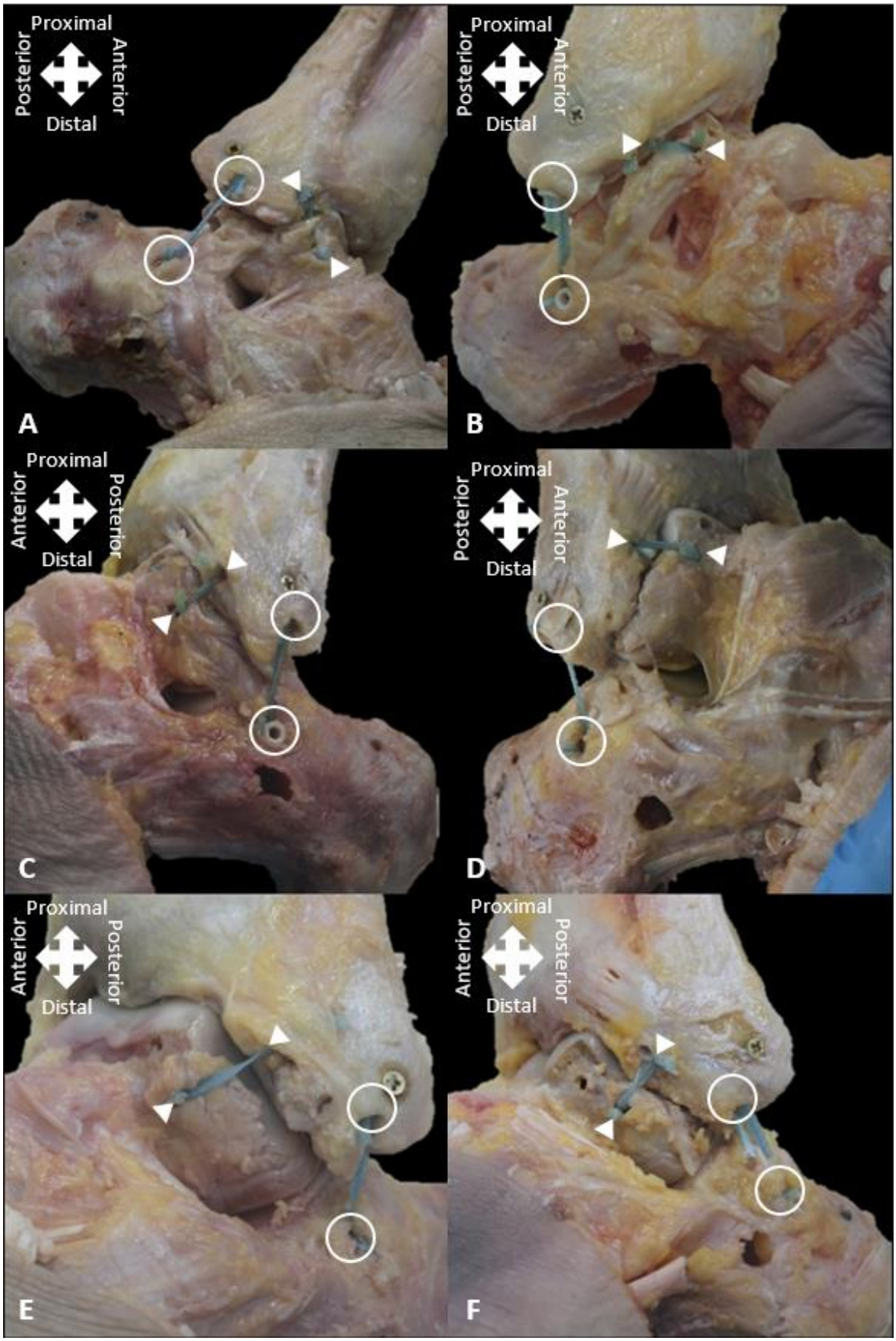

Figure 112. Anterolateral view of samples following suture tape augmentation procedure of the ATFL and CFL. A) Sample 1, B) sample 2, C) sample 3, D) sample 4, E) sample 5 and F) sample 6. White arrowheads indicate the origin and insertion points of the ATFL and white rings indicate the origin and insertion points of the CFL.

5.2.2.5 Secondary Stability Analysis

The repaired samples were defrosted for 24 hours within a 6 °C refrigerator. Once fully thawed samples were soaked in PBS for 30 minutes to maintain testing protocols between intact and repaired samples. The calcaneal tube, intramedullary rod and marker triads were implanted once again. For the stability analysis of the repaired samples, the drawer tests were performed using the same procedure described earlier in this chapter in the Stability Assessment section, in the following order; anterior, posterior, eversion and inversion drawer test. The length of the sutures tapes replacing the ATFL and CFL were measured once again using a Vernier calliper three times after all drawer tests had been completed. The intramedullary rod, calcaneal tube and marker triads were removed and samples were returned to the -80 °C freezer.

5.2.2.6 Data Analysis

The drawer tests performed in this study were each defined using the motion of the respective passive markers, shown in Table 31. Anterior and posterior drawer tests were calculated using the displacement of the anatomical marker on the posterior side of the calcaneus (PC) with respect to the anatomical marker on the medial malleolus (MM) in the y-direction. The inversion and eversion drawer tests analyse the rotations of the ankle complex, talocrural and subtalar joints independently, shown in Table 31. The convention of analysing joint motion of the distal segments in relation to proximal segments was used in this study, as in the Data Analysis section of Chapter 4.

Table 31. The passive markers used to analyse joint motion during the respective drawer tests. Wrt = with respect to.

Drawer Test	Anatomical Relation	Markers Used
Anterior/Posterior	Calcaneus wrt Tibia	PC wrt MM (y-axis)
Inversion/Eversion	Ankle Complex	C1, C2 and C3 wrt Ti1, Ti2 and Ti3
	Talocrural Joint	Ta1, Ta2 and Ta3 wrt Ti1, Ti2 and Ti3
	Subtalar Joint	C1, C2 and C3 wrt Ta1, Ta2 and Ta3

As in Chapter 4 a local coordinate system was determined for each segment of the model. The anterior and posterior drawer displacement of the ankle complex, as well as the inversion and eversion ROM of the ankle complex, subtalar and talocrural joints, were calculated. Range of motion graphs in the x-, y- and z-directions reporting the inversion/eversion, dorsi-/plantar flexion and internal/external rotation, respectively, were produced for each drawer test. The data was exported from Visual3D (C-Motion, Maryland, USA) as .txt files and imported into Microsoft Excel to be collated within a single spreadsheet.

The results for anterior and posterior drawer tests were normalised by deducting the initial displacement between the PC and the MM anatomical markers, in the anterior-posterior displacement direction (y-direction), from all results for each individual trial. The anterior and posterior displacements were then converted from metres into millimetres. Inversion and eversion results were also imported into the same Microsoft Excel spreadsheet. No normalisation or conversion was required as the ROM measurements were made by the motion capture system in degrees relative to a virtual lab.

For anterior and posterior drawer tests the maximum displacement achieved for each of the three measurements per trial was calculated. Similarly, the maximum ROM values for inversion and eversion drawer tests were calculated. An average value for each trial performed was calculated using the three maximum values of the trial. The mean and 95 % CI of all samples for each test condition and each drawer test were then calculated by averaging the mean values of each respective trial. A comparison of means was also performed between the mean values of each testing condition for individual samples. This method was necessary as comparing the overall mean values for the testing condition was not acceptable as different testing conditions had different sample sizes affecting the result.

5.2.3 Results

The average maximum ROM and displacements achieved during drawer tests performed for each testing condition are documented in their respective sub-sections which follow. The intact results are reported followed by those for the sequentially sectioned ankle and finally the synthetic repair results. Sample two was excluded from the drawer testing analysis due to the ATFL sustaining damage during dissection. The results for sample two are however still reported individually.

5.2.3.1 Intact

On average, intact samples displaced by 11.0 ± 2.3 mm and 4.7 ± 1.0 mm in anterior and posterior drawer tests, respectively. The ROM achieved by the ankle complex in inversion and eversion drawer tests was 21.3 ± 5.7 degrees and 8.2 ± 4.0 degrees, respectively. Inversion and eversion motion occurred primarily at the subtalar joint in intact specimens, shown in Table 32.

Table 32. The average maximum displacements and ROM achieved during the four drawer tests for every sample tested intact. The mean ± standard deviation (SD) for the intact test condition is shown for all drawer tests. ANT = anterior drawer, POST = posterior drawer, INV = inversion drawer, EVE = eversion drawer, AC = ankle complex, TALO = talocrural joint, SUB = subtalar joint and deg = degrees. *data not included when calculating mean values.

Sample	Test State	ANT (mm)	POST (mm)	INV AC (deg)	INV TALO (deg)	INV SUB (deg)	EVE AC (deg)	EVE TALO (deg)	EVE SUB (deg)
1	Intact	7.2	5.8	15.4	1.4	13.9	3.3	1.7	2.2
2	Intact	21.0*	6.2*	34.4*	18.4*	19.8*	3.2*	1.9*	1.4*
3	Intact	10.8	5.3	25.3	7.9	17.5	11.0	1.7	9.0
4	Intact	11.4	5.1	29.2	4.9	23.2	4.4	0.8	3.8
5	Intact	12.4	3.4	18.5	1.8	16.5	10.7	1.3	9.9
6	Intact	13.1	4.1	18.3	2.9	15.3	11.6	1.0	10.6
Mean ± SD	**Intact**	**11.0 ± 2.3**	**4.7 ± 1.0**	**21.3 ± 5.7**	**3.8 ± 2.7**	**17.3 ± 3.6**	**8.2 ± 4.0**	**1.3 ± 0.4**	**7.1 ± 3.8**

5.2.3.2 Anterior Talofibular Ligament Sectioned

Anterior and posterior drawer displacement mean values were 14.6 ± 2.3 mm and 5.4 ± 2.0 mm, respectively. A comparison of mean translations determined that sectioning of the ATFL caused a 3.6 ± 1.6 mm and 0.7 ± 1.1 mm increase in anterior and posterior displacement, respectively.

The average inversion ROM for the ankle complex increased by 1.8 ± 2.7 degrees to 23.2 ± 3.6 degrees after sectioning of the ATFL, shown in Table 33. Sectioning of the ATFL caused a 2.7 ± 2.6 degrees increase in inversion ROM at the talocrural joint and a marginal decrease of 0.7 ± 1.4 degrees at the subtalar joint. The average eversion ROM decreased negligibly by 0.2 ± 2.8 degrees to 8.0 ± 2.4 degrees after sectioning of the ATFL.

Table 33. The change in average maximum displacement and ROM from intact state achieved during the four drawer tests for every sample tested after ATFL sectioning (ATFL). The comparison of means mean ± 95 % CI result against the intact state are shown (Vs Intact). Negative values indicate a reduction in the range of motion. ANT = anterior drawer, POST = posterior drawer, INV = inversion drawer, EVE = eversion drawer, AC = ankle complex, TALO = talocrural joint, SUB = subtalar joint and deg = degrees. *data not included when calculating average values.

Sample	Test State	ANT (mm)	POST (mm)	INV AC (deg)	INV TALO (deg)	INV SUB (deg)	EVE AC (deg)	EVE TALO (deg)	EVE SUB (deg)
1	ATFL	3.6	0.7	4.3	2.1	2.1	4.3	0.4	3.4
2	ATFL	-3.8*	2.4*	6.6*	1.7*	1.7*	1.9*	-0.3*	3.9*
3	ATFL	6.0	1.8	-0.3	1.5	-1.8	-2.7	-0.2	-2.5
4	ATFL	4.2	1.8	-1.6	-0.2	-0.9	1.0	-0.3	1.6
5	ATFL	3.0	0.2	5.6	7.6	-1.3	-3.7	1.1	-4.9
6	ATFL	1.0	-1.1	1.0	2.7	-1.3	0.2	0.8	-0.2
Mean ± CI	**Vs Intact**	**3.6 ± 1.6**	**0.7 ± 1.1**	**1.8 ± 2.7**	**2.7 ± 2.6**	**-0.7 ± 1.4**	**-0.2 ± 2.8**	**0.3 ± 0.5**	**-0.5 ± 2.9**

5.2.3.3 Anterior Talofibular Ligament & Calcaneofibular Ligament Sectioned

Anterior and posterior drawer results increased further after sectioning of the CFL averaging displacements of 15.7 ± 3.0 mm and 6.0 ± 2.0 mm, respectively, shown in Table 34. The increase from the intact state as calculated using a comparison of means was 4.8 ± 2.6 mm and 1.3 ± 1.9 mm, respectively.

Eversion drawer results were similar to those of the ATFL sectioned and intact state at 7.8 ± 3.4 degrees at the ankle complex. The eversion ROM increased most at the talocrural joint with sequential sectioning by 1.2 ± 1.3 degrees, whereas a decrease of 1.6 ± 2.1 degrees was observed at the subtalar joint.

Table 34. The change in average maximum displacements and ROM from intact state achieved during the four drawer tests for every sample tested after combined ATFL and CFL sectioning (CFL). The comparison of means mean ± 95 % CI result against the intact state are shown (Vs Intact). Negative values indicate a reduction in the range of motion. ANT = anterior drawer, POST = posterior drawer, INV = inversion drawer, EVE = eversion drawer, AC = ankle complex, TALO = talocrural joint, SUB = subtalar joint and deg = degrees. *data not included when calculating average values.

Sample	Test State	ANT (mm)	POST (mm)	INV AC (deg)	INV TALO (deg)	INV SUB (deg)	EVE AC (deg)	EVE TALO (deg)	EVE SUB (deg)
1	CFL	4.8	-1.0	-	-	-	1.4	-0.7	1.8
2	CFL	-5.0*	7.8*	-	-	-	2.5*	1.4*	1.2*
3	CFL	9.7	3.2	-	-	-	0.3	3.0	-2.1
4	CFL	4.3	1.4	5.1	7.5	0.6	0.1	0.3	-0.3
5	CFL	3.0	3.6	-	-	-	-3.4	1.2	-4.7
6	CFL	2.1	-0.8	-	-	-	-0.1	2.2	-2.4
Mean ± CI	**Vs Intact**	**4.8 ± 2.6**	**1.3 ± 1.9**	**5.1 ± -**	**7.5 ± -**	**0.6 ± -**	**-0.4 ± 1.6**	**1.2 ± 1.3**	**-1.6 ± 2.1**

During the inversion drawer tests for the combined ATFL and CFL sectioned samples, the PTFL of all samples failed during testing. Samples two and four were only partially damaged, shown in Figure 113A, whereas a complete rupture or avulsion of the PTFL occurred for the other samples, shown in Figure 113B. Two complete inversion drawer tests were performed for sample four prior to failure of the PTFL, whereas all other samples failed to some extent during the first of three inversion drawer tests. A new test condition was therefore produced for complete LCL complex failure.

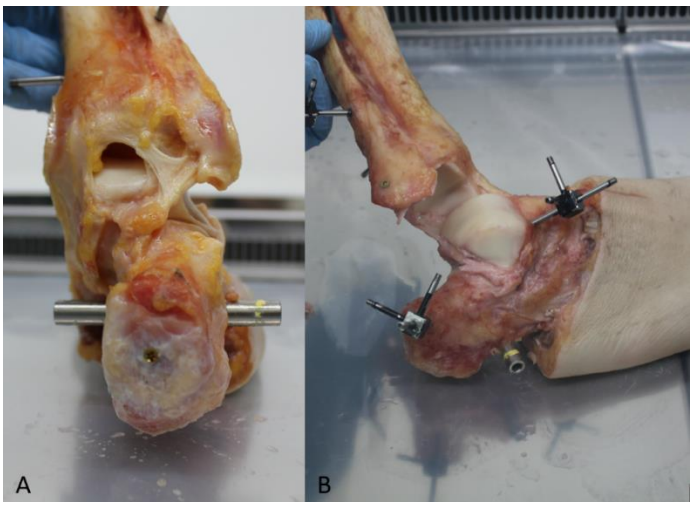

Figure 113. A) Posterior view of a partially ruptured PTFL and B) lateral view of a fully ruptured PTFL after inversion stability testing ATFL and CFL sectioned samples.

The fourth sample inverted 34.3 degrees at the ankle complex, 12.4 degrees at the talocrural joint and 23.8 degrees at the subtalar joint. The comparison of means result determined the inversion to increase at the ankle complex by 5.1 degrees, talocrural joint by 7.5 degrees and subtalar joint by 0.6 degrees after sectioning of the ATFL and CFL in comparison with the intact state.

5.2.3.4 Lateral Collateral Ligament Complex Failure

Complete LCL failure ranged from a partial rupture of the PTFL (Grade II sprain) to a complete rupture (Grade III sprain). A partial rupture of the PTFL was defined by an audible tearing of the ligament without complete macroscopic rupture being visibly evident. After PTFL failure the lateral side of the ankle was almost completely unrestrained at the talocrural joint. The inversion ROM increased by 40.1 ± 14.3 degrees at the ankle complex, 42.9 ± 22.5 degrees at the talocrural joint and 9.4 ± 6.5 degrees at the subtalar joint. The average inversion ROM values after LCL failure were 61.5 ± 13.9 degrees, 46.7 ± 25.1 degrees and 26.7 ± 10.6 degrees at the ankle complex, talocrural and subtalar joints, respectively, shown in Table 35.

Table 35. The change in average maximum displacements and ROM from intact state achieved during the inversion drawer test for every sample tested after LCL complex failure (PTFL). The comparison of means mean ± 95 % CI result against the intact state are shown (Vs Intact). Negative values indicate a reduction in the range of motion. ANT = anterior drawer, POST = posterior drawer, INV = inversion drawer, EVE = eversion drawer, AC = ankle complex, TALO = talocrural joint, SUB = subtalar joint and deg = degrees. *data not included when calculating average values.

Sample	Test State	ANT (mm)	POST (mm)	INV AC (deg)	INV TALO (deg)	INV SUB (deg)	EVE AC (deg)	EVE TALO (deg)	EVE SUB (deg)
1	PTFL	-	-	66.4	78.1	7.4	-	-	-
2	PTFL	-	-	21.5*	30.9*	-1.6*	-	-	-
3	PTFL	-	-	42.4	51.9	2.6	-	-	-
4	PTFL	-	-	26.0	10.6	22.0	-	-	-
5	PTFL	-	-	38.7	47.1	9.1	-	-	-
6	PTFL	-	-	27.1	26.9	5.9	-	-	-
Mean ± CI	**Vs Intact**	**-**	**-**	**40.1 ± 14.3**	**42.9 ± 22.5**	**9.4 ± 6.5**	**-**	**-**	**-**

5.2.3.5 Synthetic Intervention

Only two samples (1 and 3) were successfully repaired, all remaining samples experienced at least one synthetic ligament failure prior to testing or during inversion testing, shown in Figure 114. A successful repair was determined by the following two factors: the ability of the suture tape augmentation to restore joint stability to that of the intact state; and the change in length of the suture tape augmentation due to stability testing. Inversion results for repaired samples were therefore separated into successful (repaired) and unsuccessful (failed) categories.

5.2.3.5.1 Repaired

The mean maximum displacement and ROM results for the repaired samples are shown in Table 36. After repair the anterior and posterior displacements were 9.9 ± 2.1 mm and 4.5 ± 1.1 mm, respectively. The anterior displacement decreased by 0.9 ± 3.0 mm and posterior displacement decreased by 0.1 ± 0.9 mm from the intact state for the comparison of means result.

Mean eversion ROM after repair of the ATFL and CFL was 7.4 ± 1.4 degrees, 1.8 ± 0.9 degrees and 5.9 ± 2.0 degrees at the ankle complex, talocrural and subtalar joints, respectively. The ankle complex eversion ROM decreased from the intact state by 1.8 ± 4.4 degrees. Eversion ROM increased at the talocrural joint by 0.4 ± 1.1 degrees and decreased at the subtalar joint by 2.0 ± 5.4 degrees according to comparison of mean results.

The mean inversion ROM of repaired samples was 20.6 ± 2.1 degrees for the ankle complex, 1.3 ± 0.4 degrees for the talocrural joint and 19.1 ± 1.8 degrees for the subtalar joint. The comparison of means results state that the average ankle complex inversion ROM was similar to the intact state increasing by 0.2 ± 7.0 degrees. A decrease of 3.4 ± 6.8 degrees occurred at the talocrural joint and an increase of 3.4 ± 1.0 degrees occurred at the subtalar joint.

Table 36. The change in average maximum displacements and ROM from intact state achieved during the four drawer tests for every sample tested after synthetic repair with InternalBrace (repair). The comparison of means mean ± 95 % CI result against the intact state are shown (Vs Intact). Negative values indicate a reduction in the range of motion. ANT = anterior drawer, POST = posterior drawer, INV = inversion drawer, EVE = eversion drawer, AC = ankle complex, TALO = talocrural joint, SUB = subtalar joint and deg = degrees. *data not included when calculating average values.

Sample	Test State	ANT (mm)	POST (mm)	INV AC (deg)	INV TALO (deg)	INV SUB (deg)	EVE AC (deg)	EVE TALO (deg)	EVE SUB (deg)
1	Repair	1.7	0.3	3.7	0.1	3.9	4.8	-1.0	6.3
2	Repair	1.3*	-2.1*	-	-	-	1.4*	2.7*	3.3*
3	Repair	-0.1	-1.5	-3.3	-6.8	2.9	-5.6	0.0	-5.0
4	Repair	-	-	-	-	-	-	-	-
5	Repair	0.0	0.6	-	-	-	-3.4	1.6	-5.3
6	Repair	-5.4	0.0	-	-	-	-2.9	1.0	-4.0
Mean ± CI	**Vs Intact**	**-0.9 ± 3.0**	**-0.1 ± 0.9**	**0.2 ± 7.0**	**-3.4 ± 6.8**	**3.4 ± 1.0**	**-1.8 ± 4.4**	**0.4 ± 1.1**	**-2.0 ± 5.4**

Only samples one and three met the criteria to be considered successful repairs. The anterior displacement and inversion ROM of the ankle complex for sample one increased by 1.7 mm and 3.7 degrees, shown in Table 36 and Table 38. The average length of the ATFL and CFL suture tape augmentations both increased during the stability analysis by 0.2 mm and 0.5 mm, respectively, shown in Table 38. The anterior displacement and inversion ROM of the ankle complex decreased for sample three by 0.1 mm and 3.3 degrees, respectively. The ATFL and CFL suture tape augmentations for sample three increased in length by 1.5 mm and 3.1 mm, respectively.

5.2.3.5.2 Failed Repair

Samples two, four, five and six all had failed repairs, shown in Figure 114. Sample four failed prior to any repair testing being performed, when removed from the freezer the suture anchor securing the CFL suture tape into the fibula had been dislodged, shown in Figure 114D. Samples two, five and six all failed during inversion drawer tests.

When repairs failed, the average ankle complex inversion ROM was 59.9 ± 33.1 degrees ranging from 36.5 degrees to 83.3 degrees dependent on the severity of the failure, shown in Table 37. The comparison of means calculated the inversion ROM to increase by 41.5 ± 45.8

degrees, 38.9 ± 65.5 degrees and 8.3 ± 8.3 degrees for the ankle complex, talocrural and subtalar joints, respectively.

A combined ATFL and CFL failure occurred for the second sample, shown in Figure 114B. The CFL failed due to the fibular suture anchor dislodging and the ATFL failed through slippage of the suture tape whilst the suture anchors remained fixed in place. The average length of the ATFL suture tape augmentation for sample two increased from 14.0 mm to 23.6 mm, shown in Table 38. The ankle complex inverted 59.2 degrees, an increase of 24.8 degrees from the intact state.

Sample five also failed through a combined ATFL and CFL failure, shown in Figure 114E. The talar anchor of the ATFL and fibular anchor of the CFL were dislodged. The combined ATFL and CFL augmentation rupture allowed a maximum inversion ROM of 83.3 degrees, an increase of 64.8 degrees.

Only the CFL failed in sample six which occurred due to slippage of the suture tape as the calcaneal anchor was loosened, shown in Figure 114F. This caused the length of the suture tape augmentation to increase from 22.7 mm to 33.1 mm and the inversion ROM of the ankle complex to increase by 18.2 degrees to 36.5 degrees. The ATFL was not determined to have failed as the anterior displacement was lower than for the intact state and the length of the ligament only increased on average by 0.3 mm.

Table 37. The change in average maximum displacements and ROM from intact state achieved during the four drawer tests for every sample tested after synthetic repair with InternalBrace failure (Failed). The comparison of means mean ± 95 % CI result against the intact state are shown (Vs Intact). Negative values indicate a reduction in the range of motion. ANT = anterior drawer, POST = posterior drawer, INV = inversion drawer, EVE = eversion drawer, AC = ankle complex, TALO = talocrural joint, SUB = subtalar joint and deg = degrees. *data not included when calculating average values.

Sample	Test State	ANT (mm)	POST (mm)	INV AC (deg)	INV TALO (deg)	INV SUB (deg)	EVE AC (deg)	EVE TALO (deg)	EVE SUB (deg)
1	Failed	-	-	-	-	-	-	-	-
2	Failed	-	-	24.8*	19.8*	3.4*	-	-	-
3	Failed	-	-	-	-	-	-	-	-
4	Failed	-	-	-	-	-	-	-	-
5	Failed	-	-	64.8	72.3	4.0	-	-	-
6	Failed	-	-	18.2	5.5	12.6	-	-	-
Mean ± CI	**Vs Intact**	**-**	**-**	**41.5 ± 45.8**	**38.9 ± 65.5**	**8.3 ± 8.3**	**-**	**-**	**-**

Figure 114. Specimens after suture augmentation repair and stability analysis. A) Successful repair of sample 1, B) failed repair of CFL and slippage of ATFL for sample 2, C) successful repair of sample 3, D) failed repair of CFL for sample 4, E) failed repair of ATFL and CFL for sample 5, F) failed repair of CFL for sample 6. White arrowheads = point of failure.

Table 38. The average and (range) length of the synthetic ligament augmentations of the ATFL and CFL before and after stability analysis.

		Sample 1	Sample 2	Sample 3	Sample 4	Sample 5	Sample 6
Length Before Testing (mm)	**ATFL**	12.4 (12.2 – 12.6)	14.0 (13.6 – 14.7)	10.0 (9.1 – 10.6)	-	21.9 (21.6 – 22.1)	11.4 (11.0 – 11.6)
	CFL	28.2 (27.8 – 28.7)	24.7 (24.7 – 24.8)	22.4 (22.3 – 22.5)	-	25.7 (25.5 – 25.9)	22.7 (22.4 – 23.2)
Length After Testing (mm)	**ATFL**	12.6 (12.1 – 12.9)	23.6 (22.6 – 24.5)	11.5 (10.9 – 12.2)	-	-	11.7 (11.3 – 12.0)
	CFL	28.7 (28.3 – 29.4)	43.3 (42.7 – 44.3)	25.5 (24.7 – 26.1)	-	-	33.1 (32.8 – 33.6)

5.2.4 Discussion

The aims of this study were to analyse the change in ankle stability after sequential sectioning of the lateral ankle ligaments, as well as to determine the capacity of synthetic interventions to restore lateral ankle stability. The alterations in ankle stability due to injury of the ATFL, ATFL and CFL, and the entire LCL complex are compared with the intact state. In agreement with previously published findings, the anterior displacement and inversion ROM, the two key indicators of lateral ankle stability, both increased with the sequential sectioning of the LCL complex (Kerkhoffs et al., 2005; Fujii et al., 2010; Kovaleski et al., 2014; Lohrer et al., 2019). Whilst the mean and general trend in the data reflect the same pattern as the published literature this was not true for every sample.

The small overall increase in ROM after ATFL sectioning when performing an inversion drawer test highlights the difficulties faced when diagnosing ankle sprain with a talar tilt test alone (Wilkin et al., 2012). The anterior drawer test however yielded a more distinct average increase in ROM after ATFL sectioning, with anterior displacement increasing by 3.6 ± 1.6 mm. This result is above the threshold value of 3.0 mm increase in anterior displacement when compared to the contralateral limb using stress radiography (Seligson et al., 1980). The threshold value for the anterior drawer test analysed using motion capture, as in this study, would be 2.0 mm to capture 95 % of the sprains within the population when loaded with approximately 100 N force.

The inversion ROM results for some samples even demonstrated a negligible decrease after ATFL sectioning. The largest decrease in inversion ROM of the ankle complex from the intact

state was 1.6 degrees, for sample four. A small decrease could be attributed to a test error such as slightly over loading in the intact trial and/or under loading during the ATFL sectioned trial.

To the author's knowledge only one research article exists where motion capture technology has been used to analyse the stability of the ankle (Lohrer et al., 2019) and the previous study only reported anterior displacement. The inversion ROM during an inversion drawer test is however, to the author's knowledge, reported here for the first time using motion capture analysis. The use of motion capture analysis was proposed to provide a greater level of precision for stability analysis. The calibration results indicate that the system had a standard deviation for the wand length of 0.08 mm. The inter-subject variation in the results is however much higher (2.0 mm for anterior drawer of intact samples) and is likely due to the inherent natural variability between donors. The variation in the results compares well to previous studies particularly for anterior drawer tests where the variation is smaller, shown in Table 39 (Kovaleski et al., 2002).

Table 39. A comparison of results for anterior (ANT) and inversion (INV) drawer tests performed with cadaver tissue using three different calculation methods. A six DOF spatial linkage, arthrometer and motion capture analysis are compared.

	Kovaleski, 2002 Spatial Linkage		**Kovaleski, 2002 Arthrometer**		**Present study Motion Capture**	
	ANT (mm)	INV (deg)	ANT (mm)	INV (deg)	ANT (mm)	INV (deg)
Intact	7.4 ± 3.1	16.7 ± 2.4	13.8 ± 3.6	30.1 ± 4.3	11.0 ± 2.0	21.3 ± 5.0
ATFL	11.4 ± 3.8	19.1 ± 3.4	16.3 ± 3.1	34.6 ± 5.1	14.6 ± 2.0	23.2 ± 3.1
CFL	12.8 ± 4.8	25.4 ± 4.8	18.9 ± 2.7	44.1 ± 4.8	15.7 ± 2.7	34.3 ± 0.0

Differentiating between a combined ATFL and CFL sprain and an isolated ATFL sprain diagnosis is greatest when analysing the results of the inversion drawer test. The anterior drawer results for ATFL and combined ATFL and CFL sectioned samples had a large overlap in the results. The results for the inversion drawer test are more distinct, however the combined ATFL and CFL inversion result is only representative of one sample and further samples would be required to draw any meaningful inference.

When analysing the change in stability of the ankle due to increasing damage to the LCL complex it is important to compare the results of samples independently, due to the large natural variation between individuals shown in this study. Between-subject variability, among many others, exposes the issues with calculating absolute generalised population means to define ankle stability. Particularly in this study where not every sample contributed towards the average measurement for each testing condition and resulting sample sizes were small. The most appropriate way to display data therefore is as a change from the intact state

measurements. This can be achieved in patients by contrast to the contralateral limb where no previous damage to the ankle complex of the contralateral limb has occurred.

Sectioning of the ATFL and CFL considerably reduced the strength of the support on the lateral side of the ankle. Every sample in this study experienced PTFL failure during the inversion drawer tests subsequent to the sectioning of the ATFL and CFL. Failure of the PTFL occurred at loads as low as approximately 1 N.m. Failures varied in severity between a Grade II sprain, with partial tearing of the PTFL, to a Grade III sprain where complete ligament rupture occurred. As with the results of Chapter 4, this study would have benefitted from the use of medical imaging for diagnostic purposes, such as MRI or ultrasound, however these facilities were not available.

The amount of dissection performed was significant in this study with a lot of auxiliary tissue intentionally being dissected from the samples. The effect of such severe dissection would be most noticeable in the results where the entire LCL complex is damaged. The results of this study could therefore overestimate the ROM achieved when similarly loading living patients. Lateral ankle stability results however compare to those in previous studies where similar inversion loads were applied with an arthrometer and minimal soft tissue dissection was performed, shown in Table 39 (Kovaleski et al., 2002; Kovaleski et al., 2014). The severity of the dissection performed in this study could therefore have had a limited effect on lateral ankle stability as the anterior and inversion drawer results of this study lie between those reported in the two previous studies, shown in Table 39. This study did not however intend to define results for use in a clinical setting but rather define the contributions of individual ligaments to lateral ankle joint stability and how well synthetic interventions could replace such contributions. A severe dissection was therefore required to prevent other influences masking the effects of ligament damage or repair. Individuals who sustain a Grade III sprain of the ATFL and/or CFL would require treatment to prevent further long-term damage.

When successful, the suture tape augmentation procedure produced good results for the stability restoration of the LCL complex. The main issue was the success rate of the repair procedure with only two out of six samples being determined to be sufficiently repaired. Samples one and three were determined to be successfully repaired. For sample one, the anterior displacement increased by 1.7 mm from the intact state, well within the 3.0 mm threshold for stability. This small increase is likely due to the tensioning applied by the orthopaedic surgeon being different to that of the natural ligament. Slippage of the suture tape was discredited as the length of the ATFL suture tape only increased by 0.2 mm during testing. The CFL repair increased in length by 0.5 mm and inversion ROM increased by 3.7 degrees from the intact state. Whilst this level of inversion is similar to that of an ATFL rupture the small change in suture length again indicates that this could be due to surgical placement rather than the device failing. The categorisation of repair success is less clear for sample three as the suture tape length of the ATFL and CFL increased by 1.5 mm and 3.1 mm, respectively. Such an increase is more than one would expect for a static brace of the ligament. The anterior

and inversion ROM during stability tests were however in close agreement with those of the intact state. The tensioning could have been too tight for these samples causing the tape slippage to restore joint stability to intact state. This raises concerns however as to whether with continued load or higher forces suture tape slippage would continue to a point of ankle instability. The author acknowledges that sample three could be defined as either a failure or success. The decision to categorise sample three as successful was due to the stability analysis results being in such close proximity to those of the intact state and catastrophic failure of the suture tape repair not occurring.

The suture tape repair of the CFL failed frequently and under very low loads in this study. The results for the ATFL were a slight improvement with less suture tape slippage and improved joint stability. An effective brace should have a load capacity high enough to prevent overstretching of the repaired ligament. The augmented Broström procedure with InternalBrace has been reported to be "at least as strong and stiff as the native ATFL" with a strength of 315.5 ± 66.8 N (Viens et al., 2014). The strength of an augmented Broström procedure with InternalBrace has not however, to the author's knowledge, been compared to that of the modified Broström procedure. Comparing the procedure to the intact state provides opportunity for the benefits of the suture tape augmentation, or lack thereof, to be masked by the soft tissue repair performed as it is not investigating the impact of the tape alone.

Failure occurred predominantly within the CFL repair during inversion motion in this study. No study exists, to the author's knowledge, identifying the strength of an augmented repair to the CFL. The strength of the intact CFL was however reported in Chapter 3 to be greater than the augmented Broström procedure with InternalBrace of the ATFL at 367.8 ± 79.8 N. The procedure performed in this study was not an augmented Broström procedure with InternalBrace and therefore cannot question the effectiveness of the treatment. It does however raise questions as to what contribution the additional suture tape augmentation provides for the patient over the modified Broström procedure.

Clinical outcome studies do however exist comparing the augmented Broström procedure with InternalBrace to the modified Broström procedure. The anterior drawer, talar tilt, AOFAS and VAS scores have been shown to not be significantly different between the two procedures (Cho et al., 2019; Xu et al., 2019). This finding is often interpreted in the literature as a positive finding for the augmented Broström procedure with InternalBrace. The addition of a suture tape is unlikely however to lower outcome scores for the otherwise identical surgical procedure, providing no allergic reaction or over tensioning of the implant are present. Meanwhile the healthcare cost of the augmented Broström procedure with InternalBrace is 1.3 times higher than the modified Broström procedure (Cho et al., 2019). The augmented procedure has been reported to provide a quicker return to sport over a modified Broström procedure (Yoo and Yang, 2016). The post-operative patient management was different for the

two procedures however with the modified Broström patients being immobilised for two weeks and therefore this result would be expected.

These findings in addition to those reported in this study highlight relevant questions regarding what contribution the suture tape provides in an augmented Broström procedure with InternalBrace. The lack of a significant improvement in clinical outcomes and the higher cost of the augmented Broström procedure with InternalBrace suggests that the augmented procedure should not be considered over a modified Broström procedure.

Limitations to this study exist which could affect the outcome of the procedure. A suture tape augmentation procedure is typically performed on younger patients than the average age of the cohort for this study. The cadaver tissue, particularly which is from an older population, could have an inferior bone quality to that of patients typically operated on with this procedure. Other previous studies, including ATFL specific literature, have however reported no correlation between age and the mechanical properties of ligaments tested as BLB structures (St Pierre et al., 1983; Blevins et al., 1994; Johnson et al., 1994; Flahiff et al., 1995; Couppé et al., 2009). The sample size of the study was small exaggerating the percentage of failures. These factors could mostly not be avoided and requests were made with the source of the cadaver tissue to procure samples with a younger age. As with all studies within this project using human tissue, the exclusion criteria of no previous history of lower limb trauma existed but unreported sprains are frequent within society (Kemler et al., 2015). When comparing the repaired samples to intact ones it must be acknowledged that the PTFL was not repaired and some of the devices used in this study were expired. Both of these factors could have reduced the effectiveness of suture tape repair.

Sample two was excluded from the stability testing results due to damage occurring to the ATFL either during or prior to dissection of the sample as well as the presence of a small talar fracture at the location of PTFL insertion. The results for sample two were anomalous across all stability tests for the intact condition making a comparison impossible. Particularly noticeable was the excessive anterior displacement and the contribution of the talocrural joint to inversion ROM. The repair of sample four failed whilst stored within the freezer and an explanation for this occurrence is unclear. No literature exists on the effect of freezing to the structure of polylactic acid (PLLA) the polymer used to manufacture the SwiveLock suture anchors. Repairs were checked by the surgeon and an effort was made to store samples unloaded in the neutral position. Whether freezing the suture anchors affected the size of the suture anchors is unknown however it is unlikely to have altered the diameter of the suture anchor by more than the thread depth, allowing them to simply fall out.

Single plane anterior and inversion drawer tests were performed in this study rather than an anterolateral drawer test due to the use of motion capture cameras. The positioning of motion capture cameras shown in Figure 88 restricted where the examiner could be positioned to perform the drawer tests. For posterior, inversion and eversion drawer tests the examiner was

positioned on the medial side of the drop rig without restricting the view of the motion capture cameras. For the anterior drawer however this was not possible and the examiner was positioned on the anterior side of the specimen behind the motion capture cameras. Such a position prevented internal rotation motions from being applied to the specimen.

Considering the limitations the author still has serious concerns regarding the implantation of the InternalBrace using SwiveLock bone anchors as the suture tape alone provided little to no support in most samples. The results do not suggest that the augmented Broström procedure with InternalBrace is unsafe due to the absence of soft tissue repair and the severe level of dissection performed in this study. The rhetoric of the literature for the augmented Broström procedure with InternalBrace is however disconcerting as most authors appear determined to interpret the results which are dissimilar to the modified Broström procedure in favour of the augmented procedure.

5.2.5 Conclusion

Lateral ankle stability decreases as ligaments of the LCL complex are sequentially sectioned. Anterior drawer and talar tilt tests are adequate indicators of injury to the ATFL and CFL, respectively. Only well trained and highly skilled clinicians are able to identify such nuances in ankle joint stability through touch sense. Attempting to use quantitative measurement systems to evaluate lateral ankle stability raises some issues due to variations between individuals, yet is still a viable approach. The InternalBrace suture tape has been shown to independently be a sufficient stabiliser of the ATFL at times. Catastrophic failure occurred however at a high rate in this study, given the small sample size, particularly for the CFL repair during inversion motion. These results suggest further testing of the InternalBrace augmented Broström repair procedure is required to demonstrate any potential benefit over the modified Broström procedure.

5.3 The Evaluation of Synthetic Interventions to Lateral Ankle Sprain

5.3.1 Introduction

Following the unsuccessful implantation of the Infinity-Lock suture tape (Xiros Ltd, Leeds, UK) and the frequent failures of the InternalBrace suture tape (Arthrex Inc, Naples, FL, USA) investigations were made into the fixation of the suture tapes. Arthrex had previously characterised their InternalBrace FiberTape suture tape (Arthrex Inc, Naples, FL, USA) when implanted into a SawBone model using SwiveLock suture anchors (Arthrex Inc, Naples, FL, USA). The findings are reported in an article not formally published, shown in Appendix G.1 Arthrex White Paper 1. As previously mentioned, the Infinity-Lock suture tape had been successfully implanted into the same Sawbone model using SwiveLock suture anchors during in-house research at Xiros. Alternative to the methods described in Appendix G.1 Arthrex White Paper 1 the tunnel for the suture anchor was not tapped. The researchers at Xiros had previously used a 4.75 mm punch directly into the Sawbone model to create a tunnel for the suture anchor. As both the Arthrex and Xiros studies had only used a Sawbone model, a preliminary characterisation study in animal and human bone tissue was developed to characterise the fixation method and identify the potential source of implantation issues.

The first aim of this study was to identify the most suitable implantation technique for the Infinity-Lock suture tape using SwiveLock suture anchors in both Sawbone and porcine bone material. The study also aimed to evaluate the structural properties (ultimate failure load and stiffness) and failure mode of the InternalBrace when implanted into both Sawbone and porcine bone, following manufacturer guidelines. The final aim of the study was to compare the ultimate failure load, stiffness and failure mode of the Infinity-Lock suture tape to those of the InternalBrace suture tape when implanted into both Sawbone and porcine bone.

5.3.2 Method

5.3.2.1 Specimens

Artificial Sawbone blocks (Sawbones, Seattle, USA), replicating those used in the Arthrex study described in Appendix G.1 Arthrex White Paper 1, were used in this study. The structure consisted of a 40 mm deep lower density (160 $kg.m^{-3}$) polyurethane core sandwiched between two 3 mm deep higher density (320 $kg.m^{-3}$) polyurethane layers, shown in Figure 115. Three porcine right hind legs from six month old pigs, sourced from a local abattoir (Penny & Sons, Leeds, UK), were used in this study. The average weight of the pigs was 68.9 kg and ranged from 67.8 kg to 69.8 kg. Ethical approval was not required for the testing as the porcine legs were sourced from the food chain.

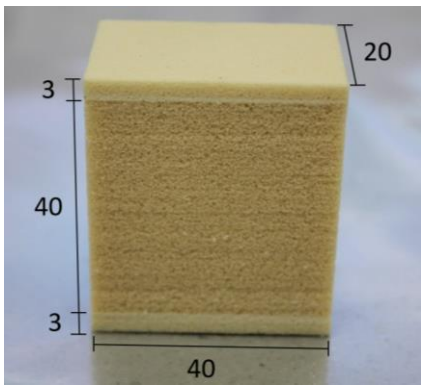

Figure 115. Artificial bone made from polyurethane foam layers of differing densities.

5.3.2.2 Sample Preparation

Three Sawbone blocks were cut with dimensions 28 x 40 x 46 mm and the bottom layer of higher density polyurethane was removed to fit within a bespoke gripping fixture. The bespoke gripping fixture had previously been used for the characterisation of similar tissues (Whitaker et al., 2019). The porcine legs arrived into the laboratory fresh from the abattoir as intact whole limbs. A transverse cut was made through the skin and muscle layers approximately 5 cm proximal to the ankle joint. Using an oscillating saw a transverse cut was made through the tibia and fibula at the same location, separating the ankle complex and trotter from the rest of the leg, shown in Figure 116.

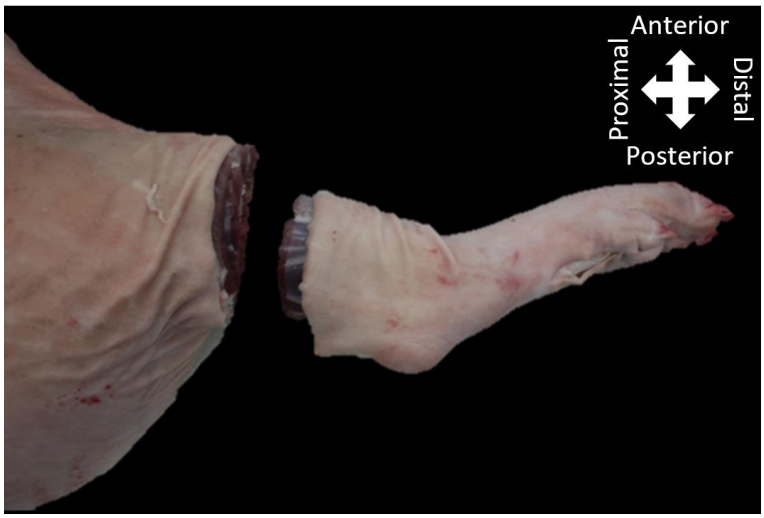

Figure 116. Lateral view of a porcine leg where the foot and ankle has been removed with a transverse cut through the skin, musculature and bone.

Using a scalpel, an anterior midsagittal cut was made through the skin distally from the proximal surface of the tibia to 5 cm distal to the ankle joint. A medial-lateral circumferential cut through the skin was then made around the trotter 5 cm distal to the ankle joint. The skin was then separated from the muscle fascia and removed exposing the ankle joint. The Achilles tendon was severed at its insertion to the calcaneus and all musculature surrounding the tibia and fibula was removed, as shown in Figure 117.

Figure 117. Lateral view of the porcine ankle joint with skin and musculature removed.

The ligaments on the medial and lateral side of the ankle were divided with a scalpel at their insertion points to the tibia and fibula, respectively. The joint capsule was dissected away from the tibia on both the anterior and posterior sides of the ankle joint allowing for the tibia and fibula to be removed from the talocrural joint, see Figure 118A. The distal tibiofibular syndesmosis ligaments were severed with a scalpel separating the fibula and tibia, see Figure 118B. The samples were wrapped in PBS (Oxoid Ltd, Basingstoke, UK) soaked tissue, sealed in airtight plastic bags and stored in a -20 °C freezer until further testing.

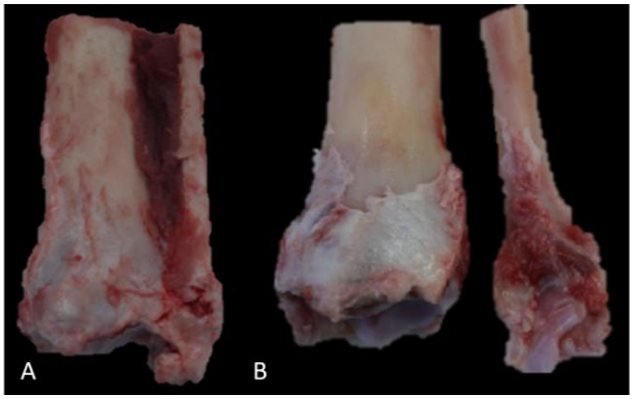

Figure 118. A) Posterior view of the distal portion of the tibia and fibula of a porcine leg. B) Posterior view of the distal portion of the tibia and medial view of the fibula separated at the distal tibiofibular syndesmosis.

Samples were defrosted overnight within a 6 °C refrigerator. Using an oscillating saw, a cut was made approximately 30 degrees inferiorly in the transverse plane through the fibula approximately 30 mm proximal to the distal tip of the fibula on the anterior side, shown in Figure 119A. Two 3 mm pilot holes were drilled all the way through the fibula from the lateral side approximately 30 mm proximal to the distal tip of the fibula. Two 4 x 20 mm screws were inserted into the pilot holes, one from the lateral side and one from the medial, as shown in Figure 119B.

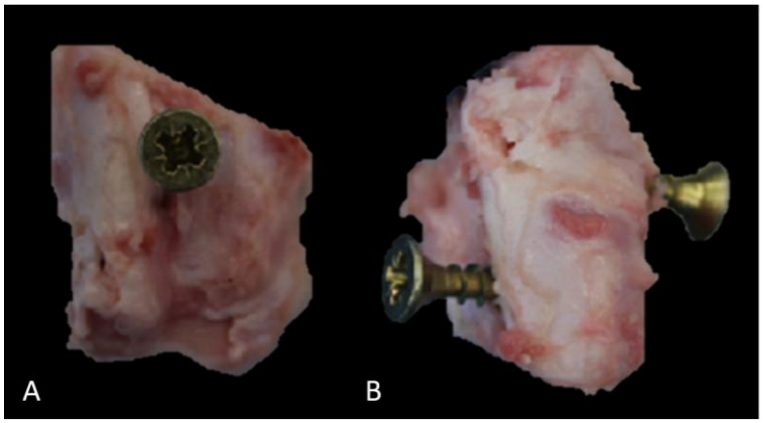

Figure 119. A) Lateral view and B) Anterior view of the distal tip of the fibula with a 4 x 20 mm screw inserted into the lateral and medial sides of the fibula.

The portions of distal fibula were then positioned within cement pots so that the 30 degree cut was parallel with the vertical walls of the pot and the anterior side of the distal tip of the fibula was facing superiorly, shown in Figure 120. The fibula was held in position within the cement pot using four locating bolts. A standard PMMA mixture (WHW Plastics, Hull, UK), created at a 2:1 ratio, was poured into the pots and left to set for 30 minutes. Once set a piece of PBS soaked tissue was placed over the fibula to reduce tissue dehydration. The samples were placed in sealed plastic bags and stored in a 6 °C refrigerator overnight.

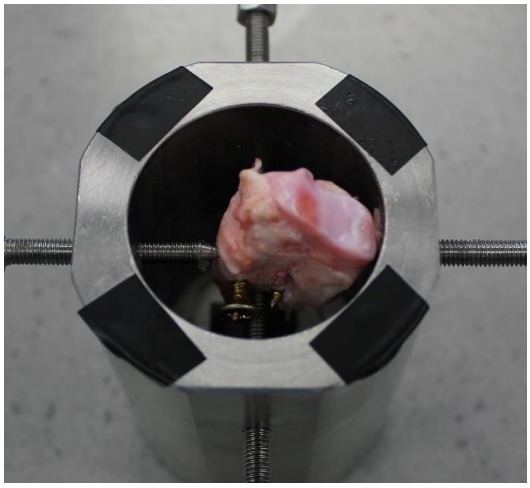

Figure 120. Superior view of the cement pot showing the distal tip of the fibula held in place prior to cementing by locating bolts.

5.3.2.3 Suture Tape Implantation

The samples were removed from the refrigerator and suture tape implantation was performed. The Infinity-Lock suture tape was implanted into both Sawbone and porcine fibula using a punched tunnel and tapped tunnel approach to suture anchor implantation. Whereas the InternalBrace FiberTape was only prepared according to manufacture guidelines, using a tapped tunnel, into both Sawbone and porcine fibula. Table 40 shows the experimental design for the testing and combinations of ligament, preparatory method of the suture anchor tunnel

and tissue implanted into. A sample size of n = 1 was used for this preliminary study due to time and resource constraints.

Table 40. Experimental design for the testing detailing ligament type, suture anchor tunnel preparation method (punch or tap) and material used.

Artificial Ligament	Hole Preparation	Tissue
Xiros Infinity-Lock (3 mm)	Punch	Sawbone
Xiros Infinity-Lock (3 mm)	Tap	Sawbone
Xiros Infinity-Lock (3 mm)	Punch	Porcine fibula
Xiros Infinity-Lock (3 mm)	Tap	Porcine fibula
Arthrex InternalBrace	Tap	Sawbone
Arthrex InternalBrace	Tap	Porcine fibula

Both the punched and tapped suture anchor tunnels were located centrally on the Sawbone and fibula specimens and orientated in the same axis of loading as the suture tapes. By orientating the suture anchor to be in the same axis as loading the results should represent the lowest loads achieved when implanted into patients where loading would occur at different angles. Testing the suture anchor fixations in this manner introduces a safety tolerance as the results should represent the worst case scenario. The punch preparation method for the suture anchor tunnel was performed by driving a 4.75 mm tapered punch (Arthrex Inc, Naples, FL, USA), shown in Figure 121A, into the specimen with a mallet. The punch was inserted up to the second black laser line producing a hole, shown in Figure 122A. The tapped procedure was performed by drilling a 3.5 mm pilot hole 20.5 mm deep into the centre of the specimen to the black laser line on the 3.5 mm drill bit (Arthrex Inc, Naples, FL, USA), shown in Figure 121B. The pilot hole was then tapped by inserting the 4.75 mm tap (Arthrex Inc, Naples, FL, USA), shown in Figure 121C, 20.5 mm into the pilot hole to the black laser line creating an internal thread for the suture anchor, shown in Figure 122B.

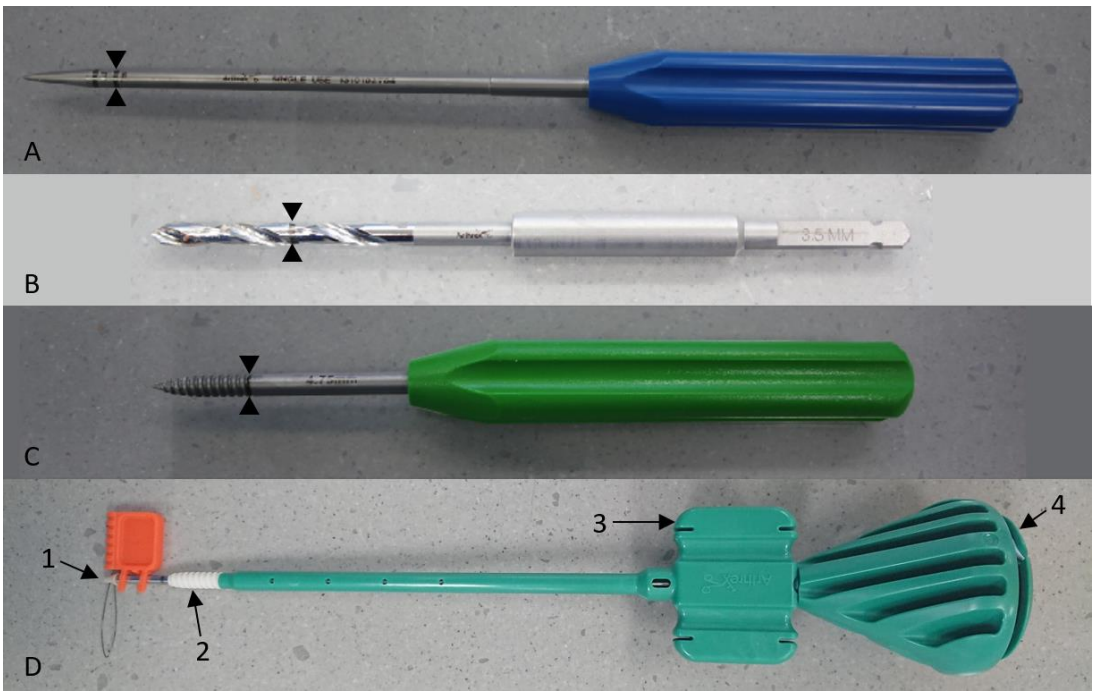

Figure 121. Arthrex tools for InternalBrace fixation with suture anchors. A) 4.75 mm punch, B) 3.5 mm drill bit, C) 4.75 mm tap driver and D) suture anchor device where 1 = closed eyelet, 2 = suture anchor, 3 = paddle and 4 = handle. Black arrowheads show the laser lines used to guide suture anchor tunnel creation.

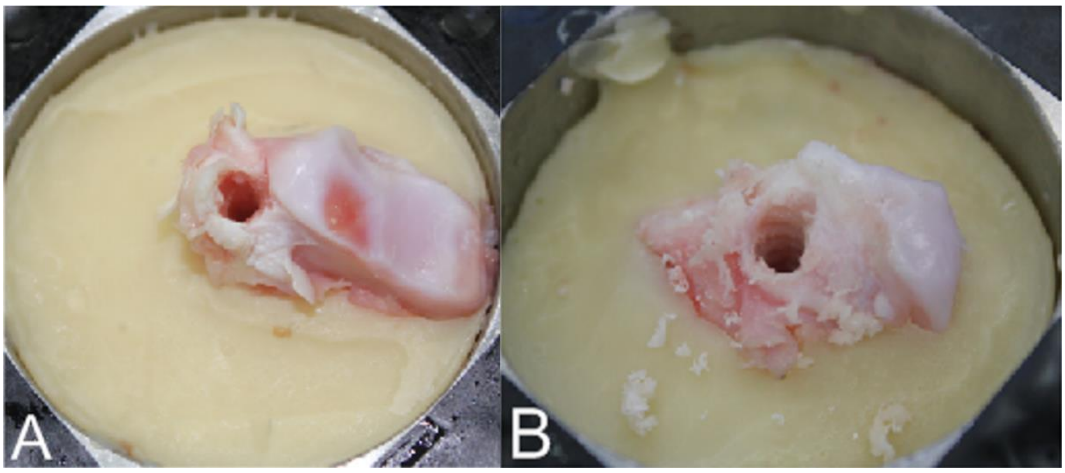

Figure 122. A) Punched and B) tapped holes in porcine fibula prior to implantation of suture anchor and suture tape.

The 4.75 mm SwiveLock suture anchors were loaded with either a 3 mm Infinity-Lock or 3 mm InternalBrace suture tape, in accordance with Table 40. The suture tapes were loaded onto the suture anchors by passing the tape through the closed eyelet, shown in Figure 121D. The anchors were seated into the prepared tunnels with a gentle tap on top of the suture anchor device with the palm of the hand, as per surgical guidelines. The suture anchors were then progressed into the tunnel by turning the suture anchor device handle clockwise whilst holding the paddle in a fixed orientation. The suture anchors were progressed until flush with the surface of the specimen, shown in Figure 123. The specimen preparation was completed by removing the FiberWire® (Arthrex Inc, Naples, FL, USA) strand(s) from the anchor, typically

used to perform the soft tissue element of the repair. The implantation of suture tapes into the Sawbone and porcine samples was scored on a scale from 1 to 5, as detailed in Table 41.

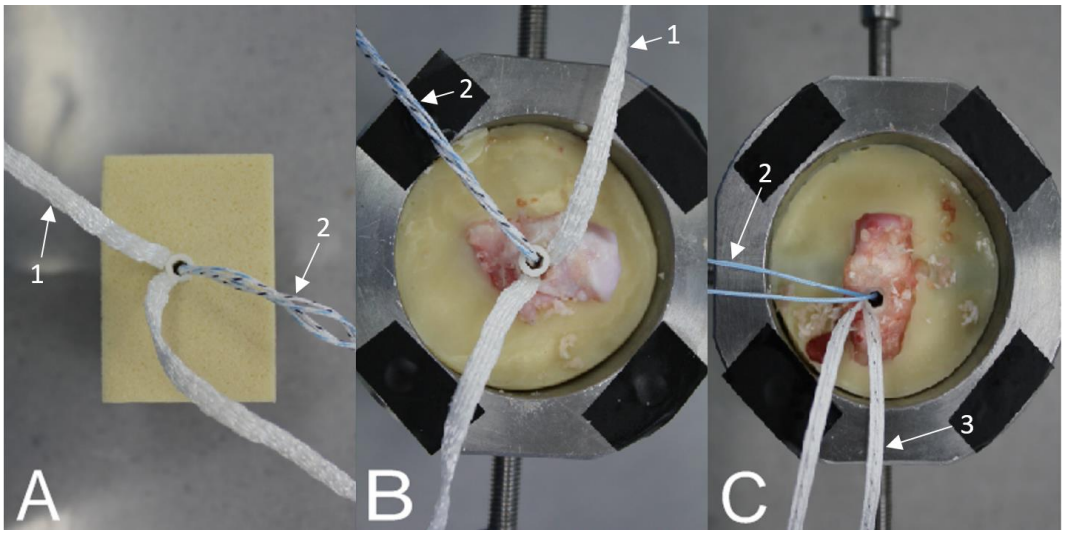

Figure 123. Specimens implanted with anchor and suture tape prior to testing. A) Infinity-Lock tape (Xiros Ltd, Leeds, UK) (1) implanted into artificial Sawbone blocks, B) Infinity-Lock (Xiros Ltd, Leeds, UK) (1) implanted into porcine fibula and C) InternalBrace (Arthrex Inc, Naples, FL, USA) (3) implanted into porcine fibula. 2 = FiberWire of the SwiveLock suture anchor (Arthrex Inc, Naples, FL, USA).

Table 41. The scoring system implemented to rank the ease of implantation of suture tapes into the samples using a SwiveLock suture anchor (Arthrex Inc, Naples, FL, USA).

Score	Description
1	Implantation not possible
2	Implantation performed with great difficulty
3	Implantation performed with some difficulty
4	Implantation performed with some ease
5	Implantation performed with great ease

5.3.2.4 Testing Protocol

Tensile pull out testing was performed using an ElectroPuls E10000 (Instron, Buckinghamshire, UK) material testing device with a 1 kN load cell. A linear pull out test was performed to enable comparisons to be drawn between the results of this study and a previously published white paper by Arthrex, shown in Appendix G.1 Arthrex White Paper 1. An x-y translating platform and universal joint, allowing 5 degrees of angular motion in any direction and 360 degrees rotation, were used to reduce potential misalignment, shown in Figure 124. The Sawbone specimens were attached to the ElectroPuls E10000 with a bespoke fixture previously developed within iMBE for testing Sawbone samples (Whitaker et al., 2019), shown in Figure 124. The fibula specimens were attached to the materials testing device using the cement

pots, as described in Chapter 2. One of the loose ends of the suture tape was held within the interference grip approximately 30 mm from the suture anchor, shown in Figure 124. The grip had two smooth crimped surfaces which were tightened using two bolts to create an interference grip of the suture tape.

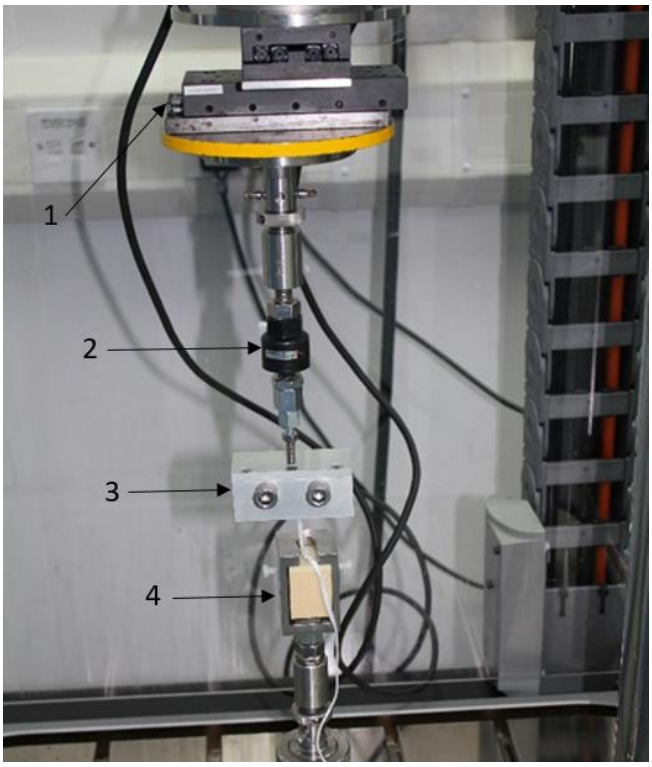

Figure 124. Testing setup showing the x-y translating platform (1), universal joint (2), interference grip (3), Infinity-Lock tape and Sawbone block within a fixed rigid grip (4).

Suture tapes were exposed to a pre-load of approximately 1 N to ensure they were taut and the x-y translating platform was correctly aligned. Exact gauge length measurements were then made using Vernier callipers accurate to 0.02 mm. The suture tapes were pre-conditioned by cyclically loading to observe if any stretching occurred. The suture tapes were exposed to 100 cycles of loading between 2 N and 100 N at a frequency of 1 Hz. A load of 100 N was determined to be a safe loading value as suture tapes were exposed to this load during anterior drawer tests performed in the previously reported study. The rate of loading was selected based on being similar to that of walking speed. All tapes were then ramped to failure at a strain rate of 1 $mm.s^{-1}$. The mode of failure was recorded and where this was not evident the sample was separated with a small hacksaw to further investigate the failure mode. The InternalBrace suture tape implanted into fibula was tested a second time with both loose ends of the suture tape gripped by the interference grip in response to slippage of the suture tape occurring in the first trial.

5.3.2.5 Data Analysis

The results from the mechanical characterisation of the suture tape implantation study were exported into, and collated in, Microsoft Excel. The pre-conditioning and load to failure results

were separated for analysis. Maximum displacements were calculated for every 10 cycles of the pre-conditioning and normalised by the gauge length of specimens. The maximum load and load at 3 mm displacement, the threshold anterior displacement value for ankle stability, were also calculated.

5.3.3 Results

5.3.3.1 Implantation

The implantation scores for each of the methods using the two different suture tapes into both Sawbone and porcine bone are shown in Table 42. The Infinity-Lock suture tape was implanted into the Sawbone material with ease using both the punch and tap suture anchor tunnel preparation methods. Implanting the Infinity-Lock suture tape into porcine bone was much more challenging. For the tapped method the anchor thread struggled to engage with the tapped thread whereas the punched method required excessive force for implantation. Implantation of the InternalBrace using the tapped method into the Sawbone was performed with great ease and with ease into porcine bone.

Table 42. The implantation ranking scores (n = 1) for the two suture tapes using either a tapped or punched suture anchor tunnel preparation method and implanting into Sawbone (SB) and porcine bone (PB).

	Xiros Infinity-Lock				Arthrex InternalBrace	
	SB Punch	SB Tap	PB Punch	PB Tap	SB Tap	PB Tap
Implantation Score	4	4	3	2	5	4

5.3.3.2 Mechanical Characterisation

5.3.3.2.1 Pre-conditioning

Cyclic loading was not completed for the Infinity-Lock suture tape implanted into porcine bone after the punch anchor tunnel preparation method as suture tape failure occurred at 44.8 N. Cyclic loading was not performed for the InternalBrace suture tape implanted into porcine bone where only one strand of the suture tape was held within the grip due to a test error.

5.3.3.2.1.1 Infinity-Lock Suture Tape

During pre-conditioning creep was experienced in all tests, shown in Figure 125. The greatest amount of creep (0.63 mm) was experienced by the Infinity-Lock suture tape implanted into Sawbone using the tapped preparation method. When the same suture tape was implanted into Sawbone using the punched preparation method the level of creep was lower (0.35 mm).

The overall displacement during the final 100 N load application for the Infinity-Lock suture tape implanted into Sawbone using the tapped and punched approach was 2.48 mm and 2.55 mm, respectively. Considerably less displacement and creep occurred when the suture tape was implanted into porcine fibula using the tapped preparation method in the single trials performed (1.22 mm and 0.18 mm, respectively).

5.3.3.2.1.2 InternalBrace Suture Tape

The InternalBrace suture tape was found to creep 0.20 mm and 0.31 mm when implanted into Sawbone and Porcine bone, respectively. Overall displacement at the final cycle of 100 N load for the suture tape was 1.44 mm and 1.68 mm when implanted into Sawbone and porcine fibula, respectively.

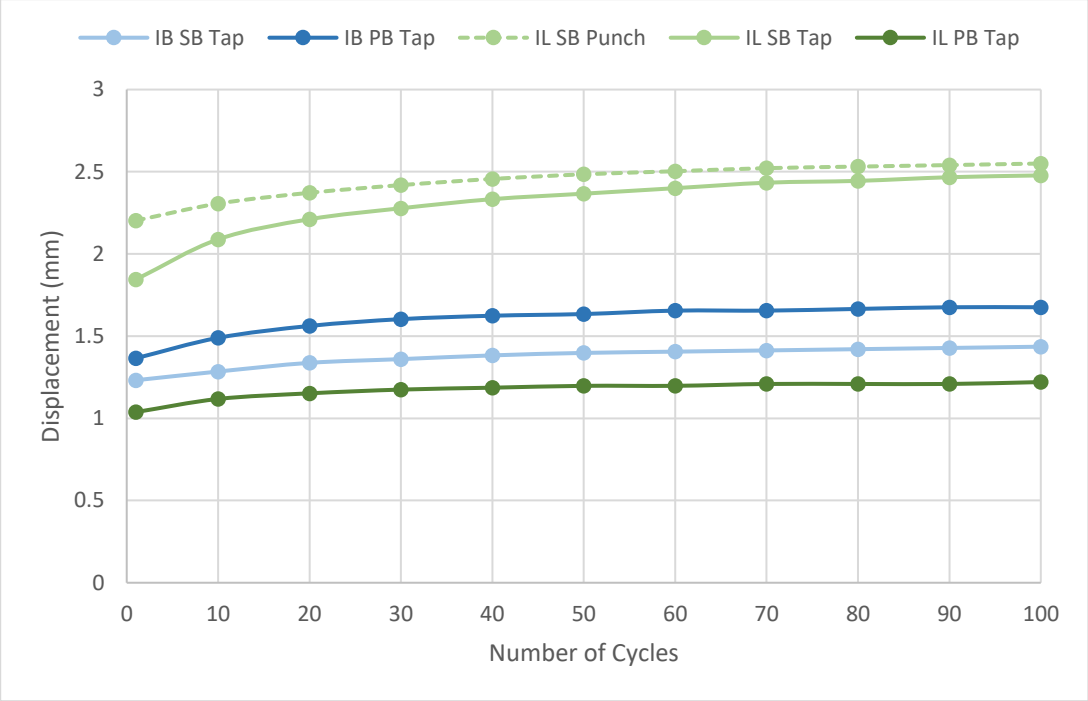

Figure 125. The displacement against number of cycles results for the cyclic loading performed (n = 1). IB = InternalBrace (blue), IL = Infinity-Lock (green), SB = Sawbone (light tone), PB = porcine bone (dark tone), Tap = tapped approach (solid line) and punch = punched approach (square dotted line).

5.3.3.2.2 Load to Failure

The failure loads of the Infinity-Lock and InternalBrace suture tapes tested are shown in Table 43 and Figure 126.

Table 43. Maximum failure load and load at 3 mm displacement of the suture tapes implanted into Sawbone (SB) and porcine bone (PB) (n = 1). Numbers within parentheses indicate the number of suture tape strands gripped.

	Xiros Infinity-Lock				Arthrex InternalBrace		
	SB Punch	SB Tap	PB Punch	PB Tap	SB Tap	PB Tap (1)	PB Tap (2)
Max Load (N)	181.7	153.0	44.8	164.9	180.8	214.0	447.8
Load at 3 mm	119.6	133.5	35.6	121.3	176.6	199.2	324.8

5.3.3.2.2.1 Infinity-Lock Suture Tape

When the Infinity-Lock suture tape was implanted into Sawbone the punched suture anchor tunnel method was stronger than the tapped method failing at 181.7 N and 153.0 N, respectively. The opposite was true for porcine tissue testing with the punched method failing at 44.8 N and the tapped method failing at 164.9 N. At the 3 mm threshold the Infinity-Lock devices implanted into porcine bone had already failed.

5.3.3.2.2.2 InternalBrace Suture Tape

The InternalBrace failed at 180.8 N and 214.0 N when implanted into Sawbone and porcine bone, respectively, when only one strand of the suture tape was gripped. Gripping both strands of the suture tape increased the failure load to 447.8 N when implanted into porcine fibula. The Internal Brace was close to failure in all three tests at the 3 mm displacement threshold but the loads were higher than the Infinity-Lock suture tapes, shown in Table 43.

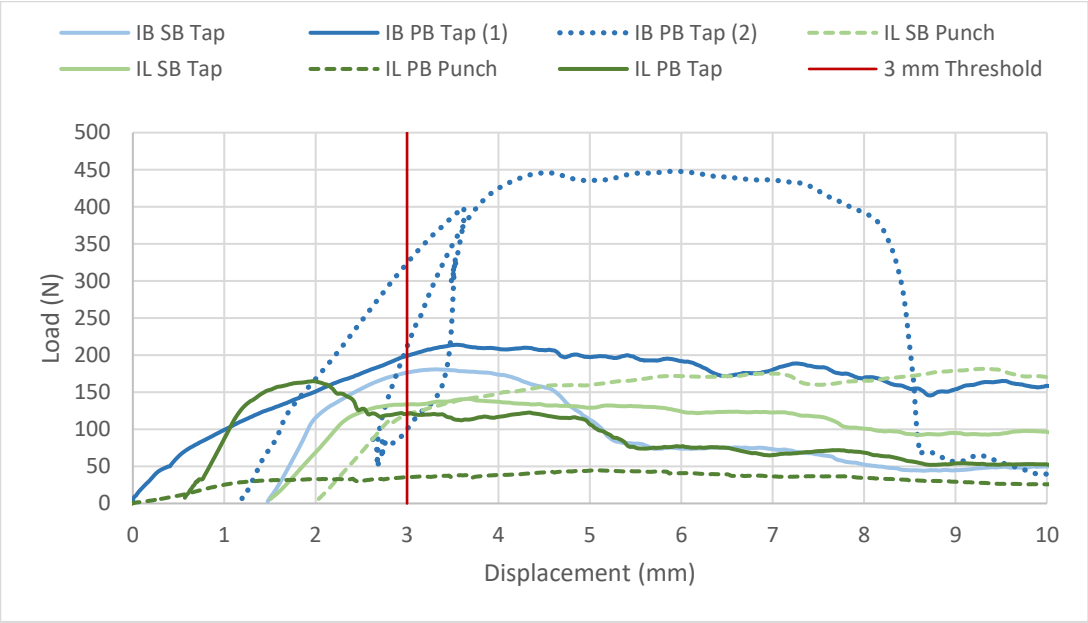

Figure 126. The load-displacement results for the load to failure pull out tests performed (n = 1). IB = InternalBrace (blue), IL = Infinity-Lock (green), SB = Sawbone (light tone), PB = porcine bone (dark tone), Tap = tapped approach (solid line), punch = punched approach (square dotted line) and the numbers within parentheses = how many strands of the suture tape were gripped (2 = round dotted line). The 3 mm stability threshold is shown (red solid line).

5.3.3.3 Failure Mode

The mode of failure differed between suture tapes, implantation method and tissue used in this study. The modes of failure for each trial are described in Table 44 and shown in Figure 127. In no cases for either suture tape did failure of the suture tape occur, all failures were an issue of suture tape fixation.

Table 44. The failure mode of each trial performed in this study.

Suture Tape	Tissue	Method	Failure Mode
Infinity-Lock	Sawbone	Punched	Eyelet fracture and suture tape slippage
		Tapped	Eyelet detachment from the anchor
	Porcine	Punched	Suture anchor fragmentation
		Tapped	Suture anchor pulled out of fibula
InternalBrace	Sawbone	Tapped	Suture anchor pulled out of Sawbone
	Porcine	Tapped (1)	Suture tape slippage
		Tapped (2)	Eyelet cracked, suture anchor deformed and suture tape slippage

5.3.3.3.1 Infinity-Lock Suture Tape

When implanted into Sawbone using the punched method the Infinity-Lock suture tape failed due to the eyelet of the SwiveLock suture anchor fracturing. Fracture of the eyelet allowed the suture tape to slip along the Sawbone-anchor interface, shown in Figure 127A. When the tapped method was used to implant the suture tape into Sawbone failure occurred due to the eyelet of the SwiveLock suture anchor dislodging from the suture anchor. The eyelet was able to pass through the low density polyurethane core to the higher density polyurethane layer, shown in Figure 127B & Figure 127C.

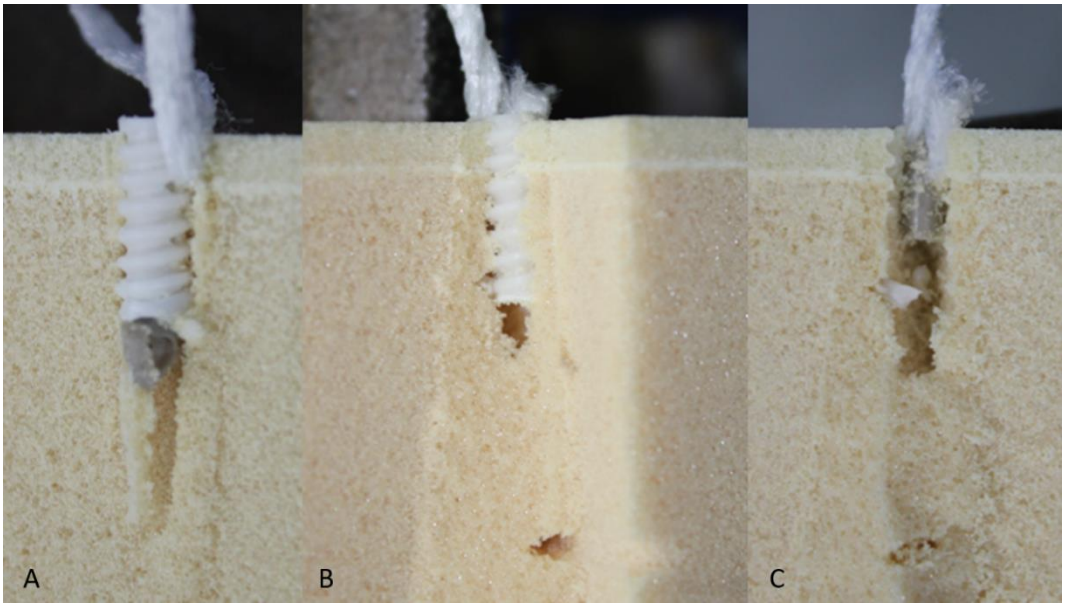

Figure 127. The failure modes of the Infinity-Lock suture tape implanted into Sawbone using the punched method (A) and tapped method (B & C). All Sawbone blocks have been cut to expose the suture anchor after testing to failure. The anchor was removed from the tapped specimen (B) to show the position of the eyelet (C).

Fragmentation of the SwiveLock suture anchor occurred when the Infinity-Lock suture tape was implanted into porcine fibula with the punched method. The anchor fractured into five separate pieces, shown in Figure 128A. Whereas, when the tapped method was used to implant the Infinity-Lock suture tape into porcine fibula the suture anchor dislodged from the tapped anchor tunnel. The SwiveLock suture anchor and Infinity-Lock suture tape were both removed from the porcine fibula without any noticeable damage, shown in Figure 128B.

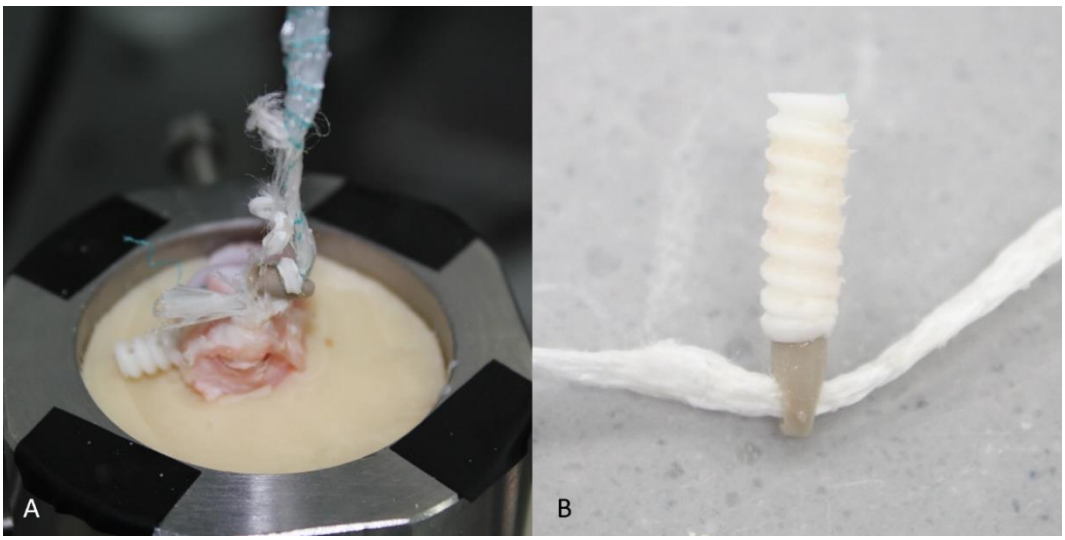

Figure 128. The failure modes of the Infinity-Lock suture tape implanted into porcine fibula using the A) punched method and B) tapped method.

5.3.3.3.2 InternalBrace Suture Tape

The InternalBrace failed through pull out of the suture anchor when implanted into Sawbone similarly to the Infinity-Lock suture tape implanted into porcine bone using the tapped method. When the InternalBrace was implanted into porcine bone slippage of the suture tape occurred when only one strand of the suture tape was gripped within the interference grip. When both strands of the InternalBrace suture tape were held in the grip failure occurred due to the eyelet fracturing allowing the suture tape to slip along the bone-anchor interface. On the surface the anchor had not moved and was still flush with the bone but the suture tape had been removed, shown in Figure 129.

Figure 129. The porcine fibula specimen after failure of the InternalBrace suture tape.

Upon further inspection by cutting into the porcine fibula it was evident that the anchor had deformed under the high failure load due to the load being applied by the eyelet onto the anchor, shown in Figure 130. The InternalBrace suture anchor showed no visible damage to its

structure other than a crimping pattern where the thread of the suture anchor had applied pressure.

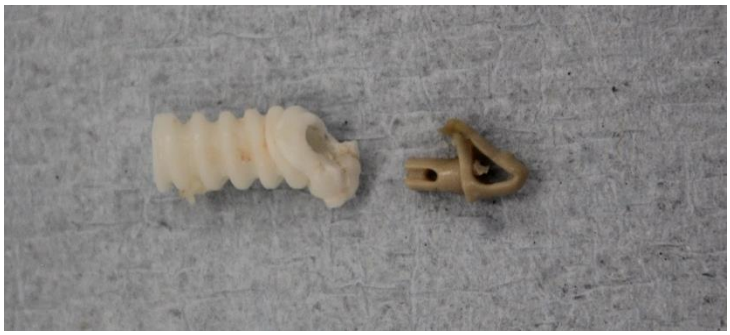

Figure 130. A failed Arthrex SwiveLock suture anchor where the eyelet has fractured and the anchor has been deformed. The suture anchor was loaded with an Arthrex InternalBrace suture tape and implanted using the tapped method described by the manufacturer.

5.3.4 Discussion

This study aimed to identify the most suitable implantation technique for the Infinity-Lock suture tape using SwiveLock suture anchors. The suture tape was implanted into both porcine bone and a custom Sawbone model. The study also aimed to mechanically characterise the InternalBrace when implanted into Sawbone and porcine bone following manufacturer guidelines. Finally the study aimed to compare the mechanical performance of the two suture tapes.

To determine the most effective method for the implantation of the suture tapes the appropriateness of the Sawbone model and porcine bone at replicating human bone must be considered. The Sawbone, although modelled on bone densities, had a very brittle core which would crumble into a fine dust when rubbed between the fingers. Implantation of the Infinity-Lock suture tape into the Sawbone model was also performed with ease, not reflecting the previously described experiences implanting into human bone. Such implantation difficulties were however evident when implanted into porcine bone. The Sawbone model was therefore determined to be a less effective model of human fibula bone than porcine fibula bone. The results of the Sawbone tests should therefore be interpreted with caution and a greater significance given to the results of the porcine bone testing.

A standard linear pull out test was performed, replicating a previous study conducted by Arthrex, shown in Appendix G.1 Arthrex White Paper 1. This produced comparable results for the Infinity-Lock suture tape to the InternalBrace suture tape using an industry established methodology. The results do not replicate failure in the ankle due to sprain and instead provide a more general understanding of the mechanical performance of various fixation methods for the two suture tapes.

5.3.4.1 Infinity-Lock Suture Tape

Based on the limited data, the highest failure load for the Infinity-Lock suture tape using a SwiveLock suture anchor was achieved when implanted into Sawbone using the punched suture anchor tunnel preparation method. The higher failure load of the punched method compared to the tapped method, when implanted into Sawbone, could have been due to the preservation and compression of Sawbone material around the thread within the suture anchor tunnel. The tapped approach involved drilling a tunnel and therefore removing some of the polyurethane whereas the punched method compressed the polyurethane material around the tunnel. The punched method would therefore have had an increased local density around the suture anchor tunnel enabling greater interaction with the suture anchor.

When implanted into porcine bone however the Infinity-Lock suture tape was considerably stronger after the tapped suture anchor tunnel preparation method had been performed. The removal of bone tissue when performing the tapped approach to suture anchor tunnel preparation reduced some of the difficulty faced implanting the Infinity-Lock suture tape into porcine bone.

The implantation of the suture anchor loaded with the Infinity-Lock suture tape was considerably more challenging when implanted into immature porcine bone than the Sawbone model for both suture anchor tunnel preparation techniques. Implantation of the Infinity-Lock suture tape into porcine bone was made difficult by the increased thickness of the suture tape compared to the InternalBrace. The thickness of the suture tape reduced the ability of the suture anchor thread to engage with the thread of the tapped bone tunnel as the suture tape was thicker than the thread depth. This could provide an explanation for the suture anchor dislodging when implanted into porcine bone following the tapped suture anchor tunnel preparation method.

Implantation into porcine bone, particularly following the punched suture anchor tunnel preparation method, required an excessive force. Deformation or even failure of the suture anchor could have occurred during implantation prior to pull out testing. This in combination with the lack of an internal thread and within the suture anchor tunnel made implantation of the suture anchor very challenging. This likely explains the reason for suture tape fraying and catastrophic failure of the suture anchor at a considerably lower load following the punched suture anchor tunnel preparation technique.

5.3.4.2 InternalBrace Suture Tape

The slim design of the InternalBrace suture tape allowed for easy implantation of the SwiveLock suture anchor into both Sawbone and porcine fibula. When one strand of the suture tape was tested in porcine fibula the fixation failed through tape slippage. Whilst the smooth and thin profile of the suture tape aids in achieving a stronger fixation of the SwiveLock anchor into bone it also appears to impact the interaction between the suture tape and suture anchor.

The InternalBrace is not branded as a synthetic ligament replacement but as a synthetic used to augment a modified Broström procedure. The effectiveness of the InternalBrace to provide additional support to the Broström repair cannot be definitively challenged by this study. The study does however raise questions regarding what strength contribution the suture tape provides in an augmented modified Broström procedure.

In response to slippage failure occurring, both strands of the suture tape were gripped to prevent slippage from occurring and the mechanical characterisation was repeated, shown in Figure 131. Equal tensioning of the suture tapes was incredibly challenging due to the enclosed design of the gripping fixture. As the tape had slipped previously it was however hypothesised that the suture tape would slip once again to self-balance the strands of the suture tape. This hypothesis was correct and after self-balancing further slippage of the suture tape was prevented. The data was normalised by removing the 4.0 mm displacement achieved at the start of the load to failure pull out test when under a load of 6.7 N. There is a noticeable anomaly in the profile of this test, shown in Figure 126, where the load reached 400 N and then plummeted along with a slight reduction in displacement. This occurred due to a safety limit for the ElectroPuls E10000 being triggered. The limit was raised to 900 N and the trial continued in a matter of seconds.

Figure 131. Arthrex SutureTape cemented into porcine fibula and both ends of the SutureTape are gripped within a mechanical grip.

When both strands of the suture tape were gripped the failure load of the InternalBrace implanted with a SwiveLock suture anchor almost doubled in the single trial performed. Typically the excess suture tape is simply cut away in the recommended procedure by the manufacturer, shown in Figure 132A. The potentially huge improvement in load capacity achieved when slippage of the suture tape is prevented is therefore not capitalised upon. This could however be achieved by attaching the loose ends of the suture tape together or to the

tensioned suture tape near the suture anchor, shown in Figure 132B. The practicalities of performing such an adaptation intraoperatively do however require some further consideration. For example, would suturing to the tensioned suture tape cause the suture tape to fail? Also to be considered is that in this pull out study the load was applied in the same axis as suture anchor orientation. This is not the reality for load application in patients who have an augmented Broström procedure with InternalBrace. The load would be applied from different angles in the fibula, talus and calcaneus as dictated by the procedure, therefore these results represent the worst case scenario.

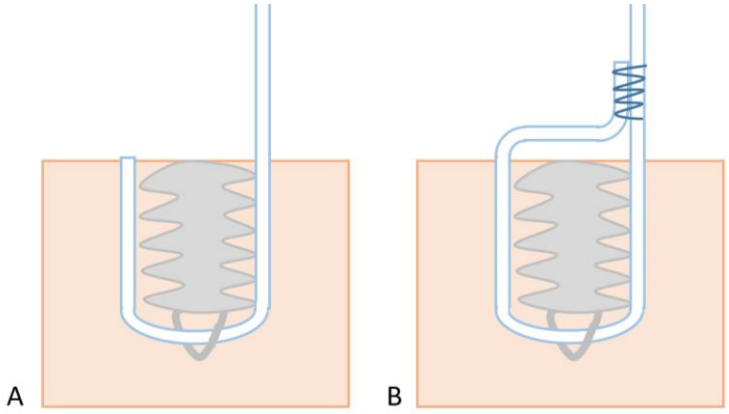

Figure 132. Illustration of InternalBrace suture tape (white with blue border) implanted into bone (beige block) using a SwiveLock suture anchor (grey threaded anchor) A) following manufacturer guidelines and B) following adaptation proposed by the author. The loose end of the suture tape is connected to the tensioned tape, in this case with a surgical suture (dark blue solid line).

5.3.4.3 General Discussion

Both the Infinity-Lock and InternalBrace suture tapes performed well under cyclic loading with minimal amounts of creep occurring. The InternalBrace failed at a higher load than the Infinity-Lock suture tape when both suture tapes were implanted into porcine bone following the Arthrex implantation guidelines of tapping the suture anchor tunnel. The InternalBrace was also easier to implant and from the limited data appeared to allow the SwiveLock suture anchor to integrate with the bone more than the Infinity-Lock suture tape. Bone integration can be interpreted by the failure mode with SwiveLock suture anchors used to implant InternalBrace suture tapes remaining within the bone whereas those implanted with the Infinity-Lock suture tape were dislodged.

The mean and 95 % CI values for failure load of the ATFL, CFL and PTFL were reported in Chapter 3 as 263.6 ± 164.3 N, 367.8 ± 79.8 N and 351.4 ± 110.8 N, respectively. Within the small sample, neither the Infinity-Lock nor the InternalBrace suture tapes were capable of achieving suitable loads when implanted with a SwiveLock suture anchor following manufacturer guidelines. Suture tape failure did not occur in any of the testing with the exception of incidental fraying of the Infinity-Lock suture tape following the punched suture anchor tunnel preparation method into porcine bone. Occurrence of fraying was likely due to

an inappropriate implantation method requiring excessive force whilst screwing the suture anchor into bone.

With a sample size of one for each investigation it is difficult to draw meaningful conclusions from the data. The thickness of the Infinity-Lock suture tape provided considerable challenge to implantation when using a SwiveLock suture anchor following the manufacturer guidelines. The small thread depth of SwiveLock suture anchors and the low tolerance between the suture anchor and the bone tunnel hinder the ability of SwiveLock suture anchors to effectively fix the Infinity-Lock suture tape. A similar approach has potential to work, however the thread depth would have to be increased and the tolerances between the suture anchor and bone tunnel refined for the specific implantation of the Infinity-Lock suture tape. Alternatively a different fixation method could be explored or perhaps the suture tape is adapted to be thinner. Should fixation of the Infinity-Lock suture tape be explored further the author recommends that it is developed and tested within natural bone tissue rather than a Sawbone model.

Failure occurred in all trials due to the fixation method, a SwiveLock suture anchor. Failure occurred in various ways and under a wide range of loads. When using a SwiveLock suture anchor the author believes that a tapped approach, as recommended by the manufacturer, is favourable over a punched approach to suture anchor tunnel preparation. This belief is based on the assumption of good quality bone stock for the patient. In patients with poor bone quality the tunnel preparation method is unlikely to influence results dramatically and the use of bone anchors has an increased potential to fail.

5.3.5 Conclusion

No suitable implantation method for the Infinity-Lock suture tape was identified within the small amount of investigations performed in this preliminary study. Future investigation of fixation methods for the Infinity-Lock suture tape should be performed using natural bone tissue opposed to the Sawbone model previously used. Within the small sample, both the Infinity-Lock and InternalBrace suture tapes failed, when implanted with a SwiveLock suture anchor, at loads lower than the natural tissue they are intended to repair. The InternalBrace cannot however be discredited as an augmentation to the Broström procedure by the findings of this study. The study does raise questions regarding the contribution that the suture tape is able to provide over the gold standard modified Broström procedure. A comparative study of the mechanical support provided by the InternalBrace during an augmented repair of the lateral ankle ligaments should be conducted. A potentially simple adaptation to limit tape slippage in the augmented Broström procedure with InternalBrace has the potential to double the load capacity of the suture tape augmentation.

Chapter 6 – Overall Discussions, Conclusions and Future Work

6.1 Overall Discussion

This project aimed to mechanically characterise the lateral ankle ligaments under conditions representative of LAS. A further aim was to analyse the biomechanics of ankle sprain and subsequent changes in joint stability through the simulation of sprain. The final aim was to evaluate the ability of synthetic interventions to restore joint stability and the effectiveness of their fixation technique.

Studies conducted were mostly of an exploratory preliminary nature due to the lack of existing knowledge and novel methodologies developed throughout the project. A great amount of insight was however still generated through the completion of the project to advance the development of synthetic interventions for LAS. The most significant finding of the project was the mechanical properties of the LCL complex were determined when characterised at strain rates representative of LAS. These results are reported in chapter three and further inform manufacturers of the mechanical requirements of synthetic interventions. A large volume of highly novel and exploratory research was conducted contributing to the development of a conceptual specification for future investigations into the simulation of LAS, detailed in chapter four. Changes in stability due to LAS were analysed and the effectiveness of synthetic interventions to restore joint stability was evaluated. The suture anchor fixation technique was mechanically characterised for both the Infinity-Lock (Xiros Ltd, Leeds, UK) and InternalBrace (Arthrex Inc, Naples, FL, USA) suture tapes and an adaptation was proposed potentially capable of doubling the failure load of the fixation technique.

6.1.1 Ligament Characterisation

6.1.1.1 Storage and Experimental Condition Effects

Cadaveric tissue if often sourced from a tissue bank and can require a large amount of dissection and sample preparation prior to testing. A preliminary study was therefore performed to identify possible effects of freeze duration and repeated freeze-thaw cycles on the mechanical properties of BLB constructs. The study also analysed the effects of testing environment conditions and strain rate on mechanical properties due to the lack of and contradictory nature of knowledge, respectively. Initial preliminary testing of the porcine patellar tendon identified that strain rate has a significant effect on the failure stress of ligaments, in agreement with previously published literature (Noyes et al., 1974; Neumann et al., 1994; Hawkins, 2002; Bonner et al., 2015; Karunaratne et al., 2018). The 40.8 % increase in failure load with increased strain rate was considerable and of importance yet determined to be statistically non-significant, likely due to the small sample size and large variation in data. This finding provides a specific novelty to the subsequent human ankle ligament characterisation study where a focus was on characterising the LCL complex at strain rates

estimated to be representative of LAS. Other storage and testing environment conditions investigated (up to four freeze-thaw cycles, freezing up to 151 days, freezing intact/dissected and tissue hydration with PBS spray/bath) were determined to have no significant effect on the mechanical properties of the patellar tendon BLB construct. A testing protocol was therefore established for future mechanical characterisation using the most time-efficient aspects investigated. These results are of particular importance for bioengineering researchers wanting to mechanically characterise tendinous and ligamentous structures of the body.

The porcine preliminary testing investigated the length of time samples were frozen for, up to 151 days (5 months). This time period covered the maximum length of time the donor tissue was expected to be stored frozen at the university. Research projects are often susceptible to change due to unforeseen circumstances preventing planned research from occurring in-line with an anticipated schedule, such as the ongoing global pandemic for example. Tissue inherited from a previous researcher was used in this study in an effort to prevent the wastage of precious human tissue and as no literature existed, to the knowledge of the author at the time, detailing the negative effect of freeze duration on the tensile mechanical properties of ligamentous structures. Research conducted after the mechanical characterisation studies highlighted the significant effect long term freezing can have on the failure load of tendinous tissue (Quirk et al., 2018). The study by Quirk et al. (2018) attributed the reduced failure load in rat Achilles tendon after 9 months of freezing to an increased collagen fibril spacing observed under electron microscopy (Quirk et al., 2018). The study raises a potential limitation not only for the mechanical characterisation study of this project but for all studies using tendinous or ligamentous tissue frozen for an extended period of time. This includes studies using human tissue from tissue banks, where the tissue is typically stored frozen for longer durations, and studies interrupted by the ongoing global pandemic. Researchers should therefore limit, as best within their control, the length of time tissues are frozen for and report the time period when publishing mechanical characterisation results to afford better interpretation.

When investigating the effects of experimental conditions on the mechanical properties of ligamentous tissues however, the use of porcine tissue as a surrogate model for human tissue is warranted. Not only does the use of porcine tissue, which is readily available, prevent the excessive and unnecessary wastage of human tissue it has also been demonstrated to be an effective model for human tissue characterisation (Kiapour et al., 2015; Cone et al., 2017). Particularly, as the inference made within this study is on what effect changes to storage conditions or testing procedures had on a particular ligamentous structure. Similarly the use of porcine tissue, considered by many to be less valuable than human tissue, is equally effective for the investigations into gripping technique development performed in this study, demonstrating responsible innovation. The main caveat to that point is that the anatomy of the model used must sufficiently reflect that of the modelled tissue. In situations where this is

not true, tissue wastage would in fact be increased for the model tissue, during model development, and the modelled tissue upon model validation.

6.1.1.2 Lateral Ankle Ligament Characterisation

The mechanical characterisation of the LCL complex was performed, at a strain rate estimated to be realistic for LAS, to determine the mechanical properties required of synthetic interventions. Should synthetic interventions be able to burden the excessive loads experienced during sprain then the augmented repair would be less prone to recurrent sprain than the repaired natural tissue. The average ultimate failure load of the ATFL was found to be noticeably lower than that of the CFL and PTFL, which had similar average ultimate failure loads, in agreement with previously published literature (Attarian et al., 1985; Siegler et al., 1988).

When the results were interpreted on an individual donor level, no systematic pattern was observed with the ATFL even being the strongest of the three ligaments of the LCL complex for some donors. Commentary on this observation has not previously been performed, to the author's knowledge, even where similar findings are present within the results of previous research articles (St Pierre et al., 1983). The relevance of this finding may not have been obvious in previous studies however in the context of ligament repair it is of great importance. It is known that the ATFL is the most frequently damaged lateral ankle ligament followed by combined ATFL and CFL injury and in a small number of very severe injuries the PTFL can also be damaged (Ferran and Maffulli, 2006; de Asla et al., 2009). Isolated cases of CFL injury have been reported but are uncommon and the occurrence is negligible in comparison to the other presentations of lateral ligament injury (Lynch, 2002; Rigby et al., 2015).

In an effort to ascertain an explanation for this phenomenon, previous researchers have assumed that the ATFL is the most frequently damaged ligament due to the fact that it is the weakest (Ferran and Maffulli, 2006; Fong et al., 2009a). Whilst this assumption could still be true for some how can it be that the ATFL is the strongest of the three ligaments of the LCL complex among some of the population? An alternative theory is that the average result for the ATFL is being reduced by the inclusion of numerous donor samples where the ATFL has been previously damaged and unreported, something that occurs very frequently (Hertel, 2002; Kemler et al., 2015). This theory could expose new understanding on the strengths of the ATFL, CFL and PTFL as well as guide an explanation for the higher frequency of ATFL ligament damage. If substantiated through further large-scale analysis, this theory would suggest that the anatomical position and insertions as well as the associated biomechanics of the ankle are more critical to the predisposition of the ATFL to have an increased injury prevalence rather than its strength (Al-Mohrej and Al-Kenani, 2016).

The advancement of synthetic ankle ligaments could optimise ligament repair treatments. The human ankle ligament characterisation findings of this study can further inform mechanical property specifications for the development of synthetic interventions. Through improved

matching of the mechanical properties, particularly the stiffness, of synthetic ligaments to their natural counterparts, joint mobility and stability have the potential to also benefit. In order for this to become a reality, novel manufacturing techniques may also be required for the production of synthetic ankle ligaments whereby varying sizes and properties of synthetic ligaments can be produced. Additional complexity is likely to be introduced when personalising medicine but even a stratified approach would surely be beneficial over a one device suits all approach.

A positive correlation between BMI and the ultimate failure load of the CFL was identified in this project within a cohort with a normal BMI (r = 0.92; p = 0.01). Further investigation with a larger sample covering a wider ranging BMI is required to corroborate this correlation. The same relationship was also observed for the ATFL and PTFL but no significant correlation was identified. This relationship is likely due to the adaptive remodelling nature of ligaments as individuals with a greater BMI are expected to apply more stress to the ligament, increasing strength over time (Hauser, 2013). This theory is supported by the findings of Taş and co-workers who identified a correlation between BMI and the thickness of the patellar tendon (Taş et al., 2017). Increased loading of tendinous tissue due to performing exercise consistently over a 12 month period has been shown to increase “tendon weight, cross-sectional area, collagen content, modulus and strength” (Woo et al., 1980; Wren et al., 2000). Likewise joint disuse can lead to a deterioration of the mechanical properties of ligaments and tendons (Yasuda and Hayashi, 1999). A patient’s BMI could therefore be an important factor when selecting the appropriate material properties of a synthetic intervention, and notably patients with a high BMI who are more often candidates for a synthetic ligament repair (Ajis et al., 2006).

The mechanical property results of this study can also be employed in computational models in the form of ligament property definitions within OpenSim or AnyBody models (AnyBody Technology A/S, Aalborg, Denmark). The data has in fact already been used in an international collaboration using a foot and ankle musculoskeletal model to understand ligament behaviour during functional movements (Boey et al., n.d.).

6.1.1.3 The Lateral Collateral Ligament Complex

An important consideration in the design and development of synthetic ligament interventions is the anatomy and structure of the ligament they intend to repair, particularly the location of the origin and insertion points. As detailed in the section of the literature review titled ‘Lateral Collateral Ligament Complex’ the anatomy of the LCL complex varies significantly between individuals. The size, orientation and number of constituent ligamentous bands forming the ATFL, CFL and PTFL have been reported to vary between individuals. With increasing inspection of the LCL complex by anatomists, the interconnected nature of the ATFL, CFL and PTFL at their fibular insertion has been observed (Golanó et al., 2016; Dalmau-Pastor et al., 2020). The same observation was made in this project and although it was discovered by

anatomists within the field over four years ago, it is yet to become common knowledge among researchers in the ankle field.

This raises a question on how we should consider the ligaments of the LCL complex. Should the ATFL, CFL and PTFL be considered as three distinct ligament structures or as a single interconnected ligamentous complex? The lateral ankle ligaments could be considered as an interconnected complex which varies depending on patient-specific factors to collectively stabilise the lateral side of the ankle joint complex and achieve the same function. Regardless of how they are considered, it appears to be growing ever more evident that there is no standard presentation of the LCL complex. Repair of the lateral ankle ligaments should therefore also be non-standardised and a patient-specific approach to anatomical repair would be preferable.

Dalmau-Pastor et al. (2020) suggests that the interconnecting fibres may play some role in the mechanical stabilisation of the lateral ankle but admits their exact function is unknown (Dalmau-Pastor et al., 2020). The mechanical properties of the interconnecting fibres were not directly reported in this project however they were retained when the entire LCL complex was characterised. No macroscopic damage to the fibular insertions of the ATFL or PTFL occurred when the CFL was ruptured, even for samples where fibular avulsion was the mode of failure. The small connecting fibres are therefore unlikely to provide a significant amount of strength to the LCL complex to aid in the stabilisation of the lateral ankle complex. Further experimentation is required to determine the exact function of the interconnecting fibres of the LCL complex. Alternatively computational modelling could be beneficial with a reverse engineering approach being adopted for the investigation into the role of the interconnecting fibres.

6.1.2 Development of a Lateral Ankle Sprain Simulation

The current understanding of ankle sprain biomechanics is poor considering the high prevalence of ankle sprains. This is in part due to the complexity of motion at the ankle complex, the likely diverse ROM combinations possible of instigating LAS and the lack of a sprain simulation methodology. Most agree that excessive inversion is a major factor to the causation of lateral ankle ligament injury with increased plantar flexion and internal rotation having the ability to increase the level of damage (Fong et al., 2009b; Mok et al., 2011; Gehring et al., 2013). The rate of loading is of importance too as sprain often occurs quicker than the reaction time of the muscles in the lower leg (Gehring et al., 2013). Less is known about the loads applied during sprain events due to the difficulty faced capturing kinetic data during sprain events.

One avenue to investigate the biomechanics of LAS is through the simulation of LAS using cadaveric tissue. To the author's knowledge, there are currently no sprain simulators capable of replicating LAS using realistic loads and strain rates. Thus the development of such a device

for cadaver testing was a central aim of this project. An iterative approach to design and development of the sprain simulation was adopted during this project, whilst simultaneously considering the three different aspects which guide motion, generate load and analyse motion. Focus was primarily on the development of a sprain platform to replicate the motions of ankle sprain whilst harmoniously combining with the loading device and motion capture system.

A robust and modular sprain platform capable of performing the motions associated with lateral, medial and distal tibiofibular syndesmosis sprain for both left and right feet was produced. The sprain platform was capable of performing up to 90 degrees of plantar flexion and inversion, individually, with zero degrees of internal rotation. Alternatively, combined plantar flexion and inversion could be performed, up to 45 degrees in each direction, generating internal rotation as a by-product of the combined universal joint motion. Higher degrees of plantar flexion (50 degrees) and inversion (45 degrees) ROM was achieved using the final hard stop design, shown in Appendix D.1.16 Base Hard Stop. The use of this style of hard stop did however reduce the adaptability of the sprain platform as a new hard stop is required to be manufactured for the investigation of different angles. Adaptability was considered a key aspect of the sprain platform given the lack of knowledge on the angles and loads required to generate LAS. In hindsight the adaptability of the platform could also have been a downfall of the design given the current stage of understanding and the investigations required. A stronger design capable of bearing higher loads could have been achieved if the ROMs tested were fixed or differed in larger increments, rather than coving the entire ROM scale.

Estimations of the required motion and loading to cause LAS were calculated from the limited literature available on the biomechanics of LAS. The data available was for unspecified or mild LASs and therefore the estimations made could have been underestimates for the generation of severe LAS. The drop-weight rig used was sufficient for applying the estimated loads required to generate LAS. A major restriction of the drop-weight rig however was that the rate of loading (strain rate applied to ligaments) could not be tailored to be specific for LAS without affecting the impact energy load. In a previous study within this project, detailed in **Error! R eference source not found.**, the importance of strain rate on the mechanical properties of lateral ankle ligaments was highlighted. Therefore, the unrealistic strain rates used in this study, as a consequence of using a drop-weight rig, could provide explanation for the difficulties faced around appropriately loading the specimen. The lack of load control offered by the drop rig throughout the sprain simulation trial was another limitation of the loading device. The inability to control load prevented the application of a consistent load at a consistent rate throughout the simulation. Rather an impact energy was applied to the sample which either caused catastrophic failure in the form of bone fracture or was absorbed by the sample with no evidence of macroscopic damage. The application of a consistent load rather than one which reduces in both magnitude and application rate during the trial could potentially have eliminated some of the challenges faced loading the sample. Of the devices

available to the author at the time the study was conducted the drop rig was however the most appropriate loading device.

Kinematic data was captured for sprain simulation efficiently using a Miqus motion capture system (Qualisys AB, Gothenburg, Sweden). An optical motion capture system was selected for biomechanical analysis due to the 3-dimensional capabilities in addition to the high capture rate. The use of motion capture presented a few obstacles for the sprain simulation study. Firstly, the line of sight of reflective markers is required by two or more motion capture cameras at all times. This initially posed a considerable design challenge for the sprain platform as a balance between structural integrity and a clear line of sight of reflective markers was required. The positioning of motion capture cameras became a specimen-specific task due to the variation in size and footedness of specimens altering the position of the reflective markers. Positioning of cameras became a time-exhaustive task due to the essentiality of obtaining a 100 % capture rate through the complete sprain motion on the first attempt.

The use of passive reflective markers also posed a separate issue in terms of hydrating the specimen throughout testing. Samples were soaked in PBS for 30 minutes prior to marker fixation in an attempt to combat dehydration effects. The fixation of markers triads into bone was also problematic and required several iterations. Difficulties arose when markers were not implanted firmly enough into bone and were either dislodged or moved/vibrated relatively to the sample. Finally 316 stainless steel marker triads implanted firmly into bone were successful in accurately tracking the motion of the ankle complex. The capture frequency of the motion capture system was determined to be critical for this study due to the high rates of loading employed. Optical motion capture was capable of capturing the fine details of ankle kinematics when motion occurred at a great rate and is therefore still recommended for ankle sprain analysis.

The simulation of sprain came close to successfully simulating LAS. Variation between donor specimens posed a significant challenge to simulating sprain, particularly as a lack of control over loading existed. The inversion ROM employed in this study was likely too low for the simulation of severe LAS. Inversion ROM closer to, or even in excess of, the 90 degree capability of the sprain platform may be required for the simulation of severe LAS as demonstrated in recently published literature (Panagiotakis et al., 2017). The load and rate of loading also needs to be closely considered, potentially at an individual donor level, when attempting to simulate ankle sprain. The sprain platform and optical motion capture system used in this project are proposed to be adequate for the successful simulation of LAS, although unproven by this study. The use of a drop-weight rig to apply load is however not recommended where more suitable devices with load control capabilities are available, such as electromechanical materials testing devices. Further research into the biomechanics of sprain through computational modelling can also potentially provide essential insight into the motions associated with ankle sprain. The computational work of Fong and their colleagues could provide answers to the current gaps in knowledge (Fong et al., 2009b).

6.1.3 Joint Stability after Lateral Ankle Sprain

Joint stability is imperative to the quality of life and ability to participate in sport with many people with CAI, where treatment has been ineffective, changing sports or stopping participation in sport entirely (Vuurberg et al., 2018a). Patients who suffer chronic lateral ankle instability can experience frequent episodes of the ankle instantaneously and unexpectedly giving way (Gribble et al., 2016b). Ankle instability is most commonly analysed through clinical assessment of the patient in the form of an anterior drawer and talar tilt tests (Song et al., 2019). Stress radiography can be used to quantify the stability of the ankle joint and an instability threshold value of 3 mm anterior displacement of the talus, relative to the contralateral limb, has been established (Seligson et al., 1980).

Individual contributions of the ankle complex, talocrural and subtalar joints to anterior-posterior displacement and inversion/eversion ROM during stability drawer tests were calculated in this project for the first time, to the knowledge of the author. The individual joint data provides insight into the effect an ATFL or combined ATFL and CFL rupture can have on the biomechanics of the ankle. Ankle stability was found to decrease with sequential sectioning of the ATFL and CFL in this project when analysed through anterior drawer and talar tilt tests measured using motion capture. Chronic ankle instability, among other factors (altered joint mechanics, congruity and malalignment), is widely accepted as a contributing factor to the progression of PTOA (McKinley et al., 2004; Saltzman et al., 2005; Valderrabano et al., 2009; Weatherall et al., 2013; Buckwalter et al., 2013; Blalock et al., 2015; Delco et al., 2017). Chronic ankle instability is however not the main cause of PTOA with up to 95 % of individuals suffering severe ankle sprain presenting with an osteochondral lesion, often on the dome of the talus (Taga et al., 1993). An osteochondral lesion lead to the development of PTOA in over 50 % of patients (Klammer et al., 2015). Increased ligament length and resulting ligament laxity, due to sprain, alters the ROM of the ankle complex, as demonstrated in the results of this study. Changes in contact stresses are therefore likely experienced in the joints, particularly in the talocrural joint after ATFL injury, exacerbating the issues associated with the osteochondral lesion present on the talar dome (Anderson et al., 2011). If an osteochondral lesion was not formed due to the primary injury during a sprain event one can arise over time due to the increased localised contact stresses experienced. This data could potentially aid in the explanation of how chronic instability can lead to the progression of PTOA.

On average the anterior drawer results increased by 3.6 ± 1.6 mm after sectioning the ATFL and by 4.8 ± 2.6 mm after combined ATFL and CFL sectioning. These findings suggest that the threshold value of 3 mm, which has been longstanding for clinical assessment of lateral ankle instability, could possibly exclude some patients who have suffered a severe ATFL rupture or even a combined ATFL and CFL rupture. Within the small sample, the variability between individuals for anterior drawer test measured using motion capture was found to be 2.0 mm in the intact condition when an anterior load of 100 N was applied. The threshold value to

determine rupture of the ATFL could therefore be lowered when using this technique to improve the accuracy of the test. A single threshold value is unlikely to be perfect for an entire population however based on the results of this project a value of 2.0 mm anterior drawer would be more suitable than 3 mm to identify severe LAS and instability. For such a value to be adopted clinically, a quantitative and equally accurate load application technique would have to be implemented. Preferably load would be applied and motion captured from the skin surface opposed to directly implanting load devices and bone pins. This would likely increase the variance in results slightly due to different levels of soft tissue depth between the bone and skin surfaces.

Motion capture was found to be a suitable tool for the evaluation of joint motion during drawer tests. The mean and variation results of the study, evaluating the validity of the motion capture and motion drawer techniques performed in this study, were comparable to two different techniques performed in a previous study (Kovaleski et al., 2002). Anterior drawer was found to be considerably more accurate than the talar tilt test for the identification of ATFL rupture in this study. Whereas the talar tilt test was much more effective at identifying combined rupture of the ATFL and CFL. Therefore the use of both the anterior drawer and talar tilt tests is recommended for the identification of LAS as well as the evaluation of repair techniques to restore joint stability, supporting the current understanding (Song et al., 2019).

6.1.4 Synthetic Repair of Lateral Ankle Ligaments

The use of synthetic interventions has recently gained some traction as an augmentation of soft tissue repair in the form of the augmented Broström procedure with InternalBrace. This type of procedure has been suggested to improve return to sport and is therefore a popular treatment for elite athletes suffering an ankle sprain (Viens et al., 2014; Coetzee et al., 2018). The use of synthetic interventions has also been proposed to be beneficial for patients with a higher than normal BMI (Cho et al., 2015).

6.1.4.1 Infinity-Lock

Testing of the Infinity-Lock suture tape, produced by the industrial sponsors of the project, was the original aim of this project. A considerable amount of resource had been spent by the industrial sponsors on the development of a strong suture tape with an open weave structure offering the opportunity for cell infiltration. An adequate strength and appropriate stiffness is imperative to the success of synthetic interventions, being able to restore joint stability, and to prevent implant failure. Unfortunately, the fixation and surgical implantation techniques for the suture tape were not sufficiently developed at the point in time of the stability analysis study for the inclusion of the Infinity-Lock suture tape.

Some initial preliminary testing was performed for the fixation of the Infinity-Lock suture tape, described in Chapter 5. Unfortunately a successful fixation technique was not developed during the preliminary testing however insight was gained surrounding the use of suture

anchors for the Infinity-Lock suture tape. Use of a SwiveLock (Arthrex Inc, Naples, FL, USA) suture anchor was determined to be unfeasible due to the inability to progress the suture anchor into the bone tunnel without the application of excessive force. The required positioning of the suture tape between the suture anchor-bone interface for the fixation technique and the thickness of the suture tape were responsible for the significant challenges faced upon implantation. The action of progressing the suture anchor into bone using a considerable torque force was also responsible for occasional fraying of the suture tape due to its fibrous and open-weave structure. The Infinity-Lock suture tape was originally developed for repair of the shoulder and fixed using a titanium alloy button (Neoligaments, n.d.). Therefore, should applications of the Infinity-Lock suture tape be pursued within the ankle, the author would recommend that a technique which does not involve a torque load being applied to the suture tape should be adopted. A considerable amount of further investigation into a suitable fixation method for the Infinity-Lock suture tape is still required. With the development of a potentially novel fixation technique the manufacturers of the Infinity-Lock suture tape would also need to consider the potential implications this would have on the surgical technique adopted.

6.1.4.2 InternalBrace

Clinical outcomes of the most routinely used synthetic repair, the augmented Broström procedure with InternalBrace, are comparable to the current gold standard procedure, the modified Broström procedure (Coetzee et al., 2018). Ascertainable benefits of the augmented procedure over the gold standard are however limited with a reduced return to sport and quicker surgical time being the standout advantages (Ulku et al., 2020). Whilst FAAM sports scores were enhanced for the augmented procedure no difference was reported during daily life (Ulku et al., 2020). The reduced return to sport is attributed to the ability to immediately partially weight-bear and subsequent earlier commencement of rehabilitation due to immobilisation within a cast for two weeks not being required as it is with the modified Broström procedure. The quicker surgical time does not translate to an increased cost effectiveness with the augmented procedures calculated to be 1.3x the cost of the gold standard even when accounting for the cost benefits of a reduced surgical time (Cho et al., 2019). No significant difference was found between the two procedures for other outcomes including FAOS, FAAM, recurrence rate of instability and stress radiographs (Cho et al., 2019).

Within this project the InternalBrace suture tape was found to adequately restore joint stability in two out of six repairs, where all other repairs failed at their fixation during inversion testing. The results for successful trials were promising considering soft tissue repair was absent from the augmented Broström procedure with InternalBrace. The high proportion and manner of fixation failures was however concerning since the suture tape is currently being implanted into patients using the same SwiveLock suture anchors. Whilst the clinical relevance of the study could be questioned due to the absence of soft tissue repair, this study exposed

potential vulnerabilities of the suture anchor fixation technique used for suture tape augmentation. Failure at relatively low loads of 4 N.m torque is unacceptable and demonstrates the inadequacy of the augmented repair for joint stability restoration when compared to the intact condition. Clinical stability analysis of ankles repaired using the augmented Broström procedure with InternalBrace produce good outcomes in patients (Ulku et al., 2020). The contribution of the suture tape augmentation to joint stability is however unknown as the soft tissue repair could be responsible for the entirety of the stability produced, which did not differ significantly from those of the modified Broström procedure (Ulku et al., 2020). The effects of the suture tape could be, and theoretically should be, masked by the soft tissue repair performed. This is due to the suture tape being implanted slightly slack to prevent impingement or stress shielding of the repaired tissue. Since the augmented procedure only differs from the gold standard procedure through the addition of the suture tape, the outcome of no significant difference between the two procedures for any outcome measure is akin to a false positive result.

In order to identify the contribution of the InternalBrace to the augmented repair procedure the strength of the fixation, identified as the weak point of the repair, was mechanically characterised. The strength of the augmented Broström procedure with InternalBrace (315.5 ± 66.8 N) (Arthrex Inc, Naples, FL, USA) has previously been reported to be as strong as the native ATFL (154.0 ± 63.7 N) it is most commonly used to replace (Viens et al., 2014). Similarly to the stability results, the published strength result of the augmented suture tape repair offers little indication of the strength provided by the suture tape due to the soft tissue repair performed simultaneously. To the author's knowledge no comparable strength data for the modified Broström procedure exists either. A comparison between the two procedures is an important one to potentially justify the use of the augmented procedure. The suture tape repair procedure performed in this study therefore excluded soft tissue repair, although less clinically relevant, to investigate more closely the ability of the suture tape to provide stability to the lateral ankle complex. The mean strength of the ATFL when characterised in this project at realistic sprain strain rates was 263.6 ± 164.3 N. Therefore, the InternalBrace is unlikely sufficiently strong enough to prevent recurrent sprain for a proportion of the population due to the overlapping of CIs. Nor is the InternalBrace strong enough to adequately replace the native CFL (367.8 ± 79.8 N) when fixed using the manufacturer's currently recommended implantation method using suture anchors, a procedure currently being performed in patients.

When fixation failure mode was further scrutinised, failures of the preliminary pull out study were not representative of those observed in the stability analysis study. A potential explanation for this could be a difference in the strength and stiffness of bone between the older human cadaver tissue compared to the immature porcine bone (Patton et al., 2019). The bone density of immature porcine bone also visually appeared to be higher than that of the human cadaver bone, although this parameter was not quantified. If the density of the aged human cadaver bone was lower, then pull out of suture anchors would be more likely as the

thread of the suture anchor would have less bone to engage with. The mean age of the stability study (47.8 ± 10.7 years) was higher than that of the peak sprain population (< 19 years) (Waterman et al., 2010), however the repair procedure is performed on a wide age range of patient's as demonstrated in a recent study (mean age of 41.94 years, (Kumar Batra et al., 2018)). In porcine bone the suture anchors were very effective at integrating with bone tissue, possibly due to an increased bone density, causing failure to occur through slippage of the suture tape. When slippage of the suture tape was prevented by clamping both strands of the suture tape within the gripping fixture the failure load almost doubled. Possible implantation techniques to prevent slippage have been proposed by the author and the findings warrant further investigation. Should a suitable method be developed where other complications are not presented and the structural integrity of the suture tape is not impaired, the strength performance of the suture tape could be sufficiently high to adequately repair the ATFL for at least 95 % of the population. Alternatively, the differences in failure mode could be related to the axis of loading applied to the fixation of the augmented repair in the two studies.

Changing from a gold standard procedure to a lesser developed surgical technique involves risk and the novel technique should therefore boast major attributes over the gold standard procedure such as reduced surgical time, cost, complication rate or return to sport/daily activity, or improved outcome scores. Since the augmented suture tape involves all aspects of the modified Broström procedure and few significant improvements in clinical outcomes have been identified to date, in addition to the frequent failure at low loads observed in this project, it is the opinion of the author that the benefits of the augmented Broström procedure with InternalBrace are unlikely to outweigh the 1.3 times cost of the procedure. Robust healthcare economics analysis is however required to substantiate such a claim.

6.1.5 Limitations

The limitations of the individual studies conducted as part of this project are discussed in detail within their respective sections of this thesis. There are however some overarching limitations to the project and some which are relevant to the conclusions drawn by the author. Firstly, the sample size of all studies was small, but pragmatic, and therefore when statistical analyses were employed they were often insufficiently powered. The statistical results are documented within this thesis to provide information to those who desire statistical analyses to be presented for engineering studies, even with a small sample size. The inferences made should however be interpreted with caution and larger scale studies, appropriately powered on the findings of this study, would be required to allow any conclusions to be drawn with conviction.

The inference made through mechanical characterisation of porcine patellar tendon may not directly correspond to the outcomes for human lateral ankle ligaments as assumed by the author. Should this be the case then the mechanical properties reported for lateral ankle ligaments could have been affected by the storage or testing conditions. This is however

considered unlikely given comparable results have been reported for other ligaments from different species. As previously discussed, use of porcine patellar tendon was deemed acceptable for reasons pertaining to minimisation of cadaver tissue wastage.

The use of cadaveric tissue comes with several limitations, particularly when the tissue is from mature adult donors, likely frozen for an extended duration and with an unknown history of sprain. Age of donors as a limitation to the study could be argued as although sprain sufferers are typically younger the age of repair patients can vary. It also appears age has no significant effect on the mechanical properties of ligaments in a healthy population (St Pierre et al., 1983; Blevins et al., 1994; Johnson et al., 1994; Flahiff et al., 1995; Couppé et al., 2009). The length of time frozen was out of the control of the author for the inherited human tissue samples and samples acquired by the author were grouped into as few transactions as possible to reduce the considerable cost implications associated with the international shipping of human tissue. Previous history of sprain was also out of the control of the author, although no prior history of lower limb trauma was a requirement of human tissue sample selection. The exclusion criteria was reliant on the patients reporting prior injuries to a medical practitioner, which often is not the case with mild/moderate ankle sprains.

A correlation between BMI and ultimate failure load was identified in this project however the finding should be interpreted with caution. In addition to a greater sample size being required the correlation was based on a donor sample with a narrow ranging BMI, with all donors within the normal category, the same correlation cannot be assumed for underweight or obese individuals.

Opinions regarding the use of suture tape augmentation are purely informed opinions of the author based on their experiences using the devices within this project. Prospective randomized studies are required to provide rigorous scientific evidence for the potential benefits of the suture tape augmentation procedure with InternalBrace. Differences in the failures observed for the fixation between studies was attributed to the difference of tissues used (human, porcine or Sawbone) however inter-surgeon differences could provide explanation.

6.2 Conclusions

Limitations aside, several meaningful and insightful conclusions can be drawn from the results of the studies performed in this project.

- Initial preliminary mechanical characterisation identified an increase in strain rate to significantly increase the failure stress and considerably increase the failure load of porcine patellar tendon, emphasising the importance of selecting an appropriate strain rate when characterising ligamentous tissue. Future ligament characterisation studies should consider carefully the strain rate used, up to 100 $\%.s^{-1}$, and select the strain rate based on the conditions being investigated. For ligament sprain or damage studies

realistic strain rates should be used or, where not published, estimates from real-world data should be made, as in this project. The study also found a high prevalence of avulsion failures to occur when ligaments were tested at strain rates representative of in vivo sprain. Therefore the consideration of structural properties of BLB complexes could be more suitable over material properties from a biomaterials engineering perspective as more than one material is being characterised. Of the other storage and testing conditions investigated no significant difference was found for the ultimate failure load and stiffness of BLB constructs. This afforded the repetitive freezing and thawing of samples for logistical purposes and determined that the use of a water bath was unnecessary, increasing the time-efficiency of the testing protocol for BLB constructs.

- Mechanical characterisation of cadaveric tissue identified no systematic difference for the ultimate failure load and stiffness of the ATFL, CFL and PTFL when investigated in isolation and in vitro. There was however, a tendency toward greater strength in people with a higher BMI. This phenomenon suggests the general understanding that the ATFL is the weakest ligament in individuals could be flawed, however a larger sized study is required. This finding has potential implications for the required mechanical properties of synthetic repair interventions as average ATFL failure loads could be underestimates for a healthy population. The maximum likely exposure loads, the BMI of the patient and the failure mode of the LCLs all appear to be factors requiring further consideration when selecting the material and repair or reconstruction technique for surgical stabilisation of the sprained ankle.
- A sprain simulation platform was produced which was capable of replicating the motions associated with LAS providing insight into the motions occurring at the ankle complex, talocrural and subtalar joints during LAS motion.
- When investigating the influence of the lateral ankle ligaments to ankle joint complex stability through the sequential sectioning of the ATFL and CFL, an increase in anterior drawer displacement and talar tilt inversion ROM was determined. Anterior drawer was most sensitive to identify ATFL rupture and the talar tilt test for combined ATFL and CFL rupture. Performing both an anterior drawer and talar tilt test can therefore assist in the clinical assessment of ankle joint stability and diagnosis of sprain. Motion capture was an effective tool to measure anterior-posterior displacements and inversion/eversion ROM when performing stability drawer tests. An anterior displacement greater than 2.0 mm could indicate ATFL rupture when analysed using optical motion capture following the technique described for anterior drawer in this project.
- The InternalBrace suture tape used in augmented repairs of the lateral ankle ligaments fail at their fixation, when implanted with SwiveLock suture anchors. Failure occurred at loads below that of the ATFL and CFL which it is intended to replace. Adapting the fixation to prevent tape slippage has the potential to double the failure load of the

synthetic repair however a larger sample size is required to confirm this finding and testing should be performed with cadaveric tissue.

- The Infinity-Lock suture tape requires further development of its fixation method as the use of SwiveLock suture anchors appear to be unsuitable. A fixation method whereby a rotational torque is not applied to the suture tape during implantation would be preferable, similar to the button fixation method used for applications in the shoulder.

6.3 Future Work

6.3.1 Mechanical Characterisation

A study into the effect of long term freezing to the structure and mechanical properties of human tissues should be conducted to address the current knowledge gap. The potential effect of long term freezing could influence the results of all tissue biomechanical studies conducted using human tissue sourced from tissue banks or where freezing durations have been extended by the ongoing global pandemic. Should an effect of long term freezing be confirmed then efforts should be made by tissue banks and researchers alike to store tissue for the minimal length of time within their control post-mortem. Freeze durations should also be recorded, supplied to researchers and reported in published results to allow for improved interpretation of results.

The possible link identified between ligament failure load and BMI requires further exploration in a larger scale study. Donor tissue used should span the BMI spectrum rather than only the normal range, as in this study, to identify whether the pattern is still observed at the extremities of BMI. Should a link be confirmed synthetic interventions to LAS could be stratified based on patient BMI to provide a closer match to the patient's mechanical requirements.

To realise the possible strength benefits of the augmented Broström procedure with InternalBrace over the gold standard modified Broström procedure a comparative mechanical characterisation study of the two repair techniques could be performed. Should the strength of the augmented procedure be significantly higher than the gold standard procedure then the benefits of the augmented procedure could be worth the increased cost of the procedure. Should, however, the results display no significant difference then the outcome should be interpreted as a 'false positive' rather than a beneficial outcome.

6.3.2 Lateral Ankle Sprain Simulation

Further research is required to fill the existing knowledge gap on the biomechanics of the LAS. Such information can be ethically sourced through the cadaveric simulation of LAS. An iterative approach to the design and development of a sprain simulation platform is recommended for those wishing to simulate LAS in the future. Adaptability of a sprain platform is required due to

the current uncertainty regarding the ROM and loads acting at the ankle complex during sprain events which can be enabled through a modular design. The sprain platform should aim to achieve plantar flexion and inversion angles up to 50 degrees to replicate mild LAS based on published data (Gehring et al., 2013). To replicate severe LAS the ROM is relatively unknown. Studies not specifying the grade of damage quote plantar flexion angles up to 52 degrees, inversion angles up to 142 degrees and internal rotation angles up to 56 degrees therefore versatility in design is essential.

Loading of specimens should be controlled and adaptable for individual specimens. Both the load and rate of loading should be tailored to individual donor specimens. Should the potential link between ligament strength and BMI be confirmed then an individual's BMI would be an effective method for the scaling of applied loads between specimens. Electromechanical testing devices, such as the ElectroPuls E10000 (Instron, Buckinghamshire, UK), have the potential to be appropriate loading devices. The working space volume required would however require careful consideration when designing a sprain platform. Alternatively, a 6 DOF robotic device could be used, similar to a robotic arm previously used for ankle motion analysis (El. Daou et al., 2018). Although the rate of loading could be a potential limitation of using such as device as strain rates associated with LAS may not be achievable.

Kinematic analysis was performed in this study using a Miqus motion capture system and is recommended for future investigation into the biomechanics of the ankle complex through sprain simulation. Although motion capture poses additional challenges to the design of a sprain simulation the capture rate is high enough to generate smooth good quality data, essential for the kinematic analysis of ankle sprain.

6.3.3 Synthetic Repair of Lateral Ankle Ligaments

The use of SwiveLock suture anchors provided significant challenge for the fixation of the Infinity-Lock suture tape. Should suture anchors be the preferred fixation method then suture anchors specifically for the Infinity-Lock suture tape should be developed. Features such as a deep and smooth thread would be beneficial to allow for improved integration with the bone tunnel thread whilst not fraying the fibrous suture tape. Alternative fixation methods may however be more preferable for the Infinity-Lock suture tape due to the fraying of the suture tape when exposed to excessive torque loads. Future fixation analysis should be explored using natural bone tissue opposed to a Sawbone model where failures appear to be unrepresentative of those within natural bone.

Ankle ligament surgical repair is behind respective treatments for the knee and hip and requires significant development, particularly when synthetic interventions are used. The future of medicine is moving towards a personalised patient-specific approach and steps have already been taken to perform such activities within the knee. The advancement of robotic assisted surgery has afforded greater precision and accelerated the development of

preoperative planning for surgical techniques. Knee arthroplasty procedures, for example, involve preoperative planning whereby imaging techniques are used to create a 3-dimensional patient-specific model to optimise the implant size and position as well as to calculate a haptic window for surgical cuts to be performed prior to the surgical procedure being performed (Kayani et al., 2018). To accomplish this standard of pre-operative planning for ligament repair procedures further understanding of the variation in ankle anatomy, ligament properties and intrinsic risk factors for LAS are required. The other main advantage of preoperative planning is that abnormalities or variations in patient anatomy can be discovered prior to surgery, of which for the ankle there are many (Aparisi Gómez et al., 2019). Potentially important is the bone density of a patient which could be calculated preoperatively to select the most suitable size, or even type, of fixation. The benefits of haptic control and intraoperative feedback during a LAS repair procedure would also be hugely beneficial to surgeons performing the procedure allowing them to adequately tension the soft-tissue repair, and synthetic intervention if used, to produce a balanced ankle joint. Correct soft-tissue tensioning is learnt through the experiences of a surgeon at present and is not measured in a quantifiable way intraoperatively. Surgeons can perform basic clinical stability assessments after the treatment has been performed but providing the results lie within the boundaries considered to be adequate for stability the repair will not be further optimised. Effective pre-operative planning is likely to improve surgical outcomes and reduce the onset of PTOA through optimisation of joint mechanics, ligament tensioning and congruity.

References

Abrahams, M. 1967. Mechanical behaviour of tendon In vitro - A preliminary report. *Medical & Biological Engineering*. **5**(5), pp.433–443.

Aerssens, J., Boonen, S., Lowet, G. and Dequeker, J. 1998. Interspecies differences in bone composition, density, and quality: Potential implications for in vivo bone research. *Endocrinology*.

Agres, A.N., Chrysanthou, M. and Raffalt, P.C. 2019. The Effect of Ankle Bracing on Kinematics in Simulated Sprain and Drop Landings: A Double-Blind, Placebo-Controlled Study. *The American journal of sports medicine*. **47**(6), pp.1480–1487.

Ahlgren, O. and Larsson, S. 1989. Reconstruction for lateral ligament injuries of the ankle. *The Journal of bone and joint surgery. British volume*. **71**(2), pp.300–3.

Ajis, A., Younger, A.S.E. and Maffulli, N. 2006. Anatomic Repair for Chronic Lateral Ankle Instability. *Foot and Ankle Clinics*. **11**(3), pp.539–545.

Al-Mohrej, O.A. and Al-Kenani, N.S. 2016. Acute ankle sprain: Conservative or surgical approach? *EFORT Open Reviews*.

Alfuth, M., Klein, D., Koch, R. and Rosenbaum, D. 2014. Biomechanical comparison of 3 ankle braces with and without free rotation in the sagittal plane. *Journal of athletic training*. **49**(5), pp.608–16.

Anderson, D.D., Van Hofwegen, C., Marsh, J.L. and Brown, T.D. 2011. Is elevated contact stress predictive of post-traumatic osteoarthritis for imprecisely reduced tibial plafond fractures? *Journal of Orthopaedic Research*.

Anderson, M.E. 1985. Reconstruction of the lateral ligaments of the ankle using the plantaris tendon. *The Journal of bone and joint surgery. American volume*. **67**(6), pp.930–4.

Aparisi Gómez, M.P., Aparisi, F., Bartoloni, A., Ferrando Fons, M.A., Battista, G., Guglielmi, G. and Bazzocchi, A. 2019. Anatomical variation in the ankle and foot: from incidental finding to inductor of pathology. Part I: ankle and hindfoot. *Insights into Imaging*.

Araoye, I., De Cesar Netto, C., Cone, B., Hudson, P., Sahranavard, B. and Shah, A. 2017. Results of lateral ankle ligament repair surgery in one hundred and nineteen patients: do surgical method and arthroscopy timing matter? *International Orthopaedics*. **41**(11), pp.2289–2295.

Arnout, N., Myncke, J., Vanlauwe, J., Labey, L., Lismont, D. and Bellemans, J. 2013. The influence of freezing on the tensile strength of tendon grafts : a biomechanical study. *undefined*.

Arthrex 2017. ATFL and CFL with InternalBraceTM Ligament Augmentation Repair. [Accessed 27 September 2020]. Available from: https://www.arthrex.com/resources/video/Tw3hDxdpq0-63gFfUAjmyA/atfl-and-cfl-with-internalbrace-ligament-augmentation-repair.

Ashton-Miller, J.A., Ottaviani, R.A., Hutchinson, C. and Wojtys, E.M. 2013. What Best Protects the Inverted Weightbearing Ankle Against Further Inversion? *The American Journal of Sports Medicine*. **24**(6), pp.800–809.

de Asla, R.J., Kozánek, M., Wan, L., Rubash, H.E. and Li, G. 2009. Function of anterior talofibular and calcaneofibular ligaments during in-vivo motion of the ankle joint complex. *Journal of Orthopaedic Surgery and Research*. **4**(1), p.7.

de Asla, R.J., Wan, L., Rubash, H.E. and Li, G. 2006. Six DOF in vivo kinematics of the ankle joint complex: Application of a combined dual-orthogonal fluoroscopic and magnetic

resonance imaging technique. *Journal of Orthopaedic Research*. **24**(5), pp.1019–1027.

Attarian, D.E., McCrackin, H.J., DeVito, D.P., McElhaney, J.H. and Garrett, W.E. 1985. Biomechanical characteristics of human ankle ligaments. *Foot and Ankle*. **6**(2), pp.54–58.

Aubin, P.M., Cowley, M.S. and Ledoux, W.R. 2008. Gait Simulation via a 6-DOF Parallel Robot With Iterative Learning Control. *IEEE Transactions on Biomedical Engineering*. **55**(3), pp.1237–1240.

Bahr, M. a and Bahr, R. 2014. Jump frequency may contribute to risk of jumper's knee: a study of interindividual and sex differences in a total of 11,943 jumps video recorded during training and matches in young elite volleyball players. *British journal of sports medicine*. **48**(17), pp.1322–6.

Bahr, R., Pena, F., Shine, J., Lew, W.D. and Engebretsen, L. 1998. Ligament force and joint motion in the intact ankle: A cadaveric study. *Knee Surgery, Sports Traumatology, Arthroscopy*. **6**(2), pp.115–121.

Barnett, C.H. and Napier, J.R. 1952. The axis of rotation at the ankle joint in man. Its influence upon the form of the talus and the mobility of the fibula. *Journal of Anatomy*. **86**(1), pp.1–9.

Baumhauer, J.F. and O'Brien, T. 2002. Surgical Considerations in the Treatment of Ankle Instability. *Journal of athletic training*. **37**(4), pp.458–462.

Baxter, J.R., Sturnick, D.R., Demetracopoulos, C.A., Ellis, S.J. and Deland, J.T. 2016. Cadaveric gait simulation reproduces foot and ankle kinematics from population-specific inputs. *Journal of Orthopaedic Research*. **34**(9), pp.1663–1668.

Behrens, S.B., Drakos, M., Lee, B.J., Paller, D., Hoffman, E., Koruprolu, S. and DiGiovanni, C.W. 2013. Biomechanical Analysis of Brostrom Versus Brostrom-Gould Lateral Ankle Instability Repairs. *Foot & Ankle International*. **34**(4), pp.587–592.

Van Den Bekerom, M.P.J., Oostra, R.J., Alvarez, P.G. and Van Dijk, C.N. 2008. The anatomy in relation to injury of the lateral collateral ligaments of the ankle: A current concepts review. *Clinical Anatomy*. **21**(7), pp.619–626.

Van Den Bekerom, M.P.J. and Raven, E.E.J. 2007. The distal fascicle of the anterior inferior tibiofibular ligament as a cause of tibiotalar impingement syndrome: A current concepts review. *Knee Surgery, Sports Traumatology, Arthroscopy*. **15**(4), pp.465–471.

Bell, S.J., Mologne, T.S., Sitler, D.F. and Cox, J.S. 2006. Twenty-six-year results after Broström procedure for chronic lateral ankle instability. *The American journal of sports medicine*. **34**(6), pp.975–8.

van Bergen, C.J.A., Kerkhoffs, G.M.M.J., Marsidi, N., Korstjens, C.M., Everts, V., van Ruijven, L.J., van Dijk, C.N. and Blankevoort, L. 2013. Osteochondral defects of the talus: a novel animal model in the goat. *Tissue engineering. Part C, Methods*. **19**(6), pp.449–57.

Best, R., Böhle, C., Mauch, F. and Brüggemann, P.G. 2016. Preventive lateral ligament tester (PLLT): a novel method to evaluate mechanical properties of lateral ankle joint ligaments in the intact ankle. *Knee Surgery, Sports Traumatology, Arthroscopy*. **24**(4), pp.963–970.

Beumer, A., Van Hemert, W.L.W., Swierstra, B.A., Jasper, L.E. and Belkoff, S.M. 2003. A biomechanical evaluation of the tibiofibular and tibiotalar ligaments of the ankle. *Foot and Ankle International*. **24**(5), pp.426–429.

Bhaskaran, D., Wortley, M., Chen, Q., Milner, C.E., Fitzhugh, E.C. and Zhang, S. 2015. Effect of a combined inversion and plantarflexion surface on ankle kinematics and EMG activities in landing. *Journal of Sport and Health Science*. **4**(4), pp.377–383.

Birch, H.L., Thorpe, C.T. and Rumian, A.P. 2013. Specialisation of extracellular matrix for

function in tendons and ligaments. *Muscles, Ligaments and Tendons Journal*. **3**(1), pp.12–22.

Bitton, R. 2009. The economic burden of osteoarthritis. *The American journal of managed care*. **15**(8 Suppl), pp.S230–S235.

Blalock, D., Miller, A., Tilley, M. and Wang, J. 2015. Joint instability and osteoarthritis. *Clinical Medicine Insights: Arthritis and Musculoskeletal Disorders*.

Blevins, F.T., Hecker, A.T., Bigler, G.T., Boland, A.L. and Hayes, W.C. 1994. The Effects of Donor Age and Strain Rate on the Biomechanical Properties of Bone-Patellar Tendon-Bone Allografts. *The American Journal of Sports Medicine*. **22**(3), pp.328–333.

Boey, H., Van Rossom, S., Rochelle, D., Brockett, C., Vander Sloten, J. and Jonkers, I. n.d. Musculoskeletal loading of the ankle and ligament behaviour during functional movements using an extended musculoskeletal foot-ankle model. *Journal of Biomechanics*.

Boey, H., Verfaillie, S., Natsakis, T., Vander Sloten, J. and Jonkers, I. 2019. Augmented Ligament Reconstruction Partially Restores Hindfoot and Midfoot Kinematics After Lateral Ligament Ruptures. *The American Journal of Sports Medicine*. **47**(8), pp.1921–1930.

Bonnel, F., Toullec, E., Mabit, C. and Tourné, Y. 2010. Chronic ankle instability: Biomechanics and pathomechanics of ligaments injury and associated lesions. *Orthopaedics and Traumatology: Surgery and Research*. **96**(4), pp.424–432.

Bonner, T.J., Newell, N., Karunaratne, A., Pullen, A.D., Amis, A.A., M.J. Bull, A. and Masouros, S.D. 2015. Strain-rate sensitivity of the lateral collateral ligament of the knee. *Journal of the Mechanical Behavior of Biomedical Materials*. **41**, pp.261–270.

Bridgman, S.A. 2003. Population based epidemiology of ankle sprains attending accident and emergency units in the West Midlands of England, and a survey of UK practice for severe ankle sprains. *Emergency Medicine Journal*. **20**(6), pp.508–510.

Brockett, C.L. and Chapman, G.J. 2016. Biomechanics of the ankle. *Orthopaedics and Trauma*. **30**(3), pp.232–238.

Broström, L. 1964. Sprained Ankles. I. Anatomic lesions in recent sprains. *Acta chirurgica Scandinavica*. **128**, pp.483–495.

Brown, A.J., Shimozono, Y., Hurley, E.T. and Kennedy, J.G. 2018. Arthroscopic Repair of Lateral Ankle Ligament for Chronic Lateral Ankle Instability: A Systematic Review. *Arthroscopy*. **34**(8), pp.2497–2503.

Buckwalter, J.A., Anderson, D.D., Brown, T.D., Tochigi, Y. and Martin, J.A. 2013. The Roles of Mechanical Stresses in the Pathogenesis of Osteoarthritis: Implications for Treatment of Joint Injuries. *Cartilage*. **4**(4), pp.286–294.

Burdett, R.G. 1982. Forces predicted at the ankle during running. *Medicine and science in sports and exercise*. **14**(4), pp.308–316.

Burks, R.T. and Morgan, J. 1994. Anatomy of the Lateral Ankle Ligaments. *The American Journal of Sports Medicine*. **22**(1), pp.72–77.

Butler, A.M. and Walsh, W.R. 2004. Mechanical Response of Ankle Ligaments at Low Loads. *Foot and Ankle International*. **25**(1), pp.8–12.

Calhoun, J.H., Li, F., Ledbetter, B.R. and Viegas, S.F. 1994. A Comprehensive Study of Pressure Distribution in the Ankle Joint with Inversion and Eversion. *Foot & Ankle International*. **15**(3), pp.125–133.

Cao, Y., Hong, Y., Xu, Y., Zhu, Y. and Xu, X. 2018. Surgical management of chronic lateral ankle instability: a meta-analysis. *Journal of Orthopaedic Surgery and Research*. **13**(1), p.159.

Carcia, C.R., Martin, R.L. and Drouin, J.M. 2008. Validity of the Foot and Ankle Ability Measure in athletes with chronic ankle instability. *Journal of athletic training*. **43**(2), pp.179–83.

Carson, M.C., Harrington, M.E., Thompson, N., O'Connor, J.J. and Theologis, T.N. 2001. Kinematic analysis of a multi-segment foot model for research and clinical applications: A repeatability analysis. *Journal of Biomechanics*. **34**(10), pp.1299–1307.

Cass, J.R. and Settles, H. 1994. Ankle Instability: In Vitro Kinematics in Response to Axial Load. *Foot & Ankle International*. **15**(3), pp.134–140.

Cawley, P.W. and France, E.P. 1991. Biomechanics of the lateral ligaments of the ankle: an evaluation of the effects of axial load and single plane motions on ligament strain patterns. *Foot Ankle*. **12**(2), pp.92–99.

Chan, Y.Y., Fong, D.T.P., Yung, P.S.H., Fung, K.Y. and Chan, K.M. 2008. *A mechanical supination sprain simulator for studying ankle supination sprain kinematics*.

Chang, S.H., Yasui, T., Taketomi, S., Matsumoto, T., Kim-Kaneyama, J.R., Omiya, T., Hosaka, Y., Inui, H., Omata, Y., Yamagami, R., Mori, D., Yano, F., Chung, U., Tanaka, S. and Saito, T. 2016. Comparison of mouse and human ankles and establishment of mouse ankle osteoarthritis models by surgically-induced instability. *Osteoarthritis and Cartilage*. **24**(4), pp.688–697.

Chen, T., Jiang, J. and Chen, S. 2015. Status and headway of the clinical application of artificial ligaments. *Asia-Pacific Journal of Sports Medicine, Arthroscopy, Rehabilitation and Technology*. **2**(1), pp.15–26.

Cho, B.-K., Kim, Y.-M., Kim, D.-S., Choi, E.-S., Shon, H.-C. and Park, K.-J. 2013. Outcomes of the Modified Brostrom Procedure Using Suture Anchors for Chronic Lateral Ankle Instability—A Prospective, Randomized Comparison between Single and Double Suture Anchors. *The Journal of Foot and Ankle Surgery*. **52**(1), pp.9–15.

Cho, B.-K., Park, J.-K., Choi, S.-M. and SooHoo, N.F. 2019. A randomized comparison between lateral ligaments augmentation using suture-tape and modified Broström repair in young female patients with chronic ankle instability. *Foot and Ankle Surgery*. **25**(2), pp.137–142.

Cho, B.-K., Park, K.-J., Kim, S.-W., Lee, H.-J. and Choi, S.-M. 2015. Minimal Invasive Suture-Tape Augmentation for Chronic Ankle Instability. *Foot & Ankle International*. **36**(11), pp.1330–1338.

Cho, B.-K., Park, K.-J., Park, J.-K. and SooHoo, N.F. 2017. Outcomes of the Modified Broström Procedure Augmented With Suture-Tape for Ankle Instability in Patients With Generalized Ligamentous Laxity. *Foot & Ankle International*. **38**(4), pp.405–411.

Chowdhury, R., Matyas, J.R. and Frank, C.B. 1991. The 'epiligament' of the rabbit medial collateral ligament: A quantitative morphological study. *Connective Tissue Research*. **27**(1), pp.33–50.

Chrisman, O.D. and Snook, G.A. 1969. Reconstruction of lateral ligament tears of the ankle. An experimental study and clinical evaluation of seven patients treated by a new modification of the Elmslie procedure. *The Journal of bone and joint surgery. American volume*. **51**(5), pp.904–12.

Coetzee, J.C., Ellington, J.K., Nilsson, L.J. and Stone McGaver, R. 2019. Ankle Ligament Reconstruction. *Techniques in Foot & Ankle Surgery*. **18**(2), pp.68–72.

Coetzee, J.C., Ellington, J.K., Ronan, J.A. and Stone, R.M. 2018. Functional Results of Open Broström Ankle Ligament Repair Augmented With a Suture Tape. *Foot & Ankle International*. **39**(3), pp.304–310.

Colville, M.R., Marder, R.A., Boyle, J.J. and Zarins, B. 1990. Strain measurement in lateral ankle ligaments. *The American Journal of Sports Medicine*. **18**(2), pp.196–200.

Cone, S.G., Warren, P.B. and Fisher, M.B. 2017. Rise of the Pigs: Utilization of the Porcine Model to Study Musculoskeletal Biomechanics and Tissue Engineering During Skeletal Growth. *Tissue Engineering Part C: Methods*.

Connexions 2013. File:Planes of Body.jpg - Wikimedia Commons. *CNX Anatomy & Physiology - OpenStax College*. [Online]. [Accessed 27 September 2020]. Available from: https://cnx.org/contents/FPtK1zmh@8.108:F-TuqKAF@5/Anatomical-Terminology.

Cooke, M.W. 2003. A survey of current consultant practice of treatment of severe ankle sprains in emergency departments in the United Kingdom. *Emergency Medicine Journal*. **20**(6), pp.505–507.

Cottom, J.M. and Rigby, R.B. 2013. The "All Inside" Arthroscopic Broström Procedure: A Prospective Study of 40 Consecutive Patients. *The Journal of Foot and Ankle Surgery*. **52**(5), pp.568–574.

Couppé, C., Hansen, P., Kongsgaard, M., Kovanen, V., Suetta, C., Aagaard, P., Kjær, M. and Magnusson, S.P. 2009. Mechanical properties and collagen cross-linking of the patellar tendon in old and young men. *Journal of Applied Physiology*. **107**(3), pp.880–886.

Crowninshield, R.D. and Pope, M.H. 1976. The strength and failure characteristics of rat medial collateral ligaments. *Journal of Trauma - Injury, Infection and Critical Care*. **16**(2), pp.99–105.

Croy, T., Saliba, S., Saliba, E., Anderson, M.W. and Hertel, J. 2012. Differences in lateral ankle laxity measured via stress ultrasonography in individuals with chronic ankle instability, ankle sprain copers, and healthy individuals. *Journal of Orthopaedic and Sports Physical Therapy*. **42**(7), pp.593–600.

Dalmau-Pastor, M., Malagelada, F., Calder, J., Manzanares, M.C. and Vega, J. 2020. The lateral ankle ligaments are interconnected: the medial connecting fibres between the anterior talofibular, calcaneofibular and posterior talofibular ligaments. *Knee Surgery, Sports Traumatology, Arthroscopy*. **28**(1), pp.34–39.

Delco, M.L., Kennedy, J.G., Bonassar, L.J. and Fortier, L.A. 2017. Post-traumatic osteoarthritis of the ankle: A distinct clinical entity requiring new research approaches. *Journal of orthopaedic research : official publication of the Orthopaedic Research Society*. **35**(3), pp.440–453.

Donatelli, R. 1985. Normal biomechanics of the foot and ankle. *Journal of Orthopaedic and Sports Physical Therapy*. **7**(3), pp.91–95.

Ebraheim, N.A., Taser, F., Shafiq, Q. and Yeasting, R.A. 2006. Anatomical evaluation and clinical importance of the tibiofibular syndesmosis ligaments. *Surgical and Radiologic Anatomy*. **28**(2), pp.142–149.

Edama, M., Kageyama, I., Kikumoto, T., Nakamura, M., Ito, W., Nakamura, E., Hirabayashi, R., Takabayashi, T., Inai, T. and Onishi, H. 2018. Morphological features of the anterior talofibular ligament by the number of fiber bundles. *Annals of Anatomy - Anatomischer Anzeiger*. **216**, pp.69–74.

Edwards, J.H., Ingham, E. and Herbert, A. 2019. Decellularisation affects the strain rate dependent and dynamic mechanical properties of a xenogeneic tendon intended for anterior cruciate ligament replacement. *Journal of the Mechanical Behavior of Biomedical Materials*.

El. Daou, H., Calder, J.D. and Stephen, J.M. 2018. Development and validation of a robotic system for ankle joint testing. *Medical Engineering & Physics*. **62**, pp.53–57.

Evans, D.L. 1953. Recurrent instability of the ankle; a method of surgical treatment. *Proceedings of the Royal Society of Medicine*. **46**(5), pp.343–4.

Ferran, N.A. and Maffulli, N. 2006. Epidemiology of Sprains of the Lateral Ankle Ligament Complex. *Foot and Ankle Clinics*.

Flahiff, C.M., Brooks, A.T., Hollis, J.M., Vander Schilden, J.L. and Nicholas, R.W. 1995. Biomechanical Analysis of Patellar Tendon Allografts as a Function of Donor Age. *The American Journal of Sports Medicine*. **23**(3), pp.354–358.

Fong, D.T.-P., Chan, Y.-Y., Mok, K.-M., Yung, P.S. and Chan, K.-M. 2009. Understanding acute ankle ligamentous sprain injury in sports. *BMC Sports Science, Medicine and Rehabilitation*. **1**(1), p.14.

Fong, D.T.-P., Chu, V.W.S. and Chan, K.M. 2012. *Myoelectric stimulation on peroneal muscles resists simulated ankle sprain motion*.

Fong, D.T.-P., Hong, Y., Shima, Y., Krosshaug, T., Yung, P.S.-H. and Chan, K.-M. 2009. Biomechanics of supination ankle sprain: a case report of an accidental injury event in the laboratory. *The American journal of sports medicine*. **37**(4), pp.822–827.

Von Forell, G.A., Hyoung, P.S. and Bowden, A.E. 2014. Failure modes and fracture toughness in partially torn ligaments and tendons. *Journal of the Mechanical Behavior of Biomedical Materials*. **35**, pp.77–84.

Franchi, M., De Pasquale, V., Martini, D., Quaranta, M., Macciocca, M., Dionisi, A. and Ottani, V. 2010. Contribution of glycosaminoglycans to the microstructural integrity of fibrillar and fiber crimps in tendons and ligaments. *TheScientificWorldJournal*.

Fregly, B.J., Besier, T.F., Lloyd, D.G., Delp, S.L., Banks, S.A., Pandy, M.G. and D'Lima, D.D. 2012. Grand challenge competition to predict in vivo knee loads. *Journal of Orthopaedic Research*.

Frey, C. 2015. Gross Anatomy of the Subtalar Joint. Available from: https://clinicalgate.com/gross-anatomy-of-the-subtalar-joint/%0A.

Fujii, T., Kitaoka, H.B., Watanabe, K., Luo, Z.-P. and An, K.-N. 2010. Ankle Stability in Simulated Lateral Ankle Ligament Injuries. *Foot & Ankle International*. **31**(6), pp.531–537.

Funk, J.R., Hall, G.W., Crandall, J.R. and Pilkey, W.D. 2000. Linear and quasi-linear viscoelastic characterization of ankle ligaments. *Journal of Biomechanical Engineering*. **122**(1), pp.15–22.

Garner, W.L., McDonald, J.A., Koo, M., Kuhn, C. 3rd and Weeks, P.M. 1989. Identification of the collagen-producing cells in healing flexor tendons. *Plastic and reconstructive surgery*. **83**(5), pp.875–879.

Gehring, D., Wissler, S., Mornieux, G. and Gollhofer, A. 2013. *How to sprain your ankle - a biomechanical case report of an inversion trauma*.

Golanó, P., Vega, J., de Leeuw, P.A.J., Malagelada, F., Manzanares, M.C., Götzens, V. and van Dijk, C.N. 2016. Anatomy of the ankle ligaments: a pictorial essay. *Knee Surgery, Sports Traumatology, Arthroscopy*. **24**(4), pp.944–956.

Golditz, T., Steib, S., Pfeifer, K., Uder, M., Gelse, K., Janka, R., Hennig, F.F. and Welsch, G.H. 2014. Functional ankle instability as a risk factor for osteoarthritis: Using T2-mapping to analyze early cartilage degeneration in the ankle joint of young athletes. *Osteoarthritis and Cartilage*. **22**(10).

Gould, N., Seligson, D. and Gassman, J. 1980. Early and late repair of lateral ligament of the ankle. *Foot & ankle*. **1**(2), pp.84–9.

Gray, H. and Lewis, W.H. 2000. *Anatomy of the human body* [Online]. Available from: www.bartleby.com/107/.

Gribble, Phillip A., Bleakley, C.M., Caulfield, B.M., Docherty, C.L., Fourchet, F., Fong, D.T.P.,

Hertel, J., Hiller, C.E., Kaminski, T.W., McKeon, P.O., Refshauge, K.M., Verhagen, E.A., Vicenzino, B.T., Wikstrom, E.A. and Delahunt, E. 2016. Evidence review for the 2016 International Ankle Consortium consensus statement on the prevalence, impact and long-term consequences of lateral ankle sprains. *British Journal of Sports Medicine*.

Gribble, Phillip A, Bleakley, C.M., Caulfield, B.M., Docherty, C.L., Fourchet, F., Tik-Pui Fong, D., Hertel, J., Hiller, C.E., Kaminski, T.W., McKeon, P.O. and Refshauge, K.M. 2016. 2016 consensus statement of the International Ankle Consortium: prevalence, impact and long-term consequences of lateral ankle sprains. *Br J Sports Med*. **50**(24), pp.1493–1495.

Grimston, S.K., Nigg, B.M., Hanley, D.A. and Engsberg, J.R. 1993. Differences in ankle joint complex range of motion as a function of age. *Foot & ankle*. **14**(4), pp.215–222.

Grond, J.T.H. 1973. The surgical treatment of injuries of the fibular collateral ligaments of the ankle. *Archivum Chirurgicum Neerlandicum*. **25**(2), pp.131–136.

Guelfi, M., Zamperetti, M., Pantalone, A., Usuelli, F.G., Salini, V. and Oliva, X.M. 2018. Open and arthroscopic lateral ligament repair for treatment of chronic ankle instability: A systematic review. *Foot and Ankle Surgery*. **24**(1), pp.11–18.

Guillo, S., Bauer, T., Lee, J.W., Takao, M., Kong, S.W., Stone, J.W., Mangone, P.G., Molloy, A., Perera, A., Pearce, C.J., Michels, F., Tourné, Y., Ghorbani, A. and Calder, J. 2013. Consensus in chronic ankle instability: Aetiology, assessment, surgical indications and place for arthroscopy. *Orthopaedics & Traumatology: Surgery & Research*. **99**(8), pp.S411–S419.

Ha, S.C.-W., Fong, D.T.-P. and Chan, K.-M. 2015. Review of ankle inversion sprain simulators in the biomechanics laboratory. *Asia-Pacific Journal of Sports Medicine, Arthroscopy, Rehabilitation and Technology*. **2**(4), pp.114–121.

Han, W.M., Nerurkar, N.L., Smith, L.J., Jacobs, N.T., Mauck, R.L. and Elliott, D.M. 2012. Multi-scale structural and tensile mechanical response of annulus fibrosus to osmotic loading. *Annals of Biomedical Engineering*. **40**(7), pp.1610–1621.

Hannafin, J.A. and Arnoczky, S.P. 1994. Effect of cyclic and static tensile loading on water content and solute diffusion in canine flexor tendons: An in Vitro study. *Journal of Orthopaedic Research*. **12**(3), pp.350–356.

Harper, M.C. 1991. The Lateral Ligamentous Support of the Subtalar Joint. *Foot & Ankle International*. **11**(6), pp.354–358.

Hassan, S., Thurston, D., Sian, T., Shah, R., Aziz, A. and Kothari, P. 2018. Clinical Outcomes of the Modified Broström Technique in the Management of Chronic Ankle Instability After Early, Intermediate, and Delayed Presentation. *The Journal of Foot and Ankle Surgery*. **57**(4), pp.685–688.

Hauser, R.A. 2013. Ligament Injury and Healing: A Review of Current Clinical Diagnostics and Therapeutics. *The Open Rehabilitation Journal*.

Hauser, R.A. and Dolan, E.E. 2011. Ligament Injury and Healing: An Overview of Current Clinical Concepts. *Journal of Prolotherapy*. **Volume 3**(Issue 4), pp.836–846.

Hawkins, D. 2002. Biomechanics of musculoskeletal tissues (online text-book).

Herbert, A., Brown, C., Rooney, P., Kearney, J., Ingham, E. and Fisher, J. 2016. Bi-linear mechanical property determination of acellular human patellar tendon grafts for use in anterior cruciate ligament replacement. *Journal of Biomechanics*. **49**(9), pp.1607–1612.

Herbert, A., Jones, G.L., Ingham, E. and Fisher, J. 2015. A biomechanical characterisation of acellular porcine super flexor tendons for use in anterior cruciate ligament replacement: Investigation into the effects of fat reduction and bioburden reduction bioprocesses. *Journal of Biomechanics*. **48**(1), pp.22–29.

Hermans, J.J., Beumer, A., De Jong, T.A.W. and Kleinrensink, G.J. 2010. Anatomy of the distal tibiofibular syndesmosis in adults: A pictorial essay with a multimodality approach. *Journal of Anatomy*. **217**(6), pp.633–645.

Hertel, J. 2002. Functional anatomy, pathomechanics, and pathophysiology of lateral ankle instability. *Journal of Athletic Training*. **37**(4), pp.364–375.

Herzog, M.M., Kerr, Z.Y., Marshall, S.W. and Wikstrom, E.A. 2019. Epidemiology of Ankle Sprains and Chronic Ankle Instability. *Journal of Athletic Training*. **54**(6), pp.603–610.

Hintermann, B., Knupp, M. and Pagenstert, G.I. 2006. Deltoid Ligament Injuries: Diagnosis and Management. *Foot and Ankle Clinics*. **11**(3), pp.625–637.

Hirose, K., Murakami, G., Minowa, T., Kura, H. and Yamashita, T. 2004. Lateral ligament injury of the ankle and associated articular cartilage degeneration in the talocrural joint: Anatomic study using elderly cadavers. *Journal of Orthopaedic Science*. **9**(1), pp.37–43.

Hoefnagels, E.M., Waites, M.D., Wing, I.D., Belkoff, S.M. and Swierstra, B.A. 2007. Biomechanical comparison of the interosseous tibiofibular ligament and the anterior tibiofibular ligament. *Foot & ankle international*. **28**(5), pp.602–4.

Hollis, J.M., Blasier, R.D., Flahiff, C.M. and Hofmann, O.E. 1995. Biomechanical comparison of reconstruction techniques in simulated lateral ankle ligament injury. *The American journal of sports medicine*. **23**(6), pp.678–82.

Hølmer, P., Søndergaard, L., Konradsen, L., Nielsen, P.T. and Jørgensen, L.N. 1994. Epidemiology of Sprains in the Lateral Ankle and Foot. *Foot & Ankle International*. **15**(2), pp.72–74.

Hope, M. and Saxby, T.S. 2007. Tendon Healing. *Foot and Ankle Clinics*. **12**(4), pp.553–567.

Huang, H., Zhang, J., Sun, K., Zhang, X. and Tian, S. 2011. Effects of repetitive multiple freeze-thaw cycles on the biomechanical properties of human flexor digitorum superficialis and flexor pollicis longus tendons. *Clinical Biomechanics*. **26**(4), pp.419–423.

Hubbard-Turner, T., Wikstrom, E.A., Guderian, S. and Turner, M.J. 2013. Acute ankle sprain in a mouse model. *Medicine and science in sports and exercise*. **45**(8), pp.1623–8.

Hurschler, C., Emmerich, J. and Wülker, N. 2003. In vitro simulation of stance phase gait part I: Model verification. *Foot & ankle international. / American Orthopaedic Foot and Ankle Society [and] Swiss Foot and Ankle Society*. **24**(8), pp.614–22.

Isman, R. and Inman, V. 1969. Anthropometric Studies of the Human Foot and Ankle. *Foot And Ankle*. **11**, pp.97–129.

Jain, T.K., Wauneka, C. and Liu, W. 2014. Unloading reaction during sudden ankle inversion in healthy adults. *Gait and Posture*. **39**(1), pp.529–533.

James, R., Kesturu, G., Balian, G. and Chhabra, A.B. 2008. Tendon: Biology, Biomechanics, Repair, Growth Factors, and Evolving Treatment Options. *Journal of Hand Surgery*. **33**(1), pp.102–112.

Johnson, G.A., Tramaglini, D.M., Levine, R.E., Ohno, K., Choi, N. -Y and L-Y. Woo, S. 1994. Tensile and viscoelastic properties of human patellar tendon. *Journal of Orthopaedic Research*. **12**(6), pp.796–803.

Johnson, M.B. and Johnson, C.L. 1993. Electromyographic response of peroneal muscles in surgical and nonsurgical injured ankles during sudden inversion. *The Journal of orthopaedic and sports physical therapy*. **18**(3), pp.497–501.

Jones, A.P., Sidhom, S. and Sefton, G. 2007. A Minimally Invasive Surgical Technique for Augmented Reconstruction of the Lateral Ankle Ligaments with Woven Polyester Tape. *Journal of Foot and Ankle Surgery*.

Juneja, S.C., Schwarz, E.M., O'Keefe, R.J. and Awad, H.A. 2013. Cellular and molecular factors in flexor tendon repair and adhesions: a histological and gene expression analysis. *Connective tissue research*. **54**(3), pp.218–26.

Jung, H.J., Vangipuram, G., Fisher, M.B., Yang, G., Hsu, S., Bianchi, J., Ronholdt, C. and Woo, S.L.Y. 2011. The effects of multiple freeze-thaw cycles on the biomechanical properties of the human bone-patellar tendon-bone allograft. *Journal of Orthopaedic Research*. **29**(8), pp.1193–1198.

Kakegawa, A., Mori, Y., Tsuchiya, A., Sumitomo, N., Fukushima, N. and Moriizumi, T. 2019. Independent Attachment of Lateral Ankle Ligaments: Anterior Talofibular and Calcaneofibular Ligaments - A Cadaveric Study. *The Journal of Foot and Ankle Surgery*. **58**(4), pp.717–722.

Kakwani, R. and Siddique, M. 2014. Sprained ankles. VI. Surgical treatment of chronic ligament ruptures. *Classic Papers in Orthopaedics*. **132**(5), pp.233–235.

Kannus, P. and Renström, P. 1991. Treatment for acute tears of the lateral ligaments of the ankle. Operation, cast, or early controlled mobilization. *The Journal of bone and joint surgery. American volume*. **73**(2), pp.305–12.

Karlsson, J., Bergsten, T., Lansinger, O. and Peterson, L. 1989. Surgical treatment of chronic lateral instability of the ankle joint. A new procedure. *The American journal of sports medicine*. **17**(2), pp.268–73; discussion 273-4.

Karlsson, J. and Peterson, L. 1991. Evaluation of ankle joint function: the use of a scoring scale. *The Foot*. **1**(1), pp.15–19.

Karunaratne, A., Li, S. and Bull, A.M.J. 2018. Nano-scale mechanisms explain the stiffening and strengthening of ligament tissue with increasing strain rate. *Scientific Reports*. **8**(1), p.3707.

Kastelic, J., Galeski, A. and Baer, E. 1978. The Multicomposite Structure of Tendon. *Connective Tissue Research*. **6**(1), pp.11–23.

Kayani, B., Konan, S., Pietrzak, J.R.T., Tahmassebi, J. and Haddad, F.S. 2018. Robotic-arm assisted total knee arthroplasty is associated with improved early functional recovery and reduced time to hospital discharge compared with conventional jig-based total knee arthroplasty. *Bone and Joint Journal*.

Kemler, E., van de Port, I., Valkenberg, H., Hoes, A.W. and Backx, F.J.G. 2015. Ankle injuries in the Netherlands: Trends over 10-25 years. *Scandinavian Journal of Medicine & Science in Sports*. **25**(3), pp.331–337.

Kerkhoffs, G.M.M.J., Blankevoort, L. and van Dijk, C.N. 2005. A measurement device for anterior laxity of the ankle joint complex. *Clinical Biomechanics*. **20**(2), pp.218–222.

Khawaji, B. and Soames, R. 2015. The anterior talofibular ligament: A detailed morphological study. *The Foot*. **25**(3), pp.141–147.

Kiapour, A.M., Shalvoy, M.R., Murray, M.M. and Fleming, B.C. 2015. Validation of Porcine Knee as a Sex-specific Model to Study Human Anterior Cruciate Ligament Disorders. *Clinical Orthopaedics and Related Research*.

King, A.I. 1984. A Technical Survey: A Review of Biomechanical Models. *Journal of Biomechanical Engineering*. **106**(2), p.97.

Kitaoka, H.B., Alexander, I.J., Adelaar, R.S., Nunley, J.A., Myerson, M.S. and Sanders, M. 1994. Clinical rating systems for the ankle-hindfoot, midfoot, hallux, and lesser toes. *Foot & ankle international*. **15**(7), pp.349–53.

Kjær, M. 2004. Role of Extracellular Matrix in Adaptation of Tendon and Skeletal Muscle to

Mechanical Loading. *Physiological Reviews*. **84**(2), pp.649–698.

Kjærsgaard-Andersen, P., Wethelund, J.O., Helmig, P. and Søballé, K. 1988. The stabilizing effect of the ligamentous structures in the sinus and canalis tarsi on movements in the hindfoot: An experimental study. *The American Journal of Sports Medicine*. **16**(5), pp.512–516.

Kjorsgaard-Andersen, P., Wethelund, J.O., Helmig, P. and Nielsen, S. 1987. Effect of the calcaneofibular ligament on hindfoot rotation in amputation specimens. *Acta Orthopaedica*. **58**(2), pp.135–138.

Klammer, G., Maquieira, G.J., Spahn, S., Vigfusson, V., Zanetti, M. and Espinosa, N. 2015. Natural history of nonoperatively treated osteochondral lesions of the talus. *Foot and Ankle International*.

Knight, A.C. and Weimar, W.H. 2012. Development of a fulcrum methodology to replicate the lateral ankle sprain mechanism and measure dynamic inversion speed. *Sports biomechanics / International Society of Biomechanics in Sports*. **11**(3), pp.402–13.

Konradsen, L. and Voigt, M. 2002. Inversion injury biomechanics in functional ankle instability: a cadaver study of simulated gait. *Scandinavian journal of medicine & science in sports*. **12**(6), pp.329–336.

Kovaleski, J.E., Gurchiek, L.R., Heitman, R.J., Hollis, J.M. and Pearsall, A.W. 1999. Instrumented Measurement of Anteroposterior and Inversion-Eversion Laxity of the Normal Ankle Joint Complex. *Foot & Ankle International*. **20**(12), pp.808–814.

Kovaleski, J.E., Heitman, R.J., Gurchiek, L.R., Hollis, J.M., Liu, W. and Pearsall IV, A.W. 2014. Joint stability characteristics of the ankle complex after lateral ligamentous injury, part I: A laboratory comparison using arthrometric measurement. *Journal of Athletic Training*. **49**(2), pp.192–197.

Kovaleski, J.E., Hollis, J.M., Heitman, R.J., Gurchiek, L.R., Pearsall, A.W. and IV 2002. Assessment of Ankle-Subtalar-Joint–Complex Laxity Using an Instrumented Ankle Arthrometer: An Experimental Cadaveric Investigation. *Journal of Athletic Training*. **37**(4), p.467.

Kristianslund, E., Bahr, R. and Krosshaug, T. 2011. Kinematics and kinetics of an accidental lateral ankle sprain. *Journal of Biomechanics*. **44**(14), pp.2576–2578.

Krosshaug, T. and Bahr, R. 2005. A model-based image-matching technique for three-dimensional reconstruction of human motion from uncalibrated video sequences. *Journal of Biomechanics*. **38**(4), pp.919–929.

Kumai, T., Takakura, Y., Rufai, A., Milz, S. and Benjamin, M. 2002. The functional anatomy of the human anterior talofibular ligament in relation to ankle sprains. *Journal of Anatomy*. **200**(5), pp.457–465.

Kumar Batra, A.V., Nicholson, D., Rao, P. and Sullivan, J.O. 2018. Clinical Outcomes of the Open Modified Brostrom Procedure with Internal Brace Augmentation for Lateral Ankle Instability. *Orthopedic & Muscular System*.

Leardini, A., Benedetti, M.G., Catani, F., Simoncini, L. and Giannini, S. 1999. An anatomically based protocol for the description of foot segment kinematics during gait. *Clinical Biomechanics*. **14**(8), pp.528–536.

Leardini, A., O'Connor, J.J. and Giannini, S. 2014. Biomechanics of the natural, arthritic, and replaced human ankle joint. *Journal of Foot and Ankle Research*. **7**(1), p.8.

Lee, D.G. and Davis, B.L. 2009. Assessment of the effects of diabetes on midfoot joint pressures using a robotic gait simulator. *Foot & ankle international*. **30**(8), pp.767–72.

Lee, S.S.M. and Piazza, S.J. 2008. Inversion-eversion moment arms of gastrocnemius and tibialis anterior measured in vivo. *Journal of Biomechanics*. **41**(16), pp.3366–3370.

Lee, W. and Jasiuk, I. 2014. Effects of freeze-thaw and micro-computed tomography irradiation on structure-property relations of porcine trabecular bone. *Journal of Biomechanics*. **47**(6), pp.1495–1498.

Li, Hong, Hua, Y., Li, Hongyun and Chen, S. 2020. Anterior talofibular ligament (ATFL) repair using two suture anchors produced better functional outcomes than using one suture anchor for the treatment of chronic lateral ankle instability. *Knee Surgery, Sports Traumatology, Arthroscopy*. **28**(1), pp.221–226.

Lohrer, H., Bonsignore, G., Dorn-Lange, N., Li, L., Gollhofer, A. and Gehring, D. 2019. Stabilizing lateral ankle instability by suture tape - a cadaver study. *Journal of orthopaedic surgery and research*. **14**(1), p.175.

Lundberg, A., Svensson, O.K., Nemeth, G. and Selvik, G. 1989. The axis of rotation of the ankle joint. *Journal of Bone & Joint Surgery, British Volume*. **71**-**B**(1), pp.94–99.

Lundgren, P., Nester, C., Liu, A., Arndt, A., Jones, R., Stacoff, A., Wolf, P. and Lundberg, A. 2008. Invasive in vivo measurement of rear-, mid- and forefoot motion during walking. *Gait and Posture*. **28**(1), pp.93–100.

Lynch, S.A. 2002. Assessment of the injured ankle in the athlete. *Journal of Athletic Training*.

Lynch, S.A., Eklund, U., Gottlieb, D., Renstrom, P.A.F.H. and Beynnon, B. 1996. Electromyographic Latency Changes in the Ankle Musculature During Inversion Moments. *The American Journal of Sports Medicine*. **24**(3), pp.362–369.

Macefield, V.G. 2005. Physiological characteristics of low-threshold mechanoreceptors in joints, muscle and skin in human subjects. *Clinical and Experimental Pharmacology and Physiology*. **32**(1–2), pp.135–144.

Maffulli, N., Del Buono, A., Maffulli, G.D., Oliva, F., Testa, V., Capasso, G. and Denaro, V. 2013. Isolated Anterior Talofibular Ligament Broström Repair for Chronic Lateral Ankle Instability. *The American Journal of Sports Medicine*. **41**(4), pp.858–864.

Magee, D.J. 2008. *Orthopedic physical assessment* [Online]. Saunders Elsevier. [Accessed 12 June 2020]. Available from: https://books.google.co.uk/books/about/Orthopedic_Physical_Assessment.html?id=J6noqxMmesQC&redir_esc=y.

Marieswaran, M., Jain, I., Garg, B., Sharma, V. and Kalyanasundaram, D. 2018. A review on biomechanics of anterior cruciate ligament and materials for reconstruction. *Applied Bionics and Biomechanics*. **2018**, p.4657824.

Martin, L.P., Wayne, J.S., Monahan, T.J. and Adelaar, R.S. 1998. Elongation behavior of calcaneofibular and cervical ligaments during inversion loads applied in an open kinetic chain. *Foot & ankle international*. **19**(4), pp.232–9.

Matsui, K., Takao, M., Tochigi, Y., Ozeki, S. and Glazebrook, M. 2017. Anatomy of anterior talofibular ligament and calcaneofibular ligament for minimally invasive surgery: a systematic review. *Knee Surgery, Sports Traumatology, Arthroscopy*. **25**(6), pp.1892–1902.

McCullough, M.B.A., Ringleb, S.I., Arai, K., Kitaoka, H.B. and Kaufman, K.R. 2011. Moment Arms of the Ankle Throughout the Range of Motion in Three Planes. *Foot & Ankle International*. **32**(03), pp.300–306.

McKinley, T.O., Rudert, M.J., Koos, D.C. and Brown, T.D. 2004. Incongruity versus instability in the etiology of posttraumatic arthritis *In*: *Clinical Orthopaedics and Related Research*.

Mellado, J.M., Ramos, A., Salvadó, E., Camins, A., Danús, M. and Saurí, A. 2003. Accessory ossicles and sesamoid bones of the ankle and foot: Imaging findings, clinical significance and differential diagnosis. *European Radiology*.

Mengiardi, B., Pfirrmann, C.W.A., Vienne, P., Hodler, J. and Zanetti, M. 2007. Medial Collateral Ligament Complex of the Ankle: MR Appearance in Asymptomatic Subjects. *Radiology*. **242**(3), pp.817–824.

Mengiardi, B., Zanetti, M., Schöttle, P.B., Vienne, P., Bode, B., Hodler, J. and Pfirrmann, C.W. a 2005. Spring ligament complex: MR imaging-anatomic correlation and findings in asymptomatic subjects. *Radiology*. **237**(1), pp.242–249.

Michael, J.M., Golshani, A., Gargac, S. and Goswami, T. 2008. Biomechanics of the ankle joint and clinical outcomes of total ankle replacement. *Journal of the Mechanical Behavior of Biomedical Materials*. **1**(4), pp.276–294.

Miller, A.G., Myers, S.H., Parks, B.G. and Guyton, G.P. 2016. Anterolateral Drawer Versus Anterior Drawer Test for Ankle Instability: A Biomechanical Model. *Foot & ankle international*. **37**(4), pp.407–10.

Miller, M.D., Peters, C.L. and Allen, B. 2006. Early Aseptic Loosening of a Total Knee Arthroplasty Due to Gore-Tex Particle-Induced Osteolysis. *Journal of Arthroplasty*.

Milner, C.E. and Soames, R.W. 1997. Anatomical variations of the anterior talofibular ligament of the human ankle joint. *Journal of anatomy*. **191 (Pt 3)**(Pt 3), pp.457–8.

Milner, C.E. and Soames, R.W. 1998. Anatomy of the collateral ligaments of the human ankle joint. *Foot and Ankle International*. **19**(11), pp.757–760.

Mitchell, A., Dyson, R., Hale, T. and Abraham, C. 2008. Biomechanics of ankle instability. Part 1: Reaction time to simulated ankle sprain. *Medicine and science in sports and exercise*. **40**(8), pp.1515–21.

Mok, K.-M., Fong, D.T.-P., Krosshaug, T., Engebretsen, L., Hung, A.S.-L., Yung, P.S.-H. and Chan, K.-M. 2011. Kinematics Analysis of Ankle Inversion Ligamentous Sprain Injuries in Sports: 2 Cases During the 2008 Beijing Olympics. *The American Journal of Sports Medicine*. **39**(7), pp.1548–1552.

Moshiri, A. and Oryan, A. 2012. Role of tissue engineering in tendon reconstructive surgery and regenerative medicine: Current concepts, approaches and concerns. *Hard Tissue*. **1**(2), pp.1–11.

Moshiri, A. and Oryan, A. 2013. Tendon and Ligament Tissue Engineering, Healing and Regenerative Medicine. *Journal of Sports Medicine & Doping Studies*. **03**(02).

Nawoczenski, D.A., Owen, M.G., Ecker, M.L., Altman, B. and Epler, M. 1985. Objective evaluation of peroneal response to sudden inversion stress. *The Journal of orthopaedic and sports physical therapy*. **7**(3), pp.107–109.

Neoligaments n.d. Infinity-LockTM Button system. [Accessed 27 September 2020]. Available from: https://www.neoligaments.com/product/infinity-lock/.

Nery, C., Raduan, F., Del Buono, A., Asaumi, I.D., Cohen, M. and Maffulli, N. 2011. Arthroscopic-assisted Broström-Gould for chronic ankle instability: a long-term follow-up. *The American journal of sports medicine*. **39**(11), pp.2381–8.

Nester, C.J., Jarvis, H.L., Jones, R.K., Bowden, P.D. and Liu, A. 2014. Movement of the human foot in 100 pain free individuals aged 18-45: Implications for understanding normal foot function. *Journal of Foot and Ankle Research*.

Nester, C.J., Liu, A.M., Ward, E., Howard, D., Cocheba, J., Derrick, T. and Patterson, P. 2007. In vitro study of foot kinematics using a dynamic walking cadaver model. *Journal of*

Biomechanics. **40**(9), pp.1927–1937.

Neumann, P., Keller, T.S., Ekström, L. and Hansson, T. 1994. Effect of Strain Rate and Bone Mineral on the Structural Properties of the Human Anterior Longitudinal Ligament. *Spine*. **19**(Supplement), pp.205–211.

Neuschwander, T.B., Indresano, A.A., Hughes, T.H. and Smith, B.W. 2013. Footprint of the lateral ligament complex of the ankle. *Foot & ankle international*. **34**(4), pp.582–6.

Noailles, T., Lopes, R., Padiolleau, G., Gouin, F. and Brilhault, J. 2018. Non-anatomical or direct anatomical repair of chronic lateral instability of the ankle: A systematic review of the literature after at least 10 years of follow-up. *Foot and Ankle Surgery*. **24**(2), pp.80–85.

Nordin, M. and Frankel, V.H. 2012. *Basic biomechanics of the musculoskeletal system* [Online]. Lippincott Williams & Wilkins. [Accessed 20 May 2020]. Available from: https://books.google.co.uk/books/about/Basic_Biomechanics_of_the_Musculoskeleta.html?id=UCxsf7mMBE0C&redir_esc=y.

Noyes, F.R., DeLucas, J.L. and Torvik, P.J. 1974. *Biomechanics of anterior cruciate ligament failure: an analysis of strain rate sensitivity and mechanisms of failure in primates* [Online]. [Accessed 25 July 2019]. Available from: www.jbjs.org.

Noyes, F.R. and Grood, E.S. 1976. The strength of the anterior cruciate ligament in humans and rhesus monkeys: Age related and species related changes. *Journal of Bone and Joint Surgery - Series A*. **58**(8), pp.1074–1082.

Oosterwaal, M., Carbes, S., Telfer, S., Woodburn, J., Tørholm, S., Al-Munajjed, A.A., van Rhijn, L. and Meijer, K. 2016. The Glasgow-Maastricht foot model, evaluation of a 26 segment kinematic model of the foot. *Journal of foot and ankle research*. **9**(1), p.19.

Ozeki, S., Kitaoka, H., Uchiyama, E., Luo, Z.-P., Kaufman, K. and An, K.-N. 2006. Ankle Ligament Tensile Forces at the End Points of Passive Circumferential Rotating Motion of the Ankle and Subtalar Joint Complex. *Foot & Ankle International*. **27**(11), pp.965–969.

Panagiotakis, E., Mok, K.-M., Fong, D.T.-P. and Bull, A.M.J. 2017. Biomechanical analysis of ankle ligamentous sprain injury cases from televised basketball games: Understanding when, how and why ligament failure occurs. *Journal of Science and Medicine in Sport*. **20**(12), pp.1057–1061.

Park, K.H., Lee, J.W., Suh, J.W., Shin, M.H. and Choi, W.J. 2016. Generalized Ligamentous Laxity Is an Independent Predictor of Poor Outcomes after the Modified Broström Procedure for Chronic Lateral Ankle Instability. *American Journal of Sports Medicine*. **44**(11).

Patton, D.M., Bigelow, E.M.R., Schlecht, S.H., Kohn, D.H., Bredbenner, T.L. and Jepsen, K.J. 2019. The relationship between whole bone stiffness and strength is age and sex dependent. *Journal of Biomechanics*. **83**, pp.125–133.

Peeters, K., Natsakis, T., Burg, J., Spaepen, P., Jonkers, I., Dereymaeker, G. and Vander Sloten, J. 2013. An in vitro approach to the evaluation of foot-ankle kinematics: performance evaluation of a custom-built gait simulator. *Proceedings of the Institution of Mechanical Engineers. Part H, Journal of engineering in medicine*. **227**(9), pp.955–67.

Pefanis, N., Karagounis, P., Tsiganos, G., Armenis, E. and Baltopoulos, P. 2009. Tibiofemoral Angle and Its Relation to Ankle Sprain Occurrence. *Foot & Ankle Specialist*.

Phisitkul, P., Chaichankul, C., Sripongsai, R., Prasitdamrong, I., Tengtrakulcharoen, P. and Suarchawaratana, S. 2009. Accuracy of anterolateral drawer test in lateral ankle instability: a cadaveric study. *Foot & ankle international*. **30**(7), pp.690–5.

Pioletti, D.P., Rakotomanana, L.R. and Leyvraz, P.F. 1999. Strain rate effect on the mechanical behavior of the anterior cruciate ligament-bone complex. *Medical Engineering and Physics*. **21**(2), pp.95–100.

Quinn, K.P. and Winkelstein, B.A. 2011. Preconditioning is correlated with altered collagen fiber alignment in ligament. *Journal of Biomechanical Engineering*. **133**(6), pp.575–579.

Quirk, N.P., Lopez De Padilla, C., De La Vega, R.E., Coenen, M.J., Tovar, A., Evans, C.H. and Müller, S.A. 2018. Effects of freeze-thaw on the biomechanical and structural properties of the rat Achilles tendon. *Journal of Biomechanics*. **81**, pp.52–57.

Rein, S., Hagert, E., Schneiders, W., Fieguth, A. and Zwipp, H. 2015. Histological analysis of the structural composition of ankle ligaments. *Foot and Ankle International*. **36**(2), pp.211–224.

Reinwald, S. and Burr, D. 2008. Review of nonprimate, large animal models for osteoporosis research. *Journal of Bone and Mineral Research*.

Renstrom, P., Wertz, M., Incavo, S., Pope, M., Ostgaard, H.C., Arms, S. and Haugh, L. 1988. Strain in the lateral ligaments of the ankle. *Foot and Ankle*. **9**(2), pp.59–63.

Rigby, R., Cottom, J.M. and Rozin, R. 2015. Isolated Calcaneofibular Ligament Injury: A Report of Two Cases. *Journal of Foot and Ankle Surgery*. **54**(3).

Rockar, P.A. 1995. The subtalar joint: Anatomy and joint motion. *The Journal of orthopaedic and sports physical therapy*. **21**(6), pp.361–72.

Rohatgi, A. n.d. WebPlot Digitizer. Available from: https://automeris.io/WebPlotDigitizer/.

Roos, E.M., Brandsson, S. and Karlsson, J. 2001. Validation of the foot and ankle outcome score for ankle ligament reconstruction. *Foot & ankle international*. **22**(10), pp.788–94.

Roos, K.G., Kerr, Z.Y., Mauntel, T.C., Djoko, A., Dompier, T.P. and Wikstrom, E.A. 2017. The Epidemiology of Lateral Ligament Complex Ankle Sprains in National Collegiate Athletic Association Sports. *American Journal of Sports Medicine*. **45**(1).

Root, M.L., Orien, W.P. and Weed, J.H. 1977. *Normal and abnormal function of the foot*.

Rowlands, A. V. and Stiles, V.H. 2012. Accelerometer counts and raw acceleration output in relation to mechanical loading. *Journal of Biomechanics*.

Rumian, A.P., Wallace, A.L. and Birch, H.L. 2007. Tendons and ligaments are anatomically distinct but overlap in molecular and morphological features—a comparative study in an ovine model. *Journal of Orthopaedic Research*. **25**(4), pp.458–464.

Russo, A., Giacchè, P., Marcantoni, E., Arrighi, A. and Molfetta, L. 2016. Treatment of chronic lateral ankle instability using the Broström-Gould procedure in athletes: long-term results. *Joints*. **4**(2), pp.94–7.

Safa, B.N., Meadows, K.D., Szczesny, S.E. and Elliott, D.M. 2017. Exposure to buffer solution alters tendon hydration and mechanics. *Journal of Biomechanics*. **61**, pp.18–25.

Safran, M.R., Benedetti, R.S., Bartolozzi, A.R. and Mandelbaum, B.R. 1999. Lateral ankle sprains: a comprehensive review: part 1: etiology, pathoanatomy, histopathogenesis, and diagnosis. *Medicine and science in sports and exercise*. **31**(7 Suppl), pp.S429-37.

Saltzman, C.L., Salamon, M.L., Blanchard, G.M., Huff, T., Hayes, A., Buckwalter, J.A. and Amendola, A. 2005. Epidemiology of ankle arthritis: report of a consecutive series of 639 patients from a tertiary orthopaedic center. *The Iowa orthopaedic journal*.

Sarrafian, S. 2011. *Sarrafians's Anatomy of the Foot and Ankle* [Online]. Wolters Kluwer Health/Lippincott Williams & Wilkins. [Accessed 18 December 2016]. Available from: https://books.google.es/books?id=I8h6bDR0SLMC.

Sarrafian, S.K. 1993. Biomechanics of the subtalar joint complex. *Clinical Orthopaedics and Related Research*. **290**(290), pp.17–26.

Schepers, T., Vogels, L.M.M. and Van Lieshout, E.M.M. 2011. Hemi-Castaing ligamentoplasty

for the treatment of chronic lateral ankle instability: A retrospective assessment of outcome. *International Orthopaedics*. **35**(12), pp.1805–1812.

Schuh, R., Benca, E., Willegger, M., Hirtler, L., Zandieh, S., Holinka, J. and Windhager, R. 2016. Comparison of Broström technique, suture anchor repair, and tape augmentation for reconstruction of the anterior talofibular ligament. *Knee Surgery, Sports Traumatology, Arthroscopy*. **24**(4), pp.1101–1107.

Screen, H.R.C., Chhaya, V.H., Greenwald, S.E., Bader, D.L., Lee, D.A. and Shelton, J.C. 2006. The influence of swelling and matrix degradation on the microstructural integrity of tendon. *Acta Biomaterialia*. **2**(5), pp.505–513.

Screen, H.R.C., Shelton, J.C., Chhaya, V.H., Kayser, M. V., Bader, D.L. and Lee, D.A. 2005. The influence of noncollagenous matrix components on the micromechanical environment of tendon fascicles. *Annals of Biomedical Engineering*. **33**(8), pp.1090–1099.

Seligson, D., Gassman, J. and Pope, M. 1980. Ankle instability: evaluation of the lateral ligaments. *The American journal of sports medicine*. **8**(1), pp.39–42.

Sharkey, N.A. and Hamel, A.J. 1998. A dynamic cadaver model of the stance phase of gait: Performance characteristics and kinetic validation. *Clinical Biomechanics*. **13**(6), pp.420–433.

Sheth, P., Yu, B., Laskowski, E.R. and An, K.N. 1997. Ankle disk training influences reaction times of selected muscles in a simulated ankle sprain. *The American journal of sports medicine*. **25**(4), pp.538–43.

Siegler, S., Block, J. and Schneck, C.D. 1988. The Mechanical Characteristics of the Collateral Ligaments of the Human Ankle Joint. *Foot & Ankle International*. **8**(5), pp.234–242.

Simpson, J.D., Stewart, E.M., Rendos, N.K., Cosio-Lima, L., Wilson, S.J., Macias, D.M., Chander, H. and Knight, A.C. 2019. Anticipating ankle inversion perturbations during a single-leg drop landing alters ankle joint and impact kinetics. *Human Movement Science*. **66**, pp.22–30.

Sinkjaer, T., Toft, E., Andreassen, S. and Hornemann, B.C. 1988. Muscle stiffness in human ankle dorsiflexors: intrinsic and reflex components. *Journal of neurophysiology*. **60**(3), pp.1110–21.

Smith, N.C., Wilson, A.M., Jespers, K.J. and Payne, R.C. 2006. Muscle architecture and functional anatomy of the pelvic limb of the ostrich (Struthio camelus). *Journal of anatomy*. **209**(6), pp.765–79.

Snedeker, J.G., Wirth, S.H. and Espinosa, N. 2012. Biomechanics of the Normal and Arthritic Ankle Joint. *Foot and Ankle Clinics*. **17**(4), pp.517–528.

Snelling, E.P., Biewener, A.A., Hu, Q., Taggart, D.A., Fuller, A., Mitchell, D., Maloney, S.K. and Seymour, R.S. 2017. Scaling of the ankle extensor muscle-tendon units and the biomechanical implications for bipedal hopping locomotion in the post-pouch kangaroo *Macropus fuliginosus*. *Journal of Anatomy*. **231**(6), pp.921–930.

Solomonow, M. 2006. Sensory - Motor control of ligaments and associated neuromuscular disorders. *Journal of Electromyography and Kinesiology*. **16**(6), pp.549–567.

Song, Y.-J. and Hua, Y.-H. 2019. Similar Outcomes at Early Term After Arthroscopic or Open Repair of Chronic Ankle Instability: A Systematic Review and Meta-Analysis. *The Journal of Foot and Ankle Surgery*. **58**(2), pp.312–319.

Song, Y., Li, H., Sun, C., Zhang, J., Gui, J., Guo, Q., Song, W., Duan, X., Wang, Xiaoqin, Wang, Xuesong, Shi, Z., Hua, Y., Tang, K., Chen, S. and Chen, S. 2019. Clinical Guidelines for the Surgical Management of Chronic Lateral Ankle Instability: A Consensus Reached by Systematic Review of the Available Data. *Orthopaedic Journal of Sports Medicine*. **7**(9),

p.232596711987385.

Spennacchio, P., Meyer, C., Karlsson, J., Seil, R., Mouton, C. and Senorski, E.H. 2020. Evaluation modalities for the anatomical repair of chronic ankle instability. *Knee Surgery, Sports Traumatology, Arthroscopy*. **28**(1), pp.163–176.

St Pierre, R.K., Rosen, J., Whitesides, T.E., Szczukowski, M., Fleming, L.L. and Hutton, W.C. 1983. The tensile strength of the anterior talofibular ligament. *Foot and Ankle*. **4**(2), pp.83–85.

Stagni, R., Leardini, A. and Ensini, A. 2004. Ligament fibre recruitment at the human ankle joint complex in passive flexion. *Journal of Biomechanics*. **37**(12), pp.1823–1829.

Stauffer, R.N., Chao, E.Y. and Brewster, R.C. 1977. Force and motion analysis of the normal, diseased, and prosthetic ankle joint. *Clin Orthop Relat Res*. (127), pp.189–196.

Stephens, M.M. and Sammarco, G.J. 1992. The stabilizing role of the lateral ligament complex around the ankle and subtalar joints. *Foot and Ankle*. **13**(3), pp.130–136.

Storen, H. 1959. A new method for operative treatment of insufficiency of the lateral ligaments of the anklejoint. *Acta chirurgica Scandinavica*. **117**, pp.501–509.

Stormont, D.M., Morrey, B.F., an, K.N. and Cass, J.R. 1985. Stability of the loaded ankle:Relation between articular restraint and primary and secondary static restraints. *The American Journal of Sports Medicine*. **13**(5), pp.295–300.

Stouffer, D.C., Butler, D.L. and Hosny, D. 1985. The relationship between crimp pattern and mechanical response of human patellar tendon-bone units. *Journal of biomechanical engineering*. **107**(2), pp.158–65.

Stovitz, S.D. and Johnson, R.J. 2003. NSAIDS and musculoskeletal treatment: What is the clinical evidence? *Physician and Sportsmedicine*. **31**(1).

Suto, K., Urabe, K., Naruse, K., Uchida, K., Matsuura, T., Mikuni-Takagaki, Y., Suto, M., Nemoto, N., Kamiya, K. and Itoman, M. 2012. Repeated freeze-thaw cycles reduce the survival rate of osteocytes in bone-tendon constructs without affecting the mechanical properties of tendons. *Cell and tissue banking*. **13**(1), pp.71–80.

Taga, I., Shino, K., Inoue, M., Nakata, K., Maeda, A. and Henry, J.H. 1993. Articular cartilage lesions in ankles with lateral ligament injury. An arthroscopic study. *American Journal of Sports Medicine*.

Tanaka, H. and Mason, L. 2011. (v) Chronic ankle instability. *Orthopaedics and Trauma*. **25**(4), pp.269–278.

Taş, S., Yilmaz, S., Onur, M.R., Soylu, A.R., Altuntaş, O. and Korkusuz, F. 2017. Patellar tendon mechanical properties change with gender, body mass index and quadriceps femoris muscle strength. *Acta Orthopaedica et Traumatologica Turcica*.

Taser, F., Shafiq, Q. and Ebraheim, N.A. 2006. Anatomy of lateral ankle ligaments and their relationship to bony landmarks. *Surgical and Radiologic Anatomy*. **28**(4), pp.391–397.

Terada, M. and Gribble, P.A. 2015. Jump Landing Biomechanics During a Laboratory Recorded Recurrent Ankle Sprain. *Foot & Ankle International*. **36**(7), pp.842–848.

Tochigi, Y., Rudert, M.J., Amendola, A., Brown, T.D. and Saltzman, C.L. 2005. Tensile Engagement of the Peri-Ankle Ligaments in Stance Phase. *Foot & Ankle International*. **26**(12), pp.1067–1073.

Tourné, Y. and Mabit, C. 2015. *La cheville instable*. ELSEVIER MASSON, VIA PALEOCAPA 7, 20121 MILANO, ITALY.

Tourné, Y. and Mabit, C. 2017. Lateral ligament reconstruction procedures for the ankle.

Orthopaedics & Traumatology: Surgery & Research. **103**(1), pp.S171–S181.

Tourné, Y., Mabit, C., Moroney, P.J., Chaussard, C. and Saragaglia, D. 2012. Long-term follow-up of lateral reconstruction with extensor retinaculum flap for chronic ankle instability. *Foot & ankle international*. **33**(12), pp.1079–86.

Tozer, S. and Duprez, D. 2005. Tendon and ligament: Development, repair and disease. *Birth Defects Research Part C - Embryo Today: Reviews*. **75**(3), pp.226–236.

Tuijthof, G.J.M., Zengerink, M., Beimers, L., Jonges, R., Maas, M., van Dijk, C.N. and Blankevoort, L. 2009. Determination of consistent patterns of range of motion in the ankle joint with a computed tomography stress-test. *Clinical Biomechanics*. **24**(6), pp.517–523.

Ulku, T.K., Kocaoglu, B., Tok, O., Irgit, K. and Nalbantoglu, U. 2020. Arthroscopic suture-tape internal bracing is safe as arthroscopic modified Broström repair in the treatment of chronic ankle instability. *Knee Surgery, Sports Traumatology, Arthroscopy*. **28**(1), pp.227–232.

Usami, N., Inokuchi, S., Hiraishi, E., Miyanaga, M. and Waseda, A. 2000. Clinical application of artificial ligament for ankle instability - Long-term follow-up. *Journal of Long-Term Effects of Medical Implants*.

Valderrabano, V., Hintermann, B., Horisberger, M. and Fung, T.S. 2006. Ligamentous Posttraumatic Ankle Osteoarthritis. *The American Journal of Sports Medicine*. **34**(4), pp.612–620.

Valderrabano, V., Horisberger, M., Russell, I., Dougall, H. and Hintermann, B. 2009. Etiology of ankle osteoarthritis. *Clinical Orthopaedics and Related Research*.

Vega, J., Malagelada, F., Manzanares Céspedes, M.C. and Dalmau-Pastor, M. 2020. The lateral fibulotalocalcaneal ligament complex: an ankle stabilizing isometric structure. *Knee Surgery, Sports Traumatology, Arthroscopy*. **28**(1), pp.8–17.

Verhagen, E.A., van Tulder, M., van der Beek, A.J., Bouter, L.M. and van Mechelen, W. 2005. An economic evaluation of a proprioceptive balance board training programme for the prevention of ankle sprains in volleyball. *Br J Sports Med*. **39**(2), pp.111–115.

Viens, N.A., Wijdicks, C.A., Campbell, K.J., LaPrade, R.F. and Clanton, T.O. 2014. Anterior Talofibular Ligament Ruptures, Part 1. *The American Journal of Sports Medicine*. **42**(2), pp.405–411.

Viladot, A., Lorenzo, J.C., Salazar, J. and Rodriguez, A. 1984. The subtalar joint: embryology and morphology. *Foot & Ankle International*. **5**(2), pp.54–66.

Voleti, P.B., Buckley, M.R. and Soslowsky, L.J. 2012. Tendon Healing: Repair and Regeneration. *Annual Review of Biomedical Engineering*. **14**(1), pp.47–71.

Vuurberg, Gwendolyn, Hoorntje, A., Wink, L.M., Van Der Doelen, B.F.W., Van Den Bekerom, M.P., Dekker, R., Van Dijk, C.N., Krips, R., Loogman, M.C.M., Ridderikhof, M.L., Smithuis, F.F., Stufkens, S.A.S., Verhagen, E.A.L.M., De Bie, R.A. and Kerkhoffs, G.M.M.J. 2018. Diagnosis, treatment and prevention of ankle sprains: Update of an evidence-based clinical guideline. *British Journal of Sports Medicine*. **52**(15), p.956.

Vuurberg, G., Pereira, H., Blankevoort, L. and van Dijk, C.N. 2018. Anatomic stabilization techniques provide superior results in terms of functional outcome in patients suffering from chronic ankle instability compared to non-anatomic techniques. *Knee Surgery, Sports Traumatology, Arthroscopy*. **26**(7), pp.2183–2195.

Waldrop, N.E., Wijdicks, C.A., Jansson, K.S., LaPrade, R.F. and Clanton, T.O. 2012. Anatomic Suture Anchor Versus the Broström Technique for Anterior Talofibular Ligament Repair. *The American Journal of Sports Medicine*. **40**(11), pp.2590–2596.

Watanabe, K., Kitaoka, H.B., Berglund, L.J., Zhao, K.D., Kaufman, K.R. and An, K.N. 2012. The role of ankle ligaments and articular geometry in stabilizing the ankle. *Clinical Biomechanics*. **27**(2), pp.189–195.

Waterman, B.R., Owens, B.D., Davey, S., Zacchilli, M.A. and Belmont, P.J. 2010. The epidemiology of ankle sprains in the United States. *Journal of Bone and Joint Surgery - Series A*.

Watson-Jones, R. 1940. *Fractures and other bone and joint injuries*. Edinburgh: E and S Livingstone Ltd.

Weatherall, J.M., Mroczek, K., McLaurin, T., Ding, B. and Tejwani, N. 2013. Post-traumatic ankle arthritis. *Bulletin of the Hospital for Joint Disease (2013)*.

Whitaker, S., Edwards, J.H., Guy, S., Ingham, E. and Herbert, A. 2019. Stratifying the mechanical performance of a decellularized xenogeneic tendon graft for anterior cruciate ligament reconstruction as a function of graft diameter. *Bone and Joint Research*.

Wikstrom, E.A., Hubbard-Turner, T., Guderian, S. and Turner, M.J. 2018. Lateral Ankle Sprain in a Mouse Model: Lifelong Sensorimotor Dysfunction. *Journal of Athletic Training*. **53**(3), pp.249–254.

Wikstrom, E.A., Hubbard-Turner, T., Woods, S., Guderian, S. and Turner, M.J. 2015. Developing a Mouse Model of Chronic Ankle Instability. *Medicine & Science in Sports & Exercise*. **47**(4), pp.866–872.

Wilkin, E.J., Hunt, A., Nightingale, E.J., Munn, J., Kilbreath, S.L. and Refshauge, K.M. 2012. Manual testing for ankle instability. *Manual Therapy*. **17**(6), pp.593–596.

Willems, T., Witvrouw, E., Delbaere, K., De Cock, A. and De Clercq, D. 2005. Relationship between gait biomechanics and inversion sprains: A prospective study of risk factors. *Gait and Posture*. **21**(4), pp.379–387.

Woo, S.L.-Y., Gomez, M.A. and Akeson, W.H. 1981. The Time and History-Dependent Viscoelastic Properties of the Canine Medial Collateral Ligament. *Journal of Biomechanical Engineering*. **103**(4), p.293.

Woo, S.L., Danto, M.I., Ohland, K.J., Lee, T.Q. and Newton, P.O. 1990. The use of a laser micrometer system to determine the cross-sectional shape and area of ligaments: a comparative study with two existing methods. *Journal of biomechanical engineering*. **112**(4), pp.426–31.

Woo, S.L.Y., Inoue, M., Mcgurk-Burleson, E. and Gomez, M.A. 1987. Treatment of the medial collateral ligament injury: II: Structure and function of canine knees in response to differing treatment regimens. *The American Journal of Sports Medicine*. **15**(1), pp.22–29.

Woo, S.L.Y., Ritter, M.A., Amiel, D., Sanders, T.M., Gomez, M.A., Kuei, S.C., Garfin, S.R. and Akeson, W.H. 1980. The biomechanical and biochemical properties of swine tendons - long term effects of exercise on the digital extensors. *Connective Tissue Research*.

Wredmark, T. and Engström, B. 1993. Five-year results of anterior cruciate ligament reconstruction with the Stryker Dacron high-strength ligament. *Knee Surgery, Sports Traumatology, Arthroscopy*.

Wren, T.A.L., Beaupré, G.S. and Carter, D.R. 2000. Tendon and ligament adaptation to exercise, immobilization, and remobilization. *Journal of Rehabilitation Research and Development*.

Wright, I.C., Neptune, R.R., Van Den Bogert, A.J. and Nigg, B.M. 2000. The influence of foot positioning on ankle sprains. *Journal of Biomechanics*. **33**(5), pp.513–519.

Xu, D., Gan, K., Li, H., Zhou, S., Lou, Z., Wang, Y., Li, G., Ruan, C., Hu, X., Chen, Y. and Ma, W. 2019. Modified Broström Repair With and Without Augmentation Using Suture Tape for

Chronic Lateral Ankle Instability. *Orthopaedic Surgery*. **11**(4), pp.671–678.

Xu, H.-X. and Lee, K.-B. 2016. Modified Broström Procedure for Chronic Lateral Ankle Instability in Patients With Generalized Joint Laxity. *The American Journal of Sports Medicine*. **44**(12), pp.3152–3157.

Yamamoto, E., Hayashi, K. and Yamamoto, N. 1999. Mechanical Properties of Collagen Fascicles From the Rabbit Patellar Tendon. *Journal of Biomechanical Engineering*. **121**(1), pp.124–131.

Yang, G., Rothrauff, B.B. and Tuan, R.S. 2013. Tendon and ligament regeneration and repair: Clinical relevance and developmental paradigm. *Birth Defects Research Part C - Embryo Today: Reviews*. **99**(3), pp.203–222.

Yasuda, K. and Hayashi, K. 1999. Changes in biomechanical properties of tendons and ligaments from joint disuse. *Osteoarthritis and Cartilage*.

Yasui, Y., Shimozono, Y. and Kennedy, J.G. 2018. Surgical Procedures for Chronic Lateral Ankle Instability. *Journal of the American Academy of Orthopaedic Surgeons*. **26**(7), pp.223–230.

Yoo, J.-S. and Yang, E.-A. 2016. Clinical results of an arthroscopic modified Brostrom operation with and without an internal brace. *Journal of Orthopaedics and Traumatology*. **17**(4), pp.353–360.

Zitnay, J.L. and Weiss, J.A. 2018. Load transfer, damage, and failure in ligaments and tendons. *Journal of Orthopaedic Research®*. **36**(12), pp.3093–3104.

Zwipp, H. and Randt, T. 1994. Ankle joint biomechanics. *Foot and Ankle Surgery*. **1**(1), pp.21–27.

Appendices

Appendix A – Lateral Collateral Ligament Complex Pot

A.1 Lateral Collateral Ligament Complex Pot Assembly Drawing

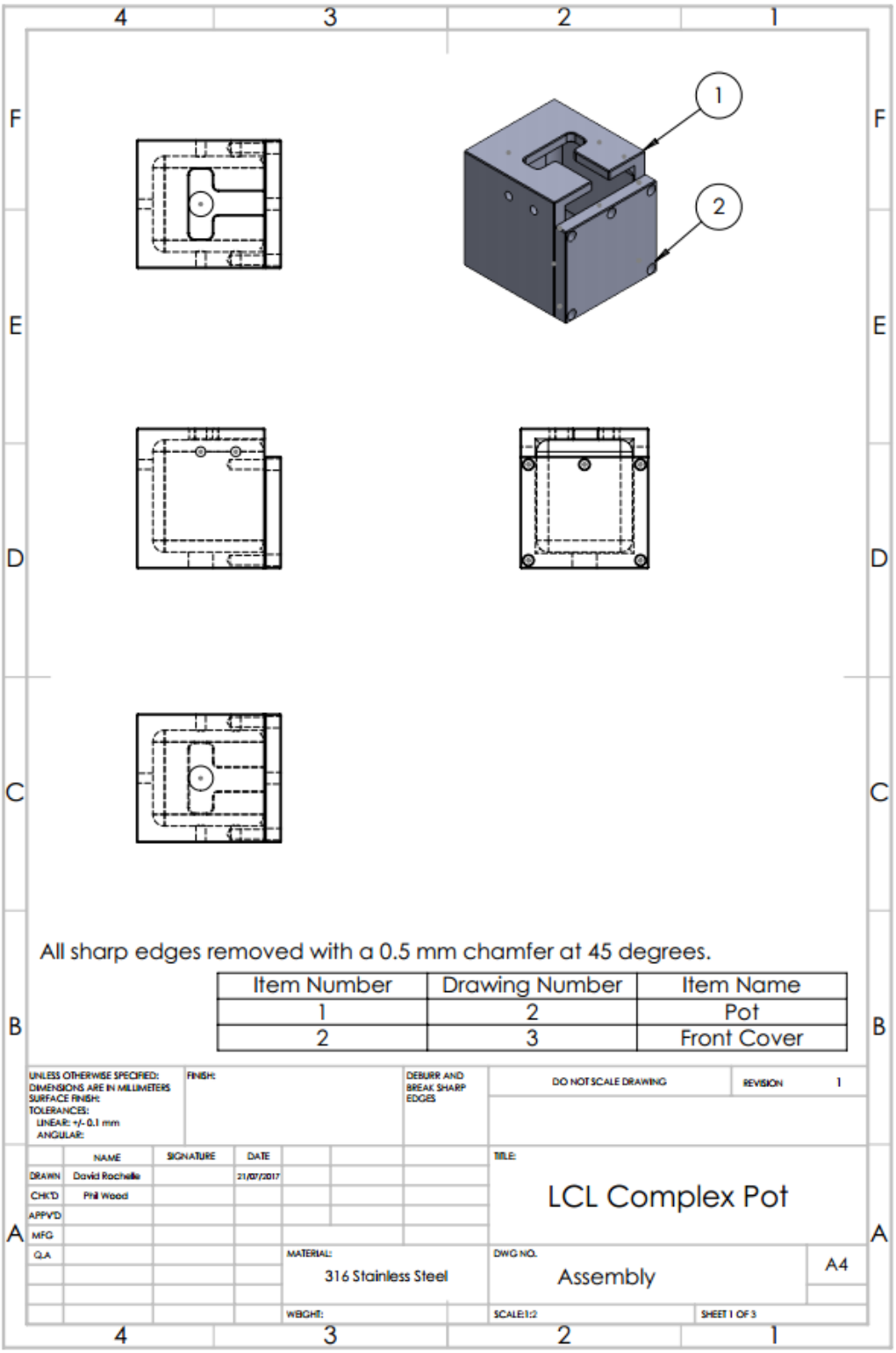

A.2 Lateral Collateral Ligament Complex Pot Drawing

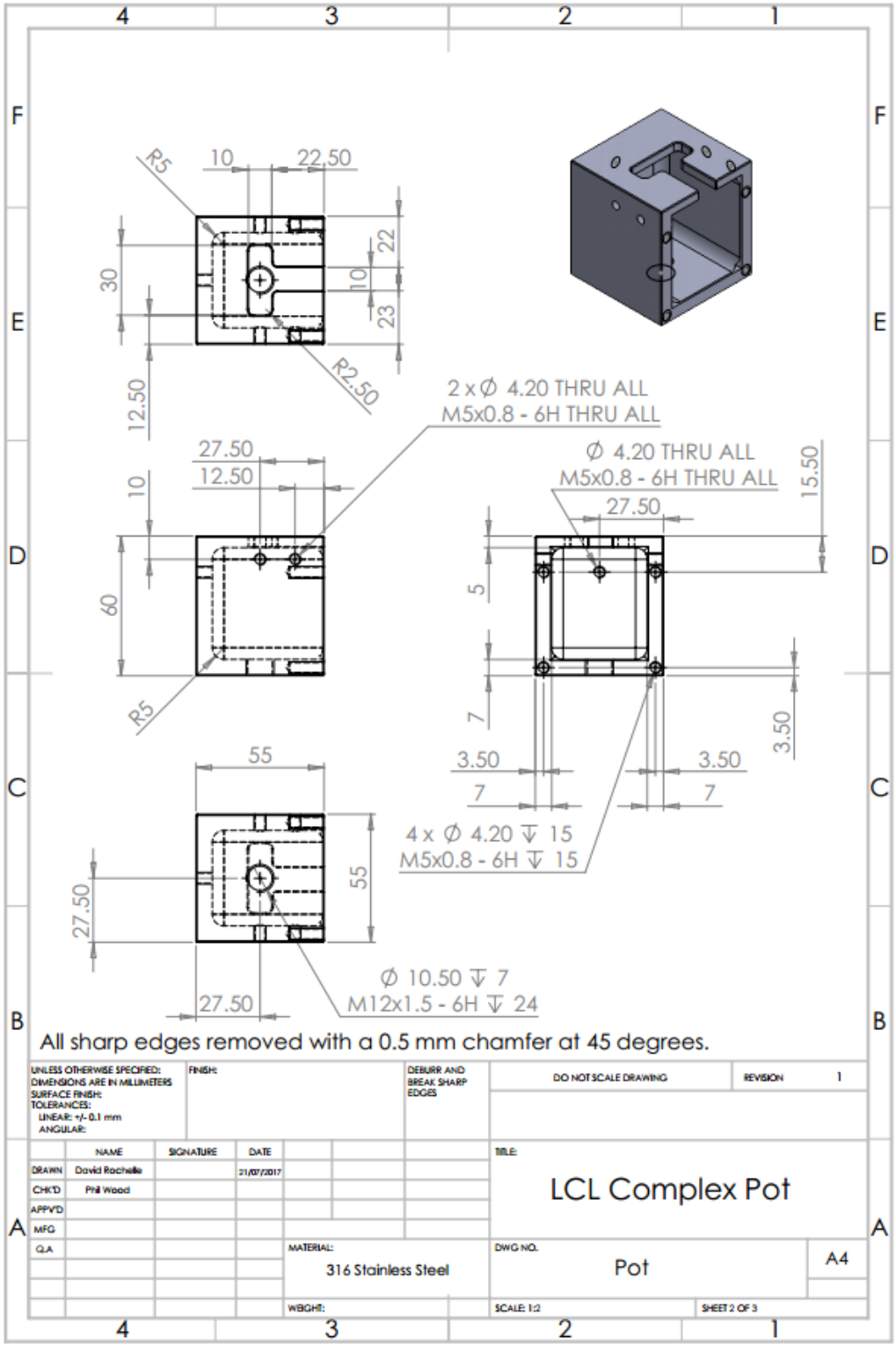

A.3 Lateral Collateral Ligament Complex Pot Front Cover Drawing

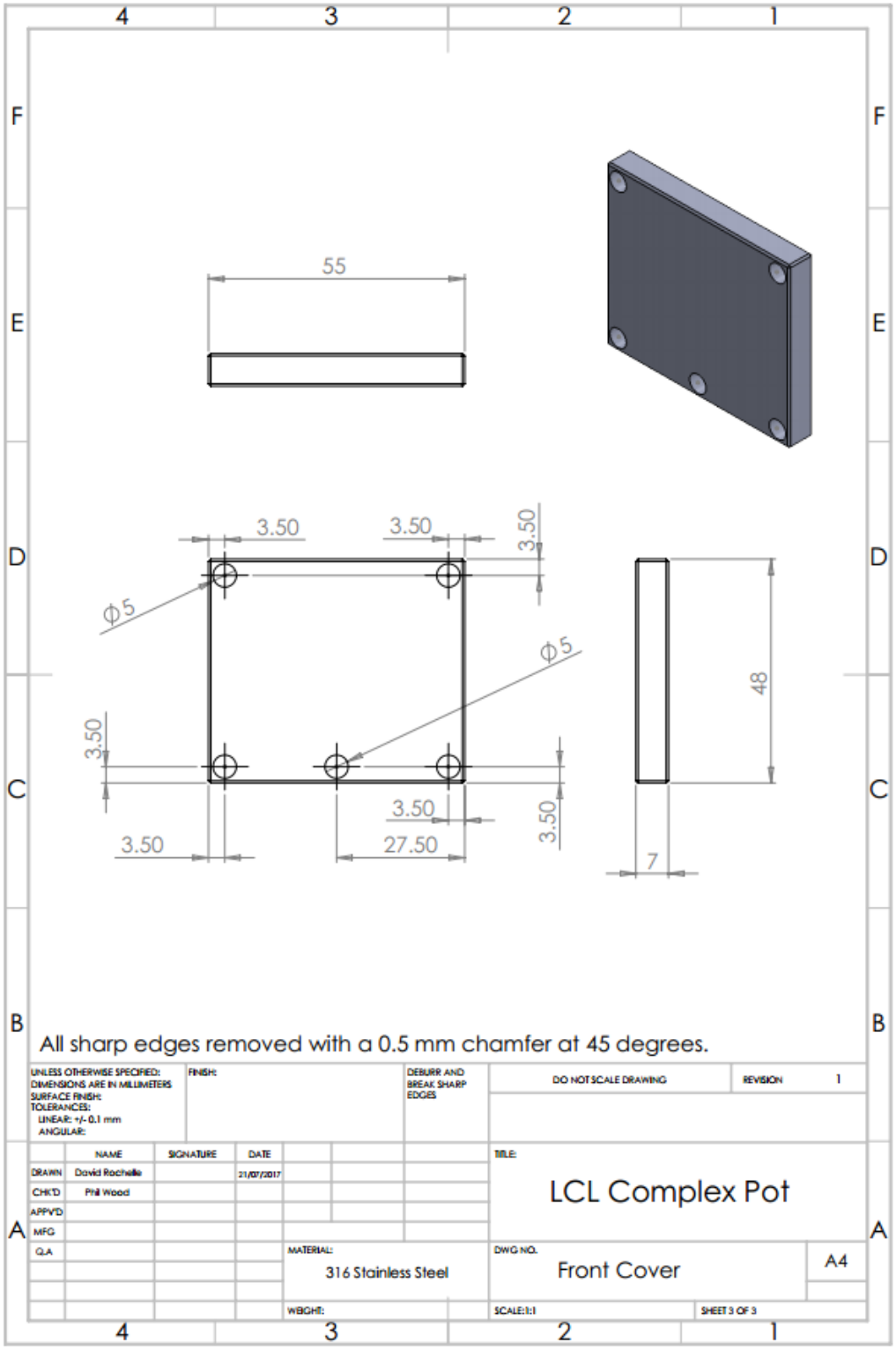

Appendix B – Syndesmosis Pot

B.1 Syndesmosis Pot Assembly

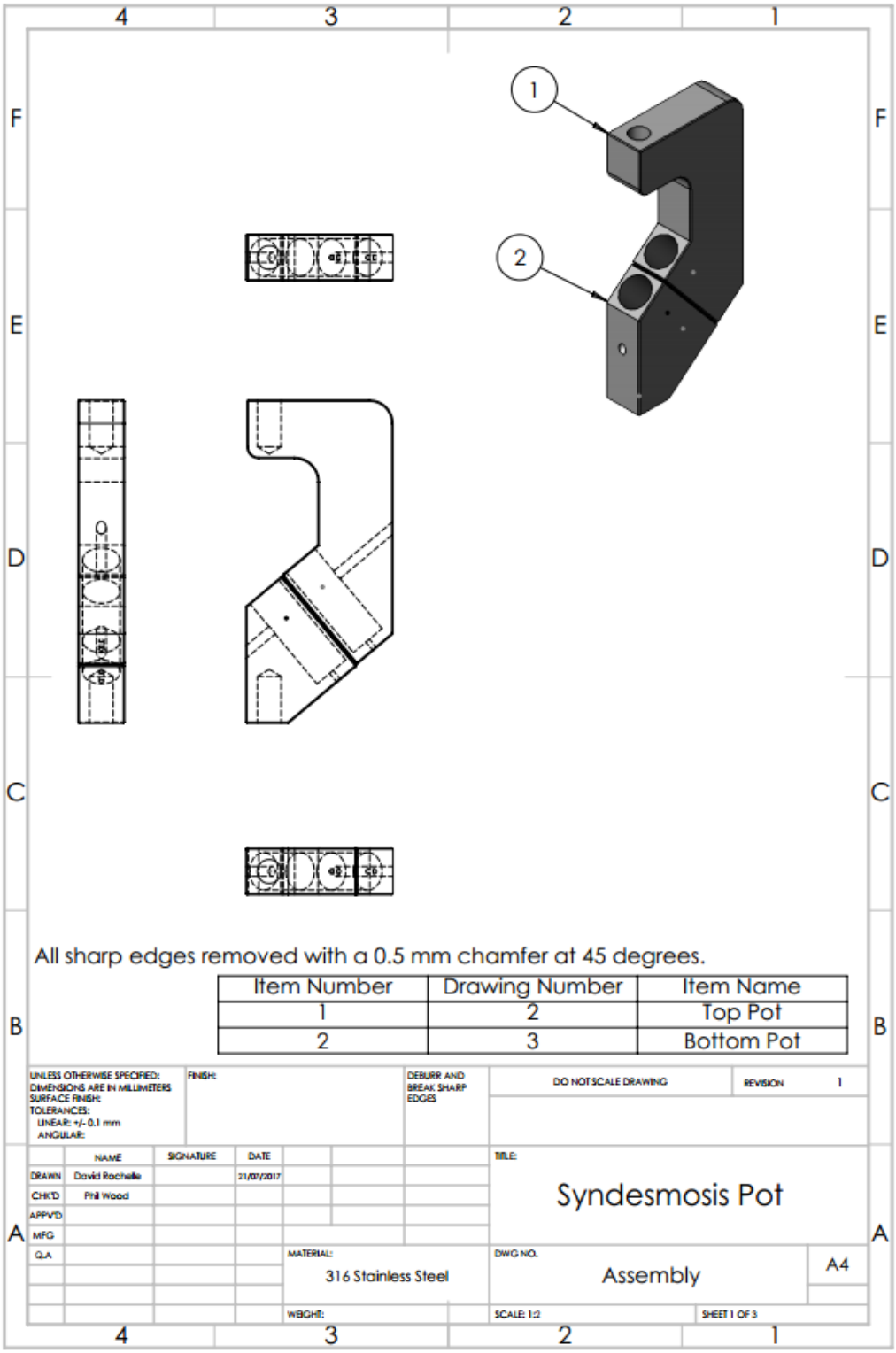

B.2 Syndesmosis Pot Top Pot

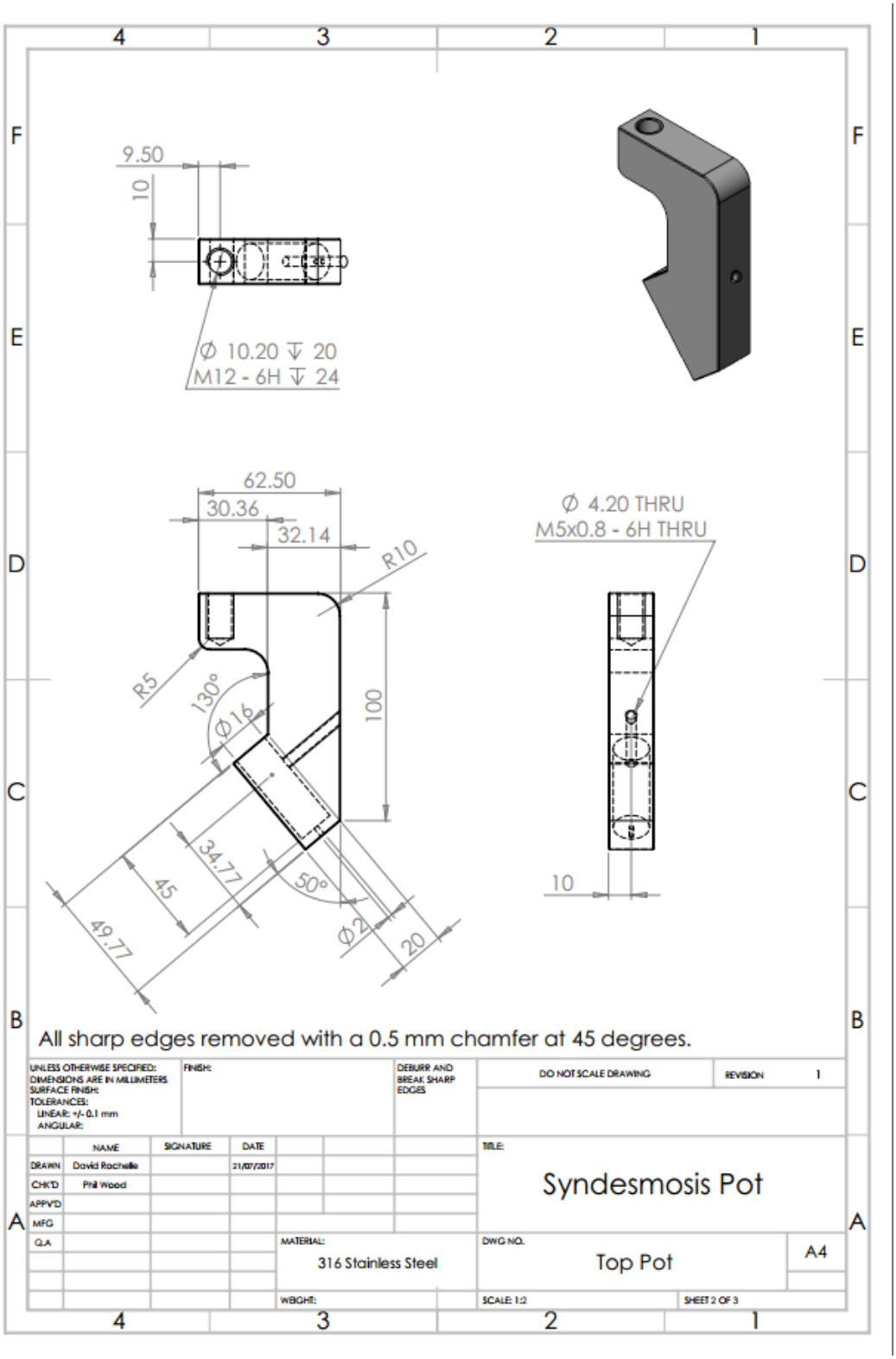

B.3 Syndesmosis Pot Bottom Pot

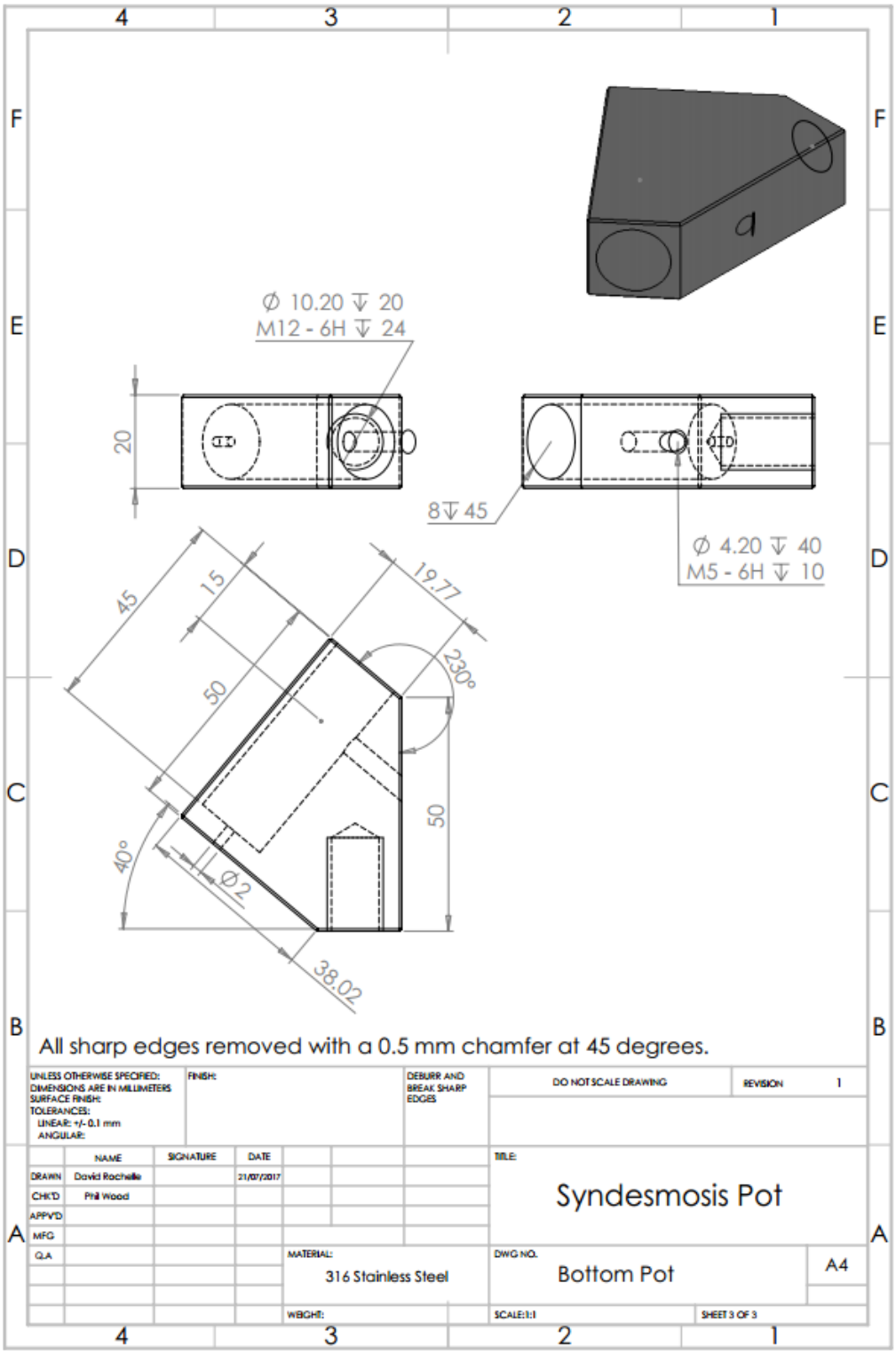

B.4 Syndesmosis Pot Cement Pot

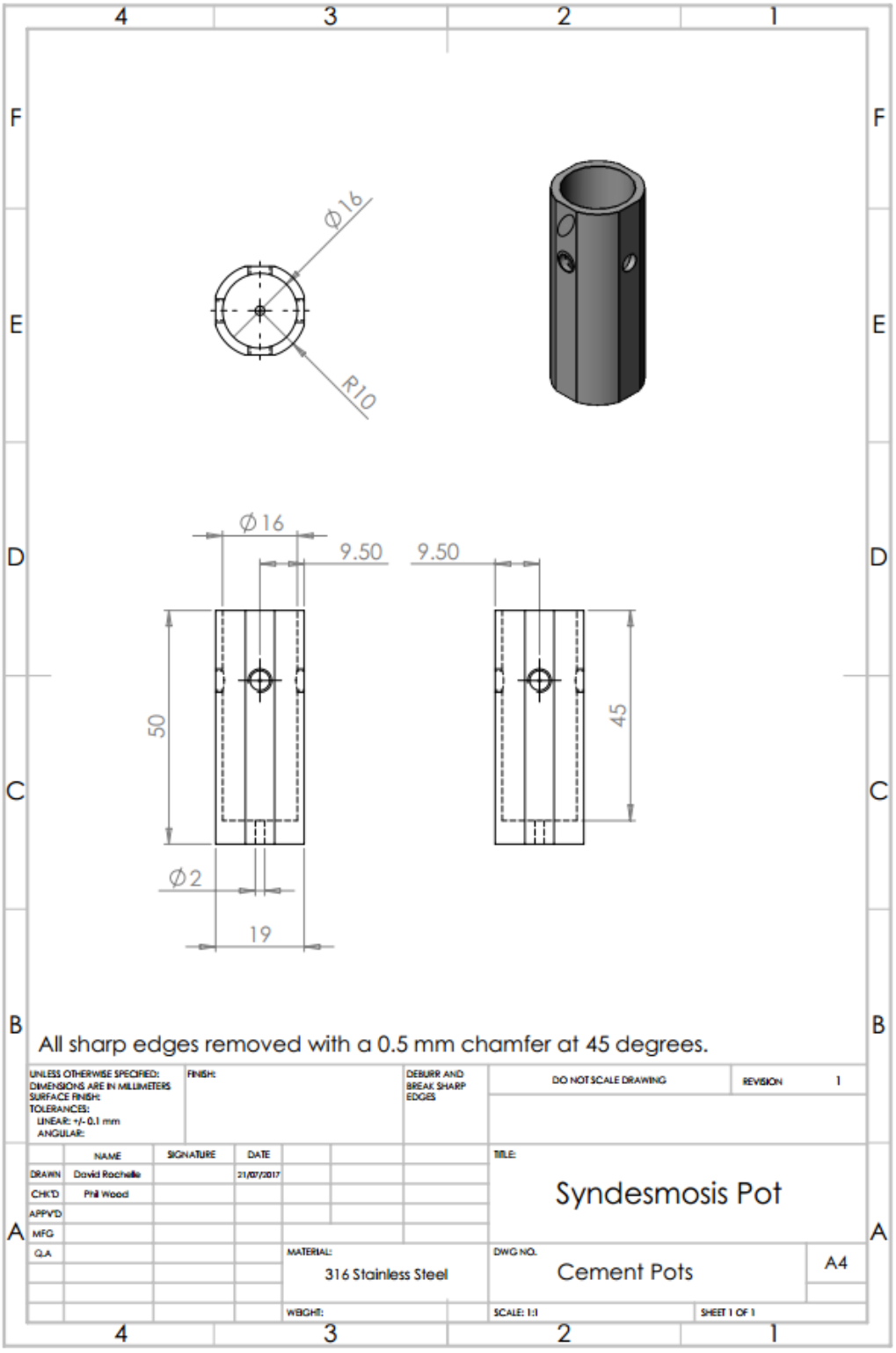

Appendix C – Human Cement Pot

C.1 Human Cement Pot Assembly

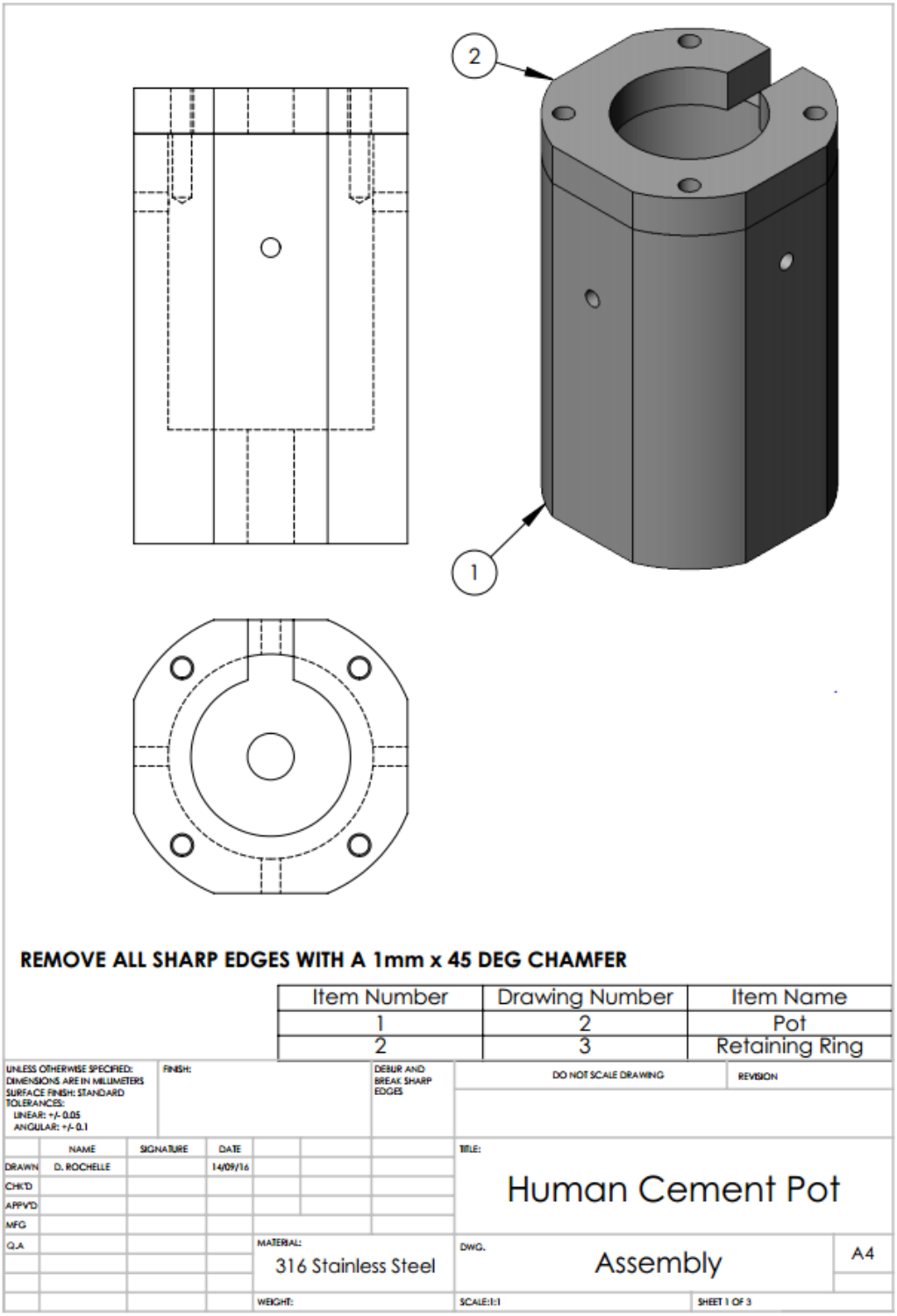

C.2 Human Cement Pot

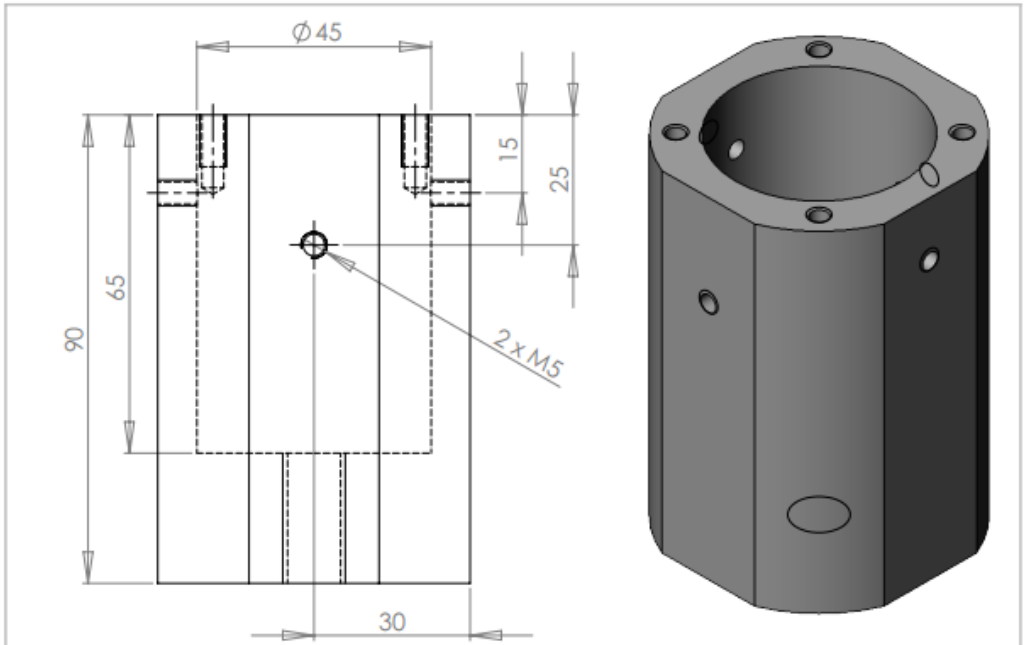

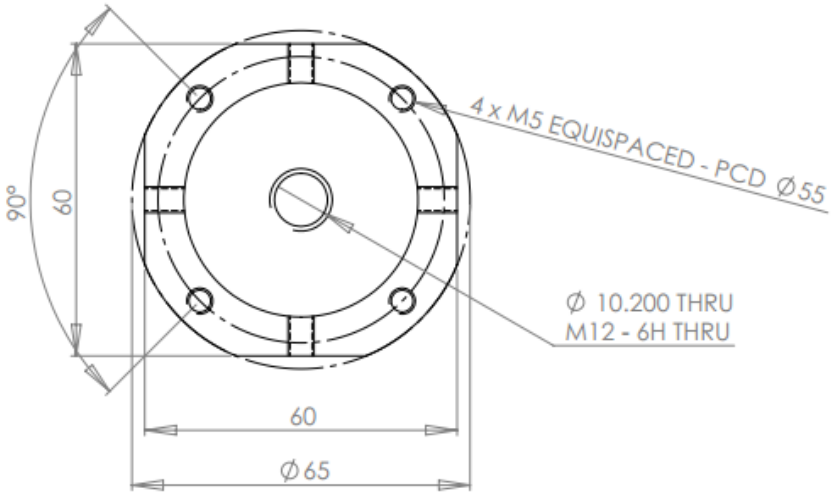

REMOVE ALL SHARP EDGES WITH A 1mm x 45 DEG CHAMFER

UNLESS OTHERWISE SPECIFIED: DIMENSIONS ARE IN MILLIMETERS SURFACE FINISH: STANDARD TOLERANCES: LINEAR: +/- 0.1 ANGULAR: +/- 0.1			FINISH:			DEBUR AND BREAK SHARP EDGES	DO NOT SCALE DRAWING	REVISION
							Quantity: 2 Off	
	NAME	SIGNATURE	DATE				TITLE: Human Cement Pot	
DRAWN	D. ROCHELLE		14/09/16					
CHK'D								
APPV'D								
MFG								
Q.A				MATERIAL: 316 STAINLESS STEEL			DWG. Pot	A4
				WEIGHT:			SCALE:1:1	SHEET 2 OF 3

C.3 Human Cement Pot Retaining Ring

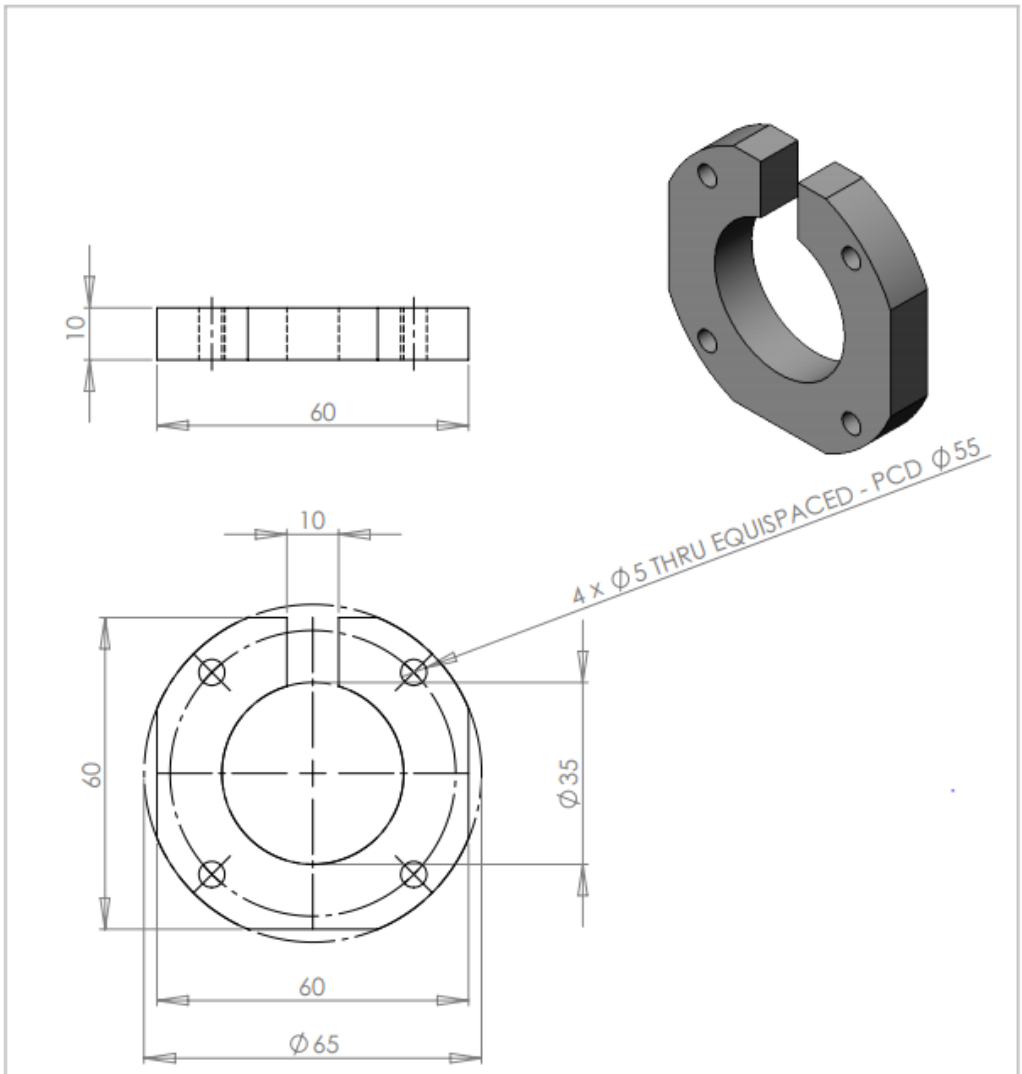

REMOVE ALL SHARP EDGES WITH A 1mm x 45 DEG CHAMFER

UNLESS OTHERWISE SPECIFIED: DIMENSIONS ARE IN MILLIMETERS SURFACE FINISH: STANDARD TOLERANCES: LINEAR: +/- 0.1 ANGULAR: +/- 0.1		FINISH:			DEBUR AND BREAK SHARP EDGES		DO NOT SCALE DRAWING	REVISION
							Quantity: 2 Off	
	NAME	SIGNATURE	DATE				TITLE: Human Cement Pot	
DRAWN	D. ROCHELLE		14/09/16					
CHK'D								
APP'D								
MFG								
Q.A				MATERIAL: 316 STAINLESS STEEL			DWG. Retaining Ring	A4
				WEIGHT:			SCALE:1:1	SHEET 3 OF 3

Appendix D – Simulation of Sprain Engineering Drawings

D.1 Sprain Platform

D.1.1 Sprain Platform Assembly v.1

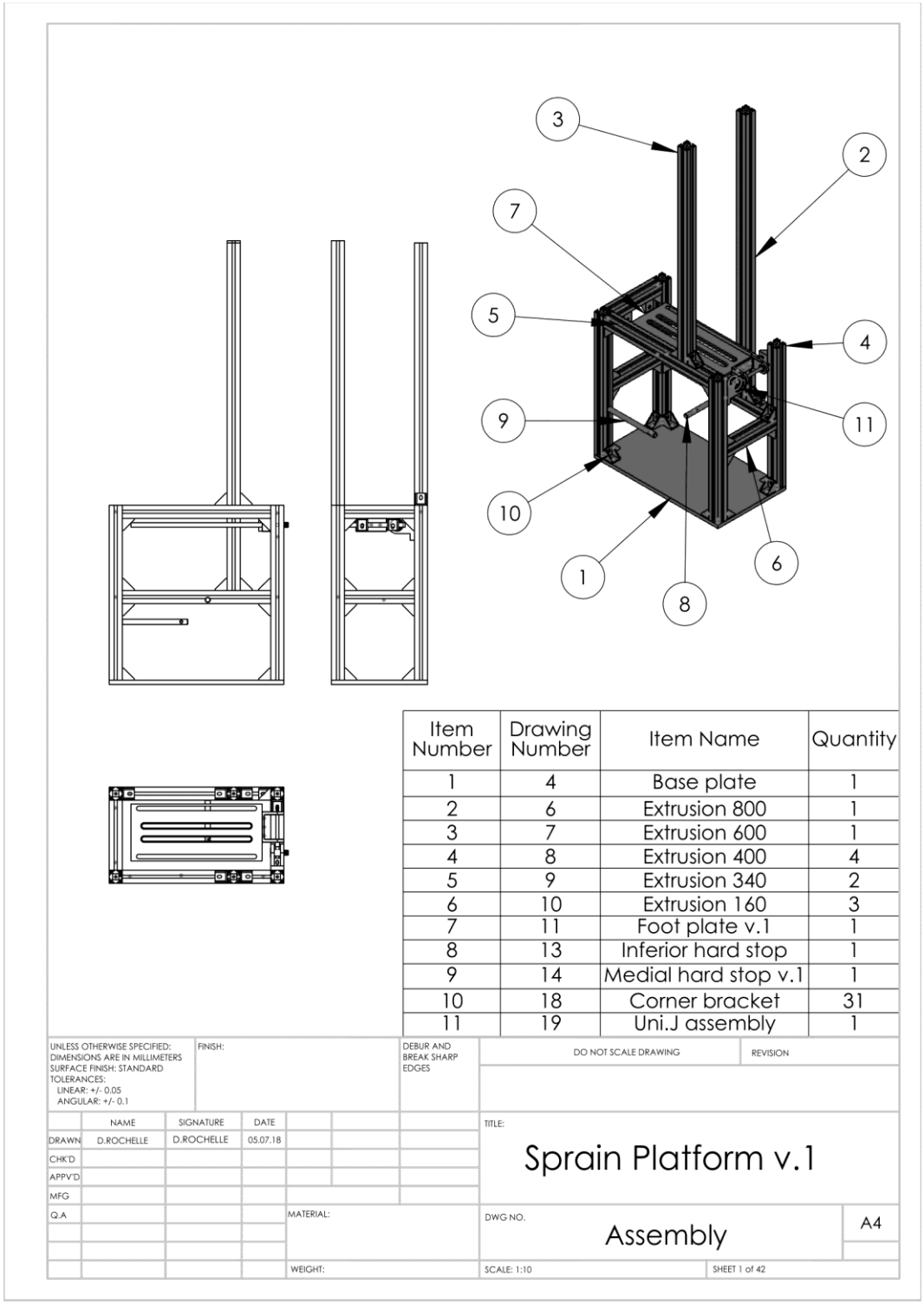

Item Number	Drawing Number	Item Name	Quantity
1	4	Base plate	1
2	6	Extrusion 800	1
3	7	Extrusion 600	1
4	8	Extrusion 400	4
5	9	Extrusion 340	2
6	10	Extrusion 160	3
7	11	Foot plate v.1	1
8	13	Inferior hard stop	1
9	14	Medial hard stop v.1	1
10	18	Corner bracket	31
11	19	Uni.J assembly	1

UNLESS OTHERWISE SPECIFIED:
DIMENSIONS ARE IN MILLIMETERS
SURFACE FINISH: STANDARD
TOLERANCES:
LINEAR: +/- 0.05
ANGULAR: +/- 0.1

FINISH:

DEBUR AND BREAK SHARP EDGES

DO NOT SCALE DRAWING

REVISION

	NAME	SIGNATURE	DATE
DRAWN	D.ROCHELLE	D.ROCHELLE	05.07.18
CHK'D			
APPV'D			
MFG			
Q.A			

MATERIAL:

WEIGHT:

TITLE:

Sprain Platform v.1

DWG NO.

Assembly

A4

SCALE: 1:10

SHEET 1 of 42

D.1.2 Sprain Platform Assembly v.2

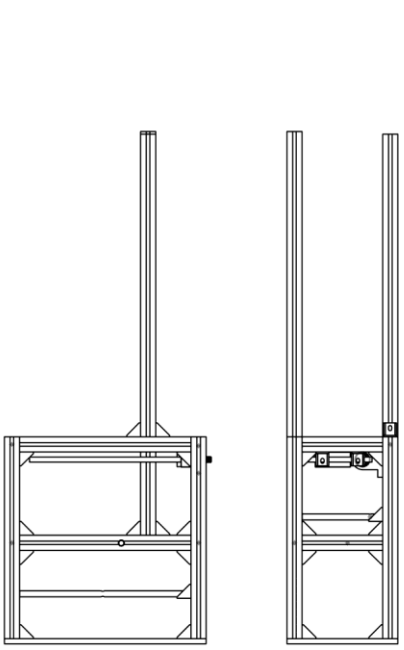

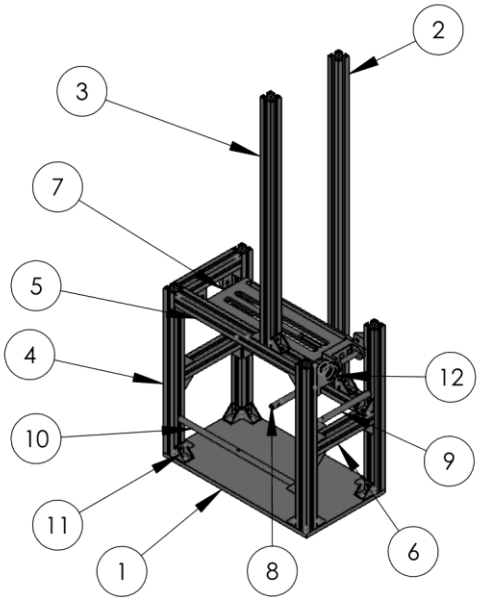

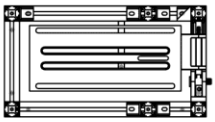

Item Number	Drawing Number	Item Name	Quantity
1	4	Base plate v.1	1
2	6	Extrusion 800	1
3	7	Extrusion 600	1
4	8	Extrusion 400	4
5	9	Extrusion 340	2
6	10	Extrusion 160	3
7	12	Foot plate v.2	1
8	13	Inferior hard stop	1
9	14	Posterior hard stop	1
10	15	Medial hard stop v.2	1
11	18	Corner bracket	33
12	20	Uni.J assembly v.2	1

UNLESS OTHERWISE SPECIFIED:
DIMENSIONS ARE IN MILLIMETERS
SURFACE FINISH: STANDARD
TOLERANCES:
LINEAR: +/- 0.05
ANGULAR: +/- 0.1

FINISH:

DEBUR AND BREAK SHARP EDGES

DO NOT SCALE DRAWING | REVISION

	NAME	SIGNATURE	DATE
DRAWN	D.ROCHELLE	D.ROCHELLE	11.12.18
CHK'D			
APPV'D			
MFG			
Q.A			

MATERIAL:

WEIGHT:

TITLE:

Sprain Platform v.2

DWG NO.

Assembly

A4

SCALE: 1:10

SHEET 2 of 42

D.1.3 Sprain Platform Assembly v.3

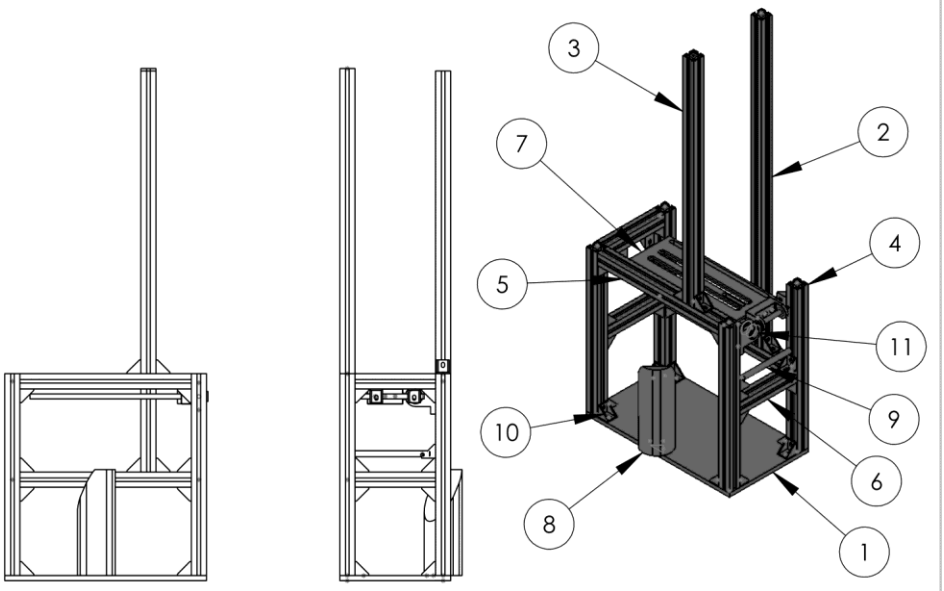

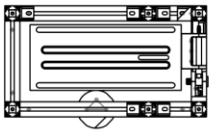

Item Number	Drawing Number	Item Name	Quantity
1	5	Base plate v.2	1
2	6	Extrusion 800	1
3	7	Extrusion 600	1
4	8	Extrusion 400	4
5	9	Extrusion 340	2
6	10	Extrusion 160	3
7	12	Foot plate v.2	1
8	16	Base hard stop	1
9	14	Posterior hard stop	1
10	18	Corner bracket	32
11	20	Uni.J assembly v.2	1

UNLESS OTHERWISE SPECIFIED:
DIMENSIONS ARE IN MILLIMETERS
SURFACE FINISH: STANDARD
TOLERANCES:
LINEAR: +/- 0.05
ANGULAR: +/- 0.1

FINISH:

DEBUR AND BREAK SHARP EDGES

DO NOT SCALE DRAWING | REVISION

	NAME	SIGNATURE	DATE
DRAWN	D.ROCHELLE	D.ROCHELLE	29.04.19
CHK'D			
APPV'D			
MFG			
Q.A			

MATERIAL:

WEIGHT:

TITLE:

Sprain Platform v.3

DWG NO.

Assembly

A4

SCALE: 1:10

SHEET 3 of 42

D.1.4 Base Plate v.1

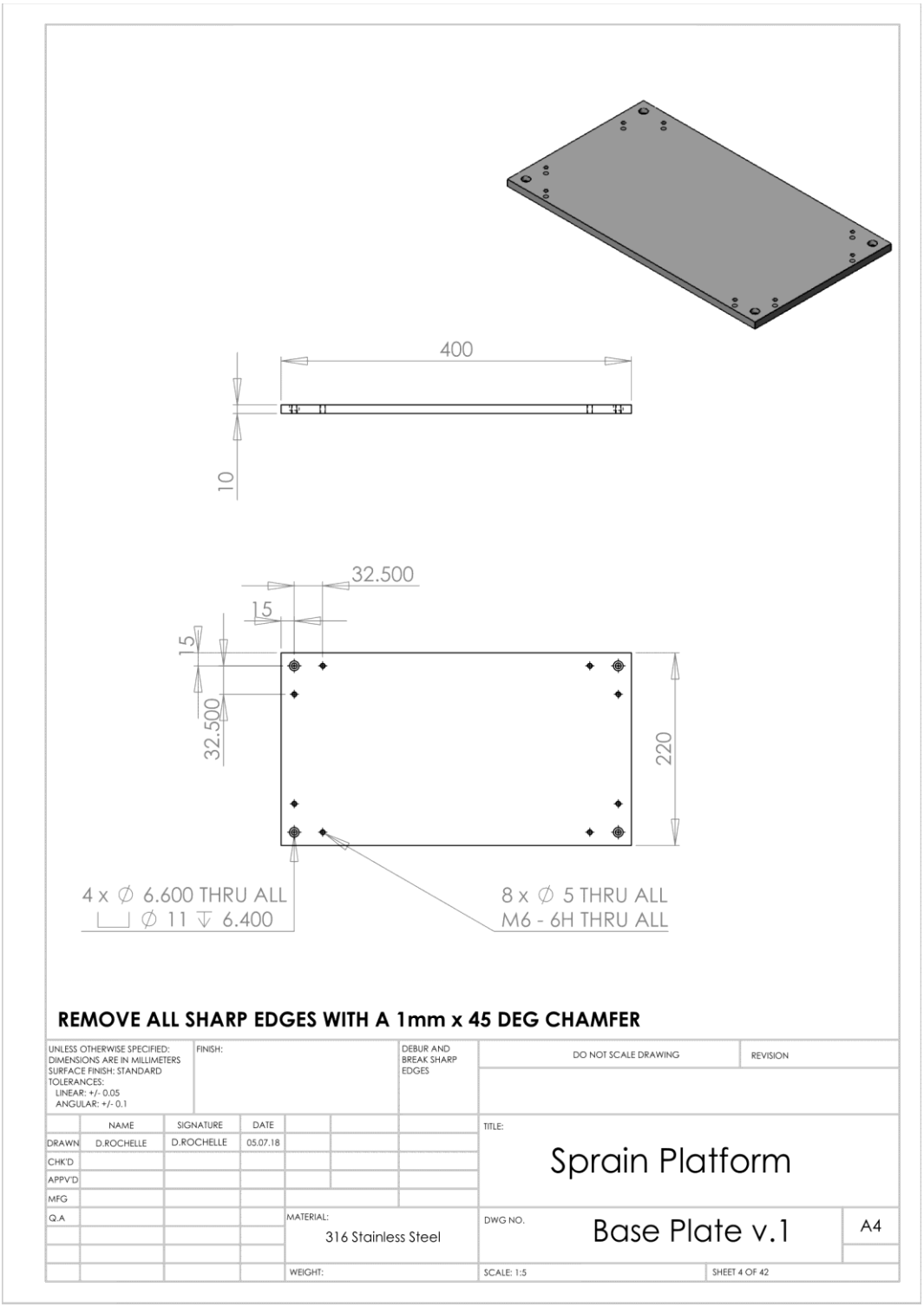

D.1.5 Base Plate v.2

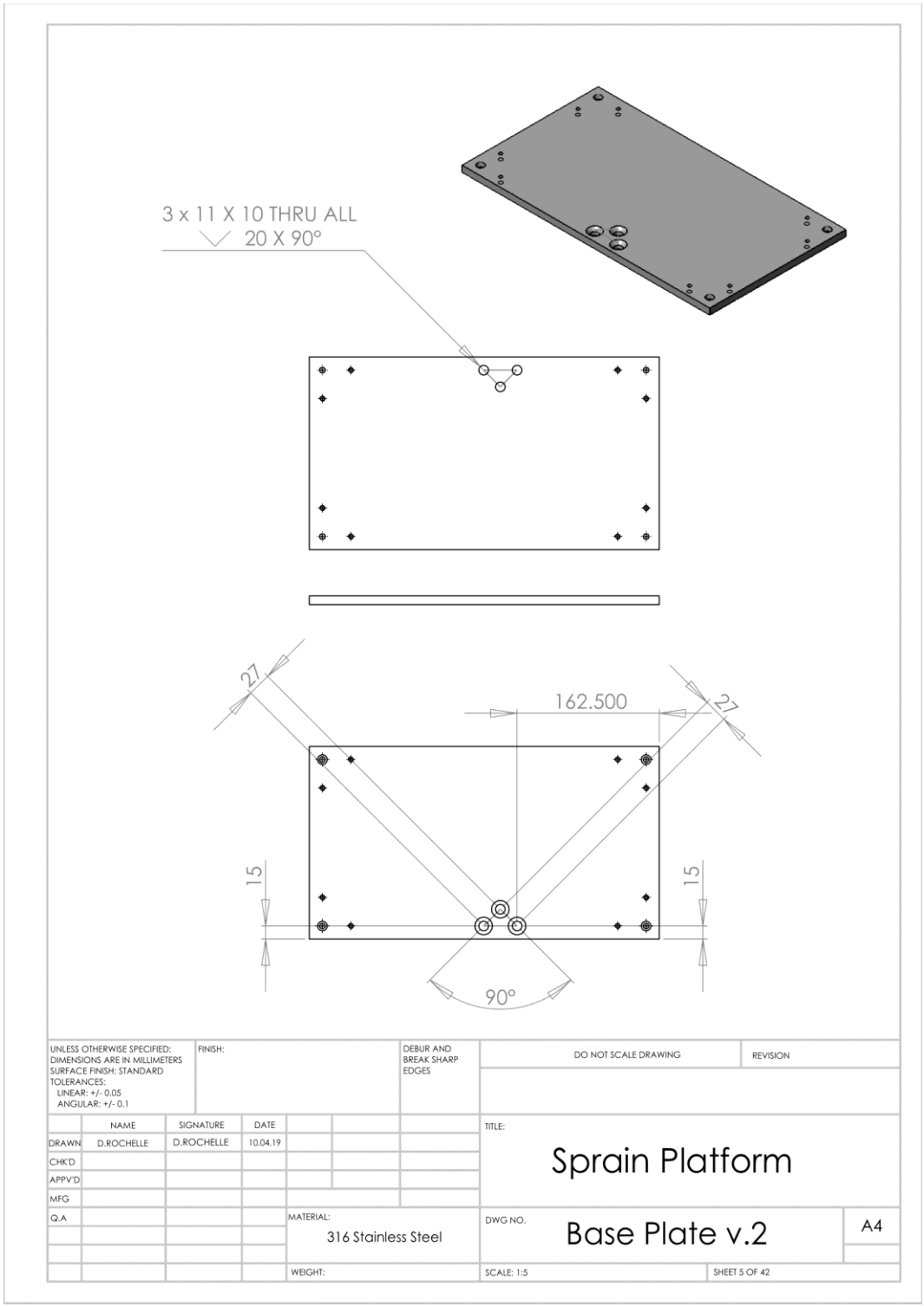

D.1.6 Extrusion 800 mm

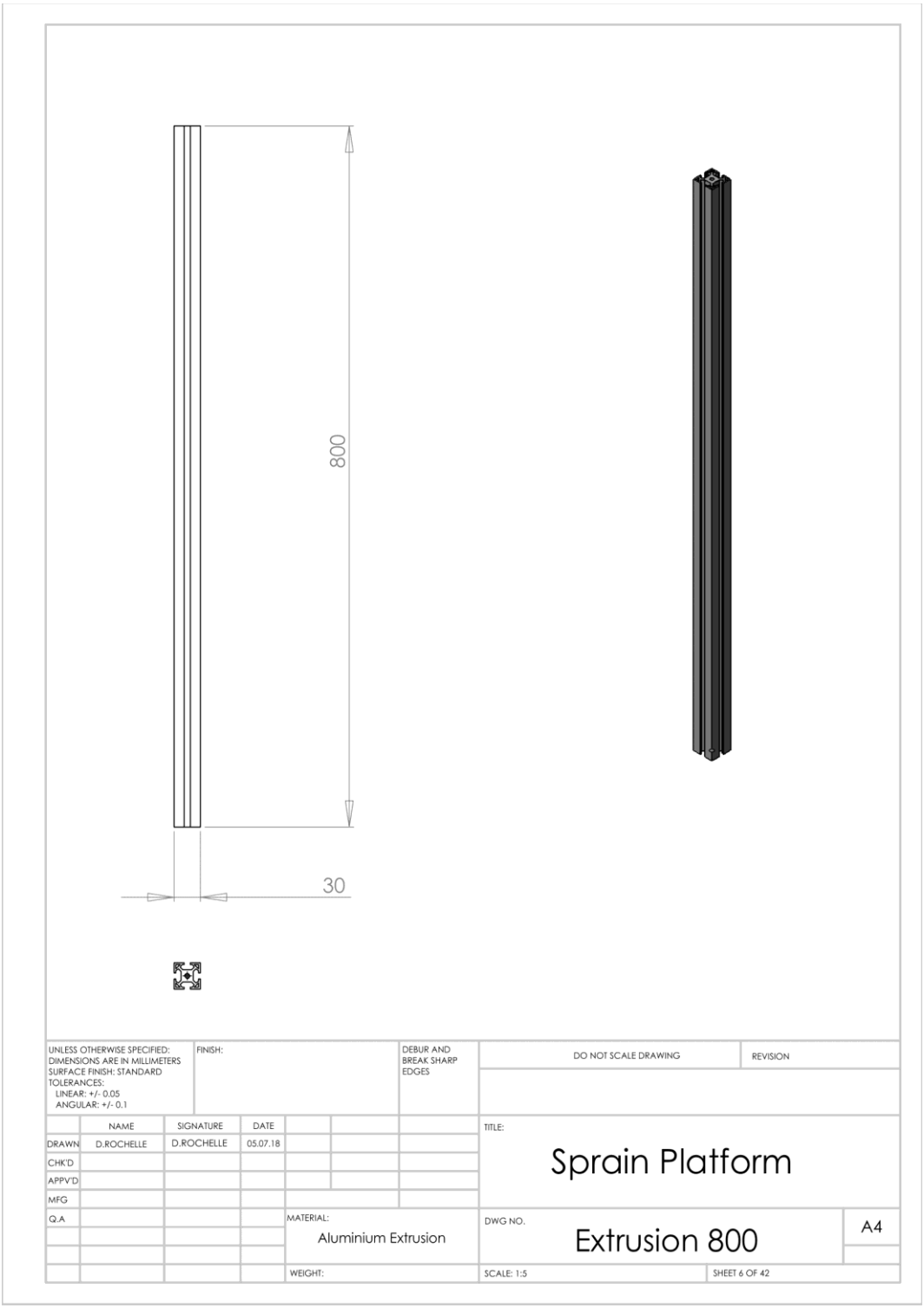

D.1.7 Extrusion 600 mm

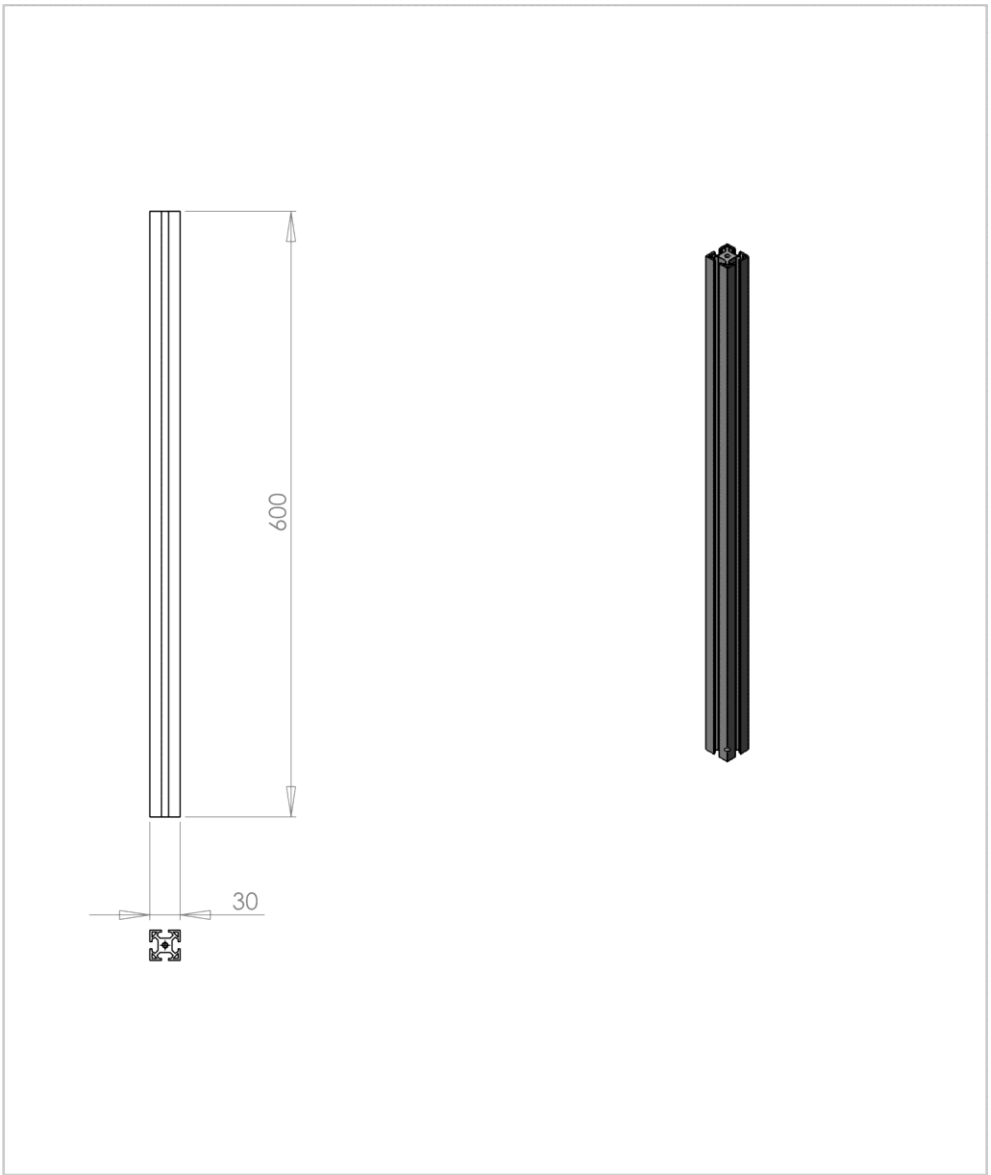

UNLESS OTHERWISE SPECIFIED: DIMENSIONS ARE IN MILLIMETERS SURFACE FINISH: STANDARD TOLERANCES: LINEAR: +/- 0.05 ANGULAR: +/- 0.1	FINISH:		DEBUR AND BREAK SHARP EDGES	DO NOT SCALE DRAWING	REVISION	
	NAME	SIGNATURE	DATE	TITLE:		
DRAWN	D.ROCHELLE	D.ROCHELLE	05.07.18	Sprain Platform		
CHK'D						
APPV'D						
MFG						
Q.A				MATERIAL:	DWG NO.	A4
				Aluminium Extrusion	Extrusion 600	
				WEIGHT:	SCALE: 1:5	SHEET 7 OF 42

D.1.8 Extrusion 400 mm

UNLESS OTHERWISE SPECIFIED: DIMENSIONS ARE IN MILLIMETERS SURFACE FINISH: STANDARD TOLERANCES: LINEAR: +/- 0.05 ANGULAR: +/- 0.1		FINISH:		DEBUR AND BREAK SHARP EDGES		DO NOT SCALE DRAWING	REVISION
	NAME	SIGNATURE	DATE			TITLE: Sprain Platform	
DRAWN	D.ROCHELLE	D.ROCHELLE	05.07.18				
CHK'D							
APPV'D							
MFG							
Q.A				MATERIAL: Aluminium Extrusion		DWG NO. Extrusion 400	A4
				WEIGHT:		SCALE: 1:5	SHEET 8 OF 42

D.1.9 Extrusion 340 mm

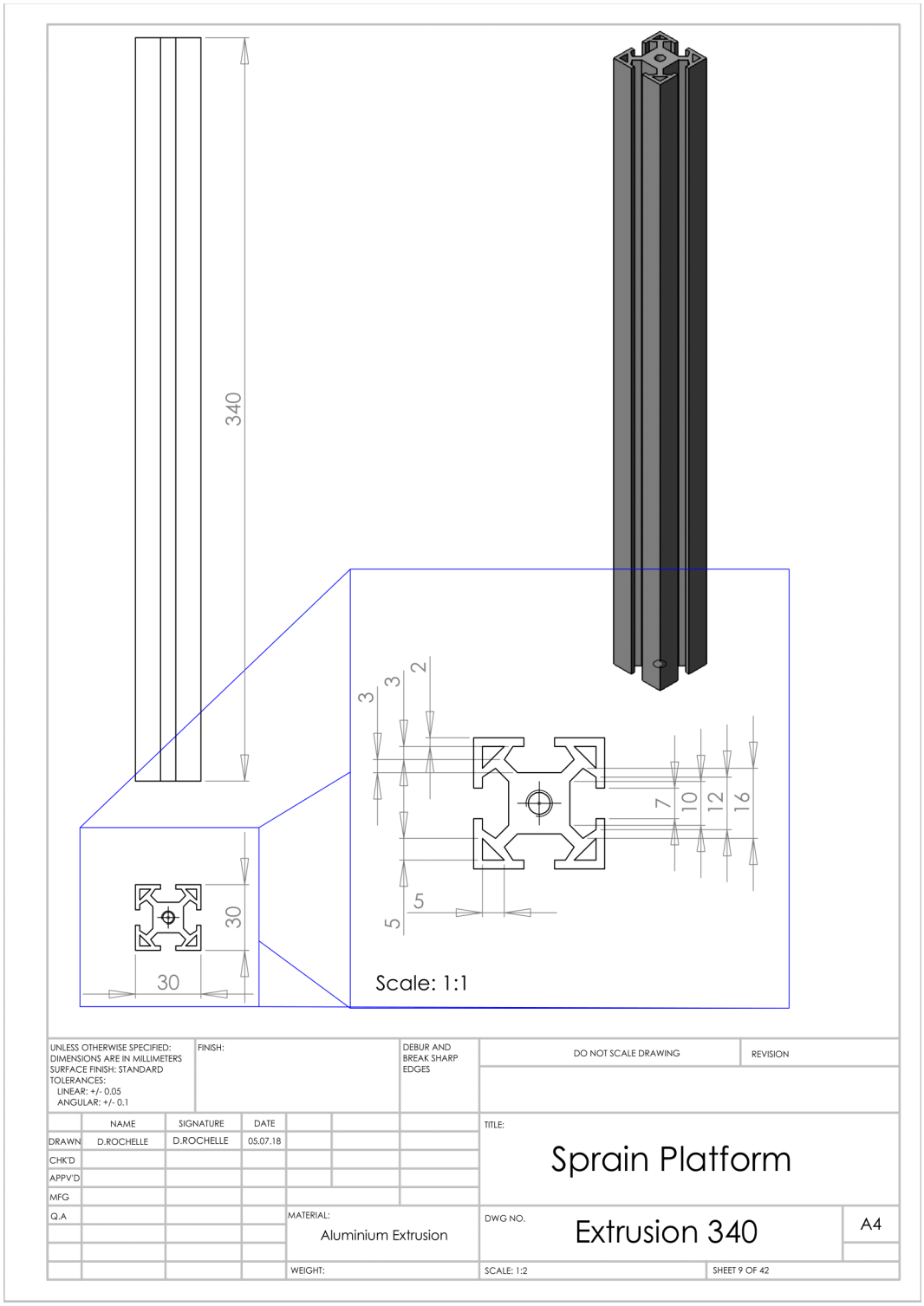

UNLESS OTHERWISE SPECIFIED: DIMENSIONS ARE IN MILLIMETERS SURFACE FINISH: STANDARD TOLERANCES: LINEAR: +/- 0.05 ANGULAR: +/- 0.1	FINISH:		DEBUR AND BREAK SHARP EDGES	DO NOT SCALE DRAWING	REVISION	
	NAME	SIGNATURE	DATE	TITLE:		
DRAWN	D.ROCHELLE	D.ROCHELLE	05.07.18	Sprain Platform		
CHK'D						
APPV'D						
MFG						
Q.A				MATERIAL: Aluminium Extrusion	DWG NO. Extrusion 340	A4
				WEIGHT:	SCALE: 1:2	SHEET 9 OF 42

D.1.10 Extrusion 160 mm

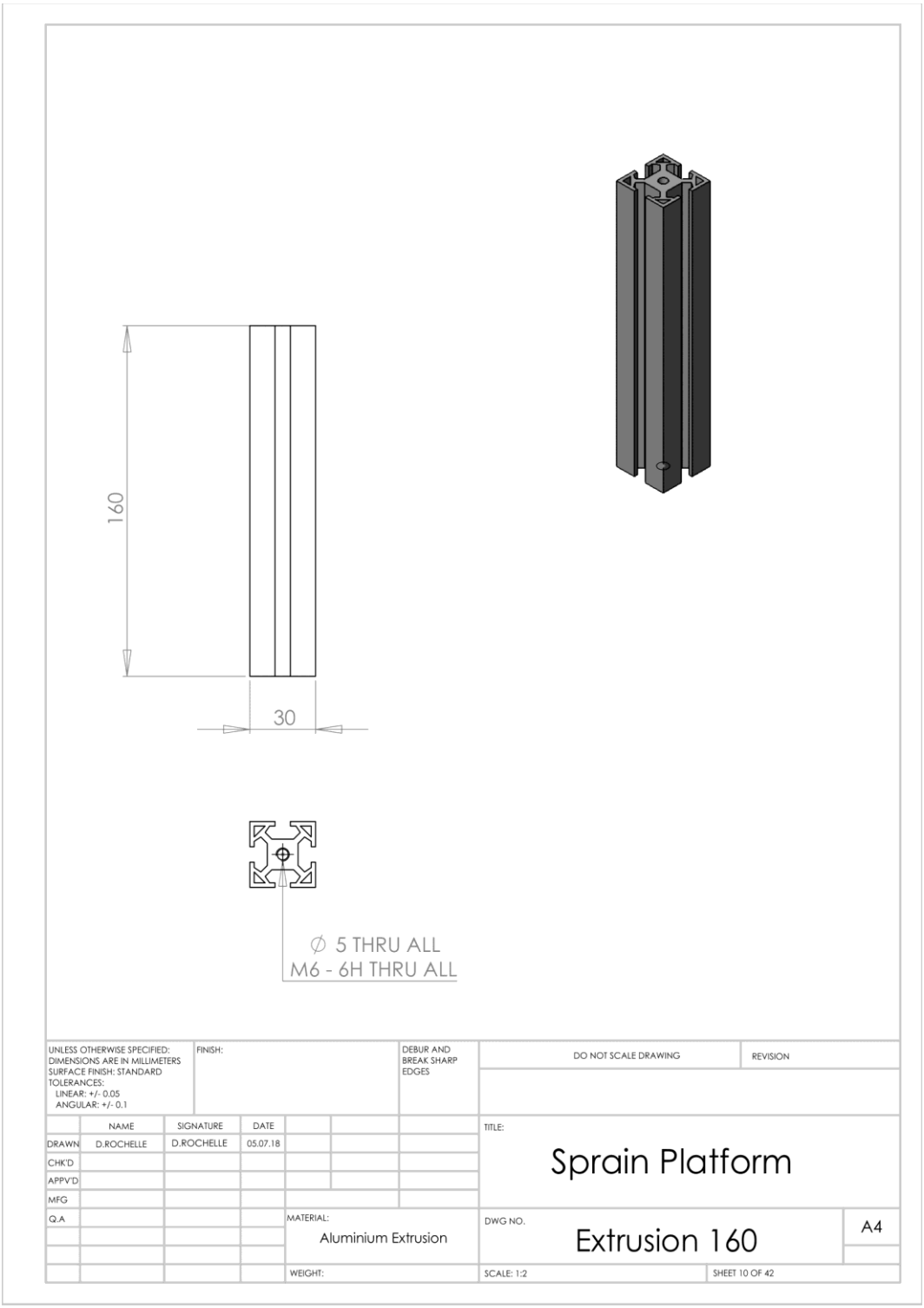

D.1.11 Foot Plate v.1

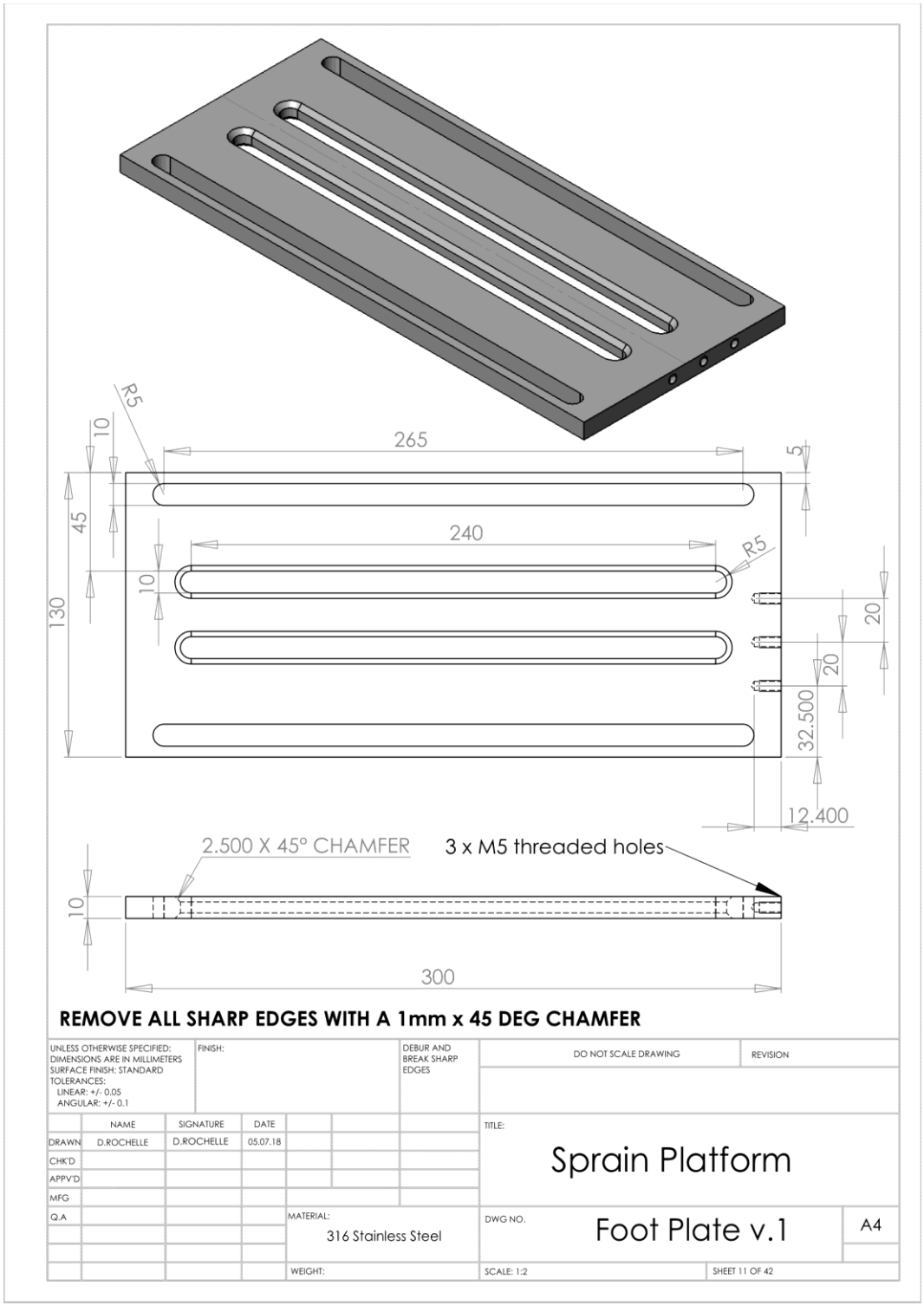

D.1.12 Foot Plate v.2

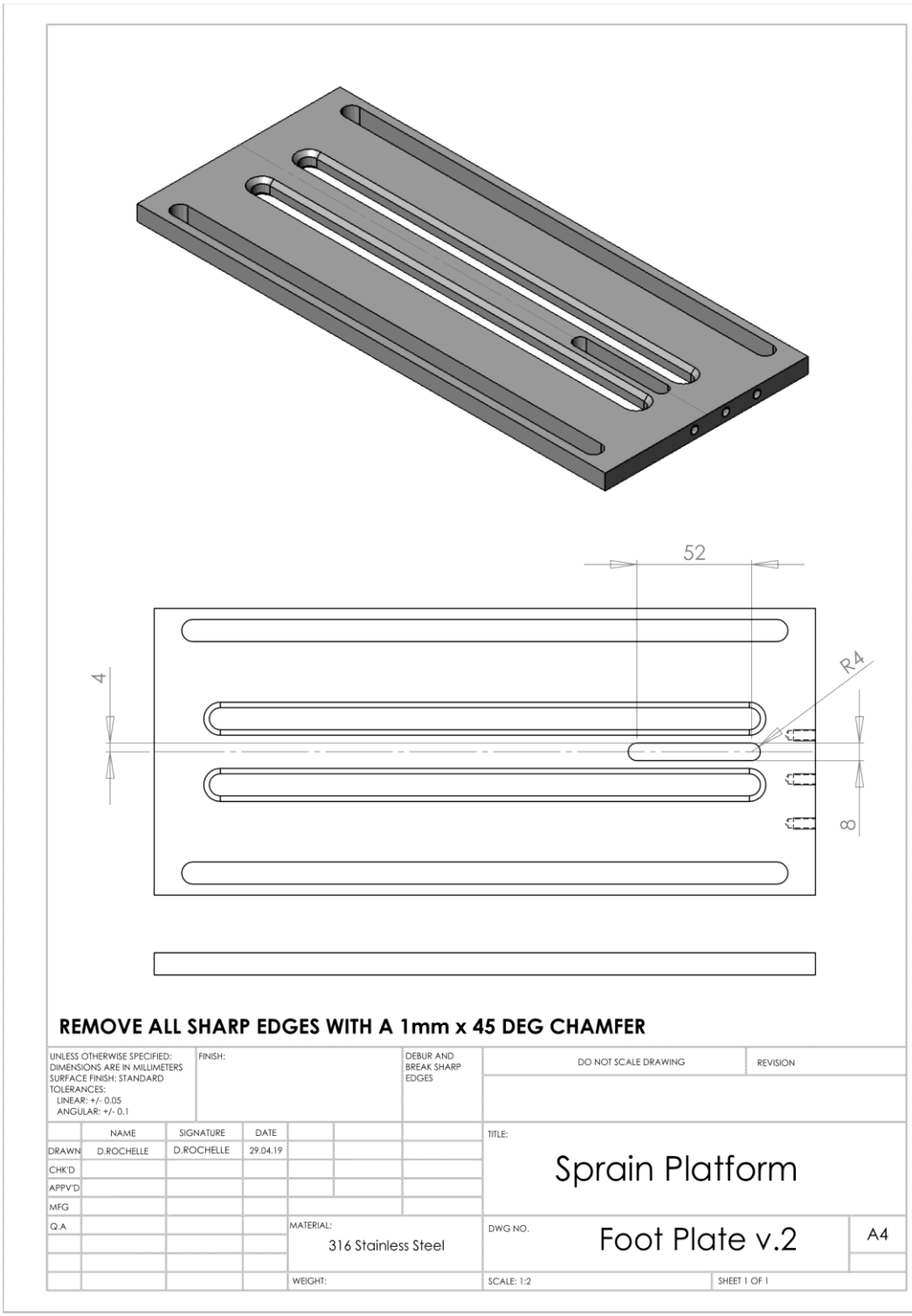

D.1.13 Inferior Hard Stop

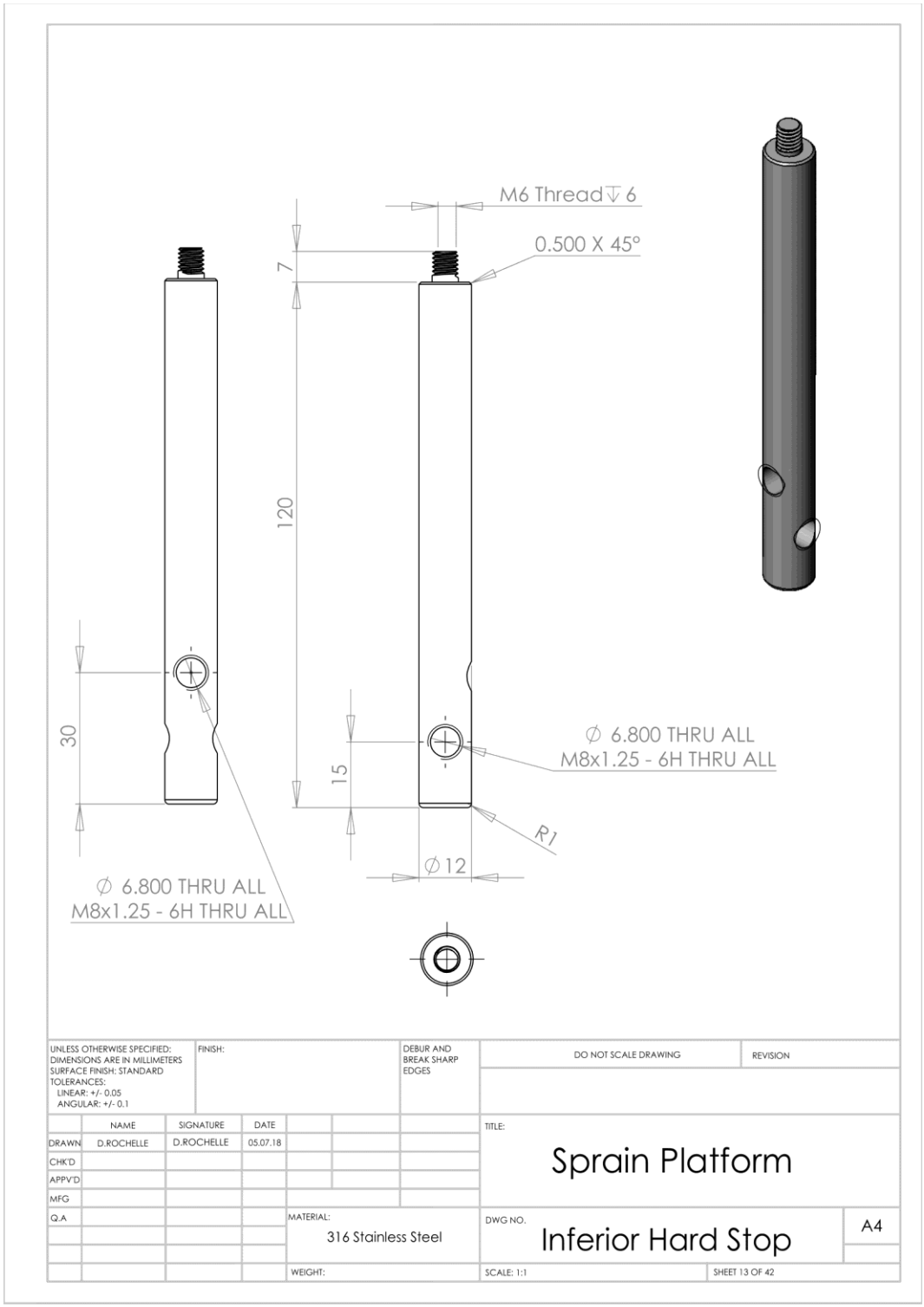

D.1.14 Medial Hard Stop v.1

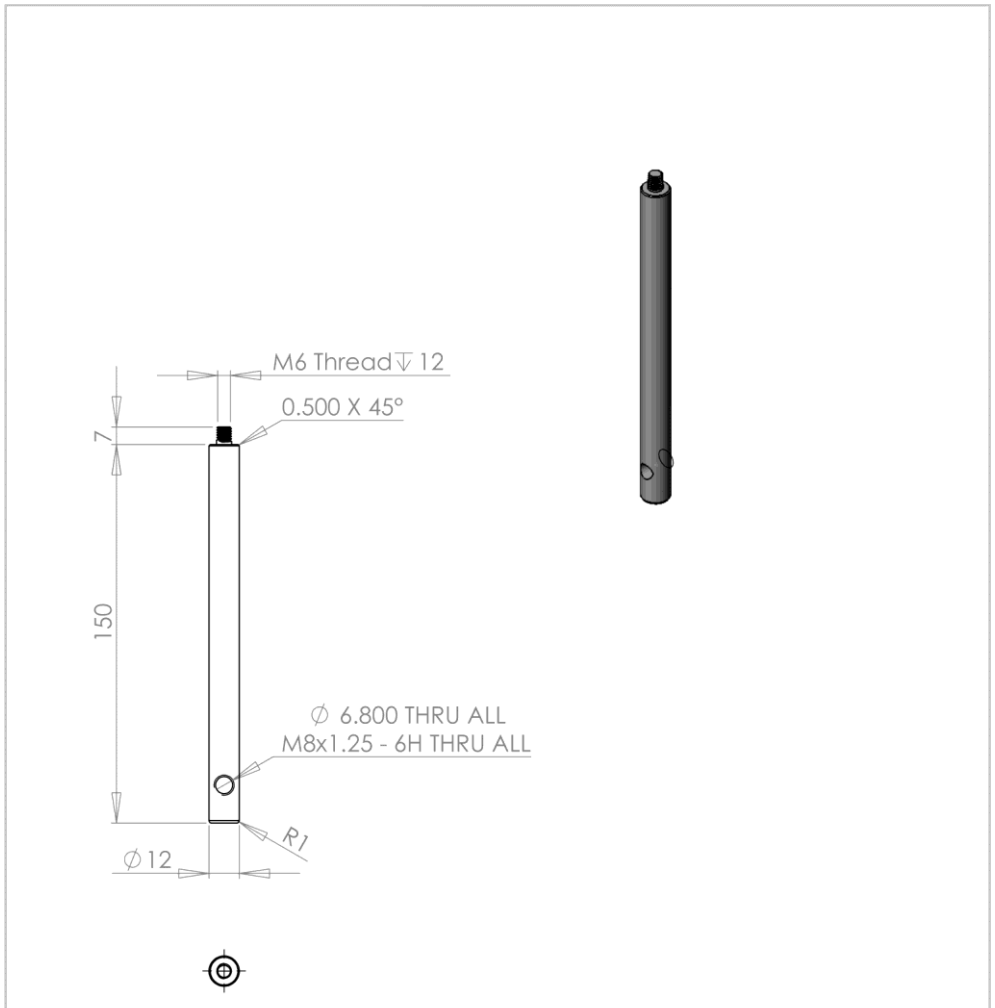

UNLESS OTHERWISE SPECIFIED: DIMENSIONS ARE IN MILLIMETERS SURFACE FINISH: STANDARD TOLERANCES: LINEAR: +/- 0.05 ANGULAR: +/- 0.1		FINISH:		DEBUR AND BREAK SHARP EDGES		DO NOT SCALE DRAWING	REVISION	
	NAME	SIGNATURE	DATE			TITLE: Sprain Platform		
DRAWN	D.ROCHELLE	D.ROCHELLE	05.07.18					
CHK'D								
APPV'D								
MFG								
Q.A				MATERIAL: 316 Stainless Steel		DWG NO. Medial Hard Stop v.1/ Posterior Hard Stop		A4
				WEIGHT:		SCALE: 1:2	SHEET 14 OF 42	

D.1.15 Medial Hard Stop v.2

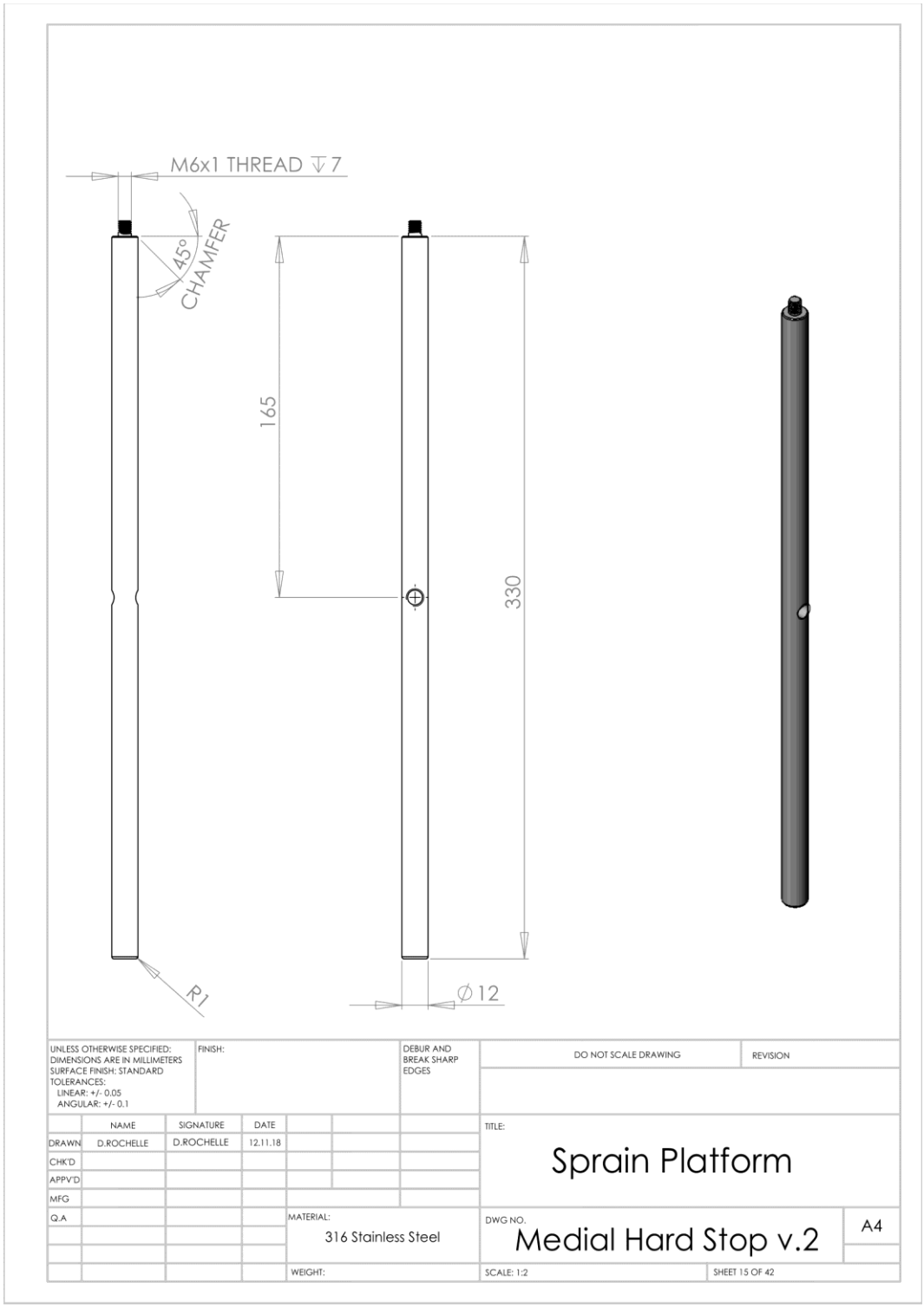

D.1.16 Base Hard Stop

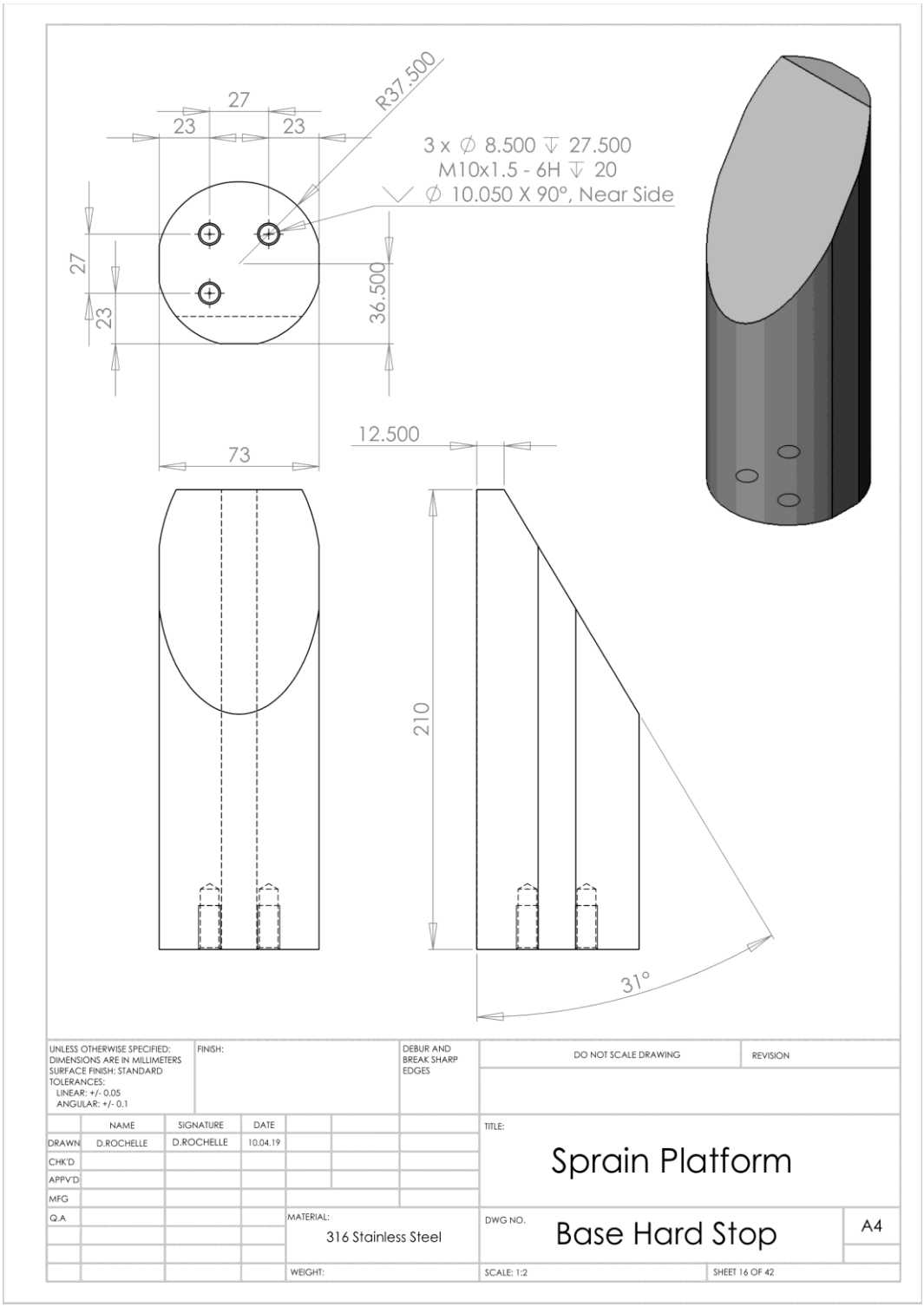

D.1.17 Calcaneal Mount

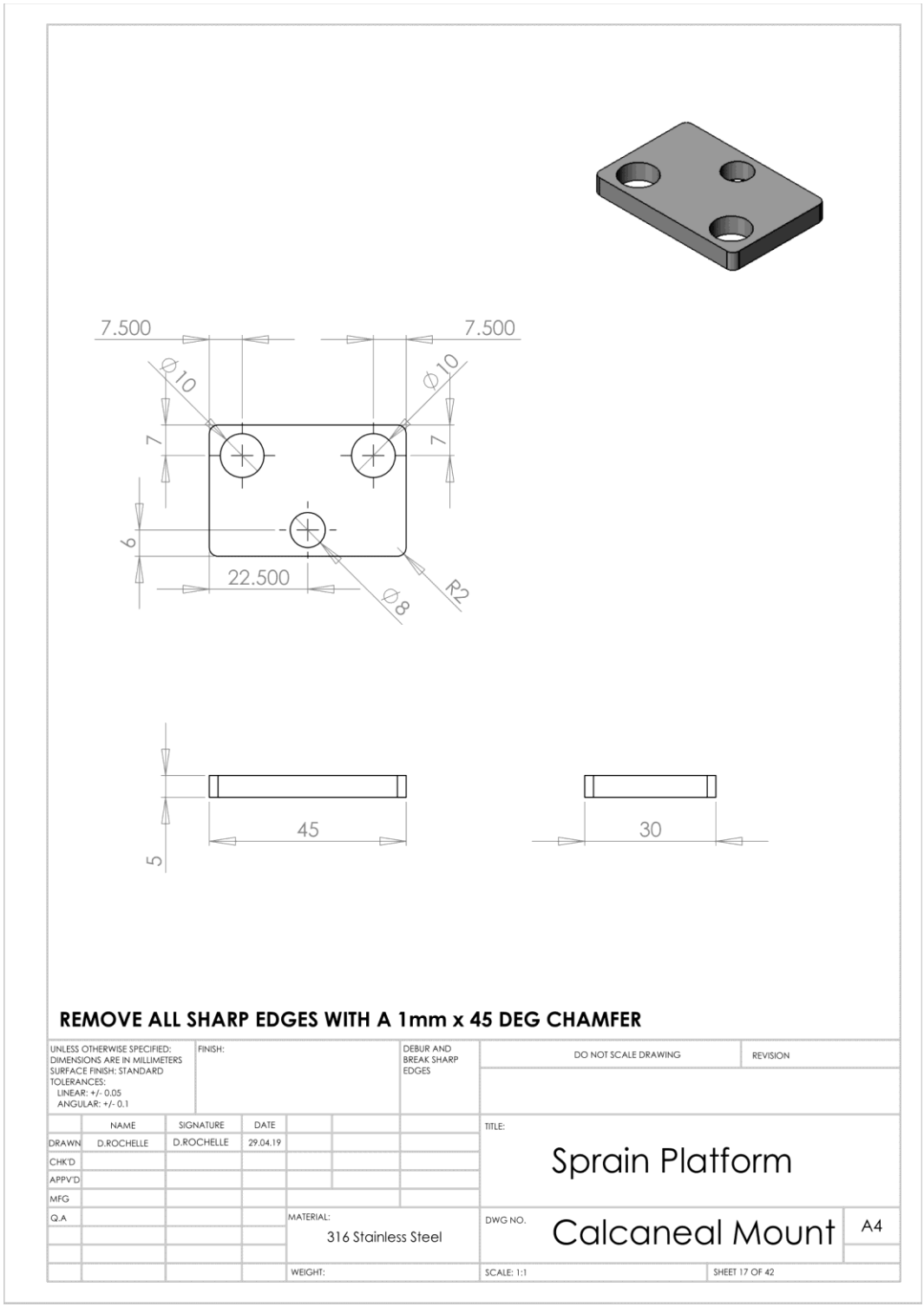

D.1.18 Corner Bracket

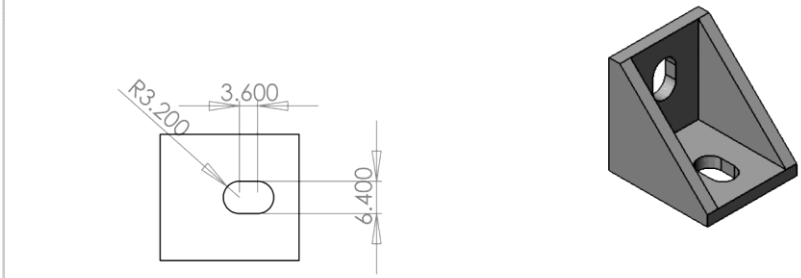

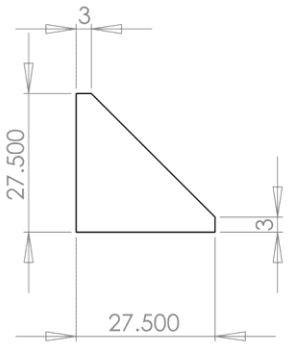

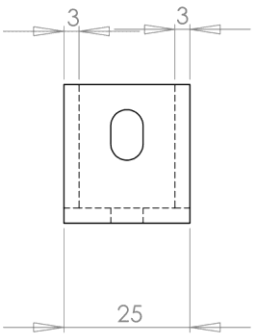

UNLESS OTHERWISE SPECIFIED: DIMENSIONS ARE IN MILLIMETERS SURFACE FINISH: STANDARD TOLERANCES: LINEAR: +/- 0.05 ANGULAR: +/- 0.1		FINISH:		DEBUR AND BREAK SHARP EDGES		DO NOT SCALE DRAWING	REVISION
	NAME	SIGNATURE	DATE			TITLE: Sprain Platform	
DRAWN	D.ROCHELLE	D.ROCHELLE	05.07.18				
CHK'D							
APPV'D							
MFG							
Q.A				MATERIAL: Aluminium Extrusion		DWG NO. Corner Bracket	A4
				WEIGHT:		SCALE: 1:1	SHEET 18 OF 42

D.1.19 Universal Joint Assembly v.1

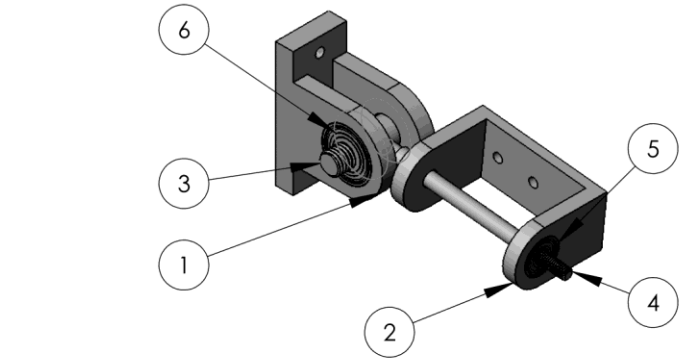

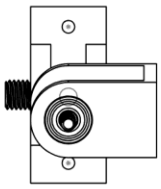

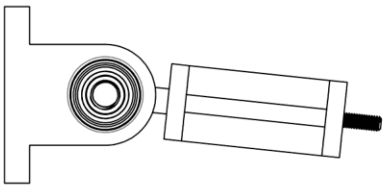

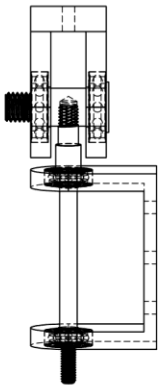

Item Number	Drawing Number	Item Name	Quantity
1	21	Uni.J Large Diameter	1
2	25	Uni.J Small Diameter v.1	1
3	23	Uni.J Arm 1 v.1	1
4	29	Uni.J Arm 2 v.1	1
5	27	Small Bearing 607-2RSH	2
6	22	Large Bearing W 61902-2RS1	2

UNLESS OTHERWISE SPECIFIED:
DIMENSIONS ARE IN MILLIMETERS
SURFACE FINISH: STANDARD
TOLERANCES:
LINEAR: +/- 0.05
ANGULAR: +/- 0.1

FINISH:

DEBUR AND BREAK SHARP EDGES

DO NOT SCALE DRAWING

REVISION

	NAME	SIGNATURE	DATE
DRAWN	D.ROCHELLE	D.ROCHELLE	05.07.18
CHK'D			
APPV'D			
MFG			
Q.A			

MATERIAL:

WEIGHT:

TITLE:

Universal Joint v.1

DWG NO.

Assembly

A4

SCALE: 1:2

SHEET 19 of 42

D.1.20 Universal Joint Assembly v.2

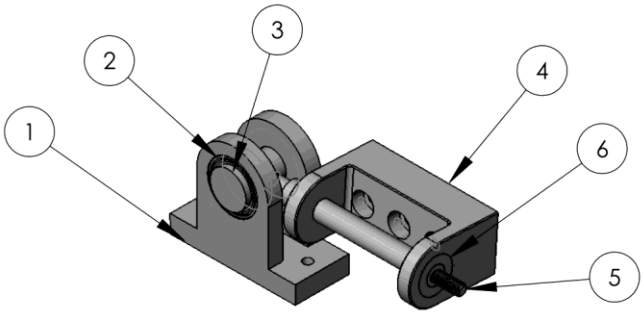

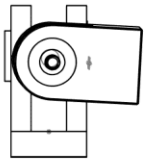

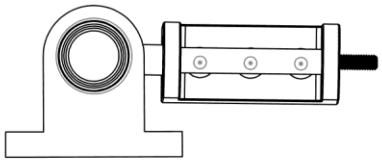

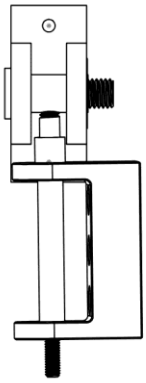

Item Number	Drawing Number	Item Name	Quantity
1	21	Uni.J Large Diameter	1
2	26	Uni.J Small Diameter v.2	1
3	24	Uni.J Arm 1 v.2	1
4	30	Uni.J Arm 2 v.2	1
5	22	Large Bearing W 61902-2RS1	2
6	28	Small Bush	2

UNLESS OTHERWISE SPECIFIED:
DIMENSIONS ARE IN MILLIMETERS
SURFACE FINISH: STANDARD
TOLERANCES:
LINEAR: +/- 0.05
ANGULAR: +/- 0.1

FINISH:

DEBUR AND BREAK SHARP EDGES

DO NOT SCALE DRAWING | REVISION

	NAME	SIGNATURE	DATE
DRAWN	D.ROCHELLE	D.ROCHELLE	11.12.18
CHK'D			
APPV'D			
MFG			
Q.A			

MATERIAL:

WEIGHT:

TITLE:

Universal Joint v.2

DWG NO.

Assembly

A4

SCALE: 1:2

SHEET 20 OF 42

D.1.21 Universal Joint Large Diameter Bracket

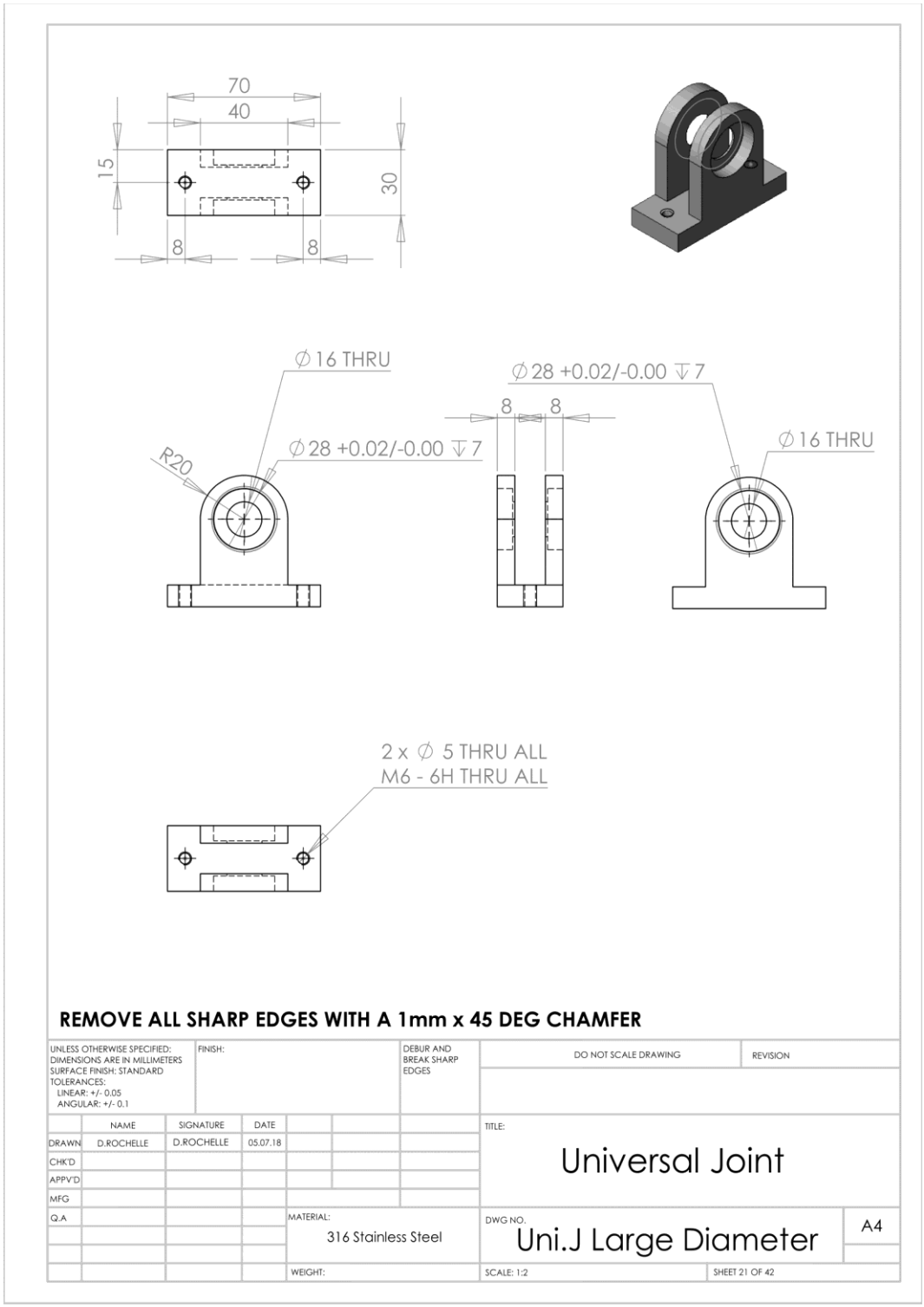

D.1.22 Universal Joint Large Bearing

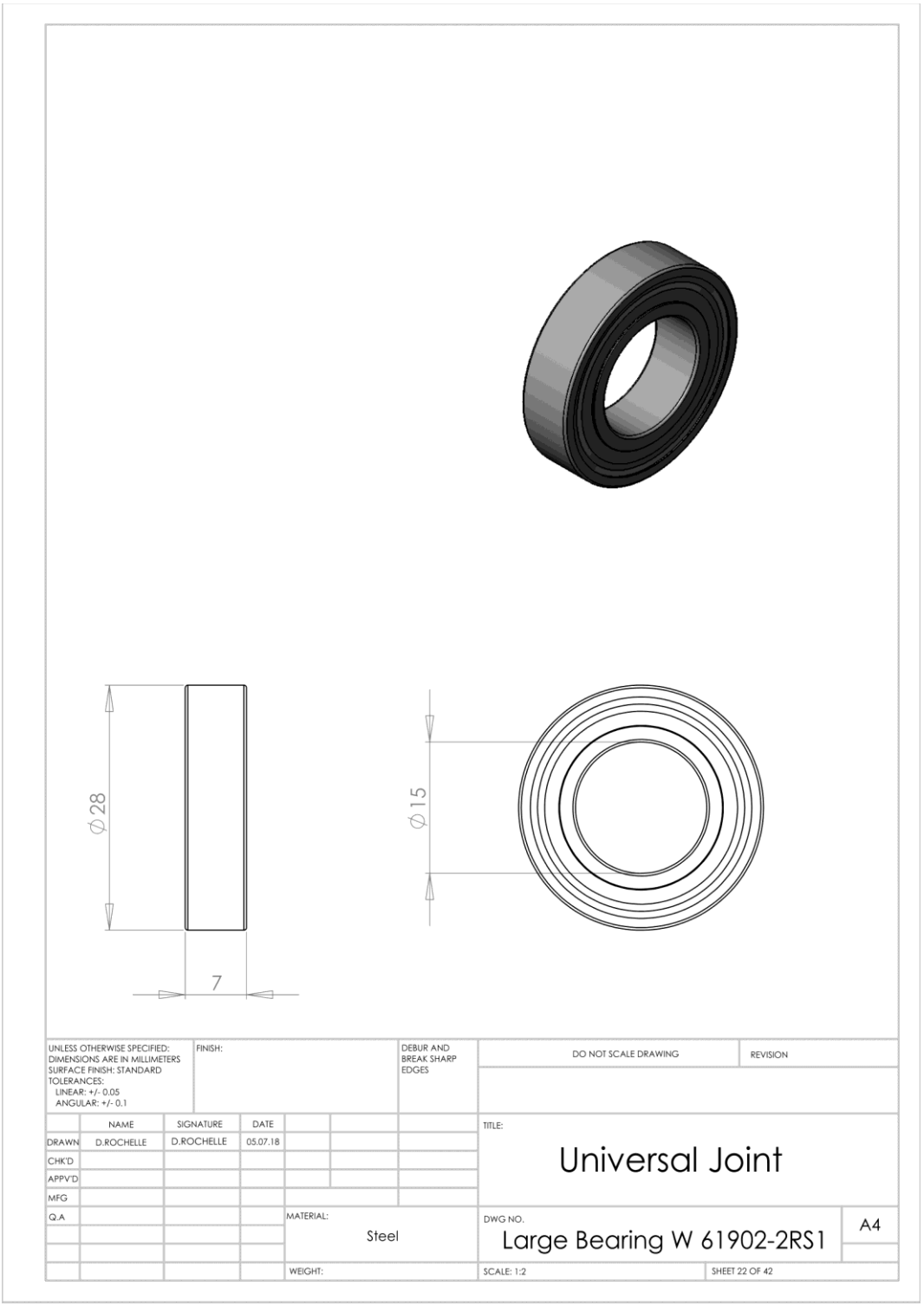

D.1.23 Universal Joint Arm 1 v.1

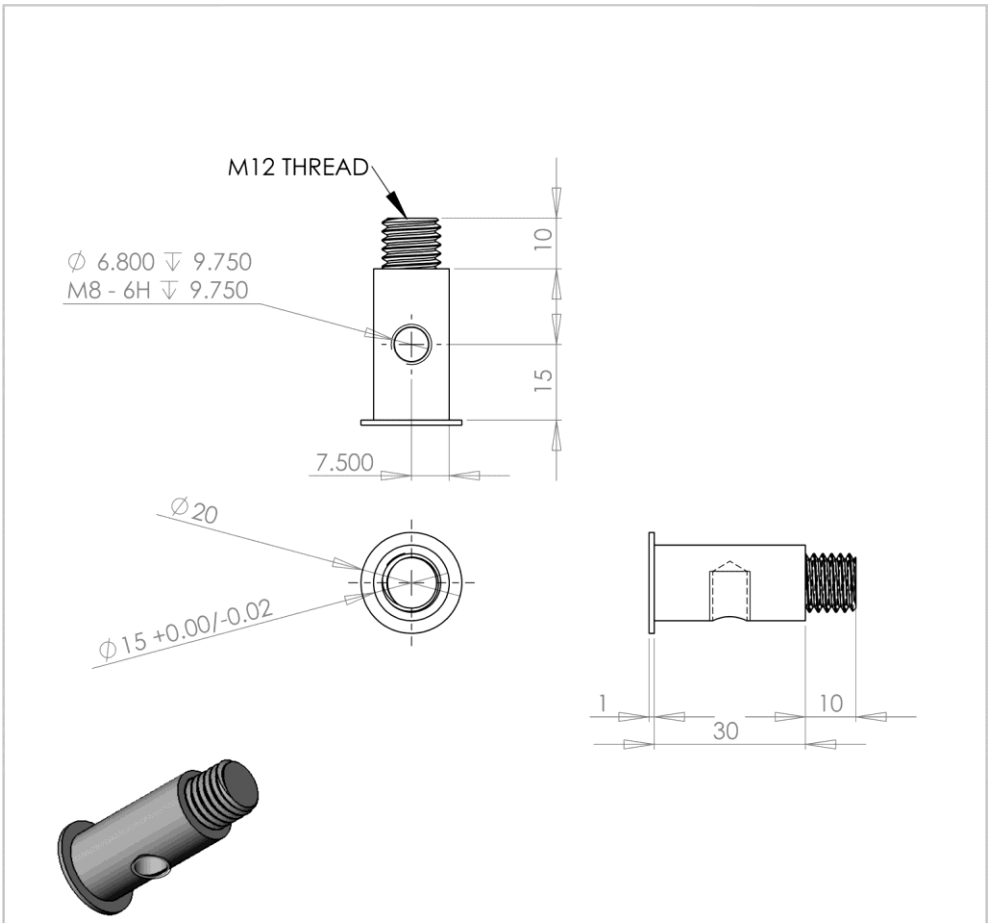

REMOVE ALL SHARP EDGES WITH A 0.25mm x 45 DEG CHAMFER

UNLESS OTHERWISE SPECIFIED: DIMENSIONS ARE IN MILLIMETERS SURFACE FINISH: STANDARD TOLERANCES: LINEAR: +/- 0.05 ANGULAR: +/- 0.1		FINISH:			DEBUR AND BREAK SHARP EDGES	DO NOT SCALE DRAWING		REVISION
	NAME	SIGNATURE	DATE			TITLE:		
DRAWN	D.ROCHELLE	D.ROCHELLE	05.07.18			Universal Joint		
CHK'D								
APPV'D								
MFG								
Q.A				MATERIAL:		DWG NO.		A4
				316 Stainless Steel		Uni.J Arm 1 v.1		
				WEIGHT:		SCALE: 1:1	SHEET 23 OF 42	

D.1.24 Universal Joint Arm 1 v.2

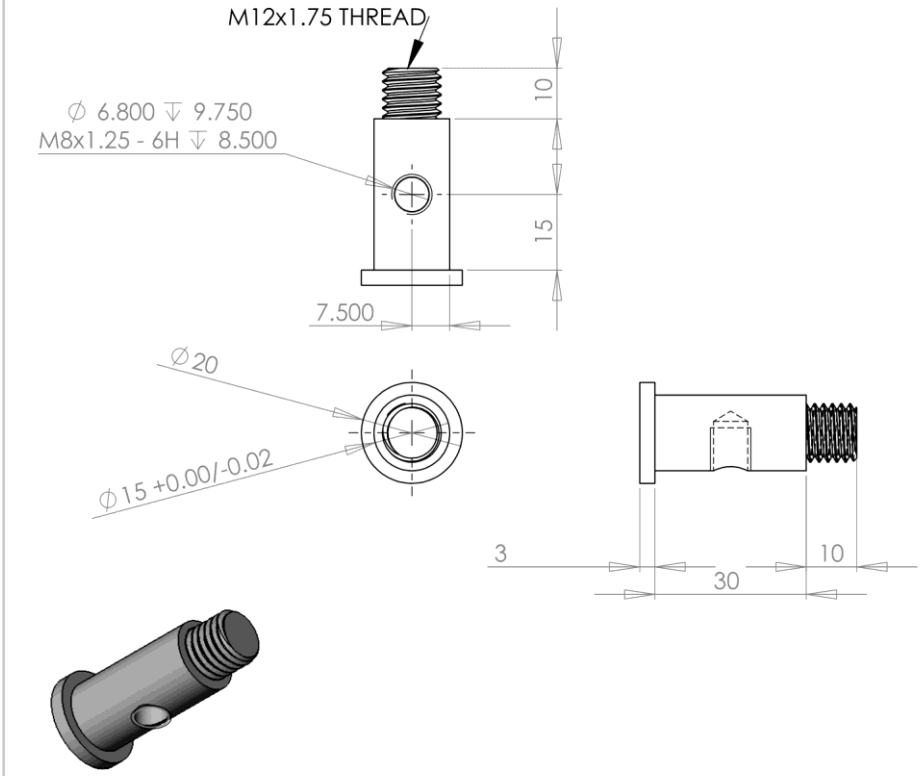

REMOVE ALL SHARP EDGES WITH A 0.25mm x 45 DEG CHAMFER

UNLESS OTHERWISE SPECIFIED: DIMENSIONS ARE IN MILLIMETERS SURFACE FINISH: STANDARD TOLERANCES: LINEAR: +/- 0.05 ANGULAR: +/- 0.1			FINISH:			DEBUR AND BREAK SHARP EDGES	DO NOT SCALE DRAWING	REVISION
	NAME	SIGNATURE	DATE				TITLE:	
DRAWN	D.ROCHELLE	D.ROCHELLE	11.12.18				Universal Joint	
CHK'D								
APPV'D								
MFG								
Q.A				MATERIAL: 316 Stainless Steel			DWG NO. Uni.J Arm 1 v.2	A4
				WEIGHT:			SCALE: 1:1	SHEET 24 OF 42

D.1.25 Universal Joint Small Bracket v.1

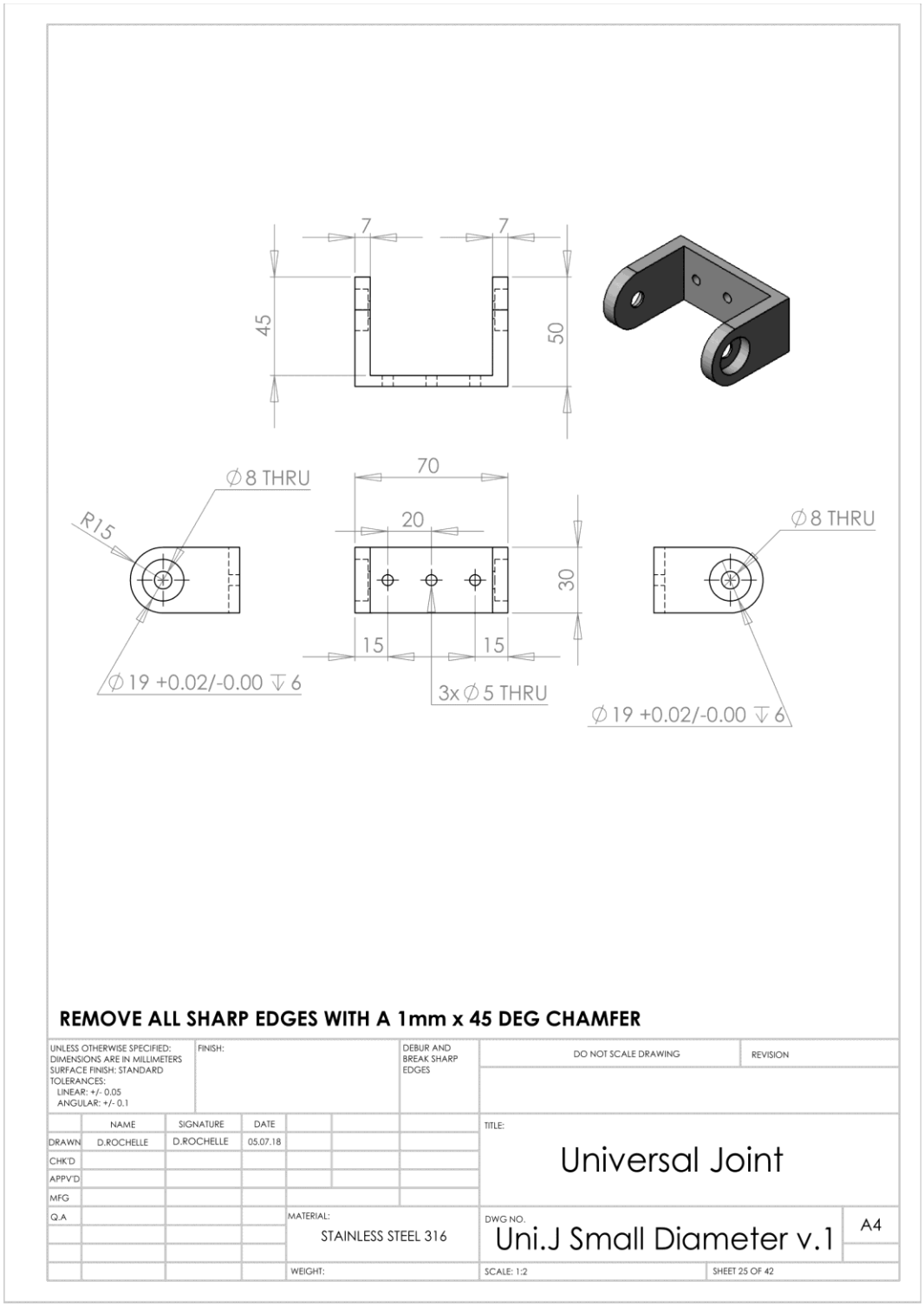

D.1.26 Universal Joint Small Bracket v.2

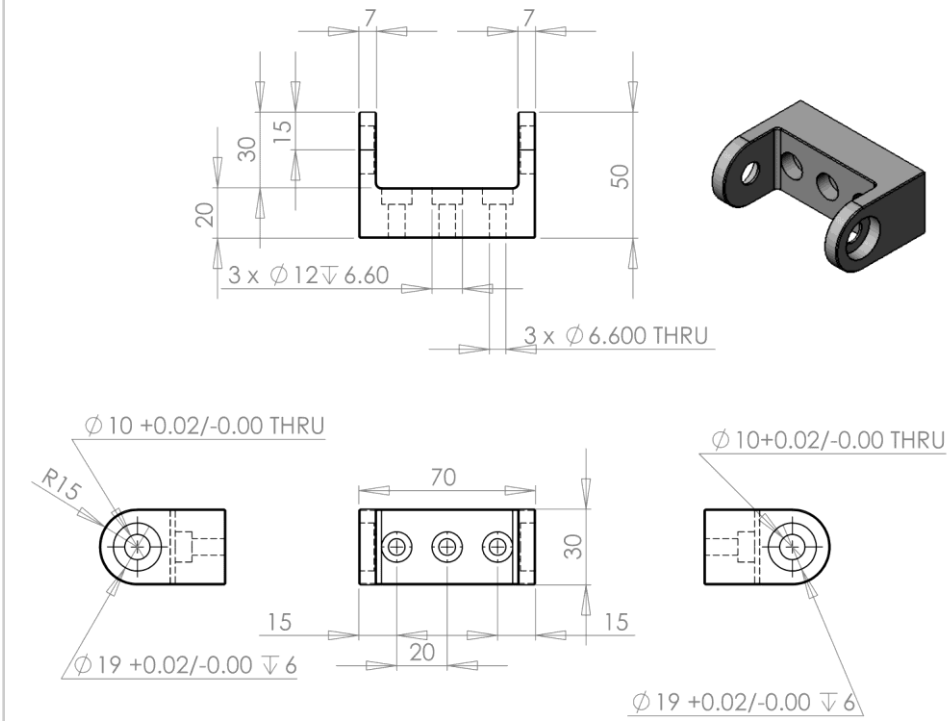

REMOVE ALL SHARP EDGES WITH A 1mm x 45 DEG CHAMFER

UNLESS OTHERWISE SPECIFIED: DIMENSIONS ARE IN MILLIMETERS SURFACE FINISH: STANDARD TOLERANCES: LINEAR: +/- 0.05 ANGULAR: +/- 0.1		FINISH:		DEBUR AND BREAK SHARP EDGES			DO NOT SCALE DRAWING	REVISION
	NAME	SIGNATURE	DATE				TITLE:	
DRAWN	D.ROCHELLE	D.ROCHELLE	11.12.18				Universal Joint	
CHK'D								
APPV'D								
MFG								
Q.A				MATERIAL: 316 Stainless Steel			DWG NO. Uni.J Small Diameter v.2	A4
				WEIGHT:			SCALE: 1:2	SHEET 26 OF 42

D.1.27 Universal Joint Small Bearing

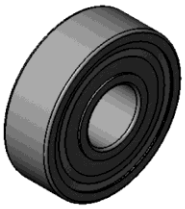

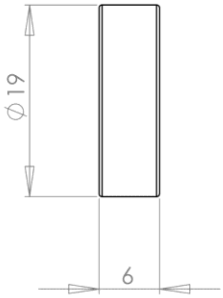

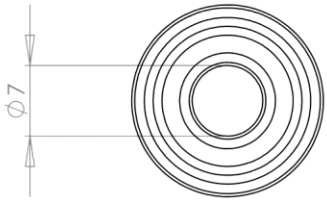

UNLESS OTHERWISE SPECIFIED: DIMENSIONS ARE IN MILLIMETERS SURFACE FINISH: STANDARD TOLERANCES: LINEAR: +/- 0.05 ANGULAR: +/- 0.1		FINISH:		DEBUR AND BREAK SHARP EDGES	DO NOT SCALE DRAWING	REVISION
	NAME	SIGNATURE	DATE		TITLE:	
DRAWN	D.ROCHELLE	D.ROCHELLE	05.07.18		Universal Joint	
CHK'D						
APPV'D						
MFG						
Q.A				MATERIAL: Steel	DWG NO. Small Bearing 607-2RSH	A4
				WEIGHT:	SCALE: 1:2	SHEET 27 OF 42

D.1.28 Universal Joint Small Bush

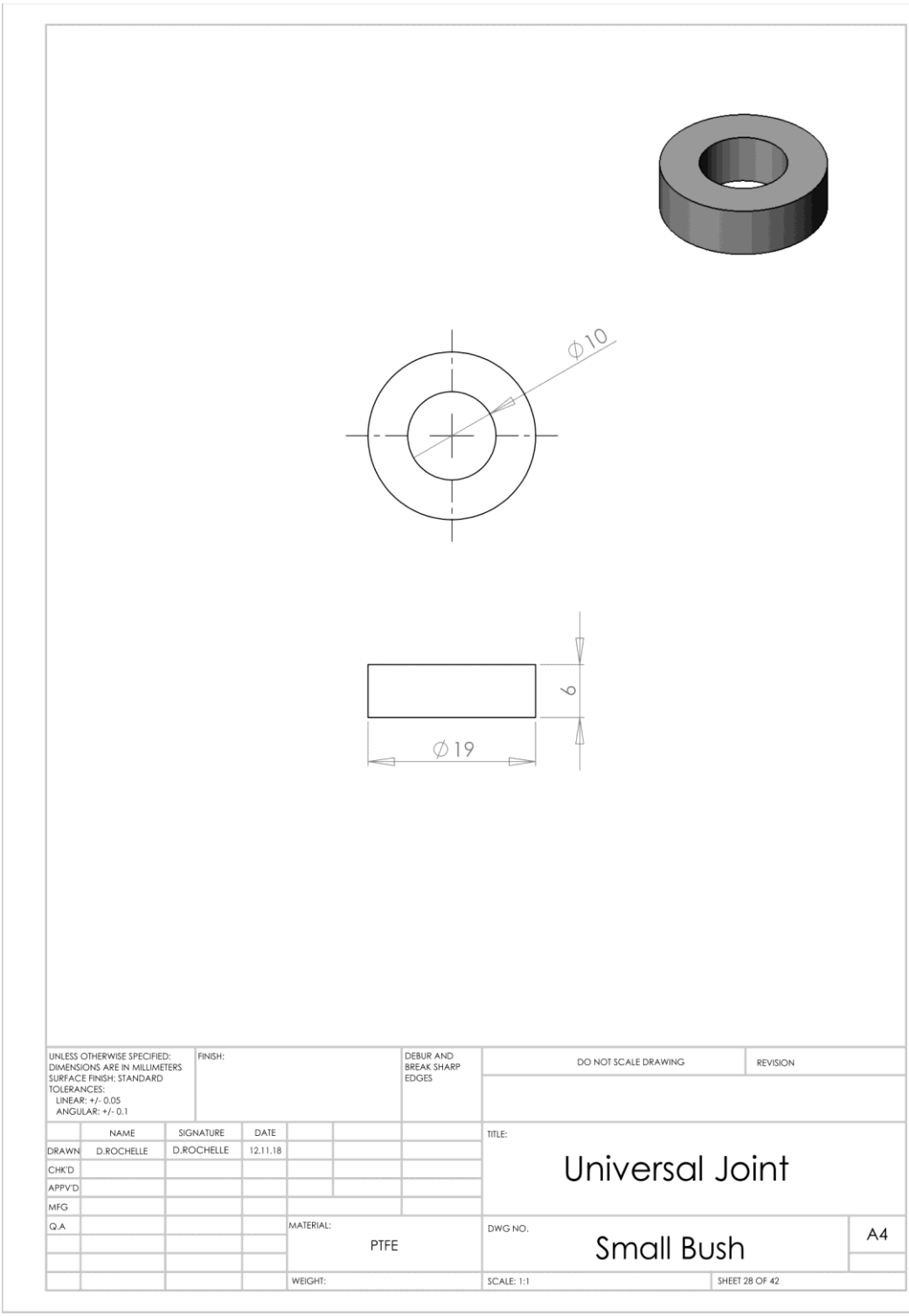

D.1.29 Universal Joint Arm 2 v.1

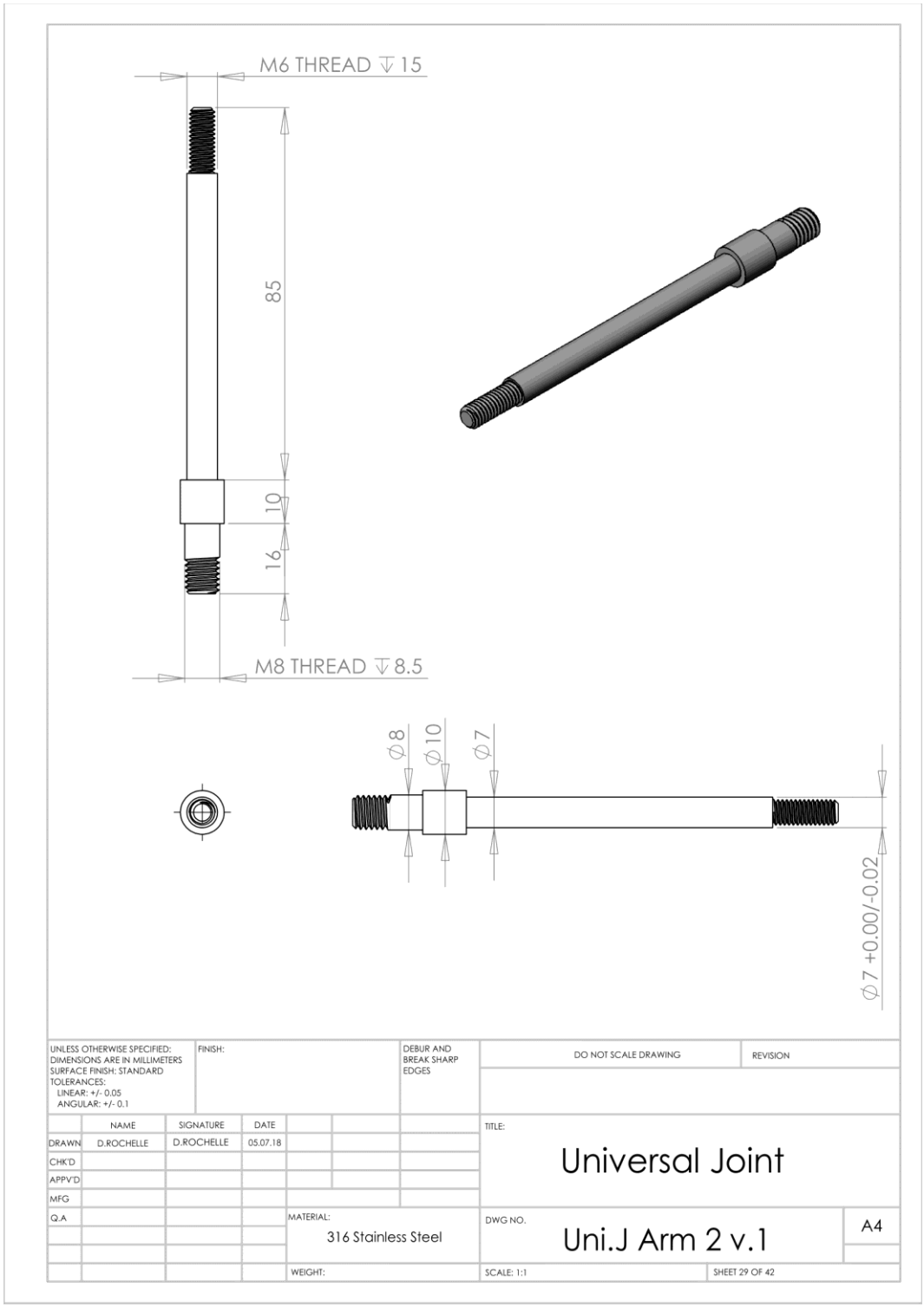

D.1.30 Universal Joint Arm 2 v.2

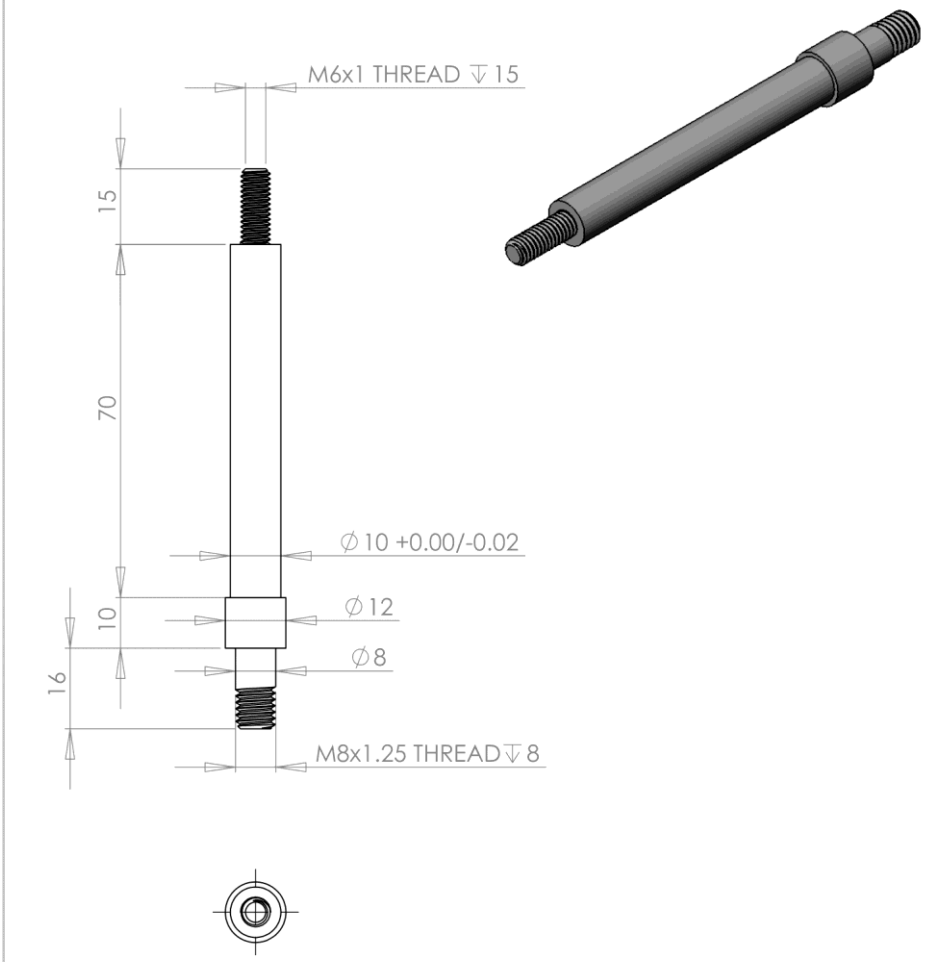

UNLESS OTHERWISE SPECIFIED: DIMENSIONS ARE IN MILLIMETERS SURFACE FINISH: STANDARD TOLERANCES: LINEAR: +/- 0.05 ANGULAR: +/- 0.1		FINISH:		DEBUR AND BREAK SHARP EDGES		DO NOT SCALE DRAWING	REVISION
	NAME	SIGNATURE	DATE			TITLE: Universal Joint	
DRAWN	D.ROCHELLE	D.ROCHELLE	12.11.18				
CHK'D							
APPV'D							
MFG							
Q.A				MATERIAL: 316 Stainless Steel		DWG NO. Uni J Arm 2 v.2	A4
				WEIGHT:		SCALE: 1:1	SHEET 30 OF 42

D.2 Marker Triads

D.2.1 Marker Triad v.1

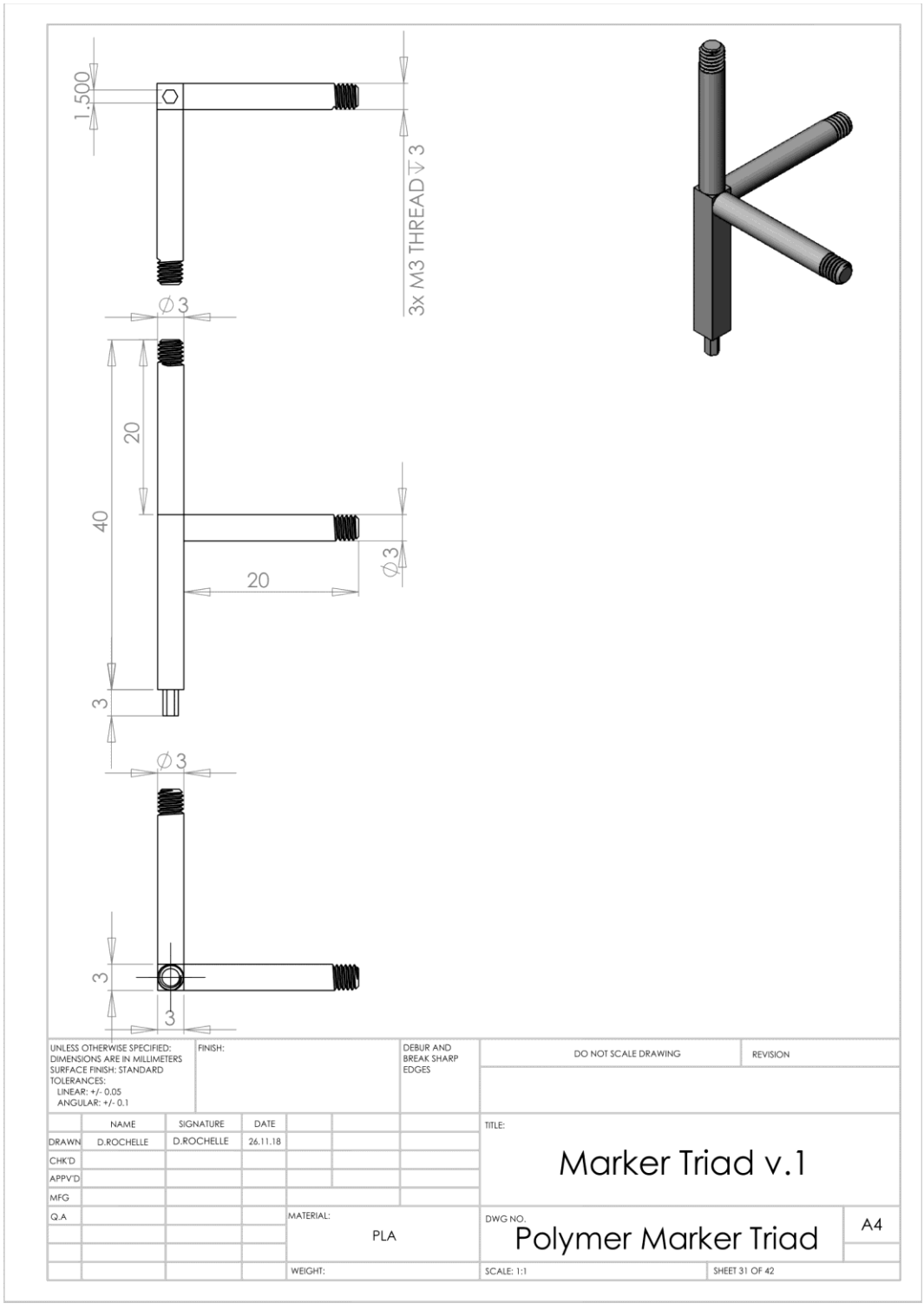

D.2.2 Marker Triad Assembly v.2

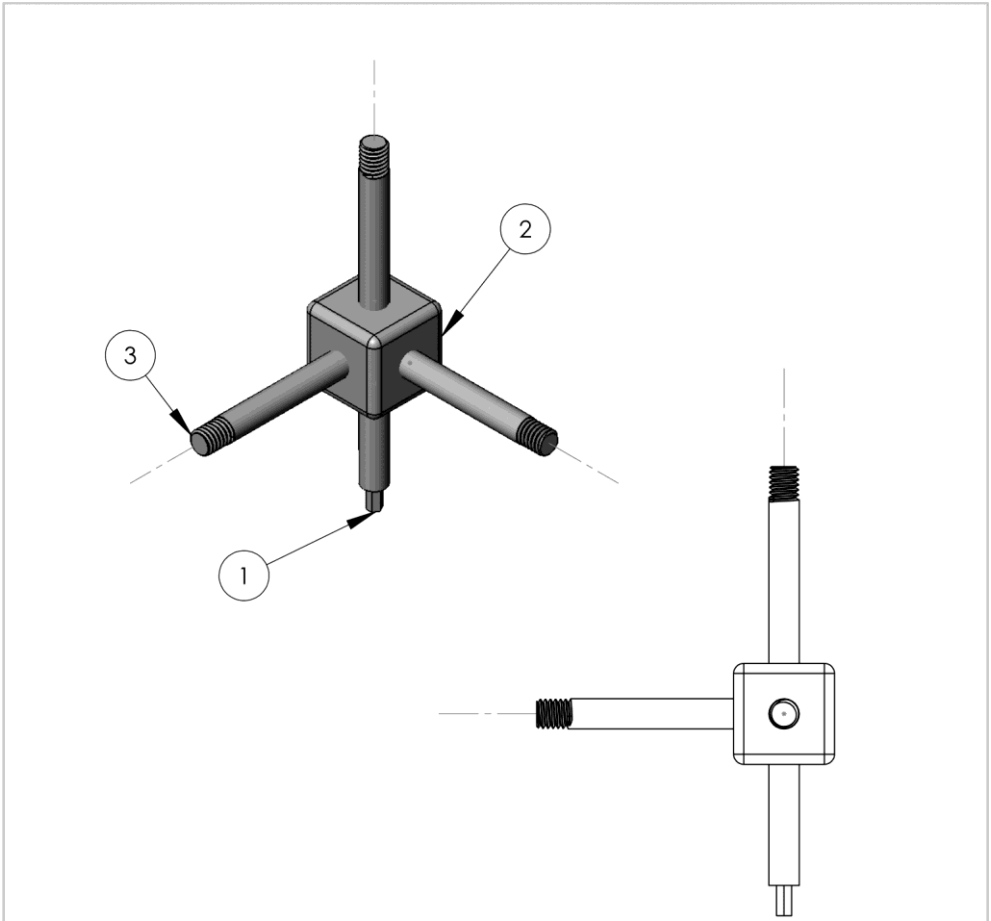

Part number	Drawing Number	Part name	Quantity
1	34	Marker Triad Base	1
2	35	Marker Triad Centre	1
3	36	Marker Triad Arm	3

UNLESS OTHERWISE SPECIFIED: DIMENSIONS ARE IN MILLIMETERS SURFACE FINISH: STANDARD TOLERANCES: LINEAR: +/- 0.05 ANGULAR: +/- 0.1		FINISH:		DEBUR AND BREAK SHARP EDGES		DO NOT SCALE DRAWING	REVISION
	NAME	SIGNATURE	DATE			TITLE:	
DRAWN	D. Rochelle	D.ROCHELLE	11/12/18			Marker Triad v.2	
CHK'D							
APPV'D							
MFG							
Q.A				MATERIAL: 316 Stainless Steel		DWG NO. Assembly	A4
				WEIGHT:		SCALE 2:1	SHEET 32 of 42

D.2.3 Marker Triad Assembly v.3

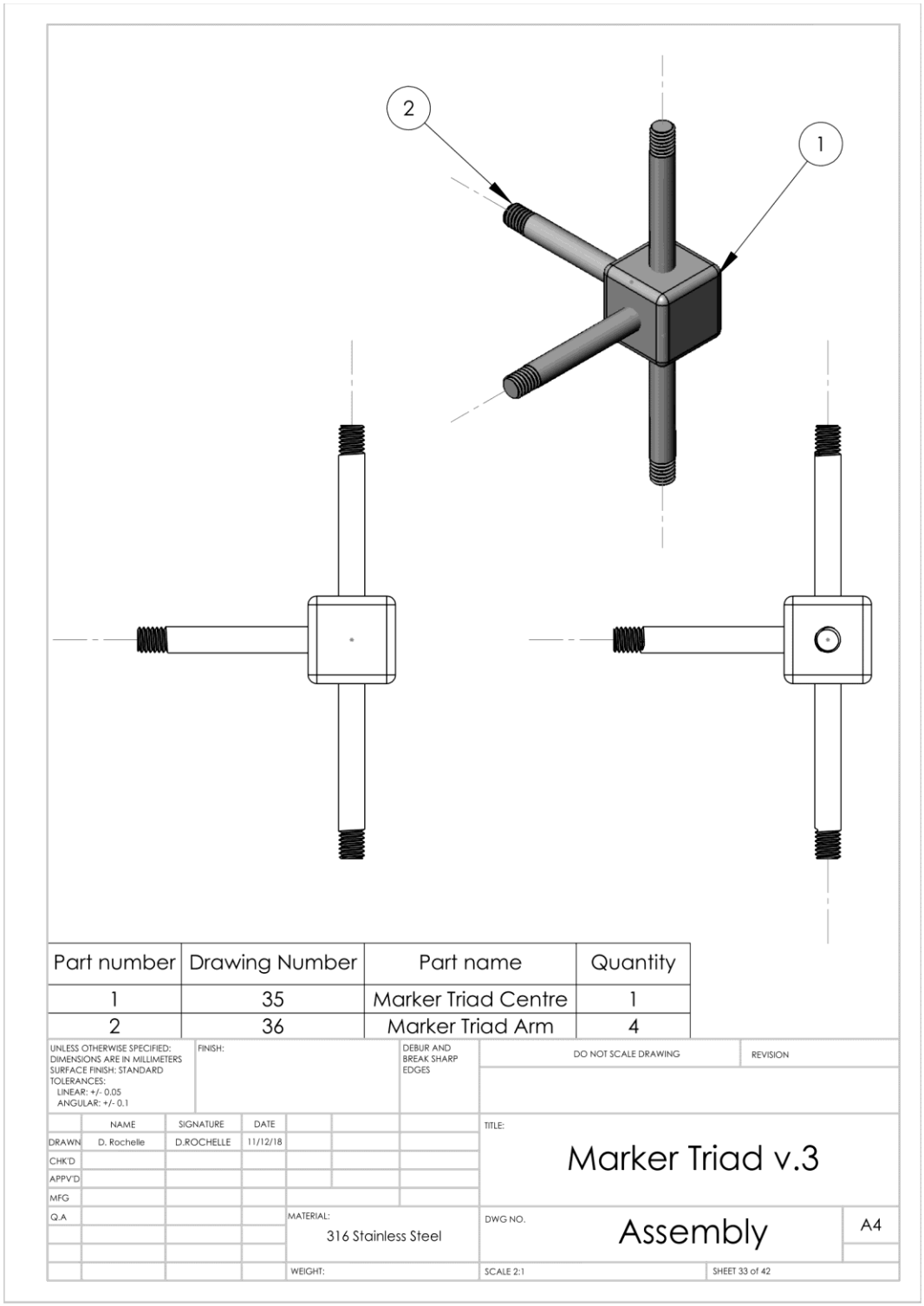

Part number	Drawing Number	Part name	Quantity
1	35	Marker Triad Centre	1
2	36	Marker Triad Arm	4

UNLESS OTHERWISE SPECIFIED: DIMENSIONS ARE IN MILLIMETERS SURFACE FINISH: STANDARD TOLERANCES: LINEAR: +/- 0.05 ANGULAR: +/- 0.1		FINISH:		DEBUR AND BREAK SHARP EDGES		DO NOT SCALE DRAWING	REVISION
	NAME	SIGNATURE	DATE			TITLE:	
DRAWN	D. Rochelle	D.ROCHELLE	11/12/18			Marker Triad v.3	
CHK'D							
APPV'D							
MFG							
Q.A				MATERIAL: 316 Stainless Steel		DWG NO. Assembly	A4
				WEIGHT:		SCALE 2:1	SHEET 33 of 42

D.2.4 Marker Triad Base

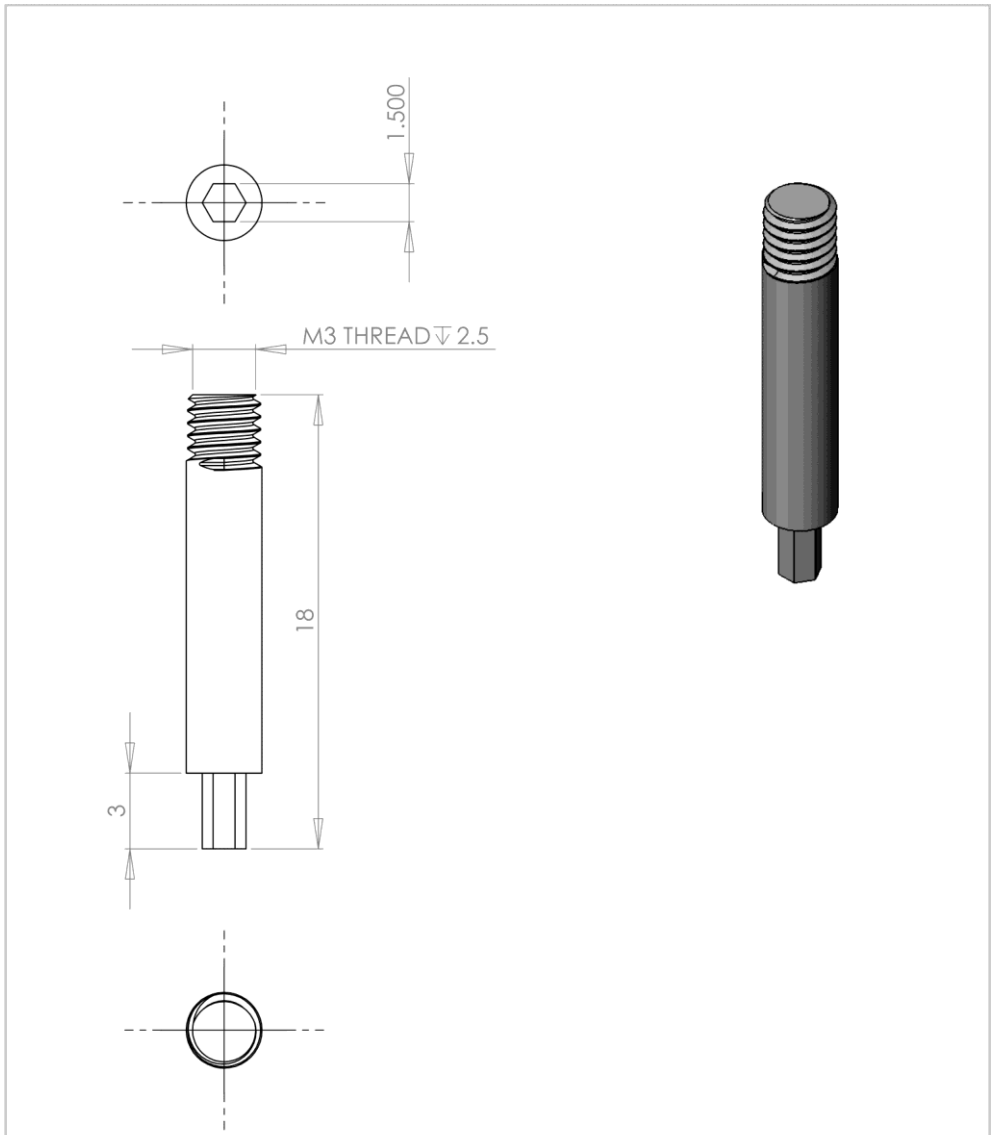

UNLESS OTHERWISE SPECIFIED: DIMENSIONS ARE IN MILLIMETERS SURFACE FINISH: STANDARD TOLERANCES: LINEAR: +/- 0.05 ANGULAR: +/- 0.1		FINISH:		DEBUR AND BREAK SHARP EDGES		DO NOT SCALE DRAWING	REVISION
	NAME	SIGNATURE	DATE			TITLE:	
DRAWN	D. Rochelle	D.ROCHELLE	11/12/18			Marker Triad	
CHK'D							
APPV'D							
MFG							
Q.A				MATERIAL: 316 Stainless Steel		DWG NO. Marker Triad Base	A4
				WEIGHT:		SCALE 5:1	SHEET 34 of 42

D.2.5 Marker Triad Centre

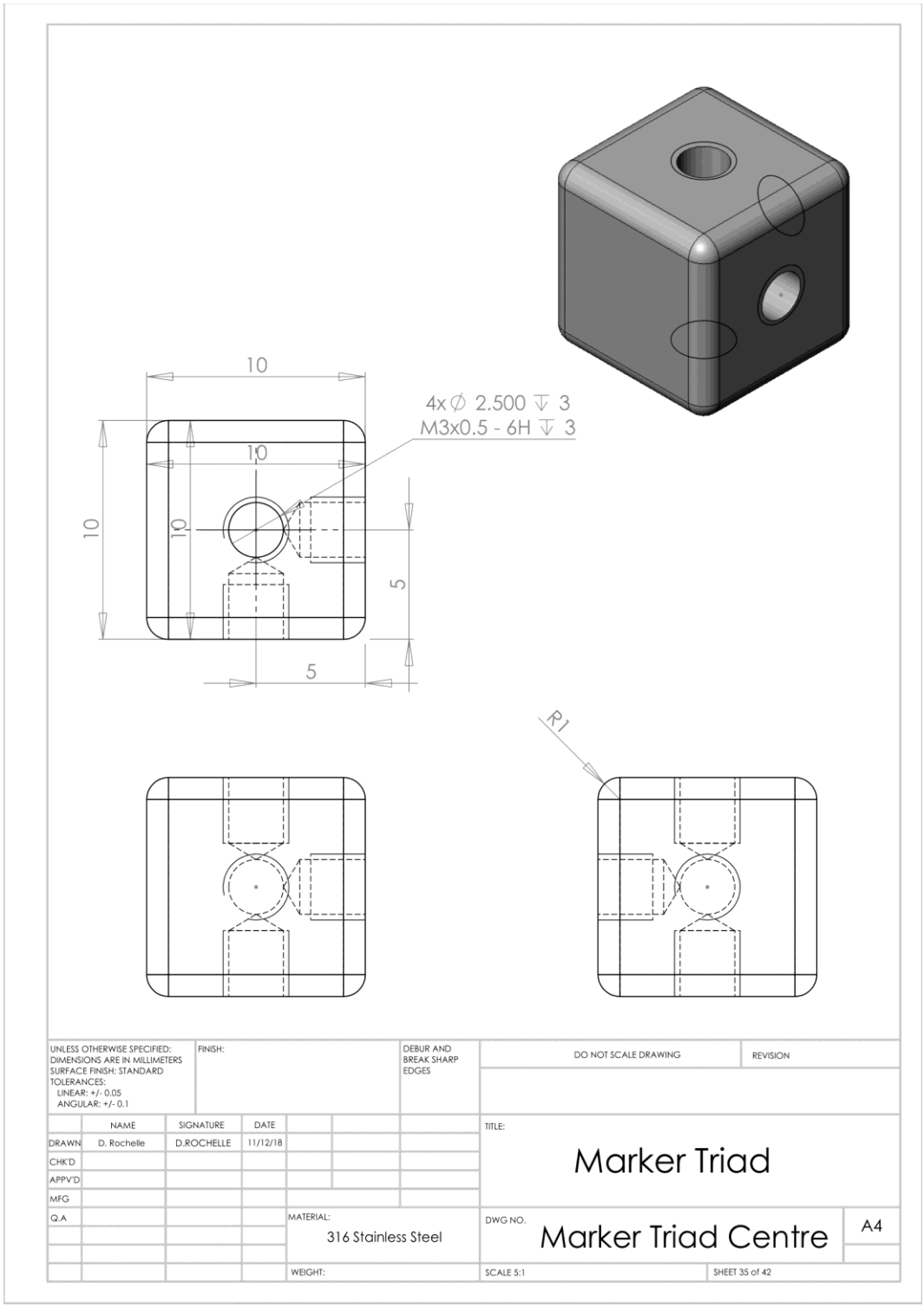

UNLESS OTHERWISE SPECIFIED: DIMENSIONS ARE IN MILLIMETERS SURFACE FINISH: STANDARD TOLERANCES: LINEAR: +/- 0.05 ANGULAR: +/- 0.1	FINISH:		DEBUR AND BREAK SHARP EDGES	DO NOT SCALE DRAWING	REVISION	
	NAME	SIGNATURE	DATE	TITLE:		
DRAWN	D. Rochelle	D.ROCHELLE	11/12/18	Marker Triad		
CHK'D						
APPV'D						
MFG						
Q.A				MATERIAL: 316 Stainless Steel	DWG NO. Marker Triad Centre	A4
				WEIGHT:	SCALE 5:1	SHEET 35 of 42

D.2.6 Marker Triad Arm

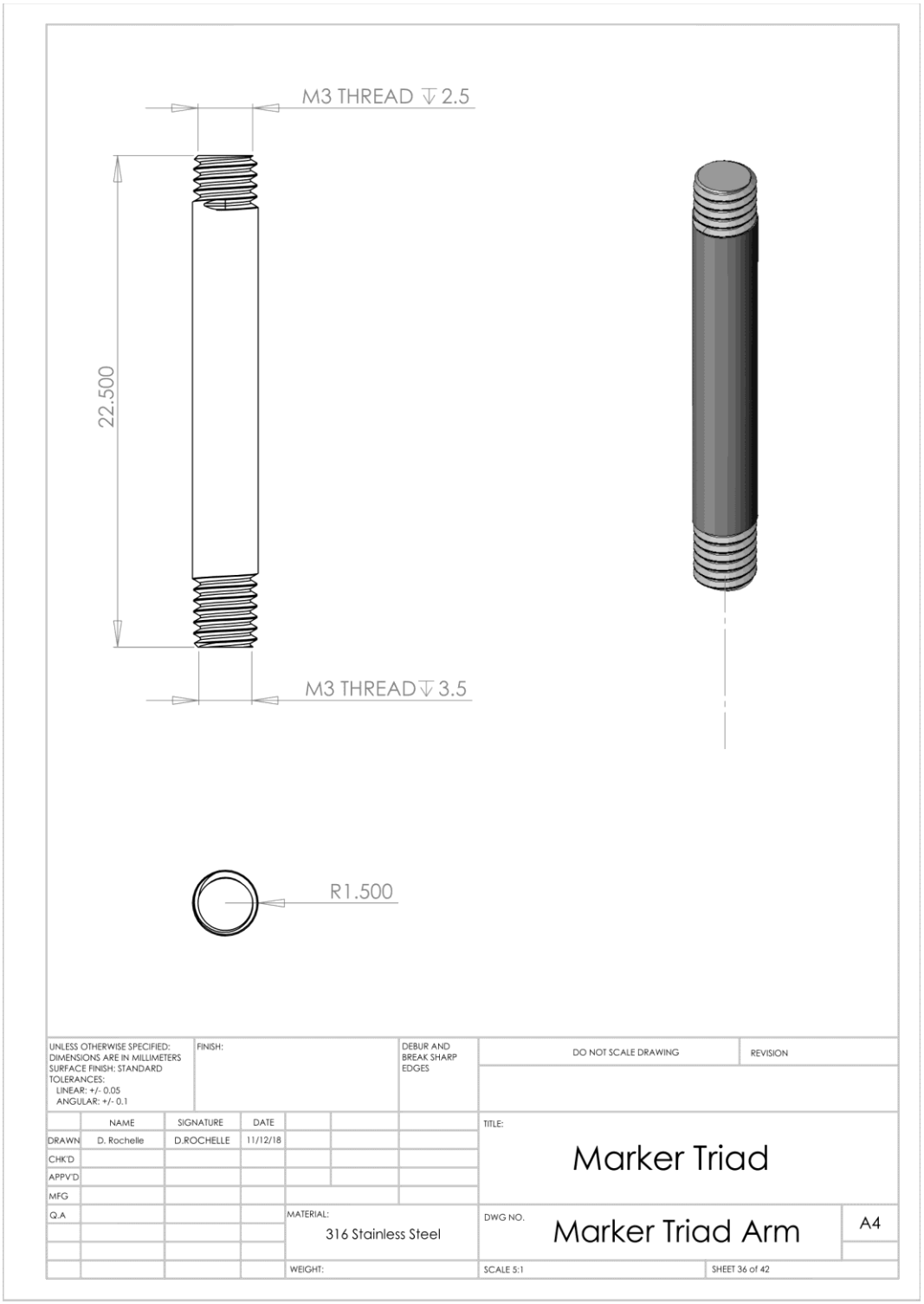

D.3 Specimen Impactor

D.3.1 Specimen Impactor Assembly v.1

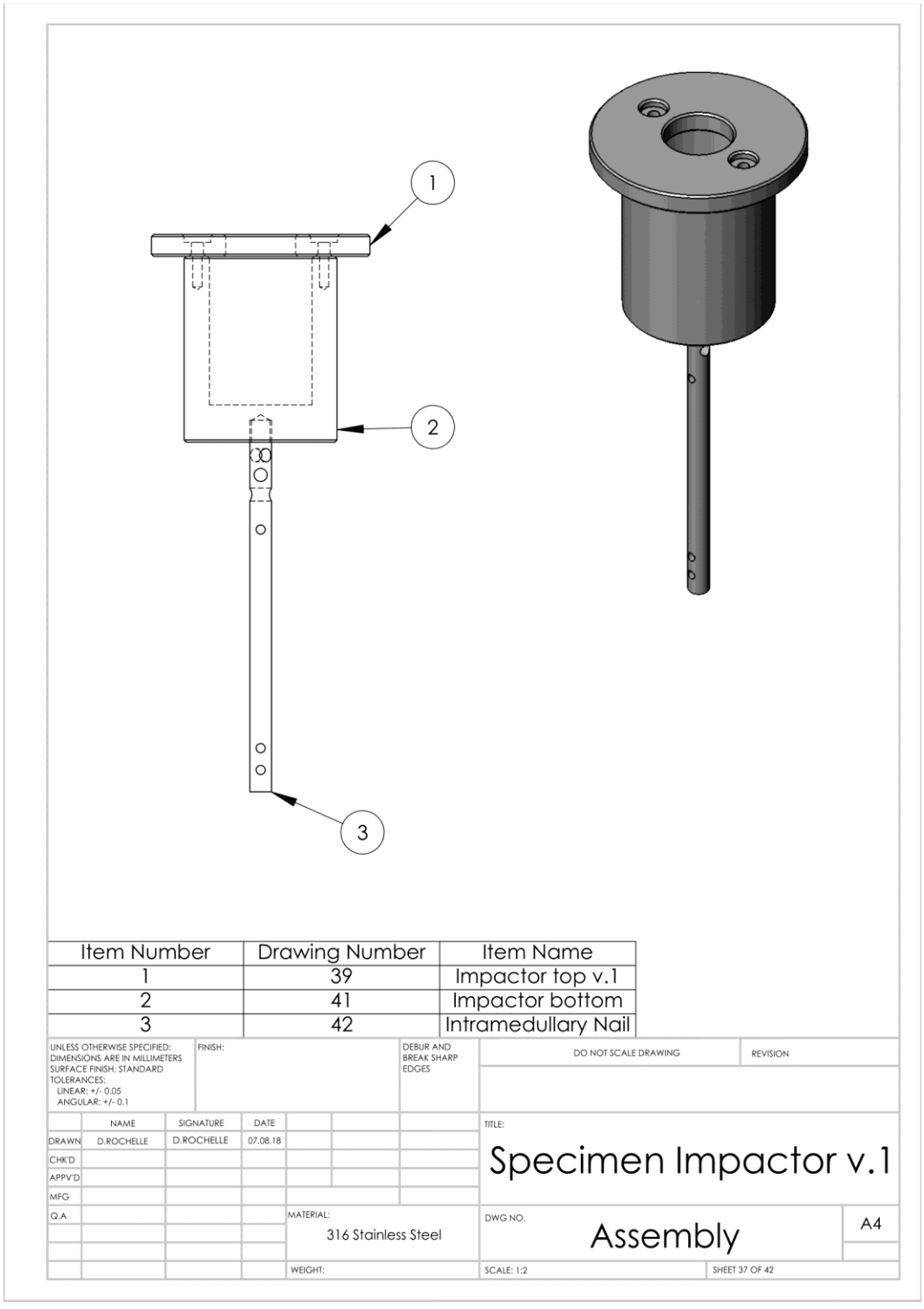

Item Number	Drawing Number	Item Name
1	39	Impactor top v.1
2	41	Impactor bottom
3	42	Intramedullary Nail

UNLESS OTHERWISE SPECIFIED: DIMENSIONS ARE IN MILLIMETERS SURFACE FINISH: STANDARD TOLERANCES: LINEAR: +/- 0.05 ANGULAR: +/- 0.1	FINISH:		DEBUR AND BREAK SHARP EDGES	DO NOT SCALE DRAWING	REVISION	
	NAME	SIGNATURE	DATE	TITLE:		
DRAWN	D.ROCHELLE	D.ROCHELLE	07.08.18	Specimen Impactor v.1		
CHK'D						
APPV'D						
MFG						
Q.A				MATERIAL: 316 Stainless Steel	DWG NO. Assembly	A4
				WEIGHT:	SCALE: 1:2	SHEET 37 OF 42

D.3.2 Specimen Impactor Assembly v.2

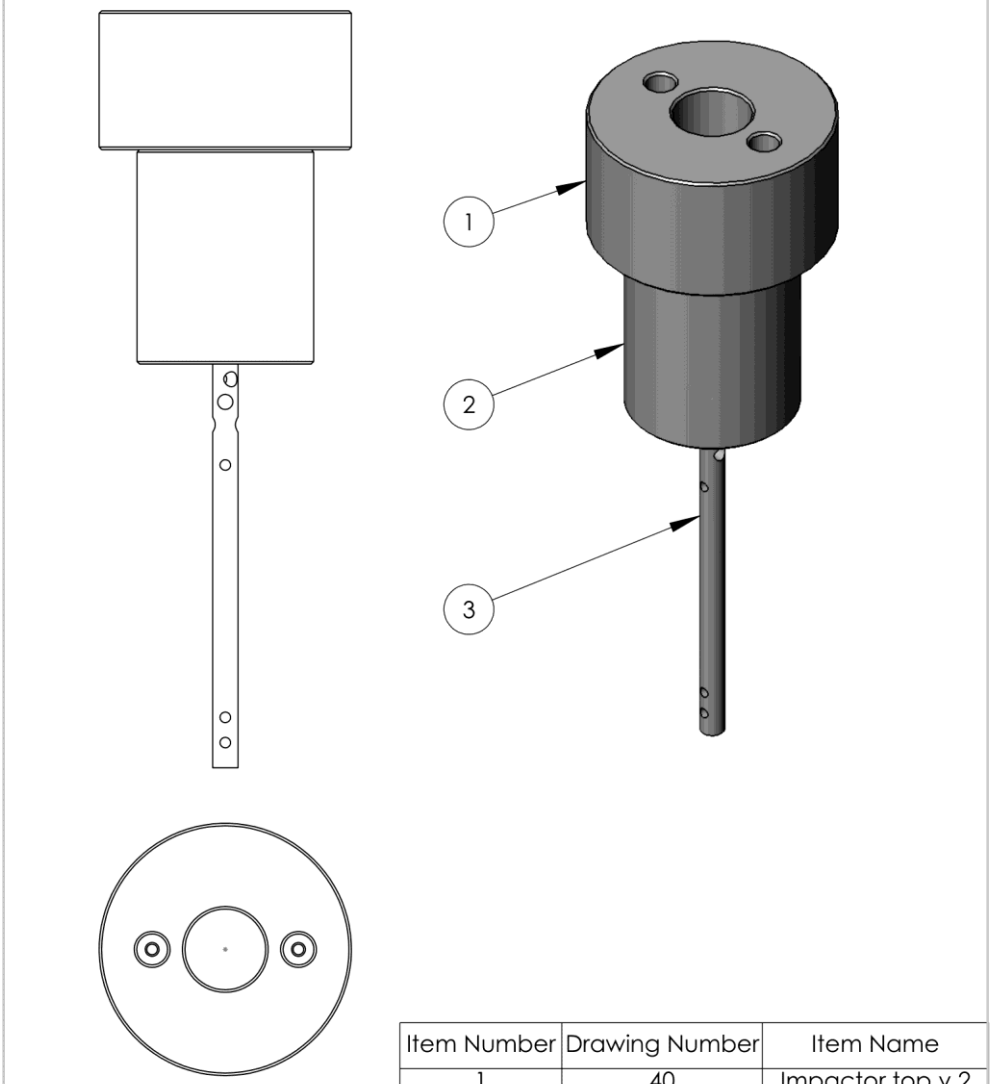

Item Number	Drawing Number	Item Name
1	40	Impactor top v.2
2	41	Impactor bottom
3	42	Intramedullary Nail

UNLESS OTHERWISE SPECIFIED:
DIMENSIONS ARE IN MILLIMETERS
SURFACE FINISH: STANDARD
TOLERANCES:
LINEAR: +/- 0.05
ANGULAR: +/- 0.1

FINISH:

DEBUR AND BREAK SHARP EDGES

DO NOT SCALE DRAWING | REVISION

	NAME	SIGNATURE	DATE
DRAWN	D.ROCHELLE	D.ROCHELLE	28.3.19
CHK'D			
APPV'D			
MFG			
Q.A			

MATERIAL: 316 Stainless Steel

WEIGHT:

TITLE: Specimen Impactor v.2

DWG NO. Assembly

A4

SCALE: 1:2

SHEET 38 OF 42

D.3.3 Specimen Impactor Top v.1

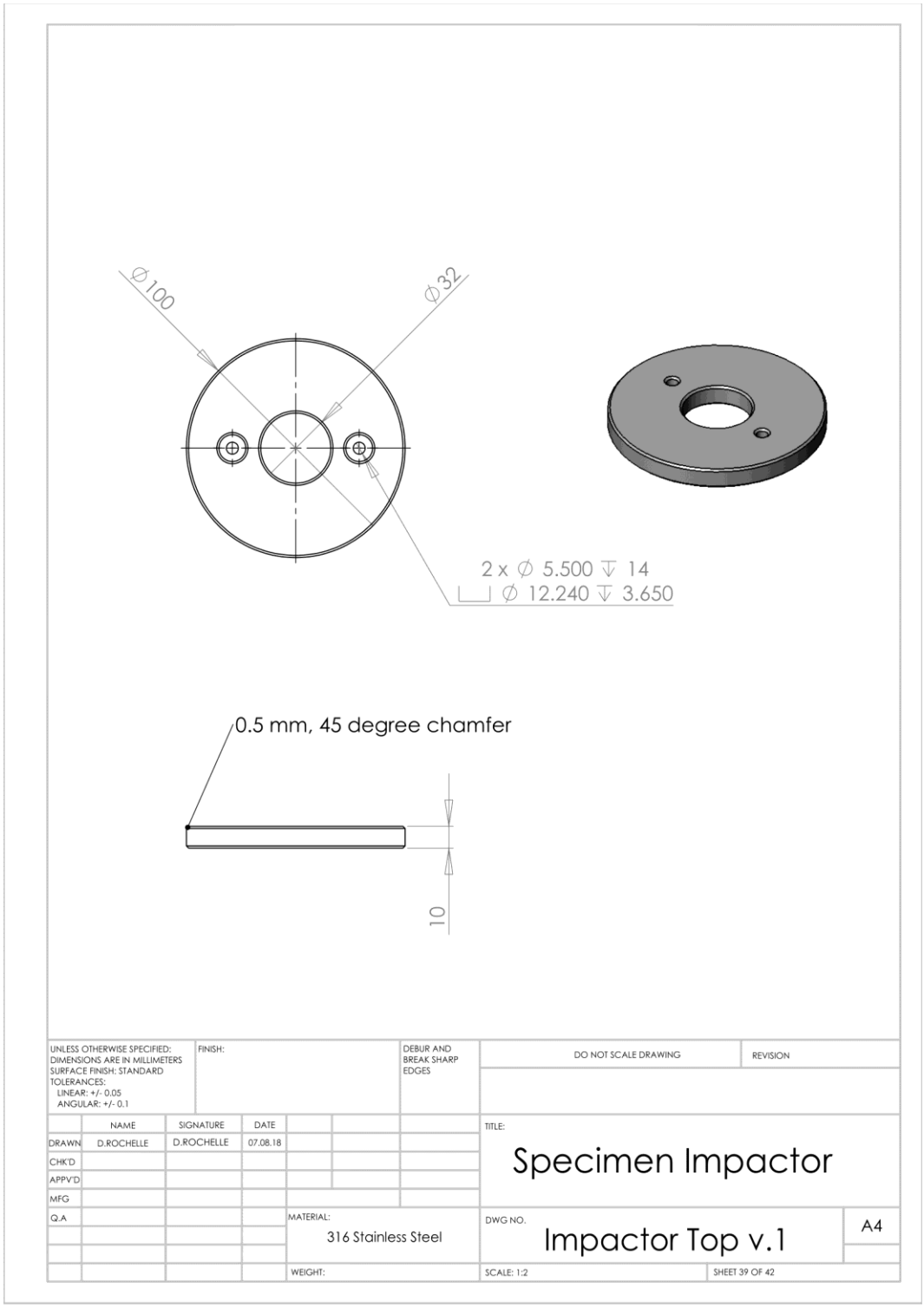

D.3.4 Specimen Impactor Top v.2

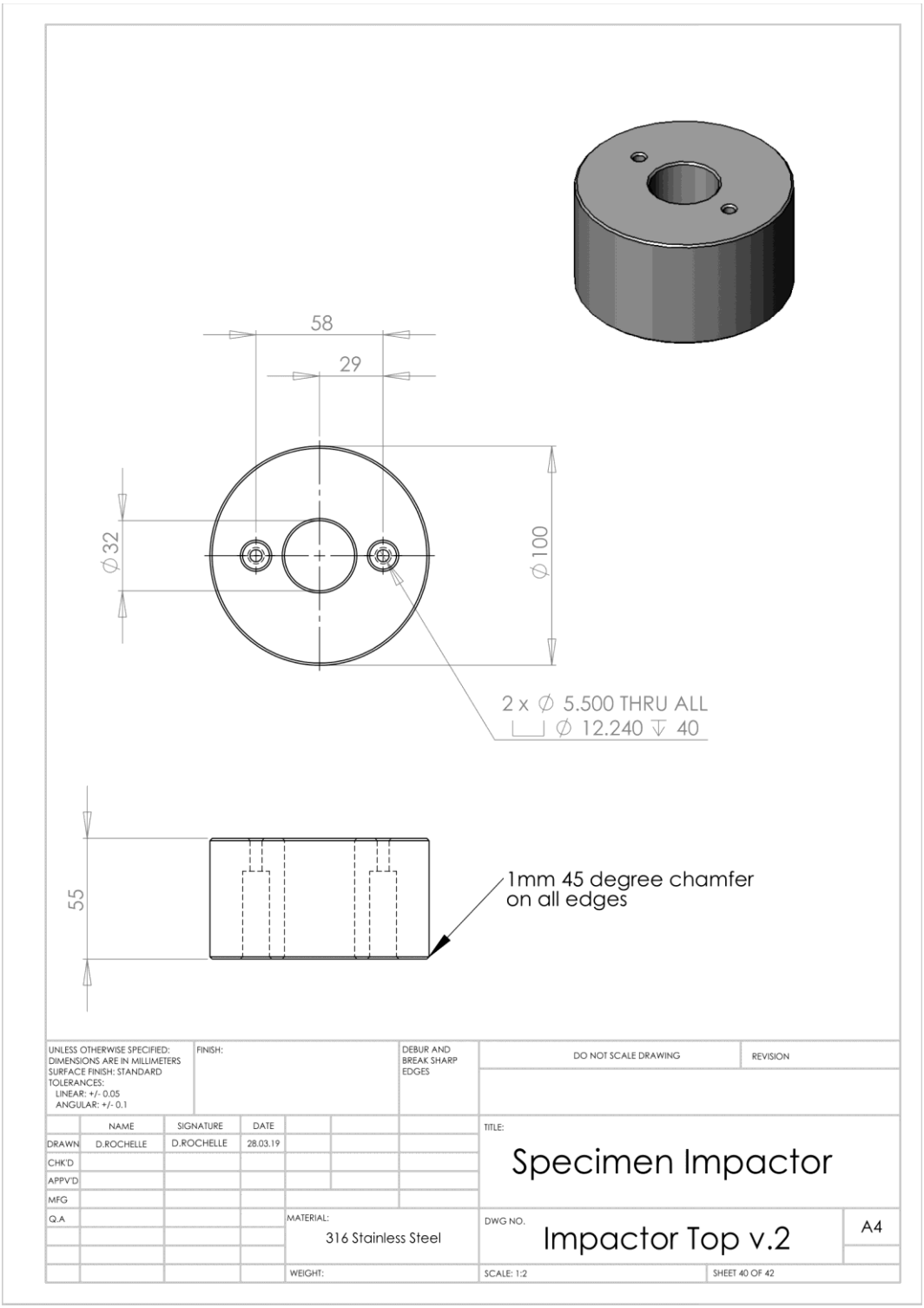

UNLESS OTHERWISE SPECIFIED: DIMENSIONS ARE IN MILLIMETERS SURFACE FINISH: STANDARD TOLERANCES: LINEAR: +/- 0.05 ANGULAR: +/- 0.1		FINISH:		DEBUR AND BREAK SHARP EDGES		DO NOT SCALE DRAWING	REVISION	
	NAME	SIGNATURE	DATE			TITLE:		
DRAWN	D.ROCHELLE	D.ROCHELLE	28.03.19			Specimen Impactor		
CHK'D								
APPV'D								
MFG								
Q.A				MATERIAL: 316 Stainless Steel		DWG NO. Impactor Top v.2		A4
				WEIGHT:		SCALE: 1:2	SHEET 40 OF 42	

D.3.5 Specimen Impactor Bottom

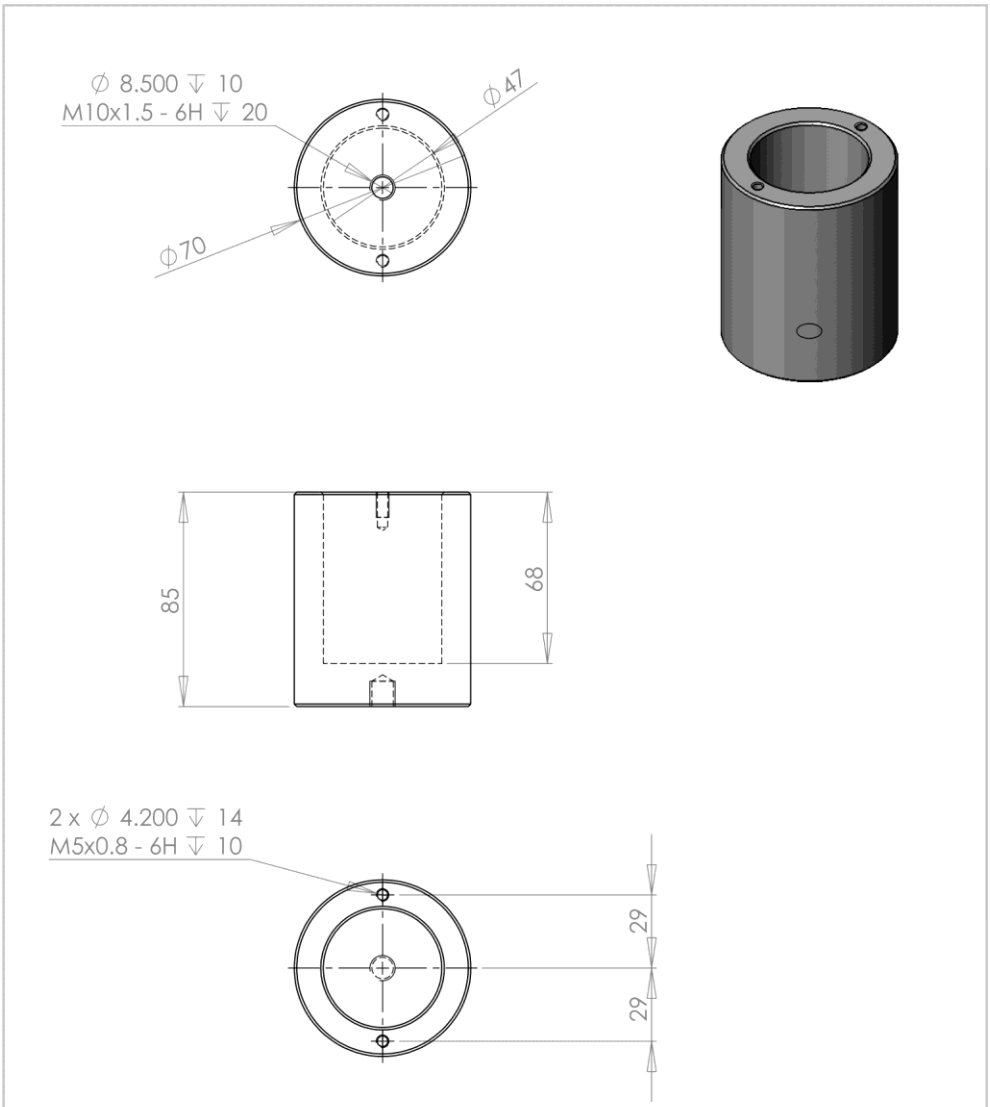

Remove all sharp edges with a 0.5 mm, 45 degree chamfer

UNLESS OTHERWISE SPECIFIED: DIMENSIONS ARE IN MILLIMETERS SURFACE FINISH: STANDARD TOLERANCES: LINEAR: +/- 0.05 ANGULAR: +/- 0.1		FINISH:			DEBUR AND BREAK SHARP EDGES	DO NOT SCALE DRAWING		REVISION
	NAME	SIGNATURE	DATE			TITLE:		
DRAWN	D.ROCHELLE	D.ROCHELLE	07.08.18			Specimen Impactor		
CHK'D								
APPV'D								
MFG								
Q.A				MATERIAL: 316 Stainless Steel		DWG NO. Impactor Bottom		A4
				WEIGHT:		SCALE: 1:2	SHEET 41 OF 42	

D.3.6 Specimen Impactor Intramedullary Nail

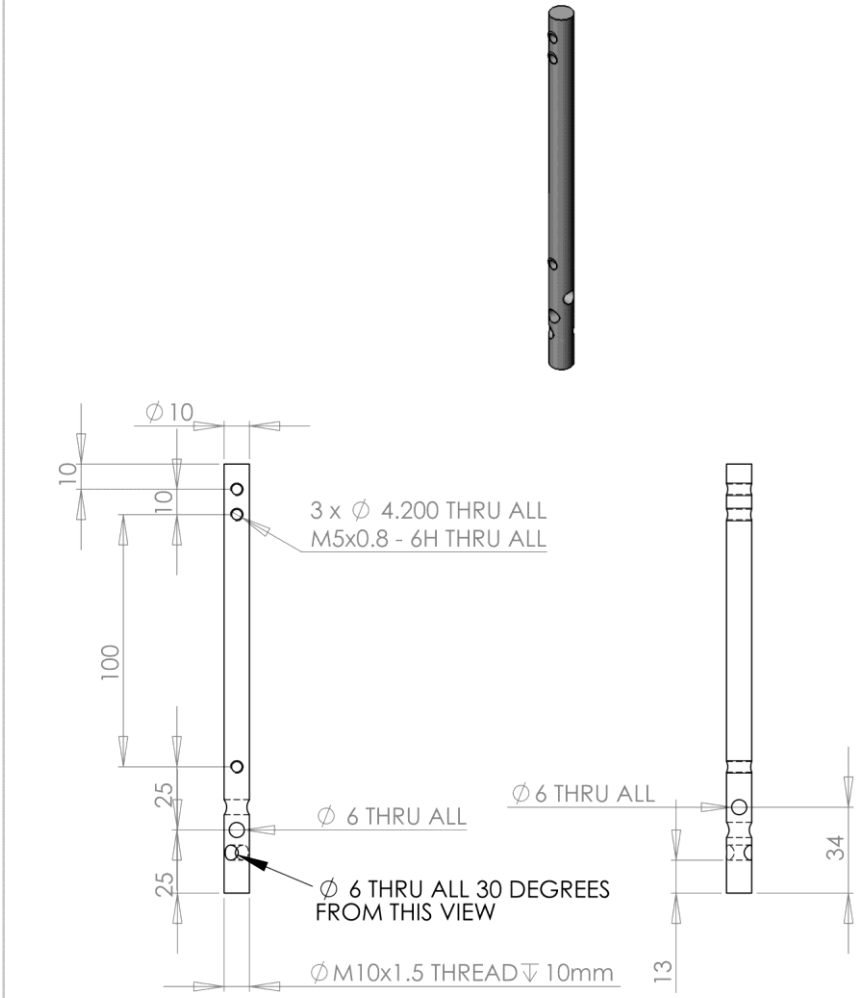

UNLESS OTHERWISE SPECIFIED: DIMENSIONS ARE IN MILLIMETERS SURFACE FINISH: STANDARD TOLERANCES: LINEAR: +/- 0.05 ANGULAR: +/- 0.05		FINISH:		DEBUR AND BREAK SHARP EDGES		DO NOT SCALE DRAWING	REVISION
	NAME	SIGNATURE	DATE			TITLE: Specimen Impactor	
DRAWN	D.ROCHELLE	D.ROCHELLE	07.08.18				
CHK'D							
APPV'D							
MFG							
Q.A				MATERIAL: 316 Stainless Steel		DWG NO. Intramedullary Nail	A4
				WEIGHT:		SCALE: 1:2	SHEET 42 OF 42

Appendix E – Simulation of Sprain Biomechanical Data

E.1 Sample 1 Trial 3

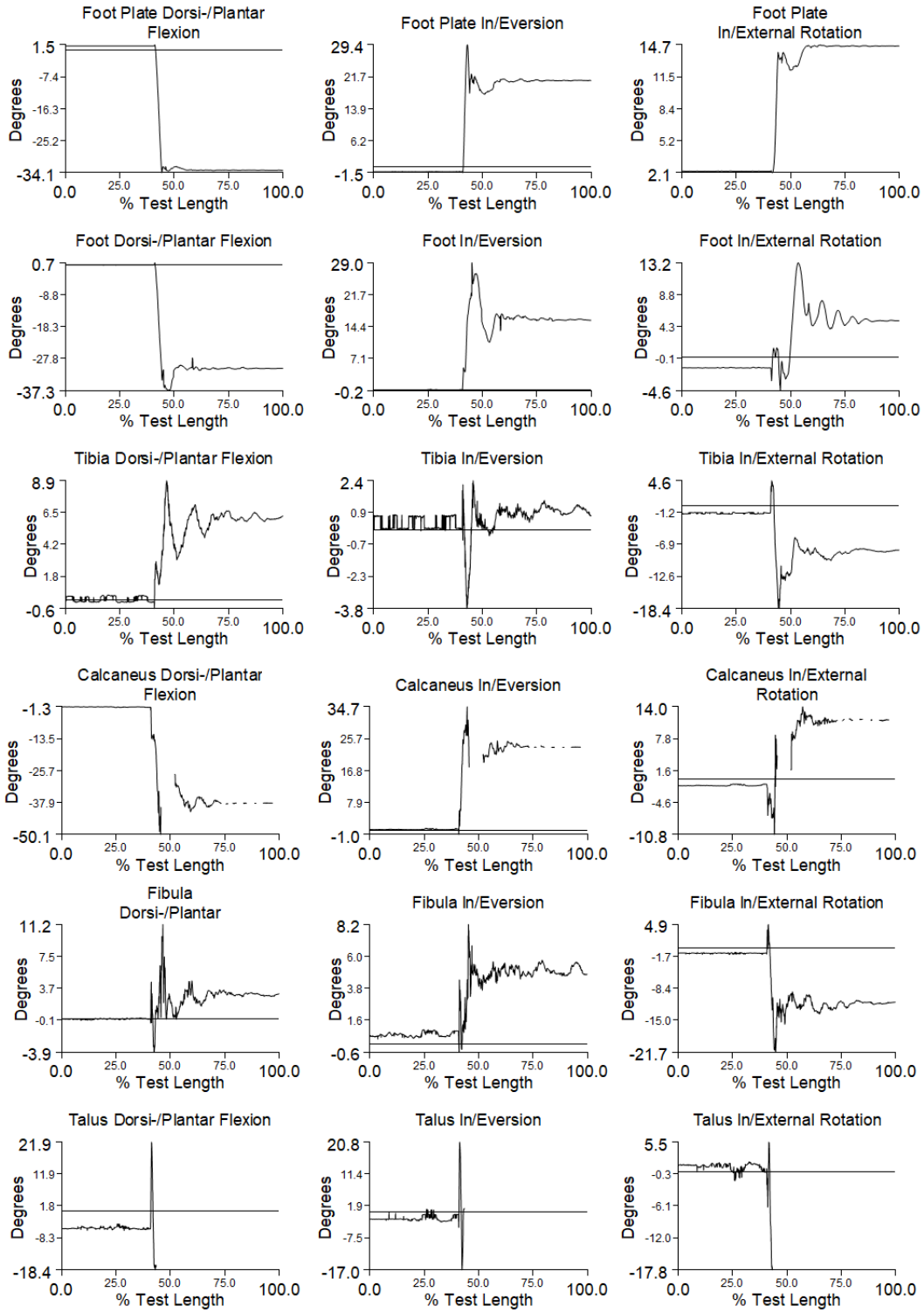

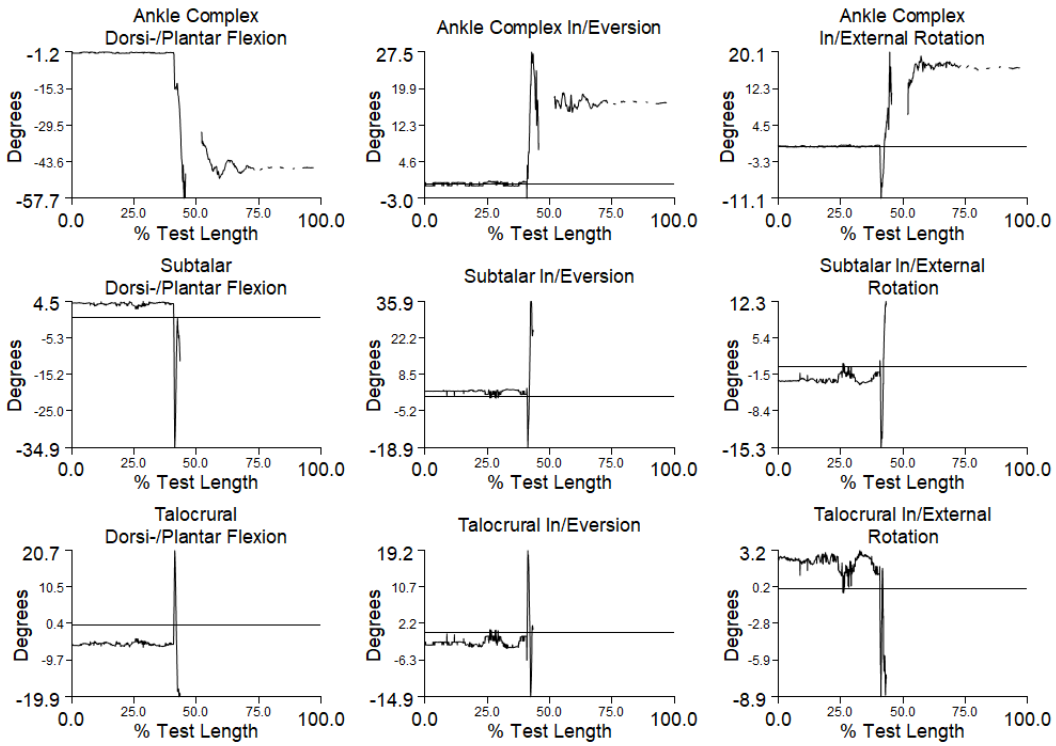

Appendix E.1. The biomechanical data output from Visual3D for the third trial of sample 1. Each column contains the data for a particular motion. The first column shows data for dorsi-/plantar flexion (dorsiflexion is positive), the second column inversion/eversion (inversion is positive) and the third column internal/external rotation (internal rotation is positive). Each row represents a section to be analysed. The first row is of the foot plate, the second is of the foot, the third is the tibia, the fourth is the calcaneus, the fifth is the fibula, the sixth is the talus, the seventh is the ankle complex, the eighth is the subtalar joint and the ninth is the talocrural joint.

E.2 Sample 2 Trial 2

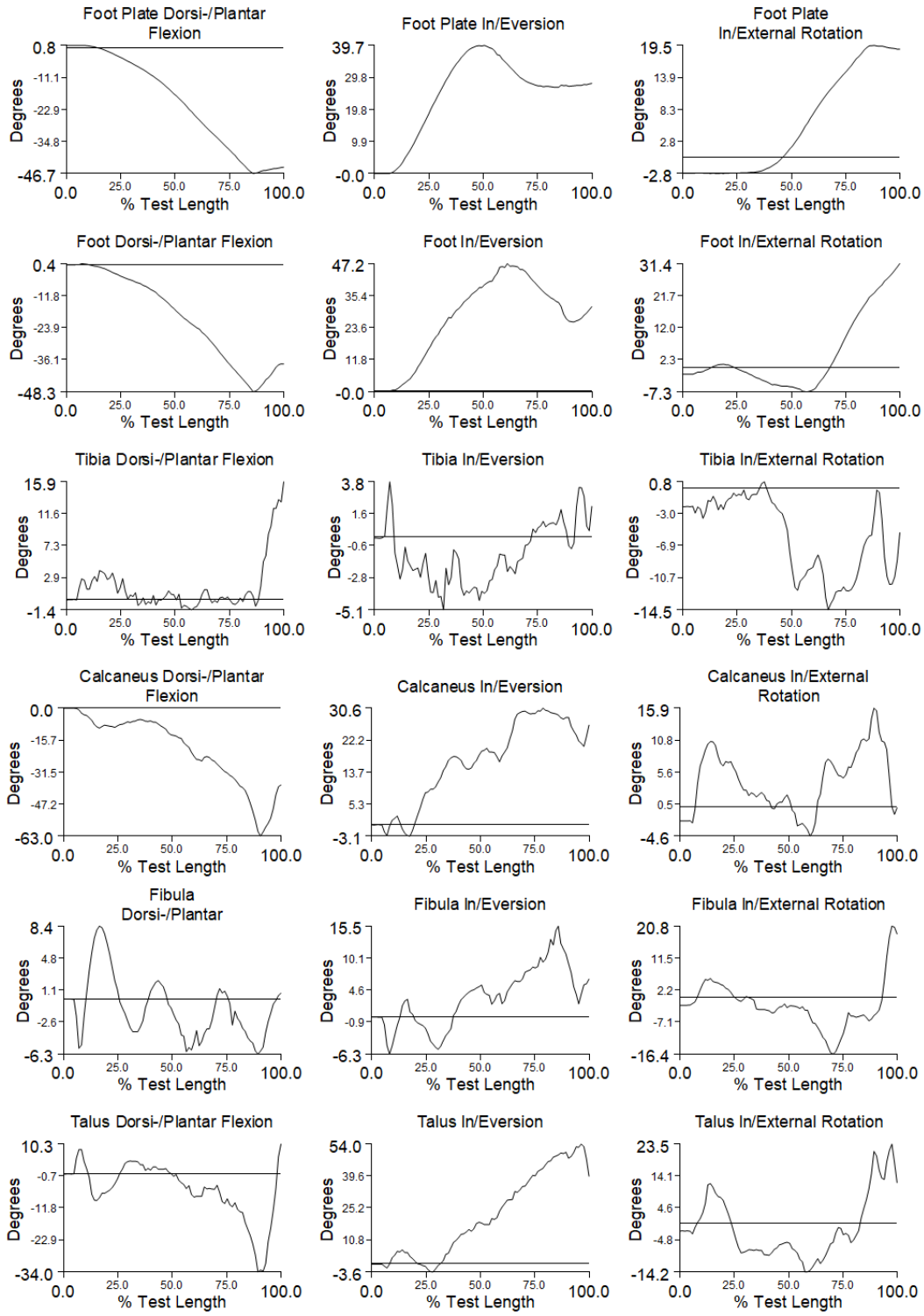

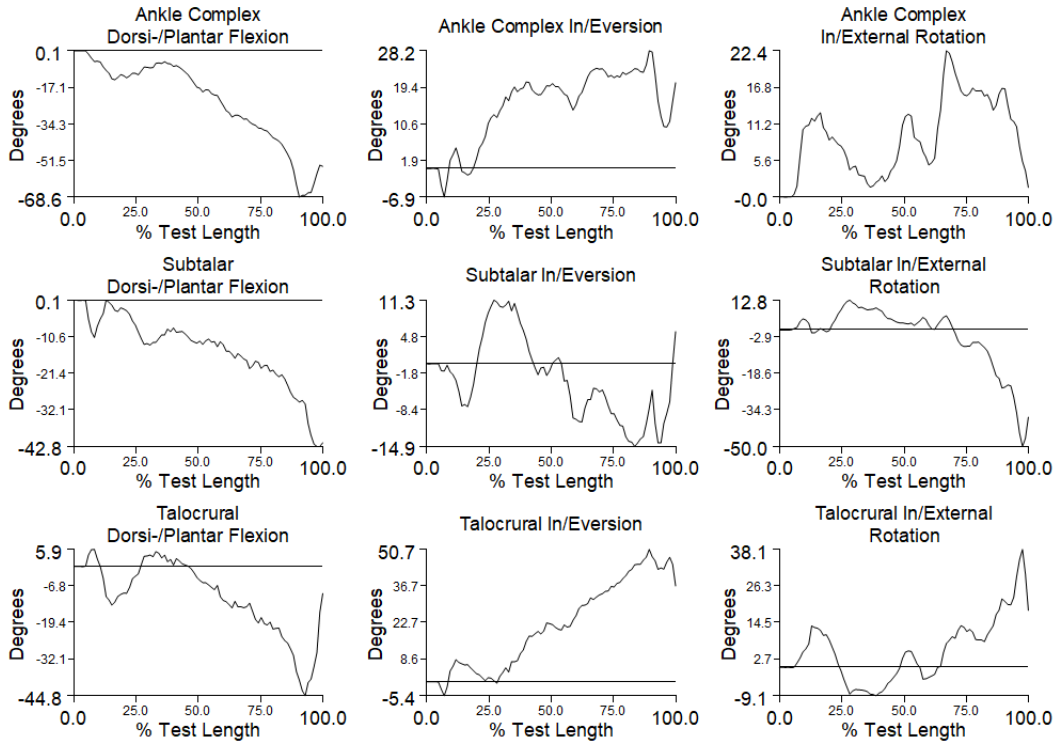

Appendix E.2. The biomechanical data output from Visual3D for the second trial of sample 2. Each column contains the data for a particular motion. The first column shows data for dorsi-/plantar flexion (dorsiflexion is positive), the second column inversion/eversion (inversion is positive) and the third column internal/external rotation (internal rotation is positive). Each row represents a section to be analysed. The first row is of the foot plate, the second is of the foot, the third is the tibia, the fourth is the calcaneus, the fifth is the fibula, the sixth is the talus, the seventh is the ankle complex, the eighth is the subtalar joint and the ninth is the talocrural joint.

Appendix F – Torque Adapter

F.1 Torque Adapter Assembly Drawing

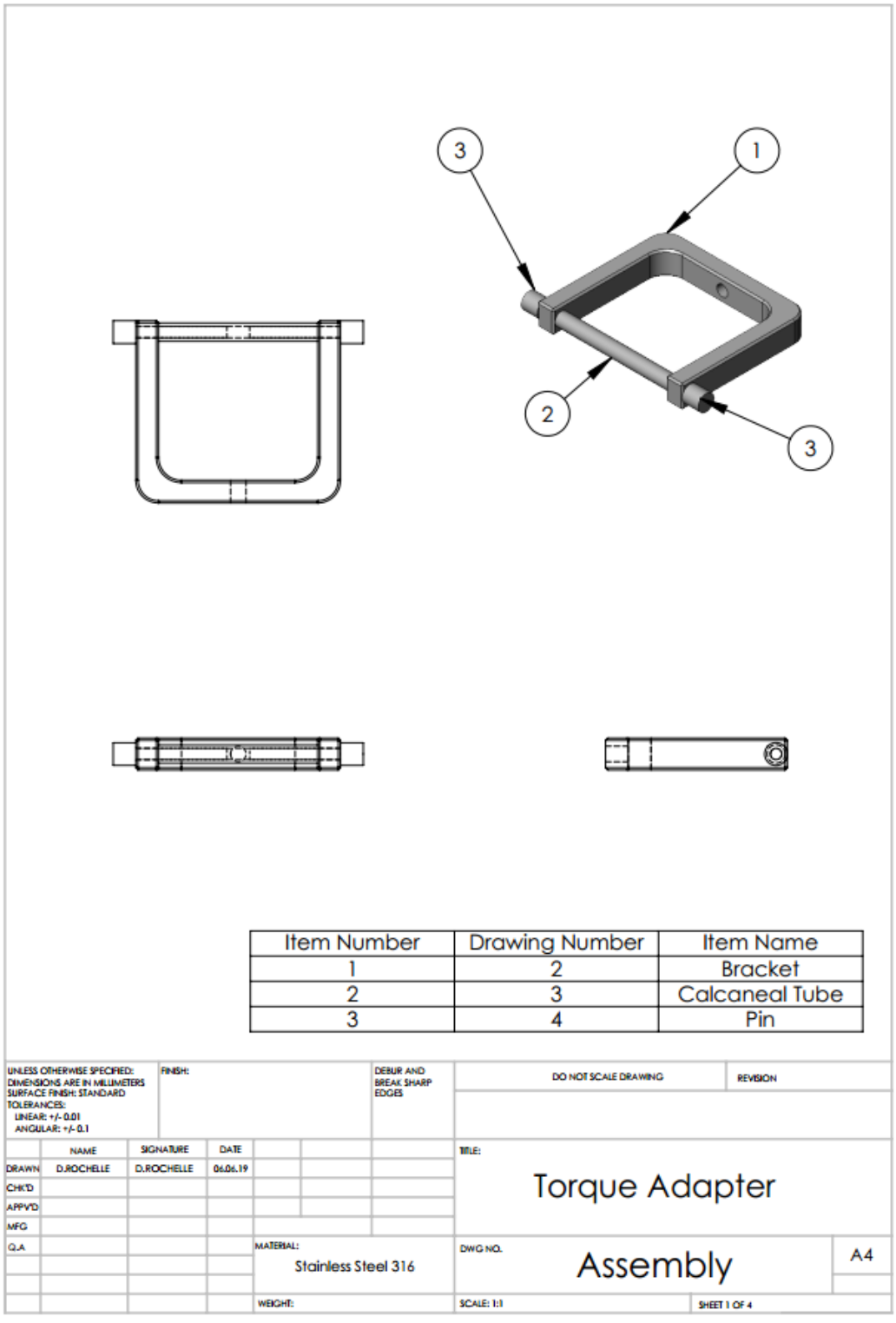

Item Number	Drawing Number	Item Name
1	2	Bracket
2	3	Calcaneal Tube
3	4	Pin

UNLESS OTHERWISE SPECIFIED: DIMENSIONS ARE IN MILLIMETERS SURFACE FINISH: STANDARD TOLERANCES: LINEAR: +/- 0.01 ANGULAR: +/- 0.1		FINISH:		DEBUR AND BREAK SHARP EDGES		DO NOT SCALE DRAWING	REVISION
	NAME	SIGNATURE	DATE			TITLE: Torque Adapter	
DRAWN	D.ROCHELLE	D.ROCHELLE	06.06.19				
CHK'D							
APPV'D							
MFG							
Q.A				MATERIAL: Stainless Steel 316		DWG NO. Assembly	A4
				WEIGHT:		SCALE: 1:1	SHEET 1 OF 4

F.2 Torque Adapter Bracket

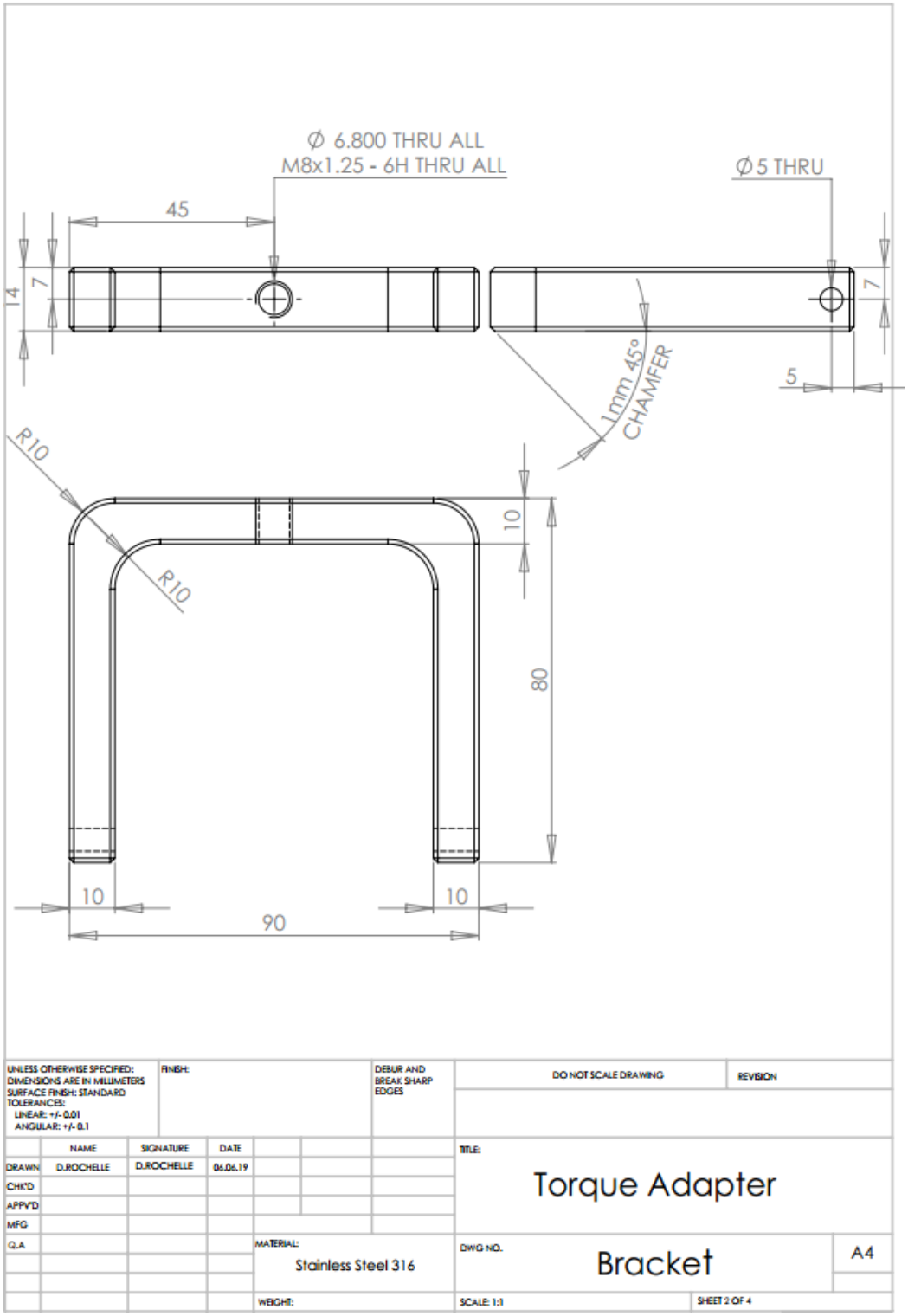

F.3 Torque Adapter Calcaneal Tube

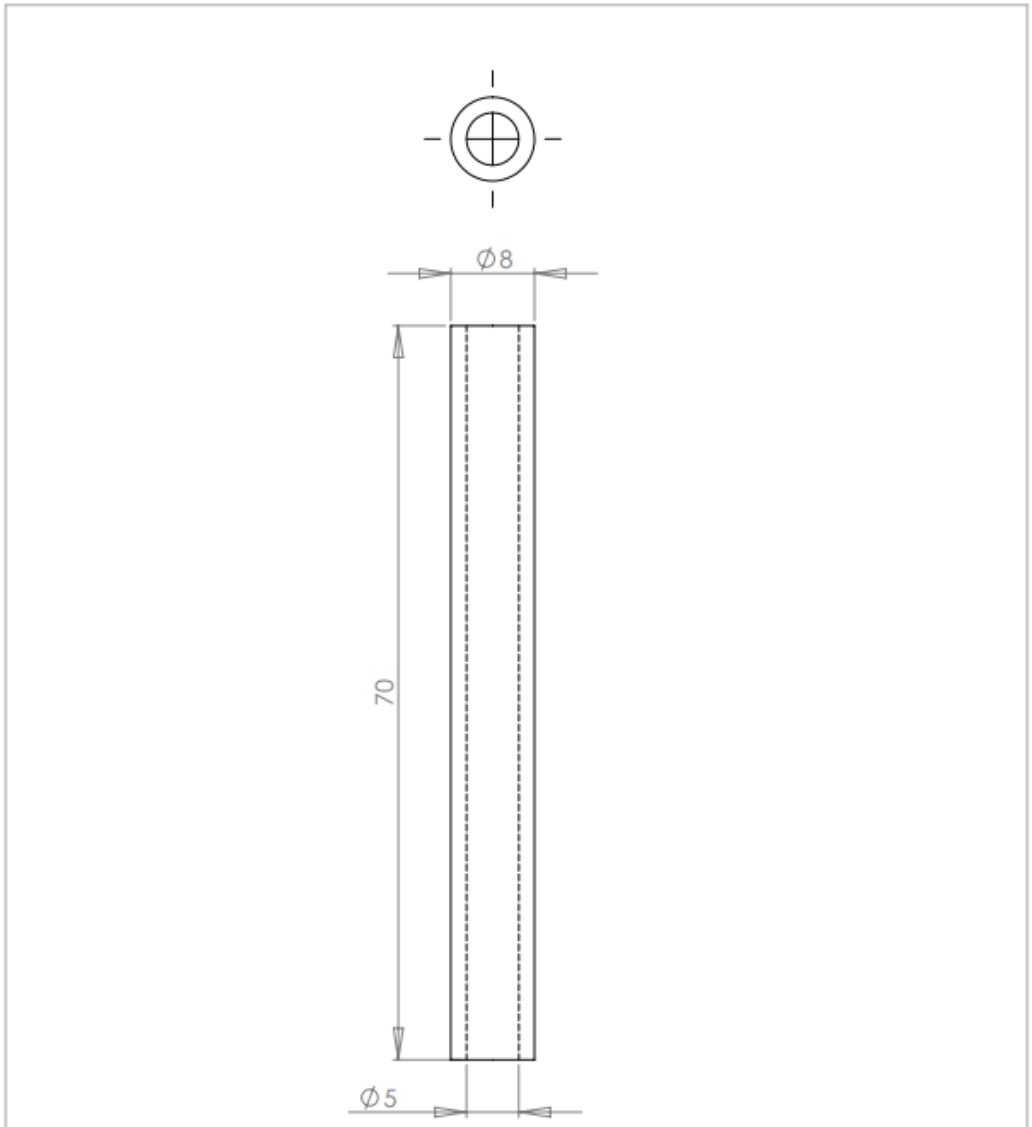

UNLESS OTHERWISE SPECIFIED: DIMENSIONS ARE IN MILLIMETERS SURFACE FINISH: STANDARD TOLERANCES: LINEAR: +/- 0.01 ANGULAR: +/- 0.1		FINISH:		DEBUR AND BREAK SHARP EDGES	DO NOT SCALE DRAWING	REVISION
	NAME	SIGNATURE	DATE		TITLE:	
DRAWN	D.ROCHELLE	D.ROCHELLE	06.06.19		Torque Adapter	
CHK'D						
APPV'D						
MFG						
Q.A				MATERIAL: Stainless Steel 316	DWG NO. Calcaneal Tube	A4
				WEIGHT:	SCALE: 2:1	SHEET 3 OF 4

F.4 Torque Adapter Pin

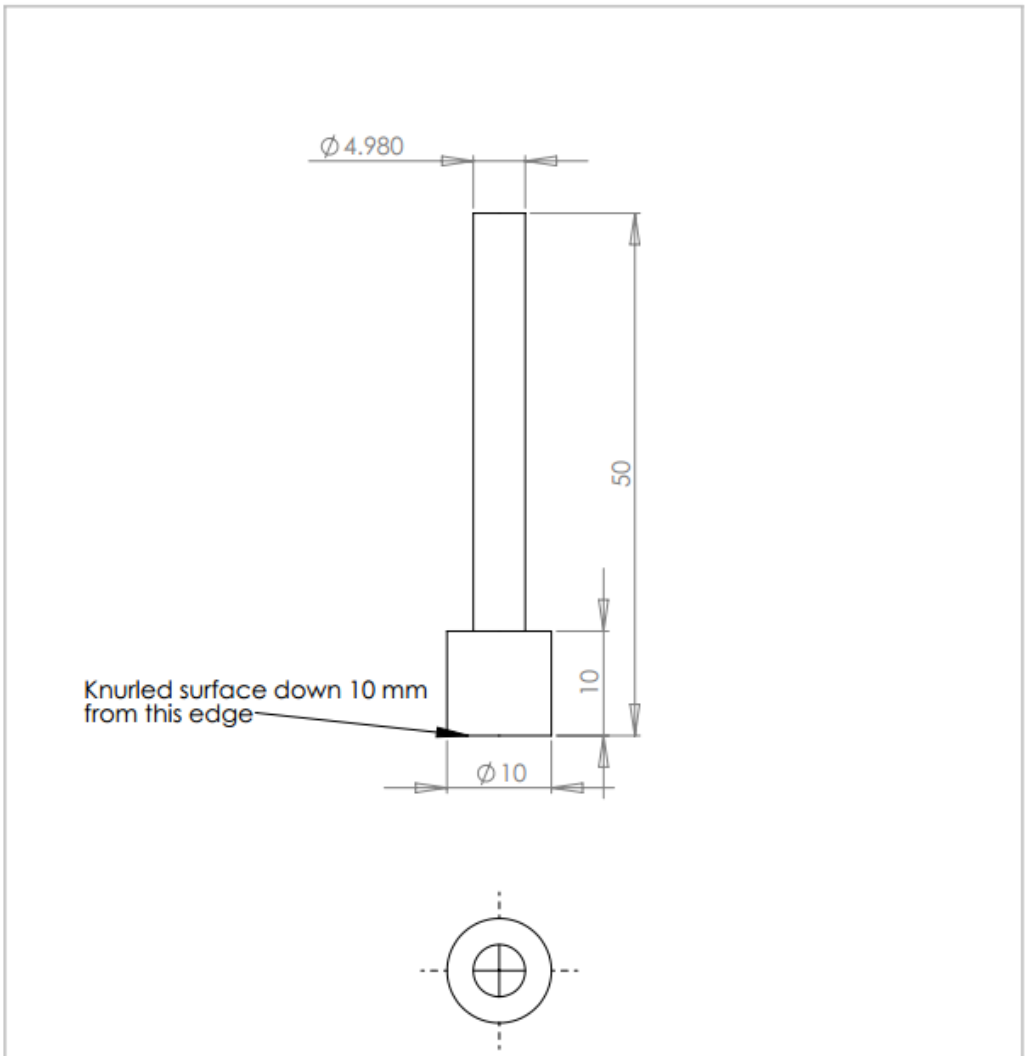

UNLESS OTHERWISE SPECIFIED: DIMENSIONS ARE IN MILLIMETERS SURFACE FINISH: STANDARD TOLERANCES: LINEAR: +/- 0.01 ANGULAR: +/- 0.1		FINISH:		DEBUR AND BREAK SHARP EDGES			DO NOT SCALE DRAWING	REVISION
	NAME	SIGNATURE	DATE				TITLE: Torque Adapter	
DRAWN	D.ROCHELLE	D.ROCHELLE	06.06.19					
CHK'D								
APPV'D								
MFG								
Q.A				MATERIAL: Stainless Steel 316			DWG NO. Pin	A4
				WEIGHT:			SCALE: 2:1	SHEET 4 OF 4

Appendix G – Arthrex White Papers

G.1 Arthrex White Paper 1

Knotted with FiberWire® #2 versus Knotless with FiberWire® #2 and Knotless with FiberTape® - A Biomechanical Study

Arthrex Research and Development

Objective

The purpose of this study was to evaluate and compare a knotted technique using FiberWire #2 to a knotless technique using either FiberTape or FiberWire #2.

Materials and Methods

Specimen Preparation:

Test blocs used in this study were made of two solid rigid polyurethane foam layers; the top layer had a density of 20 pcf and a height of 3 mm and the main layer had a density of 10 pcf and a height of 40 mm. All test blocs used in this study were prepared in the same way using a mallet and a punch as described in the surgical technique. Each surgeon performed three knotted procedures using 5.5 mm Corkscrews with their own preferred arthroscopic knots with FiberWire #2 and three knotless specimens using a 5.5 mm SwiveLock with either FiberTape or with FiberWire #2.

Mechanical Testing:

Surgeons prepared 205 specimens in total for testing (see Table 1). Testing blocs were secured to a dynamic tensile testing system (ElectroPuls E10000; Instron, UK) with the sutures attached to a hook on a metal rod (see Figure 1). Specimens were each preloaded at 5N at 1 mm/s to remove any initial slack. After preloading, each specimen was pulled to failure at a constant displacement rate of 1 mm/s. Max load was defined as the load at which the suture or eyelet failed. Point of failure was noted. Load over extension were recorded for each specimen and used to calculate load at 3 mm (termed clinical failure), max load and stiffness. Stiffness of each specimen was compared to the average construct stiffness evaluated from Burkhart et al. (2013) of 70N/mm [1].

Analysis:

Statistical analysis was performed using Sigma Plot Statistics for Windows, version 12.0 (Systat Software Inc., USA). Groups were compared using t-test. The significance level was set at P=0.05. Data analysis was performed with Matlab (R2015b, USA) for each set of data and the mean, standard deviation (std), confidence interval (C.I.), highest and lowest values were calculated.

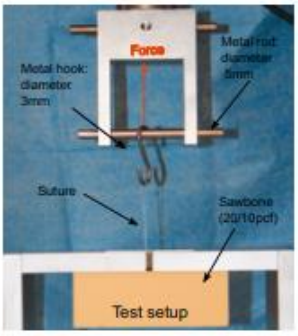

Figure 1: Test setup

Results

Technique		Load at 3mm (N)	Max Load (N)	Extension (mm)	Stiffness (N/mm)
Knotted FiberWire #2 N=105	C.I	54.0 - 64.6	132.7 - 168.9	11.1 - 14.5	24.1 - 27.3
	Mean	59.3	150.8	12.8	25.7
Knotless FiberWire #2 N=21	C.I	77.9 - 101.0	154.8 - 169.5	7.2 - 9.7	43.3 - 55.9
	Mean	89.5	162.2	8.5	49.6
Knotless FiberTape N=79	C.I	185.2 - 212.3	267.6 - 284.5	6.3 - 7.7	102.4 - 113.6
	Mean	198.7	276.1	7.0	108

Table 1: Overview for all results

Knotted FiberWire failed 62 percent of the time due to knot slippage, 36 percent due to suture rupture and less than 3 percent due to eyelet plane breakage. Knotless FiberWire mostly failed due to suture slippage as well and 10 percent of samples failed due to anchor pull-out. In the knotless FiberTape specimen, 79 percent of anchors were pulled out and other causes of failure were suture slippage and bone bloc failure. There was no statistical difference between knotted and knotless FiberWire regarding the average ultimate load (p=0.584). Differences between knotted and knotless FiberWire regarding the standard deviation were neither significant in clinical failure (p=0.693) nor extension (p=0.693). Regarding the standard deviation and mean load values of the knotless FiberTape samples, there were significant differences (all p<0.001).

Arthrex® Research

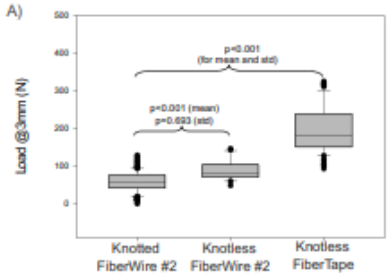

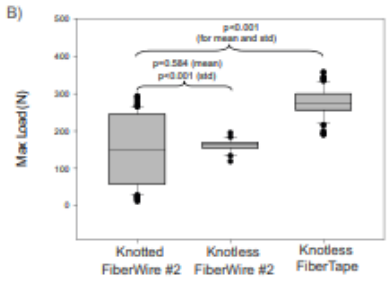

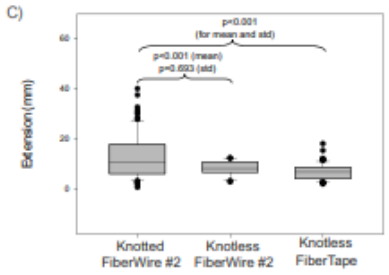

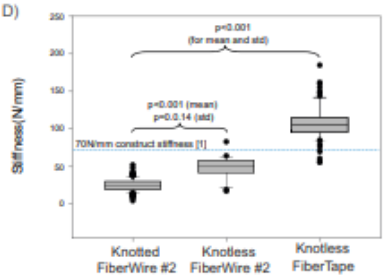

Figure 2:
Whisker bars plotted with black horizontal lines signify the median. The box extends from the 25th to the 75th percentiles, and the bars mark the 10th and 90th percentiles. Outliers are denoted as circles. For each technique the data are diagrammed for A) Mean load at 3 mm displacement B) Mean max load. C) Extension at max load and D) Stiffness.

Conclusion

Knotless technique using FiberTape withstood the highest load at clinical failure, showed the highest ultimate load in total, the least slippage and the greatest stiffness compared to all other constructs. Notably, unlike the other two techniques, the knotless anchor with FiberTape had a higher stiffness than the 70N/mm reference [1]. The ultimate load values of knotless FiberTape constructs were more consistent and therefore more reproducibility than the knotted technique which produced a large range of values. Considerable variations in knot strength between arthroscopic knots tied by surgeons is thought to be the reason for this [2].

Acknowledgments

Arthrex are grateful to the surgeons who took part in this study.

References

[1] S. B. Stephen, J. D. Patrick, K. John and H. T. Bryan, "Biomechanical Validation of Load-Sharing Rip-Stop Fixation for the Repair of Tissue-Deficient Rotator Cuff Tears," The American Journal of Sports Medicine, vol. 42, no. 457, 2013.

[2] T. H. Bryan, M. D. Jeffrey, S. Lillian, L. Walt and S. B. Stephen, "Knot Strength Varies Widely Among Expert Arthroscopists," The American Journal of Sports Medicine, vol. 42, no. 8, 2014.

Arthrex® Research

*Internal*Brace™ Ligament Augmentation: Biomechanical Testing of an Anterior Talofibular Ligament Repair, Insertion Order vs. SwiveLock Anchor Size

Arthrex Research and Development

Objective

The purpose of this study is to compare the maximum load and mode of failure of Broström anterior talofibular ligament (ATFL) repairs with *Internal*Brace Ligament Augmentation as a function of SwiveLock anchor size and insertion order in the fibula and talus.

Methods and Materials

Twelve matched pairs of fresh-frozen human cadaveric ankle specimens (average age=51±13 years) were used. The ATFL was isolated during specimen dissection and the *Internal*Brace Ligament Augmentation construct was performed by Nicholas T. Gates, MD (Edgewood, KY). A medial to lateral hole was drilled through the distal fibula, proximal to the lateral malleolus and the fibula was shortened to facilitate loading in the material testing machine. The repairs were then isolated by releasing the ATFL.

All repairs were performed using one 3.5 mm BioComposite SwiveLock and one 4.75 mm BioComposite SwiveLock (AR-2325BCC and AR-2324BCC, respectively) and the appropriate drills and taps found in Implant System, *Internal*Brace Ligament Augmentation Repair (AR-1678-CP). The repairs were categorized into one of four groups as presented in Table 1.

Table 1: Test Group Description

Testing Group Summary			
Group	**Talus Anchor Size (mm)**	**Fibular Anchor Size (mm)**	**Inserted First**
Group 1a	4.75	3.5	Fibula
Group 1b	4.75	3.5	Talus
Group 2a	3.5	4.75	Fibula
Group 2b	3.5	4.75	Talus

Following repair, each sample was strapped to a custom designed jig which held the foot in 20º of inversion and 10º of plantar flexion to simulate worst-case mechanical loading. A set screw was turned into the superior portion of the heel to prevent lift during testing and the fibula was secured to an INSTRON ElectroPuls Dynamic Testing System (INSTRON, Canton, MA) via the fibula drill hole using a clevis/pin fixture, Figure 1.

After preloading, each sample was pulled to failure at a rate of 20 mm/min. A two-way ANOVA was performed to identify any statistically significant differences in maximum load with respect to insertion order and anchor size, (α=0.05).

Figure 1: Complete testing setup

Results

The average maximum load for each group is presented in Table 2 and illustrated in Figure 2. The results of the two-way ANOVA indicated that the order in which anchors were implanted did not significantly influence maximum load (p=0.722). Additionally, a significant difference was noted in anchor size. Constructs with 4.75 mm anchors in the fibula had significantly higher maximum loads than those implanted with the 3.5 mm anchors (p=0.001). No significant interaction existed between anchor size and insertion order (p=0.156). Each of these four test groups provide maximum load values above that of native ligament (154N) and studied Broström repairs (68N & 79N). [1,2]

Table 2: Average Maximum Load Results to Failure

Tensile Testing Results Summary		
Group	**Maximum Load [N] avg ± std dev**	**Mode of failure (# of occurences)**
Group 1a: 3.5FA, 4.75TA, FF	241.57 ± 127.15	Eyelet pull-out from fibula (1), anchor pullout/suture slip from fibula (2), suture pull-out from fibula (3)
Group 1b: 3.5FA, 4.75TA, TF	181.13 ± 63.14	Anchor pull-out/suture slip from fibula (1), suture slip from fibula (5)
Group 2a: 4.75FA, 3.5TA, FF	314.67 ± 50.56	Anchor pull-out/suture slip from talus (2), suture slip from talus (2), suture slip from fibula (1), suture slip from both (1)
Group 2b: 4.75FA, 3.5TA, TF	352.31 ± 57.61	Suture slip from fibula (3), suture pull-out from talus (1), eyelet pull-out from talus (1), anchor slip from fibula (1)

Figure 2: Average Maximum Load per Group

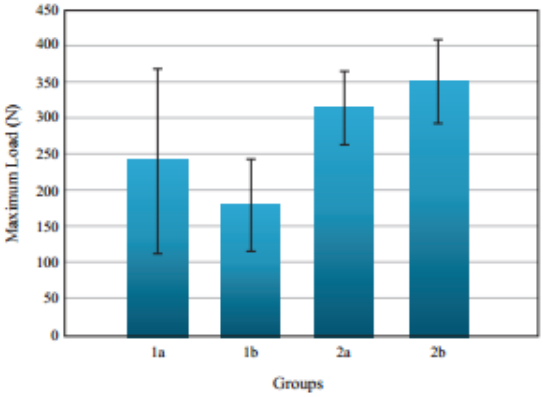

Conclusion

Insertion order did not significantly influence maximum load. Additionally, each of the constructs and insertion protocols tested in the current study demonstrated maximum load values comparable or higher than those found for native ligament (154N) and previously studied Broström repairs (68N & 79N). [1,2] Suture slip/pull-out contributed to 87.5% of the observed failures as compared to eyelet/anchor pull-out, 33%. Bone avulsion did not contribute to construct failure.

References

1. Waldrop III NE, Wijdicks CA, Jansson KS, LaPrade RF, Clanton TO. Anatomic suture anchor versus the broström technique for anterior talofibular ligament repair. *Amer. J. Sports Med.* 2012;40(11):2590 – 6.

2. Viens NA, Wijdicks CA, Campbell KJ, LaPrade RF, Clanton TO. Anterior talofibular ligament ruptures, part 1: biomechanical comparison of augmented broström repair techniques with the intact anterior talofibular ligament. *Amer. J. Sports Med.* 42(2):405 – 411.

Arthrex *Internal*Brace™ Ligament Augmentation Versus Smith & Nephew Knotless Constructs for Lateral Ankle Repairs

Troy Watson, MD, and Arthrex Research and Development

Objective

Determine the biomechanical differences on lateral ankle repair between an Arthrex *Internal*Brace ligament augmentation and a Smith & Nephew construct.

Methods and Materials

Five matched pairs of cadaver ankles were used for this testing (average age = 57 years; all male). The specimens were dissected to expose the lateral ankle joint. The tibias were removed, and an 8 mm hole was drilled through the fibula, proximal to the lateral malleolus.

All repairs were performed by Troy Watson, MD. Group 1 repairs were performed using SwiveLock® anchors, FiberTape® suture, and instrumentation contained in Arthrex's *Internal*Brace Repair Kit (AR-1688-CP). Group 2 repairs were performed with Smith & Nephew's Healicoil and Bioraptor™ anchors, Ultratape, and instrumentation. The implants for all groups were inserted according to published surgical techniques with the recommended instrumentation. All other soft tissue connecting the fibula to the talus was transected.

Mechanical testing was performed using an Instron®* machine with a 10 kN load cell. Samples were mounted on custom jigs designed to hold the foot in 20° of inversion and 10° of plantar flexion. A dowel pin was inserted through the 8 mm fibular hole to allow for superiorly directed loads to be applied to the repair, as shown in Figure 1. Samples were loaded to failure in tension at 20 mm/min.

Figure 1. Sample prepared for mechanical testing

*Instron is a registered trademark of Illinois Tool Works Inc

Results

The ultimate load of the Arthrex *Internal*Brace construct was 249 ± 47 N, and the ultimate load of the Smith & Nephew constructs was 90 ± 17 N. A paired *t* test was performed to compare differences between the 2 sample groups. The ultimate load of the Arthrex construct was significantly greater than that of the Smith & Nephew construct ($P = .001$). The results are shown in Figure 2.

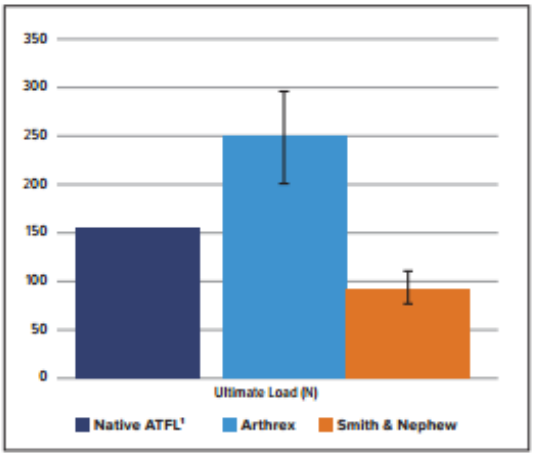

Figure 2. Mechanical testing results

Conclusions

We conclude that the Arthrex *Internal*Brace construct is biomechanically superior to the Smith & Nephew construct. At time zero, the Smith & Nephew construct offers significantly less strength than that of the native ATFL and Arthrex *Internal*Brace, 154 N and 250 N, respectively.[1,2] The lack of strength of the Smith & Nephew repair draws into question its validity as a solution to lateral ankle instability.

References

1. Viens NA, Wijdicks CA, Campbell KJ, LaPrade RF, Clanton TO. Anterior talofibular ligament ruptures, part 1: biomechanical comparison of augmented Broström repair techniques with the intact anterior talofibular ligament. *Am J Sports Med.* 2014;42(2):405-411. doi:10.1177/0363546513510141
2. Waldrop NE, Wijdicks CA, Jansson KS, LaPrade RF, Clanton TO. Anatomic suture anchor versus the Broström technique for anterior talofibular ligament repair: a biomechanical comparison. *Am J Sports Med.* 2012;40(11):2590-2596. doi:10.1177/0363546512458420

www.arthrex.com

Appendix H – Author's Journal Article

journal of the mechanical behavior of biomedical materials 102 (2020) 103473

Contents lists available at ScienceDirect

Journal of the Mechanical Behavior of Biomedical Materials

journal homepage: http://www.elsevier.com/locate/jmbbm

Mechanical characterisation of the lateral collateral ligament complex of the ankle at realistic sprain-like strain rates

David Christopher Rochelle [a,*], Anthony Herbert [a], Ioannis Ktistakis [b], Anthony Charles Redmond [c,d,e], Graham John Chapman [c,d,f], Claire Louise Brockett [a,d]

[a] Institute of Medical and Biological Engineering, University of Leeds, Leeds, LS2 9JT, UK
[b] Chapel Allerton Hospital, Chapeltown Road, Leeds, LS7 4SA, UK
[c] Institute for Rheumatic and Musculoskeletal Medicine, University of Leeds, Leeds, UK
[d] National Institute for Health Research (NIHR) Leeds Biomedical Research Centre, Leeds, UK
[e] Arthritis Research UK Centre for Sports, Exercise and Osteoarthritis, Nottingham, Oxford, Loughborough, Leeds, UK
[f] School of Sport and Health Sciences, University of Central Lancashire, Preston, PR1 2HE, UK

ARTICLE INFO

Keywords:
Characterisation
Ankle
Ligament
Sprain

ABSTRACT

Background: Synthetic interventions continue to evolve with the progression made in materials science, surgical technologies and surgical methods. To facilitate the evolution of synthetic devices for lateral ankle repair a better understanding of the mechanical properties and failure mechanisms of the lateral collateral ligament (LCL) complex is required. This study aimed to improve understanding of the mechanical properties and failure modes of the LCL complex at strain rates representative of sprain.

Method: The LCLs were dissected from six human cadavers to produce individual bone-ligament-bone specimens. A mechanical testing device uni-axially loaded the ligaments in tension. Initially, preconditioning between 2 N and a load value corresponding to 3.5% strain was conducted for 15 cycles, before extension to failure at strain rate of 100%.s^{-1}. The results were stratified by age, weight and body mass index (BMI) to explore potential correlations with ligament ultimate failure load or ligament stiffness.

Results: The mean ultimate failure loads and the 95% confidence intervals for the ATFL, calcaneofibular (CFL) and posterior talofibular (PTFL) ligaments were 263.6 ± 164.3 N, 367.8 ± 79.8 N and 351.4 ± 110.8 N, respectively. A strong positive Pearson correlation was found between BMI and ultimate failure load of the CFL ($r = 0.919$; $P = .01$). A non-significant relationship was found between the mechanical properties and both age and weight. The ATFL avulsed from the fibula four times, the CFL avulsed from the fibula twice, the PTFL avulsed from the talus twice and all remaining failures were mid-substance.

Conclusion: The results identify the forces required to induce failure of the individual ligaments of the LCL complex and the related failure modes of individual ligaments. A correlation may exist between BMI and the ultimate failure load of the CFL and PTFL, although a greater sample size is required for confirmation.

1. Introduction

The lateral collateral ligament (LCL) complex of the ankle (see Fig. 1), consists of the anterior talofibular ligament (ATFL), calcaneofibular ligament (CFL) and posterior talofibular ligament (PTFL). The LCLs of the ankle are collectively responsible for the stabilisation of the talocrural joint on the lateral side and the CFL also plays a role in the stabilisation of the subtalar joint.

The ATFL is the most frequently injured LCL in a typical lateral ankle sprain, followed by the CFL and finally the PTFL (Attarian et al., 1985; Siegler and Schneck, 1988). In cases of severe sprain or in people, such as elite athletes, wherein whom restoration of stability is important, surgical stabilisation may be performed. The current preferred standard is the Broström-Gould procedure in which ruptured ligaments are stabilised with sutures. If this approach is inadequate or has failed or if the patient has an increased BMI, general ligament laxity or is a high-demand athlete, then stabilisation with synthetic ligaments may be attempted (Ajis et al., 2006).

Abbreviation: ATFL, Anterior talofibular ligament; CFL, Calcaneofibular ligament; LCL, Lateral collateral ligament; PTFL, Posterior talofibular ligament.

* Corresponding author.
E-mail address: mndcr@leeds.ac.uk (D.C. Rochelle).

https://doi.org/10.1016/j.jmbbm.2019.103473
Received 3 June 2019; Received in revised form 2 September 2019; Accepted 2 October 2019
Available online 5 October 2019
1751-6161/

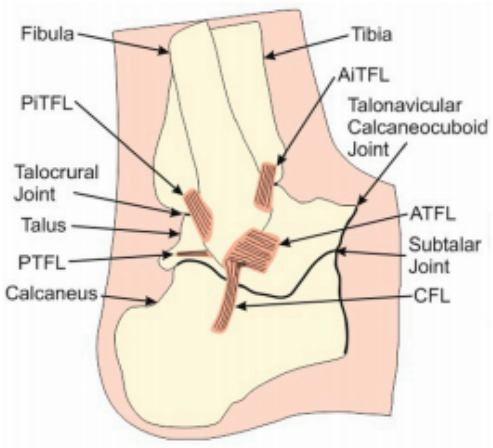

Fig. 1. Lateral view of the ankle highlighting the LCL complex (ATFL, CFL & PTFL), the syndesmosis (AiTFL & PiTFL), the talocrural joint, the subtalar joint, the talonavicular calcaneocuboid joint and the bones of the ankle (fibula, tibia, talus and calcaneus).

Natural ligaments exhibit a viscoelastic response to strain, starting with a progressively stiffer nonlinear toe region followed by a linear loading region. The response of ligamentous tissue is believed to be strain rate dependent due to the inherent viscoelastic nature of the tissue (Bonner et al., 2015). This viscoelasticity causes ligaments to display hysteresis, due to the fluid component of the ligament being redistributed and balanced by the stress carried by the solid component of the ligament. When the lateral collateral ligament of the knee was tested at strain rates greater than 100%.s^{-1}, a strain rate representative of inducing sprain in real-world events, it was found that the strain-rate dependency of the ligament can be neglected as there is insufficient time for appreciable ligament relaxation (Bonner et al., 2015). The ligaments of the ankle have been reported to be generally insensitive to strain rate (Funk et al., 2000). Conversely, the mechanical properties of the LCLs have been reported to be significantly affected by strain rates both above and below 100%.s^{-1} (Attarian et al., 1985).

Research articles detailing the mechanical characteristics of the LCL complex are scarce (Attarian et al., 1985; Funk et al., 2000; Siegler and Schneck, 1988; St Pierre et al., 1983). None of the previous papers report mechanical characteristics of the LCL complex tested at realistic sprain-like strain rates. Attarian et al. (1985) and Funk et al. (2000) characterised the LCL complex at strain rates considerably higher than those which occur during a sprain event (Attarian et al., 1985; Funk et al., 2000). Although ligaments are considered relatively insensitive to strain rates over 100%.s^{-1} the effect on the failure mode of the ligaments is not understood. The absence of literature on this topic is potentially due to the difficulty faced when gripping ankle ligament tissue, as previously reported (Siegler and Schneck, 1988). A lack of published work in this area has hindered the understanding of the mechanical requirements and failure modes of synthetic interventions for lateral ankle sprain.

This study aimed to improve understanding of the mechanical properties and failure modes of the LCL complex at strain rates representative of real-world sprain events.

2. Materials and Methods

2.1. Samples

Six fresh frozen human cadaveric feet, sourced from MedCure (USA), were used in the study. Ethical approval was granted by the University of Leeds Research Ethics Committee (MEEC 15–020). Exclusion criteria for the tissues included a reported prior lower limb trauma or surgery, or a history of diabetes. The mean (±95% confidence intervals) donor age was 56.2 ± 12.2 years, BMI was 22.3 ± 2.9 kg m^{-2} (normal) and there were three males and three females. A summary of donor information is shown in Table 1.

2.2. Sample Preparation

The feet were stored in a −80 °C freezer, compliant with the Human Tissue Act, until they were tested. Samples were thawed for 48 h at 4 °C in a refrigerator prior to dissection. After at least 24 h of thawing, each foot was imaged, at a resolution of 82 μm, using a SCANCO Medical xtreme CT scanner (SCANCO Medical, Brüttisellen, Switzerland). Each scan lasted approximately 90 min and was performed to ensure no major undiagnosed damage was present.

The LCL complex was dissected intact from each foot while preserving the syndesmosis joint for future study, as shown in Figs. 2 and 3. Firstly, all fascia and soft tissue were dissected from around the ankle by a foot and ankle specialist consultant orthopaedic surgeon. Next, the forefoot was removed by transecting along the talonavicular calcaneocuboid joint. Using an oscillating bone saw, a sagittal cut was made through the entirety of the calcaneus and talus, as shown in Fig. 2, Panel B. The lateral ankle complex was then removed by a transverse cut through the fibula, separating the LCL complex from the syndesmosis, as shown in Fig. 2, Panel C. The cut was made from in-between the attachment points of the ATFL and anterior inferior talofibular ligament (AiTFL) to in-between the attachment points of the PTFL and posterior inferior talofibular ligament (PiTFL). The talus was then split in half with a coronal cut creating an anterior and posterior bone attachment segment for the ATFL and PTFL, respectively. Finally, the calcaneus was reduced in size and shaped to fit within the gripping fixture by performing two parallel coronal cuts either side of the attachment point and one transverse cut distally to the attachment point, as shown in Fig. 3. The tissue hydration level of the ankle complex was maintained by wrapping the complex in phosphate-buffered saline (PBS) soaked paper towel (Herbert et al., 2016).

Post-dissection ligament lengths were measured using Vernier callipers with the ligaments orientated in line with their collagen fibres and the slack in the ligament was removed by hand. The ligaments were measured once, from the centre of one insertion to the centre of the other.

2.3. Testing Protocol

Each ligament of the LCL complex was tested individually whilst the complex was kept intact. The CFL was characterised first, then the ATFL followed by the PTFL. Tissue rehydration was performed to ensure the viscoelastic nature of ligaments could act efficiently during the testing. Immediately before the characterisation of the CFL, the complex was

Table 1
Tissue donor demographic details. The mean and 95% confidence interval (CI) is given for age, weight and body mass index (BMI). (M – male, F – female, A.A – African American, C – Caucasian, R – right & L – left).

Sample	Age (years)	Sex	Race	Weight (kg)	BMI (kg. m^{-2})	L/R Foot
1	72	M	A.A	71	22.4	R
2	60	F	C	53	18.9	L
3	49	F	C	49	20.9	R
4	61	M	C	66	21.4	R
5	38	M	C	85	27.0	L
6	57	F	C	61	23.2	R
Mean	56.2	–	–	64.1	22.3	–
± CI	± 12.2			± 13.8	± 2.9	

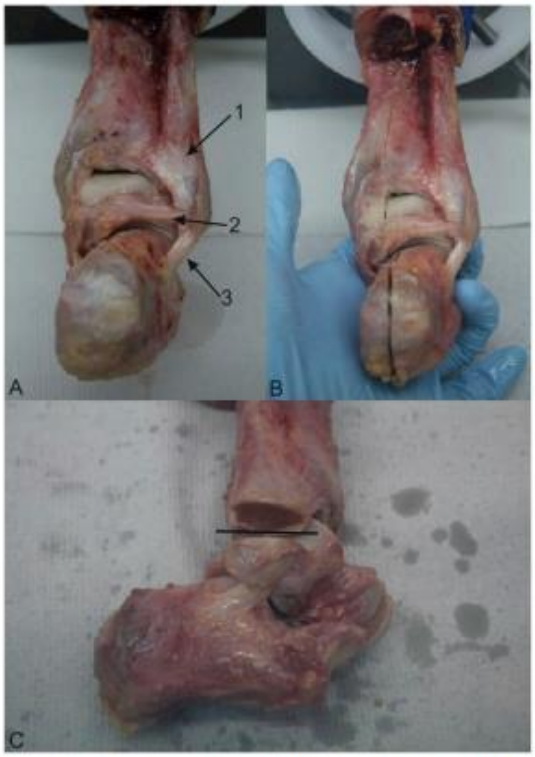

Fig. 2. The dissection protocol employed to remove the LCL complex from the rearfoot. A illustrates the intact rearfoot and provides a clear view of the PiTFL (1), PTFL (2) and CFL (3). B illustrates the sagittal cut made to separate the medial and lateral aspects of the rearfoot. C illustrates the transverse cut (black line) made through the fibula to separate the LCL complex and syndesmosis.

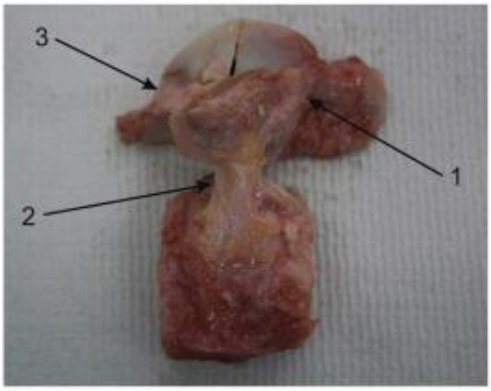

Fig. 3. The LCL complex fully dissected prior to testing. The coronal cut into talus has been performed, creating separate bone pieces for the ATFL and PTFL, and the calcaneus has been shaped to fit within the bespoke testing grip. The ATFL (1), CFL (2) and PTFL (3) are shown.

submerged in PBS for 30 min. The complex was then submerged for 15 min prior to testing the ATFL and a further 15 min prior to testing the PTFL due to the short length of time taken for each test. Testing the individual ligaments as an intact complex was facilitated by a bespoke gripping fixture. The bone segments at each end of the ligaments were fixed within the gripping fixture using six gripping bolts for each bone attachment segment ensuring collagen fibre alignment, as shown in Fig. 4.

The mechanical characterisation was performed using an Instron ElectroPuls E10000, with a 1 kN load cell (Instron, Buckinghamshire, UK). A floating joint was used to attach the top grip to the Instron to correct for any unintended malalignment within the setup.

Preconditioning was completed to ensure specimens were in an appropriate physiological state of readiness prior to failure testing and fluid redistribution had occurred within the specimens (Quinn and Winkelstein, 2011). Fifteen cycles of preconditioning following a sinusoidal waveform, ranging between 2 N and a load value corresponding to 3.5% strain, were performed at a frequency of 0.83 Hz. The 3.5% strain value represents the minimum amount of strain accumulated by any of the LCLs during one step of a normal walking cycle (10° dorsiflexion through to 20° plantarflexion) (Colville et al., 1990). The preconditioning load values representing 3.5% strain were determined in a preliminary test of each ligament tested under strain control at a rate of 10%.s^{-1}. The frequency of 0.83 Hz is equivalent to the rate of normal walking (approximately one full gait cycle per second).

Following preconditioning, the specimens were then ramp loaded to failure at a strain rate of 100%.s^{-1}. A strain rate of 100%.s^{-1} was selected to be representative of sprain, having previously been suggested to be a suitable injury strain rate for anterior cruciate ligament injury (Blevins et al., 1994). The following equation, incorporating real-world inputs, also suggests that a strain rate of 100%.s^{-1} is appropriate to replicate ankle ligament sprain.

$$\dot{\varepsilon} = \frac{\Delta L}{Lt}$$

where $\dot{\varepsilon}$ is the strain rate, ΔL is the change in length of the ATFL from neutral position to maximum plantarflexion (4.5 mm), (de Asla et al., 2009) L is the length of the ATFL in the neutral position (16.3 mm) (de Asla et al., 2009) and t is the time taken for the sprain motion of an ankle (0.3 s) (Fong et al., 2009).

2.4. Data Analysis

The mode of failure was determined via physical and visual examination of the specimens. Any specimens where the ligament had torn away from bone, torn cartilage away from bone or torn a small fragment

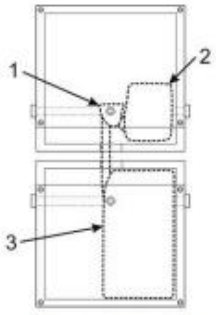

Fig. 4. The LCL complex fixed into the bespoke gripping fixture with the CFL prepared for characterisation. The ATFL and PTFL, and their bony attachments from the fibula (1) to the talus (2) are within the top pot and the calcaneus (3) is within the bottom pot.

of bone away from bone were categorised as an avulsion. Any intra-ligamentous failures were defined as mid-substance failures. After the experimental testing, post-processing was completed to calculate the ultimate failure load and stiffness of each ligament from each donor. The linear stiffness value (k1) was calculated using a custom Matlab algorithm (Herbert et al., 2016).

Mean values and 95% confidence intervals for the ligament ultimate failure load, stiffness and length, as well as the donor BMI, weight and age were calculated for the ATFL, CFL and PTFL. A repeated measures ANOVA with a Greenhouse-Geisser correction ($p < .01$) was performed to calculate any significant differences in ultimate failure load or stiffness between the ATFL, CFL and PTFL. Analysis of the data stratified by age, weight and BMI was performed to identify any potential correlations with these patient-specific factors and both ultimate failure load and stiffness. Correlations were calculated for the ATFL, CFL and PTFL individually using a two-tailed Pearson correlation test ($p < .01$).

3. Results

The post-dissection ligament lengths used to calculate the ligament specific preconditioning limits are provided in Table 2. The CFL was the longest of the three ligaments forming the LCL complex, with mean (±95% CI) length of 20.0 ± 1.9 mm. The PTFL and ATFL followed in order but were similar in length with mean lengths of 13.4 ± 3.2 mm and 12.6 ± 0.9 mm, respectively.

The mechanical characterisation results for the ATFL, CFL and PTFL are shown in Table 3. The CFL had the highest mean ultimate failure load (±95% CI) of 367.8 ± 79.8 N followed by the PTFL 351.4 ± 110.8 N, while the ATFL was the weakest 263.6 ± 164.3 N. No significant differences were found for the ultimate failure load ($p = .24$) or stiffness ($p = .30$) between the ATFL, CFL and PTFL.

The ratio of avulsions to mid-substance failures was similar for the ligament types tested, as detailed in Table 3. The ATFL avulsed from the fibula in four of the six tests, the CFL avulsed from the fibula in two of the six tests and the PTFL avulsed from the talus in two of the six tests. No systematic differences in ultimate failure load or stiffness were identified between the different failure modes. When avulsion did occur, the site of avulsion was consistent amongst ligament types (see Table 3). Fig. 5A and B illustrate clear examples of a mid-substance failure and avulsion, respectively.

The correlation results for the ultimate failure load and stiffness to the patient-specific factors: BMI, weight and age are presented in Table 4. The ultimate failure load of the CFL was found to have a significant strong positive Pearson correlation with BMI ($r = 0.92$; $p = .01$). The ultimate failure load of the ATFL and PTFL had non-significant Pearson correlation scores ($r = 0.18$; $p = .73$ and $r = 0.65$; $p = .16$, respectively). A non-significant relationship was found for both age and weight with relation to both the ultimate failure load and stiffness of the ATFL, CFL and PTFL. Any relationship identified between BMI and stiffness of the ATFL ($r = -.05$; $p = .92$), CFL ($r = 0.22$; $p = .68$) and PTFL ($r = -0.01$; $p = .98$) was also negligible.

The ultimate failure load results of the ATFL, CFL and PTFL are plotted against BMI in Fig. 6 with the results for all three ligaments of each donor aligned vertically according to the donor's BMI. There is no evidence of a systematic tendency for the ultimate failure load to vary by ligament type either within or between donors.

Table 2
Ligament lengths (mm) for each individual ligament and the mean ligament length and 95% confidence intervals (CI) for ATFL, CFL and PTFL.

Sample	ATFL	CFL	PTFL
1	11.62	17.60	10.50
2	11.76	20.66	14.66
3	12.90	19.24	10.54
4	13.50	23.00	18.34
5	12.08	20.06	14.80
6	13.54	19.66	11.66
Mean ± CI	12.6 ± 0.9	20.0 ± 1.9	13.4 ± 3.2

Table 3
The mean and 95% confidence intervals (CI) for the ultimate failure load and stiffness results of the ATFL, CFL and PTFL. As well as the failure mode (A – avulsion and M – mid-substance) and avulsion location.

	ATFL	CFL	PTFL
Mean Ultimate Failure Load ± CI (N)	263.6 ± 164.3	367.8 ± 79.8	351.4 ± 110.8
Mean Stiffness ± CI (N/mm)	44.7 ± 16.6	45.8 ± 19.0	59.0 ± 10.7
Failure Mode (A/M)	4/2	2/4	2/4
Avulsion Site	Fibula	Fibula	Talus

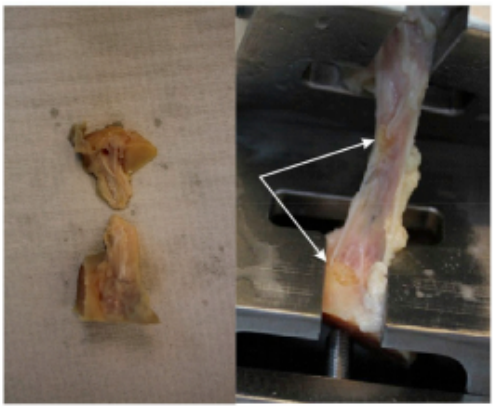

Fig. 5. A) A mid-substance failure where intra-ligamentous failure has occurred. **B)** An avulsion failure where a fragment of bone has avulsed from the bone surface (white arrows).

Table 4
The correlation (r-value) and respective significance (p-value) of both ligament ultimate failure load and ligament stiffness against the patient-specific factors (PSF): BMI, weight and age.

Ligament Property		PSF	r-value	p-value
Failure Load	ATFL	BMI	.184	.727
	CFL	BMI	.919[a]	.010
	PTFL	BMI	.650	.162
	ATFL	Weight	.516	.395
	CFL	Weight	.874	.023
	PTFL	Weight	.327	.527
	ATFL	Age	.560	.248
	CFL	Age	-.273	.600
	PTFL	Age	-.496	.317
Stiffness (k1)	ATFL	BMI	-.052	.922
	CFL	BMI	.216	.681
	PTFL	BMI	-.013	.981
	ATFL	Weight	.176	.738
	CFL	Weight	.410	.419
	PTFL	Weight	.000	.999
	ATFL	Age	.750	.086
	CFL	Age	-.397	.436
	PTFL	Age	-.340	.510

[a] Indicates result is significant at the .01 level (two-tailed).

4. Discussion

The aim of this study was to improve understanding of the mechanical properties and failure modes of the LCL complex when strained at a rate representative of ankle sprain events in real-life. The

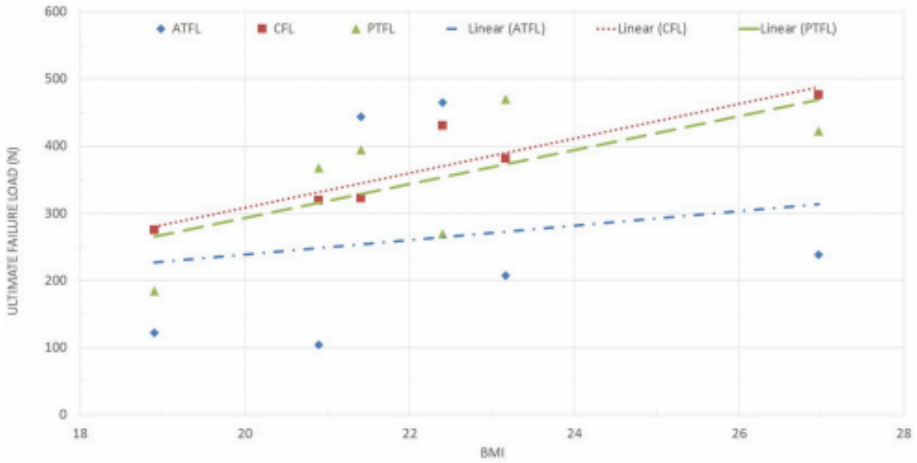

Fig. 6. A graphical representation of the relationship between BMI and ultimate failure load. The three ligaments of each donor are vertically aligned according to the BMI of the donor. The ATFL is shown by blue diamond markers, the CFL by red square markers and the PTFL by green triangle markers. Trend lines are shown for the ATFL (blue dash dot), CFL (red dotted) and PTFL (green dashed).

mechanical characteristics of the entire LCL complex when loaded at a realistic sprain-like strain rate (100%.s^{-1}) are reported. The mean ultimate failure load results concur with previously published work, that the CFL and PTFL provide similar levels of support under load and that the ATFL is the weakest (Attarian et al., 1985; Siegler and Schneck, 1988). There is however, a large amount variability between specimens, as shown in Fig. 6, and there was no clear pattern for which ligament is the strongest or weakest at an individual donor level. Whilst St Pierre et al. (1983) only reports tensile strength of the ATFL; they do so, in most cases, for each foot of each individual donor highlighting the substantial variability in ATFL failure load, ranging from 44 N to 556 N. Notably, the ATFL, which is widely established as the weakest LCL, was the strongest for two donors in this study, contradicting the general consensus (Attarian et al., 1985; Siegler and Schneck, 1988). The widely established view that the ATFL is the weakest of the LCLs could therefore be incorrect for some people. The cause of this finding is likely multifactorial and a much larger sample size and in-depth patient information is required to substantiate any hypothesis.

Stiffness results in this study are similar to those previously reported by Attarian et al. (1985) who strained the LCLs at strain rates considerably higher than 100%.s^{-1}. This paper therefore supports the theory that the strain-rate dependency of ligaments can be neglected when tested at strain rates greater than 100%.s^{-1} (Bonner et al., 2015; Funk et al., 2000). The current findings indicate a range of indicative ultimate failure loading requirements that can further inform the mechanical property specifications for synthetic ankle ligaments. Through improved matching of the mechanical properties, particularly the stiffness, of synthetic ligaments to their natural counterparts joint mobility and stability have the potential to also improve.

Both mid-substance failure and avulsion are abundantly prevalent as failure modes of the LCLs. Categorisation of the failure mode is somewhat subjective due to the fibrous nature of ligamentous failure, the difficulty faced differentiating between failure modes and the lack of a standardised definition of avulsion. The location of ligament avulsion was consistent, at the fibula for the ATFL and CFL and at the talus for the PTFL. Siegler et al. (1988) found the AFTL to avulse 58% of the time and the CFL and PTFL to avulse in 70% of tests, with remaining specimen failing mid-substance (Siegler and Schneck, 1988). Attarian et al. (1985) reported eight mid-substance failures and four talar avulsions for the ATFL, eight mid-substance failures, four calcaneal avulsions and four fibula avulsions for the CFL and four mid-substance failures for the PTFL (Attarian et al., 1985). St Pierre et al. (1983) reported 18 talar avulsions, 16 mid-substance failures and two unknown failures (St Pierre et al., 1983).

The location of ATFL avulsion in this study is inconsistent with those previously reported and an explanation as to why is unclear. Possible explanations include the status of the fibula, the orientation of the ligament or the vastly different strain rates. The fibula was intact for testing in the studies by St Pierre et al. (1983) and Attarian et al. (1985) whereas in this study the fibula was split reducing the amount of bone to be gripped. The orientation of the specimen may differ slightly between this study and the two studies highlighted due to the fibula not being intact, although all studies attempted tensile testing with fibre alignment. The prevalence of avulsion and mid-substance failures are however comparable. The high prevalence of avulsions could be due to the significantly higher local strain proximal to the attachment site of ligaments compared to the central region (Stouffer et al., 1985). The failure mechanism of a ligament is an important consideration prior to a ligament repair being performed as the fixation method may differ depending on whether the ligament needs reattaching to bone or to ligament.

A potentially noteworthy finding was the positive correlation between BMI and ultimate failure load values for the ligaments of the LCL complex, specifically the CFL. This finding, from a sample size of six, suggests that the CFL of individuals with a higher BMI have a greater load bearing capacity than those with a lower BMI. This is most likely due to the adaptive remodelling nature of ligamentous structures, as individuals with a greater BMI are likely to apply more stress to the ligament, increasing strength over time (Bonnel et al., 2010). The BMI of an individual could therefore be an important factor when selecting the appropriate material properties of a synthetic intervention, and notably people with a high BMI who are more often candidates for a synthetic ligament replacement (Ajis et al., 2006). Therefore, the load bearing capacity of the synthetic, and their fixation devices, should match the mean ultimate failure load to ensure the synthetic does not subsequently fail. The stiffness of the synthetic material, along with the tension applied upon insertion, is arguably more important. A stiffness that is too high could reduce the joint mobility and too low could affect the stability of the joint. Therefore it could be recommended that the stiffness of the synthetic material is also matched to that of the natural tissue

results reported.

The anatomy of ligaments is often depicted incorrectly in illustrations because of stylistic licence. The previously published pictorial essay does however provide detailed images of the ankle ligament anatomy (Golanó et al., 2016). Fig. 3 shows the attachment points of the ATFL and CFL to the fibula. These attachments are often illustrated as separate insertion points however as shown in Fig. 3, the two ligaments commonly attach at the same insertion point on the fibula. It is suggested that the inferior aspect of the ATFL and CFL are connected by arciform fibres (Sarrafian, 1983), thus forming the lateral fibulotalocalcaneal complex (Hertel, 2002). This observation was also made when performing the dissections for this study. The results of this study however suggest that the connecting fibres are not of a sufficient strength to cause both the ATFL and CFL to rupture simultaneously. The CFL was tested first in every instance and the results of the ATFL are still similar to those previously published, where they were tested without the arciform fibres present (Siegler and Schneck, 1988).

The limitations to the study predominantly centre on the use of human cadaveric tissue. The main limitation is the small sample size (n = 6). Research using donor cadaveric tissue should be minimised to only what is essential and performed with maximum efficiency and integrity out of respect for the donors. The characterisation of cadaveric human tissue may not reflect the same response as living tissue. However, ligamentous tissue primarily attributes its strength properties to the collagen fibres which form the majority of ligament structure. The collagen would not be greatly affected by the tissue being living or dead, providing it remains well hydrated and is stored appropriately to abate tissue degradation. Although the exclusion criteria required donors to have not reported any lower limb trauma we cannot be certain that a prior sprain had not occurred at some point during the donor's lifespan. It is estimated that ankle injury rates are approximately five and a half times higher than those registered in emergency departments (Kemler et al., 2015). This could provide some explanation for the inconsistencies in strength between ligament types (Fig. 6). Large variations in the results following the mechanical characterisation of ankle ligaments are also reported elsewhere (Siegler and Schneck, 1988). The use of elderly donor tissue to investigate sprain has previously been suggested to be a limitation of cadaver studies. An effort was therefore made when selecting donor specimens to obtain the youngest specimens possible (mean 56.2 years). A previous study however, reported no correlation between ultimate failure load and age for donors aged 17 to 54 when testing human anterior cruciate ligaments (Blevins et al., 1994). The link identified between BMI and ultimate failure load of the CFL and PTFL is based on a narrow range of BMI, with only one donor having a BMI outside of the normal range and the trend may not be reflected in a population at the extremities of the BMI scale.

5. Conclusion

Limitations aside, the conditions of this study were carefully defined to reflect those experienced by individuals who would suffer an ankle sprain, and for the first time the entire LCL complex has been characterised at realistic sprain inducing strain rates. In the current study, the ultimate failure load and stiffness of the ATFL, CFL and PTFL did not differ systematically but there was a tendency toward greater strength in people with a higher BMI. The maximum likely exposure loads, the BMI of the patient and the failure mode of the LCLs all appear to be factors to be further considered when selecting the material, repair or reconstruction technique to be used for surgical stabilisation of the sprained ankle.

Funding

This work was supported by the Engineering and Physical Sciences Research Council (EPSRC) [EP/L014823/1]; also supported by the National Institute for Health Research infrastructure at Leeds. The views expressed in this publication are those of the author(s) and not necessarily those of the NHS, the National Institute for Health Research or the Department of Health; and Xiros Ltd.

Acknowledgements

The authors would like to acknowledge Dr Nagitha Wijayathunga for his contributions to the CT scanning of the samples.

References

Ajis, A., Younger, A.S.E., Maffulli, N., 2006. Anatomic repair for chronic lateral ankle instability. Foot Ankle Clin. 11 (3), 539–545. https://doi.org/10.1016/j.fcl.2006.07.005.

de Asla, R.J., Kozanek, M., Wan, L., Rubash, H.E., Li, G., 2009. Function of anterior talofibular and calcaneofibular ligaments during in-vivo motion of the ankle joint complex. J. Orthop. Surg. Res. 4 (1), 7. https://doi.org/10.1186/1749-799X-4-7.

Attarian, D.E., McCrackin, H.J., DeVito, D.P., McElhaney, J.H., Garrett, W.E., 1985. Biomechanical characteristics of human ankle ligaments. Foot Ankle 6 (2), 54–58. https://doi.org/10.1177/107110078500600202.

Blevins, F.T., Hecker, A.T., Bigler, G.T., Boland, A.L., Hayes, W.C., 1994. The effects of donor age and strain rate on the biomechanical properties of bone-patellar tendon-bone allografts. Am. J. Sports Med. 22 (3), 328–333. https://doi.org/10.1177/036354659402200306.

Bonnel, F., Toullec, E., Mabit, C., Tourné, Y., 2010. Chronic ankle instability: biomechanics and pathomechanics of ligaments injury and associated lesions. Orthop Traumatol Surg Res 96 (4), 424–432. https://doi.org/10.1016/j.otsr.2010.04.003.

Bonner, T.J., Newell, N., Karunaratne, A., et al., 2015. Strain-rate sensitivity of the lateral collateral ligament of the knee. J. Mech. Behav. Biomed. Mater. 41, 261–270. https://doi.org/10.1016/j.jmbbm.2014.07.004.

Colville, M.R., Marder, R.A., Boyle, J.J., Zarins, B., 1990. Strain measurement in lateral ankle ligaments. Am. J. Sports Med. 18 (2), 196–200. https://doi.org/10.1177/036354659001800214.

Fong, D.T.-P., Hong, Y., Shima, Y., Krosshaug, T., Yung, P.S.-H., Chan, K.-M., 2009. Biomechanics of supination ankle sprain: a case report of an accidental injury event in the laboratory. Am. J. Sports Med. 37 (4), 822–827. https://doi.org/10.1177/0363546508328102.

Funk, J.R., Hall, G.W., Crandall, J.R., Pilkey, W.D., 2000. Linear and quasi-linear viscoelastic characterization of ankle ligaments. J. Biomech. Eng. 122 (1), 15. https://doi.org/10.1115/1.429623.

Golanó, P., Vega, J., de Leeuw, P.A.J., et al., 2016. Anatomy of the ankle ligaments: a pictorial essay. *Knee Surgery*. Sport Traumatol Arthrosc 24 (4), 944–956. https://doi.org/10.1007/s00167-016-4059-4.

Herbert, A., Brown, C., Rooney, P., Kearney, J., Ingham, E., Fisher, J., 2016. Bi-linear mechanical property determination of acellular human patellar tendon grafts for use in anterior cruciate ligament replacement. J. Biomech. 49 (9), 1607–1612. https://doi.org/10.1016/j.jbiomech.2016.03.041.

Hertel, J., 2002. Functional anatomy, pathomechanics, and pathophysiology of lateral ankle instability. J. Athl. Train. 37 (4), 364–375. https://doi.org/10.1017/CBO9781107415324.004.

Kemler, E., van de Port, I., Valkenberg, H., Hoes, A.W., Backx, F.J.G., 2015. Ankle injuries in The Netherlands: trends over 10-25 years. Scand. J. Med. Sci. Sport. 25 (3), 331–337. https://doi.org/10.1111/sms.12248.

Quinn, K.P., Winkelstein, B.A., 2011. Preconditioning is correlated with altered collagen fiber alignment in ligament. J. Biomech. Eng. 133 (6), 575–579. https://doi.org/10.1115/1.4004205.

Sarrafian, S.K., 1983. Anatomy of the Foot and Ankle. JBLippincott Co.

Siegler, S., Schneck, C.D., 1988. The mechanical characteristics of the collateral ligaments of the human ankle joint. Foot Ankle Int. 8 (5), 234–242. https://doi.org/10.1177/107110078800800502.

St Pierre, R.K., Rosen, J., Whitesides, T.E., Szczukowski, M., Fleming, L.L., Hutton, W.C., 1983. The tensile strength of the anterior talofibular ligament. Foot Ankle 4 (2), 83–85. https://doi.org/10.1177/107110078300400208.

Stouffer, D.C., Butler, D.L., Hosny, D., 1985. The relationship between crimp pattern and mechanical response of human patellar tendon-bone units. J. Biomech. Eng. 107 (2), 158–165. https://doi.org/10.1115/1.3138536.